Technical Report Documentation Page

1. Report No.	2. Government Accession No.	3. Recipient's Catalog No.
Preliminary Review Copy		

4. Title and Subtitle	5. Report Date
EXPERIMENTAL INVESTIGATION OF DESIGN METHODS FOR LARGE CANTILEVER BRIDGE BENTS	August 1997
	6. Performing Organization Code

7. Author(s)	8. Performing Organization Report No.
B.A. Wood, M.E. Kreger and J.E. Breen	Research Report 1364-3F

9. Performing Organization Name and Address	10. Work Unit No. (TRAIS)
Center for Transportation Research The University of Texas at Austin 3208 Red River, Suite 200 Austin, TX 78705-2650	11. Contract or Grant No. Research Study 0-1364

12. Sponsoring Agency Name and Address	13. Type of Report and Period Covered
Texas Department of Transportation Research and Technology Transfer Office P.O. Box 5080 Austin, TX 78763-5080	14. Sponsoring Agency Code

15. Supplementary Notes

Project conducted in cooperation with the Federal Highway Administration.

16. Abstract

During design of large cantilever bents using current AASHTO design specifications for use on recent projects, designers were faced with considerable uncertainties. Questions arose when designers attempted to satisfy both serviceability and strength requirements for a series of bent cap designs that mixed both non-prestressed and prestressed concrete solutions. The problems were further complicated because of uncertainty whether AASHTO corbel or deep beam provisions were applicable. The resulting designs were highly congested, had reduced constructibility, and high costs.

This report outlines the development of a new design approach involving the use of strut-and-tie models as well as a mix of prestressed and non-prestressed flexural reinforcement. A series of five large-scale cantilever bents were designed according to existing specifications or the proposed specifications, constructed, and tested to failure. Deflections, crack patterns and widths, reinforcement strains, and overall behavior were observed. Economic and constructibility issues were examined. T-head anchorages were incorporated in designs conforming with the proposed specifications.

A comprehensive design approach that considers both serviceability issues (deflections, cracking, crack widths, fatigue stress ranges, and side-face crack control) and strength issues (ductility, adequacy of the strut-and-tie modeling approach, and analysis of flexural capacity) was developed. Recommendations for design and detailing to improve behavior, reduce congestion, and improve constructibility are provided.

17. Key Words	18. Distribution Statement
Bridge bents, prestressed concrete, reinforced concrete, strut-and-tie models	No restrictions. This document is available to the public through the National Technical Information Service, Springfield, Virginia 22161.

19. Security Classif. (of report)	20. Security Classif. (of this page)	21. No. of pages	22. Price
Unclassified	Unclassified	316	

Form DOT F 1700.7 (8-72) Reproduction of completed page authorized

EXPERIMENTAL INVESTIGATION OF DESIGN METHODS FOR LARGE CANTILEVER BRIDGE BENTS

BY

B.A. WOOD, M.E. KREGER AND J.E. BREEN

Research Report No. 1364-3F

Research Project 0-1364

"Design of Large Structural Members Utilizing Partial Prestressing"

conducted for the

Texas Department of Transportation

IN COOPERATION WITH THE

U.S. Department of Transportation

Federal Highway Administration

by the

CENTER FOR TRANSPORTATION RESEARCH

BUREAU OF ENGINEERING RESEARCH

THE UNIVERSITY OF TEXAS AT AUSTIN

August 1997

This report was prepared in cooperation with the Texas Department of Transportation and the U.S. Department of Transportation, Federal Highway Administration.

DISCLAIMERS

The contents of this report reflect the views of the authors, who are responsible for the facts and the accuracy of the data presented herein. The contents do not necessarily reflect the official views or policies of the Federal Highway Administration or the Texas Department of Transportation. This report does not constitute a standard, specification, or regulation.

There was no invention or discovery conceived or first actually reduced to practice in the course of or under this contract, including any art, method, process, machine, manufacture, design or composition of matter, or any new and useful improvement thereof, or any variety of plant which is or may be patentable under the patent laws of the United States of America or any foreign country.

NOT INTENDED FOR CONSTRUCTION,
BIDDING, OR PERMIT PURPOSES

Michael E. Kreger, P.E. (Texas No.65541)
Research Supervisor

ACKNOWLEDGMENTS

The authors express appreciation for the guidance provided by the Texas Department of Transportation (TxDOT) Project Director, Dean Van Landuyt.

SUMMARY

During design of large cantilever bents using current AASHTO design specifications for use on recent projects, designers were faced with considerable uncertainties. Questions arose when designers attempted to satisfy both serviceability and strength requirements for a series of bent cap designs that mixed both non-prestressed and prestressed concrete solutions. The problems were further complicated because of uncertainty whether AASHTO corbel or deep beam provisions were applicable. The resulting designs were highly congested, had reduced constructibility, and high costs.

This report outlines the development of a new design approach involving the use of strut-and-tie models as well as a mix of prestressed and non-prestressed flexural reinforcement. A series of five large-scale cantilever bents were designed according to existing specifications or the proposed specifications, constructed, and tested to failure. Deflections, crack patterns and widths, reinforcement strains, and overall behavior were observed. Economic and constructibility issues were examined. T-head anchorages were incorporated in designs conforming with the proposed specifications.

A comprehensive design approach that considers both serviceability issues (deflections, cracking, crack widths, fatigue stress ranges, and side-face crack control) and strength issues (ductility, adequacy of the strut-and-tie modeling approach, and analysis of flexural capacity) was developed. Recommendations for design and detailing to improve behavior, reduce congestion, and improve constructibility are provided.

IMPLEMENTATION

Suggested design procedures are presented for design and detailing of large cantilever bents for structural concrete piers. Design procedures consider both service limit-state and strength limit-state requirements. At the service limit state, recommendations are made for crack width and distribution control for combinations of non-prestressed and prestressed reinforcement, for deformation limits, and for stress-range control to preclude fatigue failures. At the strength limit state, recommendations suggest use of approximately 75% prestressing with supplemental non-prestressed reinforcement to distribute and control cracks and to improve ductility. Strut-and-tie models are recommended for proportioning of shear reinforcement, rather than the corbel, deep beam, or shear friction rules generally used under the current AASHTO specifications. Economic studies show that reinforcement costs for such solutions will be in the range of current non-prestressed solutions, but reinforcement congestion will be greatly reduced, improving constructibility.

TABLE OF CONTENTS

TABLE OF FIGURES

TABLE OF TABLES

CHAPTER 1

INTRODUCTION

1.1 PROBLEM STATEMENT

An elevated expressway and a series of highway interchanges were constructed in San Antonio to link I-10 and I-35 and reduce traffic congestion. Because right-of-way for the ground level feeder roads and main lanes conflicted with the proposed geometry for on-ramps and off-ramps as well as several portions of the main lane elevated expressway, support piers were designed to cantilever over the existing roadways. These cantilever bents supported large prestressed concrete winged box girders, where dead load of the superstructure comprised approximately four-fifths of the design service load. Loads from the superstructure were transmitted to the substructure through two bearings located beneath the winged box girder. Location of the bearing points on the substructure varied as shown in Figure 1.1. For many of the cantilever bents, both reactions were located on the overhang.

Figure 1.1 Cantilever bents supporting entrance ramp

During design of these large bents, some confusion resulted because one reaction was often located on the overhang a short distance from the column face, resulting in a small span-to-depth (a/d) ratio less than one, and the second reaction was typically located well out on the overhang (for an a/d ratio greater than one). Current AASHTO Standard Bridge Specifications [1] state that corbel design provisions "shall apply to brackets and corbels with a shear span-to-depth ratio a/d not greater than unity," where d is measured from the column face. To be certain they were not overlooking any design provisions, designers satisfied both corbel and flexural design provisions by providing longitudinal reinforcement in the top of the overhang to resist design moments and longitudinal reinforcement near mid-depth to resist design shear friction. Because

the resulting designs were extremely congested, it was believed that the bents were substantially over-designed.

The separate treatment of reinforced concrete and prestressed concrete members in current AASHTO Standard Bridge Specifications forces engineers to perform either reinforced concrete designs or "fully prestressed" designs that are typically controlled by service-level stresses. This often results in inefficient use of the materials. For example, where the depth of a cantilever is limited by factors such as ground clearance, a fully-prestressed design is often implemented because a reinforced concrete design would be too congested. Cost associated with fully-prestressing the cantilever could be reduced if only the prestressing needed to supply the flexural capacity of the member or supplement a portion of the non-prestressed reinforcement was provided instead of fully-prestressing the cantilever. In addition, reinforced and prestressed concrete design specifications are contained in separate chapters, resulting in confusion when applying corbel design and shear friction provisions.

A research study (Project 3-5-93-1364) was commissioned by the Texas Department of Transportation and the Federal Highway Administration to develop an alternate design method for design of large structural members utilizing partial prestressing. The primary objective was to develop a design method whereby a mixture of high-strength prestressed reinforcement and mild reinforcement (often referred to as "partially prestressed concrete" and herein referred to as "structural concrete") could be used to provide both strength and adequate serviceability. Previous research conducted at The University of Texas at Austin [2] provided guidelines for structural concrete and use of strut-and-tie models (STM) for design of large concrete members.

1.2 SCOPE OF RESEARCH

Research performed as part of Project 3-5-93-1364, was divided into four phases. The first phase investigated the design of the cantilever portion of the substructure. This research was performed by Armstrong [3] and Salas [4], and their studies provided a design method for the cantilever portion of the bent. The second phase, performed by Billington [5], investigated the use of structural concrete for design of large, two-span continuous beams. Results of the study were used to validate the finite element analysis procedure for modeling continuous tendons. The third phase, reported here, investigates the behavior of the cantilever bent as a whole (overhang, pier, and joint) and proposes code language for an integrated design method for structural concrete. In this study, two San Antonio 'Y' prototype cantilever bent designs and three integrated design models were constructed and tested. It was determined during this phase that many of the San Antonio 'Y' cantilever bents were deficient due to a detailing flaw in the joint region. In order to alleviate this deficiency, the research study was extended to include a fourth phase, reported by Scott [6], in which three strengthening methods were developed, implemented on damaged test specimens, and tested.

1.3 OBJECTIVE OF RESEARCH

The objective of this research was to evaluate the behavior of large cantilever bents with a/d ratios ranging from less than one to approximately two, evaluate the behavior of the prototype design specimens and behavior of specimens containing different combinations of high-strength prestressed reinforcement and mild reinforcement, and develop a unified design method for structural concrete.

1.4 ORGANIZATION

This document is organized into seven chapters, as follows:

Chapter 2–Background	**PROVIDES BACKGROUND ON DESIGN ISSUES INVOLVED IN THE STUDY.**
Chapter 3–Experimental Program	Details the design of each specimen, testing equipment, and material properties.
Chapter 4–Test Results	Presents moment-deflection response, crack-width measurements, and failure modes.
Chapter 5–Analysis of Test Results	Compares responses of all specimens, evaluates analysis tools, and provides cost estimates for each design.
Chapter 6–Proposed Design Recommendations	Recommends changes to the AASHTO LRFD Specifications based on results of the experimental program.
Chapter 7–Conclusions	Summarizes the results of the study.

CHAPTER 2

BACKGROUND

2.1 INTRODUCTION

Investigation of the San Antonio bridge substructures was initiated when a preliminary review of the designs revealed confusion over the applicability of some of the AASHTO design provisions, and substantial congestion in the pier, overhang, and joint regions. Congestion resulted because it was not clear to designers which sections of the Standard Specifications were applicable to reinforced concrete and prestressed concrete design. In order to produce a conservative, safe design, designers applied all the provisions that were directly or remotely related to the design of the substructure elements. Application of some of these provisions will be discussed later in this chapter. Based on this experience, it was clear that an integrated design method, in the form of a specification, would simplify the design process, provide economy, and instill substantially more confidence in the users of the design specification.

2.2 DESCRIPTION OF CANTILEVER BENTS IN SAN ANTONIO

The cantilever bents in San Antonio were constructed to support a newly constructed elevated roadway for I-10 and I-35 over the existing ground-level lanes and entrance ramps. The elevated roadways were segmental prestressed winged box girders that were supported at two points on the bottom of pier segments. The massive superstructure resulted in very large dead load reactions and moments on the substructure. Approximately four-fifths of the service load reactions were attributed to the superstructure dead load component. A schematic of the cantilever bent is presented in Figure 2.1.

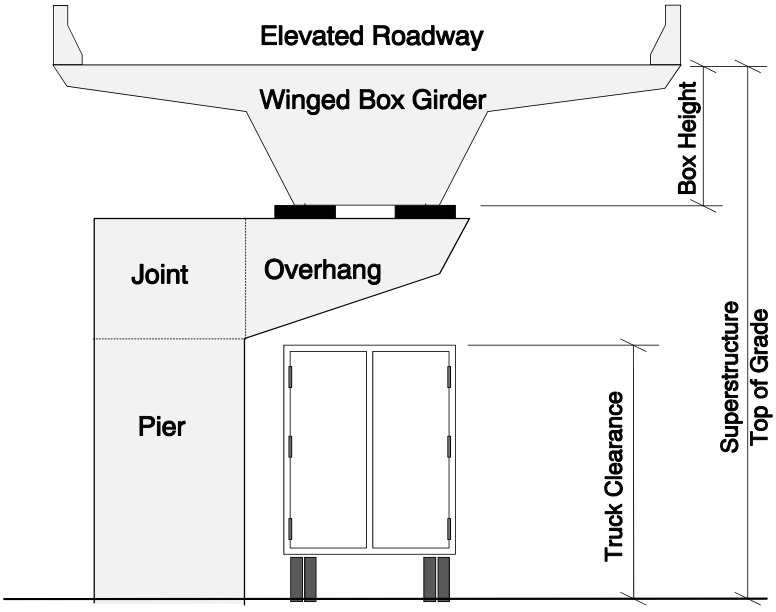

Figure 2.1 Schematic of cantilever bents in San Antonio

2.3 EVALUATION OF CURRENT DESIGN PRACTICE

Evaluation of strengths and weaknesses of the current design practice is important in the development of an integrated design method. The AASHTO Standard Specifications for Highway Bridges [7] was the code standard used for the design of the prototype bents. A more complete explanation of the mechanics and equations in the bridge design specifications is presented in Chapter 3. The convention used to describe the different regions of the bent (pier, overhang, and joint regions) is presented in Figure 2.1.

2.3.1 AASHTO Reinforced Concrete Design

The AASHTO Reinforced Concrete Design Specifications are located in Section 8 of the AASHTO Standard Specifications for Highway Bridges. The specific design requirements and procedures are detailed in Chapter 3. A general overview of the specifications is offered to provide anecdotal evidence of the ambiguity inherent in the specifications that were used to design the cantilever bents.

Sections of the specification addressing flexural design, corbel design, deep beam design, shear design, and serviceability requirements were applied to the design of prototype cantilever substructures, much as they had been applied by TxDOT designers to illustrate the conservative approach that was taken in the design of the bents.

2.3.1.1 Reinforced Concrete Overhang Design

The flexural design equations were used to determine the amount of flexural steel required to resist factored overhang moments. A reinforced concrete design was used if the amount of overhang reinforcement did not exceed the number of bars that could be placed in two rows of tension reinforcement. Otherwise, a fully-prestressed design was conducted.

Because the location of the interior load on the overhang was within a shear span-to-depth ratio (a/d) of less than one (an a/h of 0.5 is shown in Figure 2.2), corbel specifications were used to design for the inner superstructure reaction, R_i. Flexural design was used to resist the outer superstructure reaction, R_o, which was located one and one-half times the depth of the beam (1.5 h) from the column face (see Figure 2.2). The corbel design provisions require reinforcement for shear friction. This reinforcement was located near mid-depth (see Figure 2.2), and accounted for almost half of the primary tension reinforcement. The shear-friction reinforcement was not considered to contribute to the flexural strength of the section.

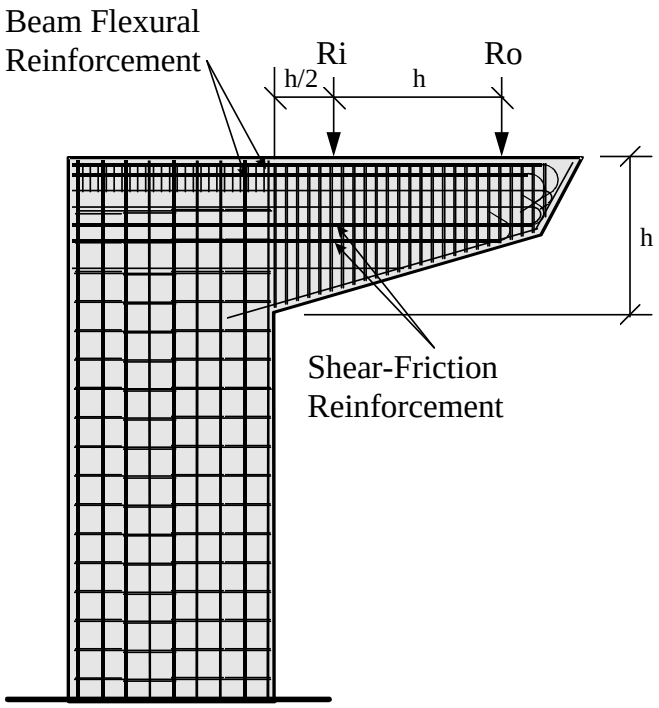

Figure 2.2 Reinforced concrete design

The quantity of transverse reinforcement required along the overhang was somewhat ambiguous due to the tapered depth of the overhang. Because the concrete component of the shear strength equation is a function of the depth of the section, a 45° failure plane propagating from the outer reaction was assumed, and the transverse reinforcement quantity necessary to intersect the diagonal crack and resist the outer reaction was computed. As will be discussed in Chapter 3, geometry of the overhang permitted a force path by which a portion of the outer reaction flowed directly into the pier. However, the shear design provisions in the Standard Specifications do not consider such force paths. In addition, the shear associated with the inner reaction was addressed through corbel design. As a result, spacing of the transverse reinforcement computed for the outer reaction was used for the entire overhang.

Fatigue stress limits in the reinforcement, and distribution of longitudinal reinforcement to control cracking were also checked for the overhang.

2.3.1.2 Reinforced Concrete Pier Design

The pier design involved the determination of minimum member size and minimum number of longitudinal reinforcing bars to resist axial forces and overturning moments. The pier designs were nearly all controlled by the AASHTO minimum longitudinal reinforcement ratio requirement of 1% ($0.01\ A_g$). Serviceability requirements such as fatigue stress limits and limits on cracking for the pier region were required by the AASHTO Standard Specifications but were typically not checked by designers of the San Antonio 'Y' substructures.

2.3.1.3 Reinforced Concrete Joint Design

The joint region for the cantilever substructure was constructed by continuing the longitudinal pier and overhang reinforcement into the joint. Column ties were placed up to the top row of overhang reinforcement, and the size of the joint was assumed to be sufficient to fully develop the longitudinal reinforcement from the critical sections of the overhang and pier regions into the joint (see Figure 2.2).

2.3.2 AASHTO Prestressed Concrete Design

The Prestressed Concrete Design Specifications are located in Section 9 of the AASHTO Standard Specifications for Highway Bridges. In addition to the reinforced and prestressed concrete specifications being located in separate sections, there is a different philosophy behind the design procedures; the prestressed design specifications assume that members are uncracked at service loads. This type of design will be referred to as "fully prestressed" in future discussion. The fully-prestressed design was performed for cantilever bents in San Antonio when it was not possible to fit a sufficient number of mild reinforcing bars into the member to resist factored loads.

In addition to separate specifications for reinforced concrete and prestressed concrete, the design process is further muddled because many sections of the prestressed specifications make reference to the reinforced concrete specifications. Shear friction design, corbel design, and design of deep beam reinforcement are not addressed in Section 9 of the AASHTO Specifications. For the cantilever substructures in the San Antonio 'Y' project, the location of the loads and magnitude of the shear forces on the overhang made these design aspects quite critical in the eyes of the designers for both the reinforced and prestressed concrete designs.

2.3.2.1 Fully Prestressed Overhang Design

The fully prestressed overhang design (Figure 2.3) was based on limiting concrete tensile stresses due to flexure of $3\sqrt{f_c'}$ at service load, and included all the design provisions assumed to be relevant, such as shear friction design, corbel design, and the design of deep beam reinforcement from the AASHTO reinforced concrete design specifications in Section 8.

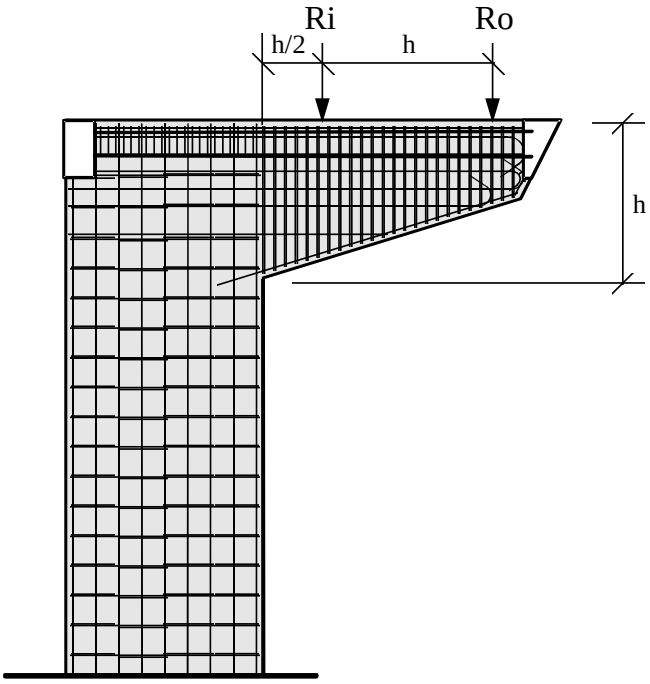

Figure 2.3 Fully prestressed overhang design with reinforced concrete pier

2.3.2.2 Fully Prestressed Pier Design

For cases where the overhang was quite long and the superstructure loading was located well onto the overhang, continuous post-tensioning through the overhang, joint, and pier was used (shown in Figure 2.4). The pier longitudinal reinforcement ratio was maintained at 1% of the gross concrete area of the pier. Flexural stresses in these piers were limited to the service load tensile stress limit of $3\sqrt{f_c'}$. Due to loss of prestress through the joint region, an additional series of tendons was placed in from the top of the joint and through the pier (shown in Figure 2.4) to provide additional prestressing. As a result, the design strength of the piers was significantly greater than required for factored loads.

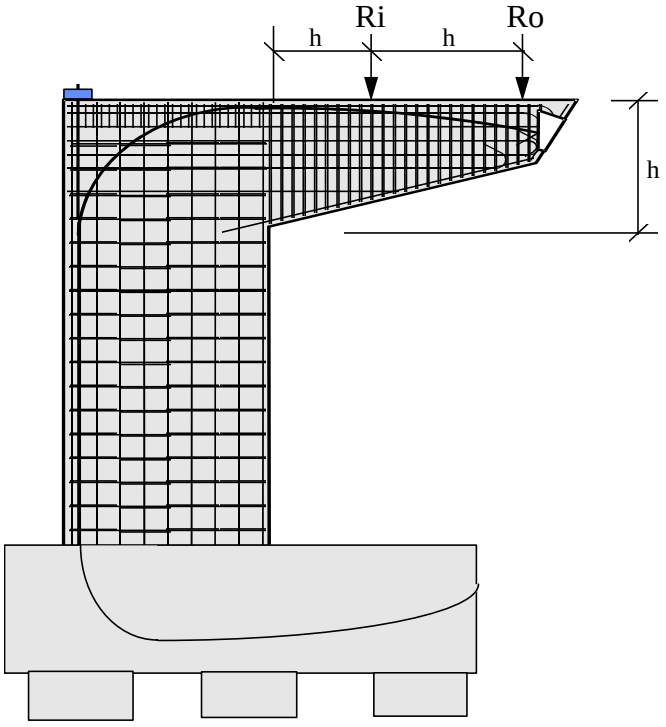

Figure 2.4 Fully prestressed substructure with continuous post tensioning

2.3.2.3 Fully Prestressed Joint Design

As in the case of the reinforced concrete joint, overhang and pier longitudinal reinforcement was continued into the joint region and anchored using straight bar development. The continuous post-tensioning through the joint region (shown in Figure 2.5) significantly reduced tensile stresses in the joint region during service loads. For cases in which only horizontal post-tensioning was provided through the overhang and the joint (shown in Figure 2.6), the longitudinal bars were terminated in the joint corner.

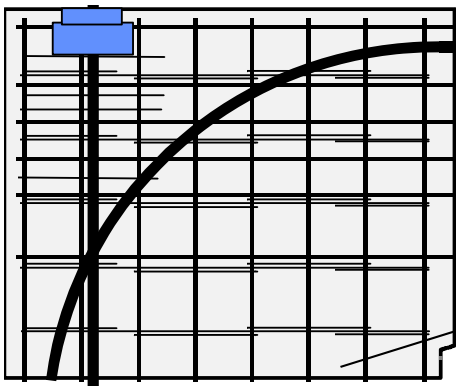

Figure 2.5 Schematic of joint region for continuous post-tensioning detail

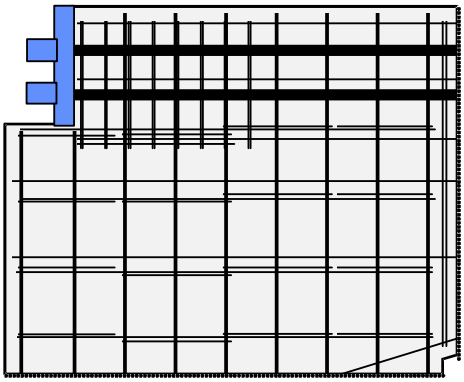

Figure 2.6 Schematic of joint region for post-tensioned overhang detail

2.4 DEVELOPMENT OF AN INTEGRATED DESIGN METHOD

Ambiguities associated with the application of the AASHTO Standard Specifications to design of large substructures, and the resulting conservative designs, were the original impetus for development of an integrated design method. Additional reasons supporting the development of an integrated design method are presented in later chapters.

Development of an integrated design method involved providing a procedure that accounts for any design contingency, is sufficiently clear for easy use by designers, and provides some guidance for use. Design of any structure must involve consideration of strength and serviceability.

The proposed integrated design method allows use of both deformed mild steel and high-strength prestressing steel for tension reinforcement. Members are allowed to crack under service loads, but the designer must control crack widths, limit fatigue stresses in the strand and mild reinforcement, and consider factors affecting long-term durability. Design will not be compartmentalized into categories such as shear design, flexural design, etc., but rather the flow of forces through members will be investigated and details provided to yield optimal performance of the structure. Good detailing practices and minimum reinforcement limits will be required to provide sufficient ductility.

2.4.1 Overview of Related Research

An overview of the previous research is presented to illustrate the tools that have been proposed and incorporated into the integrated design procedure used to develop experimental models tested as part of this study.

2.4.1.1 Strut-and-Tie Modeling

Development of strut-and-tie models for the cantilever bent specimens was greatly assisted by the PCI paper by Schlaich et al. [8]. The behavior and proposed flow of forces for many of the design examples provided insight into the development of similar strut-and-tie models for design of specimens tested in this study. The strut-and-tie model used in the design of anchorage zones in the prestressed specimens tested in this study was developed using NCHRP Report No. 356 [9].

2.4.1.2 Partial Prestressing

The history of partial prestressing is discussed in detail in a thesis by Billington [5]. The concept of partial prestressing has been applied in many ways, ranging from allowing extreme concrete tensile fibers to experience minimal tensile stresses at service loads, to permitting concrete cracking. The different incarnations of partial prestressing generally have been opposed due to concerns about fatigue in the prestressing steel, long-term corrosion durability, and large unsightly cracks in members. The use of the following tools to address these concerns should provide some confidence that the issues can be addressed and controlled using good design and detailing practices.

2.4.1.3 Deep Beam

Concerns about concrete deep beam design have historically been related to the fact that plane sections do not remain plane. The majority of deep beam designs are compounded by a lack of understanding about detailing the beam for good serviceability. Although sections might not remain plane in deep beams, the design of the primary longitudinal reinforcement can be achieved by utilizing a strut-and-tie model to compute the area of tension reinforcement required to resist factored loads. Frantz and Breen [10] developed an equation for the design of side-face cracking reinforcement, which was shown to control large cracks near mid-depth of deep members.

2.4.1.4 Limits on Column Longitudinal Reinforcement

The lower limit on column longitudinal reinforcement was developed at he University of Illinois at Urbana-Champaign and Lehigh University during the 1930's and 1940's [11]. The limit was established to preclude creep failure in concrete columns under sustained compression loads. The researchers conducted over 100 long-term column tests under a range of loads. The 1% minimum column reinforcement provision was established to prevent the onset of yielding of 276 MPa (40 ksi) mild longitudinal reinforcement under maximum expected sustained loads. The "load shedding" of the concrete to lesser quantities of mild reinforcement subjected to long-term loading could cause yielding of the column reinforcement.

Research that is currently underway at The University of Texas at Austin is investigating minimum column reinforcement for Grade 60 longitudinal reinforcement [12]. Because preliminary results of the column study were not available at the time specimens were designed and fabricated for this study, a lower limit of 0.7% for the column reinforcement ratio was used.

2.4.1.5 Design of Headed Reinforcement

The development and use of headed mild reinforcement (see Figure 2.7) provides for anchorage of reinforcement over very short embedment lengths (even for large-diameter bars). Headed reinforcement also provides a clearly defined node that can be used when designing strut-and-tie models. The development of nodes is important for redirecting the flow of forces into the desired path.

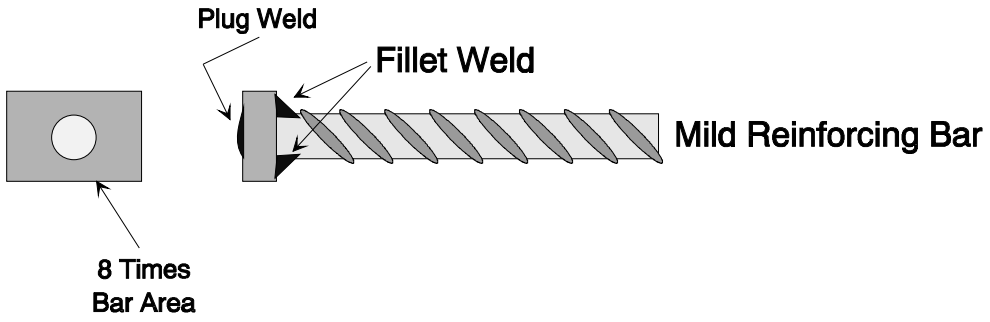

Figure 2.7 Headed bar schematic

The minimum area of the head on headed reinforcement has been studied as part of a research program at The University of Texas at Austin [13]. Previous research on headed reinforcement [14] indicated that the area of the welded plate (the head) on the end of the reinforcement should be 6 to 10 times the area of the bar. The use of a smaller plate may allow closer bar spacing and reduced concrete cover requirements for headed bars. Headed bars used in this study utilized plate areas equal to 8 times the bar area. The headed bar detail, shown in Figure 2.7, is representative of bars fabricated specifically for use in this study. Commercially-manufactured headed reinforcement in standard bar sizes was not used because test specimens utilized in the study were reduced scale and required the use of some small-scale bars.

2.4.1.6 Crack-Width Prediction

Many crack-width prediction models have been proposed for control of cracks in the design of structures in North America [15, 16, and 17]. The Building Code Requirements for Reinforced Concrete (ACI 318-93) Equation (10-4) [18] are generally accepted as the standard for providing a distribution of reinforcement that will control crack widths. However, an all-encompassing, scaleable formula has been sought that considers the effects of prestressing bars and strands, and mild reinforcement in the computation of maximum crack width. Many of the design formulas are discussed in a report by Yip [17].

The crack-width equation that was used in this study was similar to that incorporated in the AASHTO Load and Resistance Factor Design (LRFD) Specifications [19], and was developed to predict the cracking behavior of the overhang specimens studied by Armstrong [3] and Salas [4]. The crack-width formula utilized the steel stress at the tensile reinforcement centroid, the number of mild reinforcing bars, and number of bonded prestressing bars/strands in the tension zone. Crack widths predicted with the equation were in good agreement with the maximum crack widths measured in previous experiments [3, 4]. Details of the crack-width formula will be discussed in Section 3.4.1.2.

2.4.1.7 Durability and Maximum Allowable Crack Widths

Concern about durability and maximum allowable crack width has existed since the early development of reinforced concrete design. The concern with large crack widths is that chlorides can penetrate into the cracks and initiate corrosion of the reinforcement. Once a corrosion cell is

established, the reinforcement oxidizes and loses cross-sectional area. The long-term effects are loss of strength and potential premature failure of a member. Corrosion of high-strength reinforcement is of greatest concern due to the reduced corrosion resistance of small-diameter wire strands. The loss of even a small portion of the prestress can significantly degrade the service load performance and cause premature failure.

Low-permeability, high-alkaline concrete, epoxy-coated bars and strands, galvanized bars and strands, and cathodic protection have all been used to provide durable concrete structures. The long-term behavior of cracked partially-prestressed concrete is being investigated by West [20] to establish guidelines for the development of durable concrete structures. The range of different maximum crack-width limits from around the world [21] attests to the lack of a rational limit. If a maximum crack width is identified in West's study or in a subsequent study, it will be possible to use the crack-width equation to limit crack widths in members.

2.4.1.8 Scaling Model Crack Widths and Behavior

The scaled behavior of crack widths was a concern when test specimens were initially designed. The size of full-scale prototypes necessitated scaling of the test specimens to be able to economically construct and test the specimens in the laboratory. The similitude of cracking and deformation behavior for model specimens with a scale factor of 1 (full-scale), 2.5 (2/5th scale), and 4 (1/4 scale) performed by Borges and Lima [22] presented convincing evidence of crack-width similitude. The text on modeling concrete structures by Mirza [23] concluded that crack-width similitude is present for models as small as 1/10th scale.

In order to extrapolate full-scale behavior from the scale models, it was important to use mild reinforcement with the same nominal yield as used in the prototype substructures, and use scaled aggregate sizes, loads, bar spacing, and concrete cover requirements.

2.4.1.9 Fatigue Stress Limits

Previous research on partial prestressing performed by Abeles [24, 25] identified some concerns associated with cracking in prestressed concrete; specifically, fatigue of bonded mild and prestressed reinforcement. Based on the research by Wollman [26], the stress range in prestressing tendons should be kept below 100 MPa (14.5 ksi).

2.4.2 Synopsis of Previous Recommendations Used in This Study

A synopsis of the design recommendations, from the previous work on overhang specimens by Armstrong [3] and Salas [4], used in this study to design and detail test specimens is presented below.

2.4.2.1 Development of a Strut-and-Tie Model

The strut-and-tie model (STM) aids in visualizing the force path through a member from the point of load application, through the specimen, and to the structural supports. The compressive forces indicate where the concrete will direct the forces, and the tension tie forces indicate where steel should be located. By establishing a determinate geometry of compression struts and tension ties, the tension tie forces and compressive stresses can be computed. The overall model is used to design the major regions of the members, but local details such as anchorage zone bursting forces, can also be analyzed and designed. If there is any doubt as to how the forces flow through the member, a finite element model can be developed and executed to analyze the flow of stresses and forces.

2.4.2.2 Development of FEM for Cantilever Bents

Elastic analysis of the reinforced concrete sections provides the principal tensile resultants and compressive resultants that can be used to aid in construction of the strut-and-tie models. A plane stress 2D element model with concrete material properties was used throughout the research project to identify the flow of stresses through the elements. Once the flow of stresses was identified, a strut-and-tie model was fit to the envisioned stress flow to evaluate the force levels and material requirements.

The finite element models (FEM) for the prestressed specimens used external forces to apply the post-tensioning forces. It was simple to check tensile stresses at dead and service loads and to evaluate the crack-initiation loads with the FEM.

2.4.2.3 Tensile Reinforcement Requirements

The amount and approximate location of tensile reinforcement was determined using the STM. Cover requirements and the number of layers of steel often controlled the actual locations of tensile reinforcement. Once the flow of forces was established, details for various sections were checked using a linear strain compatibility model.

Design of Longitudinal Reinforcement:

Factored load capacity, crack widths, and tension steel fatigue stress ranges were checked using a strain compatibility design model that assumed a linear variation of strain over the depth of the section. The linear variation of strain was assumed because the side-face reinforcement was considered to help control non-linear deformation of the deep beam. Only minimum compressive reinforcement was provided to reduce the effects of creep and shrinkage.

Design of Transverse Reinforcement:

Transverse reinforcement was considered only for areas where tension tie forces from the STM were indicated. The amount of tensile reinforcement was reduced by considering a concrete contribution of $1\sqrt{f_c'}\, b_w d$ to the shear strength of flexural members. Minimum shear reinforcement was used for the remainder of the overhang.

Design of Anchorage Reinforcement:

The anchorage zone design utilized the design recommendations from NCHRP Report No. 356 [9]. This was essentially a STM approach for the design of the anchorage bursting and confinement reinforcing steel.

CHAPTER 3

EXPERIMENTAL PROGRAM

3.1 INTRODUCTION

Tools for the integrated design method were developed during an earlier phase of the sponsored research study investigating partially-prestressed large substructure members. Armstrong [3] and Salas [4] tested eight-1/5.5 scale-models of overhang elements with geometry similar to the cantilevers used in the San Antonio 'Y' project. A portion of their study was intended to test the efficiency of a strut-and-tie model for the design of primary tensile reinforcement and transverse reinforcement. A series of four partially-prestressed specimens with 54-100% of the flexural capacity provided by prestressed reinforcement, and models of two prototype cantilever elements were tested. Service-load performance and ultimate strength were evaluated for each specimen. During this investigation, a strain-compatibility model and crack-width prediction model for partially-prestressed concrete members were developed and evaluated. The overhang study indicated the strut-and-tie model, crack prediction model, and strain compatibility model provided reasonable prediction of specimen behavior. The same tools and similar design methodology were used to design the test specimens for this study.

Specimens investigated in this testing program were intended to study not only the behavior of the overhang, but also the behavior of the connection between the overhang and column elements. The resulting cantilever bent specimen contains a pier (column), overhang (cantilever), and joint (connection region), and will henceforth be referred to as the Pier-Overhang-Joint (POJ) specimen (see Figure 3.1 for an example of this substructure system). The study involved the construction and testing of five specimens: two models of cantilever bents designed using the same process used for the San Antonio 'Y' substructures (hereinafter referred to as the "prototype models") and three integrated design models. The two prototype models included a reinforced concrete model and a fully-prestressed overhang with a reinforced concrete pier (discussed in Chapter 2). The three integrated design models included: a reinforced concrete design with headed reinforcement, a 54% prestressed design, and a 74% prestressed design, where the percentage indicates the percent of flexural capacity provided by the prestressed reinforcement.

The Pier-Overhang-Joint experimental program was initiated to verify the experimental results from the overhang study as well as expand the use of the integrated design method to include the design of the joint and pier regions. Several studies that may impact the final recommendations of this study are currently underway at The University of Texas at Austin. Included in this group are: Minimum Mild Reinforcing Requirements for Conventionally Reinforced and Prestressed Concrete Columns [12], Durability Design of Post-Tensioning Substructure Elements [20], and Design Recommendations for Headed Reinforcement [13]. Final recommendations from this study should be reviewed once these related studies are completed.

3.2 DEVELOPMENT OF THE PIER-OVERHANG-JOINT SPECIMEN

3.2.1 Selection of Full-Scale Superstructure Loads

The San Antonio 'Y' substructures supported a variety of box girder superstructures that included: a 17.7 m (58 ft.) wide main lane box girder, a 14.6 m (48 ft.) wide transition girder, or a 7.9 m (26 ft.) wide entrance-ramp girder (shown in Figure 3.1).

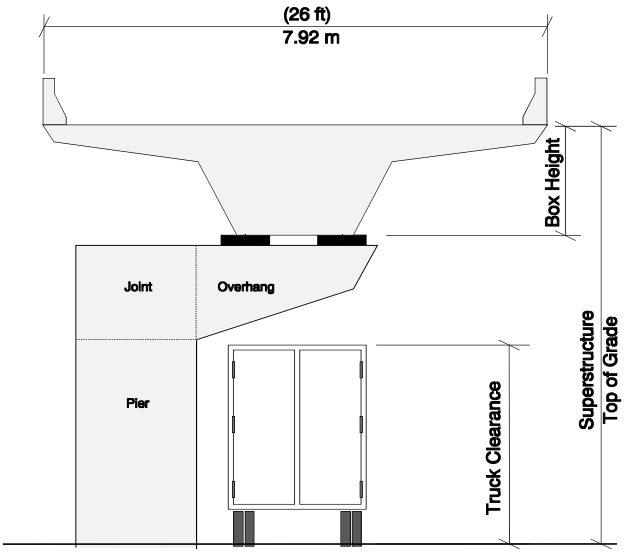

Figure 3.1 Substructure schematic

A review of the substructures supporting the 17.7 m (58 ft.) wide main lane girder indicated that when both superstructure reactions were positioned on the overhang, a fully-prestressed design was always used. A reinforced concrete substructure design was not possible given the maximum depth and width of the overhang, and the number of mild reinforcing bars that were required to resist the factored moment. As a rule, if more than two rows of closely spaced No. 11 bars were required to resist factored loads in the overhang, a fully-prestressed design was implemented. A partially-prestressed design was a viable alternative for some cases, but because a reinforced concrete design was not possible, the 17.7 m (58 ft.) wide superstructure was not modeled in this study.

A review of the substructures supporting the 7.9 m (26 ft.) wide entrance-ramp girder indicated that both reinforced concrete and fully-prestressed concrete designs were implemented. In most cases, if the two superstructure loads were positioned on the overhang, and truck clearance beneath the overhang was not a concern, designers used a reinforced concrete design. In areas where the maximum depth of the overhang was restricted, a fully-prestressed design was used. It was clear that only a small difference in the design flexural capacity of the members drove the design away from a reinforced concrete design to the more conservative fully-prestressed design. For these cases, a mixture of high-strength prestressing steel and mild reinforcing steel (partial prestressing) could be used to reduce steel congestion, provide supplemental tensile reinforcement to resist factored loads, and provide good serviceability. Based on these factors, it was decided to model the bents supporting the 7.9 m (26 ft.) wide box girder superstructure.

The design loads shown in Table 3.1 were computed for a four span continuous 7.9 m (26 ft.) box girder superstructure with spans of 33.5 m (110 ft.). The substructure under consideration in this study was the second pier. Because the superstructure was continuous, the support reactions based on a tributary span length were amplified by a 1.10 dead load continuity multiplier and a 1.22 live load continuity multiplier. The multipliers were computed for the lane loading on the bridge superstructure shown in Figure 3.2. Lane loads were applied on the box girder cross section as shown in Figure 3.3. Inside reactions (nearest the column), R_i, and outside reactions (nearest the overhang tip), R_o, for dead load (DL) and live load plus impact (LL) are listed in Figure 3.3. These reactions do not include the continuity multipliers, and were computed using the typical span length of 33.5 m (110 ft.). The reactions including continuity multipliers, are listed in Table 3.1 for five load cases.

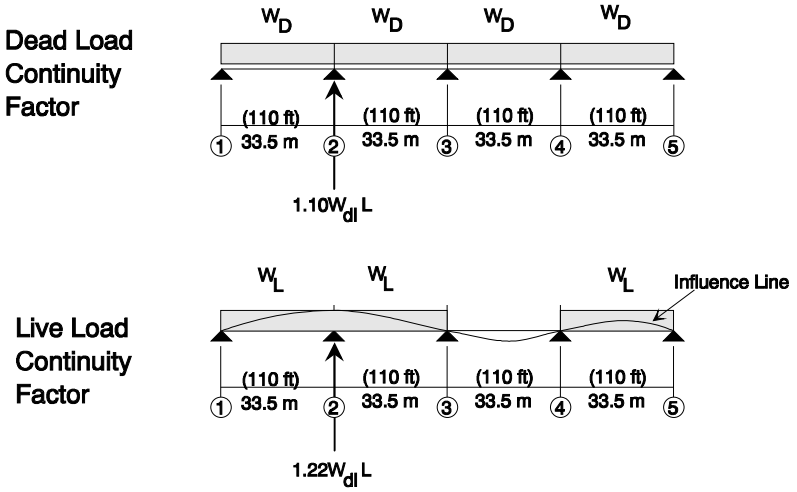

Figure 3.2 Pier location and continuity factors

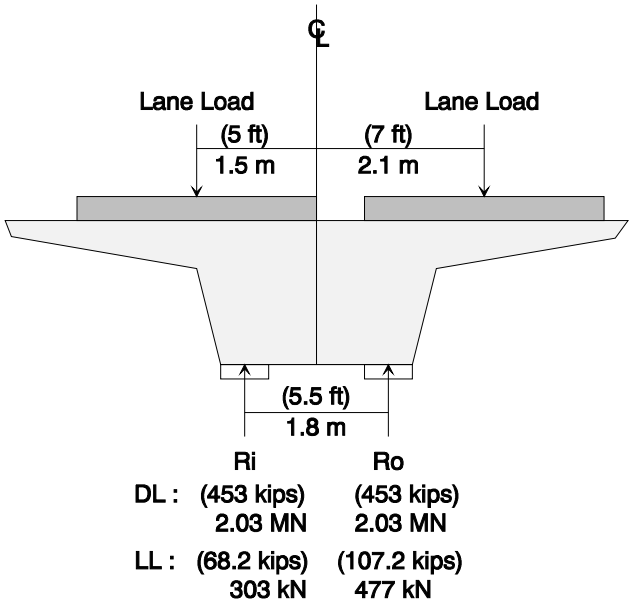

Figure 3.3 Full-scale prototype loads without continuity factors

Table 3.1 Full-scale substructure loads for a 7.9m- (26 ft.) wide girder

Load Description	Load Abbreviation	Ri		Ro	
		kN	(kips)	kN	(kips)
Dead Load	DL	2217	498.3	2217	498.3
Dead Load + 1/2 Live Load	(DL + 1/2 LL)	2362	531.1	2616	588.1
Service Load	(DL+LL)	2589	582.0	3015	677.8
Dead Load + 2 Live Load	(DL+2LL)	2961	665.7	3813	857.3
Factored Load	(1.3DL + 2.17LL)	3690	829.5	4614	1037.2
Factored Load / Φ	(1.3DL +2.17LL)/Φ	4100	921.7	5126	1152.4

3.2.2 Full-Scale Prototype Substructure Details

3.2.2.1 Reinforced Concrete Prototype Substructure–I4-C

Details for a typical reinforced concrete San Antonio 'Y' cantilever bent (Substructure I4-C) are shown in Figure 3.4. The top two layers of longitudinal reinforcement in the overhang were closely spaced No. 11 bars. The side face reinforcement consisted of No. 8 bars spaced at 30 cm (12 in.). The double No. 6 bar transverse reinforcement was spaced at 10 cm (4 in.).

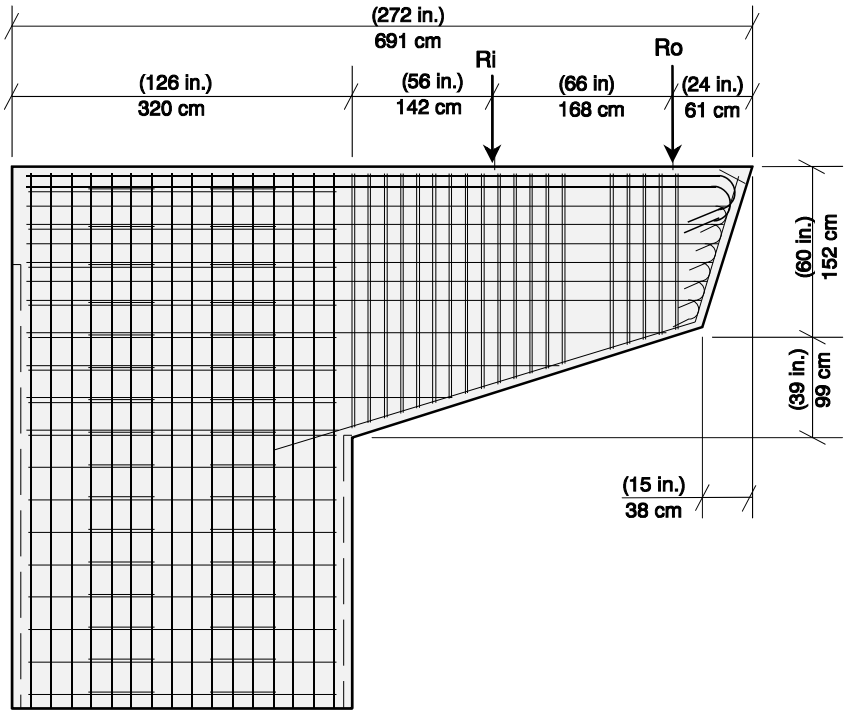

Figure 3.4 Reinforced concrete substructure I4-C details

Longitudinal pier reinforcement incorporated closely spaced No. 11 bars near extreme tension and compression fibers and No. 11 side face bars spaced at 40 cm (16 in.). The pier reinforcement ratio (area of longitudinal reinforcement / gross section area of pier) was equal to the minimum 1% required by the AASHTO Standard Specifications.

Pier and overhang longitudinal reinforcement were anchored in the joint using straight-bar anchorage instead of hooked bars. After an investigation of the bent strength (discussed by Scott [6]), field inspection of the I4-C substructure element revealed several diagonal cracks in the joint region which resulted in closure of the on-ramp until repairs were completed [27, 28].

3.2.2.2 Substructure with Fully-Prestressed Overhang–C11-C

The C11-C substructure presented in Figure 3.5 was designed utilizing a fully-prestressed overhang because the depth of the overhang at the column face was only 150 cm (60 in.) to provide adequate truck clearance beneath the cantilever bent. For the limited depth, more than two rows of mild longitudinal reinforcement would have been necessary to resist factored loads. To provide sufficient strength, the design of the overhang was changed from a reinforced concrete design to a fully-prestressed design.

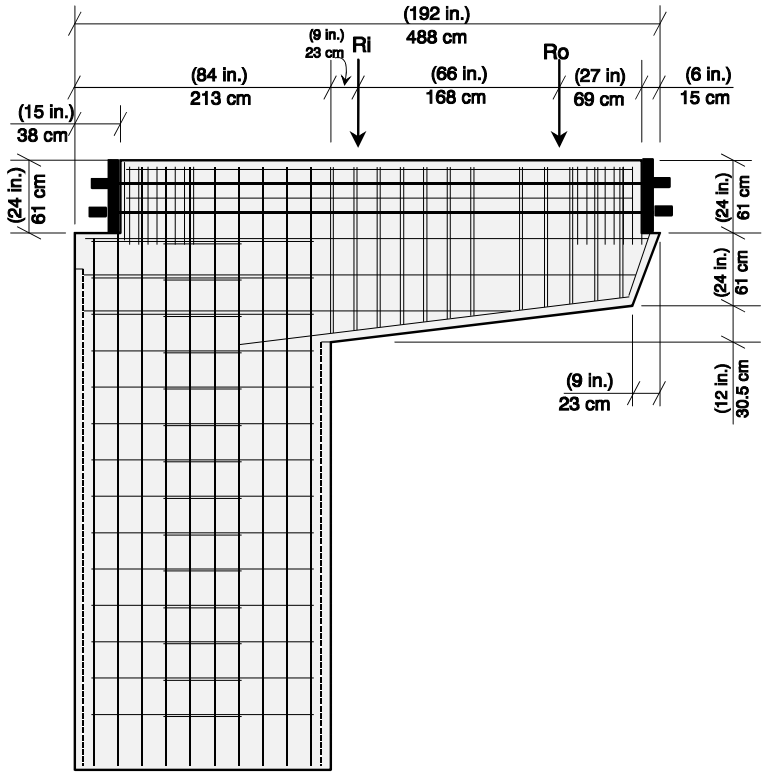

Figure 3.5 Substructure C11-C details

The post-tensioning in the overhang consisted of two rows of eight–3.49 cm (1-$^{3}/_{8}$in.) diameter deformed high-strength post-tensioning bars. The side-face reinforcement consisted of No. 8 bars spaced at 30 cm (12 in.). The double No. 6 bar transverse reinforcement was spaced at 10 cm (4 in.). The gap in the transverse reinforcement in the overhang provided a space for a drainage pipe that passed from the superstructure into the substructure.

Pier longitudinal reinforcement was closely spaced No. 11 bars on the extreme tensile and compressive fibers and No. 11 side face bars at 20 cm (8 in.) spacing. The pier reinforcement ratio was equal to the minimum 1% required by the AASHTO Specifications.

The overhang post-tensioning bars were anchored in the joint corner. As depicted in Figure 3.5, a block-out was cast into the corner to conceal the post-tensioning anchorage hardware. The pier longitudinal reinforcement on the exterior face (furthest from the overhang) was cut short to accommodate the corner block-out. No hooks were used to anchor longitudinal reinforcement in the joint region. During construction of the San Antonio 'Y' Project, as the entrance-ramp girder was placed on the C11-C substructure overhang, a large diagonal crack developed in the joint region and gradually extended until the load from the superstructure was removed. As will be explained later, the shortened pier longitudinal bars and lack of reinforcement continuity in the joint were major factors influencing the bent strength. A significant improvement in the design could have been achieved by utilizing an integrated design method that would have identified detailing problems in the joint during the design phase.

3.2.3 Selection of Scale Factor for Test Specimens

The overhang experimental study conducted by Armstrong [3] and Salas [4] utilized an interior load located at a distance of one-half the beam depth (0.5 h) from the column face and an outer load at one and one-half times the beam depth (1.5 h) from the column face. The location of these loads was a critical part of the original Overhang Specimen investigation. The proximity of the interior load to

the column face required the design to satisfy the corbel provisions, while the outer load was within a 1.5 span-to-depth ratio that required consideration of the deep beam provisions and also induced large moments. The array of different design provisions that applied due to the load positions is one of the items that can be eliminated by using an integrated design method. It was determined that the use of these load points in the present study would provide additional data on overhang behavior. Based on a review of full-scale substructures located in San Antonio, the load positions used in this study were as severe as any identified for the cantilever bents in San Antonio.

The model dimensions were determined as follows:

$$\text{Model Length} = \frac{\text{Prototype Length}}{\text{Scale Factor}}$$

$$\text{Model Area} = \frac{\text{Prototype Area}}{(\text{Scale Factor})^2}$$

$$\text{Model Force} = \frac{\text{Prototype Force}}{(\text{Scale Factor})^2}$$

Selection of the scale factor for the Pier-Overhang-Joint study (presented in Table 3.2) was made by identifying a scale factor that would allow standard size bars to be used in models while limiting scaled loads to less than 667 kN (150 kips). It was decided to limit each maximum design reaction to 667 kN (150 kips) to provide sufficient reserve capacity in the 889 kN (200 kip) rams used in the testing program to fail the specimen. Based on the combination of these factors, it was determined that a 2.75 scale factor was the smallest that satisfied both requirements. It should be noted that the selected scale factor for the test specimens was one-half the 5.5 scale factor used in the overhang study conducted by Armstrong [3] and Salas [4].

Table 3.2 Selection of scale factor, model bar diameters and load

Prototype Bar Size		**Model Bar Size SF=2.25**		**Model Bar Size SF=2.75**		**Model Bar Size SF=3.75**		**Model Bar Size SF=5.5**	
No. 14		No. 6		No. 5		~No. 4		~No. 3	
No. 11		No. 5		No. 4		No. 3		No. 2	
No. 8		~No. 4		No. 3		No. 2		7 ga. wire	
No. 6		~No. 3		No. 2		7 ga. wire		10 ga. wire	
Prototype Load		**SF=2.25**		**SF=2.75**		**SF=3.75**		**SF=5.5**	
(kN)	(kips)	kN	(kips)	kN	kips	kN	(kips)	kN	(kips)
5126	1152	1012	227	677	153	365	82	169	38

The reasons for using a 2.75 scale factor were that standard, 414 MPa (60 ksi) nominal yield deformed bars could be used, anchorage of the bars in the joint region was reasonably realistic, and 889 kN (200 kip) rams were readily available.

3.2.4 Model Loads

The 7.9 m (26 ft.) wide box-girder superstructure loads (presented in Table 3.1) were divided by the square of the scale factor [$(2.75)^2$] to determine the loads for the model specimens (presented in Table 3.3). Load steps used during testing are discussed in Section 3.8.3. The effect of the self weight of the overhang was not considered in this experimental program.

Table 3.3 Substructure design loads for a 1/2.75 scale model

Load Description	Load Abbreviation	Ri		Ro	
		kN	(kips)	kN	(kips)
Dead Load	DL	293	65.9	293	65.9
Dead Load + 1/2 Live Load	(DL + 1/2 LL)	318	71.4	344	77.4
Service Load	(DL+LL)	343	77.0	399	89.6
Dead Load + 2 Live Load	(DL+2LL)	409	92.0	496	111.4
Factored Load	(1.3DL + 2.17LL)	488	109.7	610	137.2
Factored Load / Φ	(1.3DL + 2.17LL)/Φ	543	122.1	679	152.7

3.2.5 Model Dimensions

The model dimensions shown in Figure 3.6 and Figure 3.7 were determined by scaling the 1.67 m (5.5 ft.) distance between the reactions for the 7.92 m (26 ft.) winged superstructure by the 2.75 scale factor. The distance between the model loads was 61 cm (24 in.). The interior load was positioned (0.5h) or 30.5 cm (12 in.) from the column face, and the outer load was positioned (1.5h) or 91.5 cm (36 in.) from the column face. The size of the joint was determined by multiplying the ratio of the I4-C pier-to-overhang dimensions by the depth of the model overhang, resulting in a pier depth of 76 cm (30 in.). The minimum width of the section was 61 cm (24 in.) because two rows of fourteen No. 4 reinforcing bars with a minimum bar spacing of 4.3 cm (1.7 in.) were required to resist the factored moment. The slope of the bottom face of the overhang, 12/39, and the overall dimensions of the overhang were quite similar to the overhangs tested by Armstrong [3] and Salas[4].

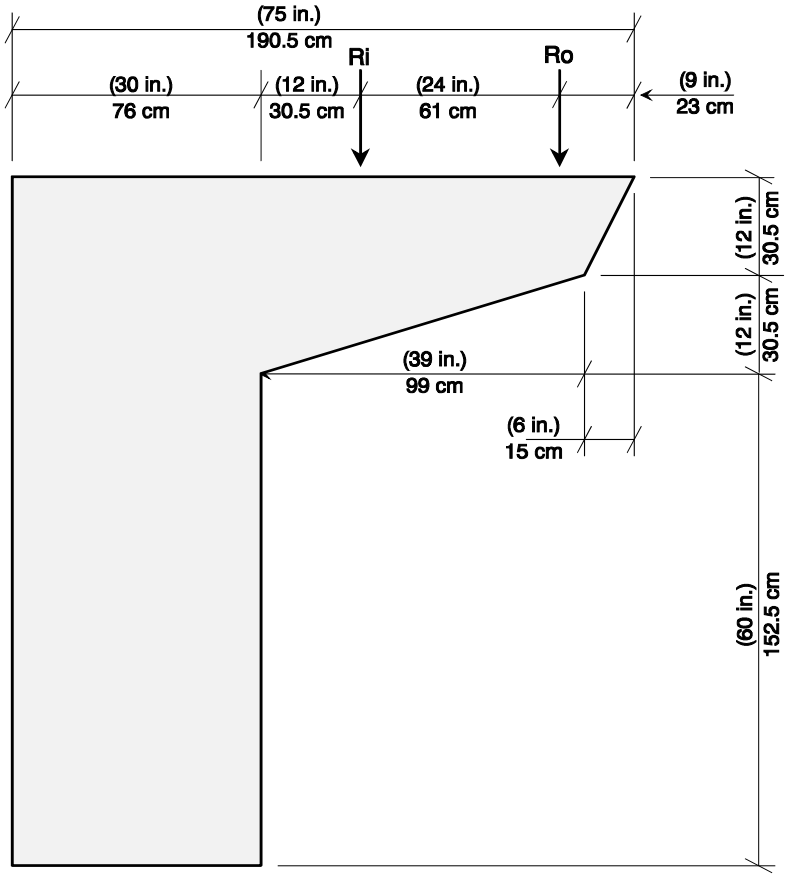

Figure 3.6 Overall dimensions for POJ specimens

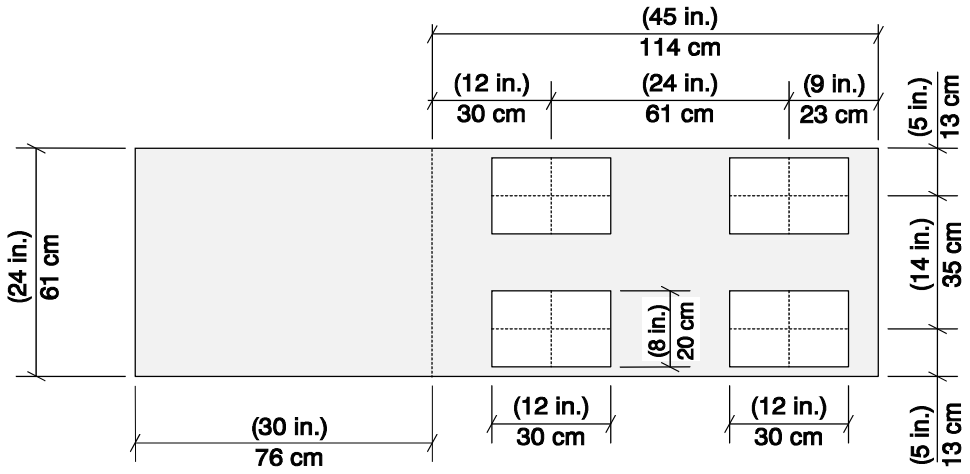

Figure 3.7 Top view of POJ specimen

3.2.5.1 Bar Development Similitude

The bar development lengths (ℓ_d) for this study were determined using the 1963 ACI Code basic bond stress capacity equation [29] to eliminate the additional factors that are inherent in the ACI-318 (1993) bar development length equations. Using the ACI-318 (1993) equations would result in larger estimates for the bar development length, and thus, underestimate the strength of the specimen. More comprehensive relationships for bar development, such as those developed by Orangun, Breen and Jirsa [30] and reported in a code format by ACI Committee 408 [31], could have been used for this discussion and in later evaluations of bent strength.

Bar development lengths (ℓ_d) were computed using the 1963 ACI Code basic bond stress equation as described in Wang and Salmon [32]:

$$\ell_d = \frac{f_y d_b}{4 u_u} \qquad [3\text{-}1]$$

where:

ℓ_d = Development Length (in.)

f_y = Reinforcing Bar Nominal Yield Stress (psi)

= 414 MPa (60,000 psi)

d_b = Reinforcing Bar Diameter (in.)

u_u = Average Unit Bond Stress Capacity (psi)

For No. 11 and Smaller $\quad u_u = \dfrac{9.5\sqrt{f'_c}}{d_b} \le$ (800 psi) 5.5 MPa $\qquad [3\text{-}2]$

For No. 14 and Larger $\quad u_u = 6\sqrt{f'_c} \le$ (800 psi) 5.5 MPa $\qquad [3\text{-}3]$

f'_c = Specified Compressive Strength of the Concrete (psi)

= (5,000 psi) 34 MPa.

The computed basic bar development lengths are tabulated in Table 3.4 for a variety of bar sizes, assuming f_y is 414 MPa (60 ksi) and a concrete compressive strength of 34 MPa (5000 psi).

Table 3.4 Computed basic bar development lengths

	Bar Diameter		Bar Area		ACI-318 (1963) Bond Stress		Development Length	
	mm	(in.)	mm^2	$(in.)^2$	MPa	(psi)	cm	(in.)
No. 2	6	0.25	30	0.048	5.5	800	12	4.7
No. 3	10	0.375	70	0.11	5.5	800	18	7.0
No. 4	13	0.50	130	0.20	5.5	800	24	9.4
No. 5	16	0.625	200	0.31	5.5	800	30	11.7
No. 6	19	0.75	280	0.44	5.5	800	36	14
No. 8	25	1.00	510	0.79	4.6	671	57	22.4
No. 11	36	1.41	1010	1.56	2.9	424	127	49.9
No. 14	43	1.693	1450	2.25	2.9	424	152	59.9

A comparison of the scaled-bar basic development lengths and the model bar basic development lengths for several bar sizes with 414 MPa (60 ksi) nominal yield in 34.4 MPa (5000 psi) concrete is shown in Table 3.5.

Table 3.5 Comparison of scaled development lengths and development lengths for model bars

Prototype Bar Size	Straight Bar Development ACI-318 -63		Scaled Bar Development SF=2.75		Model Bar Size SF=2.75	Model Bar Development ACI-318 - 63		
	cm	(in.)	cm	(in.)		cm	(in.)	% Diff.
No. 14	152	59.9	55	21.8	No. 5	30	11.7	86 %
No. 11	127	49.9	46	18.1	No. 4	24	9.4	92 %
No. 8	57	22.4	21	8.1	No. 3	18	7.0	16 %
No. 6	36	14	13	5.0	No. 2	12	4.7	6 %

Development lengths scaled from the computed development lengths for prototype bar sizes were 6 to 92% longer than development lengths for model bars. Although the bar development lengths did not scale directly, the reduced size of the joint in the model provided a similar ratio of joint dimension to development length for bars as for the I4-C joint. Using a horizontal joint dimension of 76 cm (30 in.) and a vertical joint dimension of 61 cm (24 in.) for the model, the following ratios were computed.

$$\frac{\text{Model Joint Horizontal Dimension}}{\left(\ell_d \text{ for No. 4}\right)} \stackrel{?}{=} \left[\frac{\text{I4-C Pier Depth}}{\ell_d \text{ for No. 11}}\right]$$

$$3.2 \cong 2.5$$

$$\frac{\text{Model Joint Vertical Dimension}}{\left(\ell_d \text{ for No. 5}\right)} \stackrel{?}{=} \left[\frac{\text{I4 - C Overhang Depth}}{\ell_d \text{ for No. 11}}\right]$$

$$2.1 \cong 2.0$$

The ratios imply that the model dimensions for the joint (and thus, the pier and overhang depths) provide an acceptable representation of the I4-C prototype joint. In addition, when the dimensions of the model are scaled-up to full-scale, as shown in Figure 3.8, they are very similar to the substructure C11-C dimensions shown in Figure 3.5.

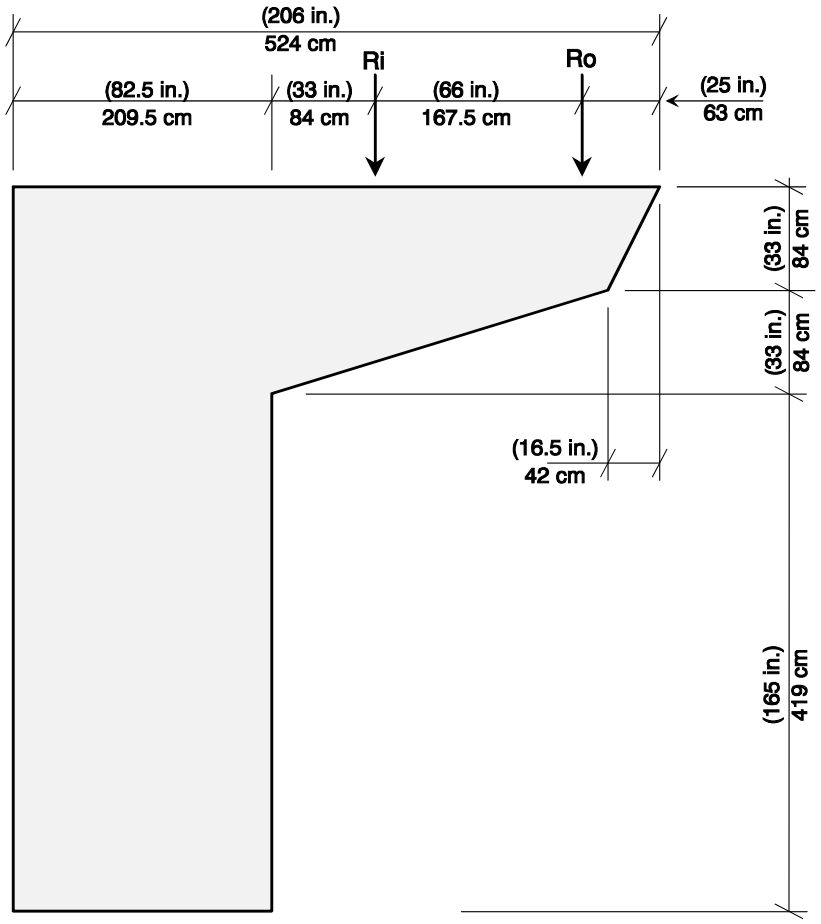

Figure 3.8 Dimensions of the model scaled-up to full-scale

3.3 DESIGN METHOD FOR PROTOTYPE PIER-OVERHANG-JOINT (POJ) TEST SPECIMENS

The prototype model designs were performed using the same the design procedures used in design of the San Antonio 'Y' substructures. The reinforced concrete and fully-prestressed concrete designs considered the shear friction and corbel design provisions, side-face cracking provisions, and minimum longitudinal column reinforcement provisions.

3.3.1 Reinforced Concrete Specimen–POJ-RC-100

The POJ-RC-100 prototype reinforced concrete specimen was designed according to the AASHTO 1986 Design Provisions using the same considerations assumed by designers of the San Antonio 'Y.'

3.3.1.1 Overhang Design - POJ-RC-100

Flexural Reinforcement for Strength:

The primary flexural reinforcement was computed by AASHTO Article 8.16.3.2, Rectangular Sections with Tension Reinforcement Only (Equation 8-15):

$$M_u \le \Phi\ M_n = \Phi\left[A_s f_y d\left(1 - \frac{0.6\rho\ f_y}{f_c'}\right)\right] \qquad [3\text{-}4]$$

where:

M_u = Factored Moment = 1.3DL+2.17LL = 706.6 kN-m (6253 k-in.)

Φ = Phi Factor for flexural members = 0.9

M_n = Nominal moment capacity = 806 kN-m (7140 k-in.)

A_s = Area of mild reinforcement = 36 cm^2 (5.6 in.^{2})

f_y = Nominal yield stress of mild steel = 414 MPa (60 ksi)

ρ = Reinforcement ratio $A_s / b_w d$ = 0.0106

d = Distance from extreme compression fiber to centroid of tension reinforcement = 56 cm (22 in.)

f_c' = Specified compressive strength of the concrete = 34 MPa (5 ksi).

Shear Friction Reinforcement:

The amount of shear friction reinforcement was specified by Article 8.16.6.4.4, Shear-Friction Design Method. The nominal shear capacity across a potential cracking plane at the column face was calculated by computing the required amount of longitudinal reinforcement placed perpendicular to the potential shear plane and applying AASHTO Equation 8-56:

$$V_u \le \Phi V_n = \Phi(A_{vf}\, f_y \mu) \qquad [3\text{-}5]$$

where:

V_u = Applied factored shear from both reactions = 1098 kN (246.9 kips)

V_n = Nominal shear friction capacity = 1292 kN (291 kips)

Φ = Phi Factor = 0.85

A_{vf} = Area of mild steel perpendicular to potential shear crack

f_y = 22.3 cm^2 (3.46 in^2)

μ = Coefficient of friction = 1.4.

Additionally, in Article 8.16.6.8.4, Special Provisions for Brackets and Corbels, an area of mild steel, A_h, shall be "uniformly distributed within two-thirds of the effective depth adjacent to A_s" where the larger of

$$A_h = \left(\frac{A_{vf}}{3}\right) = 7.4 \text{ cm}^2 \text{ (1.15 in}^2\text{)} \qquad [3\text{- }6]$$

or

$$A_h = 0.5(A_s) = 18 \text{ cm}^2 \text{ (2.8 in}^2\text{)} \qquad [3\text{- }7]$$

determined the required area of shear friction steel.

The amount of shear friction reinforcement, 18 cm^2 (2.8 in^2), was controlled by Equation 3-7. The quantity of side-face reinforcement was considered part of the required shear friction reinforcement. As a result, four of the side-face bars near mid-depth were changed to No. 3 bars. Two rows of twelve No. 3 reinforcing bars distributed near mid-depth of the section were used to satisfy the required area of shear friction steel.

Detailing of Side-Face Reinforcement:

The distribution and quantity of longitudinal skin reinforcement were determined using the equations developed by Frantz and Breen [10]. The reinforcement ratio was based on dimensions of the full-scale prototype, and the required area of reinforcement was computed using that reinforcement ratio. The reinforcement ratio was computed using:

$$\rho_{sk} \geq 0.00024(d - 30) \qquad \text{For d} \leq \text{(100 in.)} \qquad \text{[3- 8]}$$

where:

d = Full-scale distance from extreme compression fiber to main tensile reinforcement in (in.)

= 56 cm (22.1 in.) ∗ 2.75 = 154 cm (60.8 in.)

and:

$$\rho_{sk} = \frac{A_{sk}}{2[d/2 \cdot 2d_c]} \qquad \text{[3- 9]}$$

where:

ρ_{sk} = Skin reinforcement ratio = 0.007409

A_{sk} = Area of skin reinforcement = 2.4 cm^2 (0.374 in^2)

d = Distance from extreme compression fiber to main tensile reinforcement of the model = 56 cm (22.1 in.)

d_c = Distance from skin steel centroid to nearest outside face of the concrete of the model = 2.9 cm (1.14 in.).

The side-face reinforcement consisted of four No. 2 reinforcing bars equally spaced at 6 cm (2.6 in.) on each outer face of the specimen. The lower two rows of side-face reinforcement were replaced by No. 3 bars as described in the section for shear friction.

Serviceability Criteria:

The distribution of the main flexural reinforcement was checked using Article 8.16.8.4, Distribution of Flexural Reinforcement, (Equation 8-61):

$$f_s = \frac{z}{(d_c A)^{1/3}} \leq 0.6 f_y \qquad \text{[3- 10]}$$

where:

f_s = Limiting steel stress in the reinforcement at service loads in (ksi)

= 278 MPa (40.4 ksi)

z = Scaled crack distribution factor for moderate exposure conditions (170/2.75) = 62

d_c = Thickness of concrete cover from extreme tension fiber to centroid of tension reinforcement in inches 4.7 cm (1.85 in.)

A = Effective Tension Area in (in^2) surrounding the flexural tension reinforcement divided by the number of bars (in^2 / # Bars) 573 cm^2 (88.8 in^2 / 28 bars).

The computed steel stress at service load using the strain compatibility analysis was [236 MPa (34.3 ksi)], which satisfied the limiting service load stress, f_s, of [278 MPa (40.4 ksi)] computed from Equation 3-10 and the limiting value of 0.6 f_y [248 MPa (36 ksi)].

Fatigue stress limits were considered by determining the steel stresses at dead load and service load using a strain compatibility analysis considering all the flexural reinforcement. The limit stated in AASHTO Equation 8-60 is:

$$f_s < f_f = 21 - 0.33 f_{\min} + 2.4 \qquad [3\text{-}11]$$

where:

f_s = Computed Stress Range in specimen = 58 MPa (8.5 ksi)

f_f = Maximum Allowable Stress range in (ksi) for primary flexural reinforcement

$f_f \leq f_{(DL+LL+I)} - f_{(DL)} = 99$ MPa (14.4 ksi)

f_{min} = Stress level (at dead loads) in (ksi)188 MPa (27.3 ksi).

The computed stress range in the specimen of 58 MPa (8.5 ksi) was within the acceptable range computed by Equation 3-11. The resulting longitudinal reinforcement details are shown in Figure 3.9

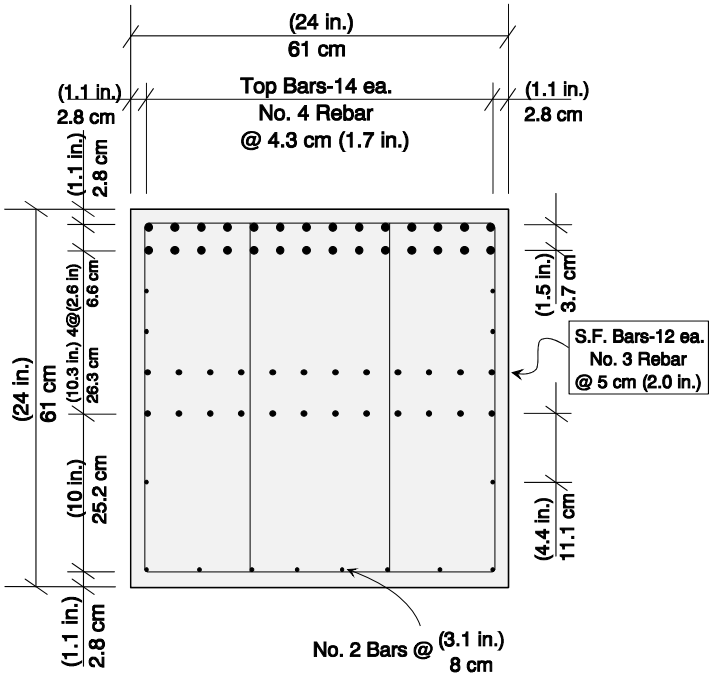

Figure 3.9 POJ-RC-100 overhang reinforcement cross-section details

Transverse Reinforcement:

The amount of transverse reinforcement was determined using AASHTO Article 8.16.6.1, Shear Strength (Equations 8-46 and 8-47):

$$V_u \leq \Phi V_n = \Phi (V_c + V_s) \quad [3\text{-}12]$$

where:

V_u = Factored Shear = 610 kN (137.2 kips)

Φ = Phi factor for Shear = 0.85

V_n = Nominal Shear Capacity = 717 kN (161.3 kips).

The nominal concrete contribution to shear strength, V_c , is defined by Equation 8-49:

$$V_c = 2\sqrt{f'_c}\, b_w\, d \quad [3\text{-}13]$$

where:

V_c = Nominal concrete contribution to shear strength = 233 kN (52.5 kips)

f_c' = Specified compressive strength of the concrete in (psi) 34 MPa (5000 psi)

b_w = Beam width = 61 cm (24 in.)

d = Beam depth at 45° angle from load point = 40 cm (15.5 in.).

The shear strength provided by stirrups, V_s, was quantified by Equation 8-53:

$$V_s = \frac{A_s f_y d}{s} \quad [3\text{-}14]$$

where:

V_s = Nominal shear strength = 484 kN (108.8 kips)

A_s = Area of stirrups = 1.2 cm^2 (0.192 $in.^2$)

f_y = Nominal yield stress of the mild steel = 414 MPa (60 ksi)

s = Spacing of the transverse reinforcement = 4 cm (1.6 in.).

The designers assumed the factored shear loading, V_u , was equal to the factored outside superstructure reaction, R_o. The depth , d , was determined at the section defined by the intersection of the extreme compression fiber and a 45° line drawn from the outer load point. This critical section was assumed to resist the entire shear force from the outer reaction. The stirrups were double No. 2 hoops with a total area of 1.2 cm^2 (0.192 in^2). The stirrup spacing, s, was determined using Equation 3-11 after subtracting the concrete contribution (Equation 3-10) from the applied factored shear. The stirrup spacing, s, of 4.2 cm (1.6 in.) was used over the entire overhang (see Figure 3.10).

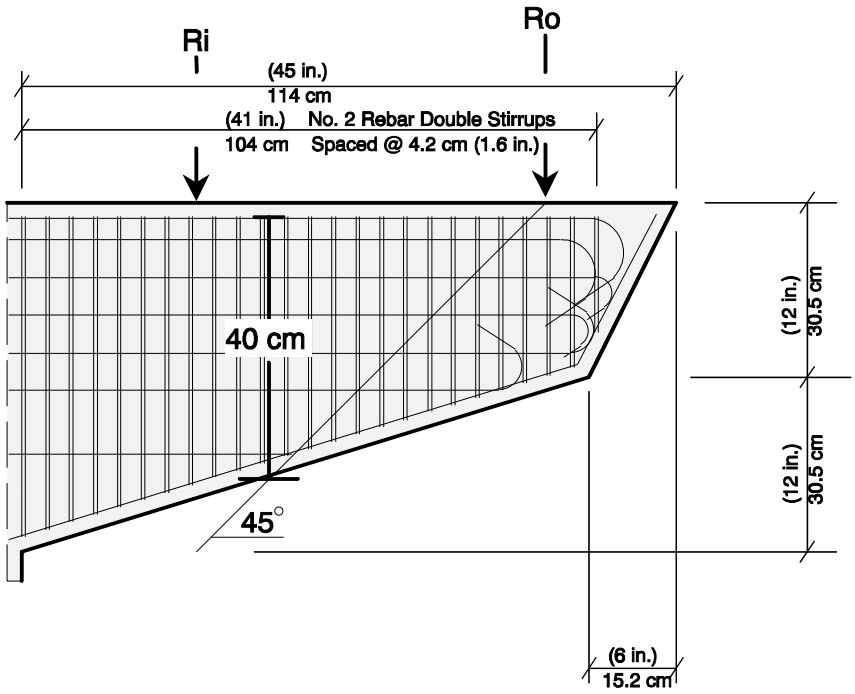

Figure 3.10 POJ-RC-100 overhang reinforcement details

3.3.1.2 Pier Design–POJ-RC-100

Flexural Reinforcement:

The amount of longitudinal reinforcement in the pier was determined using a strain compatibility analysis, allowed by Article 8.16.3.4.2, which was similar to the procedure used by the designers of the San Antonio 'Y.' The computed nominal flexural strength (M_n) was multiplied by a Φ factor and compared with the factored moment, $\Phi M_n \geq M_u$. The Φ factor increases linearly from 0.7 to 0.9 as the design axial load decreases from 0.10 $f_c' A_g$ to zero, based on the provisions in Article 8.16.1.1.2.

The required minimum percentage of longitudinal reinforcement often controlled the amount of pier reinforcement used for the San Antonio 'Y' substructures. Article 8.18.1.2 states the minimum area of longitudinal reinforcement must be greater that 0.01 A_g. In the model, the percentage of pier reinforcement was 0.0155 A_g due to the high flexural forces. The distribution of longitudinal reinforcement in the pier is shown in Figure 3.11.

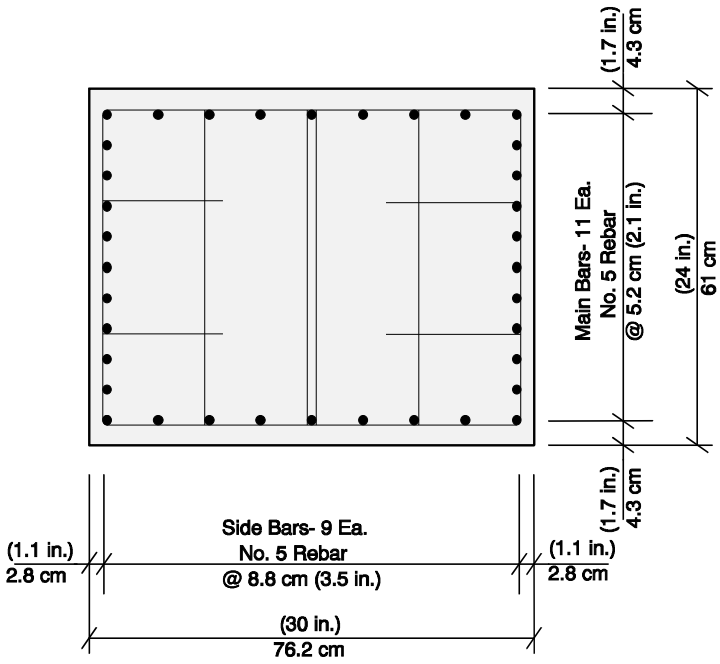

Figure 3.11 POJ-RC-100 pier reinforcement detail

Transverse Reinforcement:

Transverse reinforcement was detailed using Article 8.18.2.3. Tie spacing and bar size requirements were scaled by the 2.75 scale factor. The No. 4 ties required by AASHTO were modeled using 7 ga. wire. The minimum longitudinal spacing in the pier of 30 cm (12 in.) was divided by the 2.75 scale factor resulting in a tie spacing of 11 cm (4.4 in.). The maximum distance to a restrained bar of 61 cm (2 ft.) was divided by the 2.75 scale factor resulting in a distance of 22 cm (8.7 in.) (see Figure 3.11).

3.3.1.3 Joint Design–POJ-RC-100

Bar Anchorage:

Anchorage of the pier and overhang reinforcement in the joint was assumed to be based on straight bar development. Bar development length was compared with the available embedment from the critical moment sections of the overhang and pier to the back and top of the joint, as had been done for the San Antonio 'Y' bents. Because bars used in the model have more than twice the straight bar development required by the specifications, hooks, welded plates, and other methods of positive anchorage were not provided. An enlarged view of the reinforcement in the joint is shown in Figure 3.12 and an elevation of the reinforcement details used in Specimen POJ-RC-100 is presented in Figure 3.13.

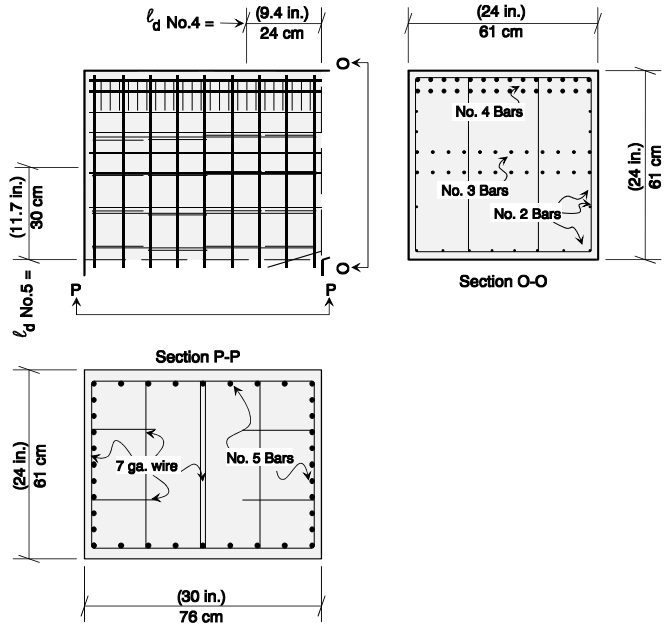

Figure 3.12 POJ-RC-100 joint reinforcement details

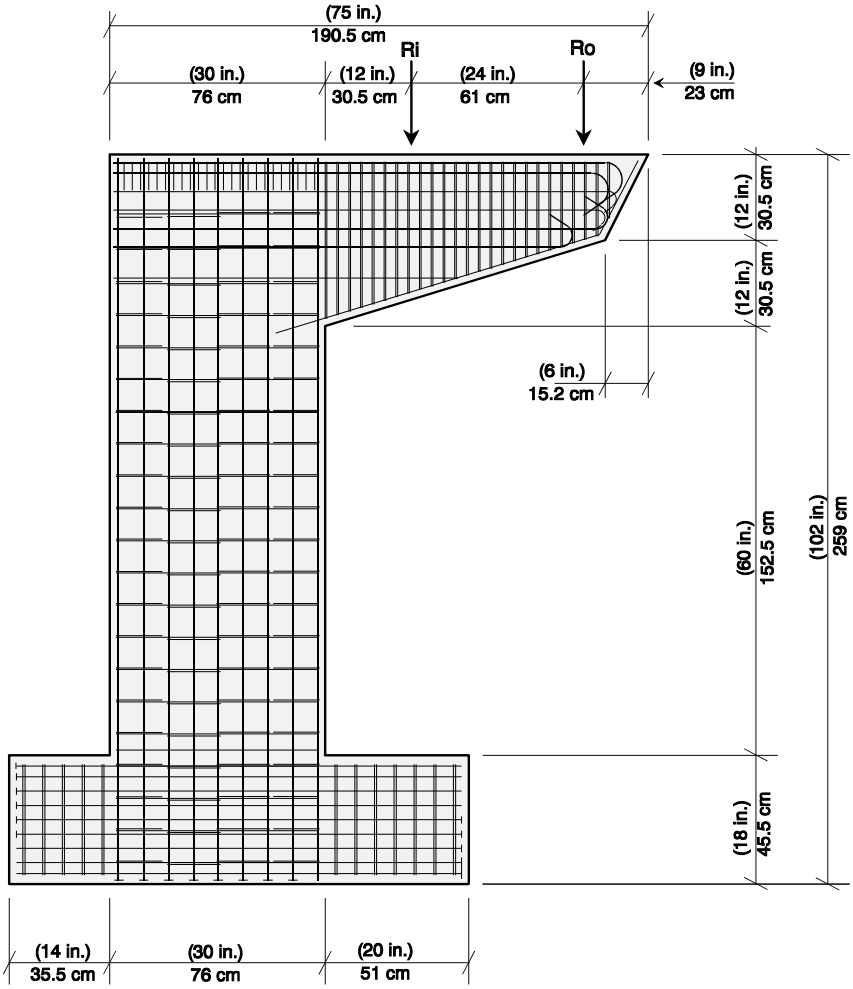

Figure 3.13 Elevation of reinforcement for POJ-RC-100

3.3.2 Specimen with Fully-Prestressed Concrete Overhang–POJ-PS-100

The pier-overhang-joint specimen with the fully-prestressed concrete overhang (Specimen POJ-PS-100) was designed according to the AASHTO 1986 Standard Specifications using the same considerations assumed by designers of the San Antonio 'Y' (see Section 2.3).

3.3.2.1 Overhang Design–POJ-PS-100

Flexural Reinforcement:

The AASHTO prestressed concrete design provisions state in Article 9.17.1 that a member may be assumed to remained uncracked at service load. The design procedure is limited by Article 9.15.2.2 which specifies a maximum allowable extreme tensile fiber stress computed by:

$$-\frac{P}{A}-\frac{Pey}{I_g}+\frac{M_{(DL+LL)}\,y}{I_g} \;\le\; 3\sqrt{f'_c} \qquad [3\text{-}15]$$

where:

P = Applied post-tensioning force = 1345 kN (302.4 kips)

A = Area of concrete = b_w h = (576 in^2) 0.371 m^2

e = Eccentricity of post-tensioning strand above beam centroid

= 19 cm (7.5 in.).

y = Distance to extreme tensile fiber from beam centroid

= 30 cm (12 in.)

I_g = Gross moment of inertia = 1/12 (b_w)(h)^3 = 0.453 m^3 (27,648 in^3)

$M_{(DL+LL)}$ = Applied service load moment = 469 kN-m (4150 k-in.).

The post-tensioning stress (P/A_{pt}) was set equal to 0.6 f_{pu} = 620 MPa (90 ksi) based on long-term losses. Twelve - 16 mm (5/8 in.) diameter Dywidag bars with an area of 1.84 cm^2 (0.28 in.^{2}) were required to satisfy Equation 3-15. The location and spacing of the post-tensioning ducts are shown in Figure 3.14.

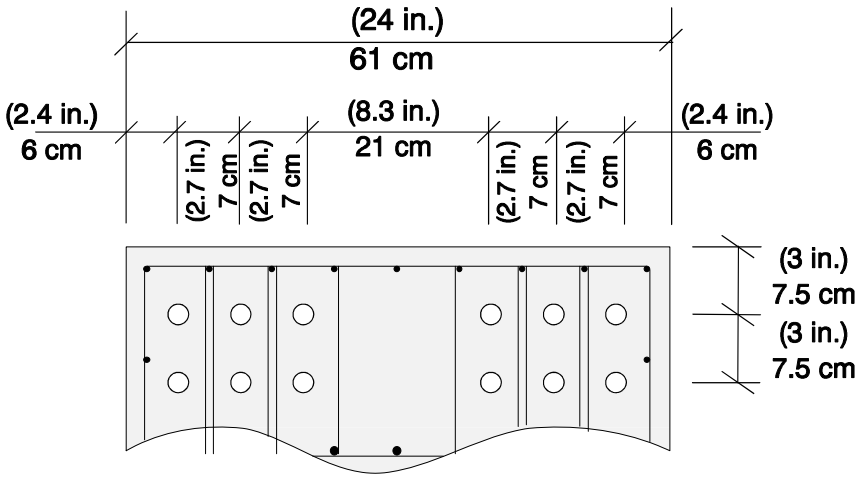

Figure 3.14 PS-100 locations of post-tensioning

Shear Friction Steel:

The concern about corbel-type shear friction behavior forced the designers to use the shear friction design method specified in Article 8.16.6.4.4. The amount of shear friction reinforcement was reduced from that specified by Article 8.16.6.4.4 to use the excess post-tensioning reinforcement beyond that required for flexural strength.

The area of post-tensioning required for ultimate strength design was computed using AASHTO Equation 9-13:

$$M_u \le \Phi M_n = \Phi \left[A_s^* f_{su}^* d \left(1 - 0.6 \frac{\rho^* f_{su}^*}{f'_c} \right) \right] \qquad [3\text{- }16]$$

and Equation 9-17:

$$f_{su}^* = f'_s \left[1 - \left(\gamma^* / B_1 \right) \left(\rho^* f'_s / f'_c \right) \right] \qquad [3\text{- }17]$$

where:

M_u = Factored moment = 706.7 kN-m (6254 k-in.)

Φ = Phi factor for flexural design of prestressed concrete = 0.95

M_n = Nominal flexural strength = 877 kN-m (7758.3 k-in.)

A_s^* = Area of prestressing steel = 22 cm^2 (3.36 in^2)

f_{su}^* = Average prestressing steel stress at ultimate load

= 923 MPa (133.8 ksi)

d = Distance from extreme compression fiber to prestressingcentroid

= 50 cm (19.5 in.)

ρ^* = Prestressing reinforcement ratio = ($A_s^* / b_w d$) = 0.007179

f_c' = Nominal concrete strength (ksi) = 34.5 MPa (5 ksi)

γ^* = Prestressing steel factor = 0.55 for prestressing bars

β_1 = Concrete factor = 0.8 for 34.5 MPa (5000 psi) concrete.

The computed capacity, ΦM_n, for the fully-prestressed overhang was 833 kN-m (7370 k-in.) that was 126 kN-m (1116 k-in.) in excess of the factored moment M_u. The excess area of post-tensioning, 2.5 cm^2 (0.392 in^2), was converted into an equi-valent area of mild steel by multiplying by [150 ksi/60 ksi]. This area of steel, 6.3 cm^2 (0.98 in^2), was considered to contribute to the shear friction steel requirement.

The amount of shear friction reinforcement was specified by Article 8.16.6.4.4, the Shear Friction Design Method. The nominal shear capacity across a potential cracking plane at the column face was calculated by considering the required amount of longitudinal reinforcement placed perpendicular to the potential shear plane and applying AASHTO Equation 8-56:

$$V_u \leq \Phi V_n = \Phi(A_{vf}\ f_y\ \mu) \qquad [3\text{-}18]$$

where:

V_u = Applied factored shear from both reactions = 1098 kN (246.9 kips)

V_n = Nominal shear friction capacity = 1292 kN (291 kips)

Φ = Phi Factor = 0.85

A_{vf} = Required area of mild steel perpendicular to potential shear crack = 22 cm^2 (3.46 in^2)

μ = Coefficient of friction = 1.4.

Additionally, in Article 8.16.6.8.4, Special Provisions for Brackets and Corbels, an area of mild steel, A_h, shall be "uniformly distributed within two-thirds of the effective depth adjacent to A_s" where the larger of

$$A_h = \left(\frac{A_{vf}}{3}\right) = 7.4 \text{ cm}^2 \text{ (1.15 in}^2\text{)} \qquad [3\text{-}19]$$

or

$$A_h = 0.5(A_s) = 18 \text{ cm}^2 \text{ (2.8 in}^2\text{)} \qquad [3\text{-}20]$$

determined the required area of shear friction steel.

The amount of shear friction reinforcement, 18 cm^2 (2.8 in^2), was reduced by the 2.4 cm^2 (0.38 in.^{2}) area of side-face reinforcement that was located near mid-depth of the section, and by the 6.3 cm^2 (0.98 in.^{2}) equivalent area of mild steel from the excess post-tensioning. Two rows of nine No. 2 bars were needed to form a portion of the confinement cages for the post-tensioning anchorage in the overhang and the joint. The lowest row was replaced by nine No. 3 bars to provide the top row of shear friction reinforcement (see Figure 3.15).

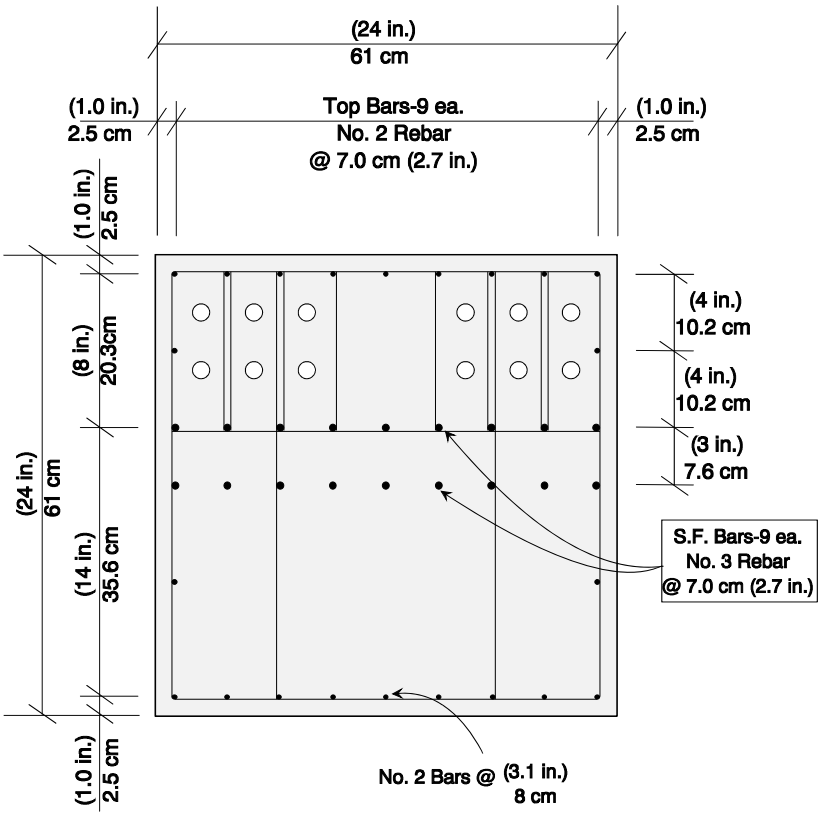

Figure 3.15 POJ-PS-100 overhang cross section

Transverse Reinforcement in the Overhang:

The design procedure used for the San Antonio 'Y' project did not consider any beneficial effects from the post-tensioning when computing the required area of transverse reinforcement in the overhang. The amount of transverse reinforcement in the overhang was computed using the same procedure as for the POJ-RC-100 test specimen.

Post-Tensioning Anchorage Reinforcement:

The amount of anchorage reinforcement was computed using the Guyon bursting stress equation:

$$T_b = \frac{P}{3}(1-\gamma) \qquad [3\text{- }21]$$

and the Guyon spalling stress equation:

$$T_s = \frac{P}{4} \qquad [3\text{- }22]$$

where:

T_b = Tensile bursting stress = 23 kN (5.2 kips)

P = Maximum post-tensioning force = 310 kN (69.8 kips)

γ = Ratio of anchorage plate height to concrete cone limit
(3.5 in. x 2)/(4.5 in. x 2) = 0.778

T_s = Maximum Tensile spalling stress = 78 kN (17.4 kips).

The area of required anchorage reinforcement was then computed by:

$$A_v = \frac{T_b}{f_s} + \frac{T_s}{f_s} \qquad [3\text{- }23]$$

where:

A_v = Area of anchorage reinforcement = 4.9 cm^2 (0.75 in^2)

f_s = Allowable tensile stress = 166 MPa (24 ksi).

The anchorage reinforcement consisted of eight sets of interlocked No. 2 ties. The anchorage ties were threaded over the No. 2 longitudinal reinforcement and spaced at 4 cm (1.6 in.) to provide reinforcement that extended beyond the limits of a 45° crack that may form from the base of the anchorage plate to the top surface of the overhang (see Figure 3.16). The same amount of anchorage reinforcement was used for both the end of the overhang as well as the joint corner.

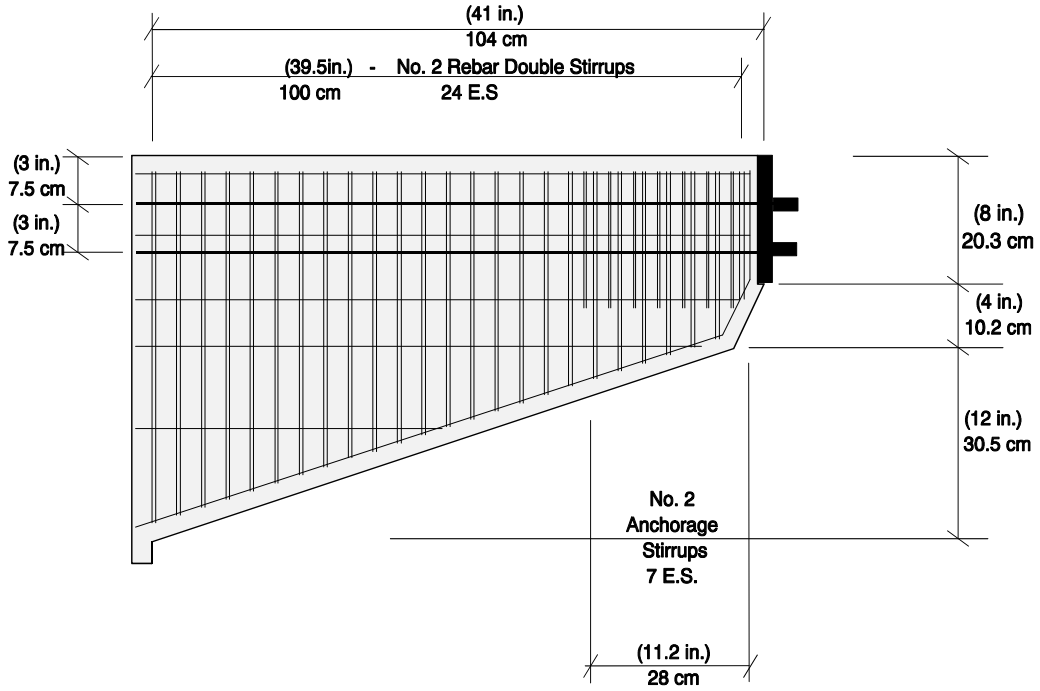

Figure 3.16 POJ-PS-100 overhang reinforcement details

3.3.2.2 Pier Design–POJ-PS-100

Flexural Reinforcement:

The amount of flexural reinforcement in the pier (see Figure 3.17) was identical to that used for the POJ-RC-100 test specimen. The percentage of pier longitudinal reinforcement, which was 0.0155 A_g, satisfied the minimum longitudinal column reinforcement ratio of 0.01 A_g.

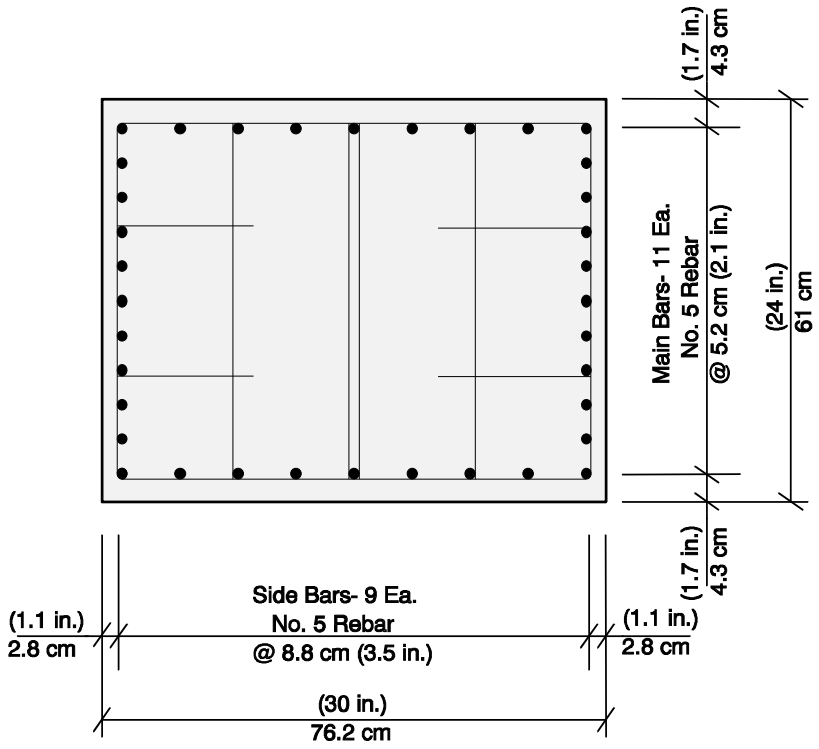

Figure 3.17 POJ-PS-100 pier reinforcement details

3.3.2.3 Joint Design–POJ-PS-100

Bar Anchorage:

Anchorage of the pier and overhang reinforcement in the joint was assumed to be based on straight bar development. The bar development length was compared with the available embedment from the critical moment sections of the overhang and pier to the back and top of the joint. Because the bars used in the model have more than twice the straight bar development required by the specifications, hooks, welded plates, and other methods of positive anchorage were not provided.

Post-tensioning bars from the overhang provided a positive anchorage for the transfer of forces into the joint region. Although the shear friction reinforcement was not hooked in the joint region, it was placed deep into the joint where it could provide some contribution to the bent capacity. A majority of pier longitudinal reinforcement (all bars on the back face and some side-face bars) was cut short to provide space for the joint corner block-out that was used to conceal the post-tensioning hardware (Figure 3.18). An elevation of the reinforcement used in Specimen POJ-PS-100 is presented in Figure 3.19.

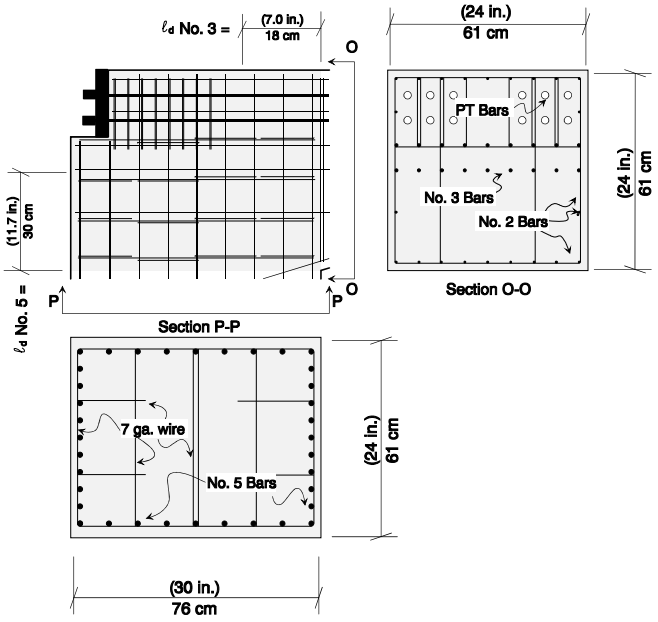

Figure 3.18 POJ-PS-100 joint reinforcement details

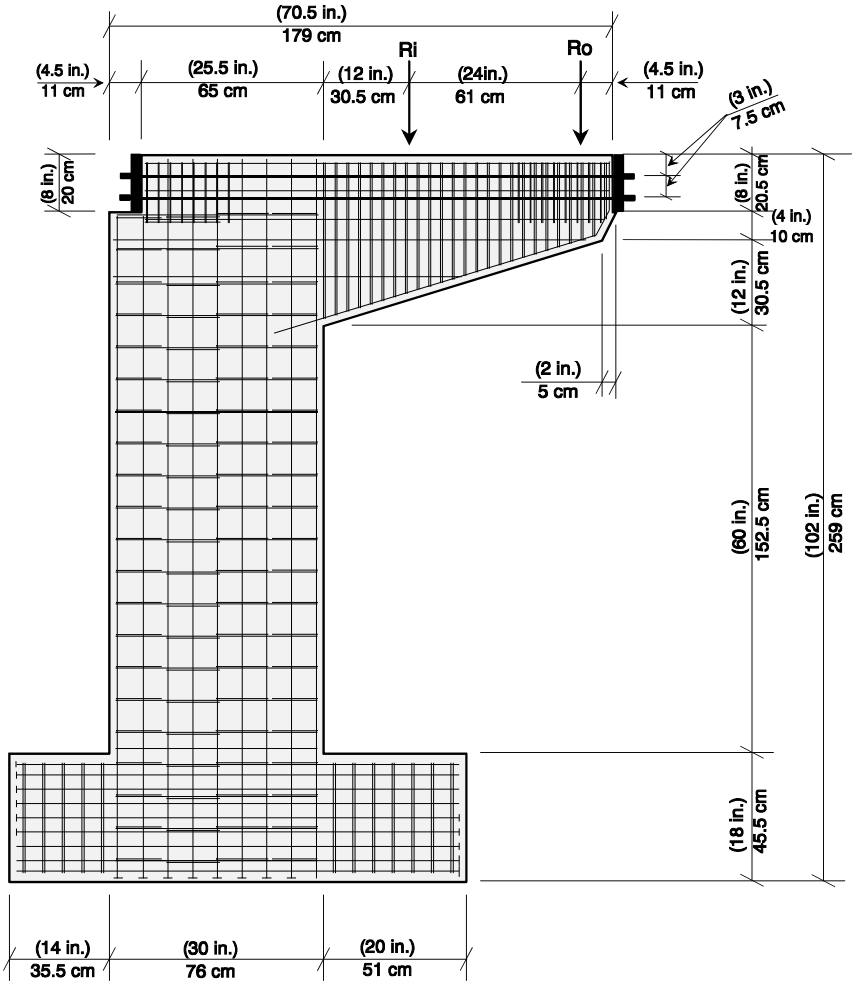

Figure 3.19 Elevation of reinforcement for POJ-PS-100

3.4 INTEGRATED DESIGN TEST SPECIMENS

The remaining three Pier-Overhang-Joint test specimens were designed with combinations of prestressed and non-prestressed (mild) reinforcement. The approach used was based on the results and recommendations of the overhang study reported by Armstrong [3] and Salas [4]. Details of the design process are reported here.

3.4.1 Overview of the Integrated Design Method

The integrated design method used a strut-and-tie model to visualize a determinate path for transfer of forces through each specimen at factored loads. Combinations of high-strength prestressed reinforcement and mild steel were used to resist the tension tie forces. The amount and distribution of reinforcement was examined to limit steel stresses and control crack widths under service loads. A planar 2D finite element analysis model was used to compute the principal tensile and compressive stresses and aid in formulation of a determinate strut-and-tie model. Once geometry of the model was established, strut-and-tie forces were computed for applied factored loads.

3.4.1.1 Factored Load Resistance

Tie forces were used to compute required quantities of tensile reinforcement, and stresses in compression struts were compared with allowable stresses. Factored resistance of struts and ties was taken as the nominal resistance (T_n) times the appropriate resistance factor or phi factor. Phi factors for flexure and shear were 0.9 and 0.85, respectively.

Strength of Tension Ties:

Tie forces (primary flexural reinforcement) were provided by combinations of prestressed steel and longitudinal mild steel. The total resistance is:

$$T_n = A_{ms} f_y + A_{ps} f_{su} \qquad [3\text{-}24]$$

where:

T_n = STM longitudinal tension tie force

A_{ms} = Area of mild steel primary flexural reinforcement

f_y = Nominal yield stress of mild reinforcement

A_{ps} = Area of prestressed primary flexural reinforcement

f_{su} = Prestressing steel stress at Ultimate Load.

Transverse tie reinforcement quantities were computed using:

$$T_n = A_{vs} f_y + 1\sqrt{f_c'}\, b_w d \qquad [3\text{-}25]$$

where:

T_n = STM tie force

A_{vs} = Total area of required shear reinforcement

f_y = Nominal yield stress of shear reinforcement

f_c' = Nominal concrete compressive stress (psi)

b_w = Beam width (in.)

d = Distance from extreme compression fiber to centroid of primary tension reinforcement at the location of the tension tie (in.).

Compression Strut Limits:

The compression stress limit at factored loads, $f_{c\,max}$, was taken to be:

$$f_{c\,max} = 0.85\, f_c' \qquad [3\text{-}26]$$

where:

f_c' = Nominal concrete compressive stress.

Reinforcement Detailing:

The area of skin reinforcement, A_{sk}, per foot of height for each side face of the overhang was based on the relationship established by Frantz and Breen [10] for control of side-face cracking:

$$A_{sk} = 0.0012\ (d - 30) \text{ for } d > 36 \text{ in.} \qquad [3\text{-}27]$$

where:

A_{sk} = Area of side face reinforcement (in^2)

d = Distance from extreme compression fiber to centroid of primary tension reinforcement at maximum depth of the member (in.).

The minimum transverse reinforcement was designed in accordance with:

$$s_{max} = \frac{A_v(f_y)}{50\, b_w} \le d/2 \ \text{ and } \frac{24(in.)}{2.75} \qquad [3\text{-}28]$$

where:

s_{max} = Maximum allowable transverse reinforcement spacing (in.)

A_v = Area of transverse reinforcement (in^2)

f_y = Nominal yield stress of transverse reinforcement (ksi)

b_w = Beam width in (in.).

The force flow indicated by the strut-and-tie model for each pier-overhang-joint specimen illustrates the need for positive anchorage of mild reinforcement in the joint region. These models will be presented later in Sections 3.4.3.2, 3.4.4.2, and 3.4.5.2. Interlocked headed mild reinforcing bars were used to provide positive anchorage in the joint region for all of the integrated design specimens.

3.4.1.2 Service Load Performance

A finite element analysis was used to compute the concrete principal tensile stresses to determine if and where cracking would occur. If the member was predicted to crack, tensile stresses were computed at dead load and service load using a cracked-section analysis to evaluate crack widths and fatigue stress ranges.

Distribution of Tension Reinforcement in Flexural Members:

The tensile stress was limited (by adjusting the amount and distribution of reinforcement) to control the width of cracks (170 / Scale Factor = 62).

Variables used for the following equation are depicted in Figure 3.20, and are defined as follows:

$$f_{sa} \le f_{sl} = \frac{Crk}{\left(d_c A\right)^{1/3}} \qquad [3\text{- }29]$$

f_{sa} = Steel tensile stress at a distance d″ from the extreme tensile fiber
= $\varepsilon_{d''}$ (29,000 ksi)

$\varepsilon_{d''}$ = Strain a distance d'' from the extreme tensile fiber based on a linear strain profile

f_{sl} = Computed limiting steel stress (ksi)

Crk = Crack width limiting factor based on exposure criteria
= (170 / 2.75) = 62

d_c = Distance from the extreme compression fiber to the centroid of the closest layer of primary tension reinforcement (in.)

A = Area of tension block (2 x d″ x b_w) divided by the number of Prestressing strands and/or mild reinforcing bars located within the tension block [in^2/# bars]

d'' = Distance from extreme tensile fiber to centroid of tensile reinforcement. (Areas of prestressed reinforcement, A_{ps}, located a distance, d_{ps}, from the extreme tensile fiber and/or areas of mild reinforcement, A_{ms}, located a distance, d_{ms}, from the extreme tensile fiber are considered in the equation.).

$$d'' = \frac{\left[\sum (A_{ps}\ f_{su})\, d_{ps} + \sum (A_{ms}\ f_y)\, d_{ms}\right]}{\left[\sum A_{ps}\ f_{su} + \sum A_{ms}\ f_y\right]} \qquad [3\text{-}30]$$

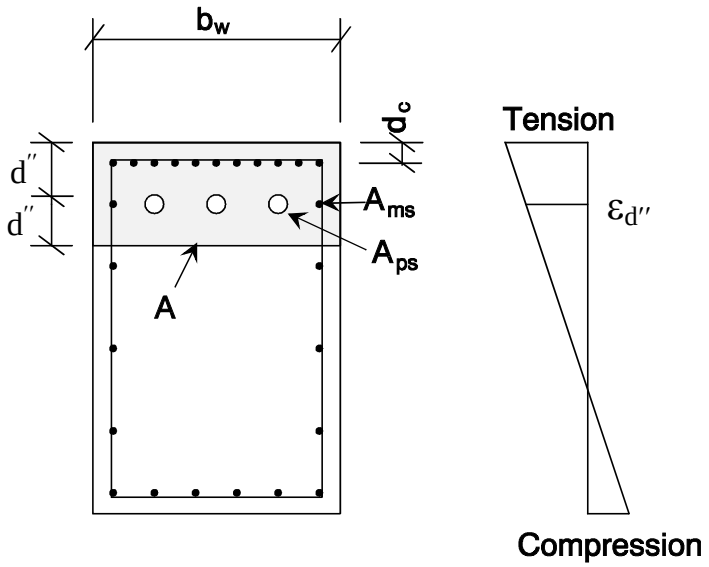

Figure 3.20 Identification of crack-width control variables

The value of f_{sa} was computed using a cracked-section analysis. Bonded prestressing steel (including estimates of long-term losses) was included in the calculation of f_{sa}. The value of f_{sa} was computed at the centroid of the primary tensile reinforcement, at a distance d′′ from the extreme tension fiber. The value of f_{sa} In order to avoid fatigue of reinforcement under service-level loads, the following stress ranges were checked for non-prestressed and prestressed reinforcement. Obviously, fatigue was not a concern during testing, but these service-level limits had the potential to change the quantity or distribution of reinforcement in each specimen.

Fatigue Stress Range:

The assumed fatigue stress range for the mild reinforcement was determined using AASHTO Equation 8-60:

$$f_f = 21 - 0.33 f_{\min} + 2.4 \qquad [3\text{-}31]$$

where:

f_f = Maximum stress range (ksi) in mild steel reinforcement

$f_{\min}$ = Minimum stress level (at dead load) in (ksi).

The allowable stress range for the post-tensioning steel was 100 MPa (14.5 ksi) based on the recommendations of Wollman, *et al.*, [26].

3.4.2 Overview of Design Details

This section reviews the steps involved in the design of the three integrated design specimens: POJ-RC-100-TH, POJ-PU-54-TH, and POJ-PU-74-TH. Finite element analyses at dead-load and service-load levels were used to visualize the flow of forces through each specimen as well as estimate the level of tensile and compressive stresses that would develop at service-load levels in each specimen. The strut-and-tie models were produced so that the struts and ties were located and aligned consistent with the larger principal stress vectors predicted by the finite element method. The detailed design used the strut-and-tie model forces to proportion and locate the primary tensile reinforcement. Cross sections and side views of each specimen are presented to document bar sizes and bar locations for each specimen.

3.4.3 Design Details for the Reinforced Concrete Specimen with Headed Bars–POJ-RC-100-TH

The reinforced concrete specimen with headed bars (POJ-RC-100-TH) utilized interlocked headed reinforcement in the joint corner to provide a tensile force path through the joint.

3.4.3.1 Finite Element Analysis–POJ-RC-100-TH

An elastic finite element analysis of the reinforced concrete specimen with headed bars was used to visualize the flow of forces from the load points into the pier. Because the analysis did not consider non-linear material properties, the level of tensile stresses in some areas was unrealistic. If the level of tensile stresses was above $7\sqrt{f_c'}$ (psi) [3.44 MPa (500 psi)], the region was considered to be cracked. Although the POJ-RC-100-TH specimen was computed to crack under dead load, the service load finite element analysis is included here to illustrate the increase in tensile stresses in the joint region. The test specimen was modeled using eight-node isoparametric elements. The finite element mesh is illustrated in Figure 3.21. Computed principal tensile and compressive stresses for dead-load and service-load levels are presented in the form of stress contours and principal tensile vectors in Figures 3.22 through 3.25. The principal tensile stress contours at dead load indicated tensile stresses in the joint were nearly $7\sqrt{f_c'}$ (psi) [3.44 MPa (500 psi)]. It was clear from Figure 3.22 that cracking in the joint would occur at loads slightly above dead load. Plots of principal tensile and compressive stress vectors aided the development of a strut-and-tie model.

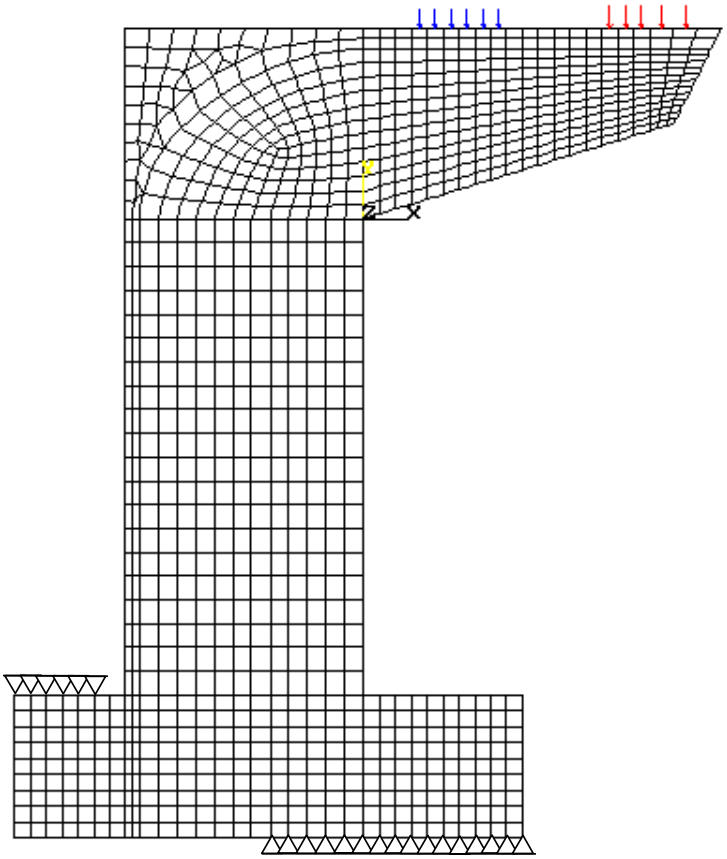

Figure 3.21 Finite element model for the POJ-RC-100-TH specimen

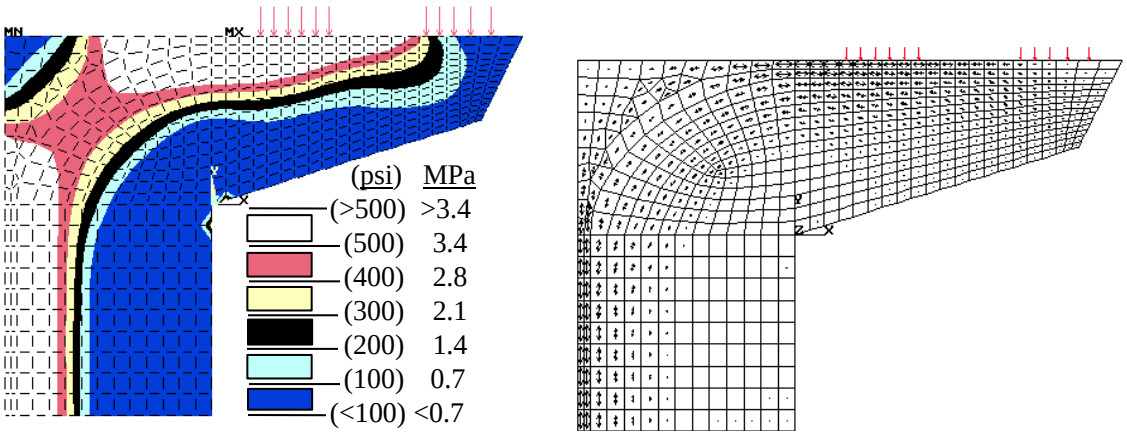

Figure 3.22 POJ-RC-100-TH principal compressive stresses and vectors at service load

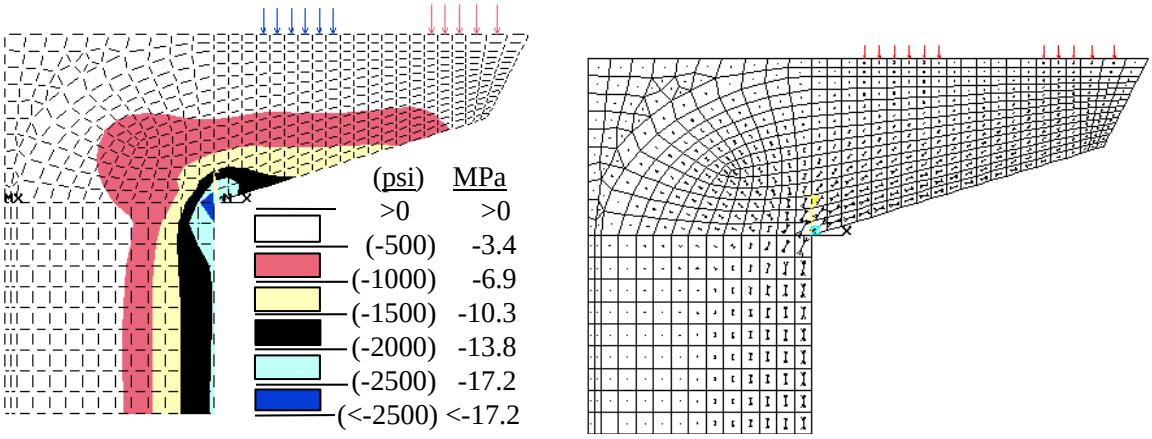

Figure 3.23 POJ-RC-100-TH principal tensile stresses and vectors at dead load

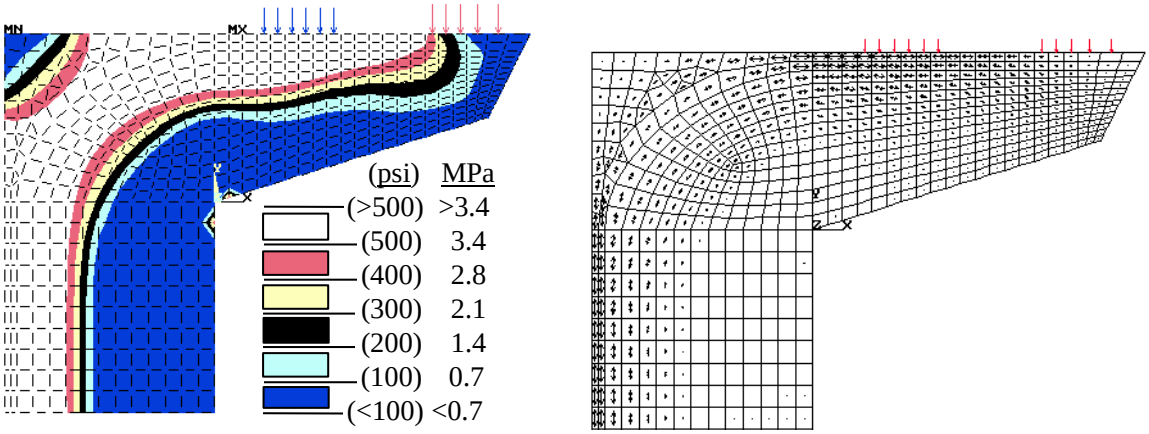

Figure 3.24 POJ-RC-100-TH principal tensile stresses and vectors at service load

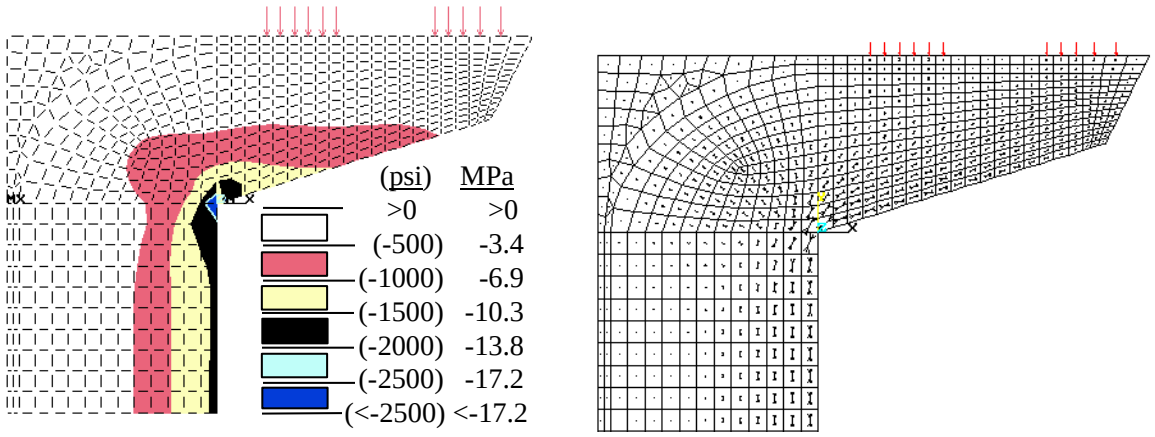

Figure 3.25 POJ-RC-100-TH principal compressive stresses and vectors at dead load

3.4.3.2 Strut-and-Tie Model–POJ-RC-100-TH

The strut-and-tie model shown in Figure 3.26 was based loosely on the principal stress vectors presented in Figures 3.24 and 3.25. Details about the computation of reinforcement corresponding with the tension ties shown in Figure 3.26 are presented in the following subsections.

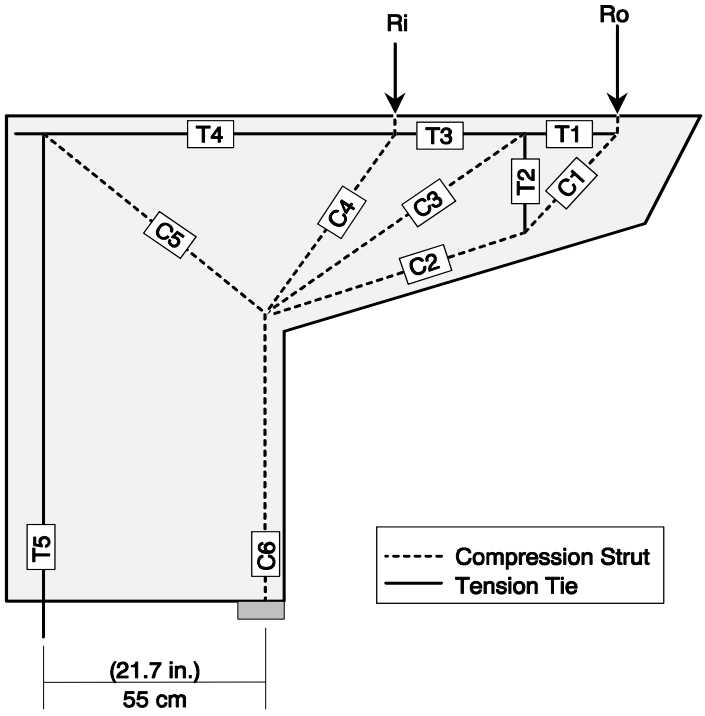

Figure 3.26 POJ-RC-100-TH strut-and-tie model

3.4.3.3 Overhang Design Details–POJ-RC-100-TH

Longitudinal Reinforcement:

The amount of longitudinal reinforcement in the overhang was determined using the maximum force in the top cord (Tension Tie T4) of the strut-and-tie model (STM). The amount of reinforcement required to resist the model factored loads was computed by:

$$T_4 \le \Phi\left(A_s f_y\right) \qquad [3\text{- }32]$$

where:

T_n = STM tension tie force = 1368 kN (307.5 kips)

Φ = Phi factor = 0.9

A_s = Area of primary flexural reinforcement = 36 cm^2 (5.6 in^2)

f_y = Nominal yield stress of mild reinforcement = 414 MPa (60 ksi).

The area of mild steel required by the equation was equal to that computed using AASHTO Equation 8-15. Based on the STM, no shear friction reinforcement was provided. Side-face reinforcement was determined using the Frantz and Breen relationship presented in Equation 3-27. The quantity of side face reinforcement was computed to be 1.3 cm^2 (0.19 in^2) per face. Details of the longitudinal reinforcement in the overhang at a cross section adjacent to the pier are shown in Figure 3.27. Once the amount of side-face reinforcement was computed, a cracked-section analysis (considering all longitudinal reinforcement) was conducted to determine the steel stresses at service and dead loads. Steel stresses were used to check crack-widths and determine the maximum stress range.

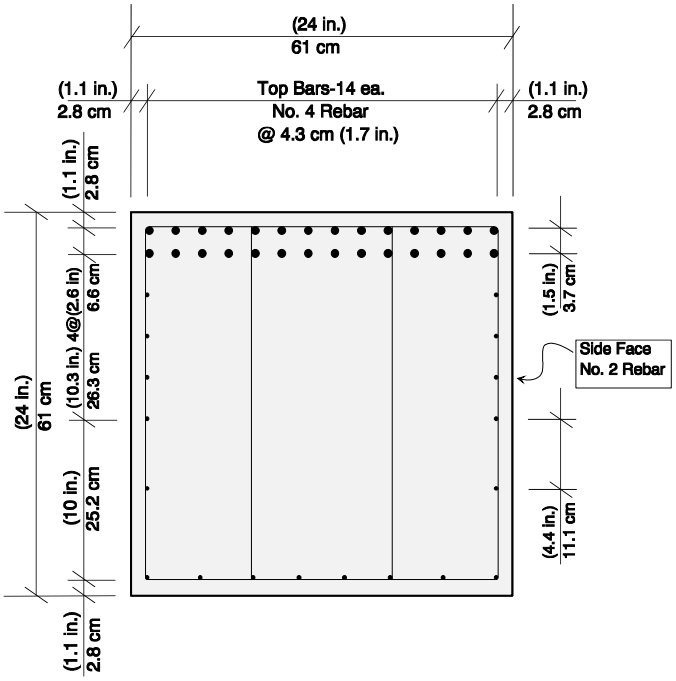

Figure 3.27 POJ-RC-100-TH overhang cross section details

Serviceability Provisions:

Crack widths were intended to be controlled by the relationship presented in Equation 3-29. The average steel stress due to service loads was computed to be 252 MPa (36.5 ksi), and was less than the stress, f_{sl}, of 278 MPa (40.3 ksi) associated with the limiting crack width.

The fatigue stress range was determined by computing the difference in steel stresses in the top-most reinforcing bars resulting from service loads and dead loads. Stress in the top reinforcing bars was 200 MPa (29.1 ksi) for dead loads and 264 MPa (38.3 ksi) due to service loads. The resulting 63 MPa (9.2 ksi) stress range was within the allowable fatigue stress range of 95 MPa (13.8 ksi) computed by Equation 3-28. The peak stress in the reinforcement was greater than 0.6 f_y = 248 MPa (36 ksi).

Transverse Reinforcement:

Only one vertical tie (Tension Tie T2) was considered in the STM. The quantity of transverse reinforcement required to resist the tension tie force (T2) of 367 kN (82.6 kips) was computed using Equation 3-25. The resulting quantity of transverse reinforcement, A_{vs}, was 7.9 cm^2 (1.22 in^2). The $[1\sqrt{f'_c}\, b_w d]$ contribution was included to account for a concrete contribution to shear strength, which reduced the required amount of transverse reinforcement. Results from the overhang study performed by Armstrong [3] and Salas [4] indicated the strut-and-tie analysis overestimated the required amount of transverse reinforcement. The inclusion of a concrete contribution significantly reduced congestion of transverse reinforcement located in the region of the T2 tension tie, and provided a more economical design with sufficient strength to resist factored loads. The tension tie reinforcement was uniformly spaced over a distance equal to the effective depth, d, of the section at the tension tie.

Minimum transverse reinforcement was provided over most of the remaining overhang according to the equation for maximum spacing (Equation 3-28). This maximum spacing was 18 cm (7 in.), and was determined for an effective depth, d, of 36 cm (14 in.) that corresponded approximately with the effective depth at the location of the vertical tie, T2 (see Figure 3.26). A slightly larger spacing of 24 cm (9.5 in.) was provided adjacent to the distributed tension-tie reinforcement. Rather than reduce the spacing of the two sets of transverse reinforcement adjacent to the column (which were spaced at $s_{max}/2$ and s_{max}) by adding an additional set, the larger space was retained to observe the effectiveness of the "slightly-less-than-minimum" reinforcement. Transverse reinforcement details are presented in Figure 3.28.

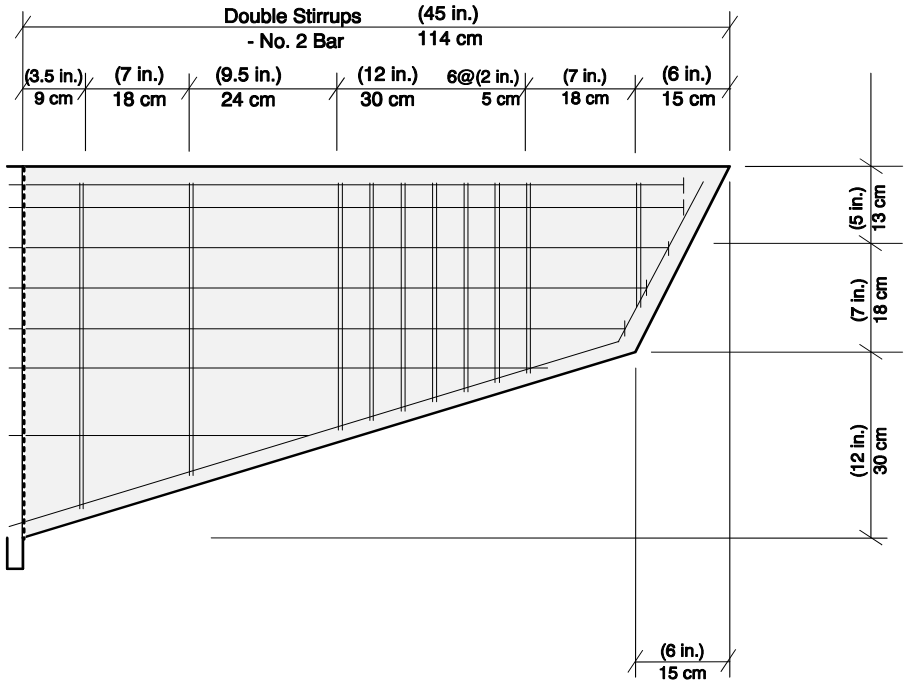

Figure 3.28 POJ-RC-100-TH transverse reinforcement details

3.4.3.4 Pier Details–POJ-RC-100-TH

Pier longitudinal reinforcement was determined using a strut-and-tie model and cracked-section analysis. The total area of longitudinal pier reinforcement for Specimen POJ-RC-100-TH was identical to that for Specimen POJ-RC-100. The distribution of longitudinal pier reinforcement was also the same to determine the effect headed reinforcement had on specimen capacity. However, it

should be noted that the distribution of longitudinal reinforcement in the pier did not satisfy serviceability requirements.

Longitudinal Reinforcement:

The quantity of longitudinal reinforcement was based on the tie force, T5, of the STM illustrated in Figure 3.26 The amount of reinforcement required to resist factored loads was computed by:

$$T_5 \le \Phi\left(A_s f_y\right) \qquad [3\text{- }33]$$

where:

T_5 = STM tension tie force = 1420 kN (319 kips)

Φ = Phi factor = 0.8 based on the level of axial load

A_s = Area of primary flexural reinforcement = 43.3 cm^2 (6.72 in^2)

f_y = Nominal yield stress of mild reinforcement = 414 MPa (60 ksi).

Transverse Reinforcement:

Transverse reinforcement was detailed using AASHTO Article 8.18.2.3. The transverse tie-spacing and bar-size requirements were divided by the 2.75 scale factor. The No. 4 minimum bar size specified in AASHTO was modeled using 7 ga. wire. The specified minimum longitudinal tie spacing of 30 cm (12 in.) was divided by the 2.75 scale factor, resulting in a tie spacing of 11 cm (4.4 in.). The specified maximum distance to a restrained bar of 61 cm (2 ft.) was divided by the 2.75 scale factor resulting in a distance of 22 cm (8.7 in.). Detailing of the transverse reinforcement and the distribution of longitudinal reinforcement in the pier is illustrated in Figure 3.29. A cracked-section analysis was conducted to determine steel stresses due to service loads and dead loads to check crack-widths and determine the maximum stress range.

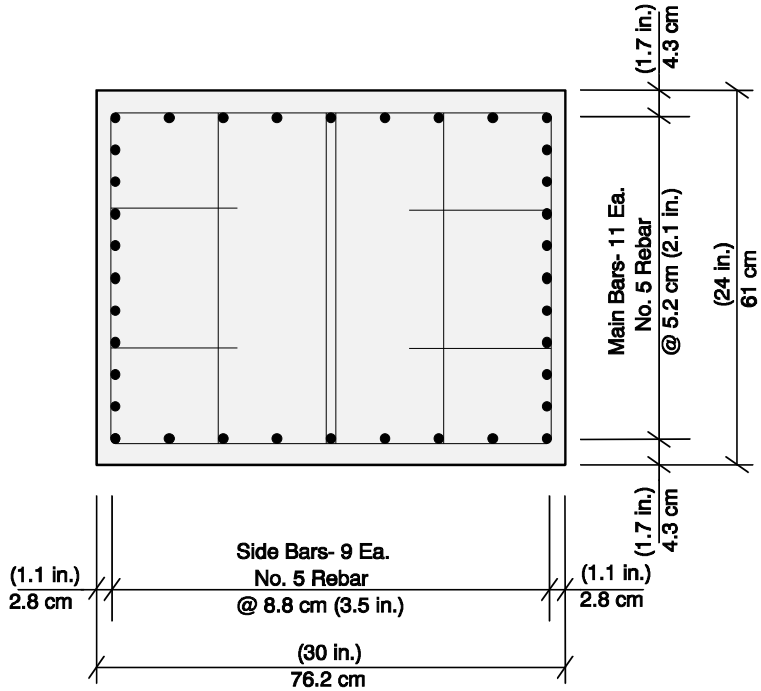

Figure 3.29 POJ-RC-100-TH pier cross-section details

Serviceability Provisions:

Crack widths were checked using the relationship presented in Equation 3-29. The average steel stress due to service loads was computed to be 203 MPa (29.4 ksi), which was greater than the stress, f_{sl}, of 165 MPa (23.9 ksi) associated with the limiting crack width. Although the equation was not satisfied, the bar distribution in the pier was not modified in order to evaluate the performance of the headed reinforcement (see Sections 3.3.1.3 and 3.4.3.5).

The fatigue stress range was determined by computing the difference in steel stresses in the extreme tensile reinforcing bars resulting from service loads and dead loads. Stress in the reinforcing bars was 213 MPa (30.9 ksi) due to dead loads and 278 MPa (40.3 ksi) due to service loads. The resulting stress range of 65 MPa (9.4 ksi) was within the allowable fatigue stress range of 112 MPa (13.2 ksi) computed by Equation 3-28. Peak stress in the reinforcement at service load was 278 MPa (40.3 ksi), which was greater than $0.6f_y$ = 248 MPa (36 ksi).

3.4.3.5 Joint Details–POJ-RC-100-TH

Bar Anchorage:

The use of headed reinforcement in the joint region assured development of the longitudinal reinforcement beginning at the face of the steel plate. This facilitated the formation of tension ties through the joint region and a diagonal compression strut between the interlocking heads and the opposite (compression) corner of the joint (see Figure 3.30).

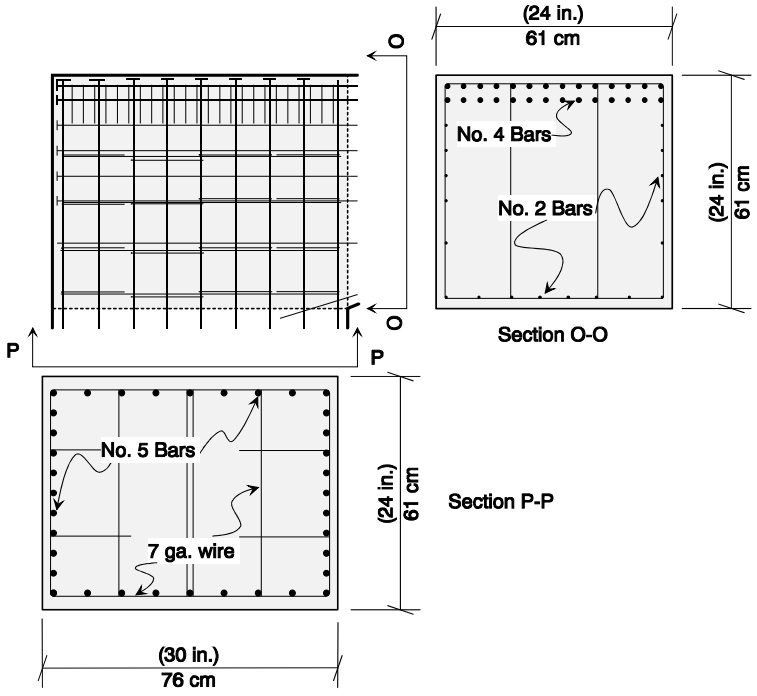

Figure 3.30 POJ-RC-100-TH joint reinforcement details

Specimen strength was computed using the model presented in Section 5.2. Because all of the primary tensile reinforcement in the overhang and pier were fully developed at the anchor head, the computed capacity was 1.26 times the strength required to resist applied factored loads. Reinforcement details for the joint and complete specimen are illustrated in Figures 3.30 and 3.31, respectively.

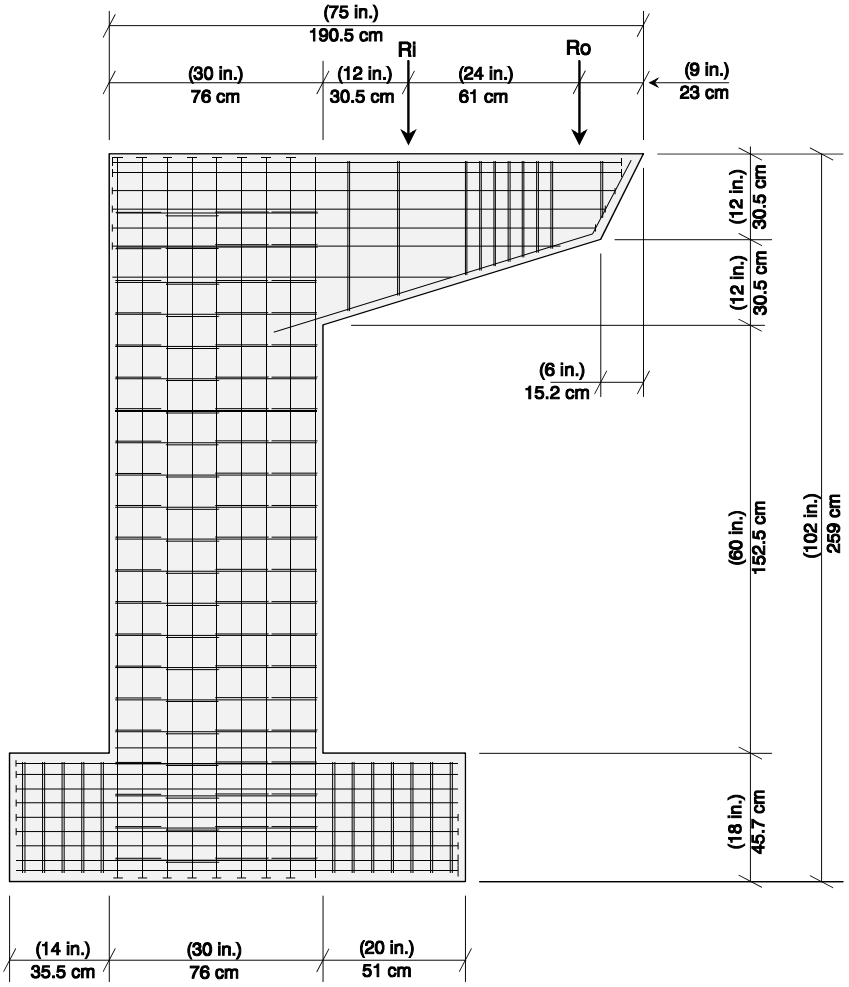

Figure 3.31 POJ-RC-100-TH complete reinforcement details

3.4.4 54% Prestressed Design with T-Headed Bars–POJ-PU-54-TH

The 54% prestressed specimen contained three post-tensioned tendons that were continuous through the overhang, joint, and pier. The percentage (54%) indicates the portion of tie force in the overhang that was provided by tendons.

3.4.4.1 Finite Element Analysis–POJ-PU-54-TH

Finite element analysis of the 54% prestressed specimen utilized a more complex ANSYS 5.0 [33] model than was used for the reinforced concrete specimen. The finite element model was developed by generating separate meshes for the post-tensioning tendon (one tendon in the FE model represented all tendons in the actual specimen) and concrete members, then introducing displacement compatibility links between the tendon nodes and concrete nodes. Tendon nodes were free to displace along the concrete mesh, but concrete and tendon nodal displacements were linked normal to the tendon path. Friction losses were not included in the finite element analysis.

Mesh boundaries were established by generating a continuous line that passed through the overhang, joint, and pier. A spline curve was used in the joint region to produce the arc. Once straight portions of the tendon path in the overhang and pier were generated, the spline arc was generated in the joint to connect the end points of the overhang and pier sections of the tendon. Ends of the spline were required to have the same slope as the connecting segments. Once tendon geometry was established, the concrete model was generated using the tendon profile as a boundary for the concrete elements.

Once the eight-node isoparametric plane-stress elements were generated, the two-node link elements were generated on a set of coincident nodes. Compatibility between the tendon and concrete was established by linking the X or Y deformations of concrete-element nodes and nodes for the tendon elements. Local-coordinate nodes on the concrete elements and tendon elements were rotated tangent to the tendon path. The tangent rotation angle was determined using an EXCEL spreadsheet [34]. If the rotation angle for the X axis was greater than 0.785 Radians (45°), the Y-axis was rotated. Once the nodes were rotated, local X or Y displacements of the coincident nodes were linked, depending on which axis was rotated and the orientation of the tendon path (see Figure 3.32).

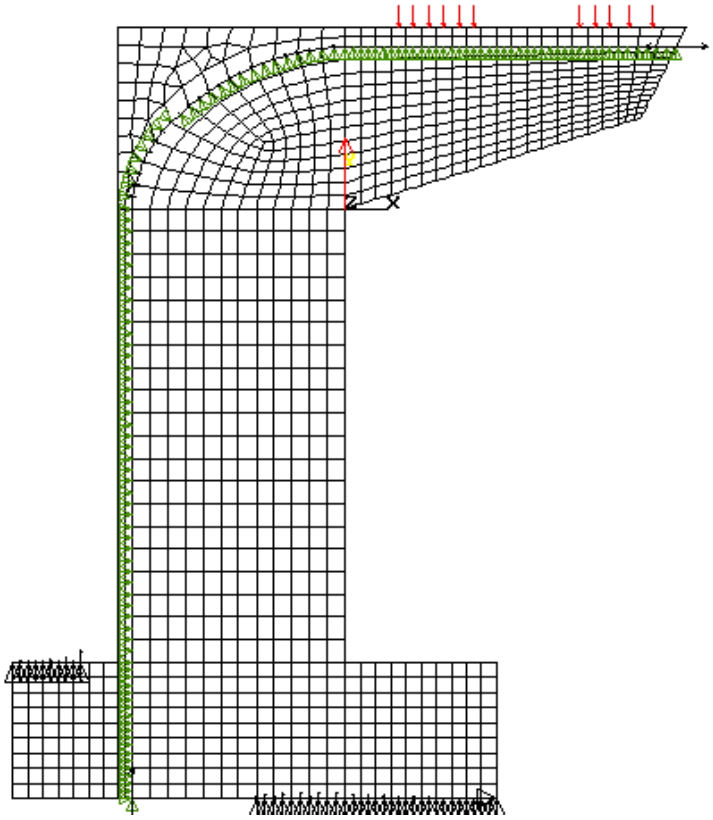

Figure 3.32 Finite element model for Specimen POJ-PU-54-TH

Tendon elements in the model were "stressed" by applying a concentrated load on the tendon at the tip of the overhang and an equal and opposite concentrated load on the specimen. Because the points on the tip of the overhang were coincident, there was no eccentricity created at the point of load application. The other end of the tendon was fixed at a point in the base of the model. The hold-down member at the base of the specimen (on the left side of Figure 3.32) was fixed against vertical displacement at the top. The base of the specimen (from a point near the center of the pier and extending to the tip of the stub on the right side of Figure 3.32) was fixed from vertical displacement at the bottom. A single point at the tip of the base member was fixed from horizontal displacement to stop rigid-body displacements.

Finite element analyses were performed for service loads and dead loads. Because the analyses did not consider non-linear material properties, tensile stresses in some areas may be over-estimated. If tensile stresses were above $7\sqrt{f_c'}$ (psi) [3.44 MPa (500 psi)], the region was considered cracked. Although the POJ-PU-54-TH specimen was computed to crack under dead loads, finite element analysis was also performed at service loads to illustrate the increase in tensile stresses in the joint. Computed principal tensile and compressive stresses for dead-load and service-load levels are

presented as stress contours and vectors in Figure 3.33 through Figure 3.36. Principal tensile contours at dead load indicated stresses in the overhang and pier were greater than the $7\sqrt{f_c'}$ (psi) [3.44 MPa (500 psi)] concrete cracking stress. However, principal tensile stresses across the joint diagonal were less than $2.8\sqrt{f_c'}$ (psi) [1.38 MPa (200 psi)] at dead load, and less than $5.6\sqrt{f_c'}$ (psi) [2.76 MPa (400 psi)] at service load. This was a significant improvement over principal tensile stresses plotted for Specimens POJ-RC-100 and POJ-RC-100-TH. As before, principal tensile and compressive stress vectors were used to aid in development of a strut-and-tie model.

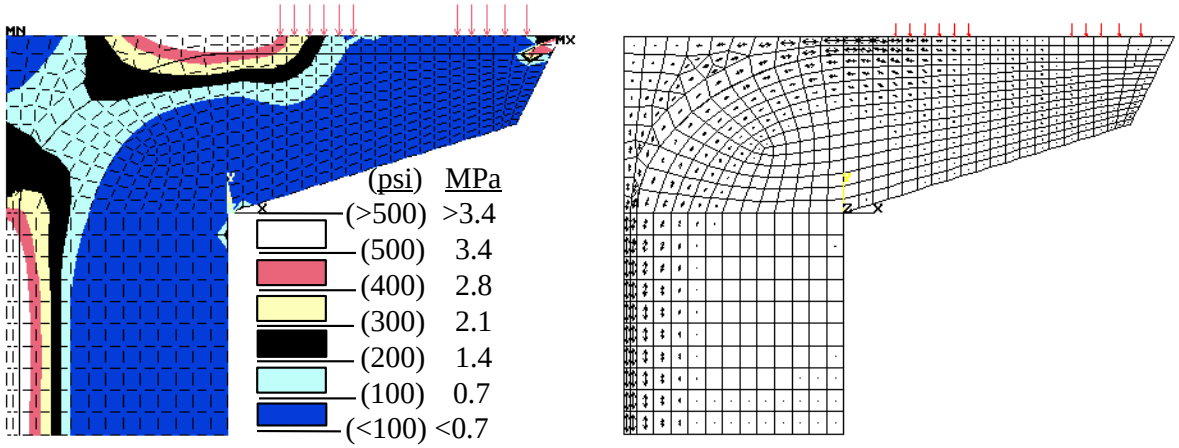

Figure 3.33 POJ-PU-54-TH principal tensile stress contours and vectors at dead load

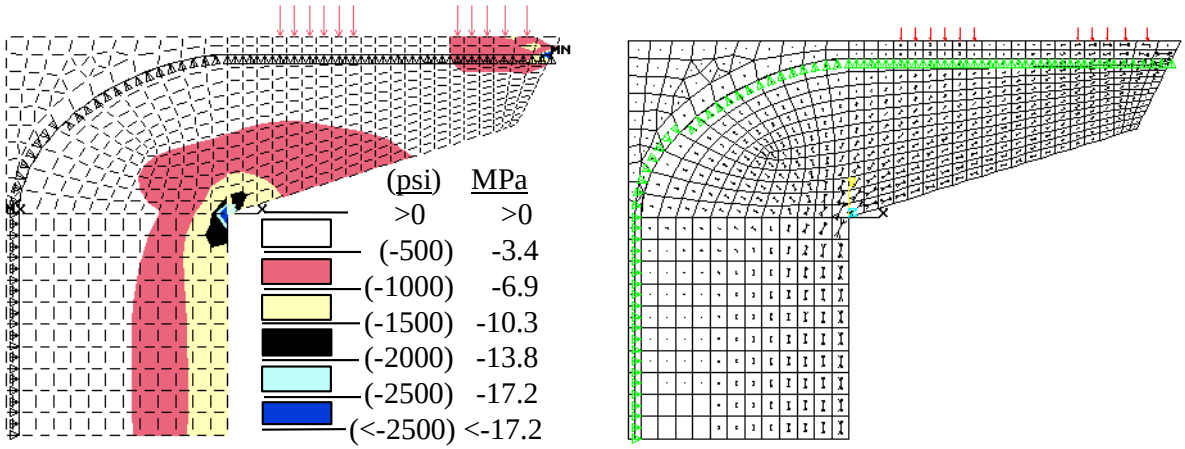

Figure 3.34 POJ-PU-54-TH principal compressive stress contours and vectors at dead load

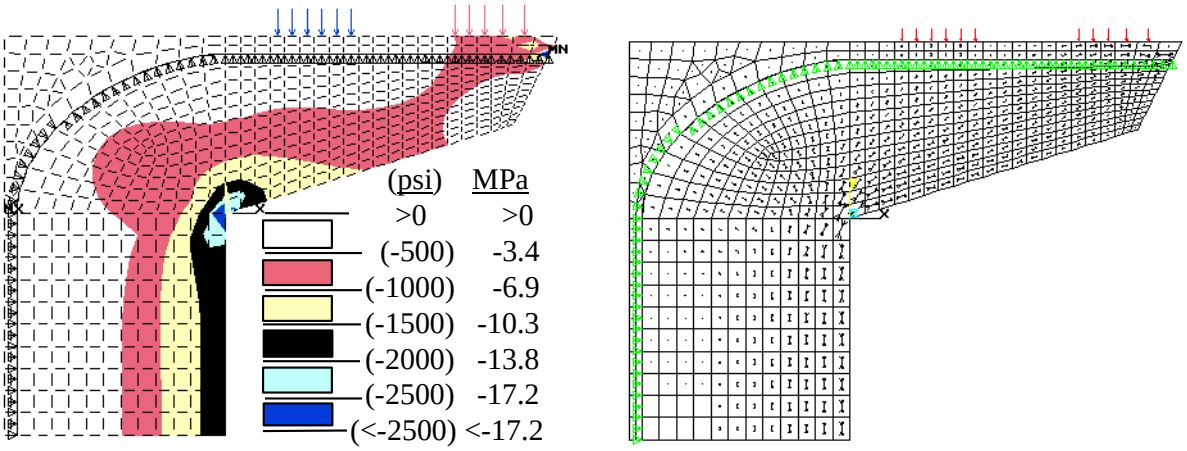

Figure 3.35 POJ-PU-54-TH principal compressive stress contours and vectors at service load

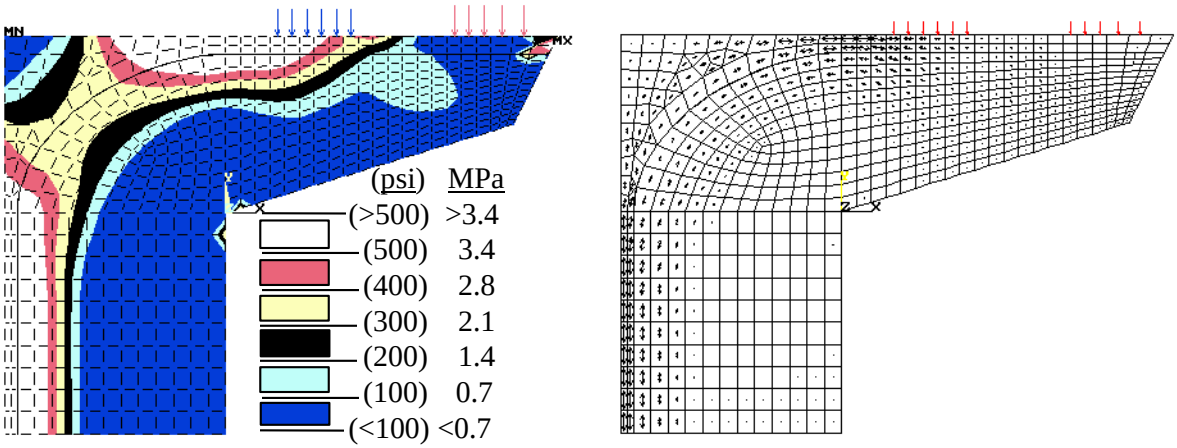

Figure 3.36 POJ-PU-54-TH principal tensile stress contours and vectors at service load

3.4.4.2 Strut-and-Tie Model - POJ-PU-54-TH

The strut-and-tie model is intended to represent the flow of forces implied by the principal stress vectors presented in Figures 3.35 and 3.36. Principal tensile and compressive stress vectors were used to aid in positioning tension ties and compression struts, respectively. Details about the computation of reinforcement corresponding with the tension ties shown in Figure 3.37 are presented in the following subsections.

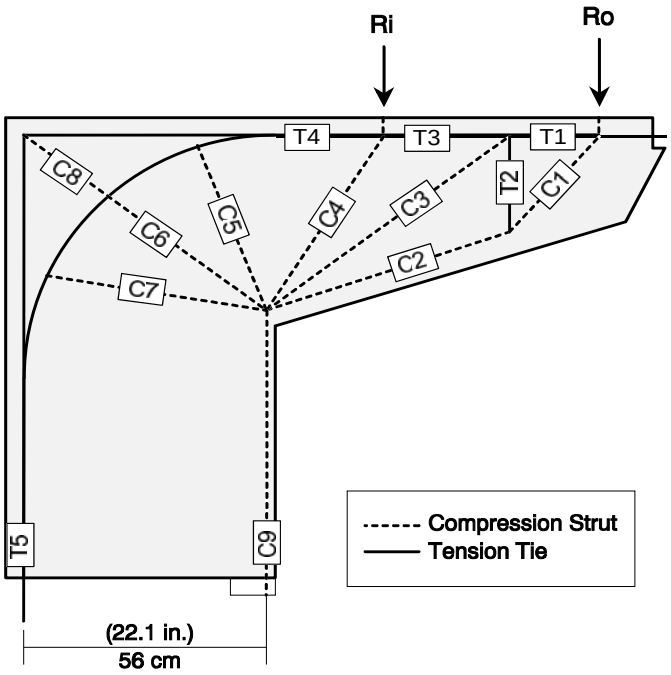

Figure 3.37 POJ-PU-54-TH strut-and-tie model

3.4.4.3 Overhead Details–POJ-PU-54-TH

Longitudinal Reinforcement:

The amount of longitudinal reinforcement in the overhang was determined using the maximum force in the top cord (Tension Tie T4) of the strut-and-tie model. The amount of reinforcement required to resist the model factored loads was computed by:

$$T_4 \le \Phi\left(A_{ms} f_y + A_{ps} f_{pu}\right) \qquad [3\text{-}34]$$

where:

T_4 = STM tension tie force =1414 kN (318 kips).

Φ = Phi factor = 0.9

A_{ms} = Area of mild steel primary flexural reinforcement

= 15.4 cm^2 (2.4 in^2)

f_y = Nominal yield stress of mild reinforcement = 414 MPa (60 ksi)

A_{ps} = Area of prestressed primary flexural reinforcement

= 4.16 cm^2 (0.645 in^2)

f_{pu} = Prestressing steel stress at Ultimate Load =1860 MPa (270 ksi).

The quantity of mild steel provided was 46% of the tension tie force (T4), and the quantity of prestressing steel provided was 54% of the tension tie force. Based on the strut-and-tie model, there was no need to provide shear-friction reinforcement. Side-face reinforcement was determined using the Frantz and Breen [10] relationship presented in Equation 3-27. The quantity of side face

reinforcement was computed to be 1.3 cm^2 (0.19 in^2) per face. Details of the longitudinal overhang reinforcement at the cross section adjacent to the pier are shown in Figure 3.39.

Selection of Post-Tensioning Reinforcement:

The quantity of post-tensioned steel was provided by three -15 mm (0.6 in.) diameter strands, located 4.8 cm (1.9 in.) from the extreme tension fiber. The location and spacing of the post-tensioned steel is presented in Figure 3.38.

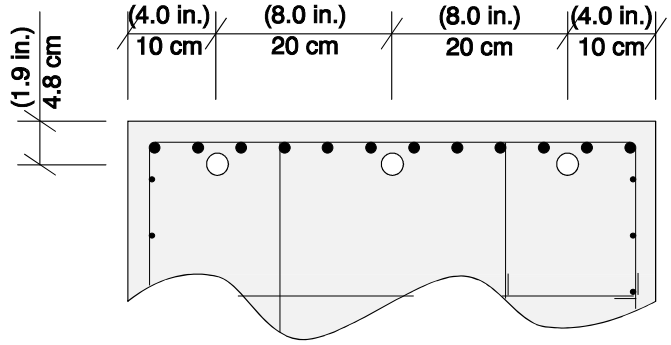

Figure 3.38 POJ-PU-54-TH location of post-tensioning tendons

Once the amount of side-face reinforcement was computed, a cracked-section analysis (considering all longitudinal reinforcement) was conducted to determine the steel stresses at service and dead loads. Steel stresses were used to check crack widths and determine the maximum stress range.

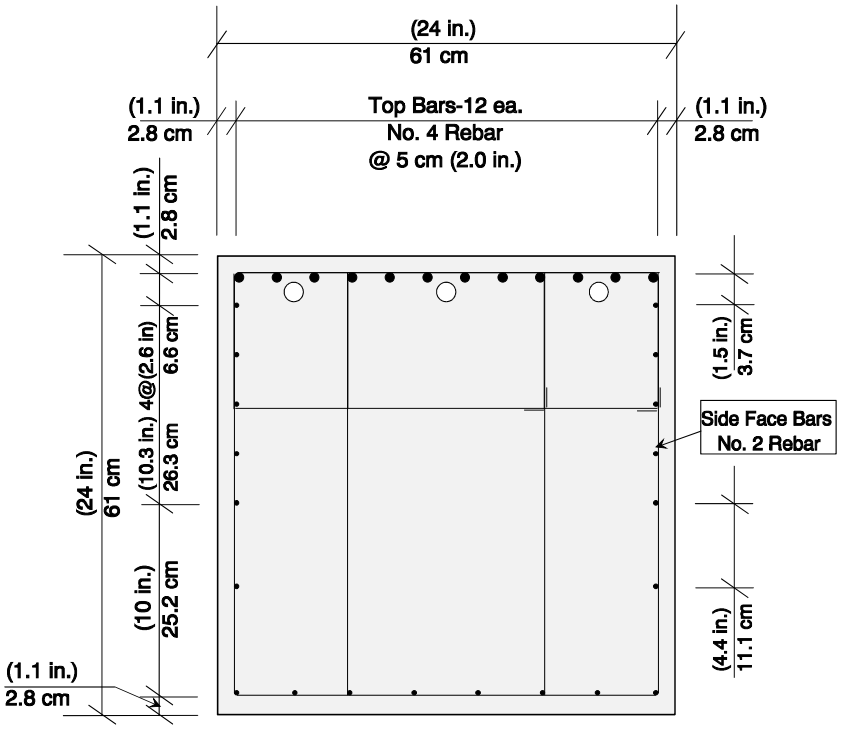

Figure 3.39 POJ-PU-54-TH overhang cross-section details

Serviceability Provisions:

Flexural crack widths were intended to be controlled by the relationship presented in Equation 3-29. The average steel stress due to service loads was computed to be 241 MPa (34.9 ksi), and was less than the stress, f_{sl} , associated with the limiting crack width.

The fatigue stress range was determined by computing the difference in steel stresses in the top-most reinforcing bars resulting from service loads and dead loads. Stress in the top reinforcing bars was 148 MPa (21.4 ksi) due to dead loads and 247 MPa (35.8 ksi) due to service loads. The resulting 99 MPa (14.4 ksi) stress range was within the allowable fatigue stress range of 122 MPa (16.3 ksi) determined by Equation 3-31. The peak stress in reinforcement was less than the 0.6 f_y = 248 MPa (36 ksi) limiting steel stress.

Stress in the prestressing tendons was 1123 MPa (162.8 ksi) due to dead loads and 1214 MPa (176.1 ksi) due to service loads. The resulting 92 MPa (13.3 ksi) stress range was within the allowable fatigue stress range of 100 MPa (14.5 ksi).

Transverse Reinforcement:

As in the POJ-RC-100-TH design, only one vertical tie was considered in the STM for the POJ-PU-54-TH overhang. The quantity of transverse reinforcement required to resist the tension tie force (T2) of 367 kN (82.6 kips) was computed using Equation 3-25. The resulting quantity of transverse reinforcement, A_{vs}, was 7.9 cm^2 (1.22 in^2). The location and quantity of transverse reinforcement was identical to that used for the POJ-RC-100-TH specimen because the post-tensioning force did not reduce the tension tie force, based on the results of the strut-and-tie model. The finite element analysis indicated tensile stresses in the overhang were reduced, but the flow of forces was the same as the STM for the POJ-RC-100-TH specimen. Tension tie T2 reinforcement was uniformly spaced over a distance equal to the effective depth, d, of the section at the tension tie.

Minimum transverse reinforcement was provided over most of the remaining overhang according to the equation for maximum spacing (Equation 3-28). This maximum spacing was 18 cm (7 in.), and was determined for an effective depth, d, of 36 cm (14 in.). Transverse reinforcement details are presented in Figure 3.40.

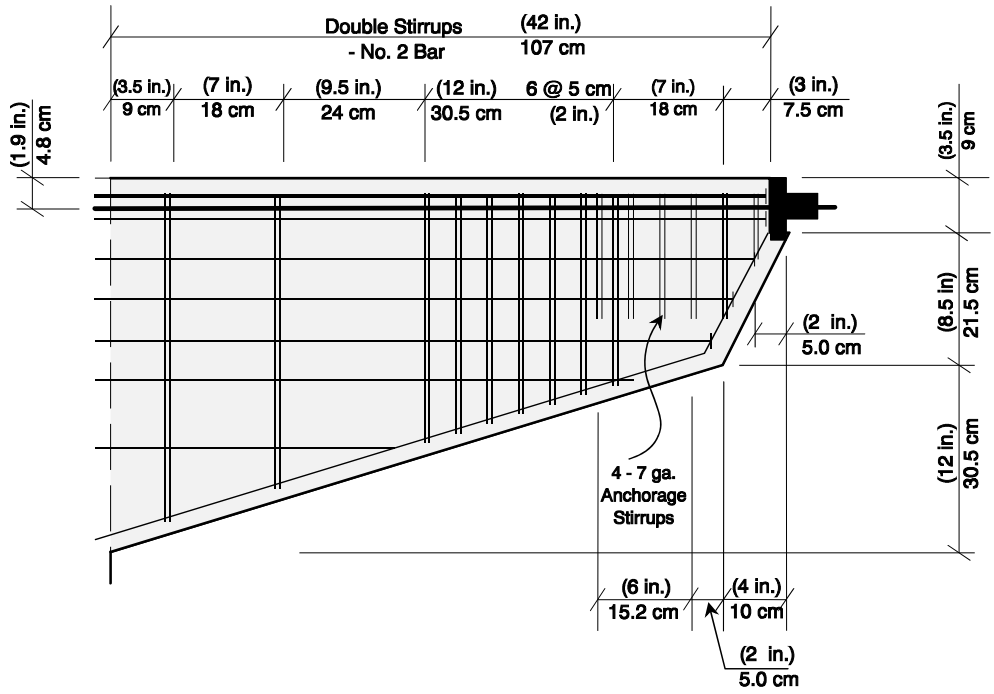

Figure 3.40 POJ-PU-54-TH transverse reinforcement details

3.4.4.4 Pier Details–POJ-PU-54-TH

Pier longitudinal reinforcement was determined using a strut-and-tie model and a cracked-section analysis. The quantity of post-tensioned steel, determined from the overhang design, was three 15 mm (0.6 in.) diameter strands. Because the prestressing tendons were continuous through the specimen, the amount of prestress in the pier accounted for less than 54% of the total tension tie force.

Longitudinal Reinforcement:

The quantity of longitudinal reinforcement was based on the tie force, T5, of the STM illustrated in Figure 3.26. The amount of reinforcement required to resist factored loads was computed by:

$$T_5 \le \Phi\left(A_{ms} f_y + A_{ps} f_{pu}\right) \qquad [3\text{-}35]$$

where:

T_5 = STM tension tie force =1393 kN (313.3 kips).

Φ = Phi factor = 0.8

A_{ms} = Area of mild steel primary flexural reinforcement

= 24 cm^2 (3.72 in^2)

f_y = Nominal yield stress of mild reinforcement = 414 MPa (60 ksi)

A_{ps} = Area of prestressed primary flexural reinforcement

= 4.16 cm^2 (0.645 in^2)

f_{pu} = Prestressing steel stress at Ultimate Load =1860 MPa (270 ksi).

The quantity of mild steel used provided 56% of the tension tie force (T4) and the quantity of prestressing steel provided 44% of the (T5) tension tie force. A cracked-section analysis was conducted to determine steel stresses due to service and dead loads to estimate crack widths and the maximum stress range. The cracked-section analysis was conducted using the reduced tendon force, T_x , at the pier-joint cross section.

The total area of longitudinal mild reinforcement in the pier, 46 cm^2 (7.13 in^2), was set equal to the minimum 1% specified by the AASHTO column design provisions.

Transverse Reinforcement:

Transverse reinforcement was detailed using AASHTO Article 8.18.2.3. Transverse tie-spacing and bar-size requirements were divided by the 2.75 scale factor. The No. 4 minimum bar size specified in AASHTO was modeled using 7 ga. wire. The specified minimum longitudinal tie spacing of 30 cm (12 in.) was divided by the 2.75 scale factor, resulting in a tie spacing of 11 cm (4.4 in.). The specified maximum distance to a restrained bar of 61 cm (2 ft.) was divided by the 2.75 scale factor resulting in a distance of 22 cm (8.7 in.). Positioning of the transverse reinforcement and distribution of longitudinal reinforcement in the pier are shown in Figure 3.41. A cracked-section analysis was conducted to determine steel stresses due to service loads and dead loads to check crack widths and determine the maximum stress range.

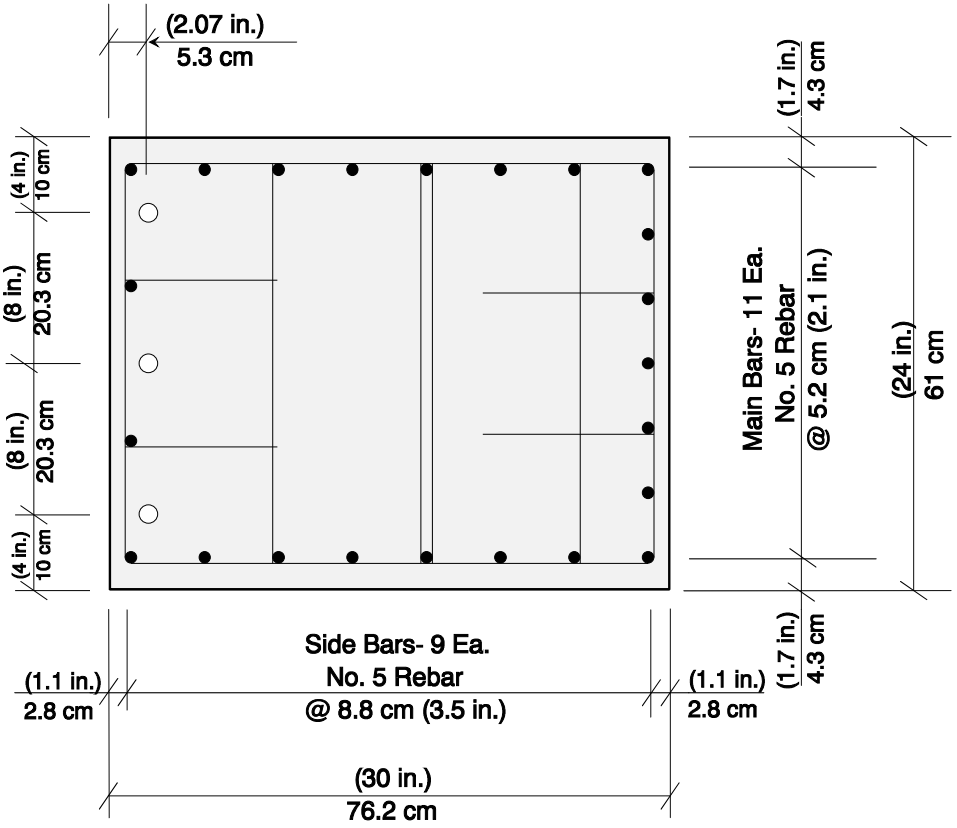

Figure 3.41 POJ-PU-54-TH pier cross-section details

Serviceability Provisions:

The post-tensioning tendon stress in the pier, after friction losses, was computed using AASHTO Equation 9-1:

$$T_x = \frac{T_o}{e^{(KL+\mu\alpha)}} \qquad [3\text{-}36]$$

where:

T_x = Prestressing force at distance (x=12 ft.) from jacking end

= 850 MPa (123.4 ksi)

T_o = Prestressing force at jacking end in (ksi) = 1396 kN (202.5 ksi)

K = Friction wobble coefficient = 0.002

μ = Coefficient of friction = 0.3

α = Total change of angle in radians = 1.5708 Rad.

L = Length (x) in (ft.) =3.7 m (12 ft.).

Crack widths in the pier were checked using the relationship presented in Equation 3-29. The average steel stress due to service loads was computed to be 243 MPa (35.2 ksi), which was greater than the limiting stress, f_{sl} , of 161 MPa (23.3 ksi) associated with the limiting crack width. The equation was not satisfied because of a miscalculation during design of the specimen. To satisfy the equation, a larger number of small-diameter reinforcing bars should have been used for the pier longitudinal reinforcement.

The fatigue stress range was determined by computing the difference in steel stresses in the extreme tensile reinforcing bars resulting from service loads and dead loads. Stress in the reinforcing bars was 205 MPa (29.8 ksi) due to dead loads and 307 MPa (44.6 ksi) due to service loads. The resulting stress range of 101 MPa (14.8 ksi) was within the allowable fatigue stress range of 103 MPa (15 ksi) computed using Equation 3-31. Peak stress in the reinforcement at service loads was 307 MPa (44.6 ksi), which was greater than 0.6 f_y =248 MPa (36 ksi).

Stress in the prestressing tendons was 851 MPa (123 ksi) due to dead loads and 994 MPa (137 ksi) due to service loads. The resulting stress range in the prestressing of 93 MPa (13.6 ksi) was within the allowable fatigue stress range of 100 MPa (14.5 ksi).

3.4.4.5 Joint Details–POJ-PU-54-TH

Bar Anchorage:

The use of headed reinforcement in the joint region assured development of longitudinal reinforcement beginning at the face of the steel plate. This facilitated the formation of tension ties through the joint region, and a diagonal compression strut between the interlocking heads and the opposite (compression) corner of the joint (see Figure 3.42).

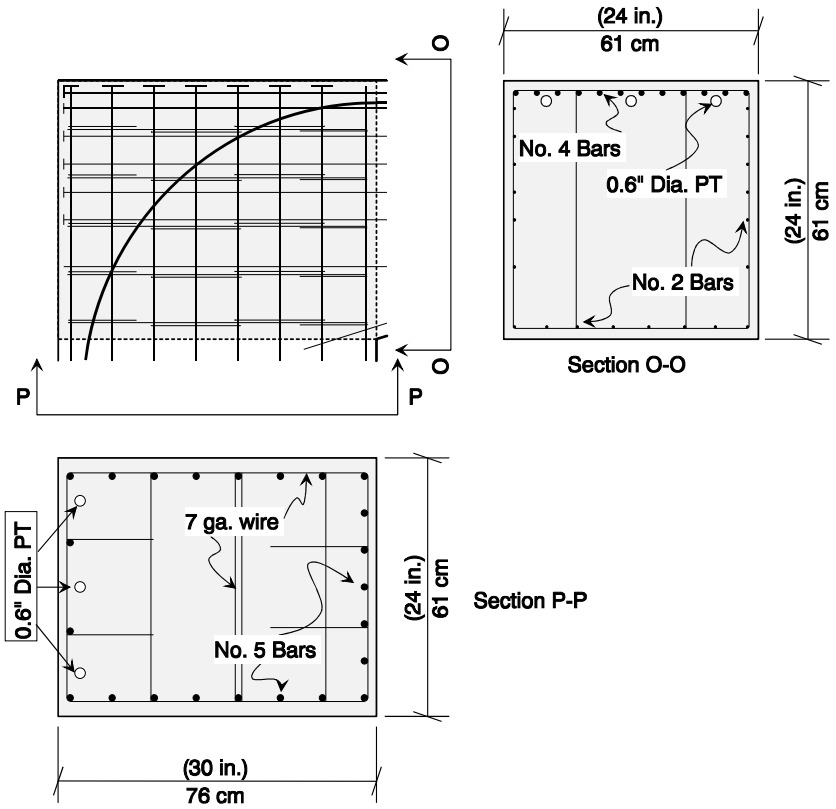

Figure 3.42 POJ-PU-54-TH joint reinforcement details

The continuous prestressing through the joint significantly reduced tensile stresses in the joint. In addition to reducing the tensile stresses, the prestressing steel provided a high-strength tensile tie across any potential diagonal joint crack. The computed specimen capacity using the model described in Section 5.2 was 1.28 times the strength required to resist applied factored loads. Reinforcement details for the joint and complete specimen are illustrated in Figure 3.42 and Figure 3.43, respectively.

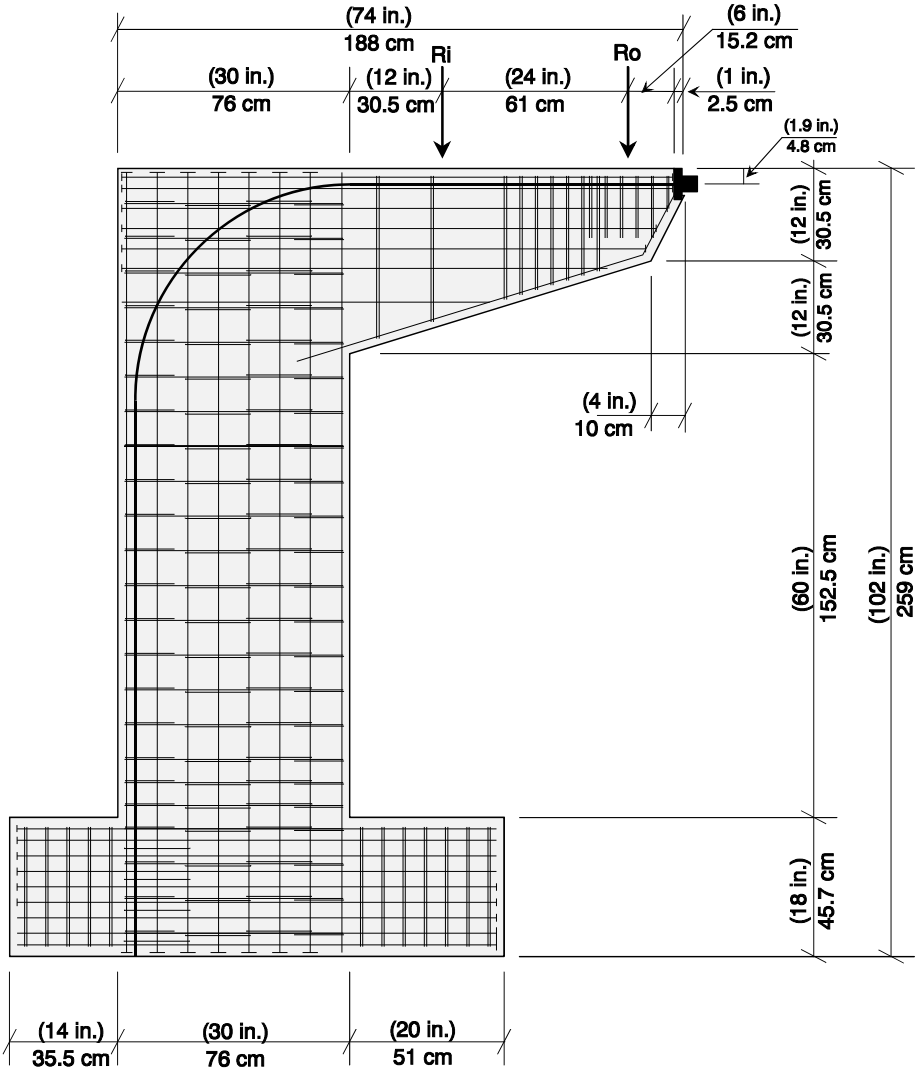

Figure 3.43 POJ-PU-54-TH overall reinforcement details

3.4.5 74% Prestressed Design with T-Head Bars–POJ-PU-74-TH

The 74% prestressed specimen (Specimen POJ-PU-74-TH) contained five post-tensioned tendons that were continuous through the overhang, joint, and pier. The percentage (74%) indicates the portion of tie force in the overhang that was provided by the tendon.

3.4.5.1 Finite Element Analysis–POJ-PU-74-TH

The finite element analysis of Specimen POJ-PU-74-TH used the same procedure used for the 54% prestressed specimen. The finite element model was developed by generating separate meshes for the post-tensioning tendon (modeled using two-node truss elements) and concrete elements (modeled using 8-node isoparametric plate elements), then introducing displacement compatibility links between the tendon nodes and concrete nodes. Nodal displacements for the concrete and tendon elements were coupled for displacements normal to the tendon axis, but were free to displace along the tendon axis. Friction losses were not included in the finite element analysis.

Tendon elements in the model were “stressed” by applying a concentrated load on the tendon at the tip of the overhang and an equal and opposite concentrated load on the specimen. Because the points

on the tip of the overhang were coincident, there was no eccentricity created at the point of load application. The other end of the tendon was fixed at a point in the base of the model. The base of the specimen was fixed from vertical displacement at the top and bottom at the locations indicated in Figure 3.32.

Finite element analyses were performed for service loads and dead loads. Because the analyses did not consider non-linear material properties, tensile stresses in some areas may be over-estimated.If tensile stresses were above $7\sqrt{f_c'}$ (psi) [3.44 MPa (500 psi)], the region was considered to be cracked. Although some regions of the POJ-PU-74-TH specimen were computed to be cracked under dead loads, finite element analysis was also performed at service loads to illustrate the increase in tensile stresses in the joint. Computed principal tensile and compressive stresses for dead-load and service-load levels are presented as stress contours and principal tensile stress vectors in Figure 3.44 through Figure 3.47.

Maximum computed principal tensile stresses for the specimen at dead load (shown in Figure 3.44) occurred in the overhang and pier, and stresses were slightly greater than the assumed concrete cracking tensile stress of $7\sqrt{f_c'}$ (psi) [3.44 MPa (500 psi)], indicating cracking would initiate at dead load. Maximum principal tensile stresses in the overhang and pier regions for Specimen POJ-PU-74-TH at dead load were slightly greater than the assumed concrete cracking tensile stress. However, principal tensile stresses in the joint region at dead load (where a critical diagonal crack could develop) were less than $1.4\sqrt{f_c'}$ (psi) [0.69 MPa (100 psi)], indicating cracking would not initiate at dead load. Additionally, principal tensile stresses in the joint region at service loads (shown in Figure 3.44) were slightly greater than $4.3\sqrt{f_c'}$ (psi) [2.07 MPa (300 psi)], indicating a critical diagonal crack would not initiate at service loads. Increased tensile stresses in the pier and overhang regions at service loads (shown in Figure 3.44) indicate that cracks initiated at dead load would extend further under the increased applied load.

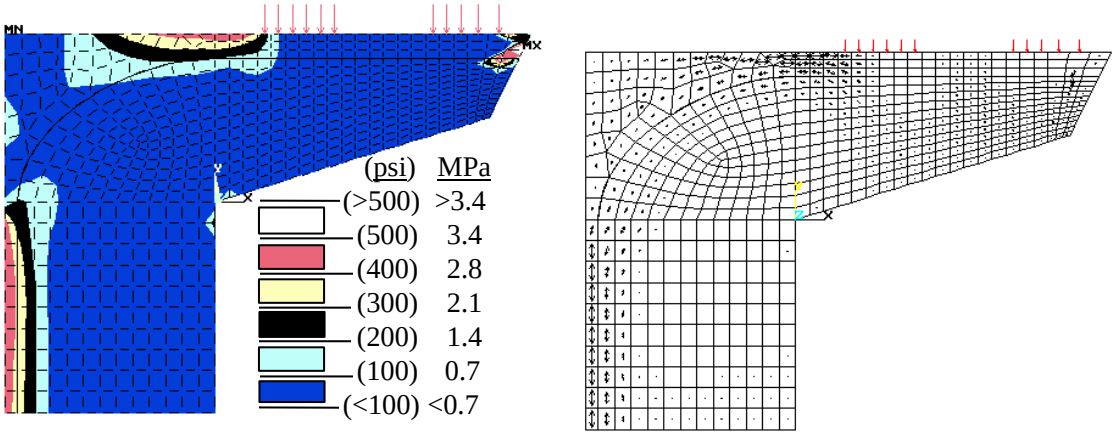

Figure 3.44 POJ-PU-74-TH principal compressive stress contours and vectors at dead load

As discussed previously, the principal tensile and compressive stress vectors (presented in Figure 3.44 through Figure 3.47) were used to aid in development of the strut-and-tie model presented in Figure 3.48.

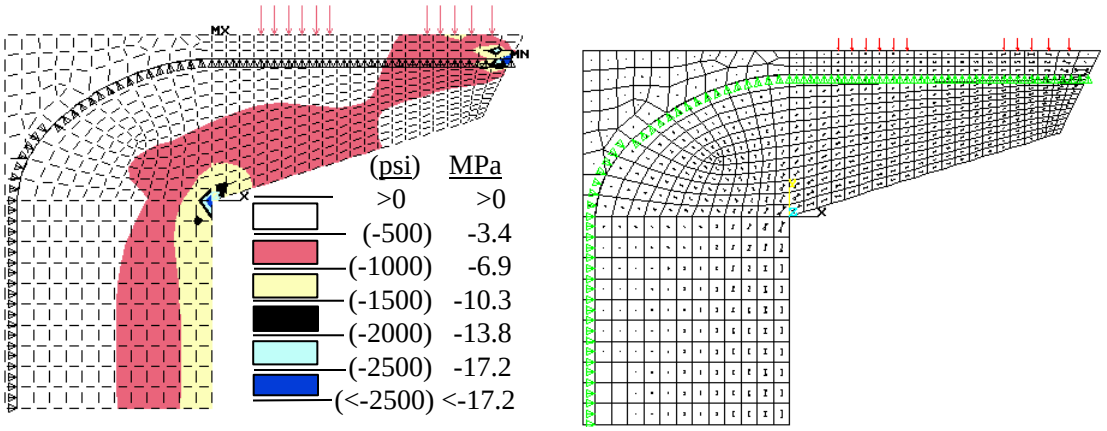

Figure 3.45 POJ-PU-74-TH principal tensile stress contours and vectors at dead load

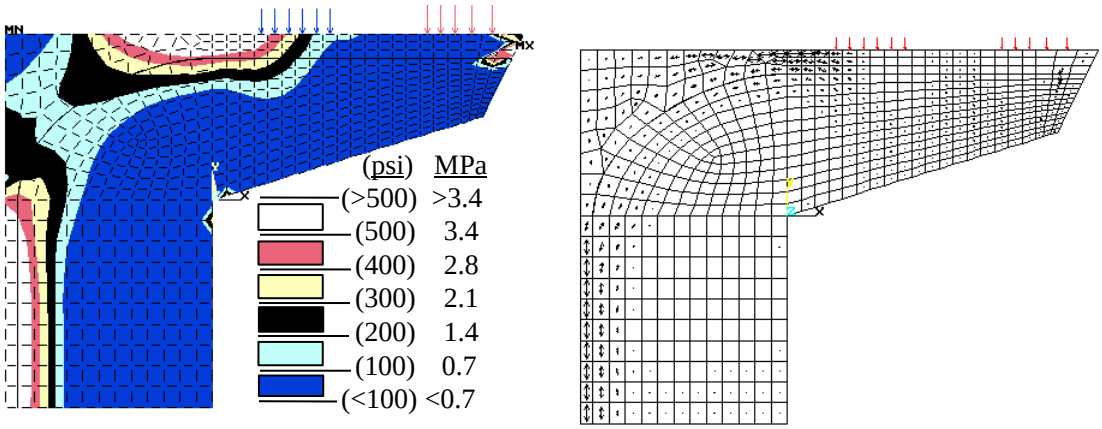

Figure 3.46 POJ-PU-74-TH principal tensile stress contours and vectors at service load

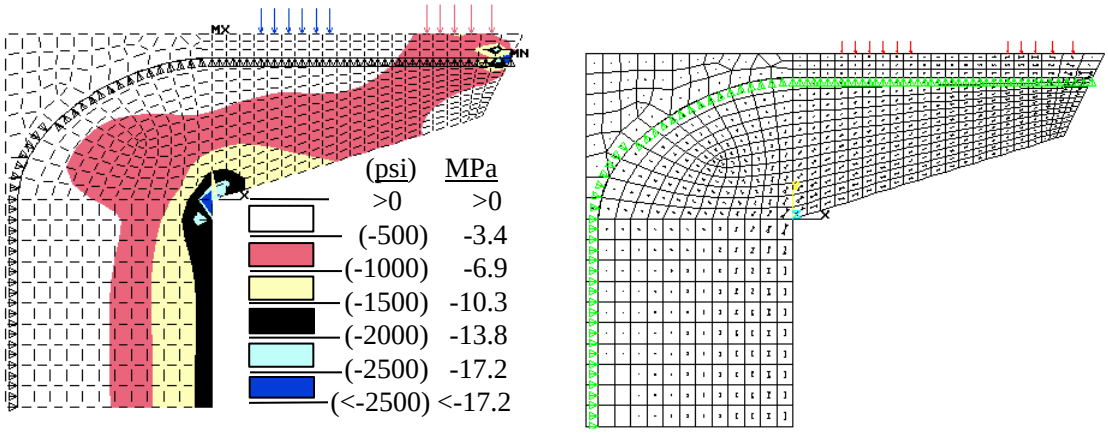

Figure 3.47 POJ-PU-74-TH principal compressive stress contours and vectors at service load

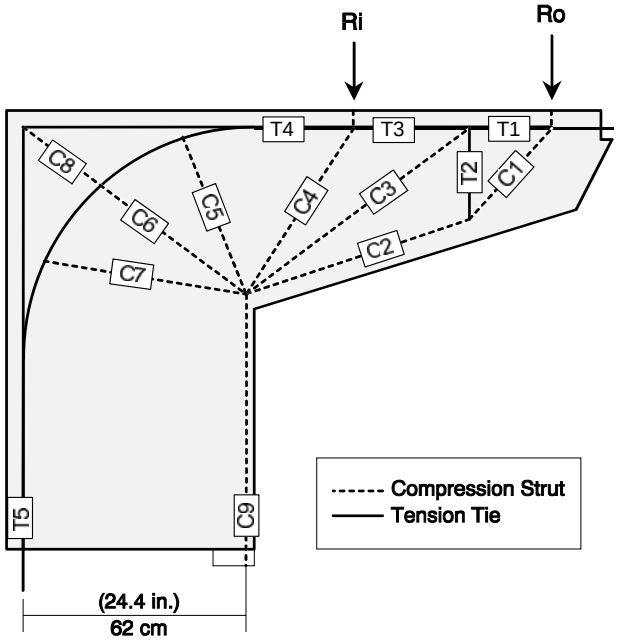

Figure 3.48 POJ-PU-74-TH strut-and-tie model

3.4.5.2 Strut-and-Tie Model–POJ-PU-74-TH

The strut-and-tie model was intended to represent the flow of stresses indicated by the principal stress vectors presented in Figure 3.46 and Figure 3.47. Principal tensile and compressive stress vectors were used to aid in positioning the tension ties and compression struts, respectively. Details about the computation of reinforcement corresponding with the tension ties shown in Figure 3.48 are presented in the following subsections.

3.4.5.3 Overhang Details–POJ-PU-74-TH

Longitudinal Reinforcement:

The amount of longitudinal reinforcement in the overhang was determined using the maximum force in the top cord (Tension Tie T4) of the strut-and-tie model (shown in Figure 3.48). The amount of reinforcement required to resist the model factored loads was computed by:

$$T4 \le \Phi\left(A_{ms} f_y + A_{ps} f_{pu}\right) \qquad [3\text{-}37]$$

where

T_4 = STM tension tie force =1439 kN (323.5 kips).

Φ = Phi factor = 0.9

A_{ms} = Area of mild steel primary flexural reinforcement

= 10.3 cm^2 (1.6 in^2)

f_y = Nominal yield stress of mild reinforcement = 414 MPa (60 ksi)

A_{ps} = Area of prestressed primary flexural reinforcement

= 6.13 cm^2 (0.951 in^2)

f_{pu} = Prestressing steel stress at Ultimate Load =1860 MPa (270 ksi).

The quantity of mild steel provided 26% of the tension tie force (T4), and the quantity of prestressing steel provided 74% of the tension tie force. Based on the strut-and-tie model, there was no need to provide shear-friction reinforcement. Side-face reinforcement was determined using the Frantz and Breen [10] relationship presented in Equation 3-27. The quantity of side-face reinforcement was computed to be 1.3 cm^2 (0.19 in^2) per face (See Fig. 3.50). Details of the longitudinal overhang reinforcement at the cross section adjacent to the pier are shown in Figure 3.53.

Selection of Post-Tensioned Reinforcement:

The quantity of post-tensioned steel was provided by three 15 mm (0.6 in.) diameter strands and two 13 mm (1/2 in.) diameter strands located 9 cm (3.5 in.) from the extreme tension fiber. The location and spacing of the post-tensioning ducts is presented in Figure 3.49.

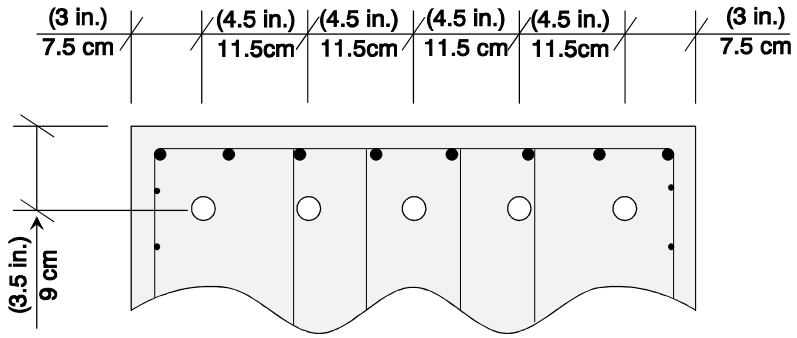

Figure 3.49 POJ-PU-74-TH post-tensioning duct locations

Once the amount of side face reinforcement was computed, a cracked-section analysis (considering all longitudinal reinforcement) was conducted to determine steel stresses at service and dead loads. Steel stresses were used to check crack widths and determine the maximum stress range.

Serviceability Provisions:

Size of crack widths was intended to be controlled by the relationship presented in Equation 3-29. The average steel stress due to service loads was computed to be 197 MPa (28.6 ksi), and was slightly greater than the stress, f_{sl} , of 196 MPa (28.4 ksi) associated with the limiting crack width.

The fatigue stress range was determined by computing the difference in steel stresses in the top-most reinforcing bars resulting from service loads and dead loads. Stress in the top reinforcing bars was 103 MPa (15 ksi) due to dead loads and 223 MPa (32.3 ksi) due to service loads. The resulting 119 MPa (17.3 ksi) stress range was within the allowable fatigue stress range of 134 MPa (19.4 ksi) determined by Equation 3-31. Peak stress in the reinforcement of 223 MPa (32.3 ksi) due to service loads was less than the 0.6 f_y = 248 MPa (36 ksi) limiting steel stress.

Stress in the prestressing strands was 1100 MPa (160 ksi) due to dead loads and 1200 MPa (174.5 ksi) due to service loads. The resulting 100 MPa (14.5 ksi) stress range was equal to the allowable fatigue stress range of 100 MPa (14.5 ksi).

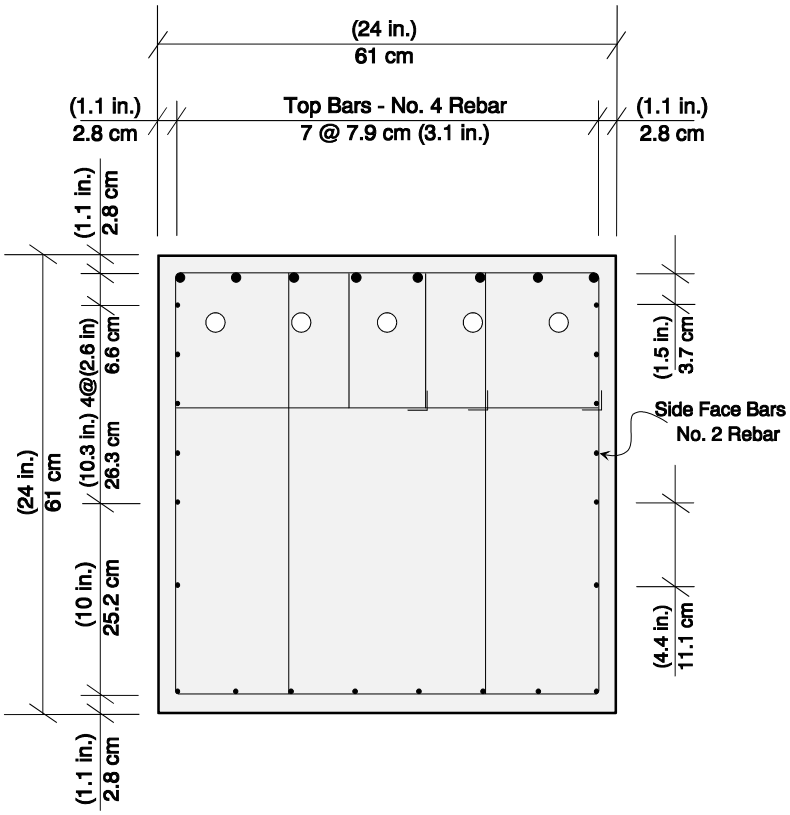

Figure 3.50 POJ-PU-74-TH overhang cross-section details

Transverse Reinforcement:

As for the POJ-PU-54-TH design, only one vertical tie was considered in the STM for the POJ-PU-74-TH overhang. The quantity of transverse reinforcement required to resist the tension tie force (T2) of 367 kN (82.6 kips) was computed using Equation 3-25. The resulting quantity of transverse reinforcement, A_{vs} , was 7.9 cm^2 (1.22 in^2). The location and quantity of transverse reinforcement was identical to that used for the POJ-PU-54-TH specimen because the different amount of post-tensioning did not reduce the tension tie force, based on the results of the strut-and-tie model. Finite element analysis indicated tensile stresses in the overhang were reduced, but the flow of forces from the STM were the same as for Specimen POJ-RC-100-TH. The tension tie reinforcement was uniformly spaced over a distance equal to the effective depth, *d*, of the section at the tension tie.

Minimum transverse reinforcement, according to the equation for maximum spacing (Equation 3-28), was provided over most of the remaining overhang. This maximum spacing was 18 cm (7 in.), and was determined for an effective depth, d, of 36 cm (14 in.). Transverse reinforcement details are presented in Figure 3.51.

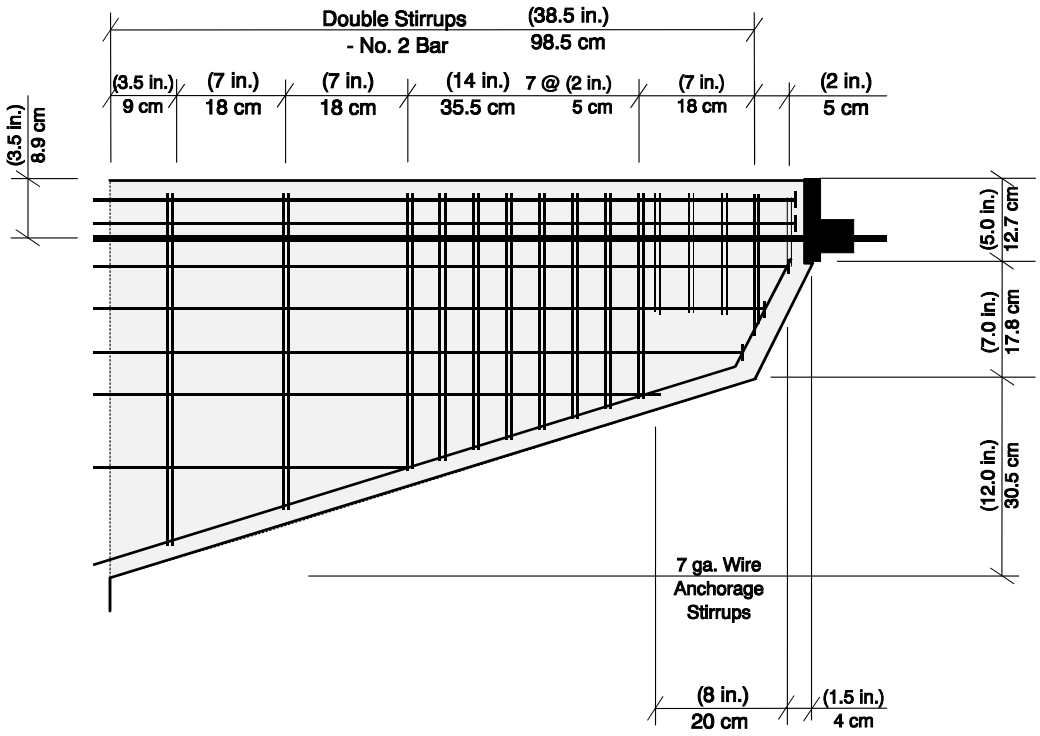

Figure 3.51 POJ-PU-74-TH overhang design details

3.4.5.4 Pier Design–POJ-PU-74-TH

Pier longitudinal reinforcement was determined using a strut-and-tie model and cracked-section analysis. The quantity of post-tensioned steel, determined from the overhang design, was three 15 mm (0.6 in.) diameter strands and two 13 mm (1/2 in.) diameter strands. Because the prestressing strands were continuous through the specimen, the percentage of prestress in the pier was less than 74% of the total tension tie force.

Longitudinal Reinforcement:

The quantity of longitudinal reinforcement in the pier was based on the tie force, T5 , of the STM illustrated in Figure 3.48. The amount of reinforcement required to resist factored loads was computed by:

$$T5 \le \Phi\left(A_{ms} f_y + A_{ps} f_{pu}\right) \qquad [3\text{-}38]$$

where

T_5 = STM tension tie force =1267 kN (285.0 kips).

Φ = Phi factor = 0.8

A_{ms} = Area of mild steel primary flexural reinforcement

= 15.5 cm^2 (2.40 in^2)

f_y = Nominal yield stress of mild reinforcement = 414 MPa (60 ksi)

A_{ps} = Area of prestressed primary flexural reinforcement

= 6.1 cm^2 (0.951 in^2)

f_{pu} = Prestressing steel stress at Ultimate Load =1860 MPa (270 ksi).

The quantity of mild steel used provided 36% of the tension tie force (T5) and the quantity of prestressing steel provided 64% of the (T5) tension tie force. A cracked-section analysis was conducted to determine steel stresses due to service and dead loads to check crack widths and maximum stress range. The cracked-section analysis was conducted using the reduced tendon force, T_x = 850 MPa (123.4 ksi), computed using Equation 3-42 in Section 3.4.4.4.

The total area of longitudinal mild reinforcement in the pier, 33.5 cm^2 (5.2 $in.^2$), provided a column reinforcement ratio of 0.72%. The design provided a realistic combination of mild reinforcement, based on a potential relaxation of the 1% minimum column reinforcement provision, and prestressing steel, based on strength design.

Transverse Reinforcement:

Transverse reinforcement was detailed using AASHTO Article 8.18.2.3. Transverse tie spacing and bar requirements were divided by the 2.75 scale factor. A 7 ga. undeformed wire was used to model the ties. Tie longitudinal spacing was 11.5 cm (4.5 in.). Detailing of transverse reinforcement and the distribution of longitudinal reinforcement are shown in Figure 3.52.

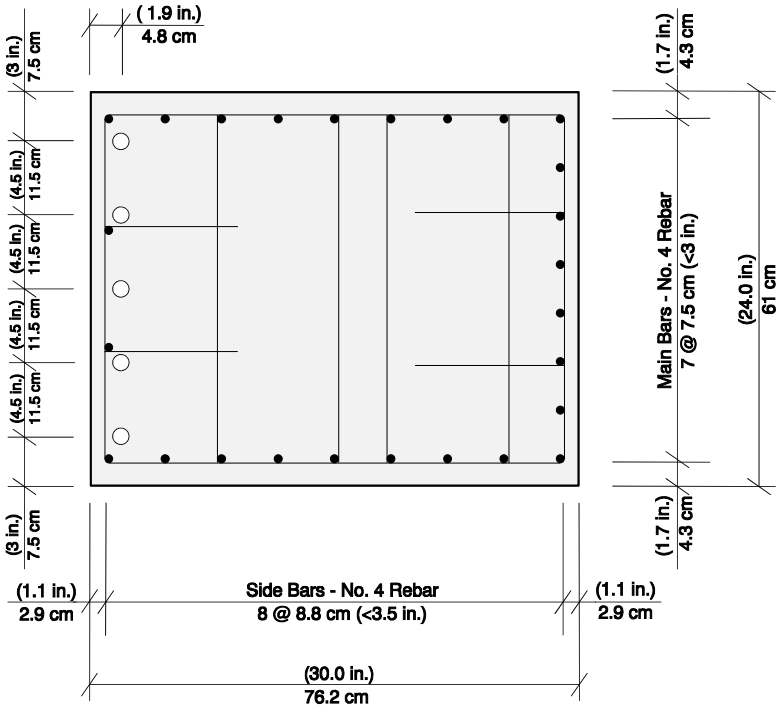

Figure 3.52 POJ-PU-74-TH pier reinforcement details

Serviceability Provisions:

Crack widths in the pier were controlled by the relationship presented in Equation 3-29. The average steel stress due to service loads was computed to be 231 MPa (33.5 ksi), which was greater than the limiting stress, f_{sl}, of 170 MPa (24.7 ksi) associated with the limiting crack width. The equation was not satisfied because of a miscalculation during design of the specimen. To satisfy the equation, a larger number of small-diameter longitudinal bars should have been used in the pier.

The fatigue stress range was determined by computing the difference in steel stresses in the extreme tensile reinforcing bars resulting from service loads and dead loads. Stress in the reinforcing bars was 149 MPa (21.6 ksi) due to dead loads and 261 MPa (37.8 ksi) due to service loads. The resulting stress range of 112 MPa (16.2 ksi) was within the allowable fatigue stress range of 126 MPa

(18.3 ksi) computed using Equation 3-31. Peak stress in the reinforcement at service loads was 261 MPa (37.8 ksi), which was greater than 0.6 f_y =248 MPa (36 ksi).

Stress in the prestressing tendons was 854 MPa (123.8 ksi) due to dead loads and 958 MPa (138.9 ksi) due to service loads. The resulting stress range in the prestressing of 104 MPa (15.1 ksi) was above the allowable fatigue stress range of 100 MPa (14.5 ksi). This limit was not satisfied because of a miscalculation that occurred during design of the specimen. To satisfy this requirement, tendons should be located further from the extreme tension fiber.

3.4.5.5 Joint Design–POJ-PU-74-TH

Bar Anchorage:

Use of headed reinforcement in the joint region assured development of longitudinal reinforcement beginning at the face of the steel plate. This facilitated the formation of tension ties through the joint region and a diagonal compression strut between the interlocking heads and opposite (compression) corner of the joint. Continuous post-tensioning through the joint reduced tensile stresses in the joint significantly. In addition to reducing tensile stresses, the post-tensioning steel provided a high-strength tensile tie across any potential diagonal joint crack. The computed specimen strength, using the analysis model described in Section 5.2, was 1.35 times the strength required to resist applied factored loads. Reinforcement details for the joint and complete specimen are illustrated in Figure 3.53 and Figure 3.54, respectively.

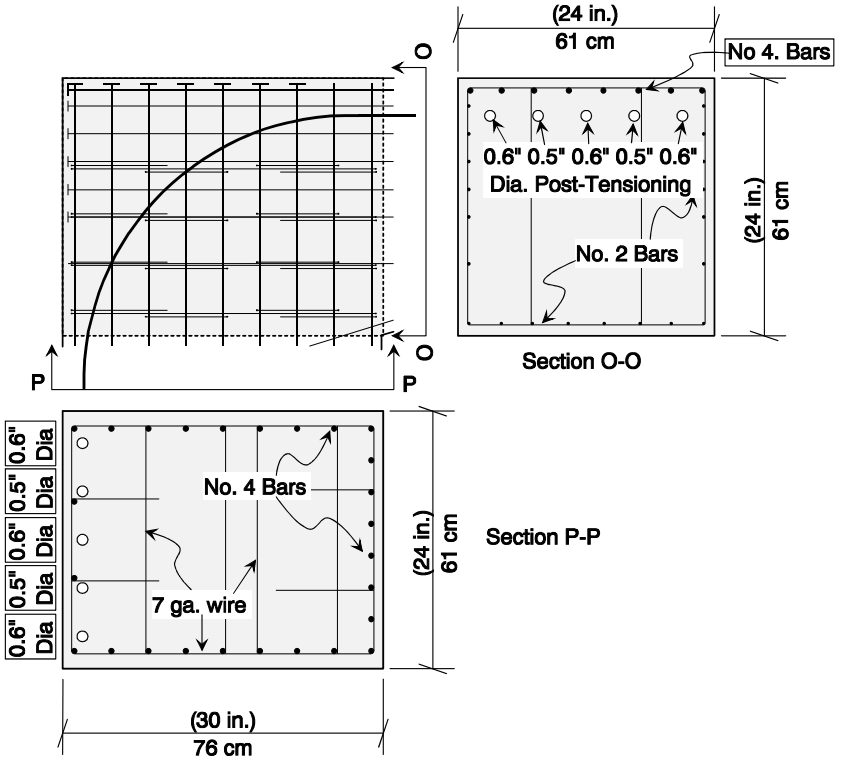

Figure 3.53 POJ-PU-74-TH joint reinforcement details

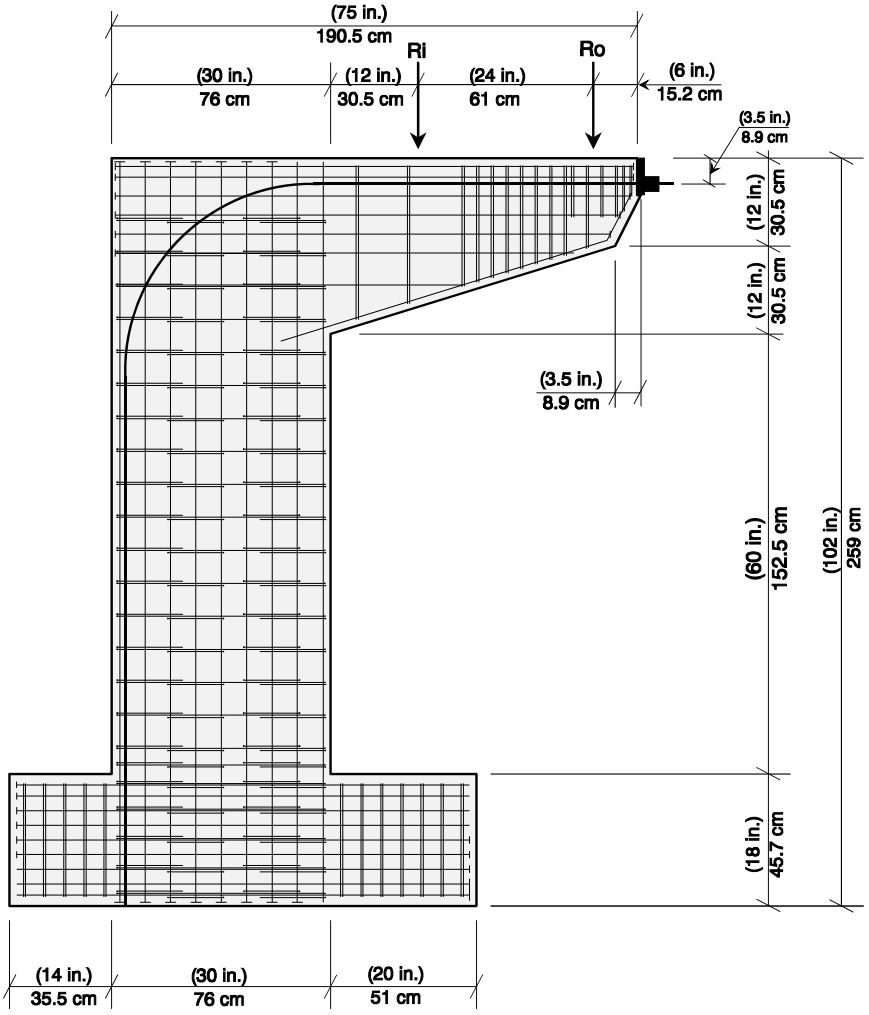

Figure 3.54 POJ-PU-74-TH overall reinforcement details

3.5 MATERIALS

3.5.1 Concrete

The concrete mix design used for the POJ specimens (shown in Table 3.6) was the same concrete design used in the overhang study conducted by Armstrong [3] and Salas [4]. The concrete mix design used a 1 cm (3/8 in.) aggregate to model 4.45 cm (1.75 in.) aggregate used in the full-scale prototype bents.

Table 3.6 Concrete mix design

Material	**Quantity**	
	SI per 1 m^3	**Customary per 1 yd^3**
Type I Cement	335 Kg	564 lb
Aggregate	867 Kg	1463 lb
Sand	968 Kg	1631 lb
Water	119 Kg	200 lb
Retarder	967 ml	25 oz.
HRWR*	1741 ml	45 oz.

*High-range water reducer (super-plasticizer)

Concrete compressive strength was anticipated to be 34.4 MPa (5000 psi) at 14 days, and a maximum of 44.8 MPa (6500 psi) at 28 days. The mix design included instructions for water to be added at the concrete batching plant if the initial slump (at the plant) was less than 13 cm (5 in.). Because the quantity of water added at the batching plant was not always measured (in violation of instructions), calculations for water-cement ratio are not presented.

The on-site slump was measured using the standard ASTM slump test procedure. If the initial slump was less than 10 cm (4 inches), water was added to increase the slump to 13 cm (5 in.). Once a slump of at least 13 cm (5 in.) was achieved, Rheobuild super-plasticizer was added to the concrete and mixed for five minutes. The resulting slump was typically between 18 and 20 cm (7 to 8 in.). Measured slumps and mix modifications completed at the laboratory are reported in Table 3.7.

Table 3.7 On-site measurements and mix modifications

Specimen	Initial Slump		Water Added		Slump		HRWR*		Final Slump	
	cm	(in.)	L	(gal)	cm	(in.)	L	(oz)	cm	(in)
POJ-RC-100	22	8.5	-	-	-	-	-	-	22	8.5
POJ-PS-100	11	4.5	-	-	-	-	1.9	64	19	7.5
POJ-RC-100-TH	5	2	38	10	9	3.5	3.8	128	22	8.5
POJ-PU-54-TH	11	4.5	-	-	-	-	3.8	128	23	9
POJ-PU-74-TH	11	4.5	-	-	-	-	3.8	128	22	8.5

*High-range water reducer (super-plasticizer)

During casting of each specimen, 24, 15.2 cm x 30.5 cm (6.0 in. x 12.0 in.) concrete cylinders were cast. These cylinders were used to measure concrete compressive strength at 1, 3, 7, 14, 21, and 28 days, at the start of testing, and when the specimen failed. Only two cylinders were tested on each specified day unless a significant deviation in strength was measured. If this occurred, a third cylinder was tested. Concrete compressive strength at time of testing, at 28 days, and at completion of the test are shown in Table 3.8.

Table 3.8 Concrete compressive strengths

Specimen	7 Day		@ Completion of Test			28 Day	
	MPa	(ksi)	Age	MPa	(ksi)	MPa	(ksi)
POJ-RC-100	28.3	4.11	23	31.7	4.60	31.7	4.60
POJ-PS-100	43.1	6.26	22	48.4	7.02	50.7	7.36
POJ-RC-100-TH	35.0	5.08	13	37.6	5.46	41.7	6.05
POJ-PU-54-TH	35.2	5.11	15	38.7	5.62	40.8	5.92
POJ-PU-74-TH	41.6	6.04	26	47.9	6.95	49.4	7.17

3.5.2 Mild Reinforcement

The mild reinforcing bars used included standard bars, deformed small-scale bars, and undeformed wire. The standard bars included: No. 3's, 4's, and 5's, and were used for primary longitudinal tension reinforcement in the pier and overhang. The No. 2 deformed small-scale bars were used for side-face reinforcement, overhang stirrups, and overhang compressive reinforcement. Undeformed 7 ga. wire was used for column ties and anchorage zone reinforcement. Material properties of the reinforcement are presented in Table 3.9.

Table 3.9 Mild reinforcement material properties

Mild Steel	Diameter		Area		Yield		Yield	Ultimate	
Size	cm	(in.)	cm^2	(in^2)	MPa	(ksi)	Strain	MPa	(ksi)
No. 5 Bar	1.58	0.625	2.0	0.31	413	59.9	0.00203	683	99.1
No. 4 Bar	1.27	0.500	1.3	0.20	416	60.3	0.00204	766	111.1
No. 3 Bar	0.95	0.375	0.71	0.11	427	62.0	0.00210	637	92.4
No. 2 Bar	0.63	0.247	0.31	0.048	512	74.2	0.00252	619	89.8
7 ga. wire	0.45	0.177	0.15	0.024	567	82.2	0.00279	596	86.4

Area of the anchor heads for headed bars was determined by using eight times the bar area. Plate sizes for the different bars are given in Table 3.10. Holes were drilled through the center of each plate, bar deformations on the tip of the reinforcing bar were ground-off, and the bar was pressed into the hole until the tip of the bar was nearly flush with the backside of the plate. A fillet weld on the front side of the plate and a button of weld material on the back side were used to attach the anchor plate to the bar (see Figure 3.55). When two T-heads were required on the same bar, the heads on the two ends were carefully aligned and welded so their orientations matched.

Table 3.10 Dimensions of T-head plates

Reinforcing Bar Size	T-Head Dimensions	
	SI cm x cm x cm	**Customary** (in.)x(in.)x(in.)
No. 2	2.5 x 2.5 x 1.3	1 x 1 x 0.5
No. 3	2.5 x 2.5 x 1.3	1 x 1 x 0.5
No. 4	3.8 x 2.5 x 1.3	1.5 x 1 x 0.5
No. 5	4.8 x 3.8 x 1.9	1.88 x 1.5 x 0.75

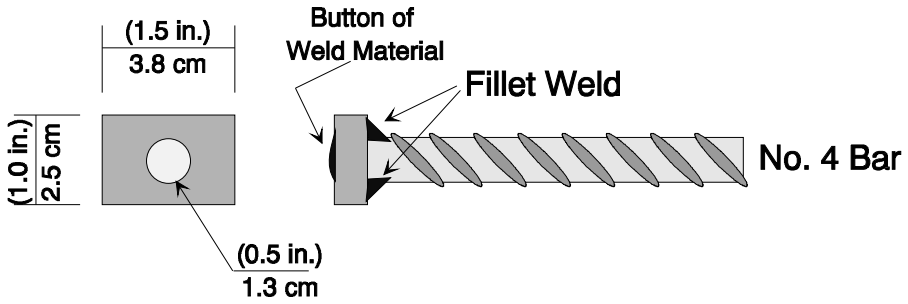

Figure 3.55 Anchor head dimensions and weld locations for a No. 4 bar

3.5.3 Post-Tensioning Steel, Duct, and Anchorage Hardware

Grade 270 Lo-Lax prestressing strands were used to prestress the integrated prestressed designs (POJ-PU-54-TH & POJ-PU-74-TH). Grade 150 Dywidag post-tensioning bars were used for the fully-prestressed specimen (POJ-PS-100).

The stress vs. strain behavior of the 13 mm (0.5 in.) and 15 mm (0.6 in.) diameter, Grade 270, seven wire strands are shown in Figure 3.56 and Figure 3.57, respectively. Anchorage hardware for the prestressing strand consisted of standard chucks and special adjustable chucks with threads for a 5.7 cm (2.25 in.) diameter nut on the live end. This made it possible to stress the strand and make fine adjustments to the final position of the anchor without having to re-seat the chucks on the strand each time an adjustment was made.

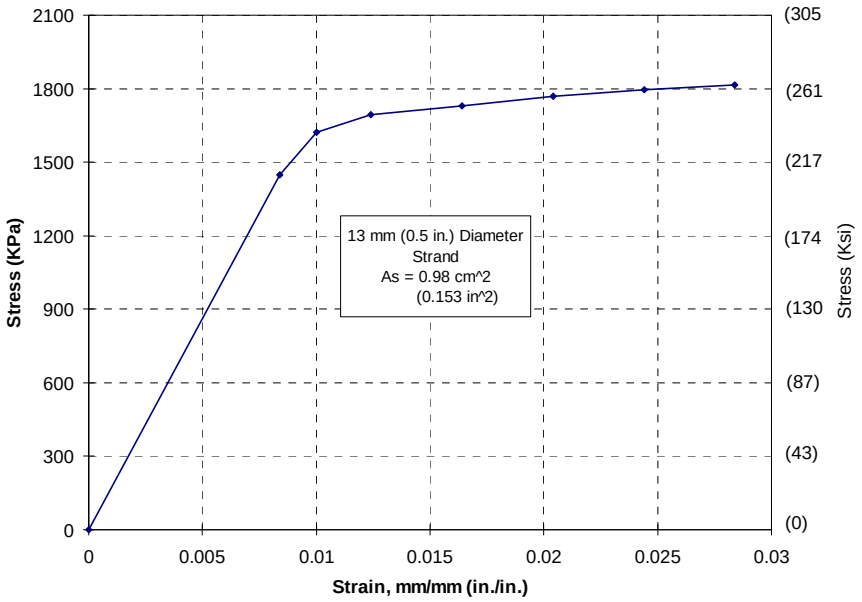

Figure 3.56 Stress-strain behavior of 13 mm (0.5-in.) diameter Grade 270 Lo-Lax strand

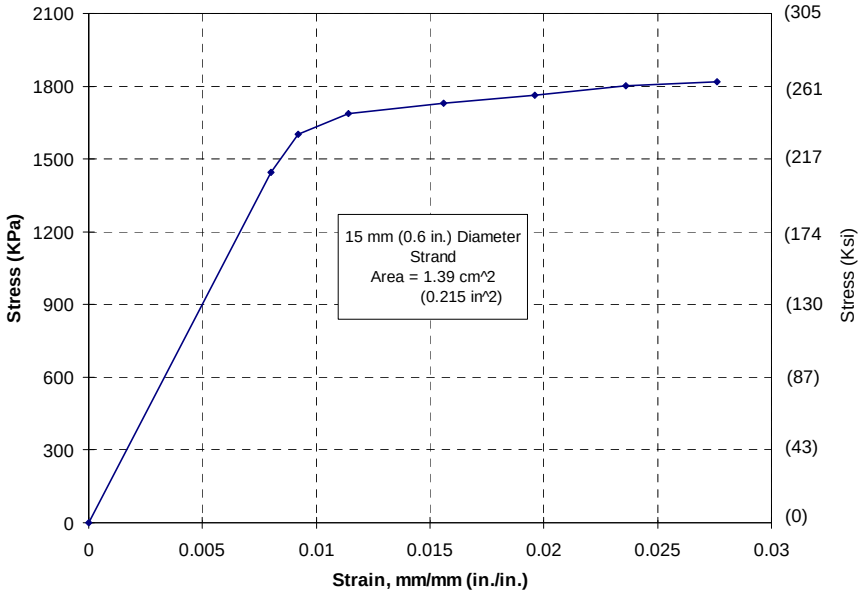

Figure 3.57 Stress-strain behavior of 15 mm (0.6-in.) diameter Grade 270 Lo-Lax strand

The stress-strain response for 16 mm (5/8 in.) diameter post-tensioning bars is shown in Figure 3.58. The Dywidag post-tensioning bar system uses a special threaded nut to anchor the bars. The nut allowed for adjustments during the stressing process, which meant that the post-tensioning force could be closely controlled.

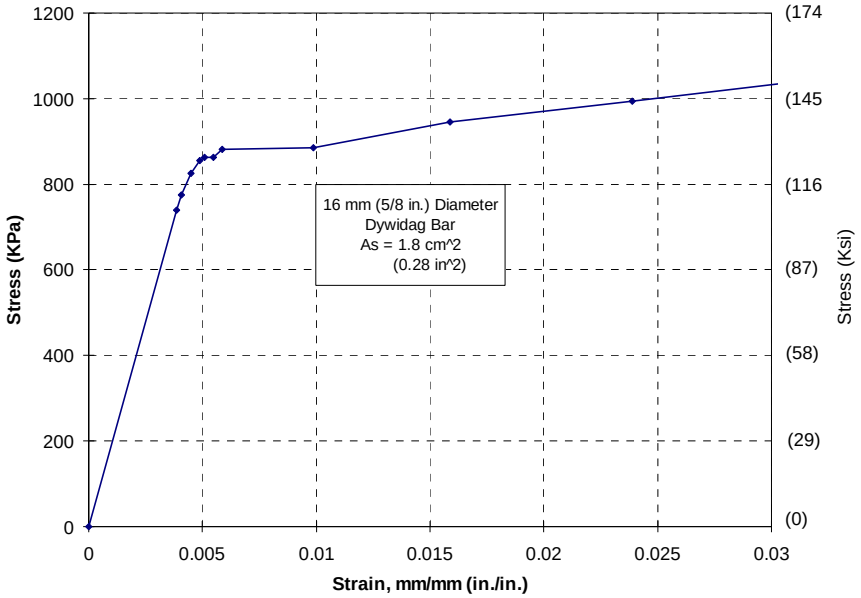

Figure 3.58 Stress-strain behavior of 16 mm (5/8-in.) diameter Grade 150 Dywidag post-tensioning bar

3.5.4 Grout

The grout mix design used throughout the project required Type I portland cement, water, and Interplast N. Interplast N is an expansive water-reducing agent that was added to offset grout shrinkage in the duct and provide a more fluid mixture that was easily injected into the ducts. Quantities used in the grout mix design, listed in Table 3.11, yielded 0.022 m^3 (0.8 $ft.^3$) of grout.

Table 3.11 Grout mix design

Material	Amount	
	kg	(lbs)
Cement	27.2	60.0
Water	13.2	29.2
Interplast N	0.27	0.6

Grout was pumped into the post-tensioning ducts through 13 mm diameter Dywidag grout ports that were cast into the specimen. After the grout was pumped, samples were placed in standard 5.1 x 5.1 x 5.1 cm (2x2x2 in.) cube forms. Grout cube strengths are presented in Table 3.12.

Table 3.12 Grout cube strengths

Specimen	1st Measurement			2nd Measurement			3rd Measurement			Age
	Age	MPa	(ksi)	Age	MPa	(ksi)	Age	MPa	(ksi)	CT*
POJ-PS-100	2	9.5	1.38	7	17.9	2.59	14	24.7	3.59	8
POJ-PU-54-TH	3	21.5	3.12	6	36.2	5.25				6
POJ-PU-74-TH	2	8.1	1.18	5	16.3	2.36	7	15.4	2.23	12

*Age of Grout (in Days) at Completion of Test

3.6 FABRICATION

Specimens were fabricated in the horizontal position. This simplified assembly of the reinforcement cage, facilitated placement of concrete, and assured that positioning of the bars would be as accurate as possible.

3.6.1 Reinforcing Cages

Components of the cages were carefully measured and bent to the dimensions specified in the designs. The 7 ga. wire column ties and anchorage reinforcement were bent on a template to assure uniformity. Stirrups were bent using a bar bending machine. Final assembly of the cage went quickly once all reinforcing bars were cut to size and stirrups and ties were bent. The T-headed bars were fabricated by drilling a hole in the steel anchor plate, welding around the bar with a 6 mm (1/4 in.) fillet weld, then filling in the annulus between the bar and plate with a "button" of weld material. Size of the anchor plates was given in Section 3.5.2.

Every effort was made to keep locations of bars in each model as close as possible to the design locations. A combination of metal wire ties and plastic ties were used to keep bars fixed firmly in position.

For prestressed specimens, the 2.5 cm (1 in.) diameter galvanized electrical conduit (used as post-tensioning duct) was placed in the cage after the majority of overhang and pier reinforcement was tied in place. Strands were instrumented with 2 mm electrical strain gages, water-proofed, and carefully threaded into the galvanized duct. Once the strand was in the duct, the duct was positioned inside the cage. In the joint region, the inner radius of the duct was tied in place so that the strand, when pulled tight against the duct during stressing, would be in the specified location. The ducts were held in place by short pieces of No. 2 reinforcing bar tied to the reinforcing cage at closely-spaced intervals.

Once a cage was assembled, the forms were oiled with form-release compound, and eight to ten 1.9 cm (0.75 in.) diameter PVC spacers were placed on the bottom of the form to support the weight of the cage and provide the specified clear cover.

Prestressed specimens had holes drilled in the forms to allow prestressing strands to pass though the formwork. Special plywood components were constructed to provide the stressing shelf and anchorage plate lip. Silicon caulk was placed around the holes in the formwork and galvanized conduit to prevent water and paste seepage.

3.6.2 Placement and Consolidation of Concrete

Concrete was designed with a high slump to ensure good consolidation and workability. After the desired slump was achieved, a large hopper, lifted by the overhead crane, was used to transport concrete to the forms. Each specimen was cast in three layers and consolidated using two hand-held pencil vibrators and two formwork vibrators. Concrete cylinders were filled in three layers and each layer was tamped 25 times with a smooth steel rod. Excess concrete was removed by rolling the steel rod over the top of the cylinder.

Once water bleeding stopped, tops of cylinders were finished and covered with a thin plastic sheet. The specimens often took four to five hours to reach an initial set. At this time the surface of the concrete was finished with a trowel. Several short wood poles were nailed to the formwork and used to "tent" the plastic sheet covering the specimen. Three hours after initial set, water was pooled on the specimen. The top surface was wetted several times a day until concrete temperature decreased.

3.6.3 Curing and Form Removal

After three days of wetting the top surface of the specimen and checking the surface temperature, the forms were removed and the specimen was prepared for installation in the testing frame.

3.7 TEST SET-UP

The test set-up consisted of two frames, a stiff load beam with two 890 kN (200 kip) capacity hydraulic rams, and two restraining beams for fixing the base of the specimen.

3.7.1 Loading Frame and Rams

The loading frame with a test specimen in place is shown in Figure 3.59. Columns for each frame were spaced 2.4 m (8 ft.) apart, and the frames were spaced 1.2 m (4 ft.) apart. Distances were dictated by the 1.2 m x 1.2 m (4 ft. x 4 ft.) spacing of the testing floor anchor locations. Four 2.5 cm (1.0 in.) diameter high-strength threaded rods were used to secure each W12 x 65 steel column to the testing floor. The base of each column was not tensioned to the floor to allow some lateral motion to occur, thus reducing any restraining forces caused by deflection of the member. The 3.9 m (13 ft.) long W30 x 108 steel cross beams were bolted to each column with twelve 2.4 cm (1.0 in.) diameter ASTM 325 bolts. The W12 X 145 longitudinal load beam with the attached rams was fastened into place with steel clamps.

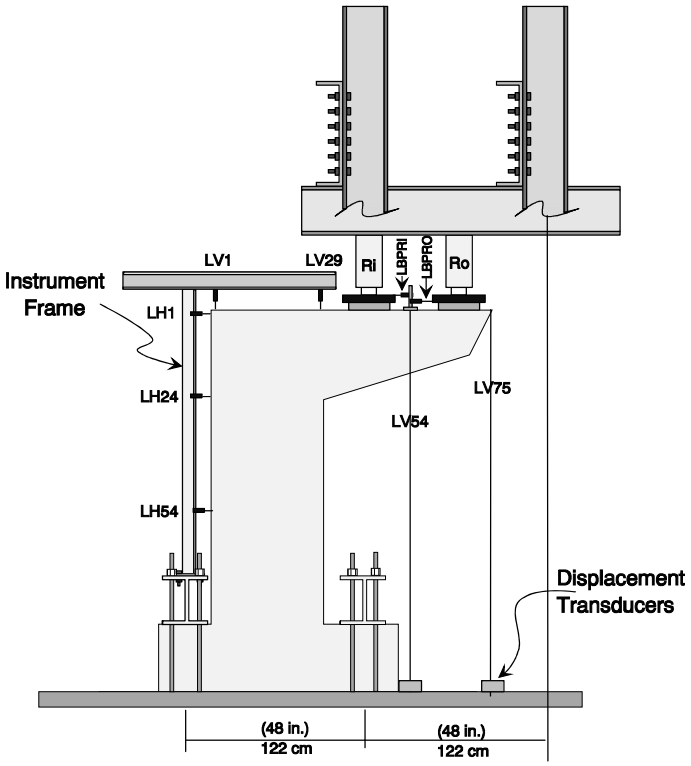

Figure 3.59 Test setup and location of displacement transducers

Each of the rams on the longitudinal load beam was held in position by four 2.5 cm (1 in.) diameter threaded rods that were threaded into nuts welded to the bottom flange of the beam. The outside of the ram casing was held tight against the bottom flange of the beam by tightening nuts against the outer-face of a 10 mm (3/8 in.) thick steel plate with a 10 cm (4 in.) hole located in the center (for the ram piston).Both the inside ram and the outside ram had a capacity of 890 kN (200 kips) with an effective ram area of 137 cm^2 (21.3 in^2).

3.7.2 Anchorage of Test Specimen to Floor

Each test specimen was anchored to the floor with a 3.96 m (13 ft.) long W12 x 145 steel beam on the back side of the specimen and a 2.28 m (9 ft.) long W12 x 145 steel beam on the front side of the specimen. The beams had a nominal yield stress of 344 MPa (50 ksi). The longer beam on the back

side of the specimen was tied down using 12–2.5 cm (1.0 in.) diameter high-strength threaded rods. This side of the specimen was clamped to the test floor with a total of 1495 kN (336 kips). The shorter tie-down beam was tied to the floor by wrench-tightening the anchor bolts. The high-strength rods were threaded into floor anchors that were embedded approximately 120 cm (4 ft.) inside the reaction floor. Placement of the beams is shown in Figure 3.59 and Figure 3.60.

3.7.3 Instrumentation and Data Collection

3.7.3.1 Data Acquisition System

The data acquisition system was a 140-channel Hewlett Packard 3497A scanner controlled by an IBM-compatible Hewlett Packard XT personal computer. Software to control the scanner and record the data was a Ferguson Laboratory computer program (HPDAS2). The system allowed different types of gages to be identified and read by the scanner. Pressure transducers, linear potentiometers, and displacement transducers were connected using a full-bridge circuit having a 10-volt excitation that was, in turn, connected to the scanner to measure output voltage. Strain gages were connected to quarter-bridge circuits having a 2 volt excitation.

3.7.3.2 Pressure Transducers

The two pressure transducers used for measuring applied ram loads had a 10 V/mV accuracy with a maximum range of 69 MPa (10,000 psi).

3.7.3.3 Linear Potentiometers and Displacement Transducers

The position and designations for the displacement-measuring devices are shown in Figure 3.59. The first test (POJ-RC-100) used a combination of 15 cm (6.0 in.) and 5 cm (2 in.) linear potentiometers to measure pier and joint deformations, and a combination of 13 cm (5 in.) and 38 cm (15 in.) displacement transducers to measure overhang displacements. Because the long wires for the LV1 and LV29 displacement transducers were disturbed during crack readings, only 5 cm (2 in.) linear potentiometers with an accuracy of 0.03 mm (±0.001 in.) were used to measure pier and joint displacements for subsequent tests. In addition, overhang displacements were measured using 13 cm (5 in.) displacement transducers with an accuracy of 0.03 mm (±0.001 in.).

3.7.3.4 Strain Gages

Two sizes of electrical-resistance strain gages were used to measure steel strains in specimens. Five-mm-wide strain gages with pre-soldered two wire, 5 m leads were used to measure strains in the No. 5, No. 4, and No. 3 bars and 5/8″ dia. Dywidag bars. Two mm-wide strain gages with pre-soldered two wire, 5 m leads were used to measure strains in the No. 2 bars and prestressing strand.

3.8 TESTING PROCEDURE

3.8.1 Installation of Specimen

Each specimen had four lifting inserts cast into the top of the specimen and one lifting insert in the side of the pier. The four top lifting inserts were positioned to enable lifting through the center of gravity of the specimen. To install the specimen, the model was lifted off the form using the top lifting hooks and the 178 kN (20 ton) overhead crane. Before the specimen was lifted off the floor, the centerline of the pier was marked on the top, bottom, and mid-thickness of the base member at the front and back end of the member. Because the prestressing chucks at the base of the POJ-PU-54-TH and POJ-PU-74-TH specimens were not accessible once the specimens were placed in the test setup, strain-gage leads exiting from the base of each specimen had to be protected, and a minimal stress had to be applied to the post-tensioning strands to seat the post-tensioning anchorages. For the POJ-PU-74-TH and POJ-PU-54-TH specimens, grooves were ground into the anchorage plates to provide a

path for the strand strain gage wires to pass. Ends of the ducts were sealed with silicon caulk, and anchorage plates were also sealed to the specimen to prevent grout seepage. Once the ducts were sealed, strands were stressed to 0.05 f_{pu} to seat the post-tensioning chucks.

Once the specimen was fully prepared, lifting cleavises were attached to the lifting inserts, and the specimen was transported from the casting site to the testing area. The east loading frame cross beam (see Figure 3.60) was removed for the installation procedure. The specimen was centered over the testing area and hydrostone was pooled into a form slightly larger than the base of the specimen. Ten cm (4 in.) thick steel plates with small gaps to accommodate the post-tensioning chucks were placed under the specimen. The steel plates were not necessary for the POJ-RC-100 and POJ-RC-100-TH specimens.

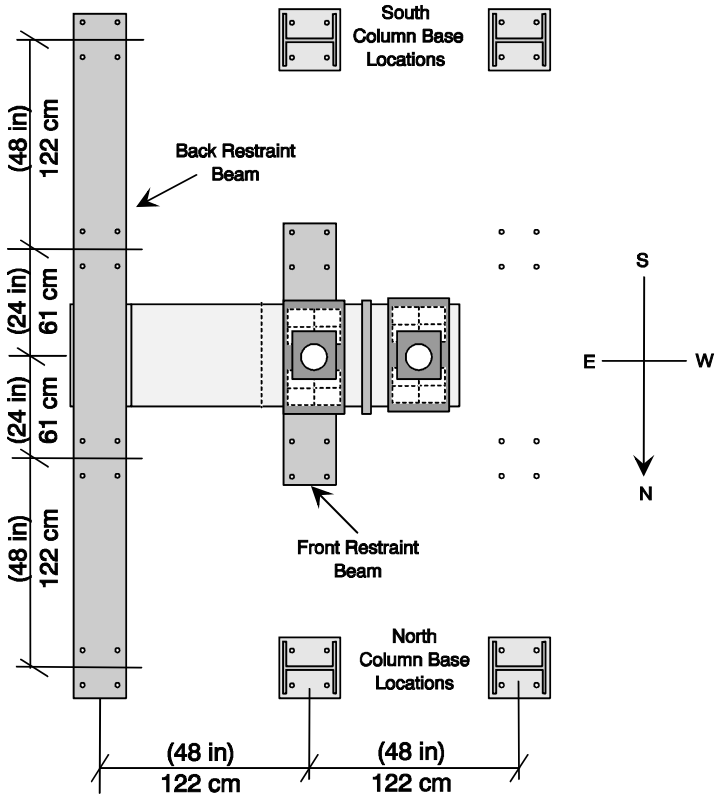

Figure 3.60 Top view of test setup

The specimen was then guided into position by four people as it was lowered into the hydrostone. Marks on the floor and specimen centerlines on the N, S, E, and W sides were used to position the specimen relative to the testing frame. Minor adjustments to ram locations were often made to correct for small misalignments.

Once the hydrostone hardened, the restraint beams were installed. First, a ring of silicon was placed on top of the east end of the base member of the specimen, and hydrostone was pooled in the ring. The east restraint beam was lowered slowly into position using the crane, then was leveled using the threaded floor anchor rods. The west beam used the same procedure except it was lowered into position using an electric forklift. The west beam was not stressed; the four anchor rods were hand-tightened using a wrench. After a day, the east restraint beam was stressed against the specimen. Twelve floor anchor rods were each stressed to 125 kN (28 kips) to provide the required resistance.

After the specimen was anchored to the floor, the load bearings, which consisted of four 28cmx20cm (11 in. x 8 in.) steel laminated elastomeric bearings, were positioned on the specimen. Two bearings were located at 30.5 cm (12 in.) from the face of the pier for the interior load, Ri, and two bearings were located at 91.5 cm (36 in.) from the face of the pier for the outside load, Ro. A stiffened steel plate was centered on top of the bearings to transfer ram forces equally to the two bearing pads. Torsional loads were not applied to the specimen.

Load plates on top of the specimen were used to center the load beam and rams over the specimen. The beam was lowered into position using the crane and adjusted using hammers until the rams and load beam were positioned directly over the two load plates. Once the position was correct, the load beam and ram assembly was clamped to the loading frame with four heavy steel clamps.

Linear potentiometers for the pier and east face of the joint were attached to a vertical steel section that was bolted to the prestressed restraint beam. Linear potentiometers for the top of the joint were attached to a horizontal channel section connected to the vertical steel section and a steel structural column in the laboratory (column not depicted in Figure 3.59). Displacement transducers were attached to the floor and connected by a piano wire to the specimen. Two displacement transducers were used to measured overhang deformations at the two locations shown in Figure 3.59. At each location, one transducer was located on the north side and the south side. The POJ-RC-100 test specimen utilized steel-wire displacement transducers to measure all vertical displacements. This approach was discontinued for subsequent specimens because the piano wires in the joint region were disturbed many times while measuring crack widths.

Pressure transducers were connected to the hydraulic lines of two independent pumps. One pump was used to control the inside load (Ri) and another controlled the outside load (Ro). Multimeters were connected to the pressure transducers so the individual applying load to the specimen could accurately control the load steps. An X-Y plotter was used to monitor the tip deflection and outside ram pressure transducer (and thus, Ro). The X-Y plot was used to monitor the load and tip deflection, and control displacement steps after ultimate load was reached.

3.8.2 Post-Tensioning Operation

Post-tensioning was carried out on Specimens POJ-PS-100, POJ-PU-54, and POJ-PU-74. The procedure involved the use of a 267 kN (60 kip) ram, a 69.0 MPa (10,000 psi) pressure transducer, and a 5 cm (2 in.) linear potentiometer. Once the specimen was in place, the design stressing sequence was used to safely stress the specimen. The stressing sequence was different for each specimen, but the main objective was to stress all tendons to 0.6 f_{pu} [1.10 GPa (160 ksi)] while keeping maximum flexural tension stresses below $3\sqrt{f'_c}$ [1.46 MPa (212 psi)]. Flexural tensile stresses were computed using the following equation:

$$-\frac{P_{tx}}{A}-\frac{P_{tx}\,e\,y}{I_g}+\frac{M_{(applied)x}\,y}{I_g}\ \le 3\sqrt{f'_c} \qquad [3\text{- }39]$$

where:

P_{tx} = Total applied post-tensioning force at stage of stressing

A = Area of concrete = $b_w\ h$

e = Eccentricity of post-tensioning strand above beam centroid

y = Distance to extreme tensile fiber from beam centroid

I_g = Gross moment of inertia = 1/12 (b_w)(h)^3

$M_{(applied)x}$ = Applied overhang moment at stage of stressing.

Both the top and bottom-fiber tensile stresses were evaluated along the length of the member at all stages of post-tensioning.

All post-tensioning strands were "overstressed" to 0.9 f_y to overcome friction losses in each tendon. The prestressing operation was carried out at the overhang tip because the chuck on the bottom of the specimen was not accessible, and it would not be possible to stress tendons in the pier region of a full-scale bent to 0.6 f_{pu} because of losses that would occur in the curved portion of the tendon. As stated earlier, the computed post-tensioning losses in the pier region were considered in design of the pier.

Once tendons were initially stressed, a lift-off test was conducted to verify tendon tension. A lift-off test is conducted by monitoring movement of an anchorage device while pulling against the tendon (strand). Lift-off (a sudden increase in movement) of the tendon anchor occurs when load in the ram used to perform the lift-off test reaches a load exceeding the initial tendon force. The sudden increase in deformation at lift off occurs because the length of tendon that elongates changes suddenly from the length inside the ram and anchor device to the free (unbonded) length of the tendon.

Lift-off tests performed on tendons in Specimens POJ-PU-54-TH and POJ-PU-74-TH did not yield definitive information about tendon forces. Because a portion of the post-tensioning ducts was curved, tendons were in contact with the curved portion of the ducts as well as some portion of the straight duct leading into the curved portion. After lift off, the free length of tendon changed incrementally as contact friction along the tendon was gradually overcome. Gradual elongation of tendons instead of a sudden increase in elongation made it difficult to discern the lift-off force for each tendon. Because accuracy of the lift-off procedure was in question, a simpler procedure for determining lift-off was developed.

The adjustable chucks used for anchoring the post-tensioned strands had a large nut that was used to make fine adjustments in the chuck position without having to re-seat the chuck. After the initial lift-off test was performed, each tendon was slowly stressed again and the adjusting nut was tapped with a hammer while the ram load was monitored. When the nut turned, the lift-off load was determined. If the tendon force was too low, the strand was fully stressed to 0.6 f_{pu}, the nut was tightened, and the ram load was released. The strand was then stressed again, and the nut was again tapped to determine the lift-off load.

Once the tendons were stressed, holes in the anchorage plates were filled with silicon caulk. After the caulk set, cement, water, and Interplast N were weighed, divided in half, and placed in separate five gallon buckets. Grout was mixed using a hand-held electric drill and mixing bit. The mixer was

started in the bucket containing water, then cement was slowly added. After cement and water were mixed, Interplast N was added. Consistency of the mixture was noticeably more fluid with Interplast N. The bucket of grout was poured into the electric grout pump, and the grout hose was attached to the bottom grout port. The grout pump was switched on and off in spurts to keep the grout pressure below 0.28 MPa (40 psi) to avoid rupture or separation of the hose connections.

During the grouting procedure, flow of grout from the port in the tip of the overhang was monitored. The pump was switched off and grout ports closed when grout flowing from the port in the tip of the overhang was free of air bubbles. The procedure was repeated until all ducts were grouted. The grouting procedure had to be completed quickly, and small quantities were mixed because the grout was noticeably less fluid after only 10 minutes.

Three grout cubes were made from each grout mix. Cube compressive strengths were tested four days and six days after grouting the specimen, and on the day testing was completed. Once the grout reached a compressive strength of 10.3 MPa (1500 psi), each specimen was tested.

3.8.3 Static Load Steps

The testing procedure was similar to the procedure used in the overhang study by Armstrong [3] and Salas [4]. Major events in the loading history and number of load steps corresponding with each event are listed in Table 3.13.

Table 3.13 Events in load history, corresponding load steps, and applied loads

Load Step	Load Event	Load Abbreviation	Ri		Ro	
			kN	(kips)	kN	(kips)
20	Dead Load	DL	293	65.9	293	65.9
27	Dead Load + 1/2 Live Load	(DL + 1/2 LL)	318	71.4	344	77.4
34	Service Load	(DL+LL)	343	77.0	399	89.6
35	Dead Load	(DL)	318	65.9	293	65.9
49	Service Load	(DL+LL)	343	77.0	344	89.6
60	Dead Load + 2 Live Loads	(DL+2LL)	409	92.0	496	111.4
73	Factored Load	(1.3DL + 2.17LL)	488	109.7	610	137.2
80	Factored Load / Φ	(1.3DL + 2.17LL)/Φ	543	122.1	679	152.7
100	Maximum Applied Load	1.44 x Factored Load	701	157.7	877	197.1

The load steps started with 0 (no load), and equal-size steps were applied between each load event. After every two load steps, the specimen was examined for new cracks. During initial load steps, once a crack was observed in the pier, overhang, or joint, it was marked on the specimen, the width was measured using a 0.013 mm (±0.0005 in.) optical crack-width comparitor, and photographs were taken. Crack widths were measured at the outer fibers and at grid locations shown in Figure 3.61. Loads and crack widths corresponding with first cracking were recorded for the pier, overhang, and joint sections. Once first cracking occurred in a region, cracks were examined every two load steps to identify new cracks or crack extensions. Cracks were marked with a magic-marker on the surface of the specimen, numbered according to the load step, and recorded on a map of the north and south side of the specimen.

Photographs were taken and all visible cracks in the overhang, joint, and pier were numbered and measured separately at the major load events listed in Table 3.13. Crack widths were not measured after load step 60 (DL+2LL) was reached, but cracks were still identified and marked on the specimen.

Loads steps were continued beyond Factored Load / Φ in the same increments applied between load steps 73 to 80. Reinforcement strains, deflections, and pressure transducer readings were scanned by

the data acquisition system at every load step. After ultimate load was reached, the X-Y plotter was used to monitor displacement increments in the post-ultimate range. Cracks were no longer marked on the specimen because of safety concerns.

All specimens were loaded as far as possible into the post-ultimate range without damaging the test setup or rams. Once a test was concluded, any new cracks that formed were marked and photographs were taken to record the final state of the specimen.

3.8.4 Crack Identification and Marking Procedure

A crack identification and marking procedure was developed to keep a record of cracks as they formed. All marked cracks have a unique identification number that was used to identify respective crack widths. Figure 3.61 illustrates the rules used to identify each crack.

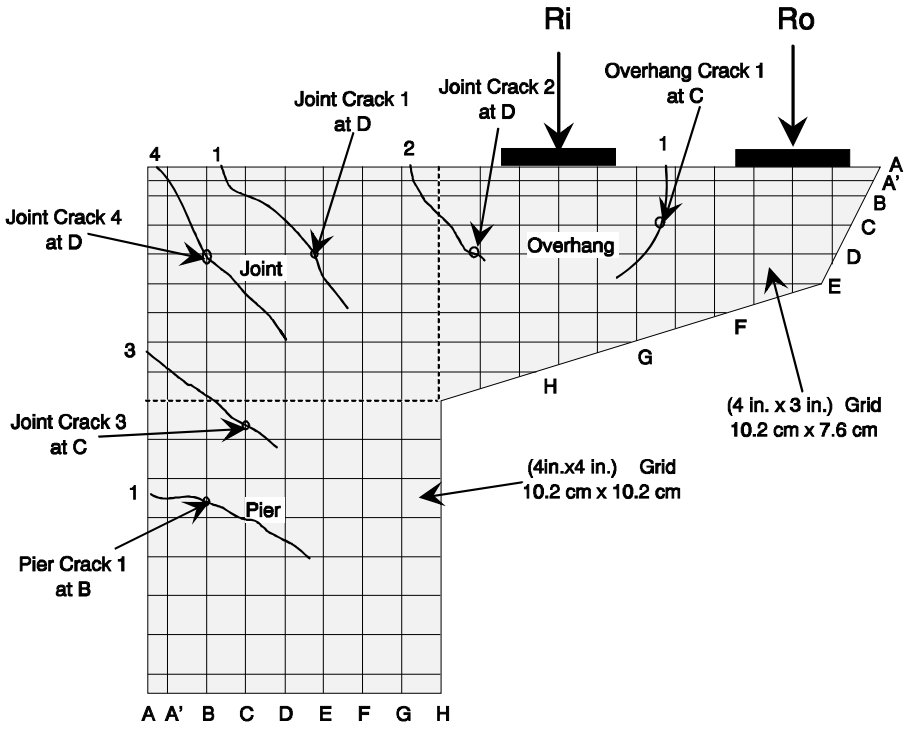

Figure 3.61 Crack identification procedure

As stated in the previous section, cracks were measured at specific load steps. The object of this was to keep the test progressing because, on average, it required two hours to measure all the crack widths. Cracks were associated with different specimen regions to facilitate evaluation of the cracking performance. Each crack was always associated with the region in which it initiated, regardless of where it propagated later in the test.

All crack identifications incorporated a load step number, but the letter portion of the crack width depended on the orientation of the crack. If the crack initiated on the horizontal top face of the overhang or joint, the horizontal grid lines and corresponding letter labels applied. If the crack initiated on the outside face of the pier or joint, the vertical grid lines and corresponding letter labels applied. This convention was used regardless of the final orientation of the crack. Cracking patterns and crack widths for all the specimens are presented in Chapter 4 and Section 5.2.

CHAPTER 4

PRESENTATION OF TEST RESULTS

4.1 INTRODUCTION

Presentation and discussion of experimental results is divided into two separate sections. Response of models of "prototype" specimens (POJ-RC-100 & POJ-PS-100) is presented first, followed by response of the integrated design models (POJ-RC-100-TH, POJ-PU-54-TH, and POJ-PU-74-TH).

Specimen responses that are presented include crack-width measurements, moment versus displacement response, and moment versus strain readings. Crack-width measurements at dead load (DL), service load (DL+LL), and DL+2LL are discussed, and overall cracking patterns are presented. Crack widths were measured in units of inches using an optical device with an internal gage that has an accuracy of ±0.013 mm (±0.0005 in.). The maximum crack-width readings were measured at grid lines scribed on each specimen, as shown in Figure 3.61, at vertical and horizontal spacings of (4 in. x 4 in.) 10.2 cm x 10.2 cm for the pier, and (4 in. x 3 in.) 10.2 cm x 7.6 cm for the overhang and joint regions. Maximum crack width for each crack was recorded in a table, and the grid location of the maximum crack width was listed next to the measurement. The scaled limiting crack width at service loads was 0.14 mm (0.0055 in.), which corresponded to a Z factor of 170 [1] divided by the scale factor of 2.75. Cracks on the north and south faces of each specimen were identified in the overhang, joint, and pier regions. Dashed lines on crack-width drawings indicate boundaries of the different regions. Cracks that originated in one zone and later extended into a different zone were identified/associated with the region in which they originated. Overall cracking patterns at dead load and service load illustrate the appearance of specimens at operational loads. Cracks and local concrete crushing associated with the failure mechanism at ultimate load are highlighted on crack drawings with heavier lines.

Vertical displacement response at the overhang (cantilever) tip, at mid-span of the overhang, at the top surface of the joint, and horizontal displacement response of the pier at three elevations, and bearing pad shear displacements are plotted as a function of the applied moment (at the column face). Moment vs. displacement plots provide insight into specimen behavior at service loads and ductility at failure.

Strain measurements were used to identify yielding of mild reinforcement at factored loads, and to determine peak strains in tension reinforcement around the joint region. Strain data at service and factored loads from primary flexural reinforcement in the overhang and pier provided information about the level of forces in mild reinforcement and the effectiveness of the partially-prestressed designs. Strain data from transverse reinforcement were used to assess the adequacy of shear reinforcement. The intended load history for test specimens is presented in Table 4.1.

Table 4.1 Intended load history for pier-overhang-joint specimens

Load Step	Load Description	Load Abbreviation	Ri		Ro	
			Kn	(kips)	Kn	(kips)
20	Dead Load	DL	293	65.9	293	65.9
27	Dead Load+½ Live Load	(DL+½LL)	318	71.4	344	77.4
34	Service Load	(DL+LL)	343	77.0	399	89.6
35	Dead Load	(DL)	293	65.9	293	65.9
49	Service Load	(DL+LL)	343	77.0	399	89.6
60	Dead Load+2 Live Loads	(DL+2LL)	409	92.0	496	111.4
73	Factored Load	(1.3DL+2.17LL)	488	109.7	610	137.2
80	Factored Load / Φ	(1.3DL+2.17LL)/Φ	543	122.1	679	152.7
100	Maximum Applied Load	1.44 x Factored Load	701	157.7	877	197.1

Loads listed in Table 4.1 were applied incrementally. The number of equal load-step increments used to load (or unload) from one level in Table 4.1 to another can be inferred from the left-hand column. Plots of moment vs. displacement were non-dimensionalized by dividing the applied overhang moment at the face of the column by the moment at the face of the column produced by applying design factored flexure loads. Dimensionless units on the vertical axis provided a quicker understanding of the ultimate load state relative to factored loads.

4.2 PROTOTYPE MODEL TEST SPECIMENS

The prototype test specimens, POJ-RC-100 and POJ-PS-100, were 2.75 scale models of cantilever substructure elements used in the San Antonio 'Y' project. The same design and detailing procedures used by designers of the San Antonio 'Y' substructures were used for these specimens. A research study conducted by Armstrong [3] and Salas [4] concluded that the overhang portion of the substructure was significantly stronger than the required strengths associated with factored load design. Over-strength was attributed to the inclusion of all reinforcement requirements specified in the AASHTO Bridge Standard Specification [1] associated with deep beam, corbel, and if applicable, prestressed concrete design. The overhang study recommended the use of a strut and tie/strength-based design for reinforced and prestressed concrete. The study also recommended the elimination of shear-friction reinforcement, and a reduction of stirrups for shear reinforcement.

4.2.1 Reinforced Concrete Prototype Specimen–POJ-RC-100

Specimen POJ-RC-100 was installed in the testing frame and tested over a four day period. Initial cracking occurred at a load level less than DL/2 (between load steps 7 and 8). During loading from DL to DL+½LL, a large number of cracks were identified in the joint region. The critical diagonal crack had not developed at this point. A complete diagonal crack in the joint region formed at DL+LL (service load). Crack widths were measured at this point. Loads were sustained throughout the crack-width measurement process. Next, applied load was reduced to DL and crack widths were again measured at DL, DL+½LL, and DL+LL (service load). A photograph of cracks on the north face of Specimen POJ-RC-100 is presented in Figure 4.1.

Figure 4.1 Photograph of north face of Specimen POJ-RC-100 at service load

After crack widths were measured, applied loads were increased toward DL+2LL. It was apparent that the critical diagonal crack in the joint was growing rapidly from load step to load step. Maximum load resisted by the specimen was DL+1.62LL, which was equal to an overhang moment of 538.6 kN-m (4767 k-in.). After reaching ultimate load, the tip of the cantilever was subjected to incremental displacements. Electronic gages were scanned and recorded immediately after each desired displacement was reached and again several minutes later when the load stabilized. Loads measured at these instances were referred to as dynamic and static loads, respectively.

Loads dropped off immediately after the capacity was attained, but deteriorated relatively slowly to 0.6 times factored loads at a tip displacement of 40 mm (1.57 in.). Testing was discontinued at this point and load was removed from the specimen. A large residual displacement and a large diagonal crack in the joint [approximately 13 mm (0.5 in.)] were visible after load was removed. A photograph of the north face of the specimen is presented in Figure 4.2, and a close-up of the joint failure is presented in Figure 4.3.

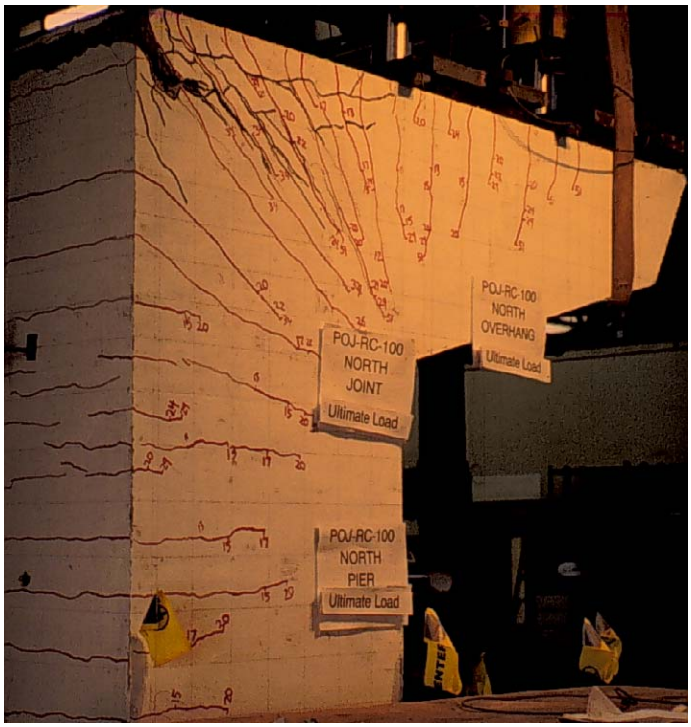

Figure 4.2 Photograph of north face of Specimen POJ-RC-100 at failure

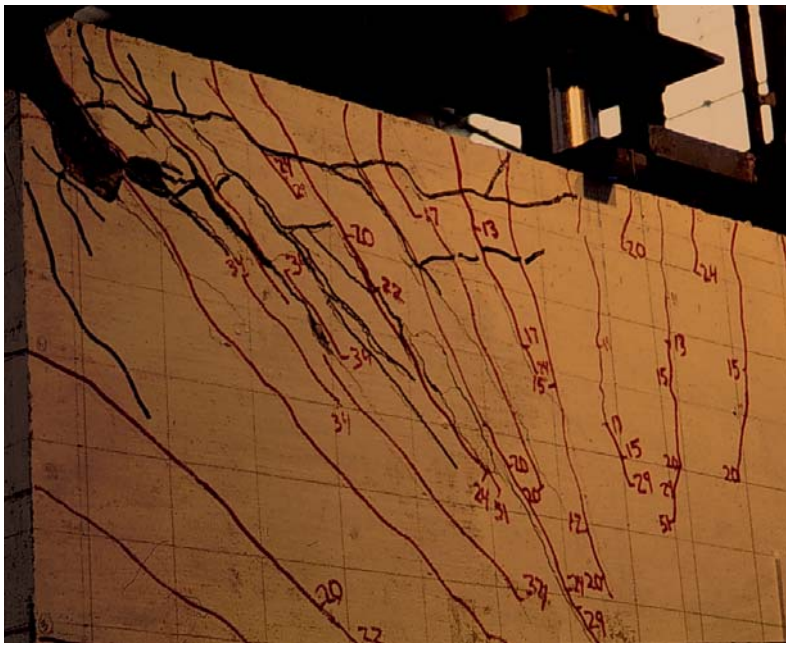

Figure 4.3 Photograph of joint region on north face of Specimen POJ-RC-100 at failure

4.2.1.1 Cracking Patterns and Maximum Crack Width Measurements–POJ-RC-100

Cracking patterns for Specimen POJ-RC-100 were quite important because they were used to evaluate the level of distress in the San Antonio 'Y' substructures.

The overall cracking patterns at dead load for the north and south sides of Specimen POJ-RC-100 are shown in Figure 4.4 and Figure 4.5, respectively. The cracking patterns on the north and south sides of the specimen at service level loads (Figure 4.6 and Figure 4.7, respectively) show the development of the diagonal crack and the fan-shape nature of the cracks from the compression node to the tensile fibers. Critical diagonal cracks in the joint associated with failure of the specimen are identified with heavy lines in Figure 4.8 and Figure 4.9 (joint crack 10 in Figure 4.8 and joint crack 8 in Figure 4.9).

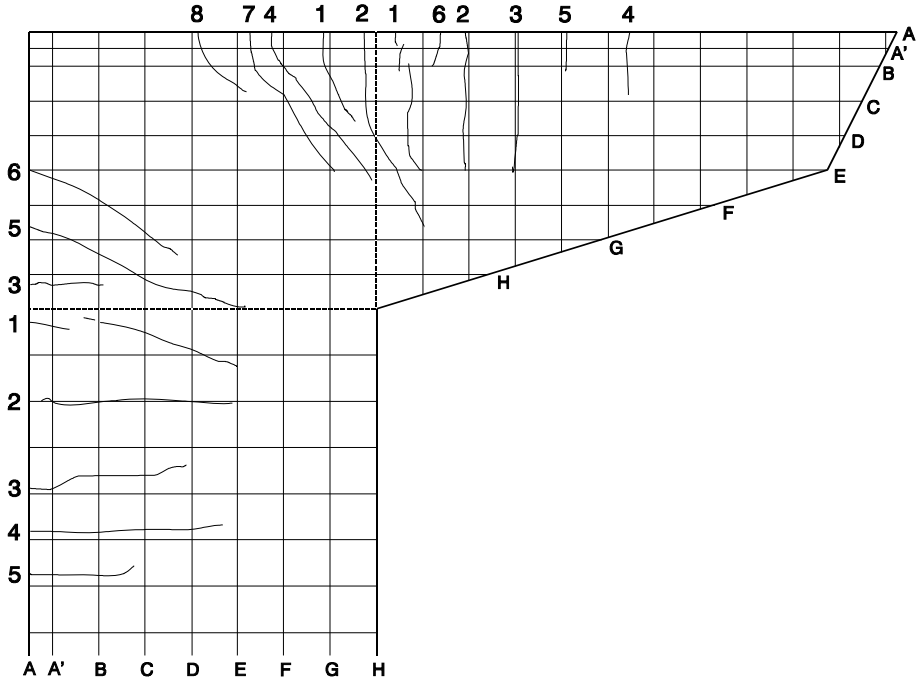

Figure 4.4 POJ-RC-100 cracking pattern on north face of specimen at dead load

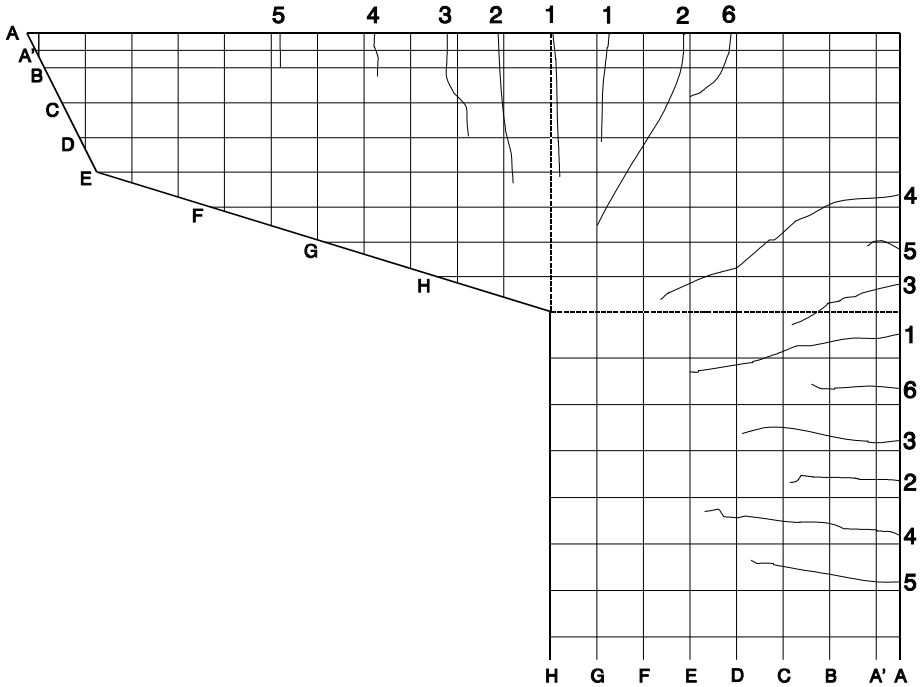

Figure 4.5 POJ-RC-100 cracking pattern on south face of specimen at dead load

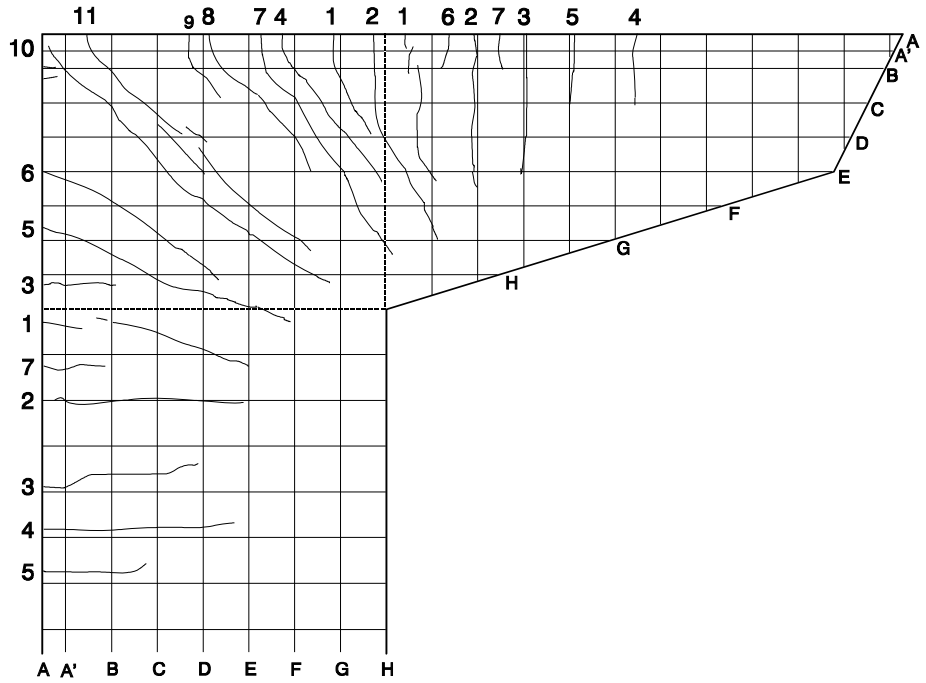

Figure 4.6 POJ-RC-100 cracking pattern on north face of specimen at service load

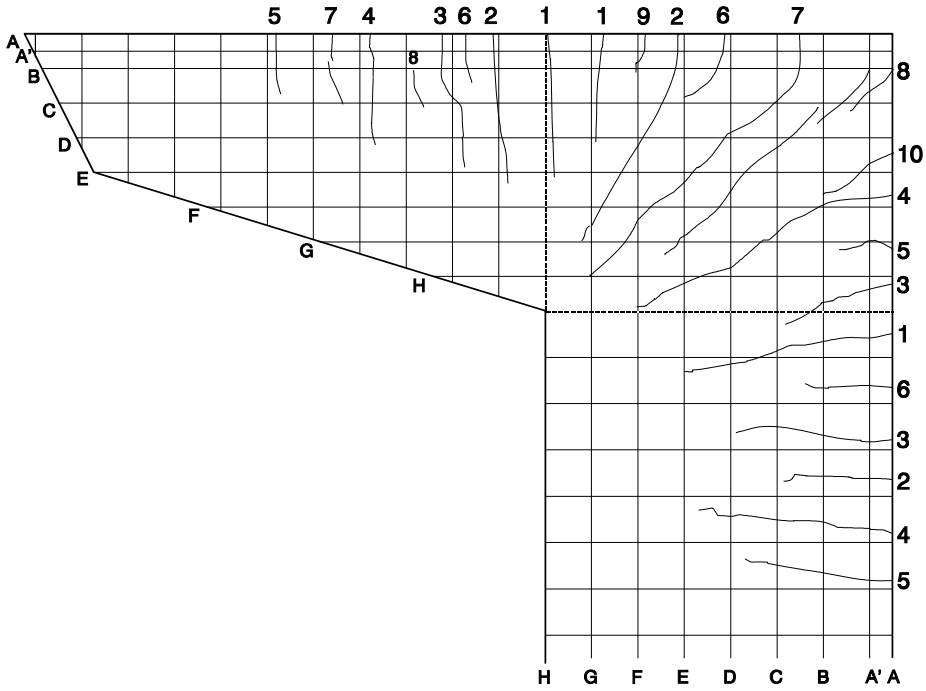

Figure 4.7 POJ-RC-100 cracking pattern on south face of specimen at service load

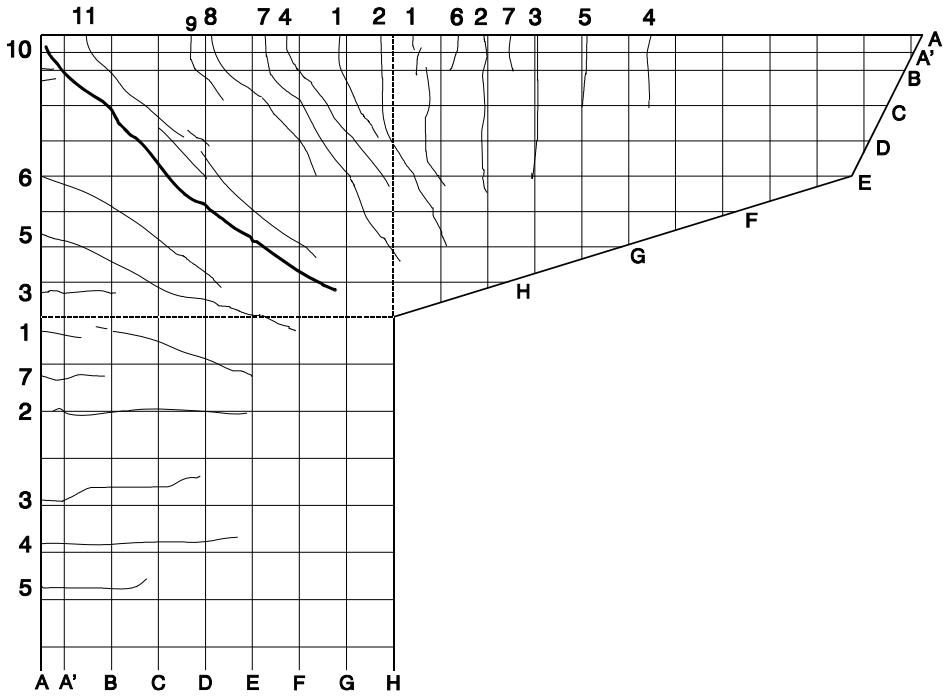

Figure 4.8 POJ-RC-100 cracking pattern on north face of specimen at failure

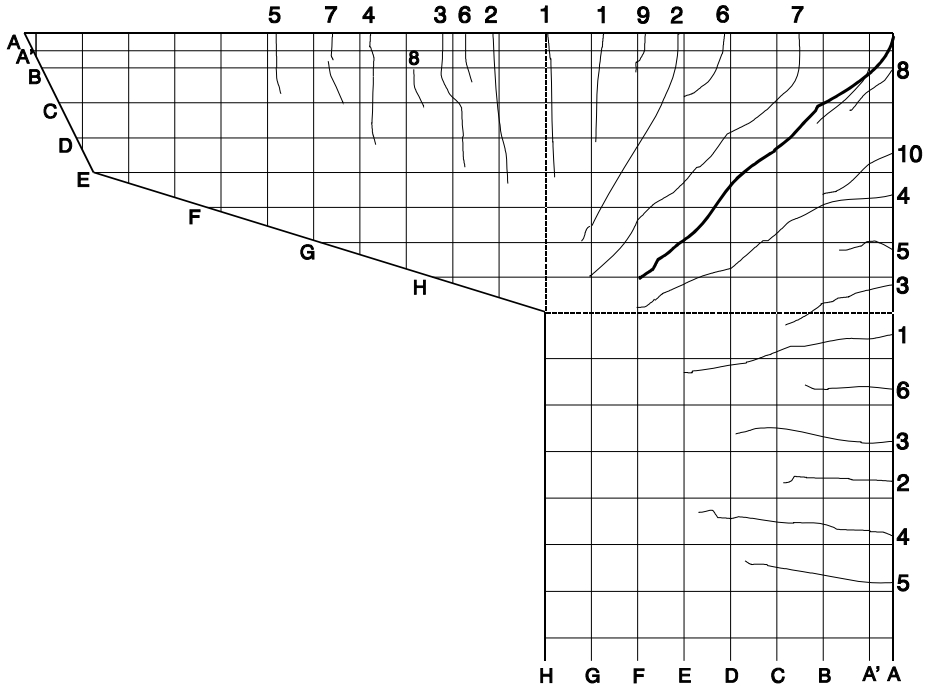

Figure 4.9 POJ-RC-100 cracking pattern on south face of specimen at failure

Crack widths in the overhang region were well-controlled throughout testing. Cracking patterns at dead load and service load for the north face of the overhang are shown in Figure 4.10 and Figure 4.11, respectively. Maximum crack widths in the overhang are presented in millimeters and inches in Table A.1 and Table A.2, respectively. Cracking patterns at dead load and service load for the south face of the overhang are shown in Figure 4.12 and Figure 4.13, respectively. Maximum crack widths in the south face of the overhang are presented in millimeters and inches in Table A.3 and Table A.4,

respectively. The maximum crack width of 0.10 mm (0.0040 in.) occurred in three cracks at service load. None of the overhang cracks were larger than the limiting crack width of 0.14 mm (0.0055 in.). Small crack widths can be attributed to the shear friction steel located near mid-depth of the section.

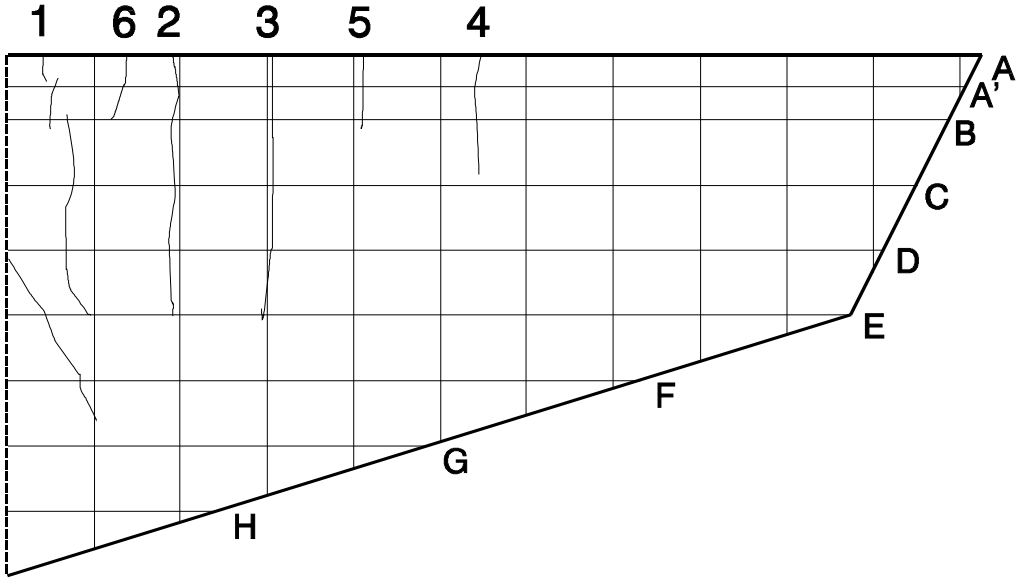

Figure 4.10 POJ-RC-100 cracking pattern on north face of overhang at dead load

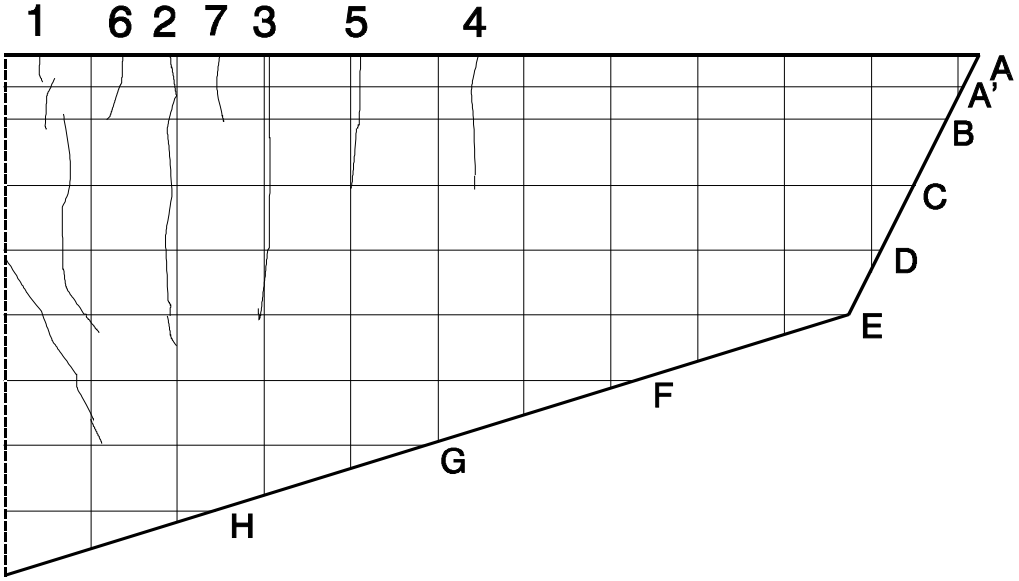

Figure 4.11 POJ-RC-100 cracking pattern on north face of overhang at service load

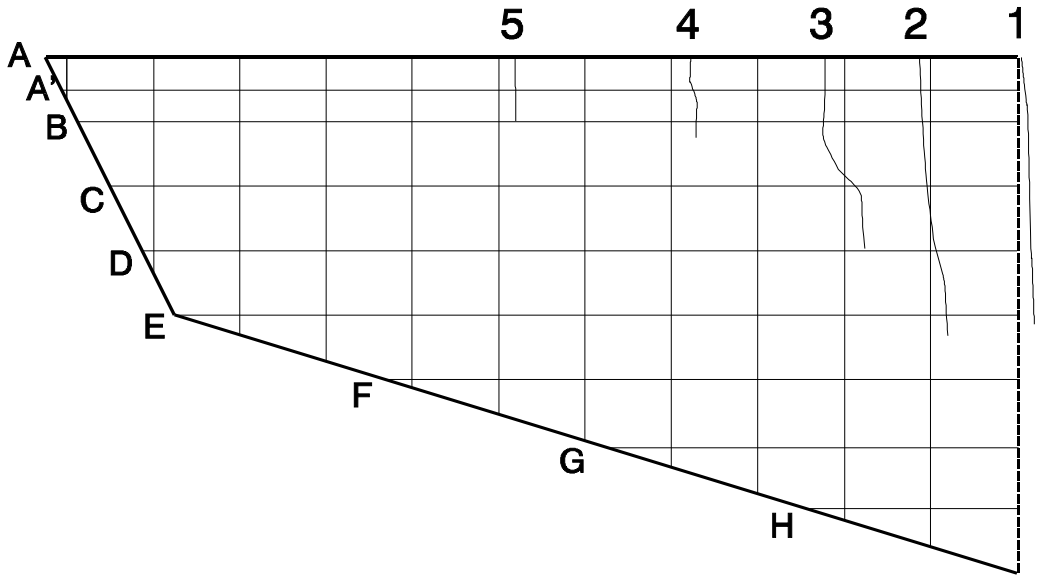

Figure 4.12 POJ-RC-100 cracking pattern on south face of overhang at dead load

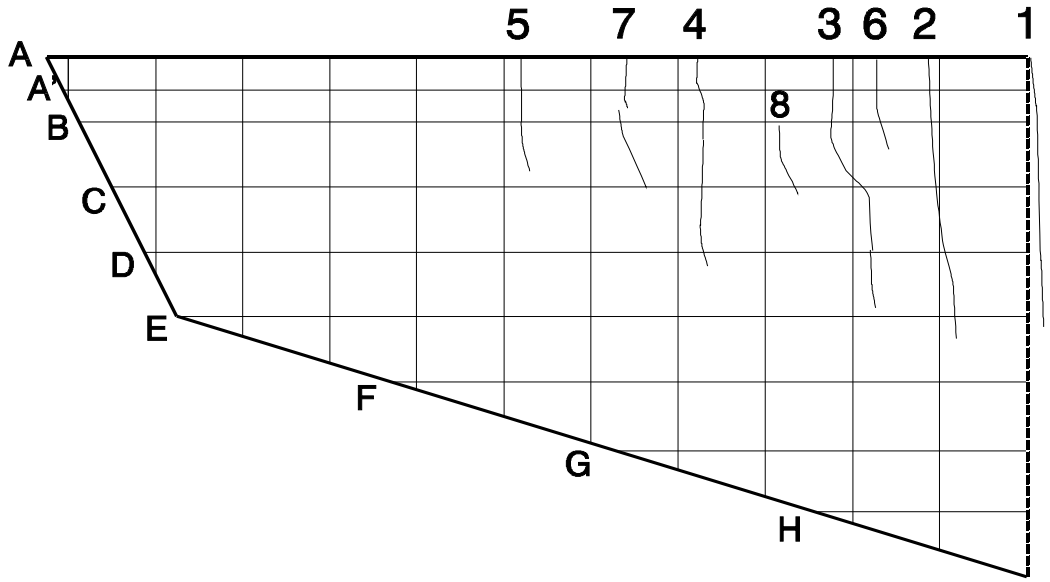

Figure 4.13 POJ-RC-100 cracking pattern on south face of overhang at service load

Joint cracks initiated in the pier and overhang regions and propagated toward the outer joint corner with increased loads. Growth of cracks toward the joint corner was an indicator of the level of joint distress. As tensile stresses in the joint region exceeded tensile strength of the concrete, cracks propagated toward the corner. Cracking patterns at dead load and service load for the north face of the joint are shown in Figure 4.14 and Figure 4.15, respectively. Maximum crack widths for the north face of the joint are presented in millimeters and inches in Table A.5 and Table A.6, respectively. Cracking patterns at dead load and service load for the south face of the joint are shown in Figure 4.16 and Figure 4.17, respectively. Maximum crack widths for the south face of the joint are presented in millimeters and inches in Table A.7 and Table A.8, respectively. The maximum crack width of 0.43 mm (0.017 in.) occurred on the north face of the joint and corresponded with a crack that originated at the joint corner. A total of 14 joint cracks exhibited widths at service load larger than the limiting crack width.

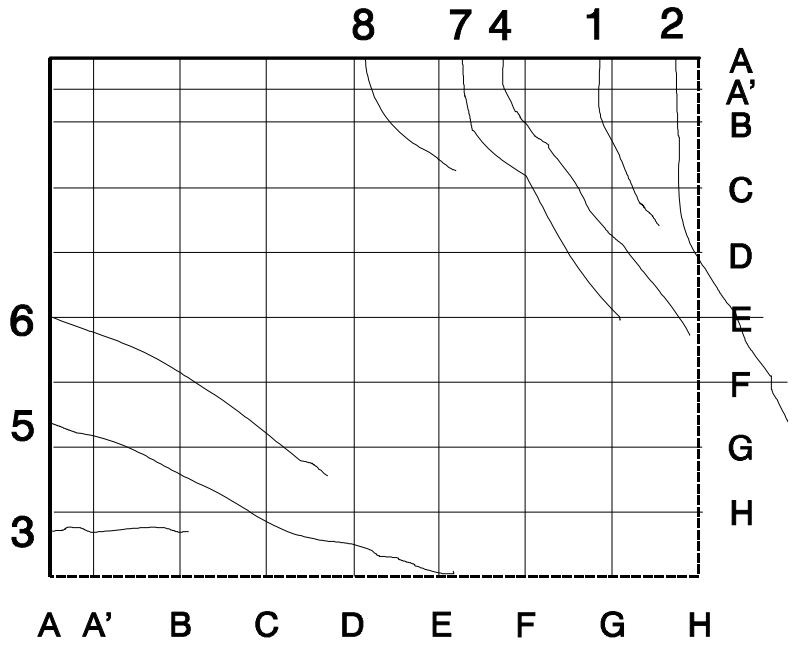

Figure 4.14 POJ-RC-100 cracking pattern on north face of joint at dead load

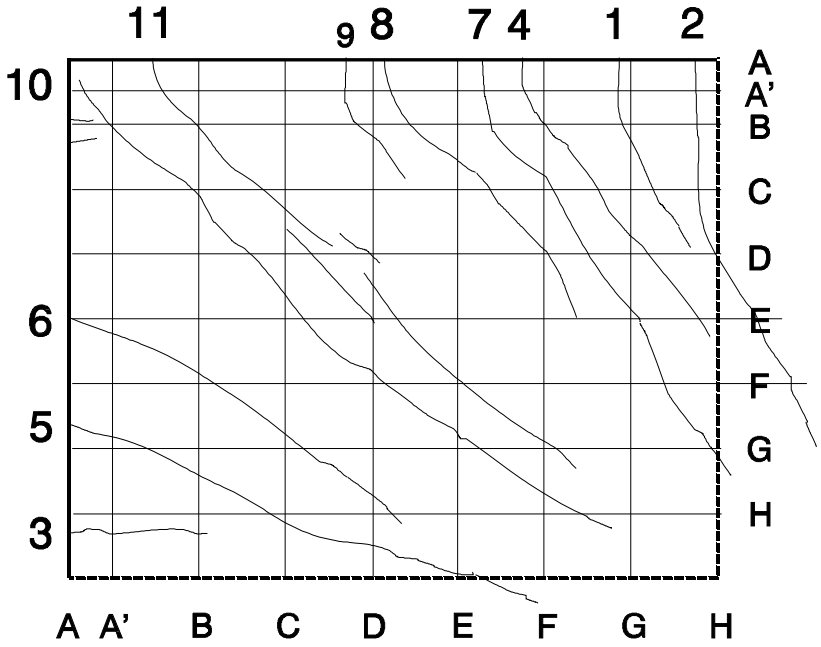

Figure 4.15 POJ-RC-100 cracking pattern on north face of joint at service load

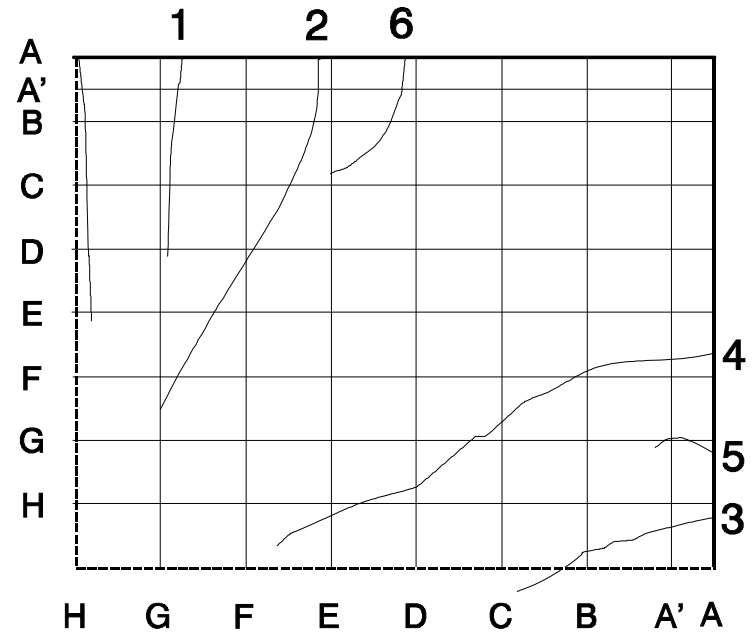

Figure 4.16 POJ-RC-100 cracking pattern on south face of joint at dead load

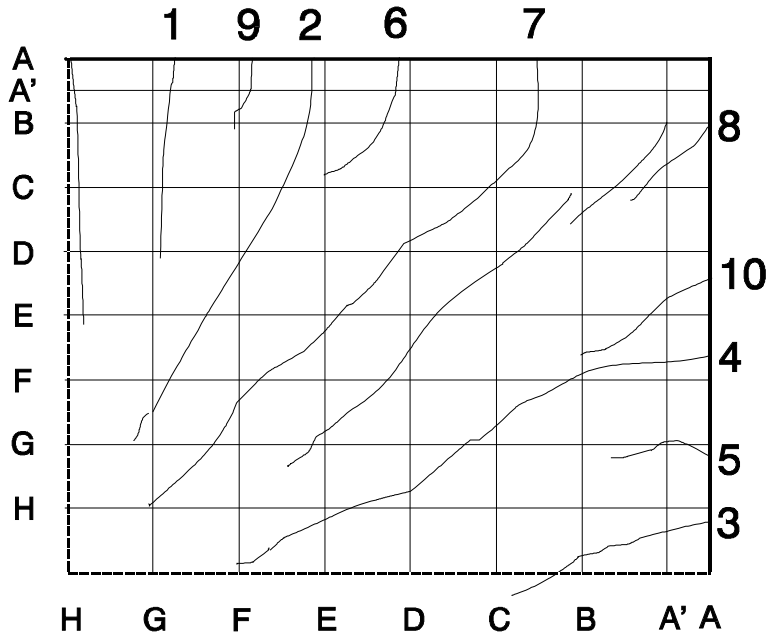

Figure 4.17 POJ-RC-100 cracking pattern on south face of joint at service load

Cracking patterns at dead load and service load for the north face of the pier are shown in Figure 4.18 and Figure 4.19, respectively. Maximum crack widths for the north face of the pier are presented in millimeters and inches in Table A.9 and Table A.10. Cracking patterns and maximum crack widths for the south face of the pier are presented in Figure 4.20 and Figure 4.21, and Table A.11 and Table A.12. Crack widths in the pier region exceeded the maximum allowable crack width. The maximum service load crack width of 0.18 mm (0.007 in.) occurred at two locations for crack number 1 on the north face of the pier. A total of three crack measurements at service load were larger than the limiting crack width.

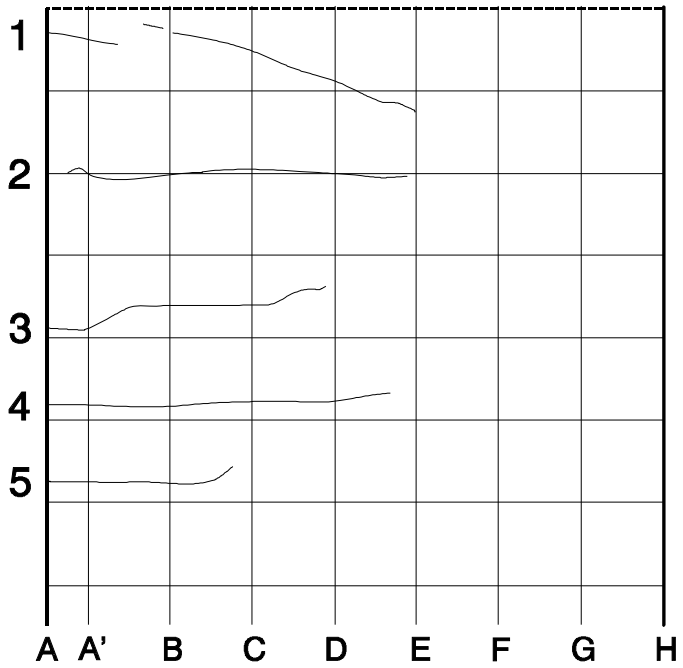

Figure 4.18 POJ-RC-100 cracking pattern for north face of pier at dead load

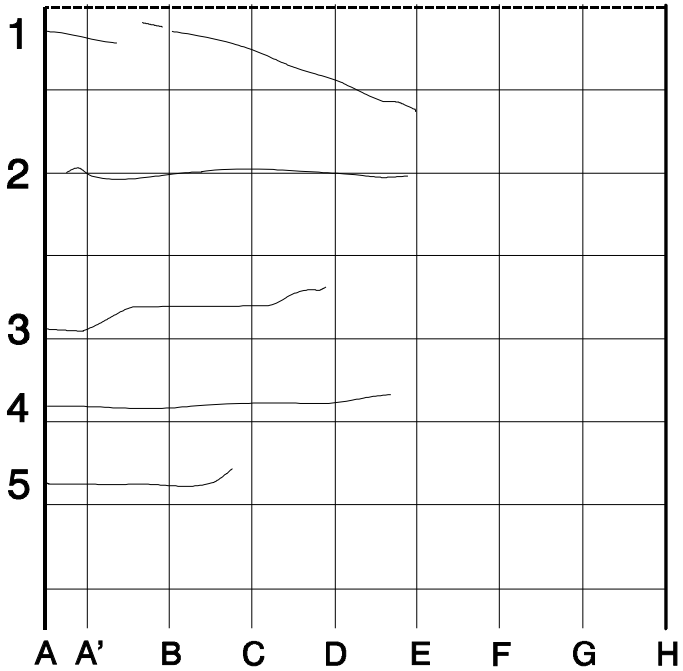

Figure 4.19 POJ-RC-100 cracking pattern for north face of pier at service load

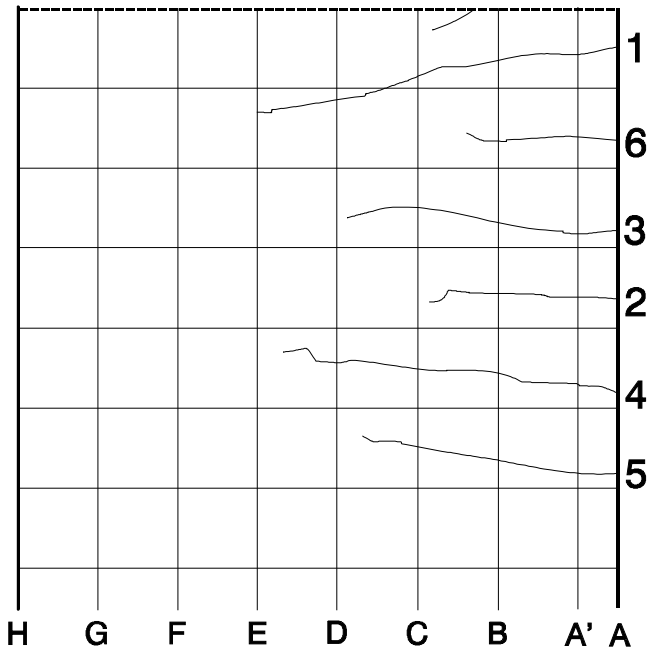

Figure 4.20 POJ-RC-100 cracking pattern on south face of pier at dead load

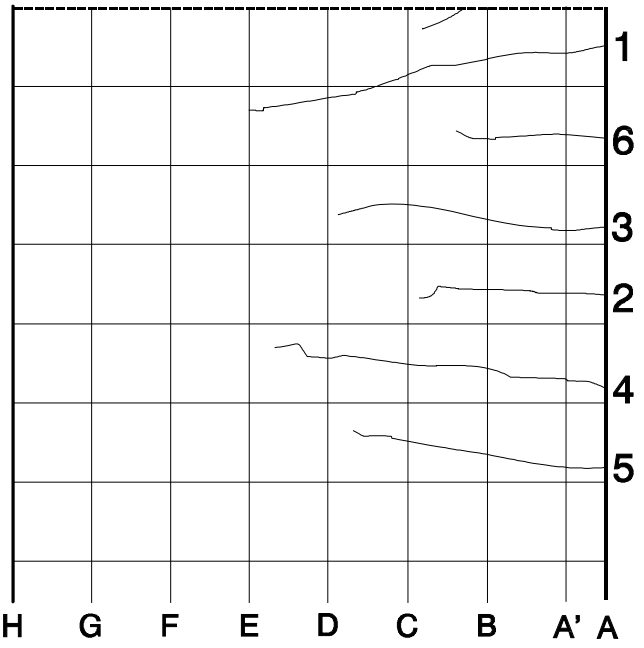

Figure 4.21 POJ-RC-100 cracking pattern on south face of pier service load

4.2.1.2 Applied Moment vs. Deflection Behavior–POJ-RC-100

Plots of applied moment vs. deflection response for Specimen POJ-RC-100 are presented in Figure 4.23 through Figure 4.26. The overhang moment is plotted as a fraction of the factored moment. Displacements are labeled in both SI and customary units. Locations of the displacement transducers are shown in Figure 4.22. Transducers labeled A (i.e., LV-75A) were located on the north side of the specimen, while gages labeled C (i.e., LV-75C) were located on the south side of the specimen.

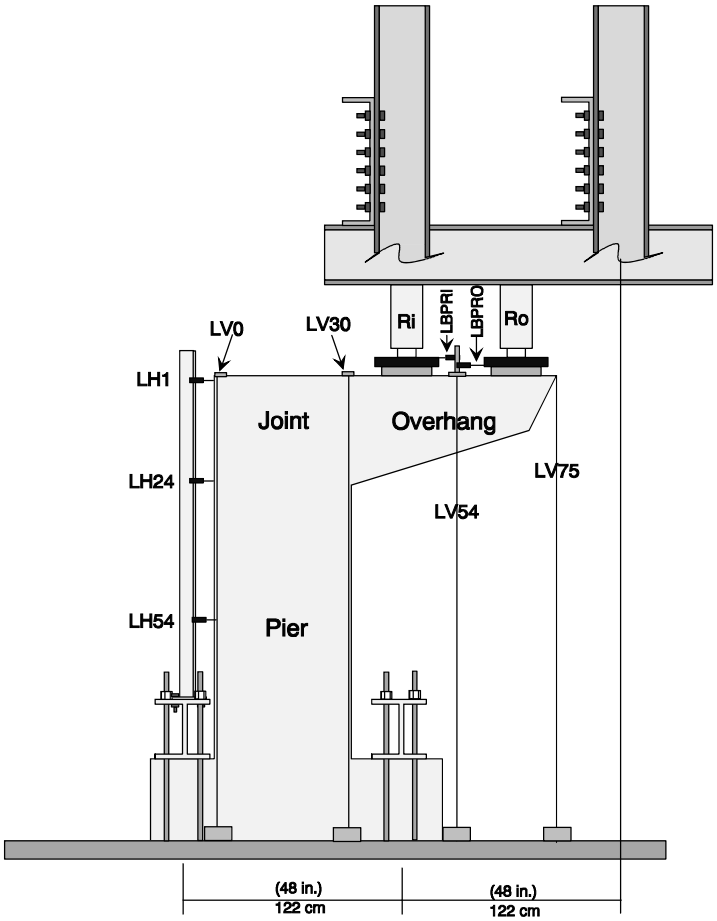

Figure 4.22 POJ-RC-100 locations of displacement transducers

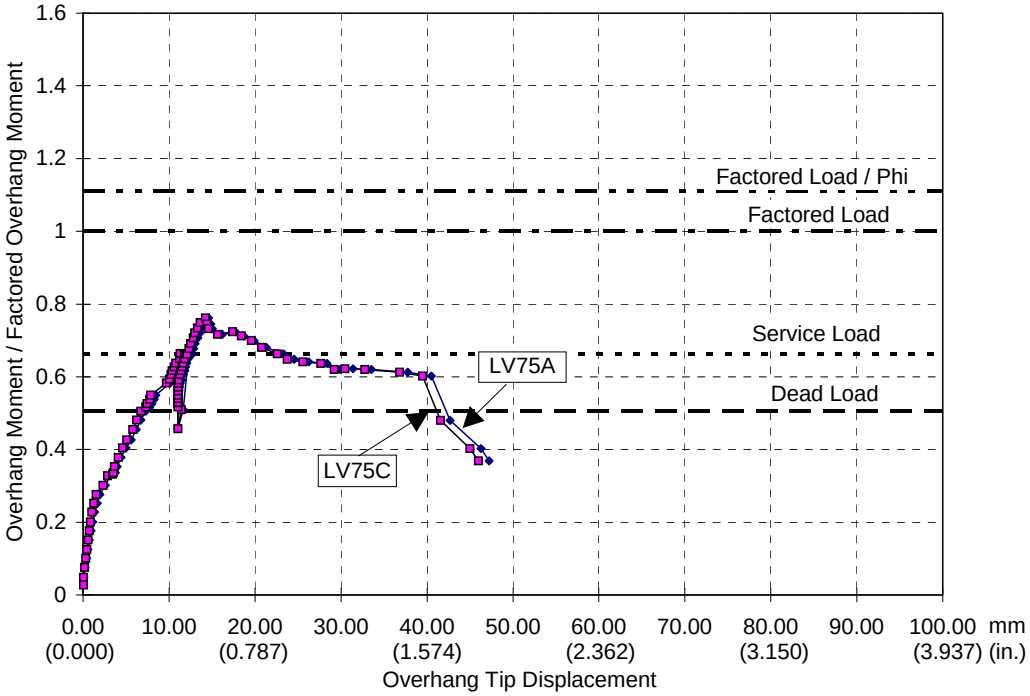

Figure 4.23 POJ-RC-100 tip deflection (LV-75)

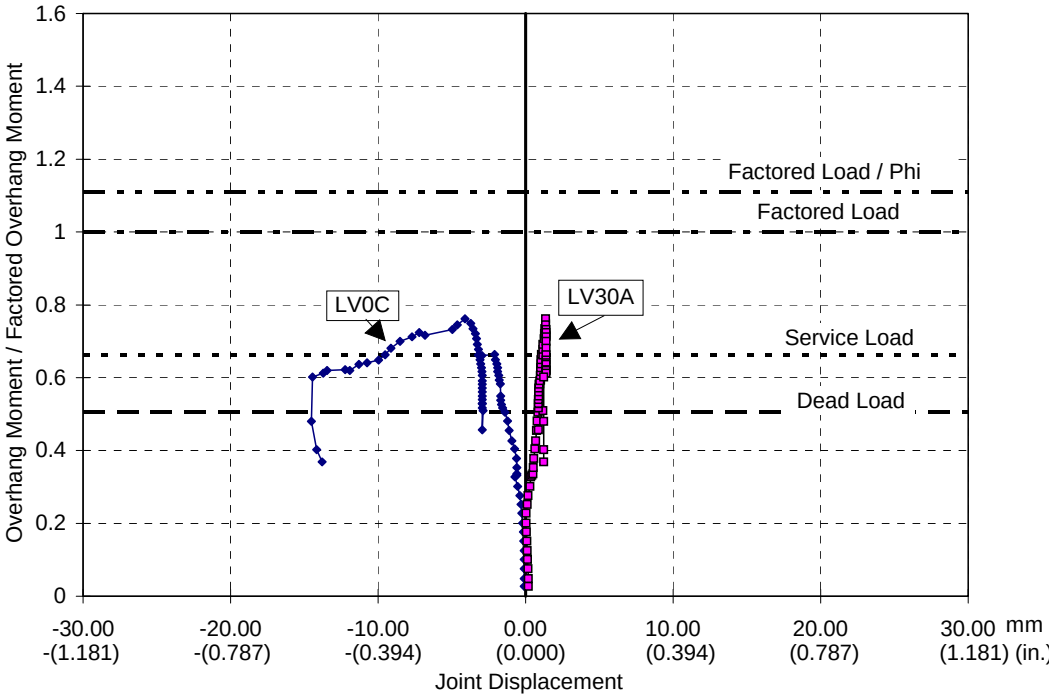

Figure 4.24 POJ-RC-100 top joint deflection

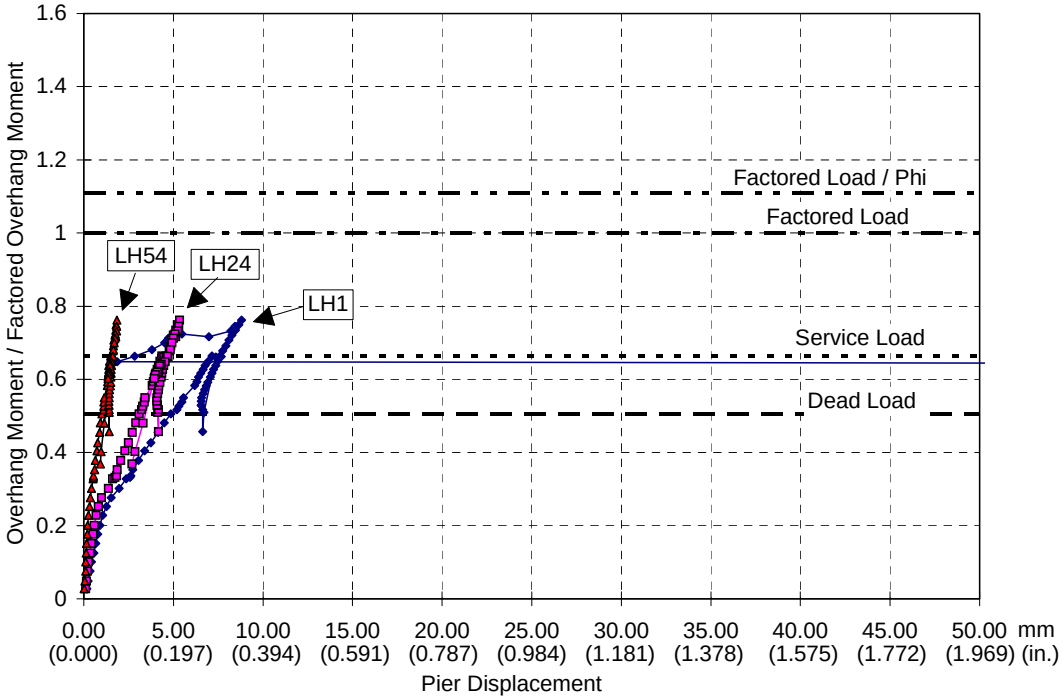

Figure 4.25 POJ-RC-100 pier horizontal deflections

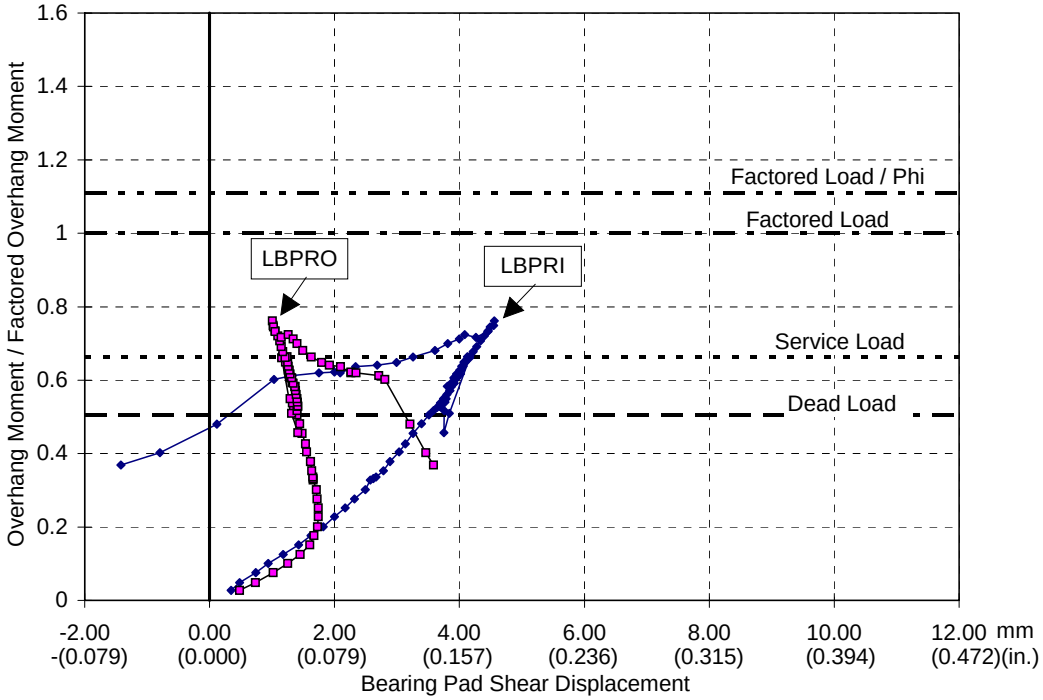

Figure 4.26 POJ-RC-100 bearing pad displacements

The overhang tip deflection (LV-75) shown in Figure 4.23, illustrates the result of premature failure of bar anchorage in the joint region. First cracking is evident in the moment-displacement plot at a moment ratio (overhang moment/factored moment) of approximately 0.3, or 50% of dead load. Failure of anchorage in the joint corresponded with the peak load, and occurred at a tip displacement of only 14.5 mm (0.57 in.). After the reduction in load, the specimen was incrementally displaced to a peak tip displacement of 40 mm (1.57 in.) before the specimen lost capacity to carry any significant load. One of the vertical joint displacement responses shown in Figure 4.24 (LVOC) depicts the vertical displacement of the joint corner due to opening of the critical diagonal crack in the joint. A displacement of 14.5 mm was recorded before the specimen was unloaded. The plot of the pier horizontal displacements in Figure 4.25 also illustrates the change in stiffness associated with first cracking. The LH1 transducer became detached and did not record the opening of the joint after maximum load. Displacement transducers connected to the bearing pads measured small shear displacements in the pads that were only 10-50% of the lateral displacement measured at the top of the pier. The two bearing pad displacements (shown in Figure 4.26) confirm that the loading frame swayed during testing. The load frame swayed because the center of applied force was located eccentrically with respect to the centerline of the frame. Because bearing pad shear displacements were small, the forces were not considered in the moment calculation.

4.2.1.3 Location and Identification of Strain Gages–POJ-RC-100

Strain gages were located at a number of locations to determine strain distributions across each section, and to provide redundancy of gages in case a gage was defective. There were layers of strain gages at several levels to measure strain gradients through the depth of the overhang and pier sections. Gages were located in the joint region to evaluate anchorage of mild reinforcement in the joint.

Strain gage labels utilize combinations of letters and distances (measured in inches) associated with an X-Y-Z coordinate system to identify the location of each gage (see Figure 4.27). The origin of the X, Y, and Z axes was located at the exterior corner of the joint corresponding with the casting surface

(south face of the specimen). The X axis increased positively in the direction of the overhang tip. The Z axis increased positively from the joint corner to the pier base. Values associated with the Y axis increased with depth of the strain gage from the casting surface. Locations associated with the X and Z axes were specified by the number of inches from the origin. Distances from the casting surface were indicated by the letter A (~ 1.5 inches from the casting surface), A' (~ 4 in.), B (~ 12 in.), or C (~ 22.5 in.). Labels and gage locations are illustrated in Figure 4.27 through Figure 4.30. The 'M,' 'T,' and 'C' prefixes correspond to the reinforcement type: primary '**M**ain' overhang longitudinal reinforcement, overhang side-face '**T**ie' longitudinal reinforcement, and Pier '**C**olumn' longitudinal reinforcement, respectively ('P' was reserved for '**P**ost-tensioned' reinforcement and 'S' for Overhang Transverse '**S**hear' reinforcement). These letter labels were required because X-Y-Z coordinates for a gage on longitudinal overhang reinforcement often corresponded to gages located on longitudinal pier reinforcement or transverse reinforcement in the overhang. Specifying the bar type being gaged avoided mistakes during construction and processing of data following testing.

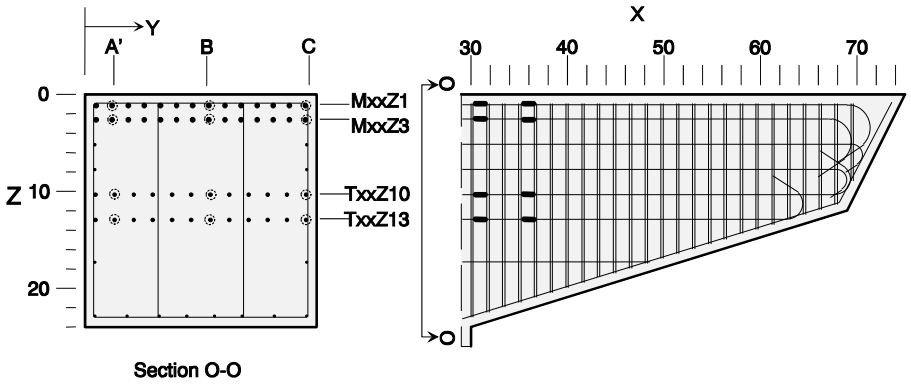

Overhang Longitudinal Reinforcement	Section X=30			Section X=35		
	A'	**B**	**C**	**A'**	**B**	**C**
Layer Z=1	M30Z1A'	M30Z1B	M30Z1C	M35Z1A'	M35Z1B	M35Z1C
Layer Z=3	M30Z3A'	M30Z3B	M30Z3C	M35Z3A'	M35Z3B	M35Z3C
Layer Z=10	T30Z10A'	T30Z10B	T30Z10C	T35Z10A'	T35Z10B	T35Z10C
Layer Z=13		T30Z13B			T35Z13B	

Figure 4.27 POJ-RC-100 overhang strain gage locations and labels

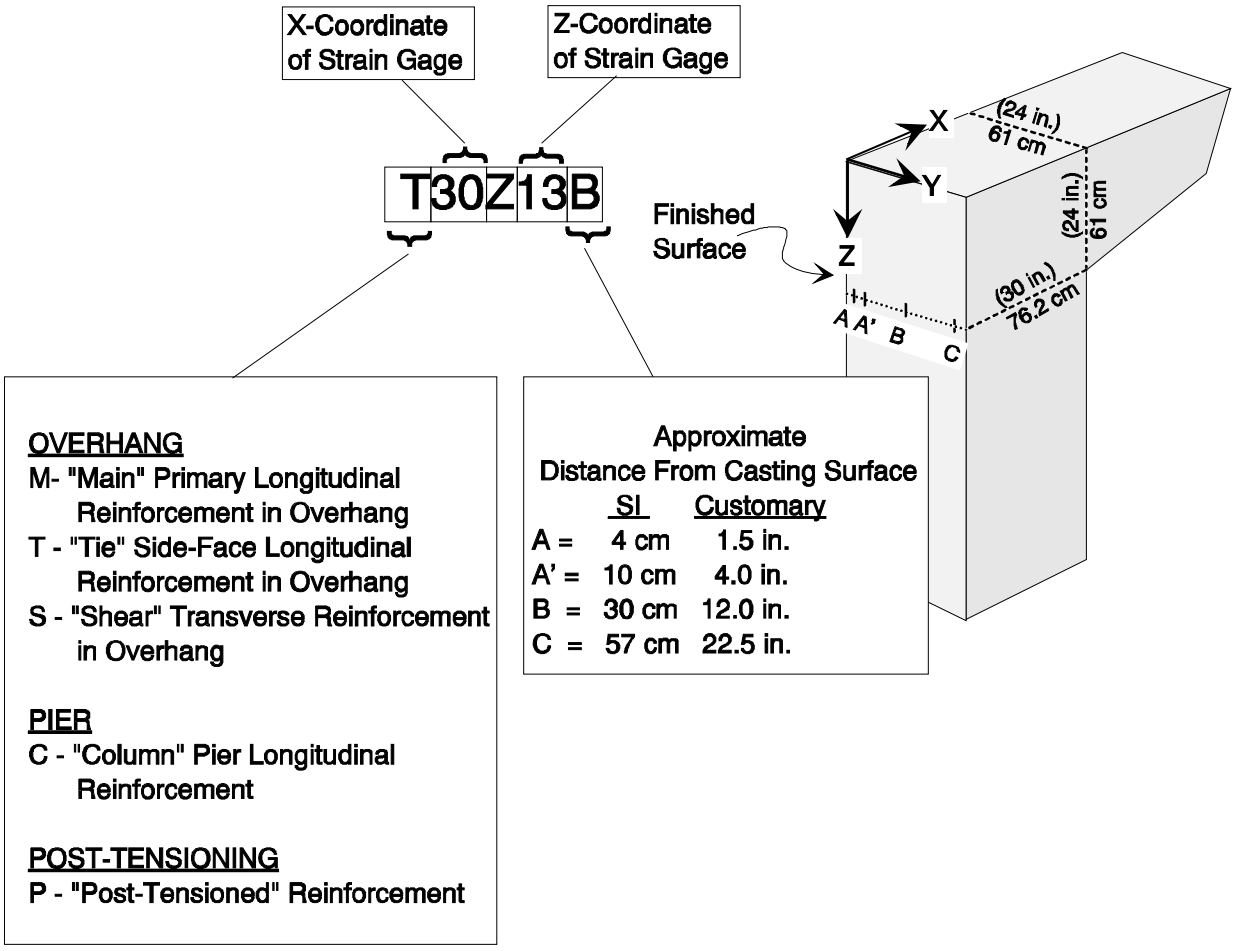

Figure 4.28 Strain gage labeling scheme

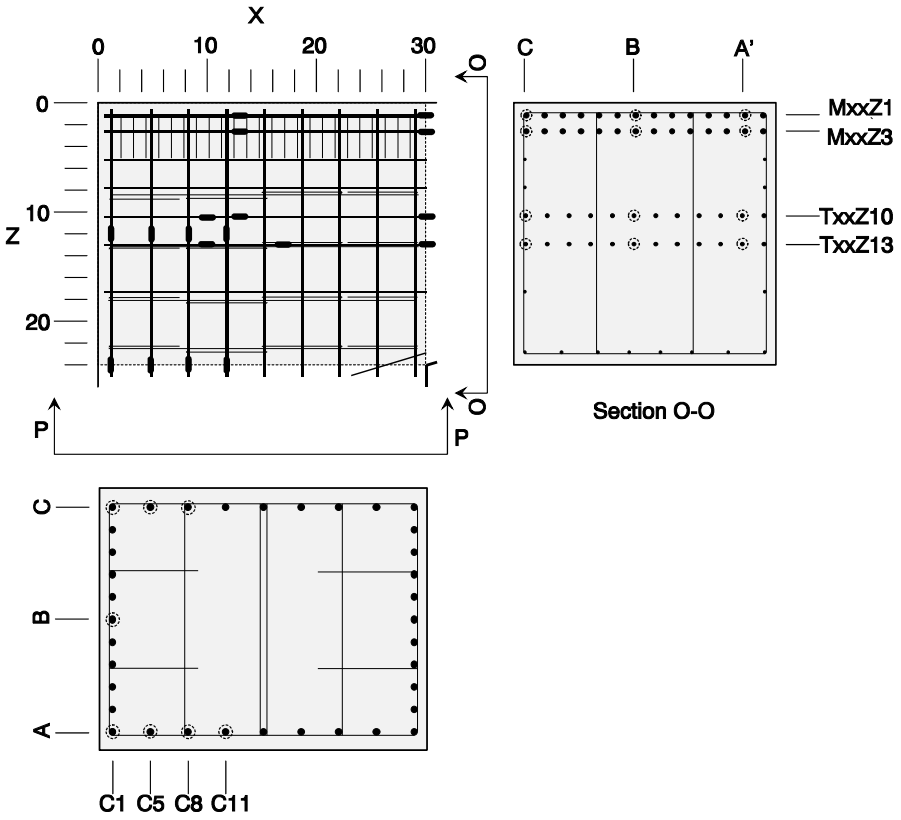

Overhang Longitudinal Reinforcement	Section X=10	Section X=13			Section X=17		Section X=30		
	B	A'	B	C		B	A'	B	C
Layer Z=1		M13Z1A'	M13Z1B	M13Z1C			M30Z1A'	M30Z1B	M30Z1C
Layer Z=3		M13Z3A'	M13Z3B	M13Z3C			M30Z3A'	M30Z3B	M30Z3C
Layer Z=10	T10Z10B	T13Z10A'	T13Z10B	T13Z10C			T30Z10A'	T30Z10B	T30Z10C
Layer Z=13	T10Z13B				T17Z13A’	T17Z13B		T30Z13B	

Pier Longitudinal Reinforcement	Section Z=12			Section Z=24		
	A	B	C	A	B	C
Layer X=1	C1Z12A	C1Z12B		C1Z24A	C1Z24B	C1Z24C
Layer X=5	C5Z12A			C5Z24A		C5Z24C
Layer X=8	C8Z12A			C8Z24A		C8Z24C
Layer X=11	C11Z12A			C11Z24A		C11Z24C

Figure 4.29 POJ-RC-100 joint strain gage locations and labels

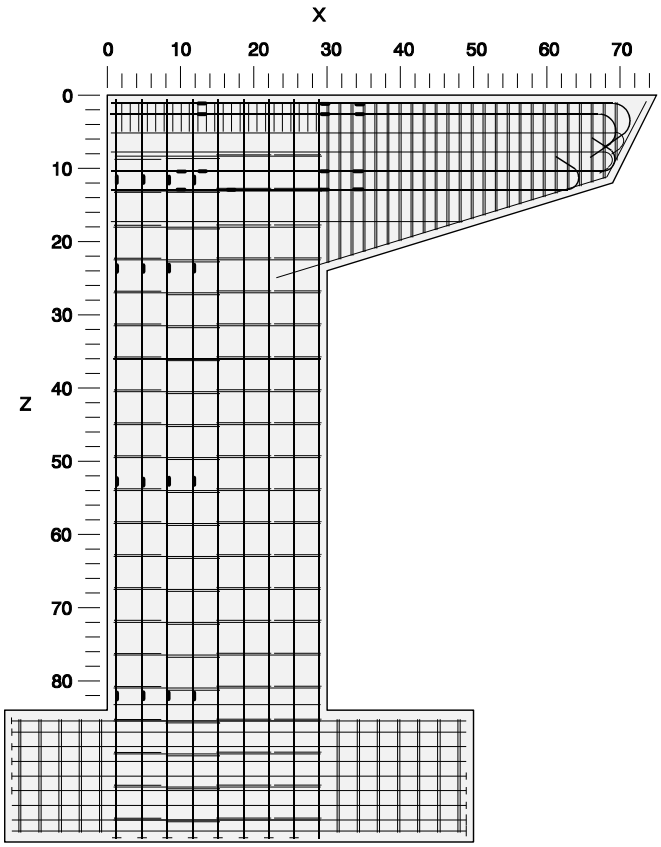

Pier Longitudinal Reinforcement	Section Z=54			Section Z=81		
	A	**B**	**C**	**A**	**B**	**C**
Layer X=1	C1Z54A	C1Z54B	C1Z54C	C1Z81A	C1Z81B	C1Z81C
Layer X=5	C5Z54A		C5Z54C	C5Z81A		C5Z81C
Layer X=8	C8Z54A		C8Z54C	C8Z81A		C8Z81C
Layer X=11	C11Z54A		C11Z54C	C11Z81A		C11Z81C

Figure 4.30 POJ-RC-100 overall strain gage locations and pier strain gage labels

An example of the labeling scheme is presented in Figure 4.28 for strain gage T30Z13B. Reading the label from left to right, T indicates the strain gage was attached to side-face reinforcement in the overhang, was located ~30 inches (~76.2 cm) from the exterior corner of the joint, was ~13 inches (33 cm) below the top of the overhang, and was ~ 12 inches (30.5 cm) from the casting surface (south side of the specimen).

4.2.1.4 Applied Moment vs. Strain Response–POJ-RC-100

The applied moment vs. strain plots for Specimen POJ-RC-100 included: longitudinal bar strains for the overhang and pier reinforcement and strain distributions across the cross section.

Strain gages on overhang longitudinal reinforcement indicated abrupt changes in strain when cracking occurred in the vicinity of each of the gages (see Figure 4.31 through Figure 4.38). Due to premature failure of the specimen in the joint region, strains in the primary longitudinal reinforcement in the overhang and pier did not exceed 75% of yield. Following failure of bond in the joint, strains in the top two layers of longitudinal reinforcement in the overhang and No. 5 bars in the pier decreased as displacements at the tip of the overhang increased. The strain reductions were consistent with reductions in applied load that occurred because of the loss of anchorage in the joint for primary

longitudinal reinforcement in the overhang and pier. Even though bars 11 inches from the exterior face of the pier (X=11) were closer to the neutral axis than the other instrumented bars in the pier, strains measured 12 inches below the top of the joint (Z=12) for a bar 11inches from the exterior face (X=11 in.) were greater than strains measured at the same depth (Z=12 in.) for other bars because of the longer embedment length available beyond the critical diagonal crack in the joint.

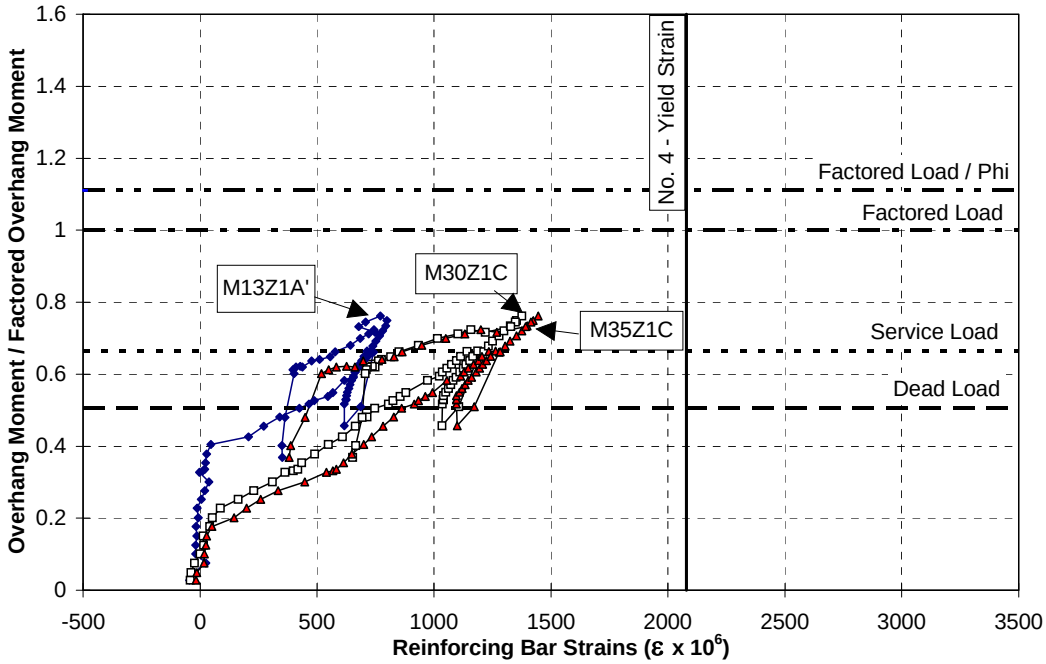

Figure 4.31 POJ-RC-100 strains in primary longitudinal reinforcement at Layer Z=1 in the overhang

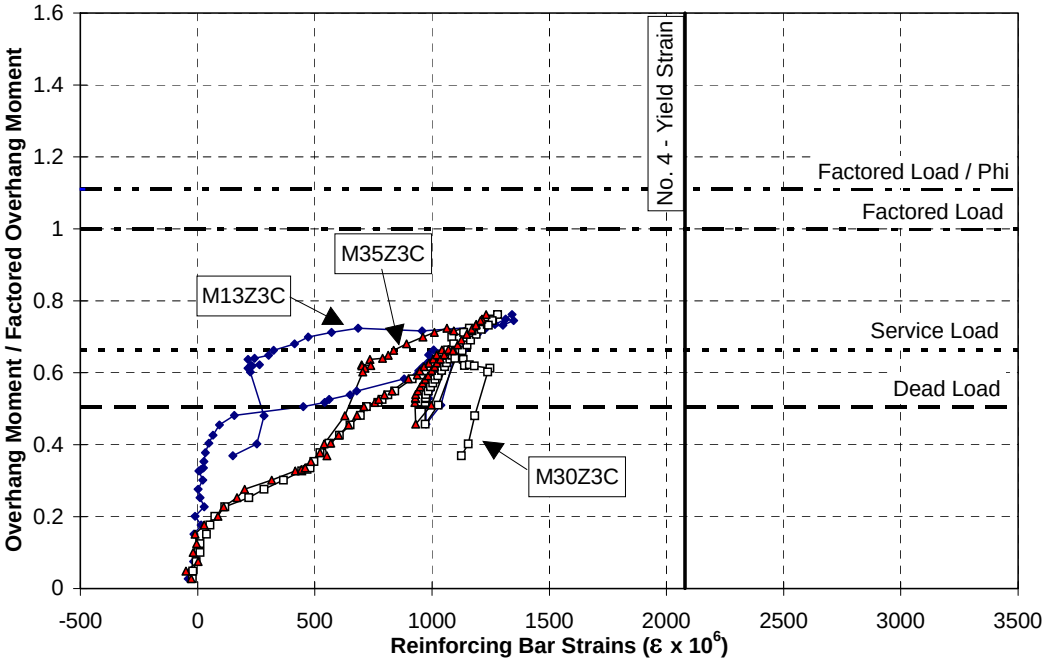

Figure 4.32 POJ-RC-100 strains in primary longitudinal reinforcement at Layer Z=3 in the overhang

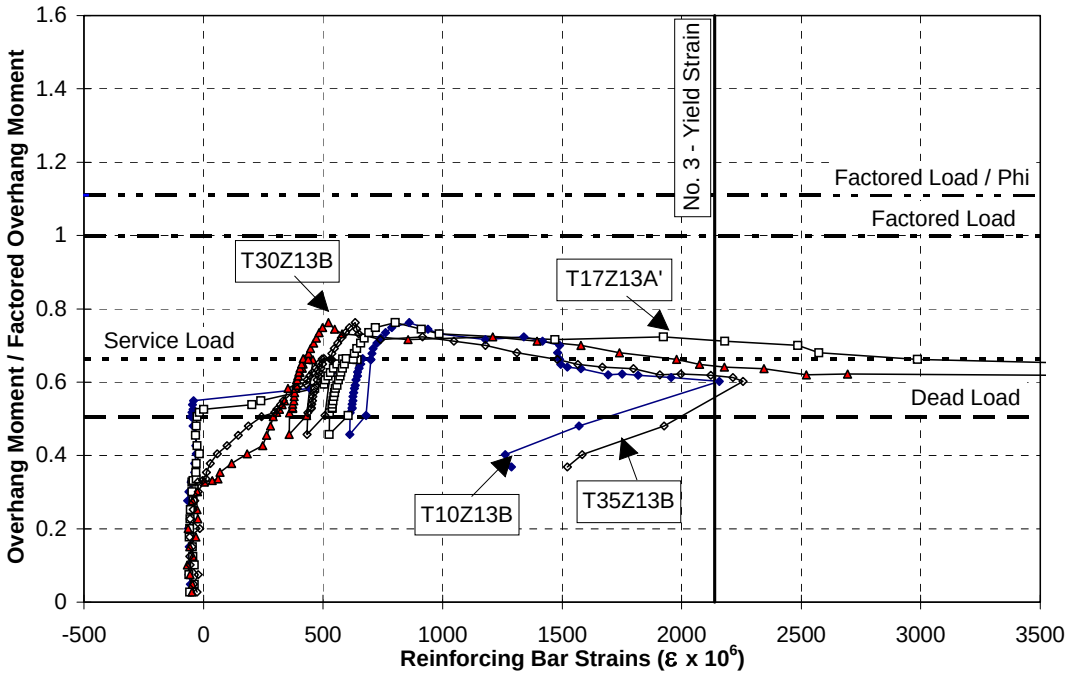

Figure 4.33 POJ-RC-100 strains in primary longitudinal reinforcement at Layer Z=13 in the overhang

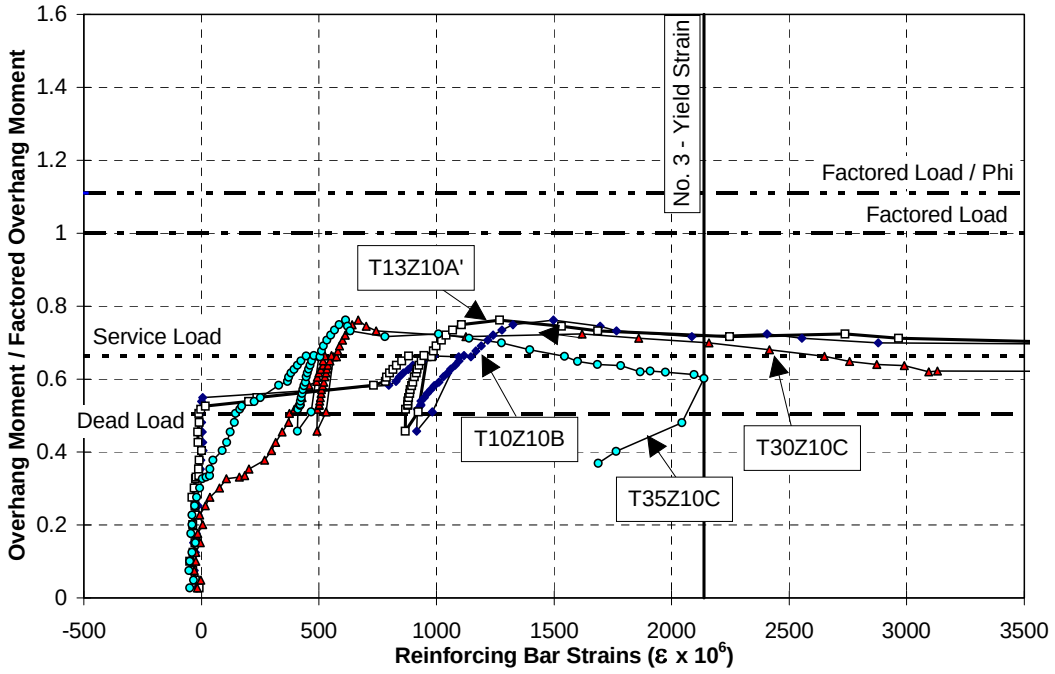

Figure 4.34 POJ-RC-100 strains in primary longitudinal reinforcement at Layer Z=10 in the overhang

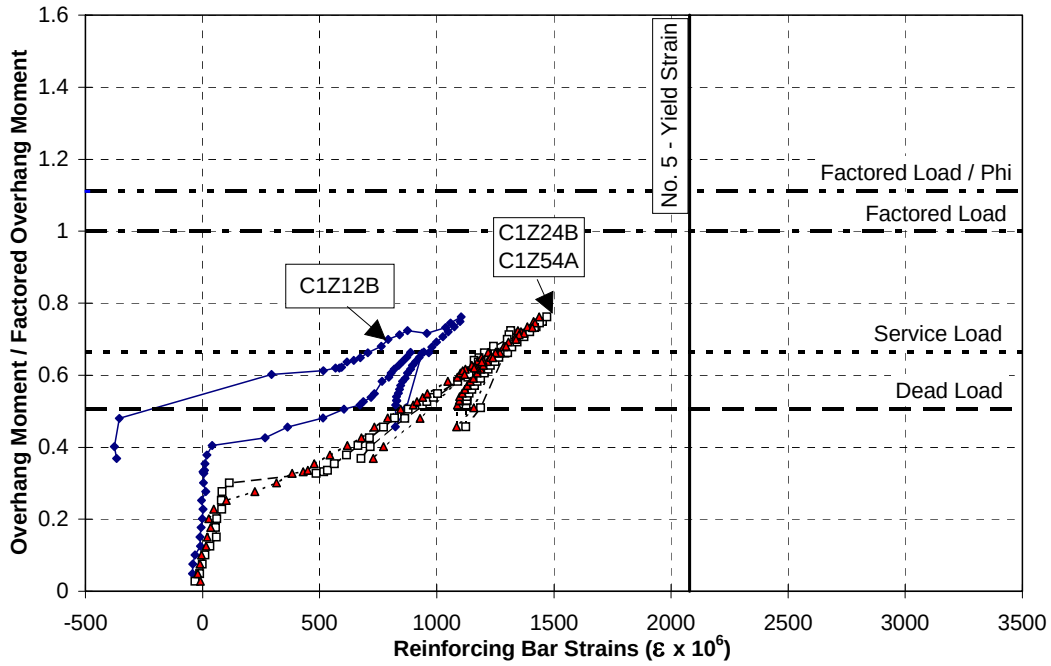

Figure 4.35 POJ-RC-100 strains in pier longitudinal reinforcement at Layer X=1

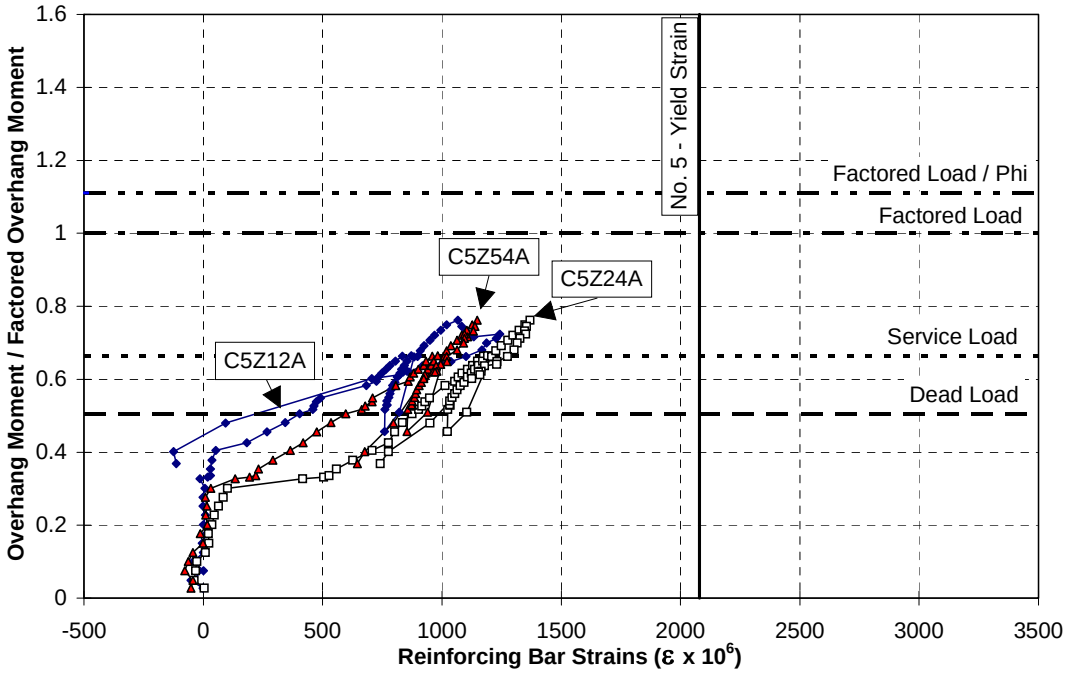

Figure 4.36 POJ-RC-100 strains in pier longitudinal reinforcement at Layer X=5

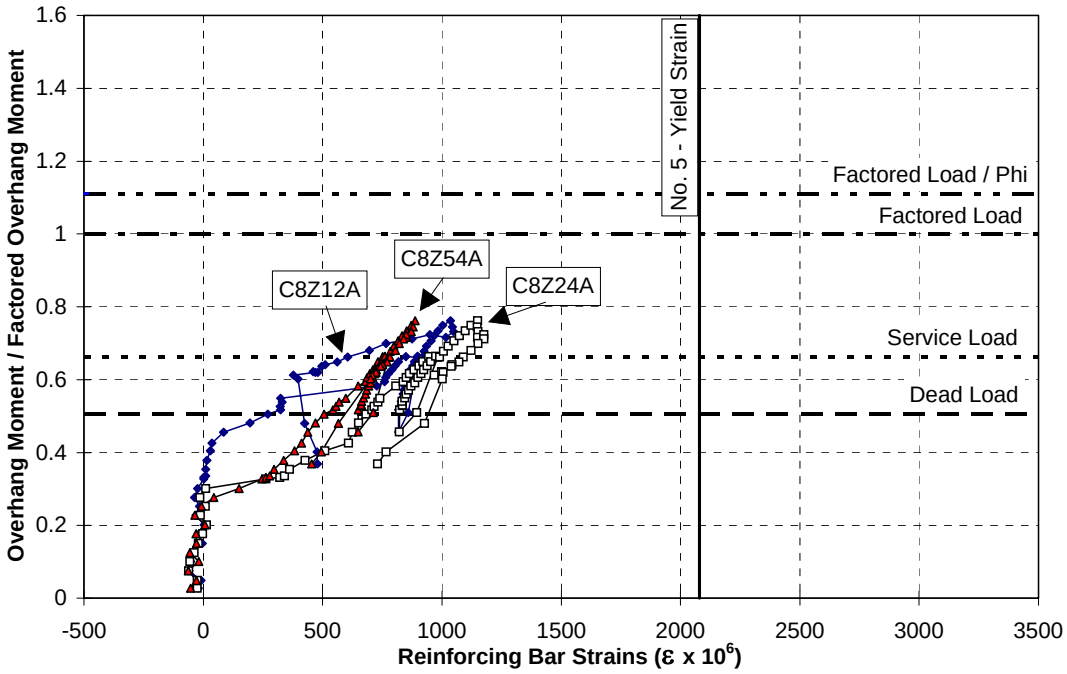

Figure 4.37 POJ-RC-100 strains in pier longitudinal reinforcement at Layer X=8

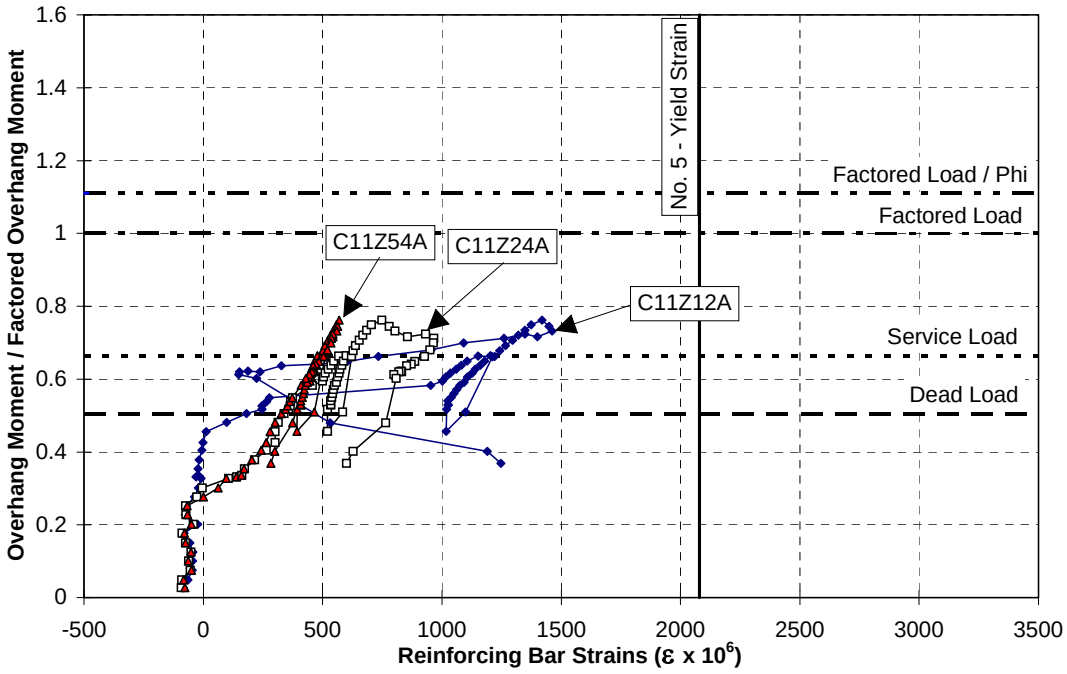

Figure 4.38 POJ-RC-100 strains in pier longitudinal reinforcement at Layer X=11

The sudden increase in strains measured by gages, T13Z10A', T10Z13B, T17Z13A', and T10Z10B (see Figure 4.29) at loads approximately equal to DL+½LL indicated the onset of cracking in the joint and transfer of tensile stresses into the mild reinforcement. As expected, strains increased at a lower load level for gages T30Z10C, T35Z10C, T30Z13B, and T35Z13B (Figure 4.33 and Figure 4.34) because flexure-shear cracks occurred near the inside face of the pier before cracks formed in the

joint. The moment vs. strain plots in Figure 4.33 and Figure 4.34 also indicate that shear friction reinforcement was anchored sufficiently to develop yield strength of the bars.

4.2.1.5 Overhang and Pier Section Strain Profiles

Strain profiles over the depth of the overhang and pier at a number of cross sections are illustrated in Figure 4.39 through Figure 4.43, for loads up to and including failure. The strain profiles for the overhang member (Figure 4.39 and Figure 4.40) were approximately linear up to failure. This observation was also true for strain profiles in the pier at a cross section 54 inches from the top surface of the specimen (Z=54, shown in Figure 4.43). Strain profiles from mid-depth of the joint (Figure 4.41) were highly nonlinear. Strains in pier longitudinal reinforcement located in the central portion of the pier demonstrated the largest increases in strain because of the longer embedment of the bars beyond the critical diagonal crack in the joint.

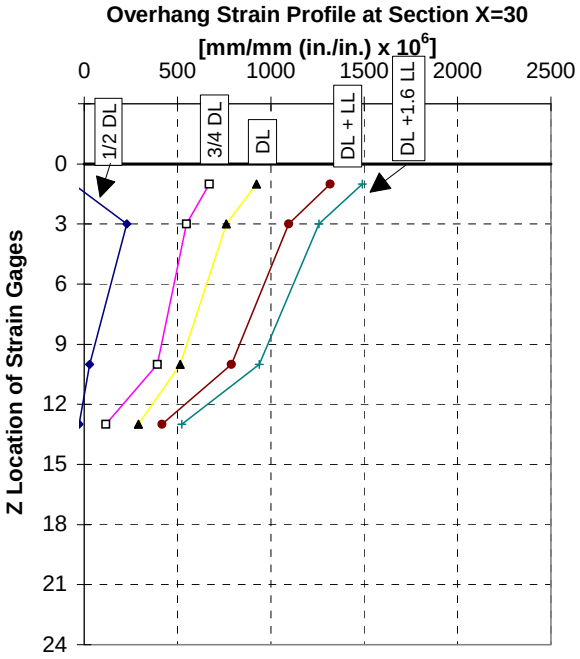

Figure 4.39 POJ-RC-100 strain profiles in overhang at Section X=30

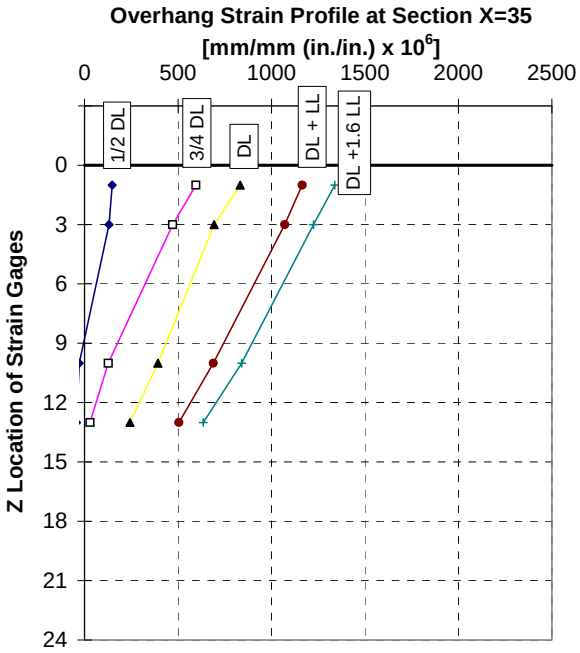

Figure 4.40 POJ-RC-100 strain profiles in overhang at Section X=35

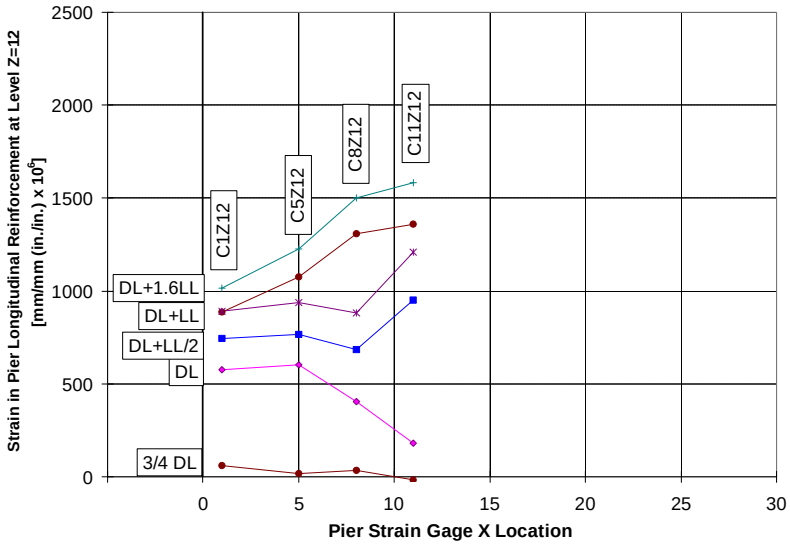

Figure 4.41 POJ-RC-100 strain profiles in joint at Section Z=12

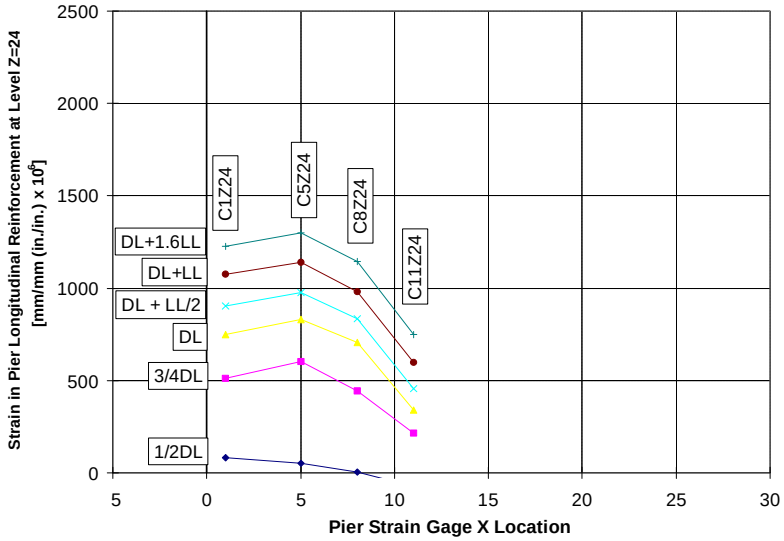

Figure 4.42 POJ-RC-100 strain profiles in pier at Section Z=24

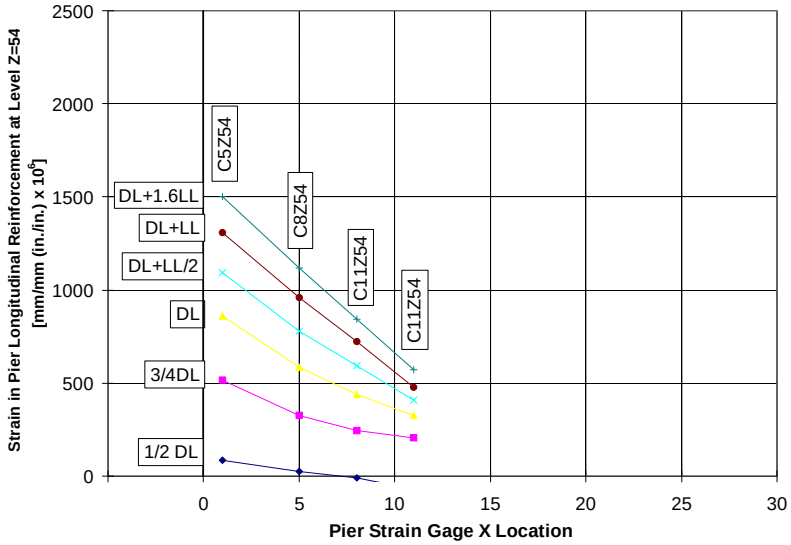

Figure 4.43 POJ-RC-100 strain profiles in pier at Section Z=54

4.2.2 Prestressed Concrete Design - POJ-PS-100

Specimen POJ-PS-100 was a model of a prototype fully-prestressed overhang bent designed according to the AASHTO 1986 Standard Design Provisions using the same considerations assumed by the designers of the San Antonio 'Y'. Specimen POJ-PS-100 was similar to the C11-C substructure in both shape and design.

Two rows of Dywidag longitudinal post-tensioning bars were located in the top of the overhang and anchored in the corner of the joint (shown in Figure 4.44). Shear friction reinforcement was located near mid-depth of the overhang. The prestressed overhang section was designed to remain uncracked at service loads. Extreme tensile fiber stresses in the pier were expected to be greater than the concrete cracking tensile stress under applied service level loads.

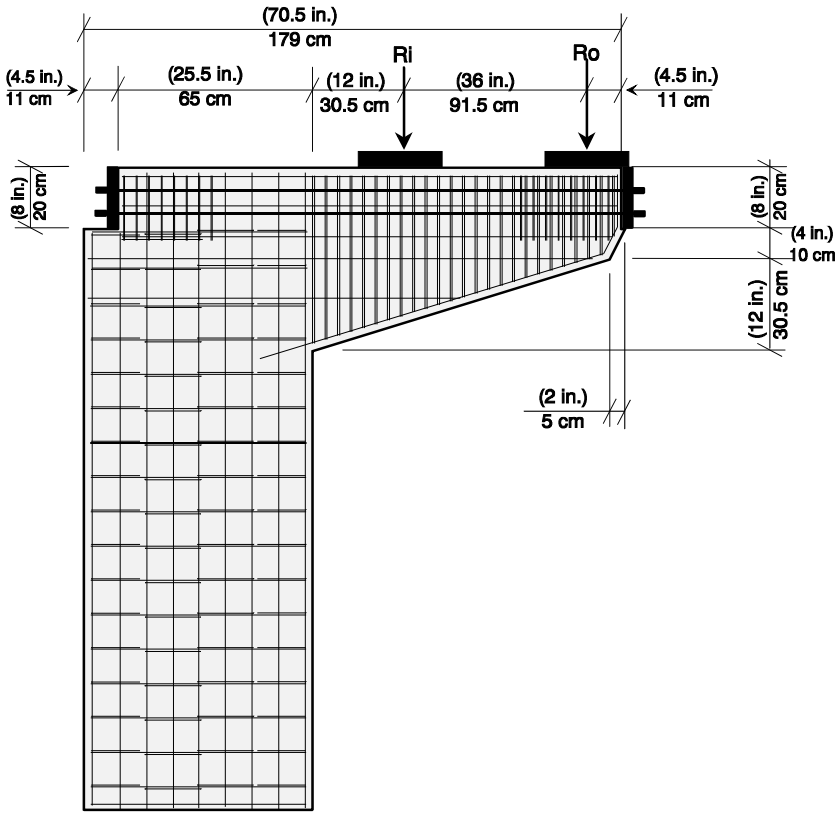

Figure 4.44 POJ-PS-100 reinforcing details

The block-out was cast into the specimen and all the extreme tensile longitudinal reinforcing bars in the pier were terminated to provide space for the block-out. The pier reinforcing bars at layer X=8 and greater were outside the post-tensioning block-out and were sufficiently embedded in the joint to provide some resistance. The shear friction reinforcement at layer Z=9 and Z=12 also provided some resistance for moments transferred through the joint.

Construction of the specimen was made more difficult due to the closely spaced anchorage reinforcement in the joint region and tip of the overhang. The location of the lifting anchors in the top of the joint used to move the specimen were located in a region where they would not provide additional specimen capacity. Detailing of the joint closely followed that for the full-scale bents.

Once the specimen was constructed and cast, the model was fixed into the loading frame and the gages were attached and checked. The stressing operation for the specimen was quite complex due to the multiple stressing stages that were required to ensure the extreme tensile fiber stresses did not exceed $3\sqrt{f'_c}$ 1.46 MPa (212 psi). The lower layer of six 16mm (5/8 in.) diameter Dywidag post-tensioning bars was stressed to 1103 MPa (160 ksi) with no load applied to the overhang. After the bars were stressed, the specimen was loaded in steps to ½ dead load, and the specimen was inspected for cracks after every load step. At ½ dead load, the top layer of 6–16mm (5/8 in.) diameter Dywidag post-tensioning bars was stressed to 1103 MPa (160 ksi). Final stress in the bars was checked by performing lift-off tests. After the stressing operation was completed the post-tensioning ducts were grouted. Once the grouting operation was completed a crack on the north and south faces was identified in the joint corner (crack 1 in Figure 4.45 and Figure 4.46, respectively). Crack widths were recorded and the crack was marked on the specimen.

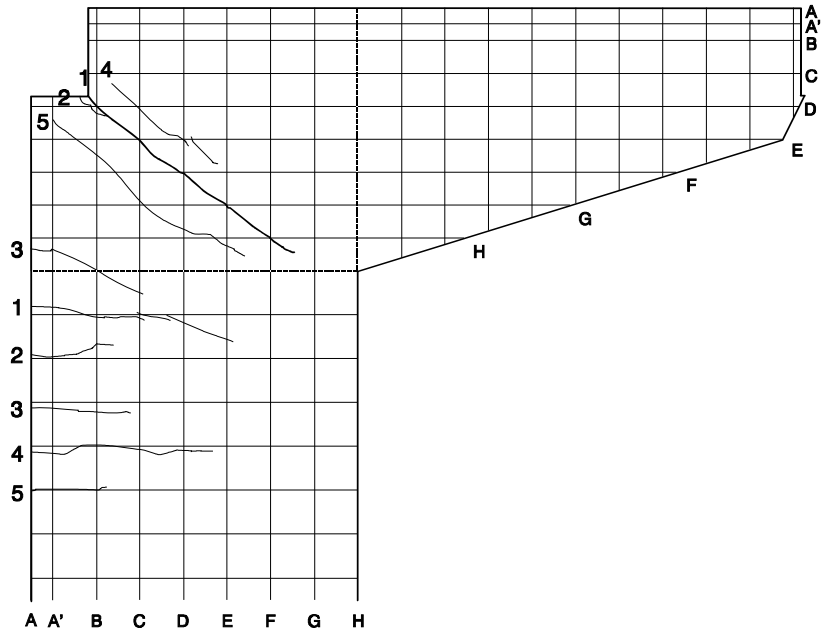

Figure 4.45 POJ-PS-100 cracking pattern on north face of specimen at dead load

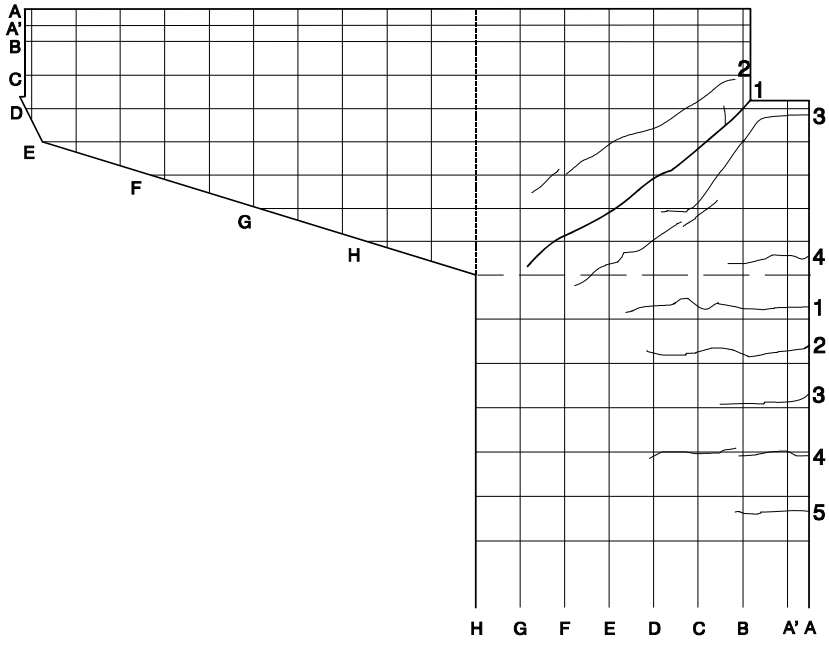

Figure 4.46 POJ-PS-100 cracking pattern on south face of specimen at dead load

The specimen was left under half-dead load until the grout attained a cube compressive strength of 6.8 MPa (1000 psi). After three days the specimen was loaded incrementally to dead load. During the loading procedure, cracks were marked at every load step and measured every other load step. It was apparent that the critical diagonal crack in the joint was growing rapidly from load step to load step. In order to preserve the specimen for the repair study, the test was stopped after applying full dead load.

After the repair study load tests were completed, the specimen was left at ½ dead load and the repair hardware was removed. Because the tip displacement transducers were not disturbed during removal

of the repair hardware, tip deflection readings were used as the new starting point for displacements. However, joint and pier displacement transducers were moved in order to remove the repair, therefore the origin of joint and pier displacement curves were assumed to be the point where the first test ended (i.e., the last recorded displacement at ½ DL for the unrepaired specimen). Most of the strain gages were not functioning after the repair study was completed, so strain gage results are plotted only for the first test (up to dead load).

The specimen was loaded incrementally to dead load and the displacement was monitored using an X-Y plotter. The peak load was 0.58 times factored load (DL+0.47LL). The joint crack grew rapidly with increasing overhang displacement. The specimen was loaded in displacement increments to a total tip displacement of 37 mm (1.46 in.). The test was stopped due to the large overhang displacement. A photograph of the failure mode viewed from the north side is presented in Figure 4.47, and close-ups of the anchorage failure are presented in Figure 4.48 and Figure 4.49.

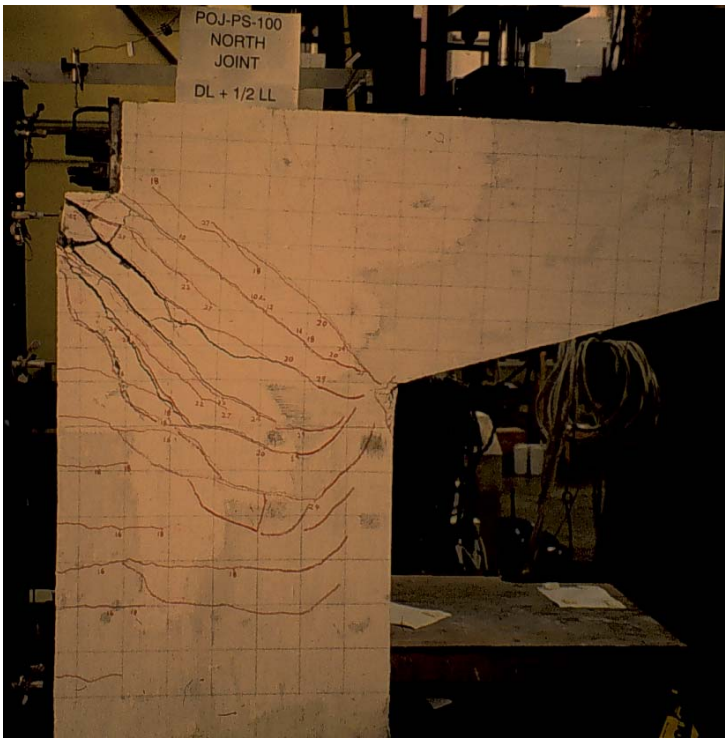

Figure 4.47 Photograph of Specimen POJ-PS-100 failure mode viewed from the north

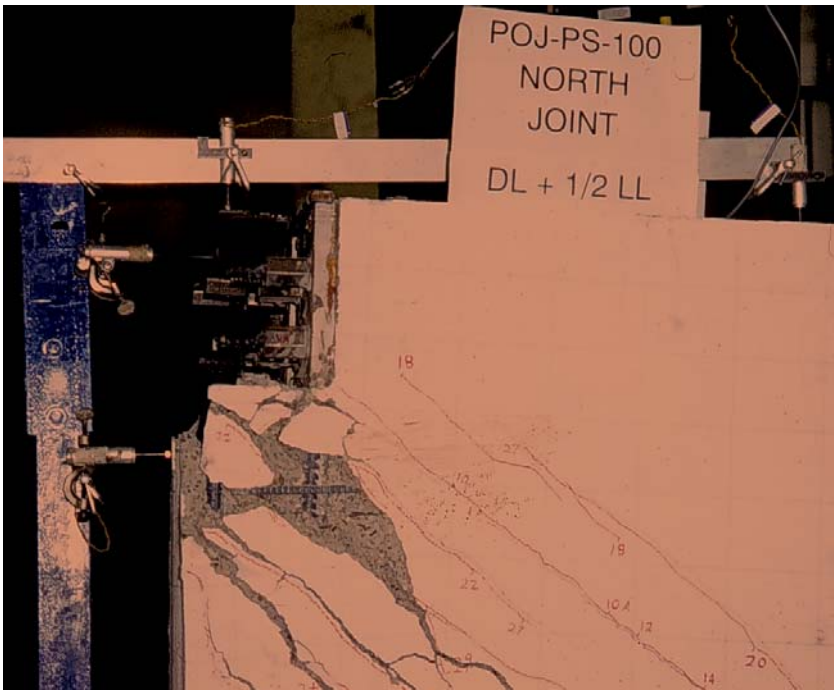

Figure 4.48 Photograph of Specimen POJ-PS-100 bar anchorage failure

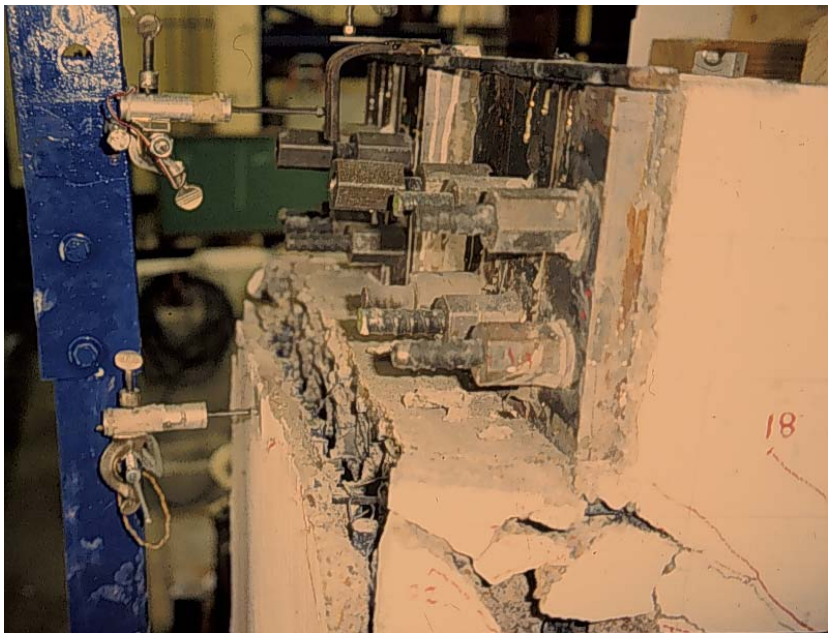

Figure 4.49 Photograph of joint crack opening in Specimen POJ-PS-100

4.2.2.1 Cracking Patterns and Maximum Crack Width Measurements–POJ-PS-100

Cracking patterns and maximum crack-width measurements are presented only for the first test of Specimen POJ-PS-100 up to dead loads. Crack-width measurements for the test to failure are not presented because the specimen was proof loaded to factored loads/phi twice during the repair study.

Cracks in Specimen POJ-PS-100 were concentrated in the joint and pier regions. No cracks were identified in the overhang region because the flexural stresses resulting from the peak applied

moment were not great enough to overcome the compressive stress provided by the post-tensioning. The joint region developed a diagonal crack which originated at the corner of the post-tensioning anchorage pocket during the post-tensioning operation (at applied loads equivalent to ½ DL of the superstructure). Cracking patterns in the pier region were similar to those obtained during the POJ-RC-100 test.

The overall cracking patterns at dead load for the north and south sides of Specimen POJ-PS-100 are presented in Figure 4.45 and Figure 4.46, respectively. The critical diagonal crack associated with failure of the specimen (crack 1 on the north and south face of the specimen) is identified with a heavy line in Figure 4.45 and Figure 4.46.

Cracking patterns on the north face and south face of the joint at dead load are presented in Figure 4.50 and Figure 4.51, respectively. Maximum crack widths for the north face of the joint are presented in millimeters and inches in Table A.13 and Table A.14, respectively. Maximum crack widths for the south face of the joint are presented in millimeters and inches in Table A.15 and Table A.16, respectively. The maximum crack width of 1.12 mm (0.0440 in.) occurred for crack 2 on the north face of the specimen at dead load. Dead load (equivalent to dead load of the superstructure) was applied to the specimen overnight to determine if crack widths would grow with time. Maximum measured crack widths in the joint increased under sustained dead loads. It should be noted that the outer surface of crack 2 at grid location 'B' collapsed into the crack overnight, and the resulting maximum measured crack width for crack 2 was 0.71 mm (0.028 in.) at grid line 'D'.

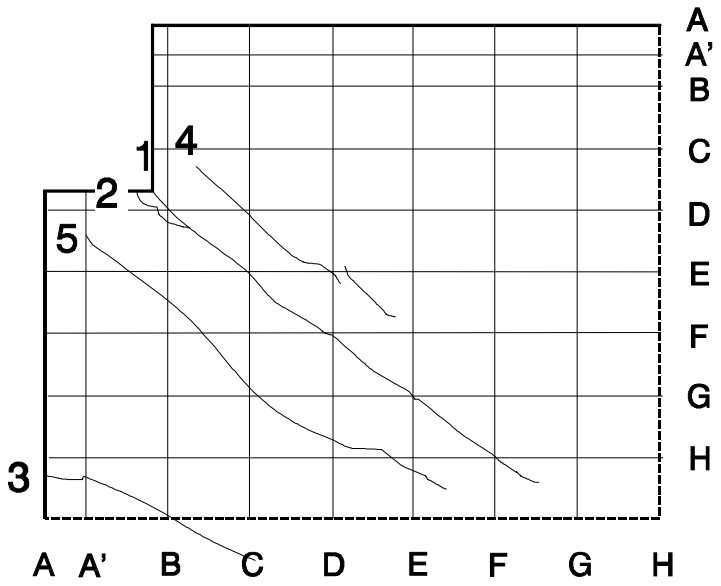

Figure 4.50 POJ-PS-100 cracking pattern on north face of joint at dead load

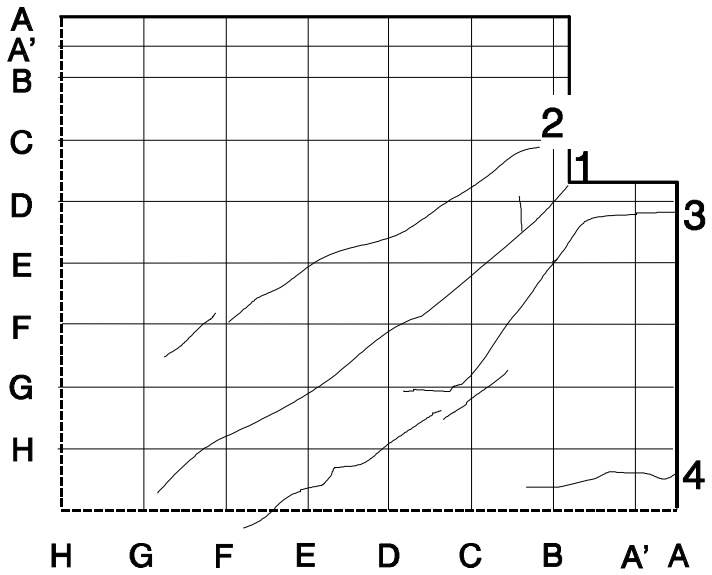

Figure 4.51 POJ-PS-100 cracking patterns on south face of joint at dead load

Cracking patterns on the north and south face of the pier at dead load are presented in Figure 4.52 and Figure 4.53, respectively. Maximum crack widths for the north face of the pier are presented in millimeters and inches in Table A.17 and Table A.18, respectively. Maximum crack widths for the south face of the pier are presented in Table A.19 and Table A.20 in millimeters and inches, respectively. A maximum crack width of 0.10 mm (0.0040 in.) occurred for crack 2 on the north and south face of the pier.

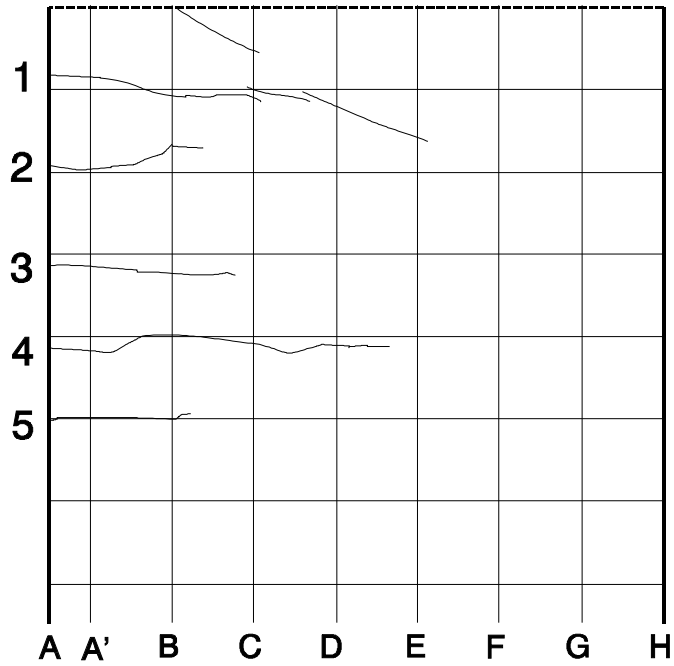

Figure 4.52 POJ-PS-100 cracking patterns on north face of pier at dead load

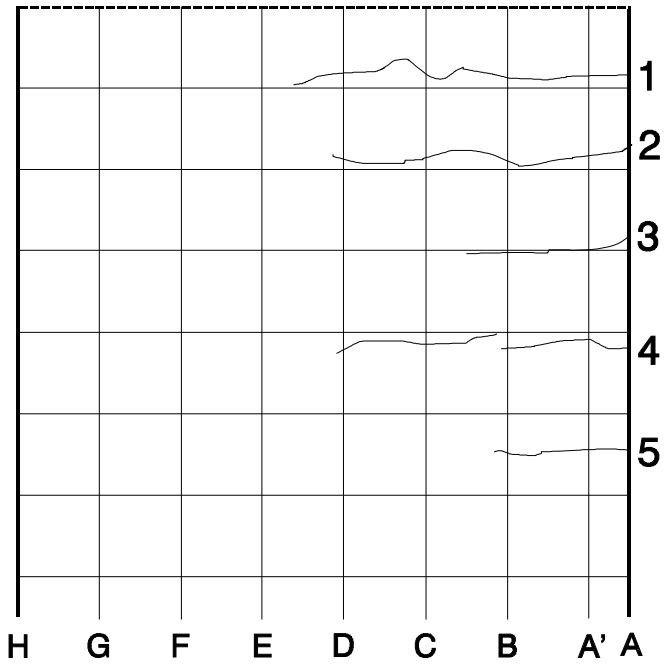

Figure 4.53 POJ-PS-100 cracking patterns on south face of pier at dead load

4.2.2.2 Applied Moment vs. Deflection Response–POJ-PS-100

Locations of the displacement transducers for the test of Specimen POJ-PS-100 are shown in Figure 4.54. Transducers labeled A (i.e., LV-75A) were located on the south side of the specimen, while transducers labeled C (i.e., LV-75C) were located on the north side of the specimen. Displacement transducers LH1, LH9, LH24, LH54, LV1 and LV29 were located along the centerline of the specimen. A steel bracket was located in the joint corner and on the north and south face of the overhang tip in order to measure displacements at points consistent with the other specimens.

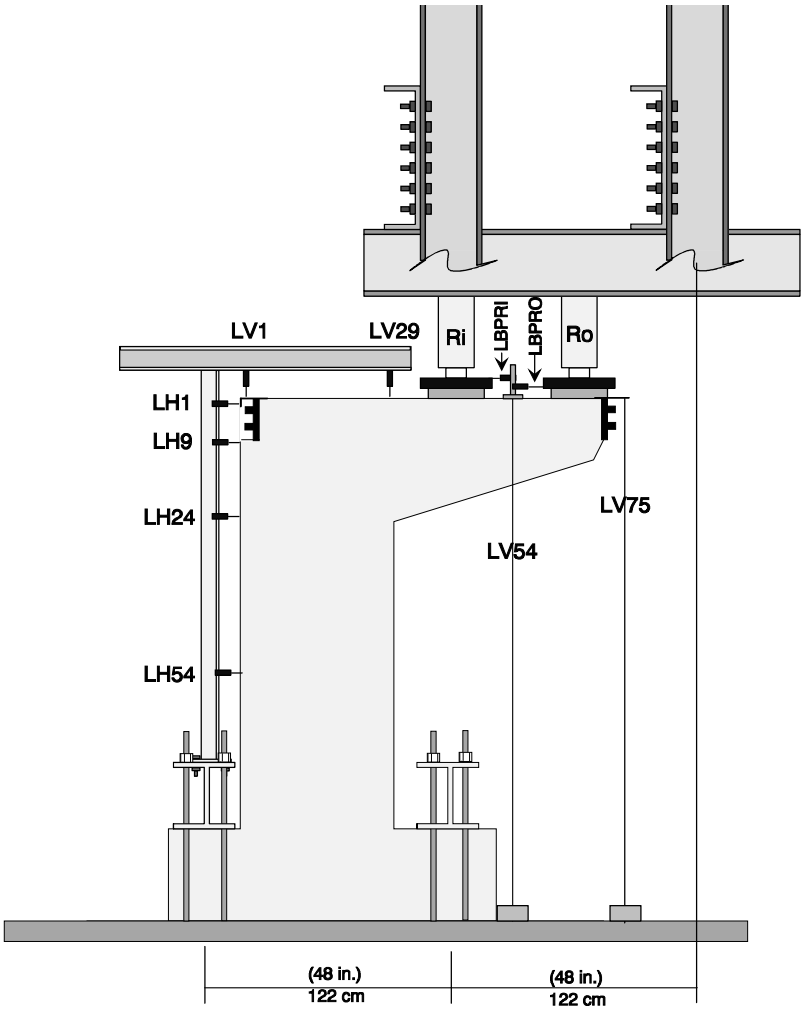

Figure 4.54 POJ-PS-100 location of displacement transducers

Plots of applied moment vs. deflection response for Specimen POJ-PS-100 are presented in Figure 4.55 through Figure 4.58. The overhang moment is plotted as a fraction of the factored moment. Displacements are labeled in both SI and customary units. As stated earlier, the plots of moment vs. deflection are a composite of the initial loading of the specimen to dead load, and the subsequent loading to failure after the repair study was completed. The overhang tip deflection near DL/2 (shown in Figure 4.54) corresponds to the displacement transducer reading at the start of the test to failure. First cracking is evident in the moment displacement plot at a moment ratio (overhang moment/factored moment) of approximately 0.3, or DL/2. A large increase in overhang tip deflection occurred under a sustained load equivalent to 0.45 times factored loads (0.89 DL) while crack widths were measured, which was an indicator that the specimen was approaching ultimate load. The specimen was loaded to dead load, crack widths were measured, applied load was sustained overnight, and crack widths were measured the following morning. Specimen POJ-PS-100 was unloaded to DL/2 to preserve the specimen for the repair study.

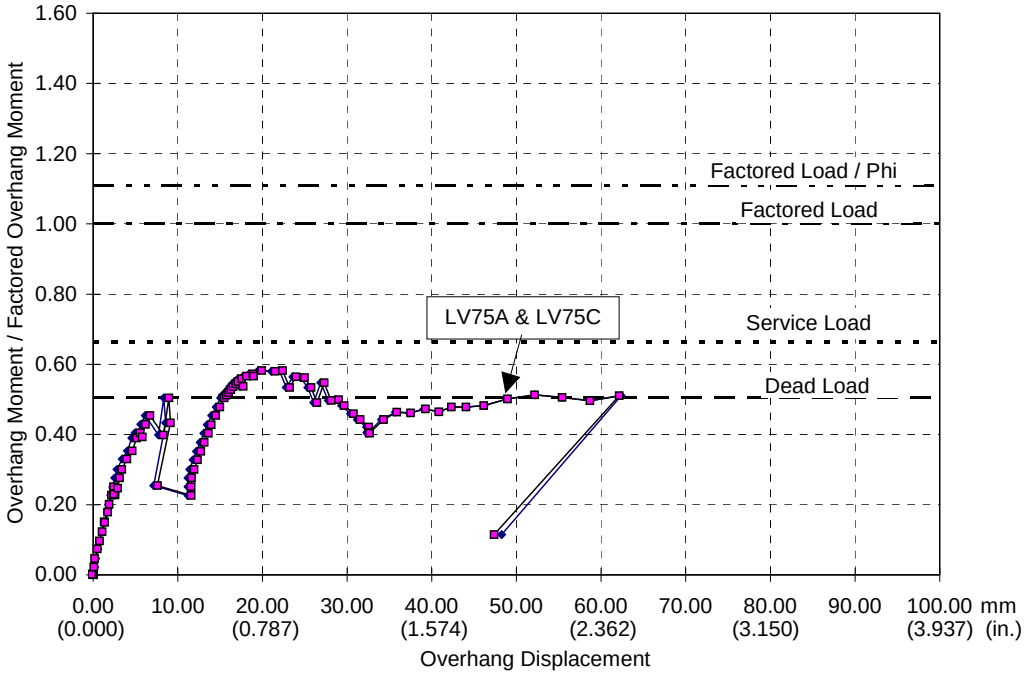

Figure 4.55 POJ-PS-100 tip deflection (LV 75)

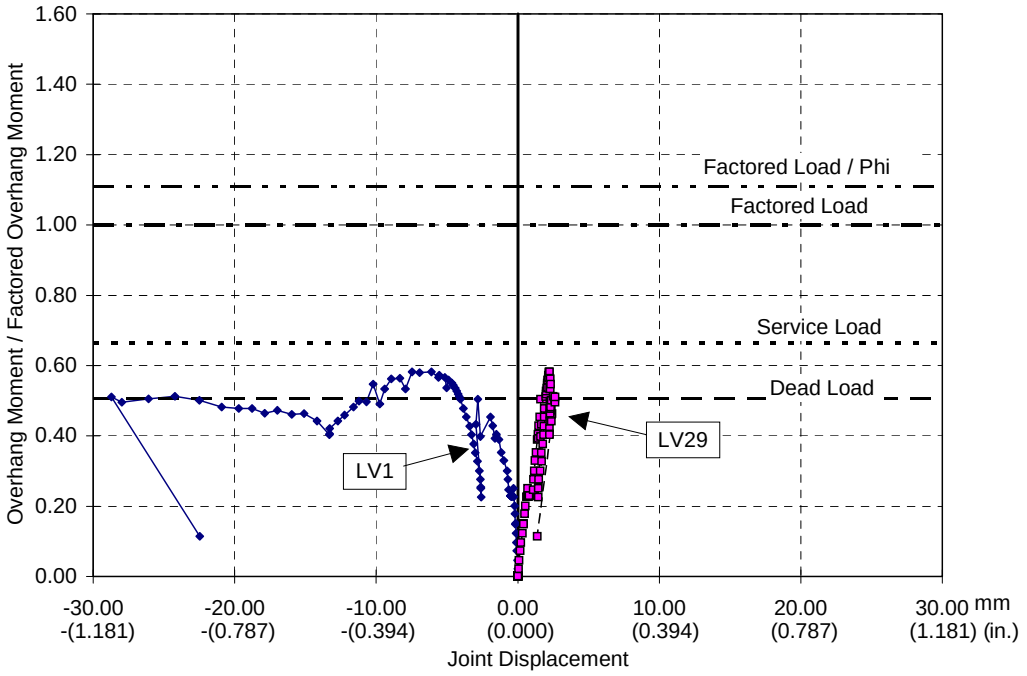

Figure 4.56 POJ-PS-100 vertical displacement of top of joint

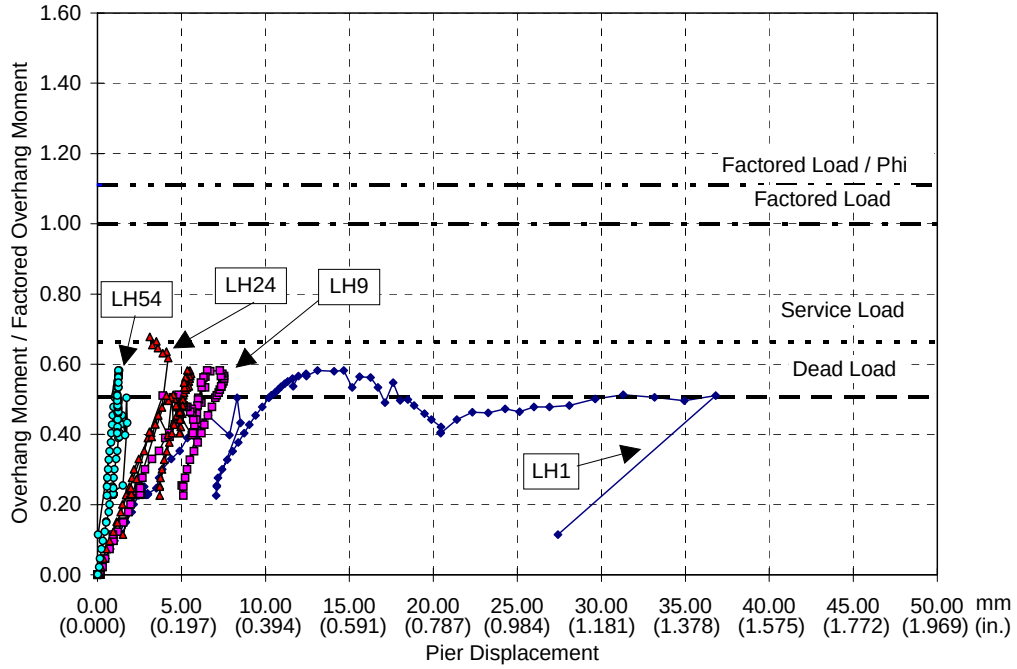

Figure 4.57 POJ-PS-100 pier horizontal deflections

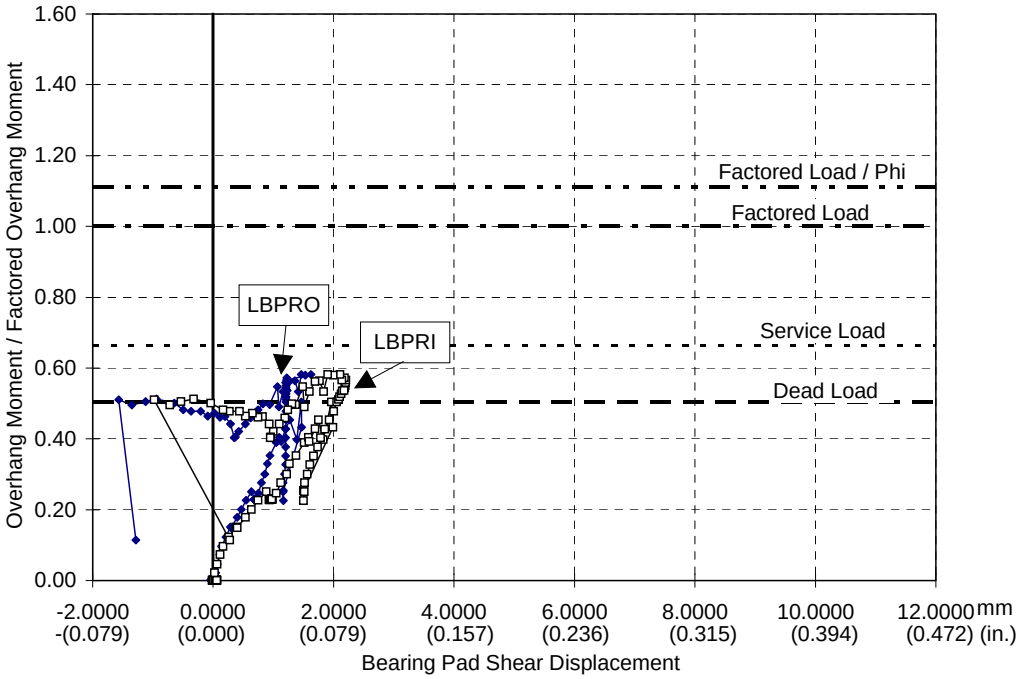

Figure 4.58 POJ-PS-100 bearing pad shear displacements

After the repair study was completed, the specimen was loaded to failure. Failure of anchorage in the joint corresponds with an applied load equivalent to 0.58 times factored load (DL+0.47LL), and occurred at a tip displacement of 20 mm (0.787 in.). The specimen was displaced incrementally, but the load remained approximately at dead load until the test was stopped due to excessive tip deflections. Displacement transducers LV1 and LH1 recorded the vertical and horizontal components of displacement associated with opening of the critical diagonal joint crack (see Figure 4.56 and Figure 4.57). Displacements measured at transducer LH9 indicated the pier unloaded elastically after

maximum applied loads were reached. Bearing pad displacements (plotted in Figure 4.58) indicated the load frame did not apply a large restraining force, which would have influenced the moment capacity of the specimen.

4.2.2.3 Location and Identification of Strain Gages–POJ-PS-100

Strain gages for Specimen POJ-PS-100 were concentrated in the joint region to measure reinforcement strains at bond failure in the joint. It was anticipated that strains in the longitudinal bars anchored in the joint would provide a measure of the bar force at failure. Computed bar forces could then be compared with the bar forces computed from the strength analysis model. Strain gage locations and labels for the joint region are presented in Figure 4.59. Overall strain gage locations and labels for strain gages located in the pier are presented in Figure 4.60. The labeling convention is the same as that described in Section 4.2.1.3.

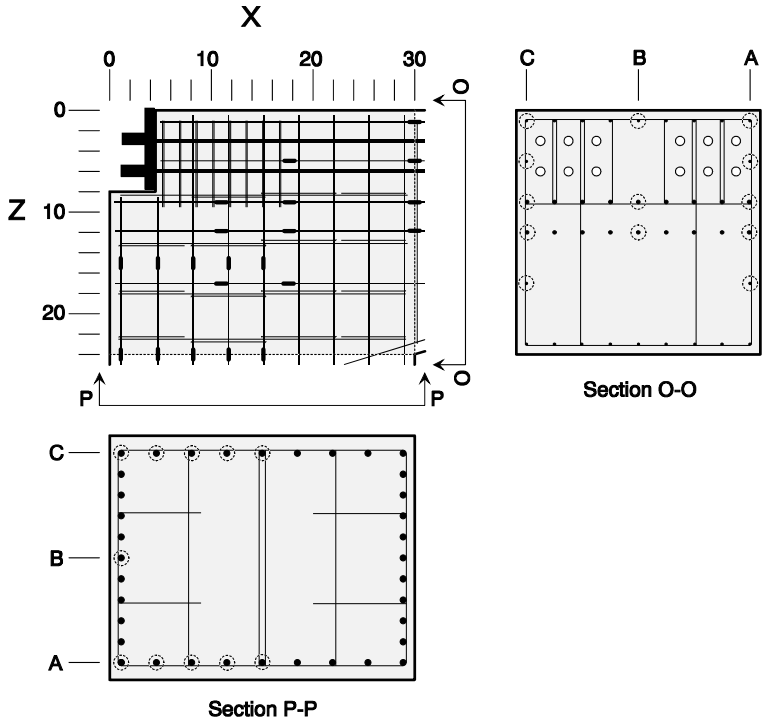

Overhang Longitudinal Reinforcement	Section X=10			Section X=17			Section X=30		
	A	B	C	A	B	C	A	B	C
Layer Z=1							T31Z1A	T31Z1B	T31Z1C
Layer Z=5				T17Z3A			T31Z5A		
Layer Z=9	T10Z9A	T10Z9B	T10Z9C	T17Z9A	T17Z9B	T17Z9C	T31Z9A	T31Z9B	T31Z9C
Layer Z=12	T10Z12A	T10Z12B	T10Z12C	T17Z12A	T17Z12B	T17Z12C	T31Z12A	T31Z12B	T31Z12C
Layer Z=17	T10Z17A			T17Z17A					

Pier Longitudinal Reinforcement	Section Z=12			Section Z=24		
	A	B	C	A	B	C
Layer X=1	C1Z12A	C1Z12B	C1Z12C	C1Z24A	C1Z24B	C1Z24C
Layer X=5	C5Z12A		C5Z12C	C5Z24A		C5Z24C
Layer X=8	C8Z12A		C8Z12C	C8Z24A		C8Z24C
Layer X=11	C11Z12A		C11Z12C	C11Z24A		C11Z24C
Layer X=15	C15Z12A		C15Z12C	C15Z24A		C15Z24C

Figure 4.59 POJ-PS-100 joint strain gage locations and labels

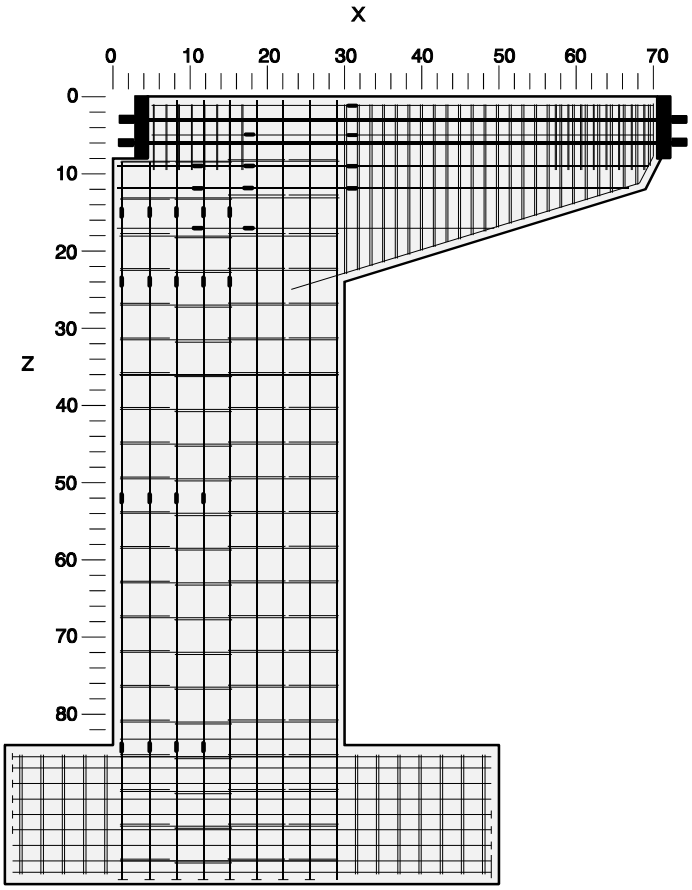

Pier Longitudinal Reinforcement	Section Z=54			Section Z=84		
	A	**B**	**C**	**A**	**B**	**C**
Layer X=1	C1Z54A	C1Z54B	C1Z54C	C1Z83A	C1Z83B	C1Z83C
Layer X=5	C5Z54A		C5Z54C	C5Z83A		C5Z83C
Layer X=8	C8Z54A		C8Z54C	C8Z83A		C8Z83C
Layer X=11	C11Z54A		C11Z54C	C11Z83A		C11Z83C

Figure 4.60 POJ-PS-100 overall strain gage locations and pier strain gage labels

Strain gages were attached to the overhang Dywidag post-tensioning bars before the bars were inserted into the reinforcing cage (prior to casting). After the stressing operation was completed, none of the gages attached to the post-tensioning bars were functional.

4.2.2.4 Applied Moment vs. Strain Response–POJ-PS-100

The applied moment vs. strain plots for Specimen POJ-PS-100 include responses measured with strain gages attached to longitudinal overhang reinforcement (Figure 4.61 through Figure 4.63) and longitudinal pier reinforcement (Figure 4.64 through Figure 4.65). Strain gages indicated abrupt changes in strain when cracking occurred in the vicinity of the gages. It should be noted that strain gage responses are presented for the first test of the specimen only up to dead load because strain gages were no longer functioning after the repair study was completed.

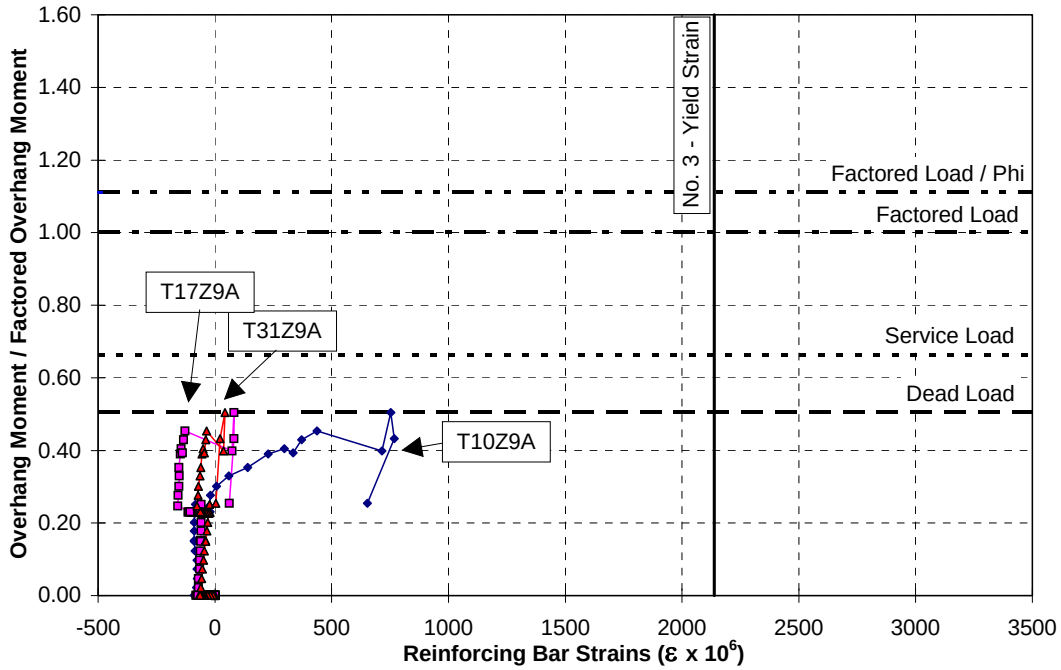

Figure 4.61 POJ-PS-100 strains in secondary overhang reinforcement at Layer Z=9

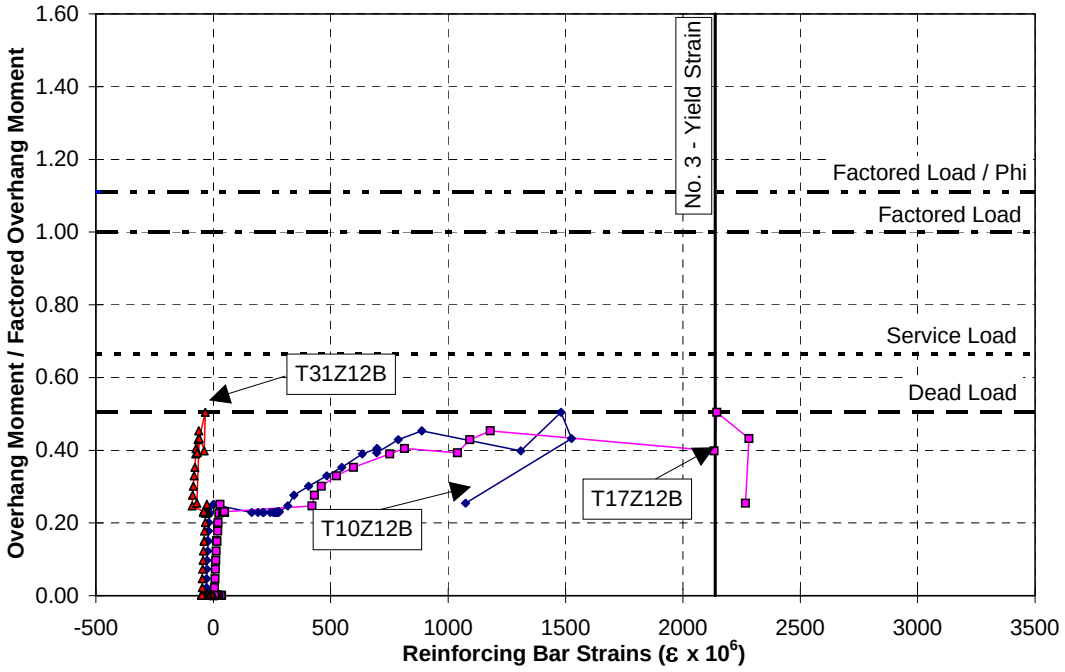

Figure 4.62 POJ-PS-100 strains in secondary overhang reinforcement at Layer Z=12

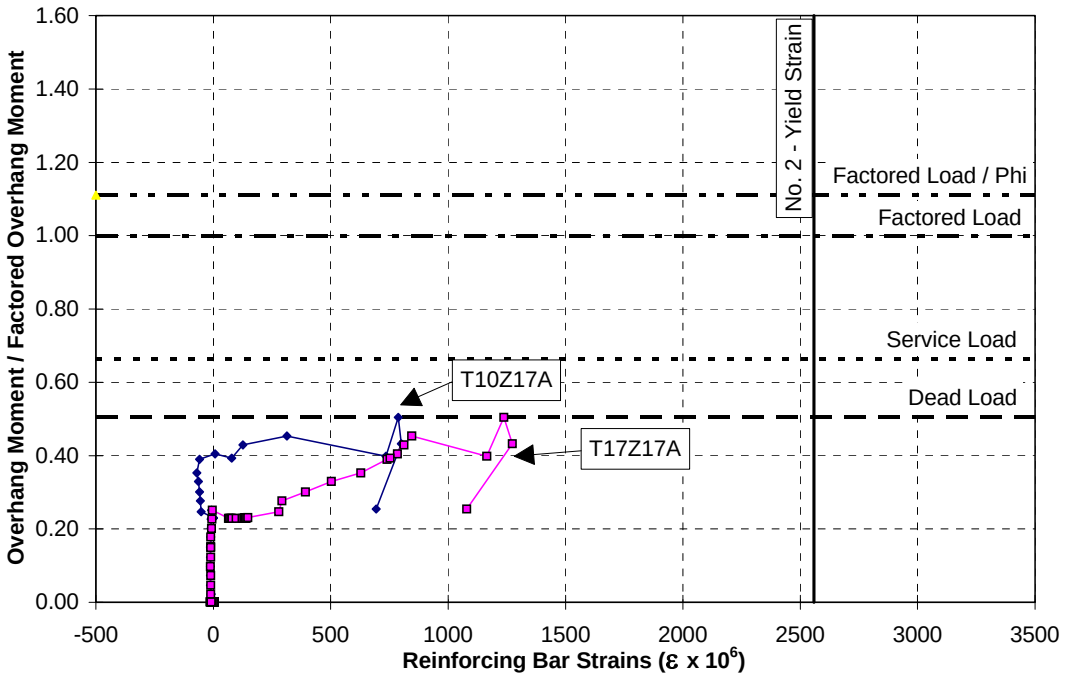

Figure 4.63 POJ-PS-100 strains in secondary overhang reinforcement at Layer Z=17

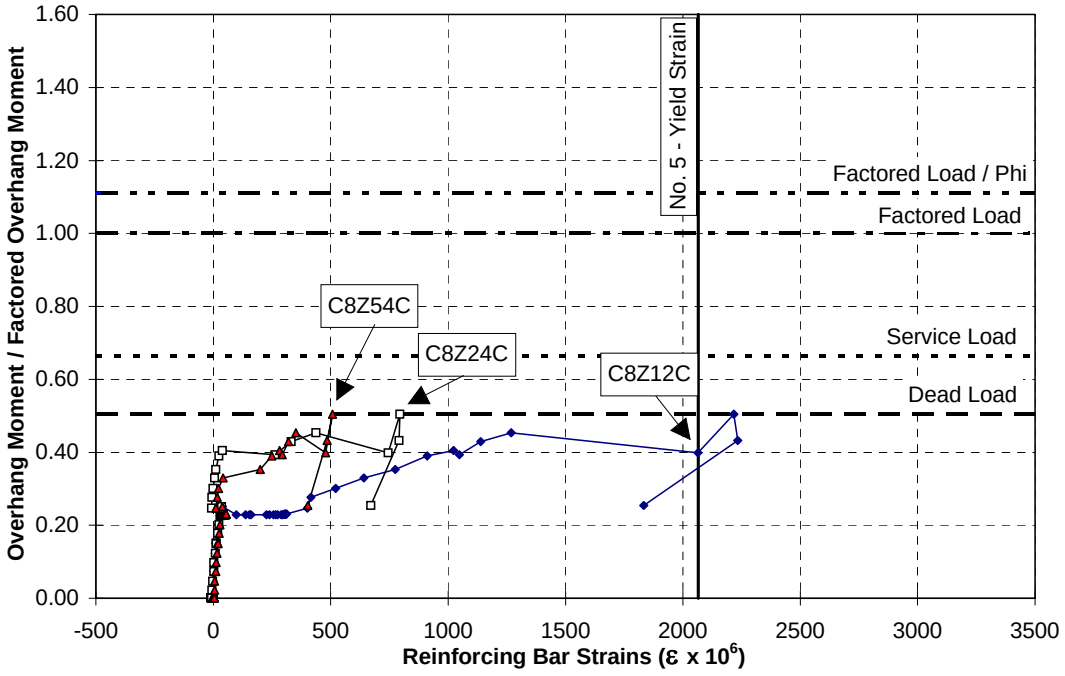

Figure 4.64 POJ-PS-100 strains in pier longitudinal reinforcement at Layer X=8

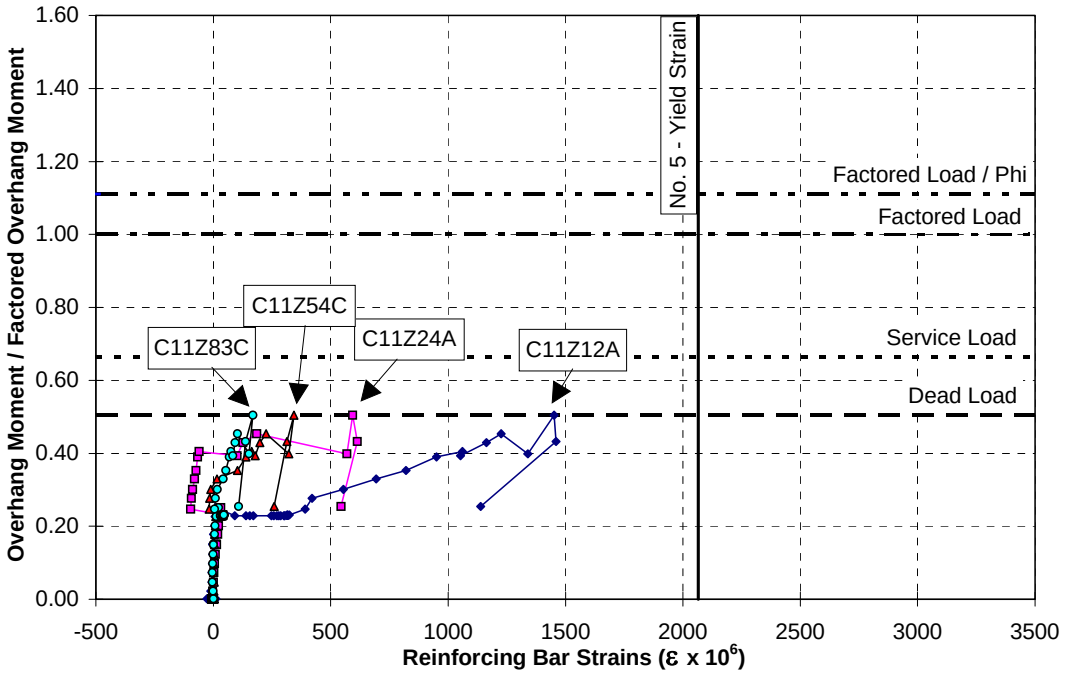

Figure 4.65 POJ-PS-100 strains in pier longitudinal reinforcement at Layer X=11

Strain gages concentrated in the joint region confirmed early cracking at a moment ratio (overhang moment/factored moment) of 0.25, or ½ DL. Strains measured in the longitudinal overhang reinforcement at layer Z=12 (12 inches from the top surface) indicated shear friction reinforcement yielded as crack widths were measured at load step 18, as shown in Figure 4.62. Gages located at layer Z=9 and layer Z=17 of the longitudinal overhang reinforcement (9 and 17 inches from the top surface, respectively) had large increases in strain with small increases in applied load, as shown in Figure 4.61 and Figure 4.63, respectively, but the measured strains were less than 50% of yield.

Measured strains in the pier longitudinal reinforcement indicated layers X=1 and X=5 did not contribute to the capacity of the joint. Measured strains in the pier longitudinal reinforcement at layers X=8, 11, and 15 increased significantly after ½DL. Strain measurements for gage C8Z12C located at the critical diagonal joint crack (plotted in Figure 4.64) indicated the No. 5 longitudinal reinforcement yielded during load step 19 (after crack widths were measured). Strain measurements for gage C11Z12A (plotted in Figure 4.65) were nearly 70% of yield at dead load.

4.2.2.5 Strain Profiles for the Pier at Various Cross Sections–POJ-PS-100

Strain profiles over the depth (in positive X direction) of the pier for cross sections located 12 inches, 24 inches, and 54 inches from the top surface of the joint are illustrated in Figure 4.66 through Figure 4.68, respectively. As before, the strain profiles were developed by averaging the strains for gages at the same layer (*i.e.*, strain readings for gages C5Z12A and C5Z12C). Strain profiles are presented for one-half dead load (DL/2), three-quarters dead load (¾DL), and dead load, where applied dead load is equivalent to the weight of the superstructure. The strain profile through cross section Z=12 (shown in Figure 4.66) confirms the supposition that the longitudinal pier reinforcement at layers X=1 and X=5 did not contribute to the joint capacity. Pier longitudinal reinforcement at layers X=8, 12, and 15 had sufficient bar anchorage beyond the critical diagonal joint crack to fully develop. Strain profiles through cross section Z=24 illustrate the increase in strain for gages on the X=1 and 5 layers of pier longitudinal reinforcement as crack 3 on the north face and crack 4 on the south face of the specimen developed at load step 16. Cross-section Z=54, located 54 inches from the top surface of the joint, exhibited strain profiles and peak strains similar to those from Specimen POJ-RC-100.

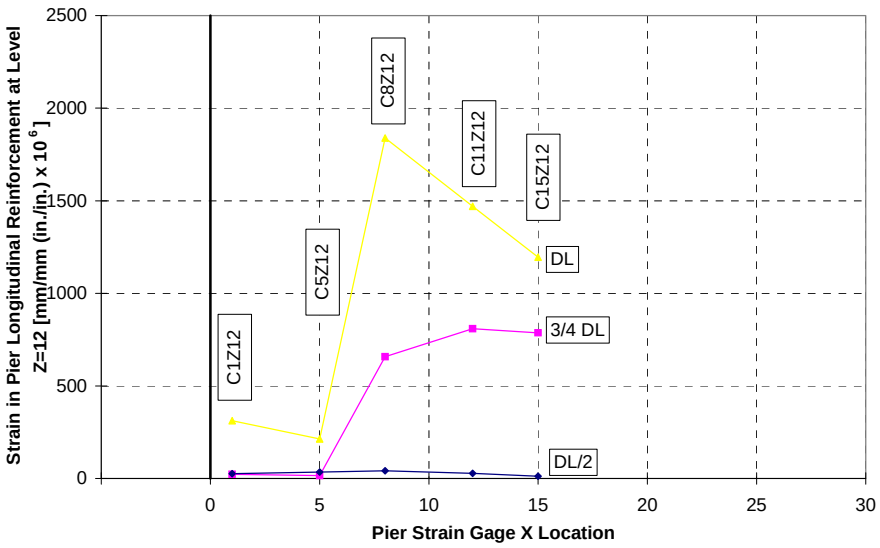

Figure 4.66 POJ-PS-100 strain profiles in pier at Section Z=12

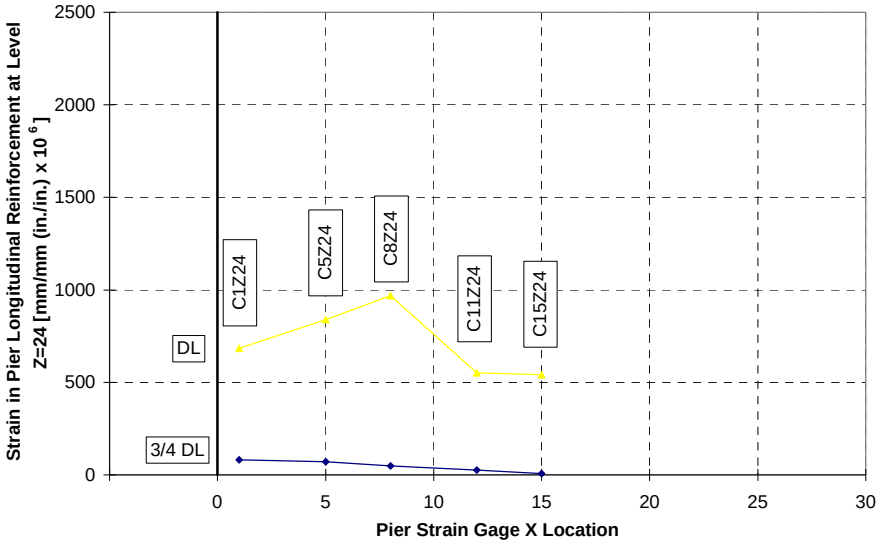

Figure 4.67 POJ-PS-100 strain profiles in pier at Section Z=24

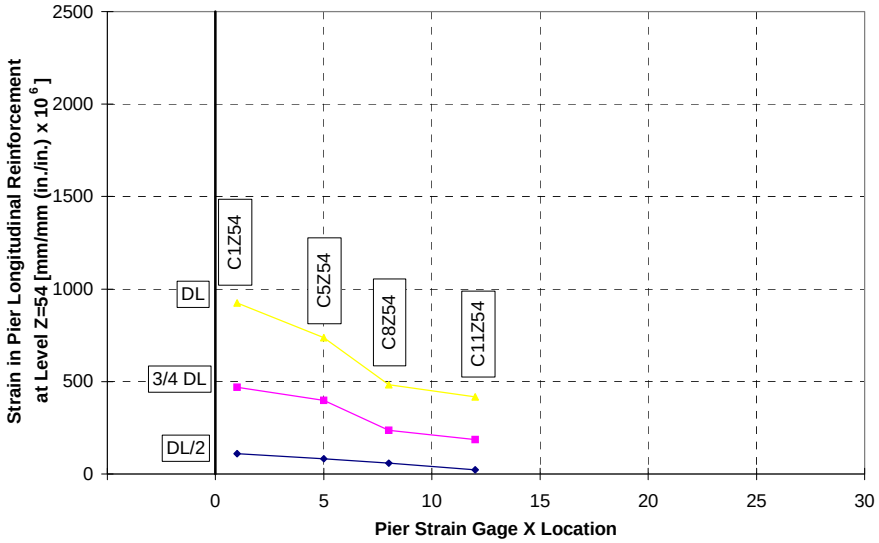

Figure 4.68 POJ-PS-100 strain profiles in pier at Section Z=54

4.3 INTEGRATED DESIGN METHOD POJ TEST SPECIMENS

4.3.1 Reinforced Concrete Design with T-Headed Bars–POJ-RC-100-TH

Specimen POJ-RC-100-TH utilized the integrated strut-and-tie design method (detailed in Chapter 3) to proportion and locate tensile reinforcement. The purpose of the test was to verify factored load resistance and service-level crack-width performance of POJ-RC-100-TH. Reinforcing details for POJ-RC-100-TH are presented in Figure 4.69.

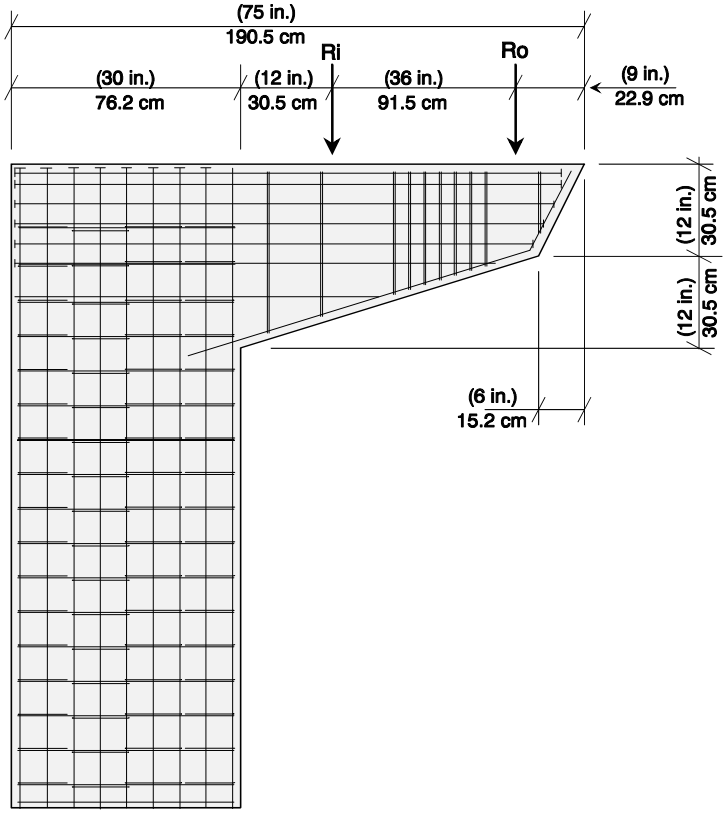

Figure 4.69 POJ-RC-100-TH reinforcing details

An important feature of the specimen was the use of T-headed longitudinal reinforcement in the overhang and pier that extended to the exterior corner of the joint (see Figure 4.70). The strut-and-tie model indicated the tensile force path from the overhang, through the joint, and into the pier was continuous. In order to provide a continuous force path, the tensile forces from the primary longitudinal reinforcement in the overhang (the top two layers of mild steel reinforcement) needed to be transferred into the pier longitudinal reinforcement. The T-heads for the longitudinal pier reinforcement were placed on top of the overhang longitudinal reinforcement (shown in Figure 4.70) to form a node which was used to develop a diagonal compression strut in the joint. When tensile stresses in the joint exceeded the concrete tensile strength, the interlocked heads prevented a tensile crack from propagating fully to the corner of the joint.

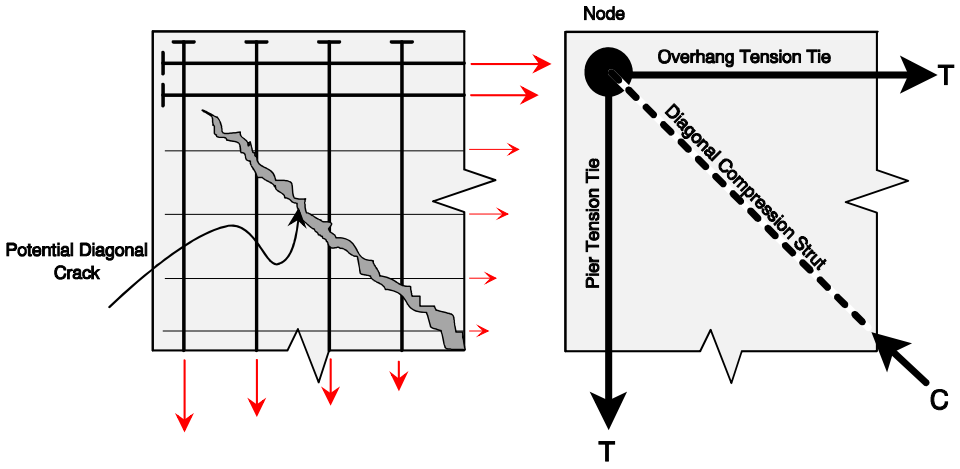

Figure 4.70 POJ-RC-100-TH joint corner detail

After Specimen POJ-RC-100-TH was cast and installed in the testing frame, the testing required eight days to complete. The specimen was loaded incrementally and examined every other load step for cracks. The first visible cracks in the overhang and joint were found at load step 9. Applied load was maintained while the crack widths were measured. Applied load was increased in steps to load step 12, at which time cracks on the south face of the pier were identified. Cracks on the north face of the pier were not visible until dead load was applied. All visible cracks from the different areas were measured and recorded at applied loads equivalent to ¾ Dead Load and Dead Load of the superstructure. A significant diagonal crack developed in the joint at an applied load equivalent to DL+0.14LL (load step 22), but it did not propagate into the corner where the interlocked T-headed bars formed a compression node. Applied load on the specimen was increased incrementally to DL+½LL and DL+LL (Service Load), at which point crack widths were measured. After measuring crack widths at DL+LL, the applied load was reduced to a load equivalent to Dead Load of the superstructure. At Dead Load, the reduction of crack widths was determined by measuring the crack widths. Crack widths were again measured at DL+½LL and DL+LL, and applied load was incrementally increased to DL+2LL, where crack widths were measured and recorded for the last time.

After cracks were measured at DL+2LL, applied loads on Specimen POJ-RC-100-TH were increased incrementally to a load equivalent to applied Factored Load. Cracking patterns on the north and south faces of the specimen were marked on the specimen (north face shown in Figure 4.71) and recorded on a pencil sketch of the specimen. Growth of the major joint crack was noted during loading, but further crack measurements were not taken.

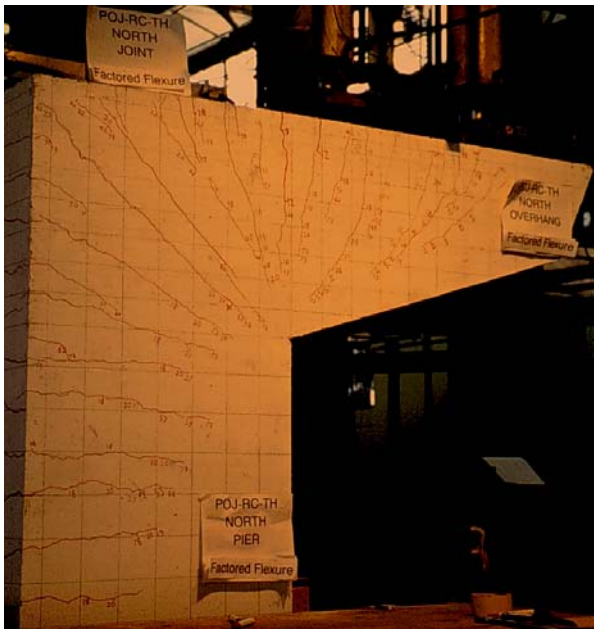

Figure 4.71 POJ-RC-100-TH photograph of cracking pattern on north face of specimen at factored load

At an applied load equivalent to DL+5LL, spalling of the side-face concrete in the joint was noted. Maximum applied load for Specimen POJ-RC-100-TH (shown in Figure 4.72) was equivalent to DL+6LL (1.47 Factored Load), after which point a sharp drop in load and significant increase in tip displacement was recorded. After examining the joint, it was determined the extensive spalling of the side-face concrete had reduced the effectiveness of the headed bars located in the joint corner (shown in Figure 4.73). With the loss of bar anchorage, the recorded load continued to reduce with increased overhang tip deflection. Specimen POJ-RC-100-TH was loaded to a maximum tip displacement of 87 mm (3.42 in.) which corresponds with an applied load equivalent to DL+2LL. Applied load on the specimen was removed in steps, and a large residual tip displacement was noted. After the test was completed, the spalled, side-face concrete was removed to provide a view of the crumbled concrete inside the joint and the placement of the headed bars (shown in Figure 4.74).

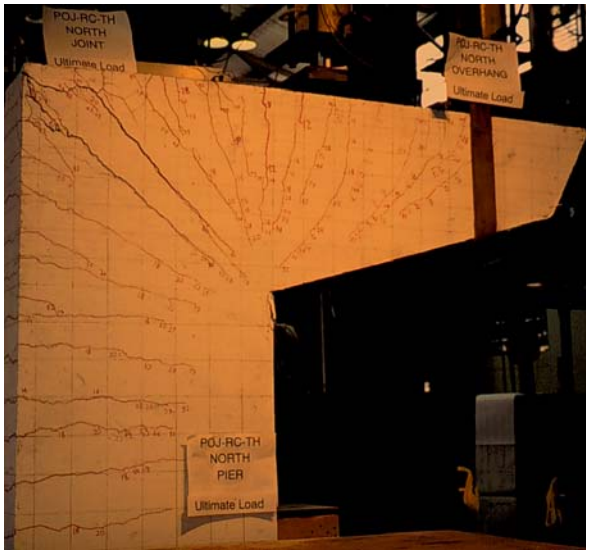

Figure 4.72 POJ-RC-100-TH photograph of cracking pattern on north face of specimen at ultimate load

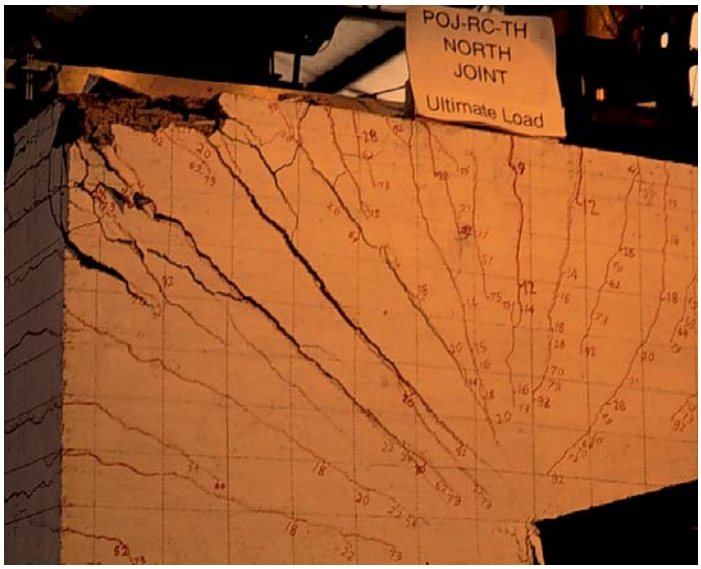

Figure 4.73 POJ-RC-100-TH photograph of concrete spalling in joint region at end of test

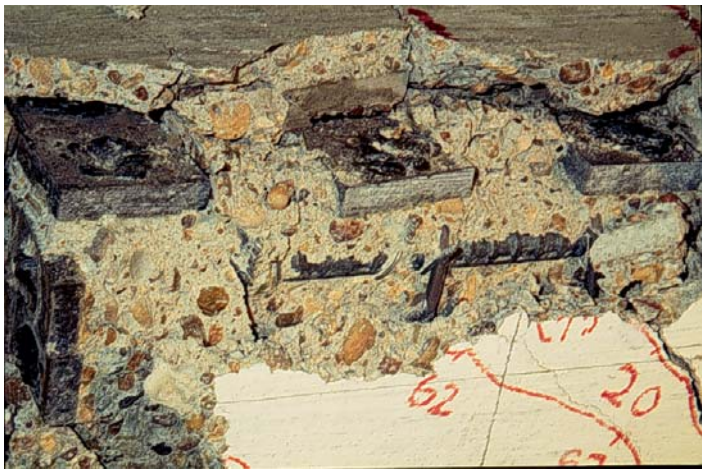

Figure 4.74 POJ-RC-100-TH photograph of exposed headed bars after concrete spalled in joint region

4.3.1.1 Cracking Patterns and Maximum Crack-Width Measurements–POJ-RC-100-TH

Cracking patterns and maximum measured crack widths for the north and south faces of Specimen POJ-RC-100-TH are presented in the following section. Overall cracking patterns at dead load for the north and south faces of the specimen (presented in Figure 4.75 and Figure 4.76, respectively) and cracking patterns at service load (presented in Figure 4.77 and Figure 4.78, respectively) are similar to those recorded for Specimen POJ-RC-100 (Figures 4.1 through 4.4, respectively). The critical diagonal crack in the joint associated with failure of the specimen is identified with heavy lines in Figure 4.79 and Figure 4.80 (joint crack (9) in Figure 4.79 and joint crack (10) in Figure 4.80).

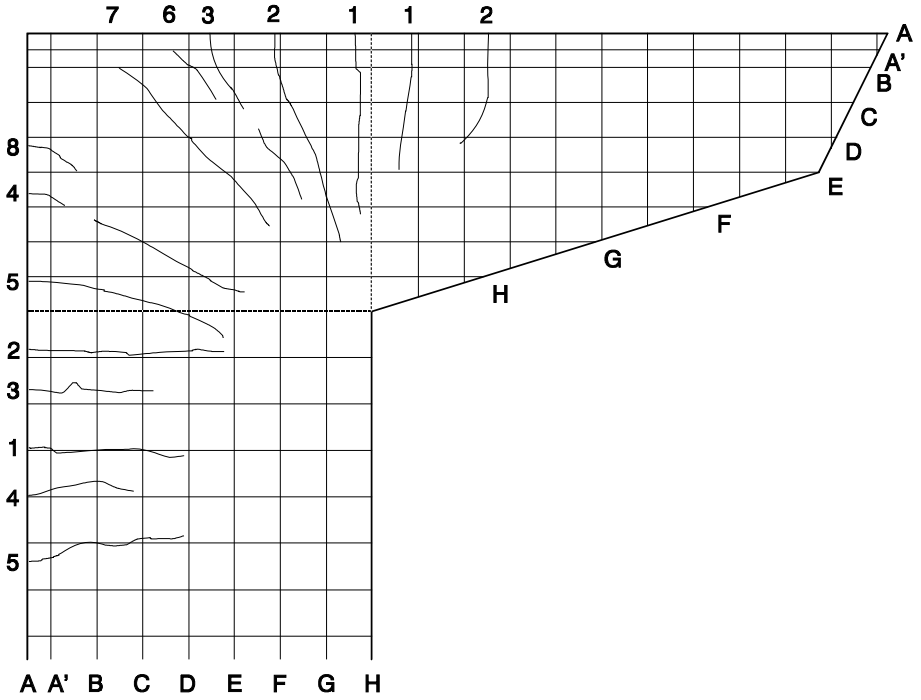

Figure 4.75 POJ-RC-100-TH cracking pattern on north face of specimen at dead load

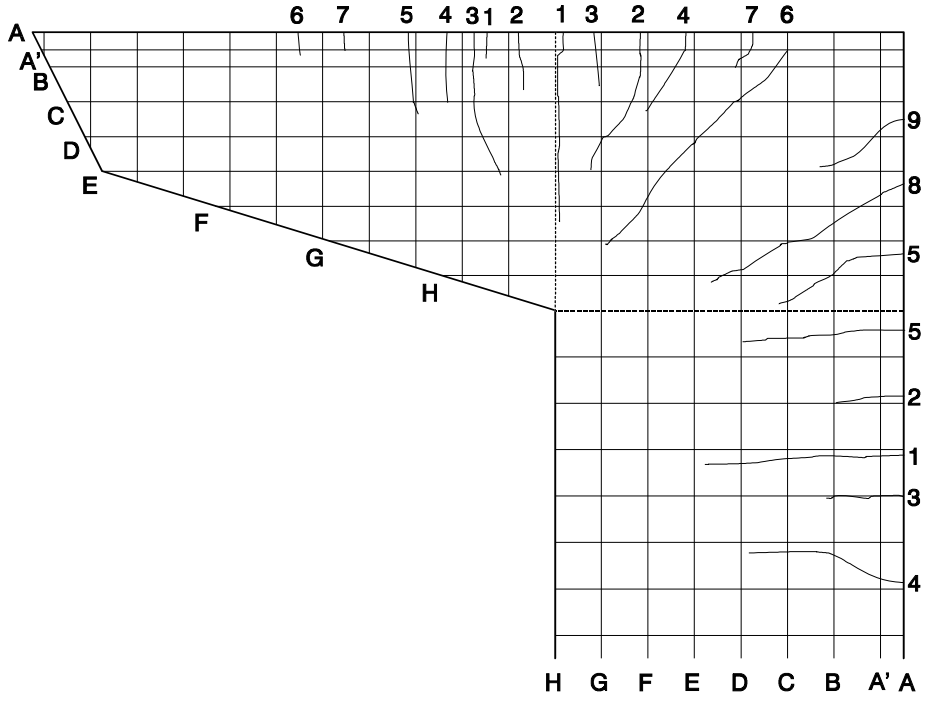

Figure 4.76 POJ-RC-100-TH cracking pattern on south face of specimen at dead load

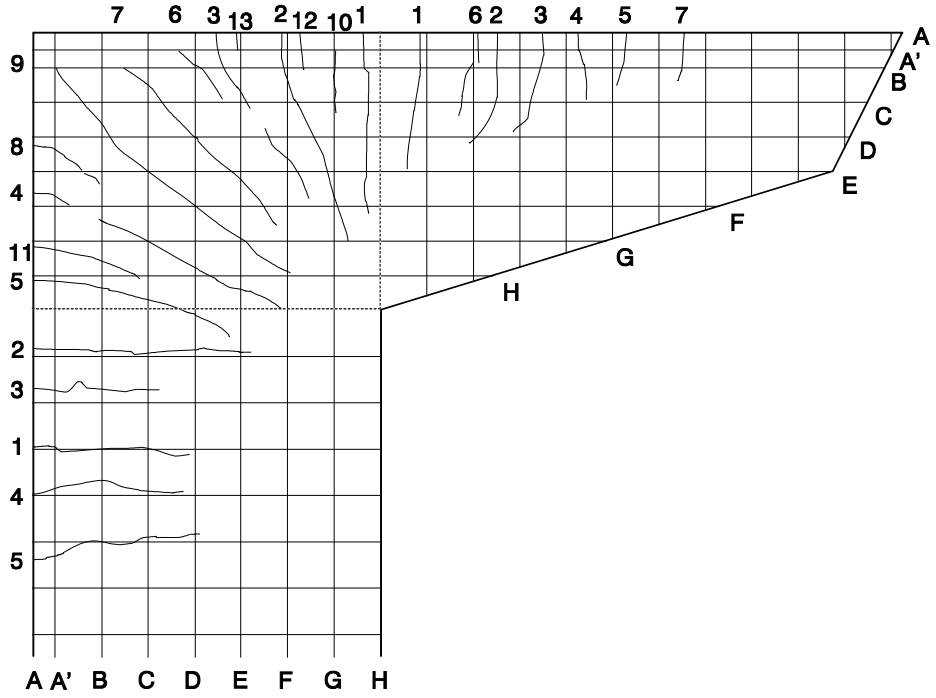

Figure 4.77 POJ-RC-100-TH cracking pattern on north face of specimen at service load

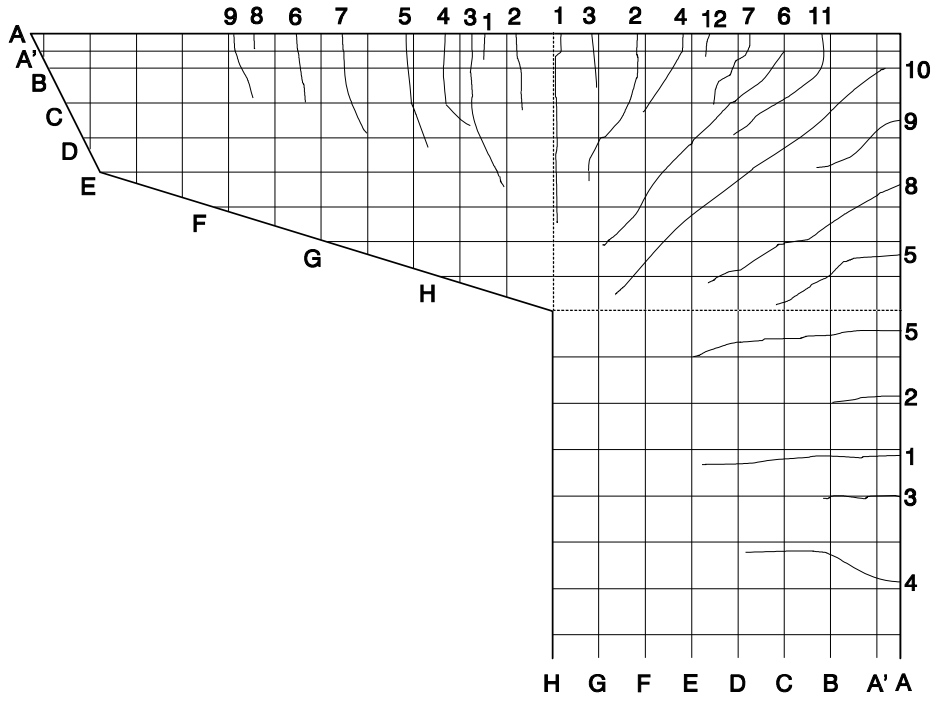

Figure 4.78 POJ-RC-100-TH cracking pattern on south face of specimen at service load

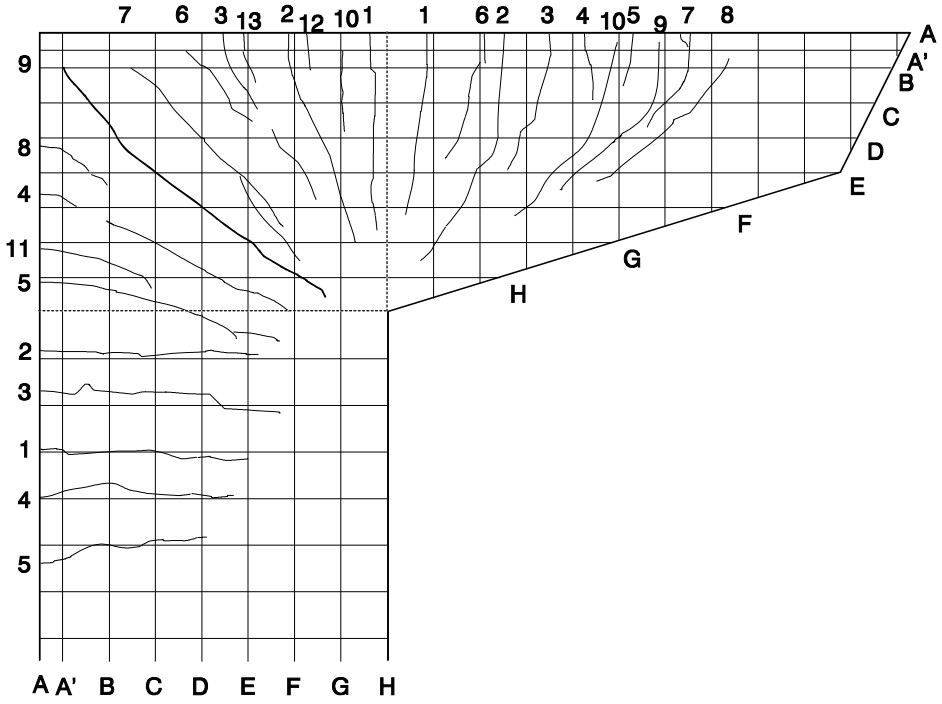

Figure 4.79 POJ-RC-100-TH cracking pattern on north face of specimen at failure

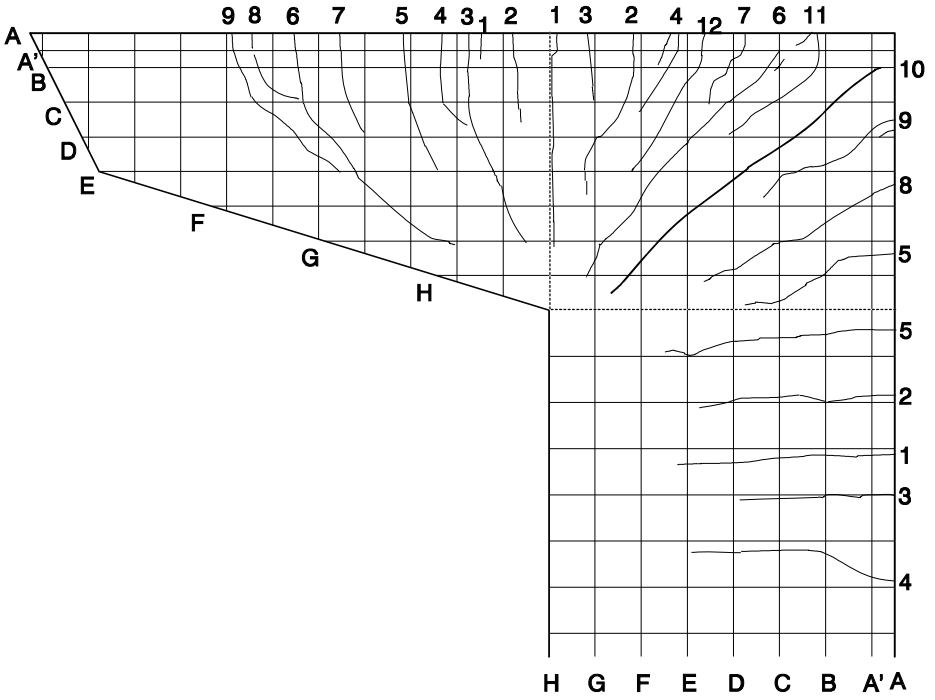

Figure 4.80 POJ-RC-100-TH cracking pattern on south face of specimen at failure

Discussion of maximum measured crack widths for Specimen POJ-RC-100-TH is divided into evaluation of cracking in the component elements: overhang, joint, and pier, respectively.

Cracking patterns at dead load for the north and south faces of the overhang are presented in Figure 4.81 and Figure 4.83, respectively, and cracking patterns in the overhang at service load are presented in Figure 4.82 and Figure 4.84, respectively. Maximum measured crack widths for the north face of

the overhang are presented in Table A.21 and Table A.22, in SI and customary units, respectively, and Table A.23 and Table A.24, in SI and customary units, respectively, for the south face of the overhang. Crack widths in the overhang, in general were well controlled, but crack (1) at level A on the north face of the overhang (shown in Table A.21 and Table A.22) proved to be the largest crack in the overhang. This crack formed at load step (9), and at DL+½LL the measured crack width was 0.18 mm (0.0070 in.), which was greater than the acceptable crack width of 0.14 mm (0.0055 in.). It should be noted that the measured crack width remained constant with increased applied load, to a load equivalent to DL+2LL. The next largest crack width was crack (2) on the south face of the overhang, which had a measured maximum crack width of 0.13 mm (0.0050 in.), which was within the acceptable crack size limit.

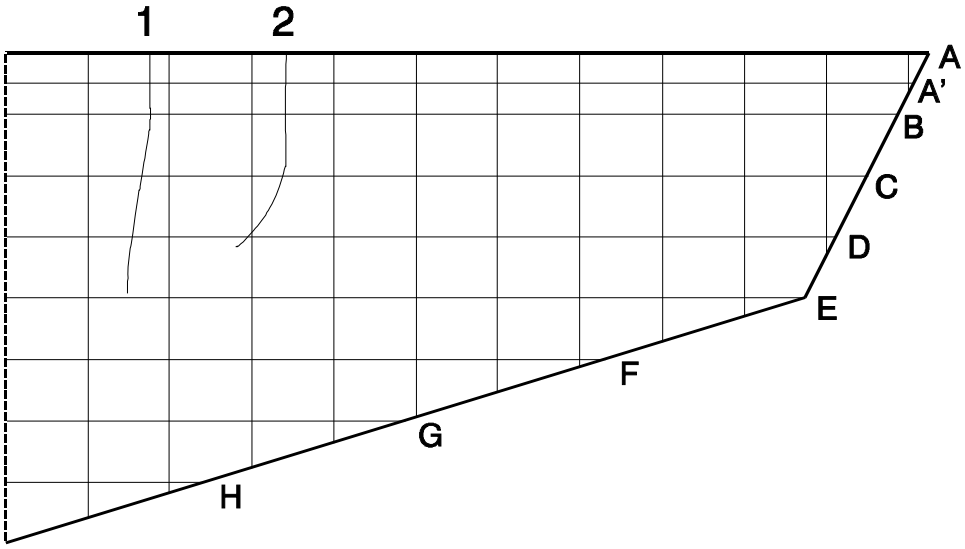

Figure 4.81 POJ-RC-100-TH cracking pattern on north face of overhang at dead load

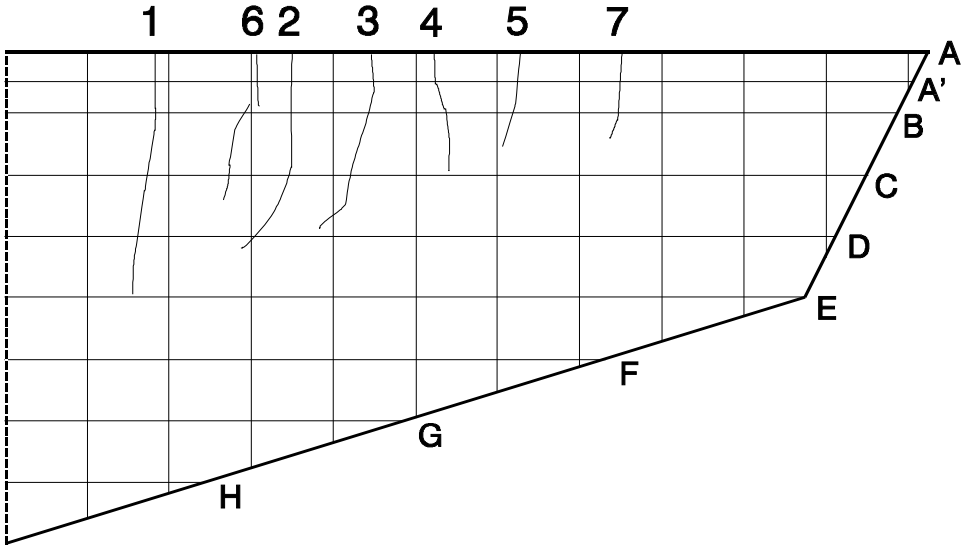

Figure 4.82 POJ-RC-100-TH cracking pattern on north face of overhang at service load

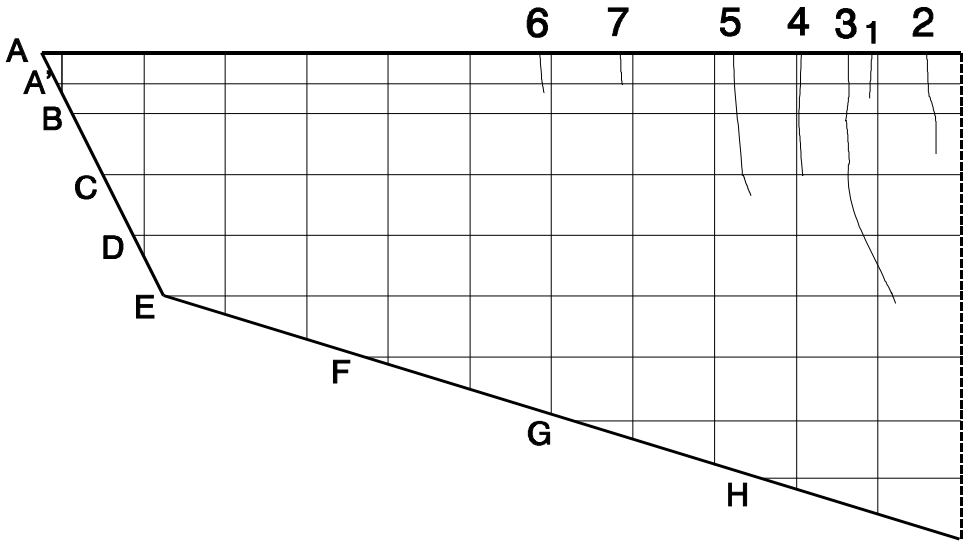

Figure 4.83 POJ-RC-100-TH cracking pattern on south face of overhang at dead load

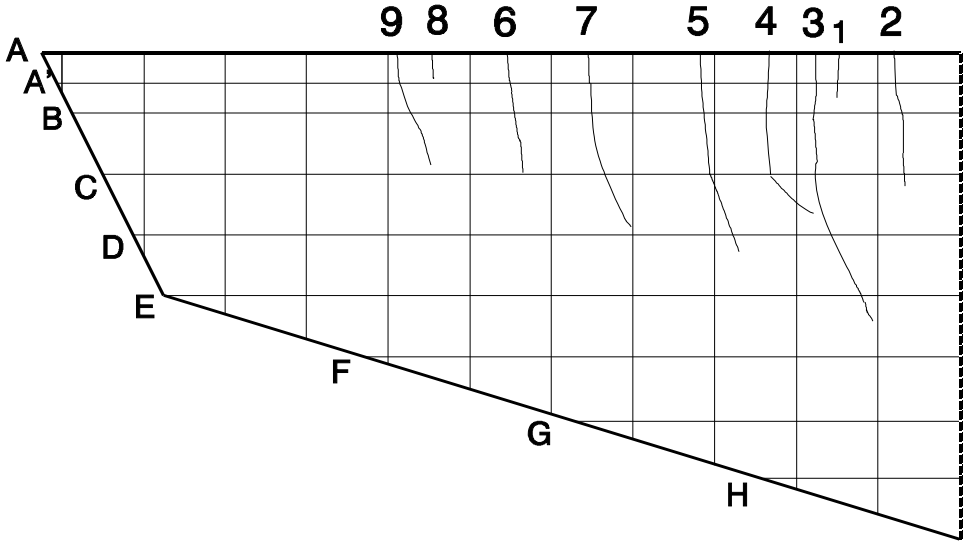

Figure 4.84 POJ-RC-100-TH cracking pattern on south face of overhang at service load

Cracking patterns at dead load for the north and south faces of the joint are presented in Figure 4.85 and Figure 4.87, respectively, and cracking patterns in the overhang at service load are presented in Figure 4.86 and Figure 4.88, respectively. Maximum measured crack widths for the north face of the joint are presented in Table A.25 and Table A.26, in SI and customary units, respectively, and Table A.27 and Table A.28, in SI and customary units, respectively, for the south face of the joint. The joint cracks were well distributed over the joint region, but the main diagonal joint cracks, crack (9) on the north face and crack (10) on the south face of the joint, each with a crack width of 0.28 mm (0.011 in.) at grid level C, were much larger than the acceptable crack width of 0.14 mm (0.0055 in.). As stated earlier, a diagonal joint crack was anticipated because of the large principal tensile stresses in the joint, but additional side face reinforcement was not provided to limit crack widths in order to test the T-headed bar corner detail. A revised design that introduced short T-Headed bars, oriented perpendicular to the diagonal joint crack, would have controlled crack widths in the joint. Further discussion of this detail is presented in Chapter 5.

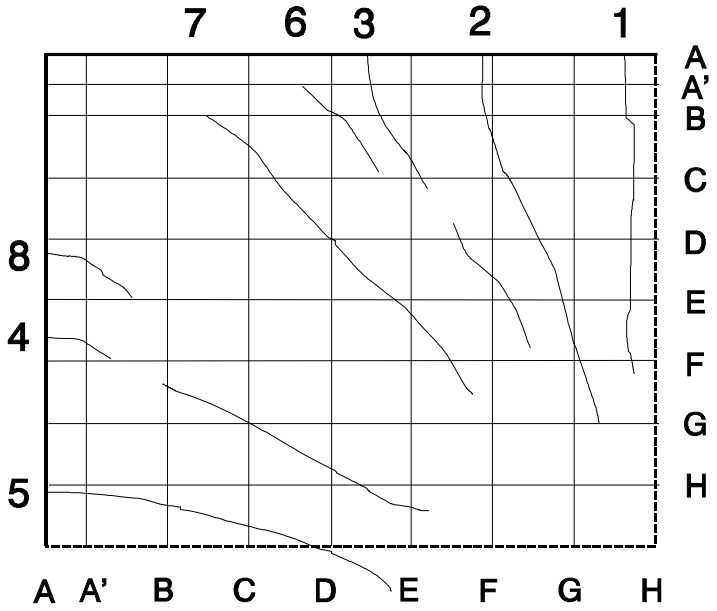

Figure 4.85 POJ-RC-100-TH cracking pattern on north face of joint at dead load

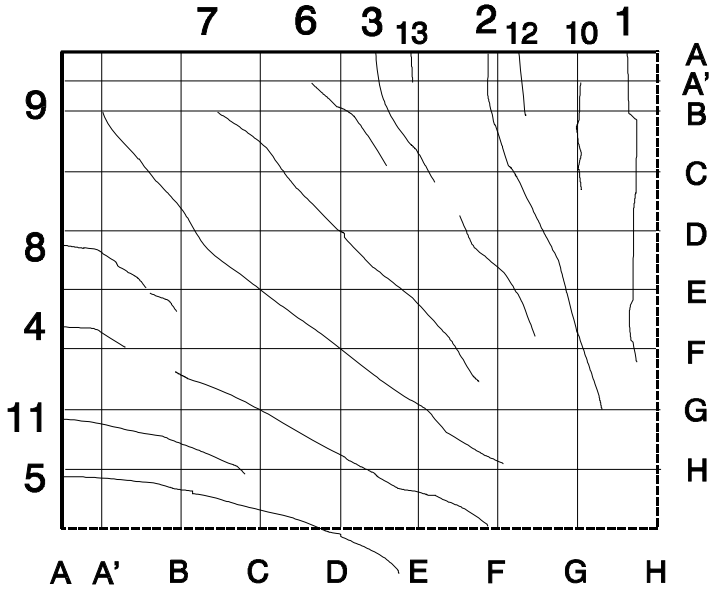

Figure 4.86 POJ-RC-100-TH cracking pattern on north face of joint at service load

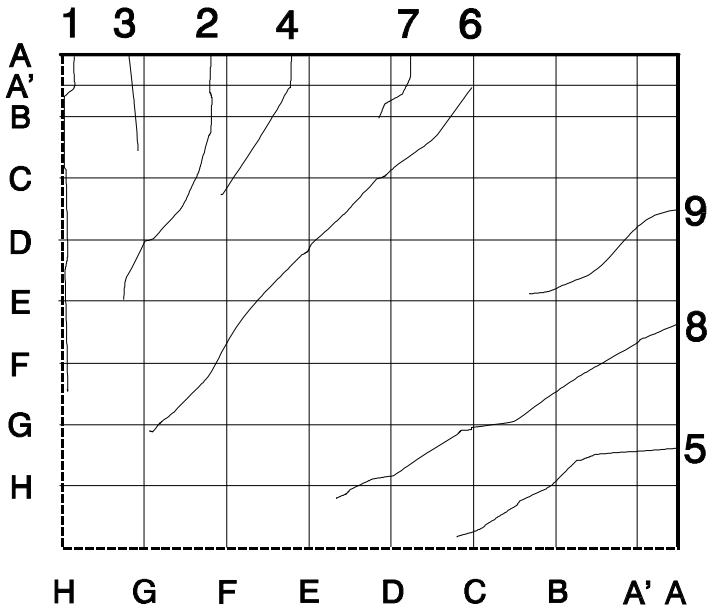

Figure 4.87 POJ-RC-100-TH cracking pattern on south face of joint at dead load

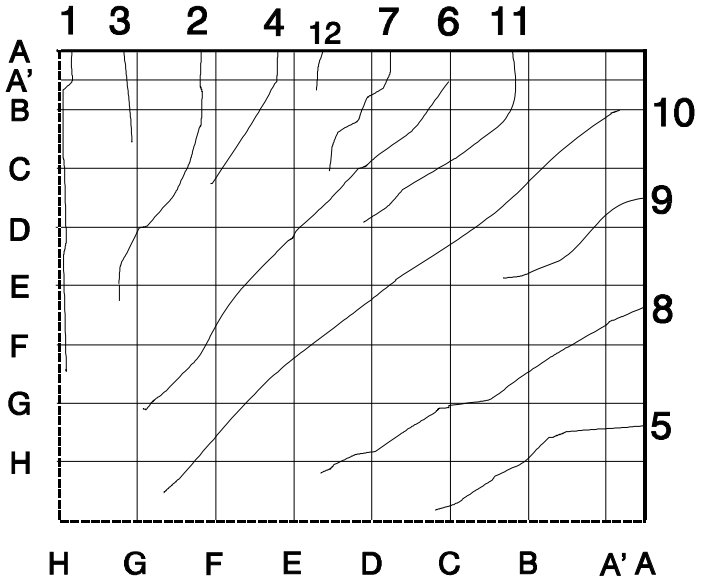

Figure 4.88 POJ-RC-100-TH cracking pattern on south face of joint at service load

Cracking patterns at dead load for the north and south faces of the pier are presented in Figure 4.89 and Figure 4.91, respectively, and cracking patterns in the overhang at service load are presented in Figure 4.90 and Figure 4.92, respectively. Maximum measured crack widths for the north face of the joint are presented in Table A.29 and Table A.30, in SI and customary units, respectively, and Table A.31 and Table A.32, in SI and customary units respectively, for the south face of the joint. The pier design was identical to the previous models to verify the effects of T-headed bars in the joint corner, and the pier region exhibited the same cracking behavior as the POJ-RC-100 and POJ-PS-100 test specimens. Crack (5) on the north side and cracks (2, 3, and 4) on the south side had maximum crack

widths larger than the acceptable crack width. The integrated design method would have replaced the pier longitudinal reinforcement with a greater number of smaller-diameter longitudinal bars, to control crack widths.

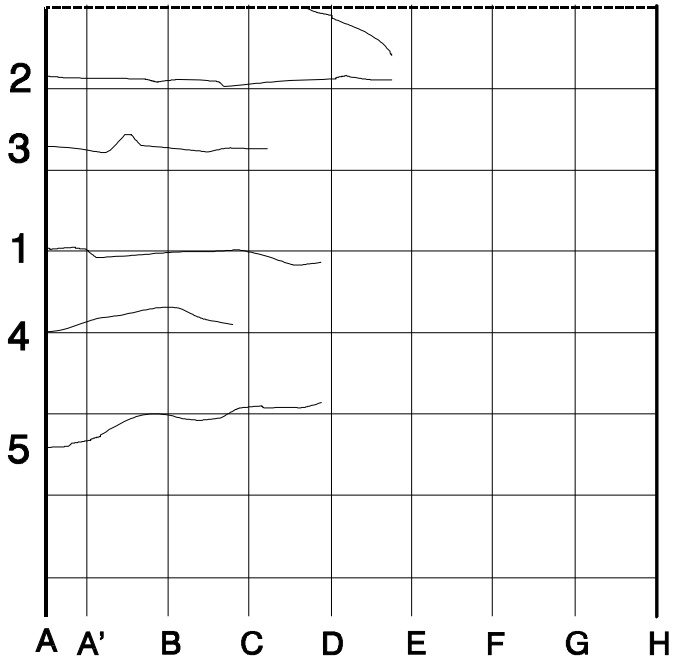

Figure 4.89 POJ-RC-100-TH cracking pattern on north face of pier at dead load

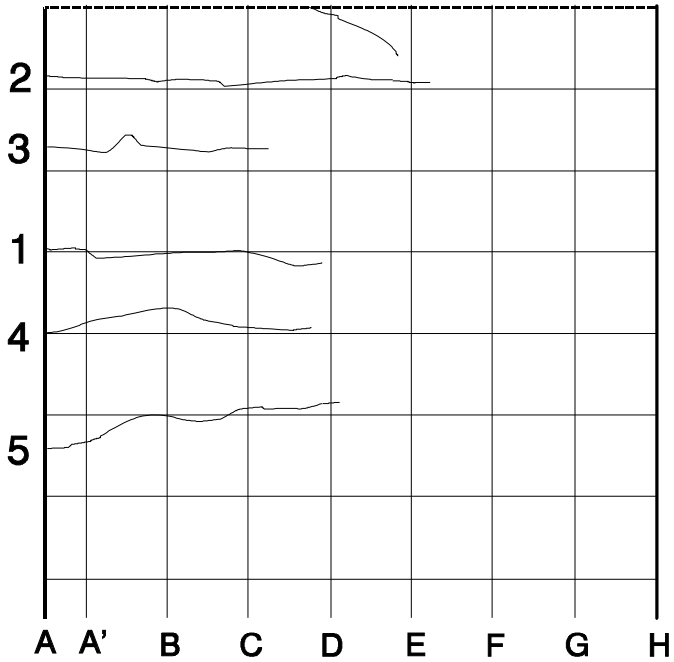

Figure 4.90 POJ-RC-100-TH cracking pattern on north face of pier at service load

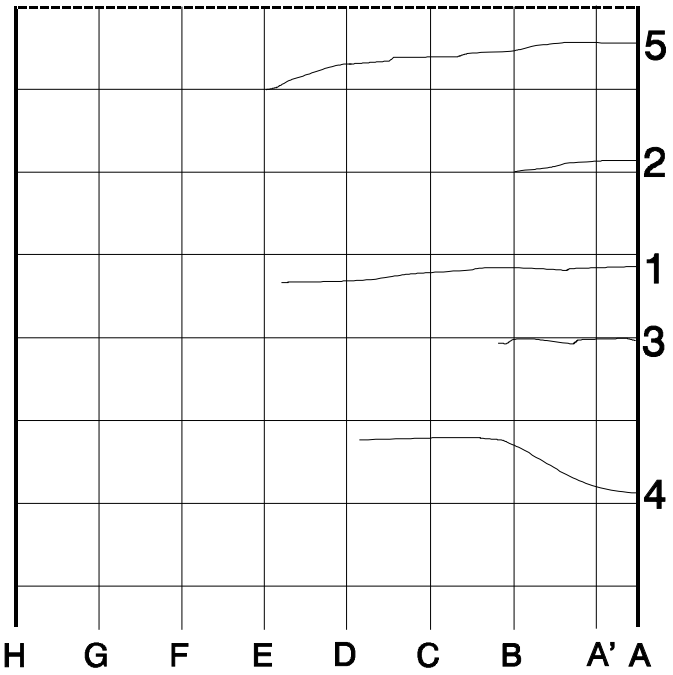

Figure 4.91 POJ-RC-100-TH cracking pattern on south face of pier at dead load

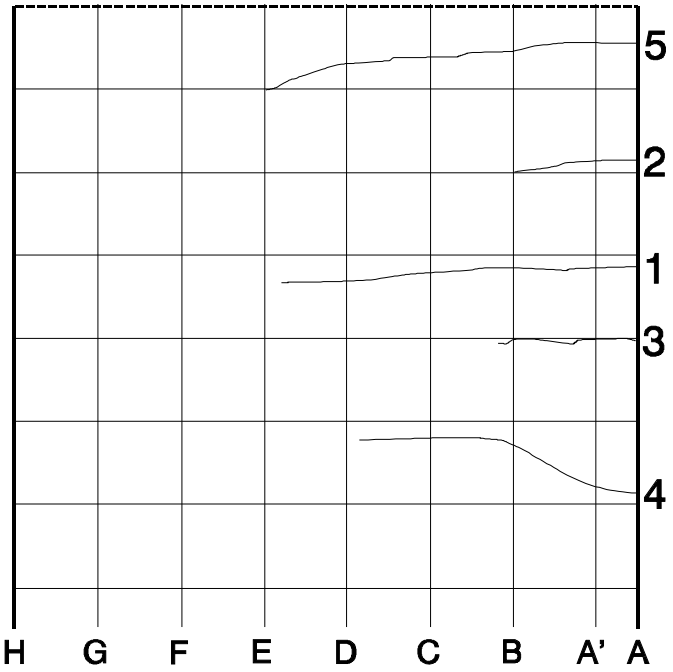

Figure 4.92 POJ-RC-100-TH cracking pattern on south face of pier at service load

4.3.1.2 Applied Moment vs. Deflection Response–POJ-RC-100-TH

Locations of displacement transducers for Specimen POJ-RC-100-TH are shown in Figure 4.93. Transducers labeled 'A' (*i.e.*, LV-75 A) were located on the south side of the specimen, transducers labeled 'B' (*i.e.*, LH1B) were located along the centerline of the specimen, and transducers labeled 'C' (*i.e.*, LV-75C) were located on the north side of the specimen.

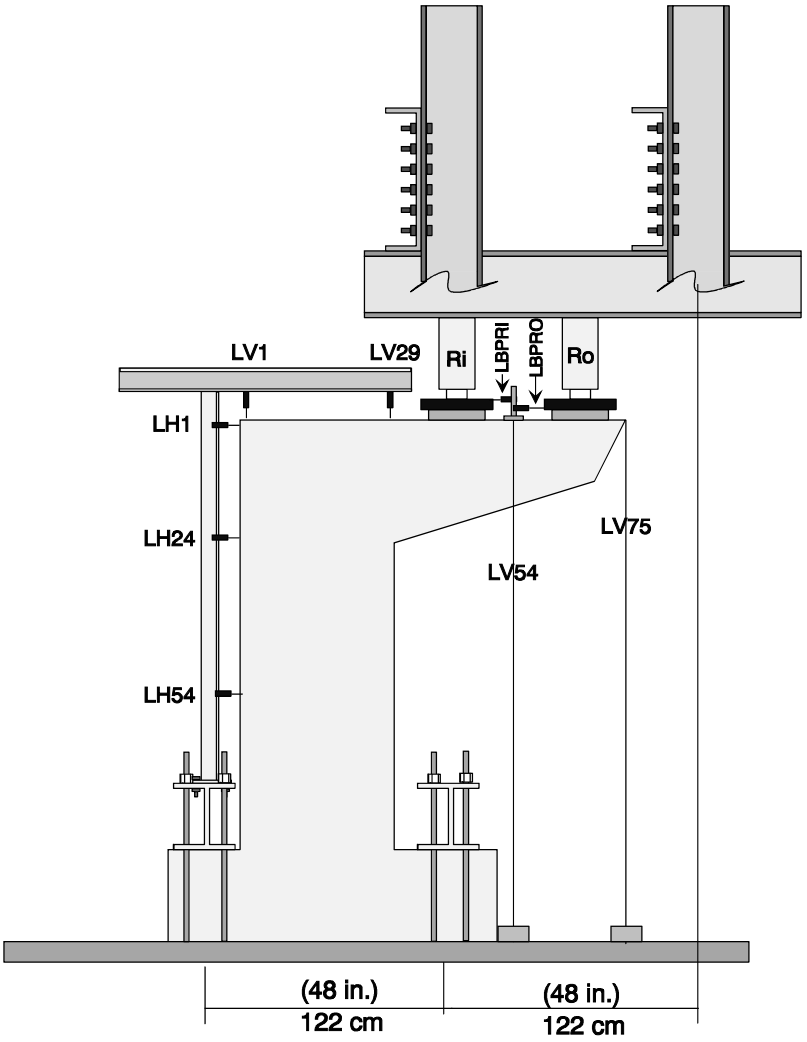

Figure 4.93 POJ-RC-100-TH location of displacement transducers

Plots of applied moment vs. deflection response for Specimen POJ-RC-100-TH are presented in Figure 4.94 through Figure 4.97. As before, overhang moment is plotted as a fraction of factored moment. Displacements are labeled in both SI and customary units.

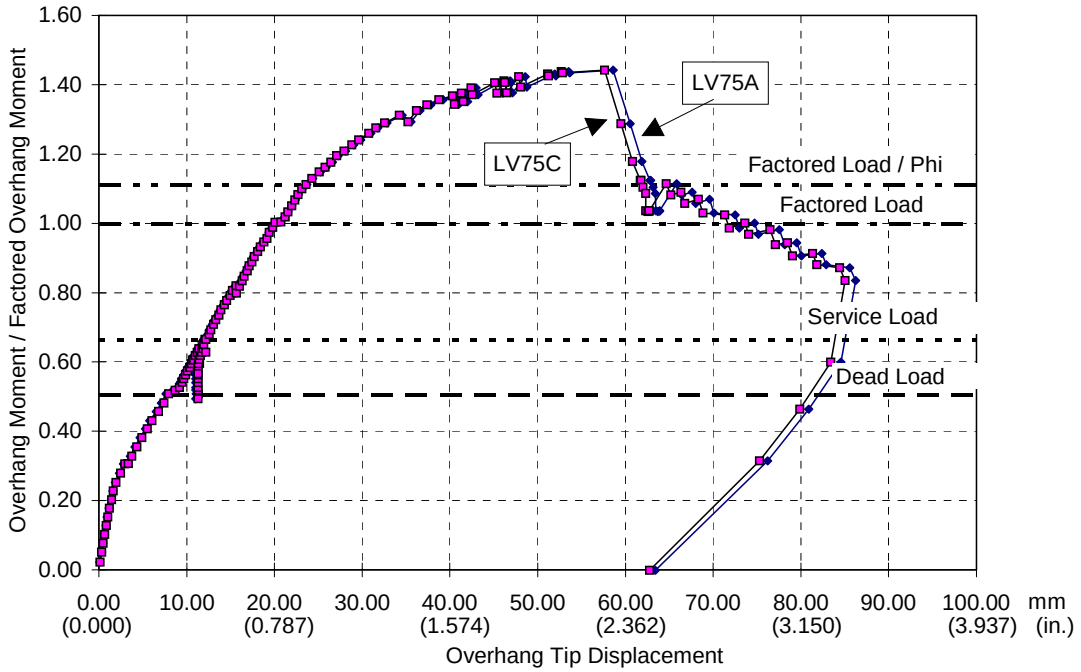

Figure 4.94 POJ-RC-100-TH tip deflection (LV 75)

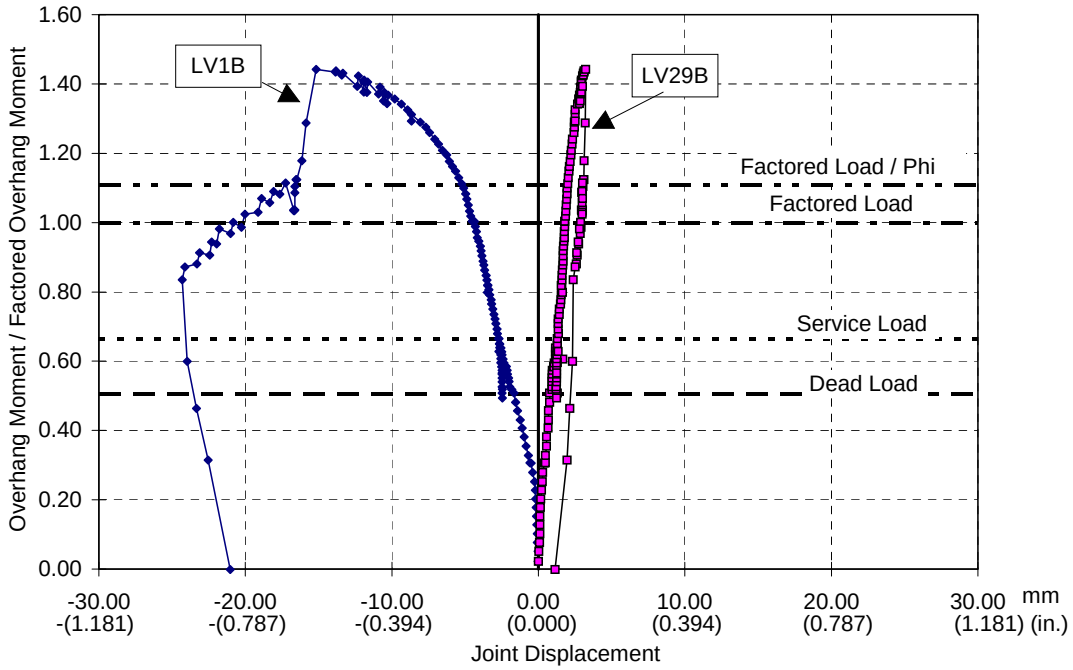

Figure 4.95 POJ-RC-100-TH joint vertical displacement

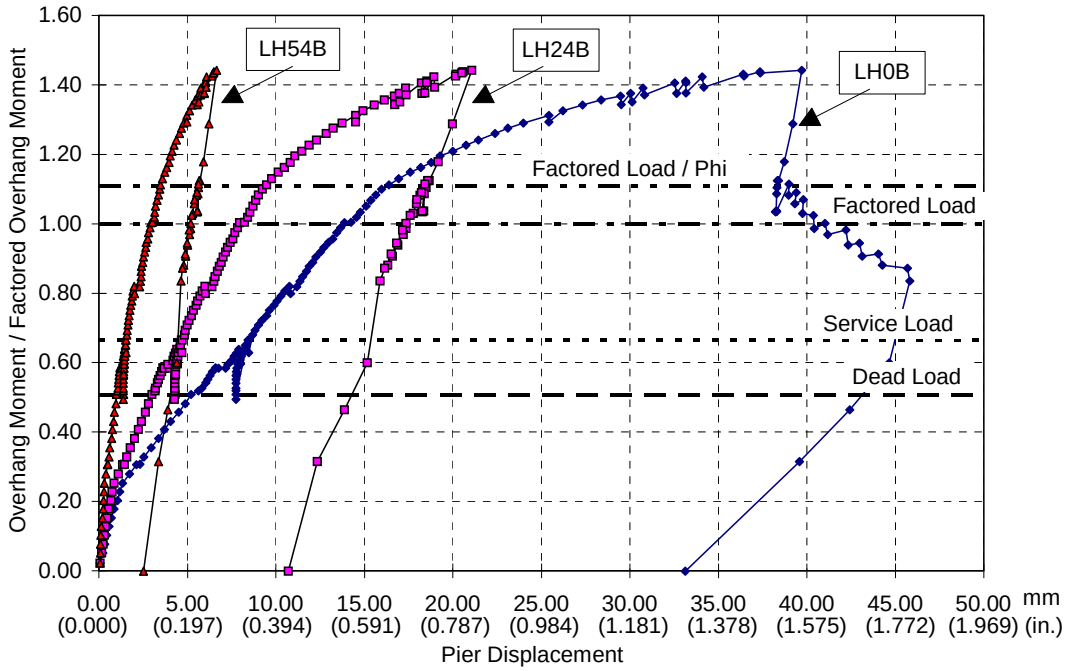

Figure 4.96 POJ-RC-100-TH pier horizontal deflection

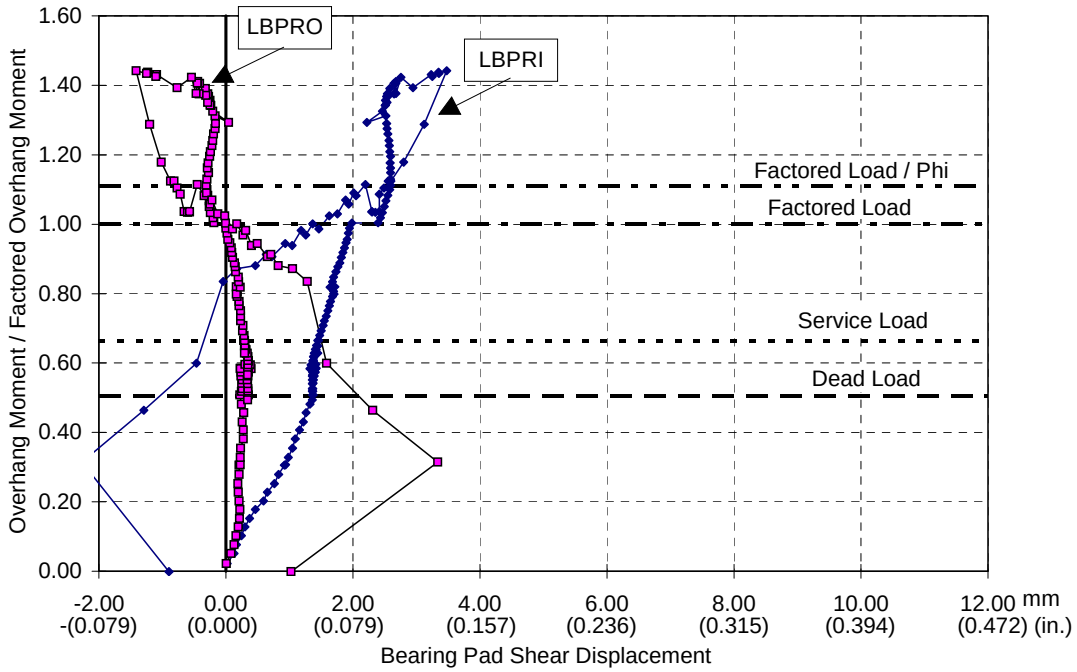

Figure 4.97 POJ-RC-100-TH bearing pad horizontal displacement

The overhang tip deflection response (LV-75) shown in Figure 4.94 illustrates the high level of strength that was attained using interlocked T-headed bars in the joint corner. The sharp drop in moment resistance at a displacement of 58 mm (2.28 in.) when spalling of the joint side-face concrete occurred, resulted in the loss of anchorage of the T-headed pier side face reinforcement. The sharp drop in load was not accompanied by a significant displacement because the hydraulic rams unloaded themselves before a large displacement could occur. The post-ultimate behavior indicated the

specimen had some reserve strength, but the accompanying tip displacement and joint opening were quite large.

Joint vertical displacements shown in Figure 4.95, were consistent with the response of the overhang section. As the critical diagonal joint crack opened after the peak load, vertical and horizontal displacements of the joint corner (measured by displacement transducers LV1B and LH0B, in Figure 4.95 and Figure 4.96, respectively) increased. Post-ultimate horizontal displacements of the pier measured by transducers LH24B and LH54B (shown in Figure 4.96) decreased elastically with increased overhang tip deflection (and corresponding decreased applied load). This indicated the lower portions of the pier were not failing. The bearing pad gages were erratic but, in general, only small shear displacements were measured, indicating the load frame did not apply large restraining forces, which would have influenced the specimen capacity.

4.3.1.3 Location and Identification of Strain Gages–POJ-RC-100-TH

Strain gages for Specimen POJ-RC-100-TH were distributed throughout the specimen to measure strain in the longitudinal and transverse reinforcement. Multiple strain gages were located at the same layer of reinforcement (i.e., strain gages M30Z1A', B, and C, as shown in Figure 4.98) to determine strain patterns across each section, and to provide redundancy in case a gage was defective. Strain gages were located at several layers for a given cross section (i.e., M30Z1A', M30Z3A', etc.) to measure strain gradients through the depth of the overhang or pier section. This information was used to evaluate the linear strain profile assumption that was used for the analytical model. Gages located on side-face longitudinal and transverse overhang reinforcement (over the region X=40 to X=62) were used to measure reinforcement strains in the event a shear crack developed. There was concern of a shear failure occurring because the number of closed ties in the overhang was intentionally reduced to account for tensile strength of the concrete. The overhang and pier T-headed longitudinal reinforcement were gaged at several locations in the joint region to evaluate bar development from the overhang/joint and pier/joint interfaces to the exterior corner of the joint.

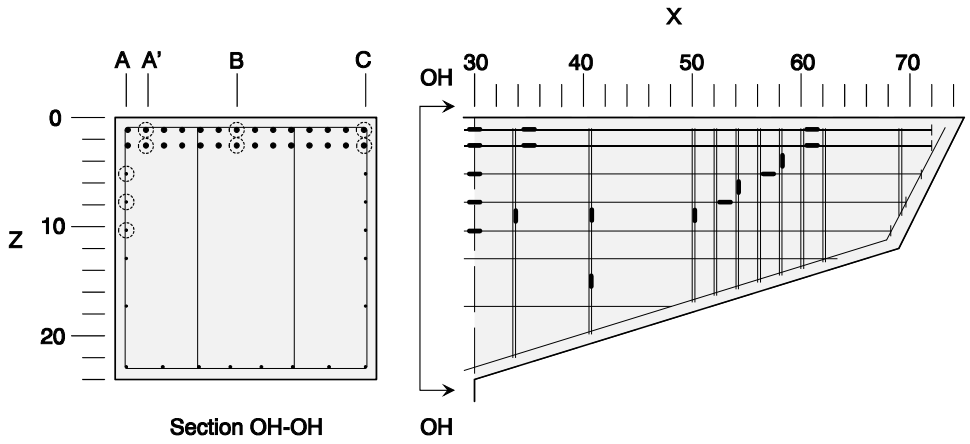

Overhang Primary Longitudinal Reinforcement	Section X=30			Section X=35		
	A'	B	C	A'	B	C
Layer Z=1	M30Z1A'	M30Z1B	M30Z1C	M35Z1A'	M35Z1B	M35Z1C
Layer Z=3	M30Z3A'	M30Z3B	M30Z3C	M35Z3A'	M35Z3B	M35Z3C

Overhang Side-Face Reinforcement	Section X=30	Section X=53	Section X=57
Layer Z=5	T30Z5A		T57Z5A
Layer Z=8	T30Z8A	T53Z8A	
Layer Z=10	T30Z10A		

Overhang Transverse Reinforcement	Section X=34	Section X=41	Section X=50	Section X=54	Section X=58
Level Z=4					S58Z4A
Level Z=6				S54Z6A	
Level Z=9	S34Z9A	S41Z9A	S50Z9A		
Level Z=15		S41Z15A			

Figure 4.98 POJ-RC-100-TH overhang strain gage locations and labels

The location and identification of each strain gage for Specimen POJ-RC-100-TH are shown in Figure 4.98 through Figure 4.100. Plots in Section 4.3.1.4 use these labels to identify the responses being plotted. The general labeling terminology was described in Section 4.2.1.3 (Figure 4.28).

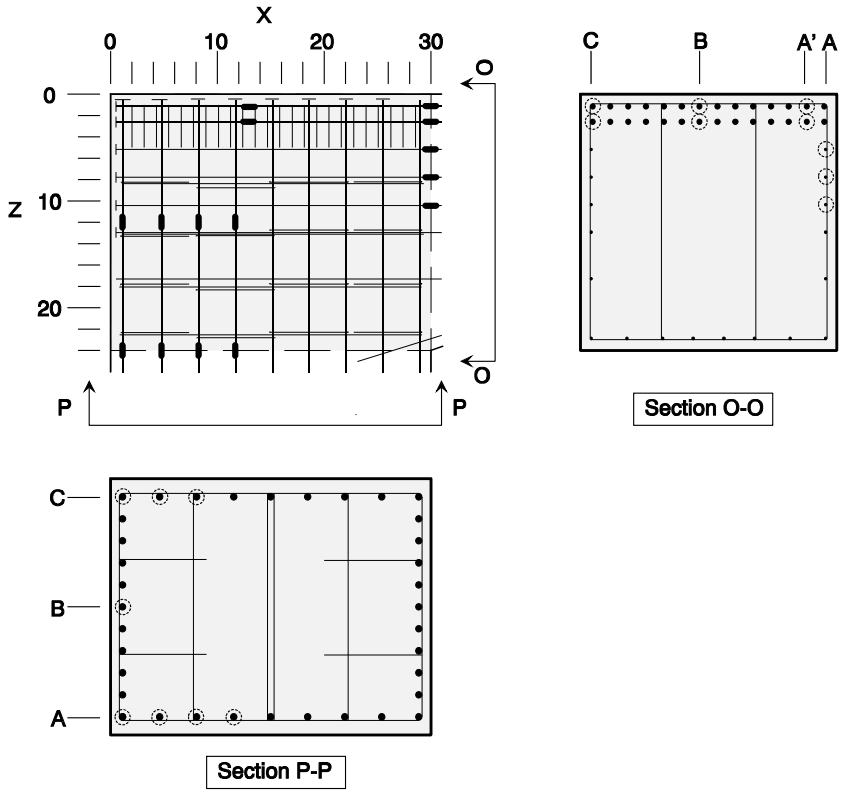

Overhang Longitudinal Reinforcement	Section X=13			Section X=30		
	A'	B	C	A'	B	C
Layer Z=1	M13Z1A'	M13Z1B	M13Z1C	M30Z1A'	M30Z1B	M30Z1C
Layer Z=3	M13Z3A'	M13Z3B	M13Z3C	M30Z3A'	M30Z3B	M30Z3C
Layer Z=8				T30Z8A		
Layer Z=10				T30Z10A		
Layer Z=13				T30Z13A		

Pier Longitudinal Reinforcement	Section Z=12			Section Z=24		
	A	B	C	A	B	C
Layer X=1	C1Z12A	C1Z12B	C1Z12C	C1Z24A	C1Z24B	C1Z24C
Layer X=5	C5Z12A			C5Z24A		C5Z24C
Layer X=8	C8Z12A			C8Z24A		C8Z24C
Layer X=11	C11Z12A			C11Z24A		

Figure 4.99 POJ-RC-100-TH Joint Strain Gage Locations and Labels

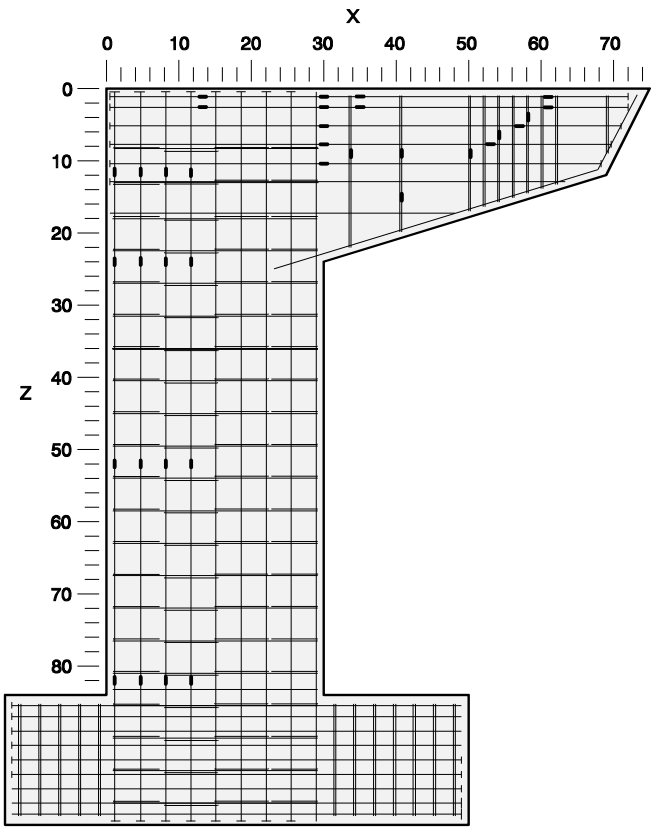

Pier Longitudinal Reinforcement	Section Z=54			Section Z=81		
	A	**B**	**C**	**A**	**B**	**C**
Layer X=1	C1Z54A	C1Z54B	C1Z54C	C1Z81A	C1Z81B	C1Z81C
Layer X=5	C5Z54A		C5Z54C	C5Z81A		C5Z81C
Layer X=8	C8Z54A		C8Z54C	C8Z81A		C8Z81C
Layer X=11	C11Z54A			C11Z81A		

Figure 4.100 POJ-RC-100-TH overall strain gage locations and pier strain gage labels

4.3.1.4 Applied Moment vs. Strain Response–POJ-RC-100-TH

Applied moment vs. strain plots for Specimen POJ-RC-100-TH included response for strain gages attached to longitudinal overhang reinforcement (Figure 4.101 and Figure 4.102), transverse overhang reinforcement (Figure 4.103), and several layers of longitudinal pier reinforcement (Figure 4.104 through Figure 4.107). Strain gages indicated abrupt changes in strain when cracking occurred in the vicinity of each of the gages.

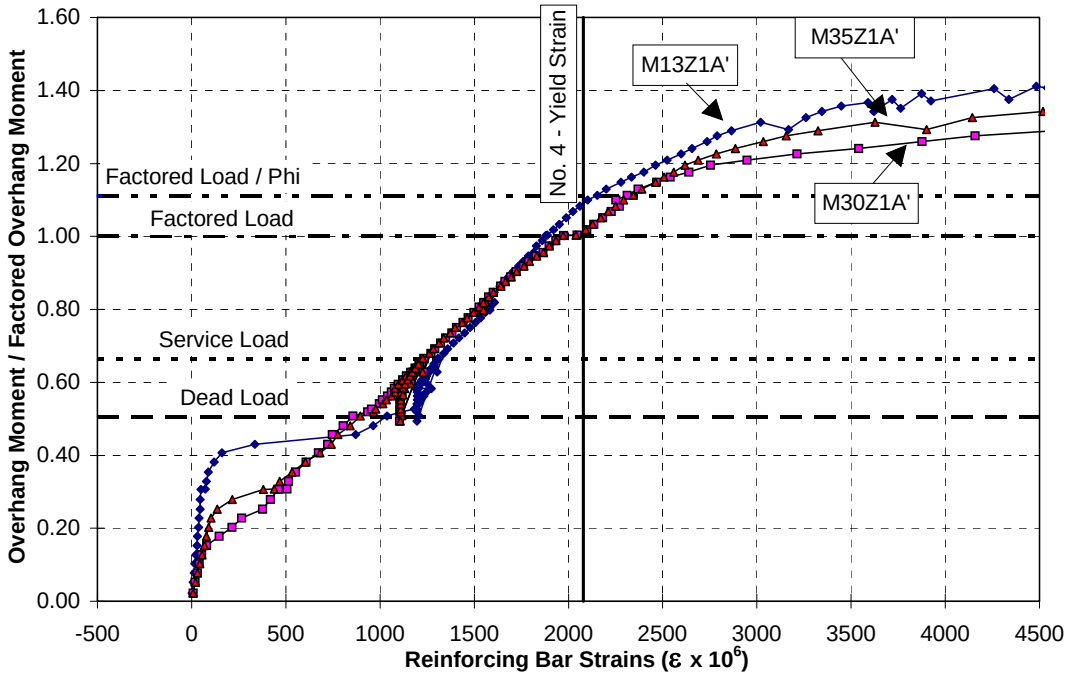

Figure 4.101 POJ-RC-100-TH strains in primary longitudinal reinforcement at Layer Z=1 in the overhang

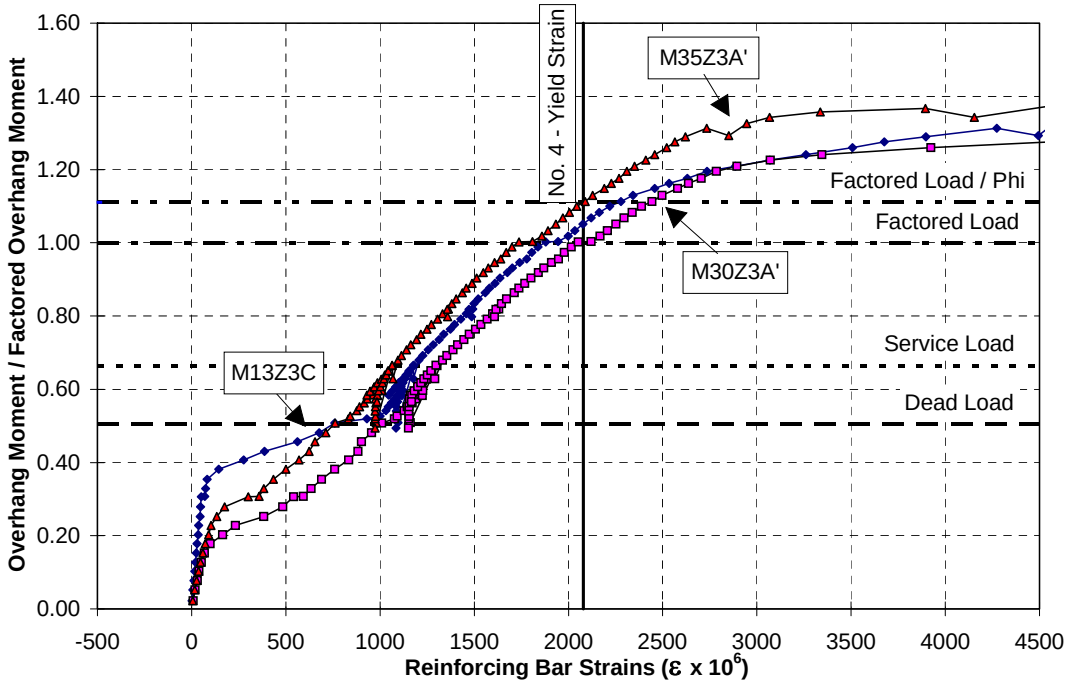

Figure 4.102 POJ-RC-100-TH strains in primary longitudinal reinforcement at Layer Z=3 in the overhang

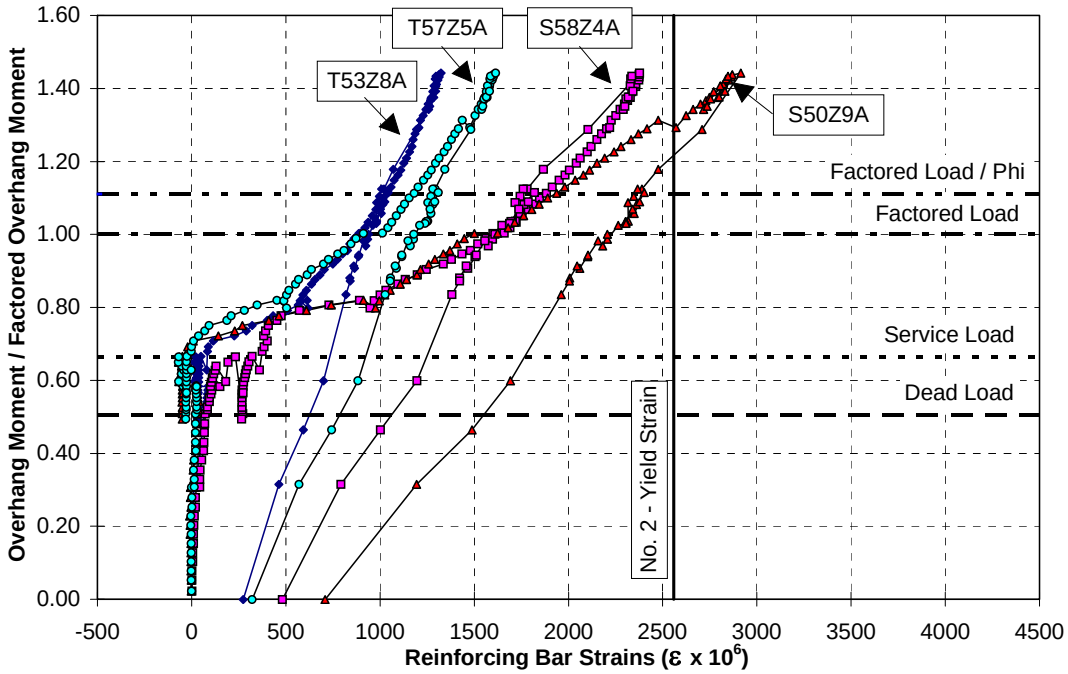

Figure 4.103 POJ-RC-100-TH strains in transverse and side-face reinforcement in the overhang

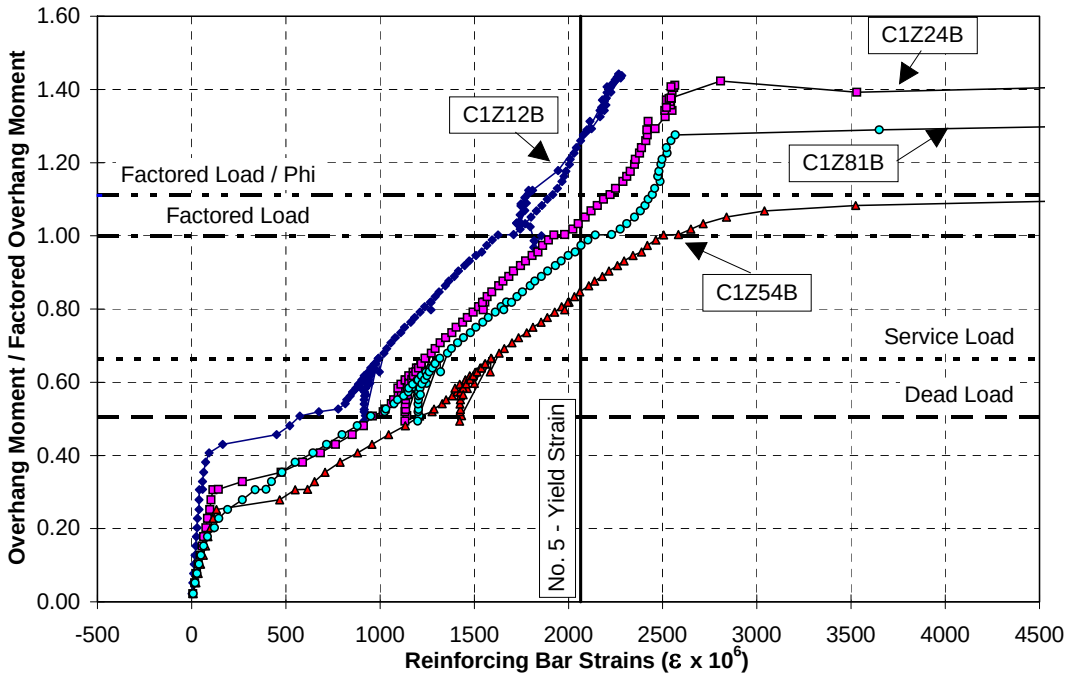

Figure 4.104 POJ-RC-100-TH strains in pier longitudinal reinforcement at Layer X=1

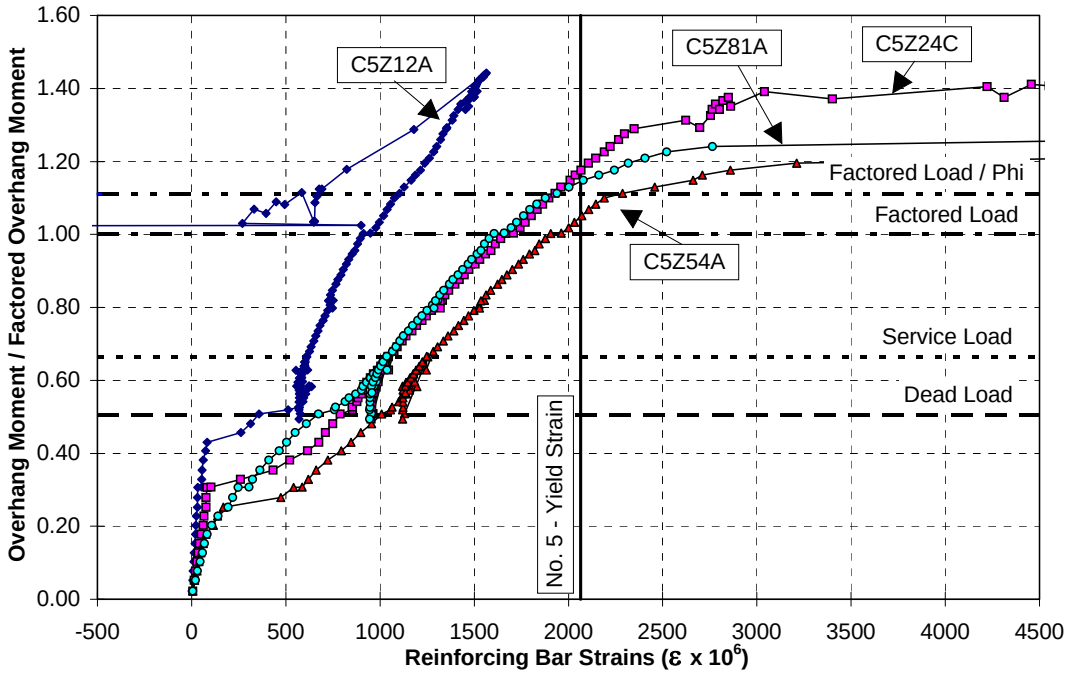

Figure 4.105 POJ-RC-100-TH strains in pier longitudinal reinforcement at Layer X=5

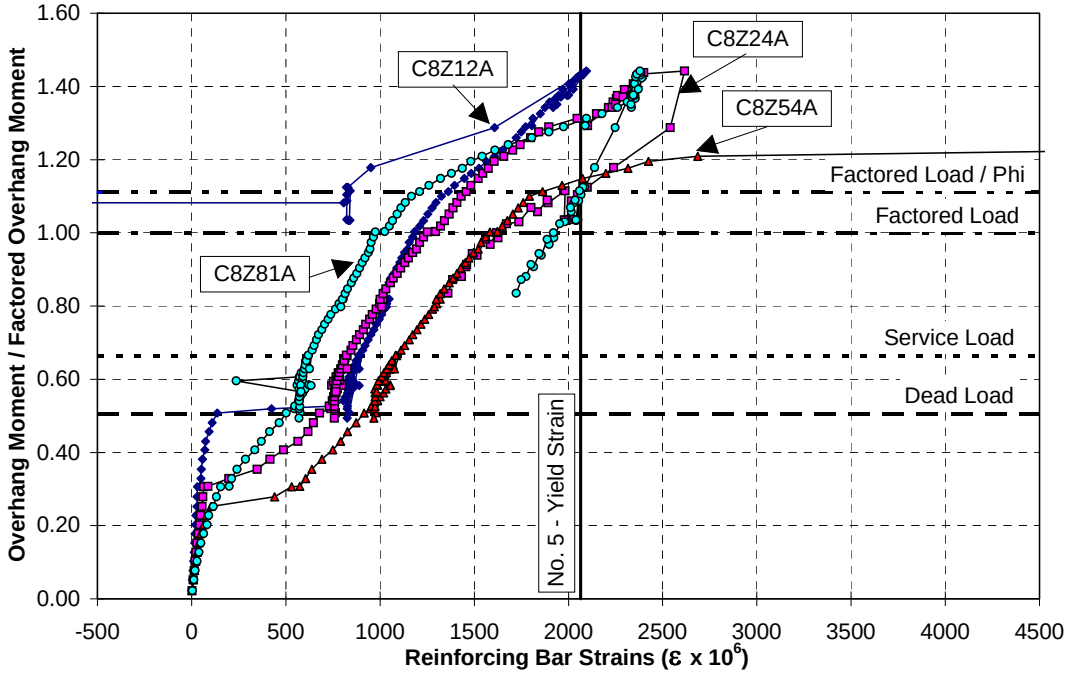

Figure 4.106 POJ-RC-100-TH strains in pier longitudinal reinforcement at Layer X=8

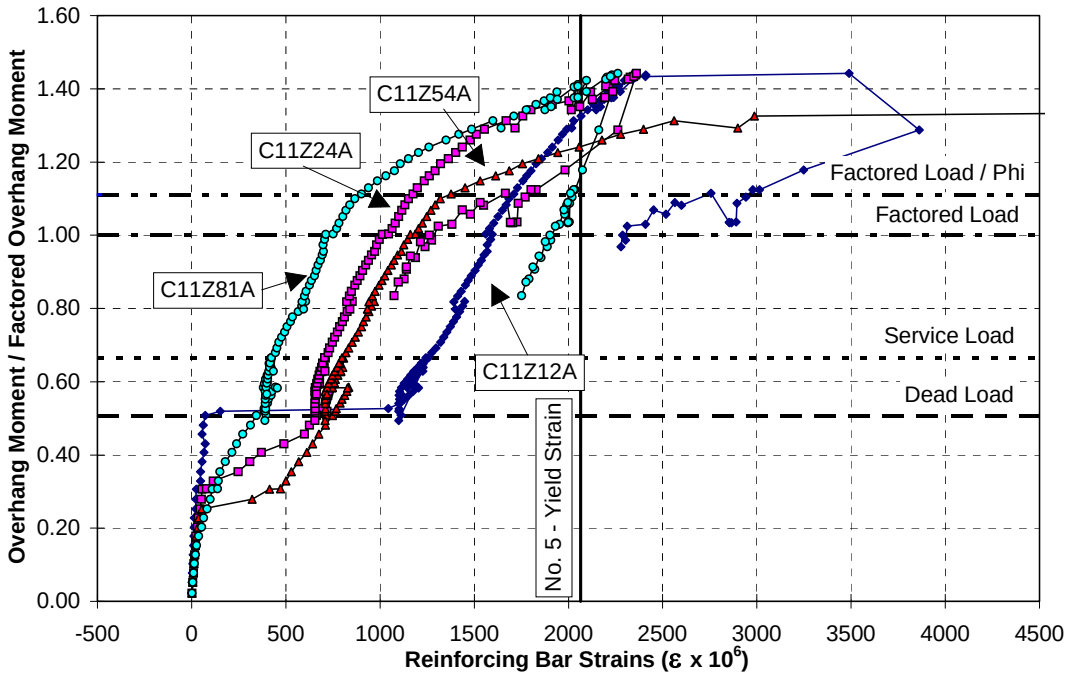

Figure 4.107 POJ-RC-100-TH strains in pier longitudinal reinforcement at Layer X=11

The moment-strain response for strain gages attached to the primary longitudinal overhang reinforcement (Layers Z=1 and Z=3, shown in Figure 4.101 and Figure 4.102, respectively) indicated the reinforcement strain was nearly constant from the face of the pier, back into the joint. This confirmed the strut-and-tie model assumption that the tensile force path extended to the extreme corner of the joint. The moment-strain plots also indicate the primary overhang reinforcement reached yield strain at a moment ratio (overhang moment/factored moment) of 1.0, or factored load. The long strain plateau indicated the reinforcement experienced very large strains before failure occurred at a moment ratio of 1.47.

The moment-strain response for gages attached to the overhang transverse reinforcement (shown in Figure 4.103) indicated a sharp increase in strain after first cracking occurred at service load. The strain gage located on a transverse tie near the outer applied load (strain gage S50Z9A) yielded at a moment ratio of 1.33. Because transverse reinforcement was designed assuming a nominal yield stress of 413 MPa (60.0 ksi), it should be noted that the reinforcement reached nominal yield at a moment ratio of 1.15 (slightly larger than factored flexure/phi). Although large loads were applied to the test specimen and an overhang shear failure did not occur, there is concern that the amount of conservatism associated with the shear design is small.

Moment-strain responses for gages attached to the pier longitudinal reinforcement (shown in Figure 4.104 through Figure 4.107) clearly show first cracking and yielding of the reinforcement at moment ratios above 1.0 (factored loads). Although reinforcement strains varied along the length of the longitudinal pier reinforcement, it was clear the reinforcement needed to be fully anchored at the joint corner. Anchorage failure of the pier longitudinal reinforcement (located on the side faces) can be seen in Figure 4.105 through Figure 4.107, where gages located near the critical diagonal joint crack (gages C5Z12A, C8Z12A, and C11Z12A) have significant reductions in recorded strain after the maximum moment ration of 1.47. In contrast, gages attached to pier longitudinal reinforcement located in the interior of the specimen (gage C1Z12B) show elastic unloading of the reinforcement. This indicated spalling of the side-face concrete resulted in loss of anchorage of the pier

reinforcement located on the side faces, but did not influence the bars near the center of the specimen. Closer examination of the joint after the test was completed confirmed this conclusion.

4.3.1.5 Overhang and Pier Section Strain Profiles

Strain profiles are presented for the overhang cross section nearest the column face (X=30), and for pier cross sections located 12 inches, 24 inches, and 54 inches from the top surface of the joint (Sections Z=12, Z=24, and Z=54, respectively). Strain profiles were developed by averaging the strains for gages at the same layer (for example, recorded strains for gages C5Z24A and C5Z24C were averaged).

Strain profiles for the cross section closest to the column face are presented in Figure 4.108. The overhang strain profiles at section X=30 were fairly uniform with increased depth. This was quite different from the overhang strain profiles obtained for Specimen POJ-RC-100 (shown in Fig. 4.36) where the strain varied linearly with increased depth. The large measured strains in the overhang cross section, specifically at Layers Z=5, 10, and Z=13, were attributed to crack widths that were not controlled by the quantity of side-face reinforcement that was provided.

Strain profiles at the pier cross section located 12 inches from the top surface (Z=12) (presented in Figure 4.109) had a jagged profile due to the location of the cracks in the joint region. The strain profile was expected to be fairly uniform based on the failure mechanism. The addition of the T-headed anchorage enabled pier longitudinal reinforcement at the exterior face to achieve larger strains than those recorded for Specimen POJ-RC-100 (shown in Fig. 4.39). Strain profiles for the pier cross sections located 24 inches and 54 inches from the top of the joint (Z=24 and Z=54, shown in Figure 4.110 and Figure 4.111, respectively) had nearly linear strain profiles as a function of distance across the pier. As expected, strain profiles for the various cross sections were similar because bending moment was constant over the height of the pier.

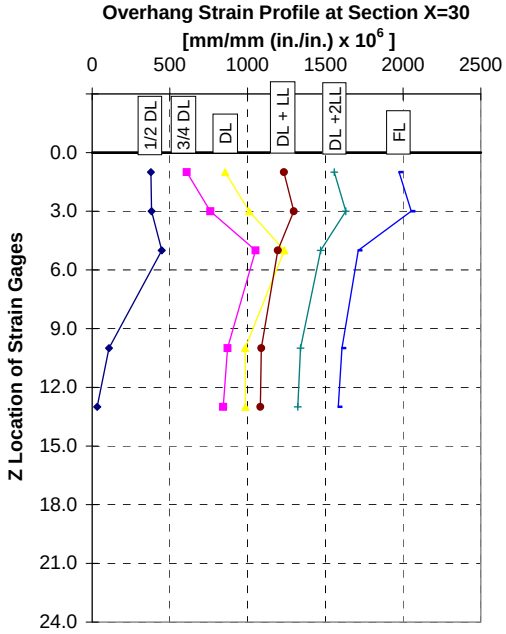

Figure 4.108 POJ-RC-100-TH overhang strain profile at Section X=30

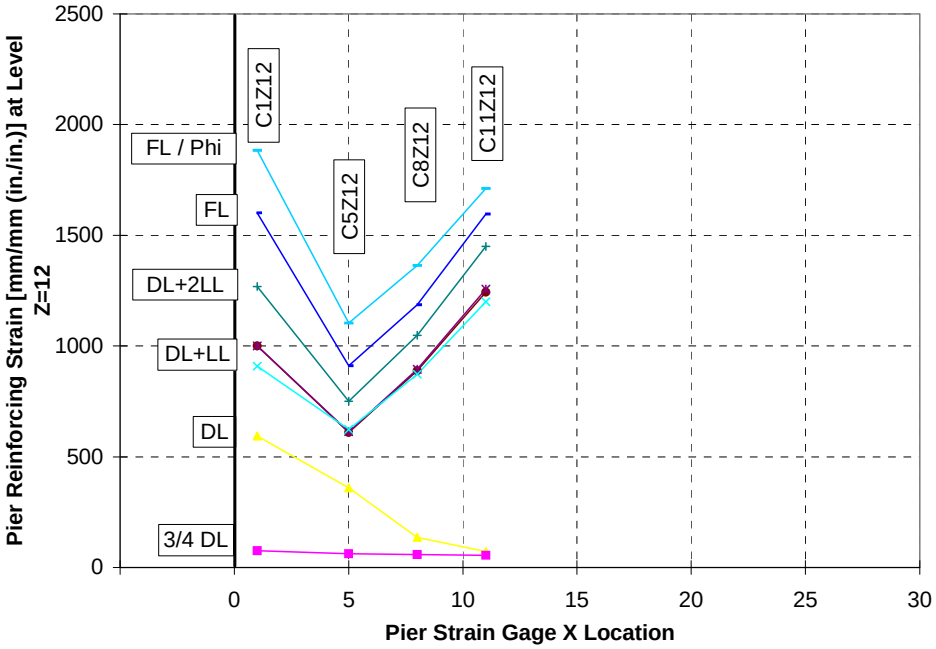

Figure 4.109 POJ-RC-100-TH joint strain profile at Section Z=12

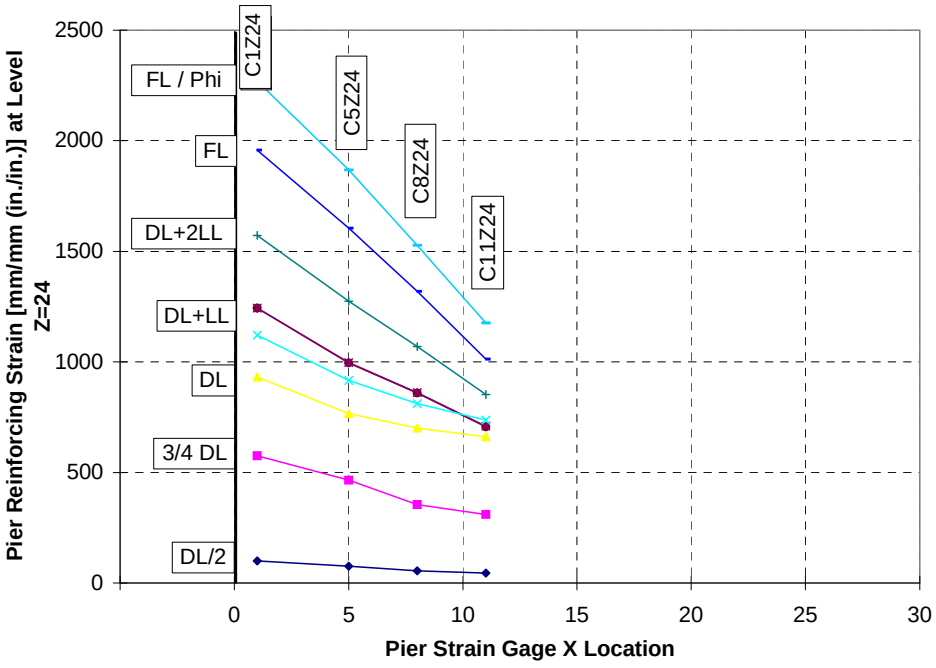

Figure 4.110 POJ-RC-100-TH pier strain profile at Section Z=24

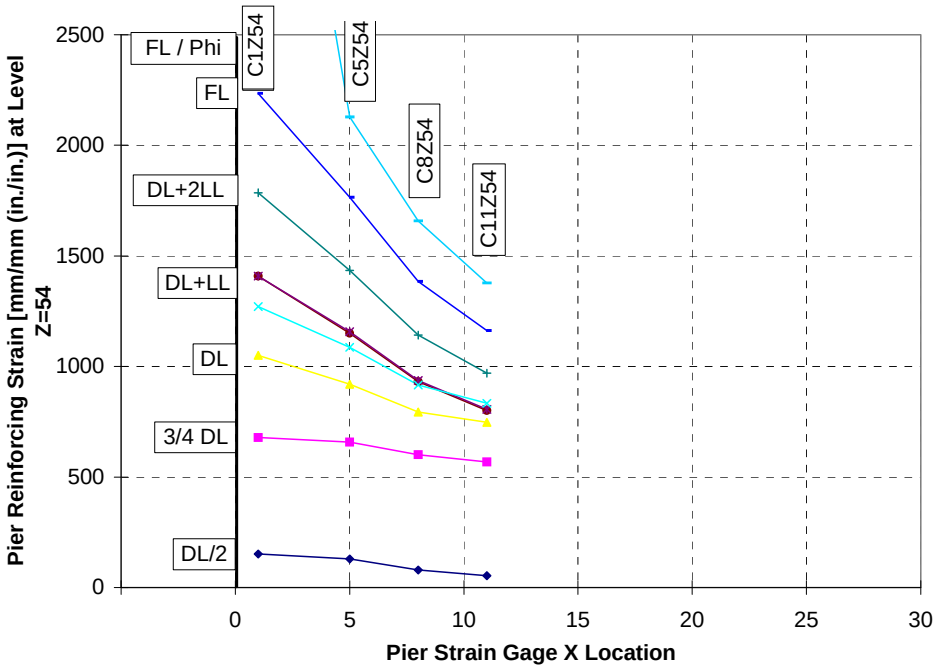

Figure 4.111 POJ-RC-100-TH pier strain profile at Section Z=54

4.3.2 54% Prestressed Design with T-Headed Reinforcement–POJ-PU-54-TH

Specimen POJ-PU-54-TH was designed using a strength-based design method (detailed in Chapter 3) which combined continuous post-tensioning and T-headed longitudinal reinforcement to resist factored loads and provide good serviceability at design loads.

For Specimen POJ-PU-54-TH, 54% of the tension tie force required for strength was provided by Lo-Lax prestressing strand with an ultimate tensile stress of 1.8 GPa (270 ksi), and 46% was provided by T-Headed mild reinforcement with a nominal yield stress of 413 MPa (60 ksi). A small amount of post-tensioning was selected in order to reduce reinforcement congestion, delay the onset of cracking, and to identify problems associated with the use of partial prestressing.

Interlaced T-headed reinforcement and continuous post-tensioning in the joint corner (shown in Figure 4.112) provided a continuous force path to transfer forces into the pier (see Figure 4.113). Continuous post-tensioning through the joint region reduced the level of concrete tensile stresses in the joint, provided strength, and helped control crack widths. Headed mild reinforcement controlled crack widths and provided strength when the critical diagonal joint crack developed. A finite element analysis (shown in Figure 4.114 and Figure 4.115) confirmed post-tensioning reduced tensile stresses at service load, and illustrates the flow of forces through the joint. Cracks were expected to form in the joint at loads below dead load, but the distribution of mild reinforcement and the position of post-tensioned reinforcement were designed to limit the width of cracks that formed.

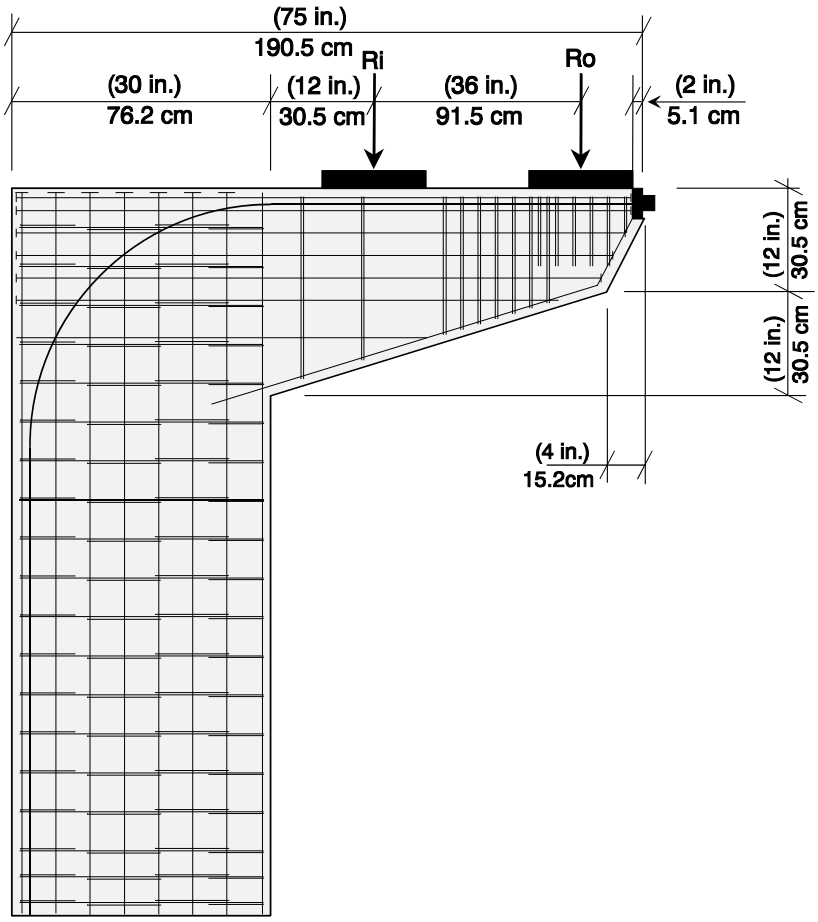

Figure 4.112 Reinforcing details for Specimen POJ-PU-54-TH

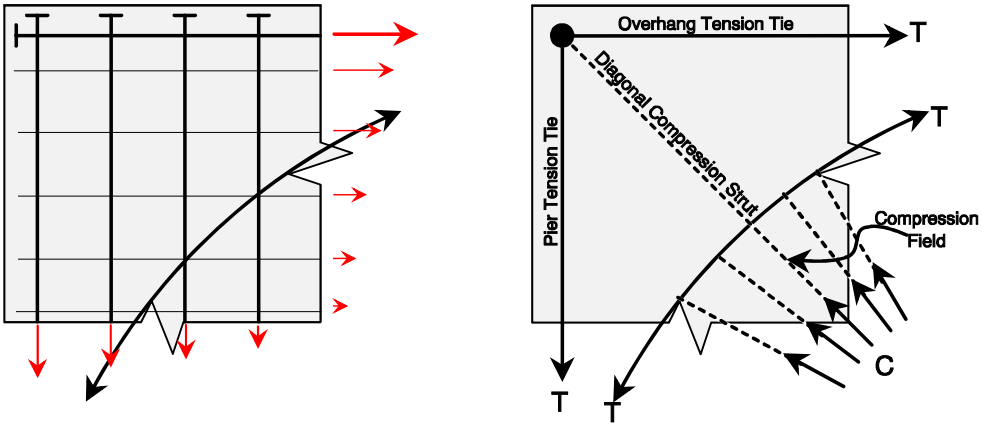

Figure 4.113 Joint corner detail for Specimen POJ-PU-54-TH

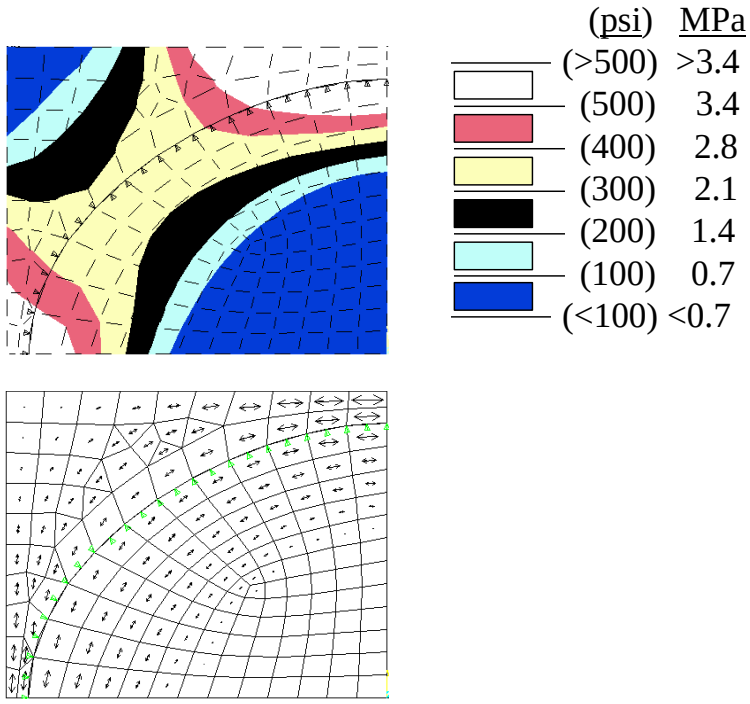

Figure 4.114 POJ-PU-54-TH joint principal tensile stresses and vectors at service load

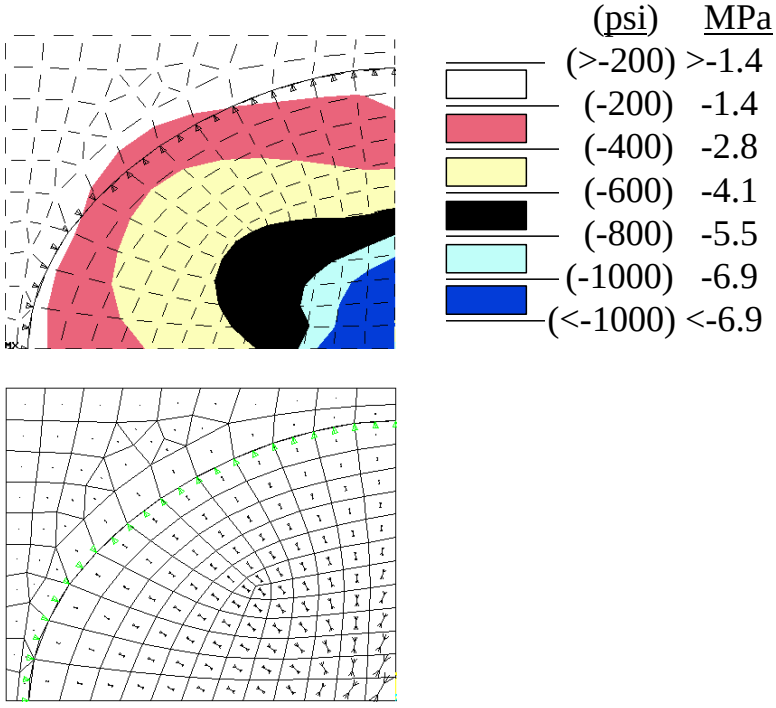

Figure 4.115 POJ-PU-54-TH joint principal compressive stresses and vectors at service load

After Specimen POJ-PU-54-TH was cast and installed in the testing frame, the specimen was post-tensioned. Each tendon was gaged with 2 mm strain gages at several points along the length, and

each gage was protected with mastic and a water-resistant coating. Despite the precautions that were taken, only a few of the tendon gages survived the post-tensioning operation.

The post-tensioning operation involved stressing the two outer tendons to 1.1 GPa (160 ksi) and applying ½DL before stressing the center tendon. This procedure reduced the risk of cracking the underside of the overhang and inner face of the pier. It was determined that the two outer tendons could be stressed to 1.1GPa (160 ksi) before a tensile stress of $6\sqrt{f'_c}$ [2.9 MPa (425 psi)] would be reached in the pier. Once the outer two strands were stressed, applied load on the specimen was increased incrementally until a load equivalent to one-half the dead load of the superstructure was applied. The specimen was inspected for cracks after every load step, and once ½ DL was applied, the center strand was stressed to 1.1 GPa (160 ksi). After a lift-off test was performed for each strand (to ensure the final post-tensioning load), the post-tensioning ducts were grouted. Testing was continued once the grout reached a cube compressive strength of 10 MPa (1500 psi).

Three days after grouting the post-tensioning ducts, Specimen POJ-PU-54-TH was loaded incrementally to Dead Load. An X-Y plotter was used to monitor applied load vs. overhang tip displacement during the test. The specimen was inspected for cracks after every load step, and at load step 13, cracks were identified on the south overhang, pier, and joint sections. After first cracking, cracks were marked every other load step on the specimen and on a pencil sketch. Crack widths were measured at loads equivalent to DL+½LL and DL+LL (Service Load). After crack widths were measured at DL+LL, applied load was reduced to DL, and crack widths were measured. Crack widths were measured at DL+½LL and DL+LL, and the last crack width measurements were taken at DL+2LL. Cracks were marked on the specimen at every other load step until failure was imminent. Photographs taken of Specimen POJ-PU-54-TH at an applied load equivalent to factored load (shown in Figure 4.116) indicate the extent of cracking in the joint and overhang.

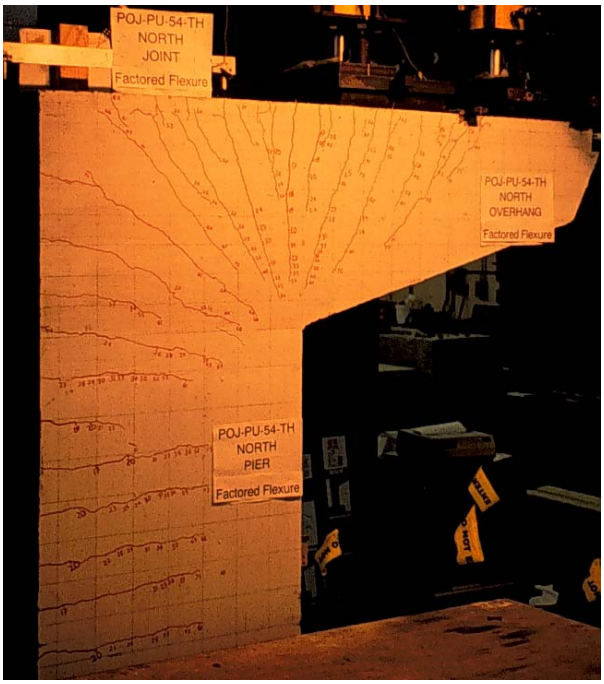

Figure 4.116 Photograph of cracking patterns on north face of Specimen POJ-PU-54-TH at factored load

Large cracks were noted in the overhang as loads were increased past factored load. At load step 90 (DL+4.7LL), initial concrete spalling was noted on the underside of the overhang. As applied load

was increased, cracks in the overhang at the cross section closest to the column face (crack (1) on the north face and crack (3) on the south face, shown in Figure 4.117) extended nearly the full depth of the overhang. After a large section of cover concrete spalled from the underside of the overhang (shown in Figure 4.118), crack (8) (which extended from the outer load to the column face) extended the full depth of the overhang, causing the outer portion of the overhang to fail. Consideration of the strut-and-tie model indicated that once the compression strut from the outer load was lost, the entire outer load had to be resisted by the vertical tension tie force. Because the transverse reinforcement in the overhang was not designed to resist the entire outer load, the overhang failed.

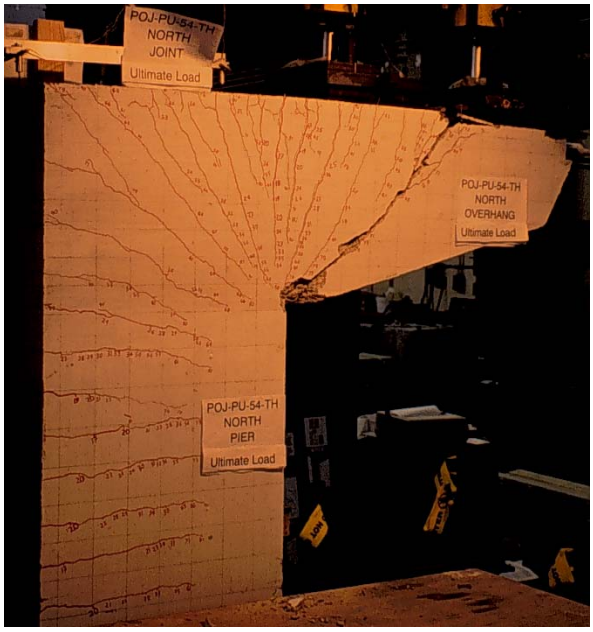

Figure 4.117 Photograph of cracking pattern on north face of Specimen POJ-PU-54-TH at ultimate load

Figure 4.118 Photograph of concrete spalling on underside of overhang for Specimen POJ-PU-54-TH

Failure of the overhang section may have been prevented by providing additional longitudinal reinforcement and closed transverse reinforcement in the compression zone of the overhang, increasing

the ductility of the compression node. The brittle failure mode provided valuable information on the design of the transverse reinforcement. However, it should be noted that the failure occurred at an applied load equivalent to 1.41 times factored load (DL+5.7LL).

4.3.2.1 Cracking Patterns and Maximum Crack Width Measurements–POJ-PU-54-TH

The overall cracking pattern on the north and south faces of Specimen POJ-PU-54-TH at dead load (presented in Figure 4.119 and Figure 4.120, respectively) and service load (presented in Figure 4.121 and Figure 4.122, respectively) indicated the post-tensioning helped reduce the number of cracks observed under operational loads. The crack associated with failure of the specimen is identified with a heavy line (overhang crack (8) on the north face and overhang crack (6) on the south face of the specimen, respectively), and the spall location is denoted by the shaded region in Figure 4.123 and Figure 4.124. Specimen POJ-PU-54-TH had a well-distributed cracking pattern, and individual cracks in the overhang and joint did not dominate until applied load was greater than factored load. Cracking patterns and maximum measured crack widths for the overhang, joint, and pier are detailed below.

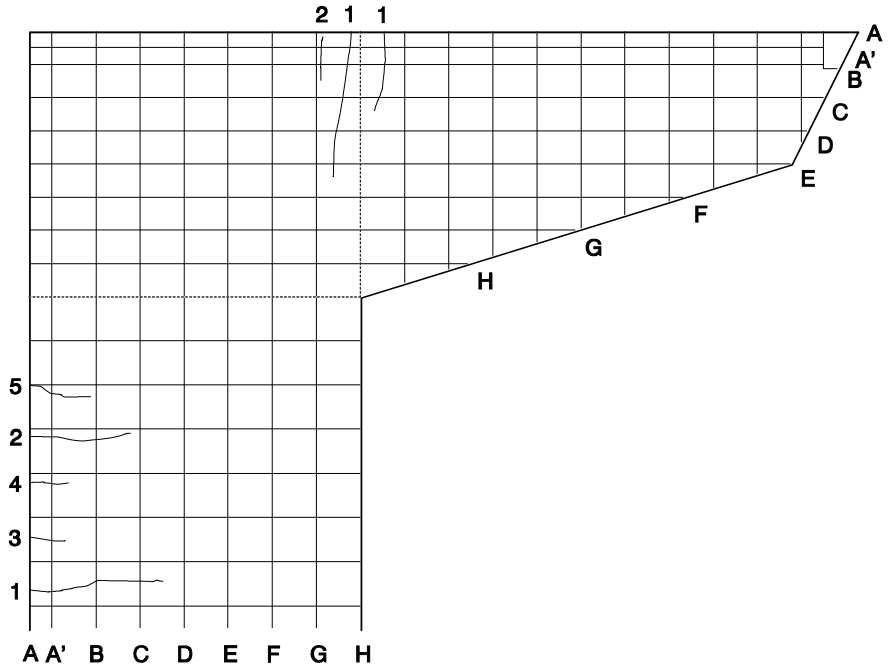

Figure 4.119 Cracking pattern on north face of Specimen POJ-PU-54-TH at dead load

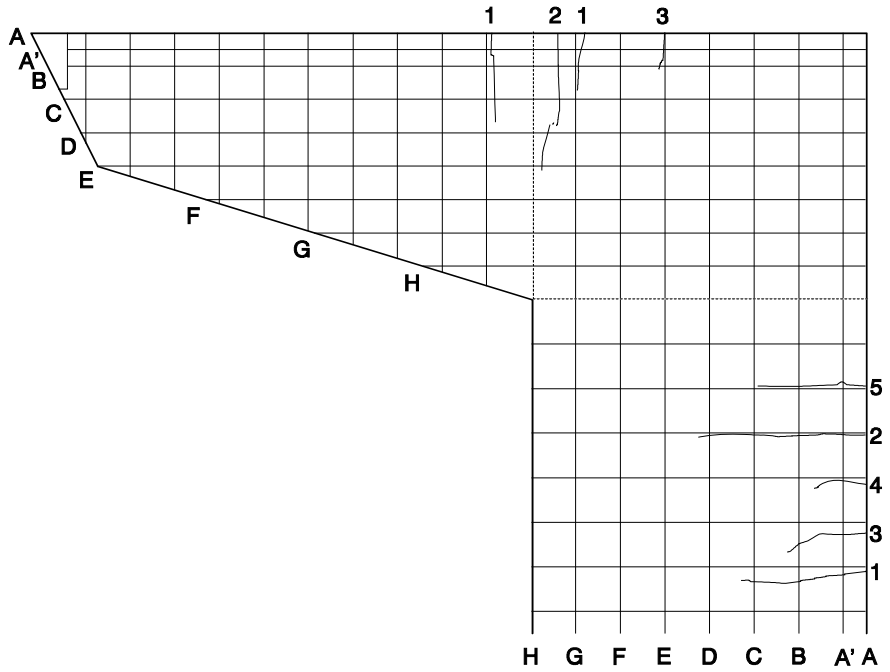

Figure 4.120 Cracking pattern on south face of Specimen POJ-PU-54-TH at dead load

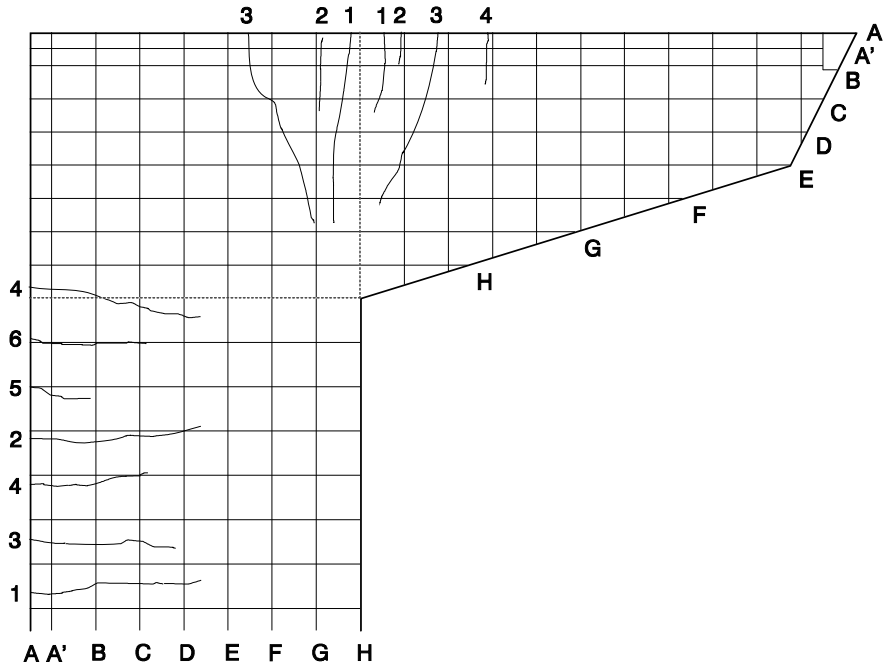

Figure 4.121 Cracking pattern on north face of Specimen POJ-PU-54-TH at service load

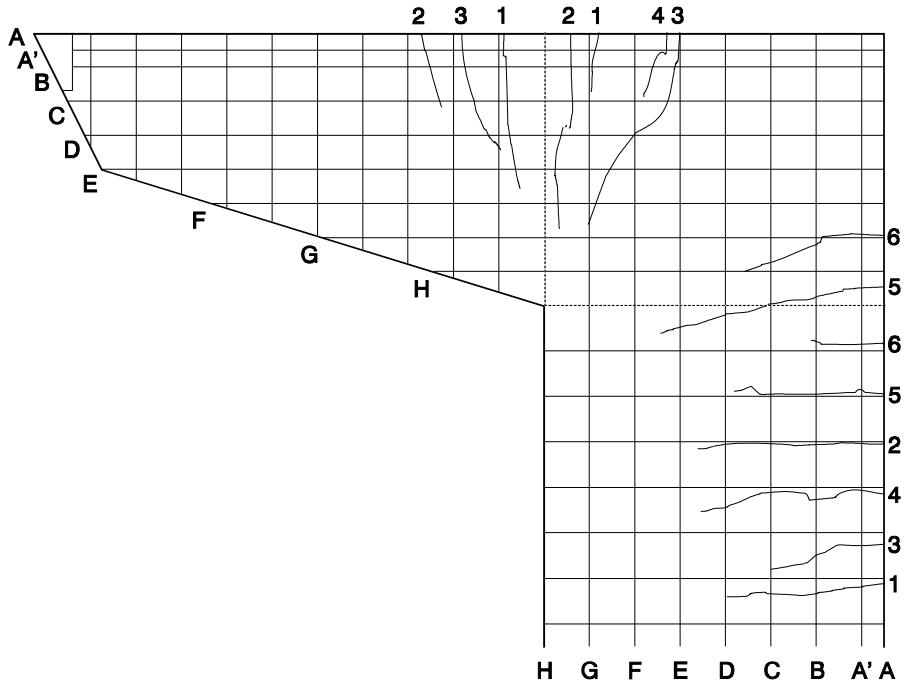

Figure 4.122 Cracking pattern on south face of Specimen POJ-PU-54-TH at service load

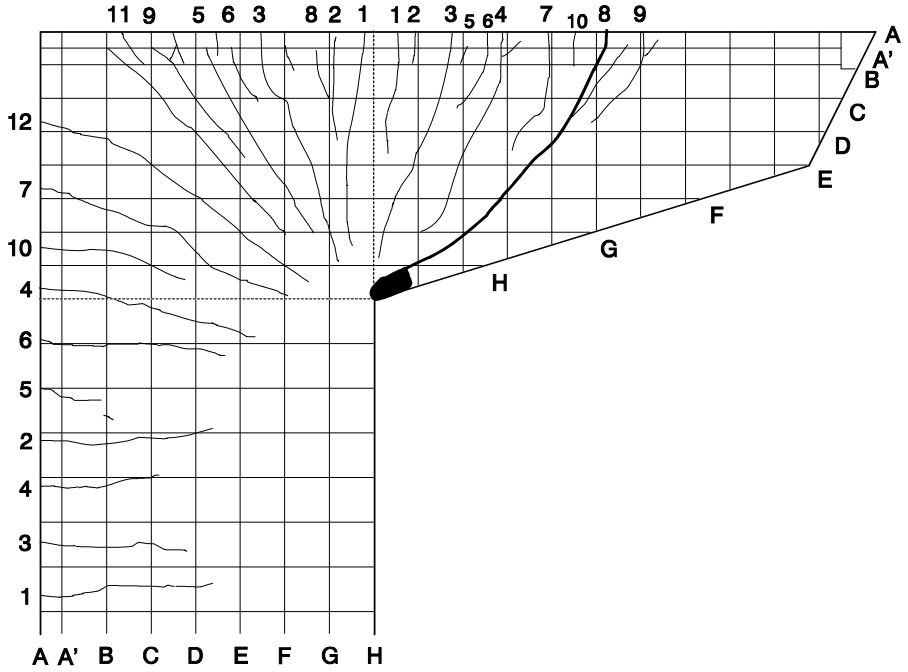

Figure 4.123 Cracking pattern on north face of Specimen POJ-PU-54-TH at failure

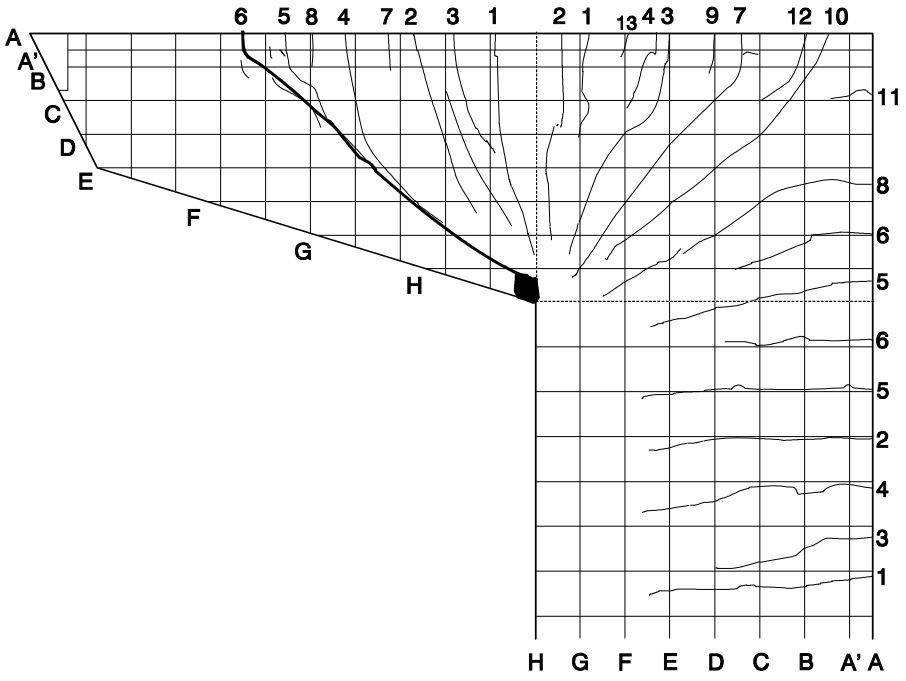

Figure 4.124 Cracking pattern on south face of Specimen POJ-PU-54-TH at failure

Cracking patterns for the north and south faces of the overhang at dead load are presented in Figure 4.125 and Figure 4.127, respectively, and cracking patterns at service load are presented in Figure 4.126 and Figure 4.128, respectively. Maximum measured crack widths for the north face of the overhang are presented in Table A.33 and Table A.34 in SI and customary units, respectively. Maximum measured crack widths for the south face of the overhang are presented in Table A.35 and Table A.36 in SI and customary units, respectively. Crack widths in the overhang at service load, in general, were well controlled, and the largest measured crack width of 0.15 mm (0.006 in.) occurred for crack (1) on the south face. This was only slightly larger than the maximum acceptable crack width of 0.14 mm (0.0055 in.).

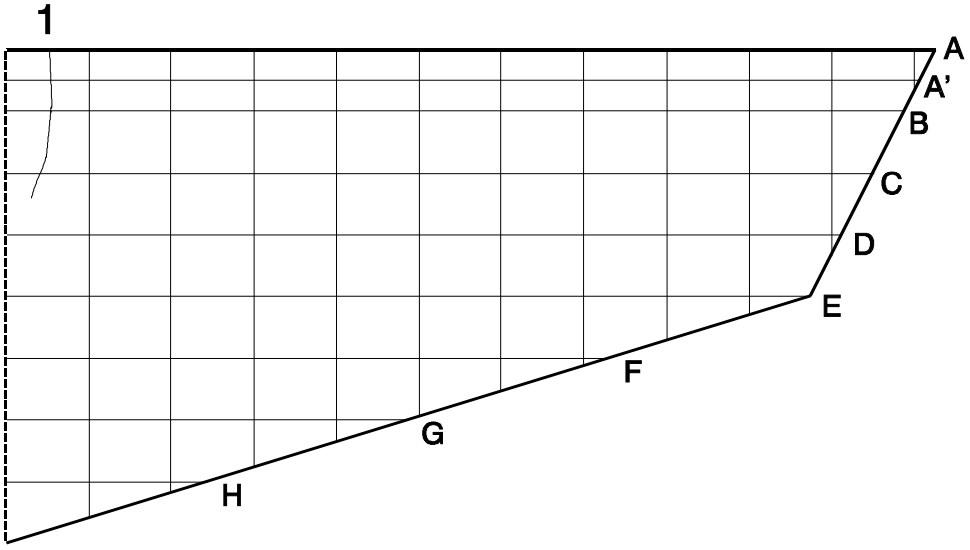

Figure 4.125 POJ-PU-54-TH cracking pattern on north face of overhang at dead load

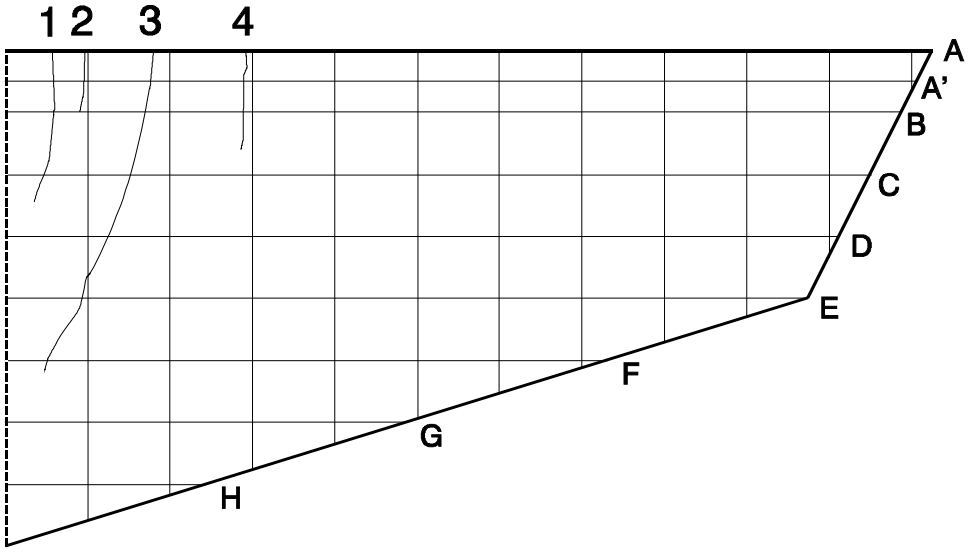

Figure 4.126 POJ-PU-54-TH cracking pattern on north face of overhang at service load

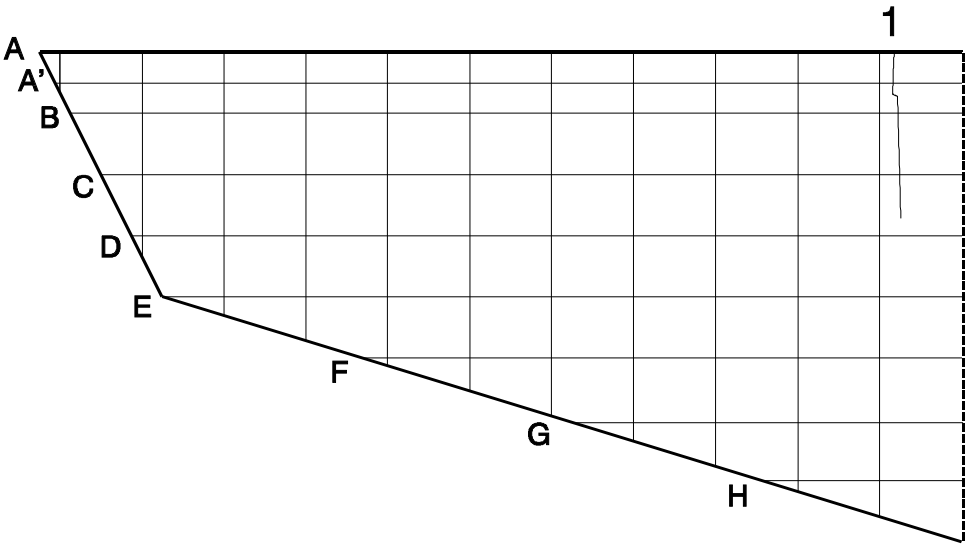

Figure 4.127 POJ-PU-54-TH cracking pattern on south face of overhang at dead load

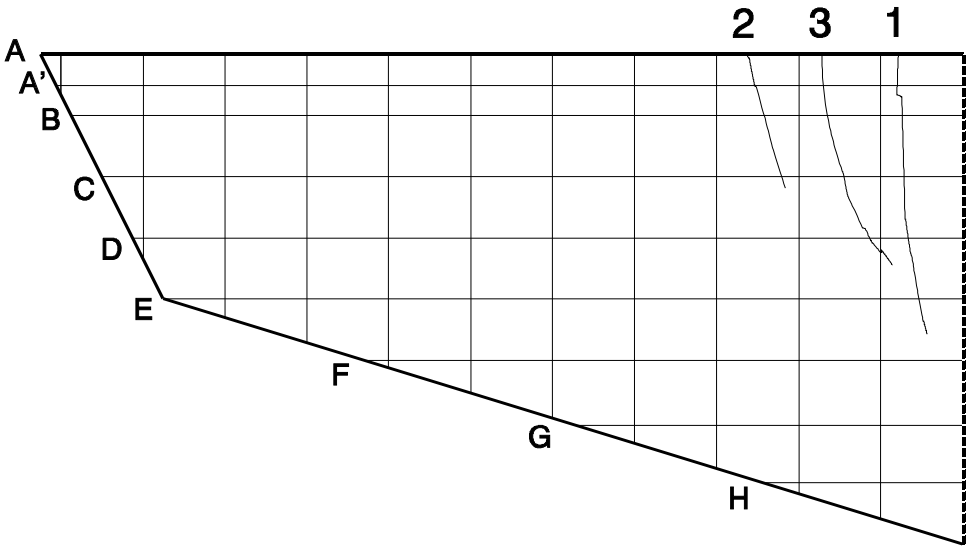

Figure 4.128 POJ-PU-54-TH cracking pattern on south face of overhang at service load

Cracking patterns for the north and south faces of the joint at dead load are presented in Figure 4.129 and Figure 4.131, respectively, and cracking patterns at service load are presented in Figure 4.130 and Figure 4.132, respectively. Maximum measured crack widths for the north face of the overhang are presented in Table A.37 and Table A.38 in SI and customary units, respectively. Maximum measured crack widths for the south face of the overhang are presented in Table A.39 and Table A.40 in SI and customary units, respectively. Maximum measured crack widths for crack (4) on the north face and crack (5) on the south face of the joint (0.17 mm (0.0065 in.) were larger than the maximum acceptable crack width of 0.14 mm (0.0055 in.). Maximum measured crack widths for the other cracks were large. A large diagonal crack developed at loads slightly larger than DL+2LL (crack (11) on the north face and crack (10) on the south face, as shown in Figure 4.123 and Figure 4.124, respectively).

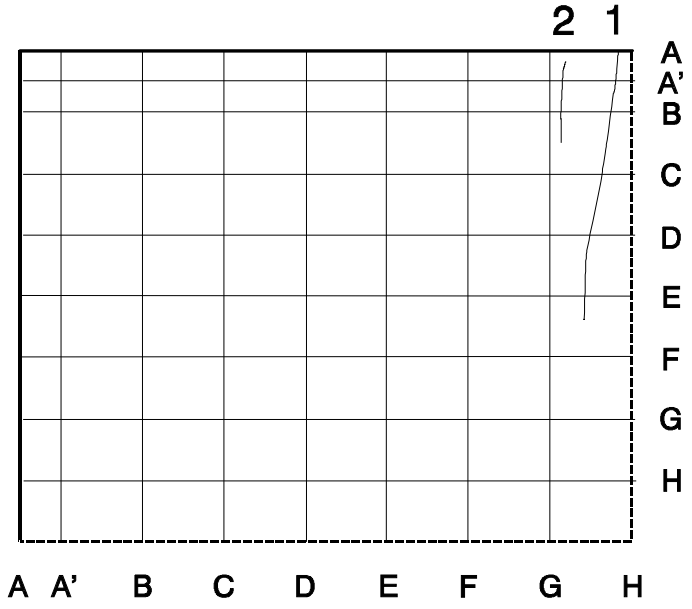

Figure 4.129 POJ-PU-54-TH cracking pattern on north face of joint at dead load

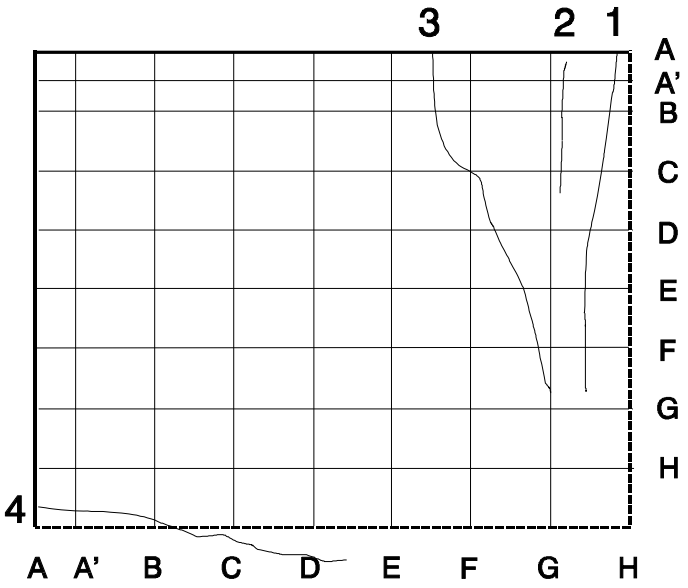

Figure 4.130 POJ-PU-54-TH cracking pattern on north face of joint at service load

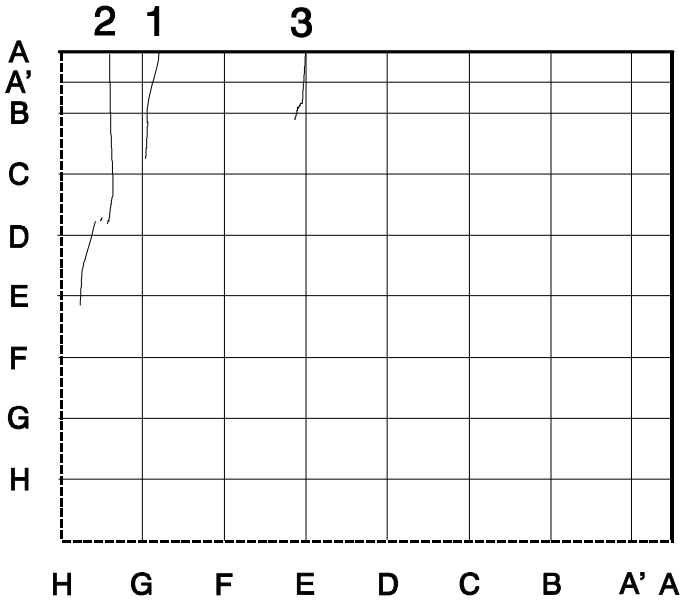

Figure 4.131 POJ-PU-54-TH cracking pattern on south face of joint at dead load

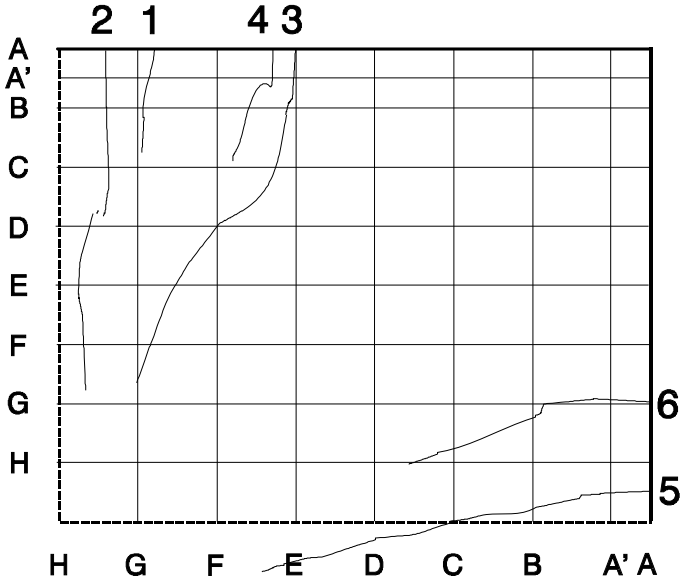

Figure 4.132 POJ-PU-54-TH cracking pattern on south face of joint at service load

Cracking patterns at dead load for the north and south faces of the pier are presented in Figure 4.133 and Figure 4.135, respectively. Cracking patterns in the pier at service load are presented in Figure 4.134 and Figure 4.136, respectively. Maximum measured crack widths for the north face of the pier are presented in Table A.41 and Table A.42 in SI and customary units, respectively. Maximum measured cracks for the south face of the pier are presented in Table A.43 and Table A.44 in SI and customary units, respectively. Crack widths in the pier were controlled, and the largest measured crack width (crack (1) on the south face of the pier) was equal to the maximum acceptable crack width of 0.14 mm (0.0055 in.).

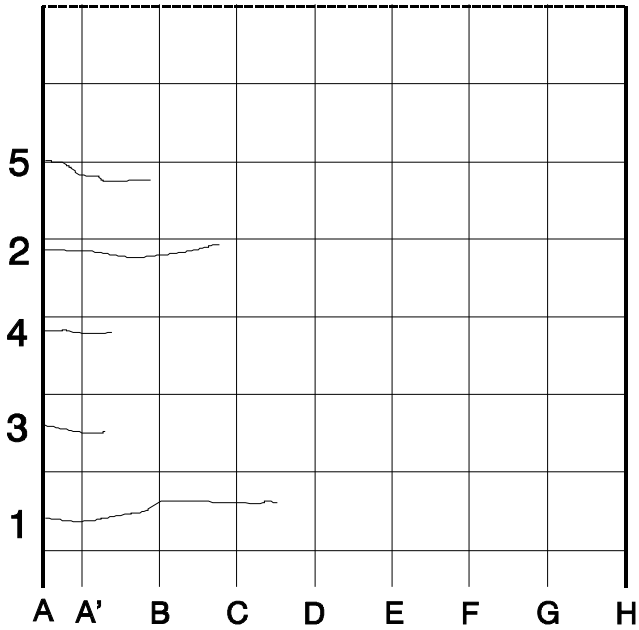

Figure 4.133 POJ-PU-54-TH cracking pattern on north face of pier at dead load

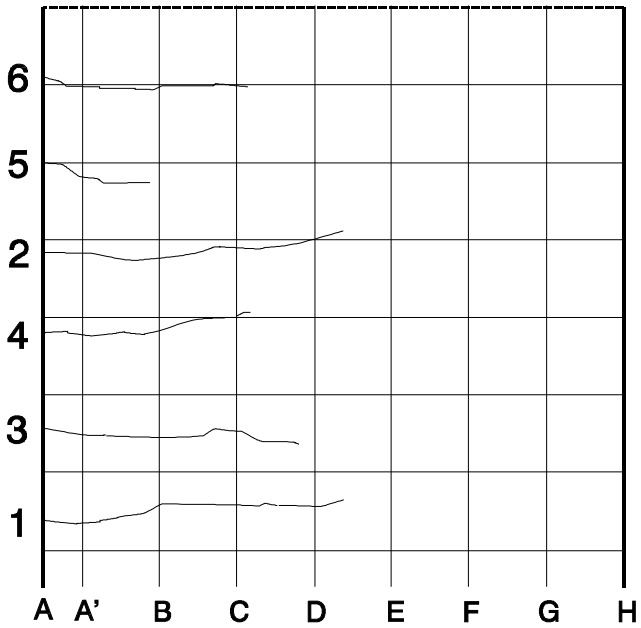

Figure 4.134 POJ-PU-54-TH cracking pattern on north face of pier at service load

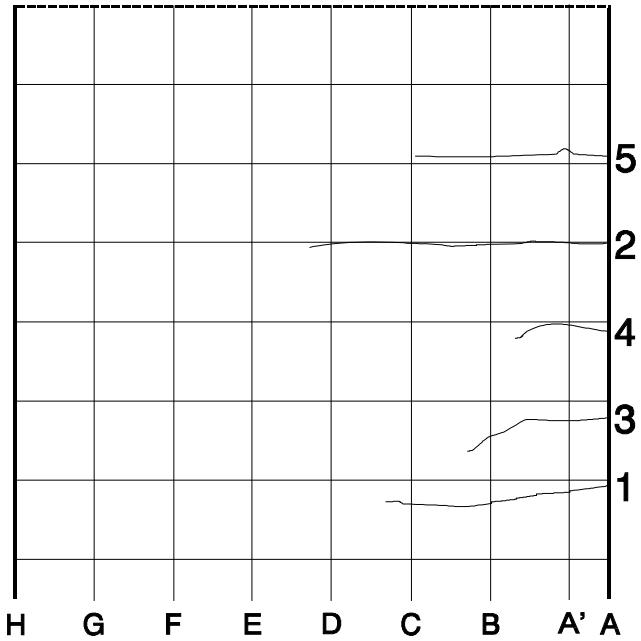

Figure 4.135 POJ-PU-54-TH cracking pattern on south face of pier at dead load

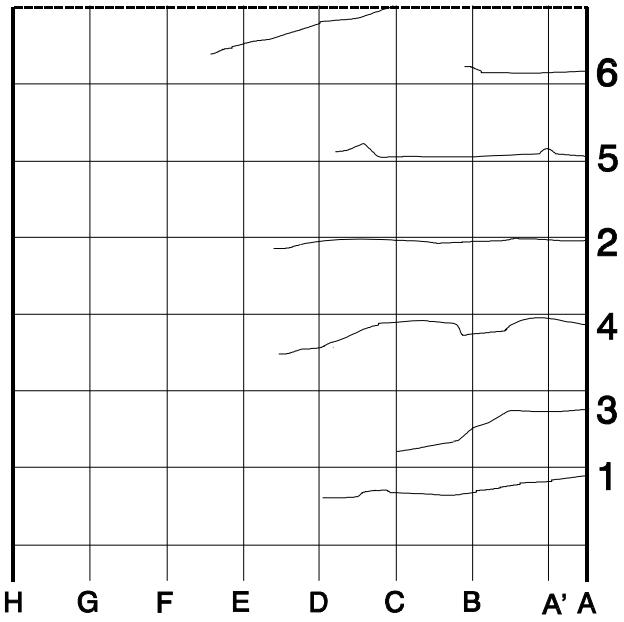

Figure 4.136 POJ-PU-54-TH cracking pattern on south face of pier at service load

4.3.2.2 Applied Overhang Moment vs. Deflection Response–POJ-PU-54-TH

Locations of the displacement transducers for Specimen POJ-PU-54-TH are shown in Figure 4.137. Transducers labeled A, B, or C were located on the south side, center line, or north side of the specimen, respectively.

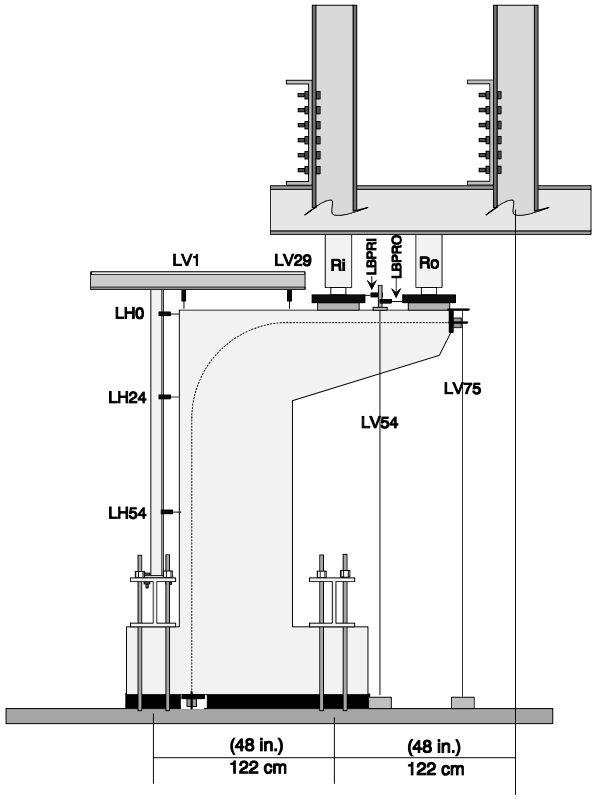

Figure 4.137 Location of displacement transducers for Specimen POJ-PU-54-TH

Plots of applied moment vs. deflection response for Specimen POJ-PU-54-TH are presented in Figure 4.138 through Figure 4.141. As before, the applied overhang moment is plotted as a fraction of factored moment. Displacements are labeled in both SI and customary units.

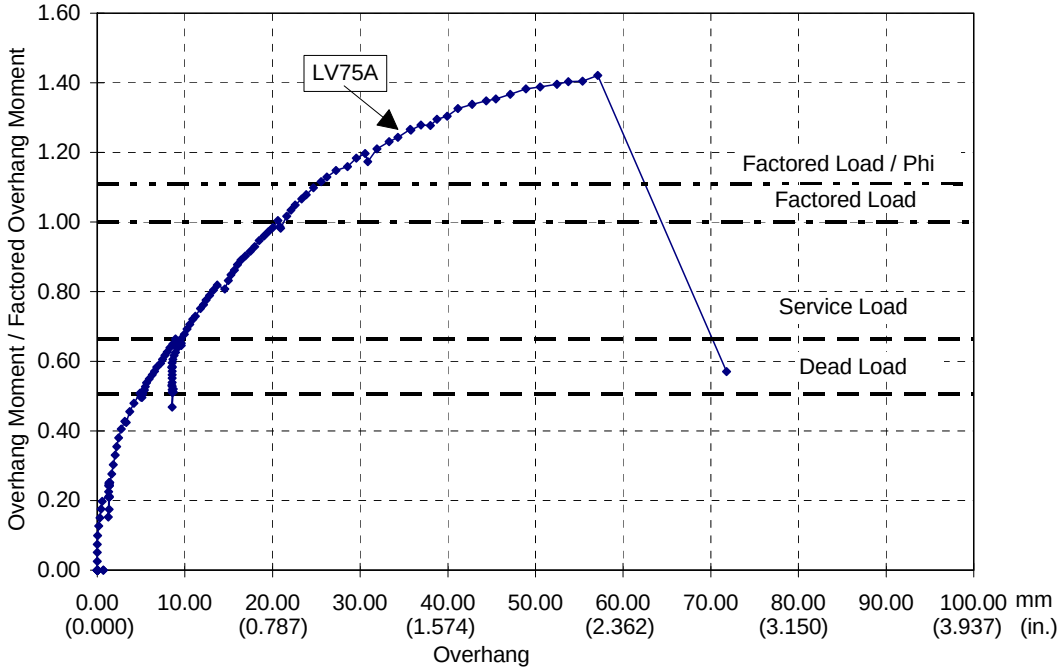

Figure 4.138 POJ-PU-54-TH tip deflection (LV 75)

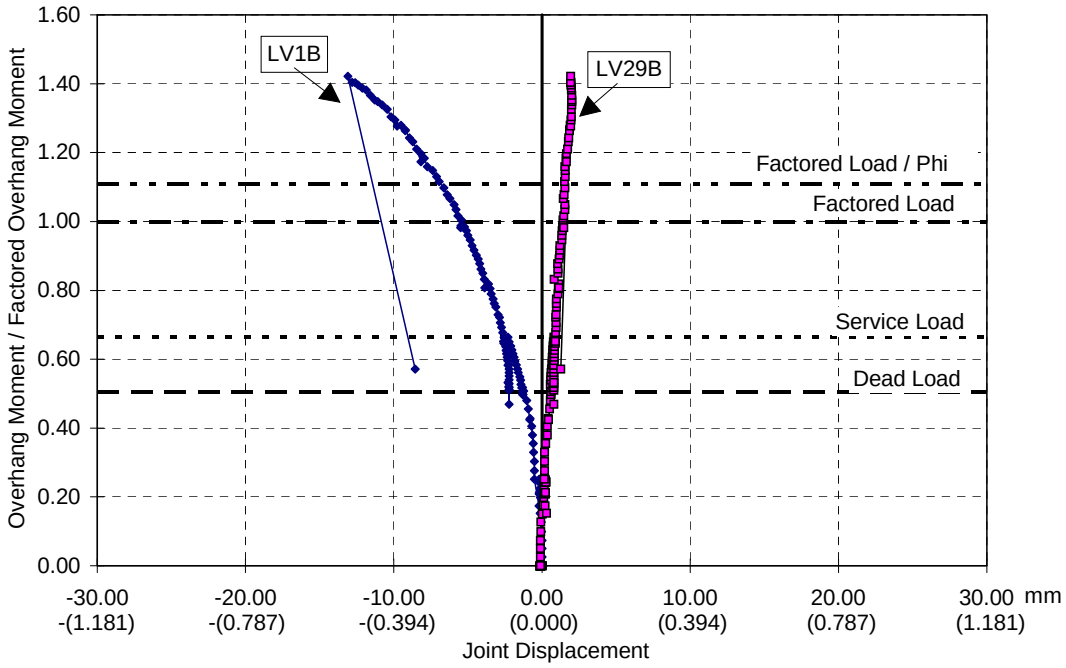

Figure 4.139 POJ-PU-54-TH joint vertical displacement

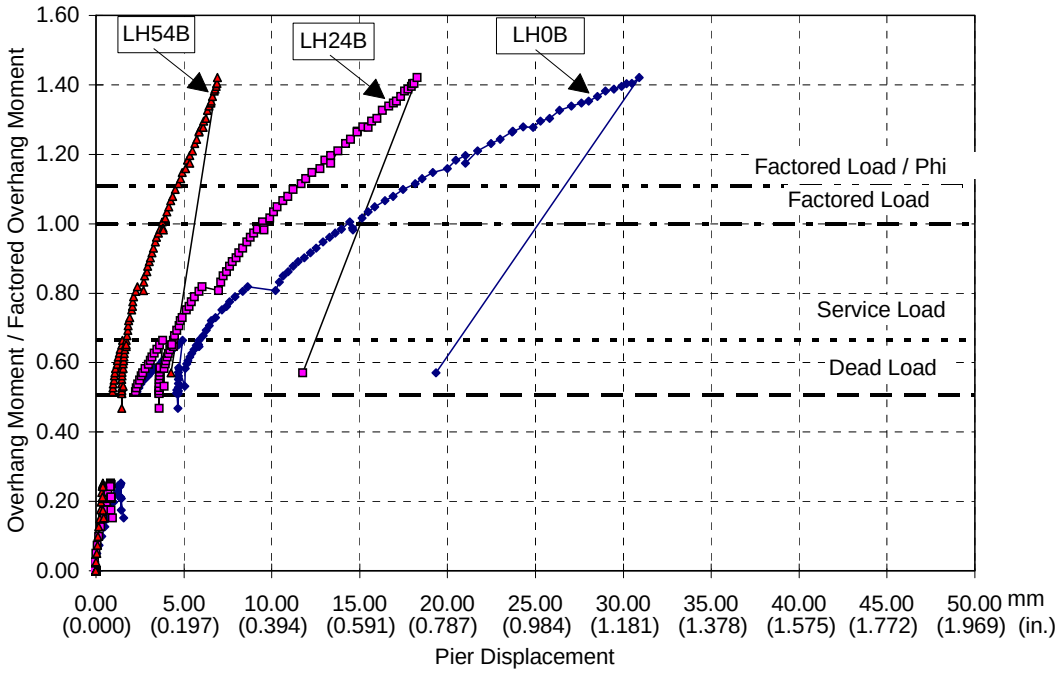

Figure 4.140 POJ-PU-54-TH pier horizontal deflection

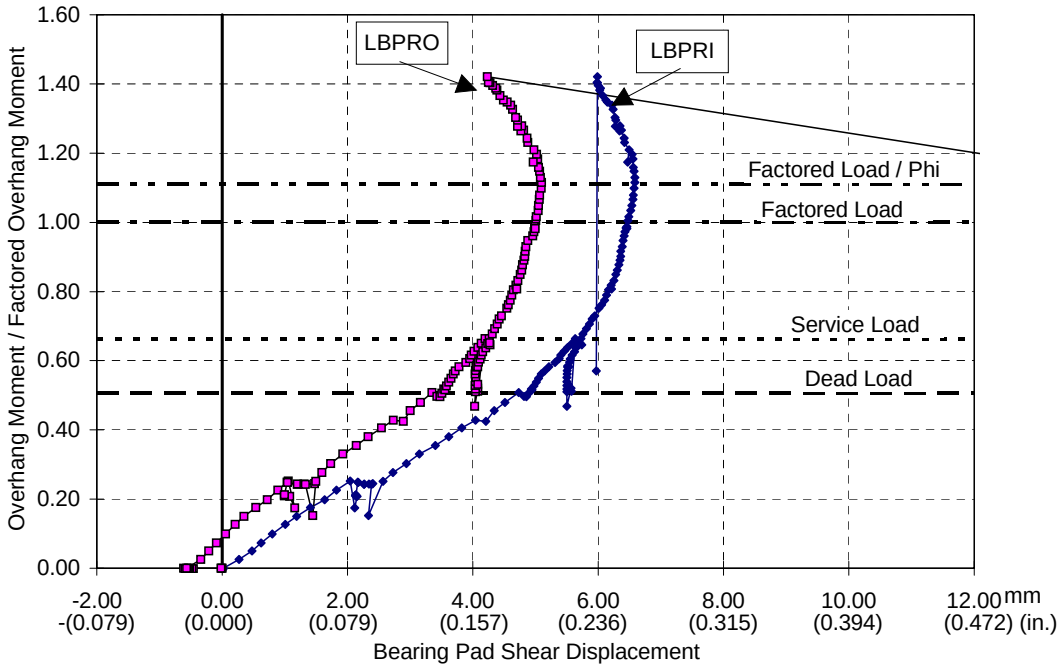

Figure 4.141 POJ-PU-54-TH bearing pad shear displacement

First cracking and loading to service load followed by unloading to dead load are clearly illustrated in Figure 4.138. The abrupt drop in load and sudden increase in overhang tip displacement occurred when the overhang failed. The overhang tip displacement of 57 mm (2.24 in.) at maximum applied load was quite close to displacement at failure of Specimen POJ-RC-100-TH. Vertical displacement of the exterior corner of the joint, measured by transducer LV1B (plotted in Figure 4.139), indicated a gradual decrease of stiffness with increased applied load. This may have been attributed to the large horizontal deflections of the pier for loads above factored load. The plot of pier horizontal deflections, shown in Figure 4.140, has a gap where the displacement transducers failed to function. The bearing pad shear displacements, shown in Figure 4.141, indicated larger shear deformations than those recorded for the previous tests. It is apparent the eccentric loads applied to the loading frame (see Figure 4.137) caused the loading frame to sway away from the bent with increased applied load. The increased sway of the test frame, in this test and the test of Specimen POJ-PU-74-TH, was attributed to damage of some of the strong-floor hold-down bolts. The increase in applied moment on the specimen (computed using the shear stiffness of the bearing pad [1.7 kN/mm (9.6 kip/in.)] and the measured shear displacement [6.60 mm (0.260 in.)]) was small, and was not included in the moment calculations.

4.3.2.3 Location and Identification of Strain Gage—POJ-PU-54-TH

Strain gages for Specimen POJ-PU-54-TH were attached to the longitudinal and transverse reinforcement at points similar to those selected for Specimen POJ-RC-100-TH. Strain gage locations and labels for Specimen POJ-PU-54-TH are presented in Figure 4.142 through Figure 4.144. As before, multiple strain gages were located at the same layer of reinforcement (*i.e.*, Strain gages M30Z1A, B, and C, shown in Figure 4.142) to provide redundancy in case a strain gage malfunctioned. The primary mild longitudinal reinforcement in the pier and overhang were gaged at several points along the length to measure bar development. Additionally, pier and overhang longitudinal reinforcement were gaged at several cross sections to determine strain profiles across the sections. Strain gages were attached to transverse and longitudinal reinforcement in the overhang (over the region X=40 to X=62) to measure reinforcement strains in the event a shear crack developed. As for Specimen POJ-RC-100-TH, there was concern that a shear failure might develop because the number of closed transverse ties in the overhang was intentionally reduced. Plots in Section 4.3.2.4 use the following notation to identify which strain gage results are being plotted.

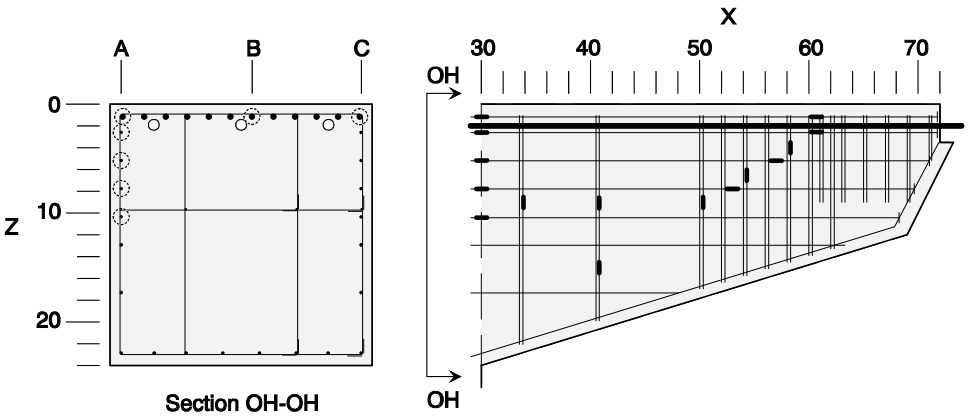

Overhang Primary Longitudinal Reinforcement	Section X=30			Section X=35			Section X=61
	A	B	C	A	B	C	A
Layer Z=1	M30Z1A	M30Z1B	M30Z1C	M35Z1A	M35Z1B	M35Z1C	M61Z1A

Longitudinal Side-Face Reinforcement	Section X=30	Section X=53	Section X=57	Section X=61
Layer Z=3	T30Z3A			T61Z3A
Layer Z=5	T30Z5A		T57Z5A	
Layer Z=8	T30Z8A	T53Z8A		
Layer Z=10	T30Z10A			

4

Overhang Transverse Reinforcement	Section X=34	Section X=41	Section X=50	Section X=58
Level Z=4				S58Z4A
Level Z=6			S50Z6A	
Level Z=9	S34Z9A	S40Z9A	S50Z9A	
Level Z=15		S40Z15A		

Figure 4.142 POJ-PU-54-TH overhang strain gage locations and labels

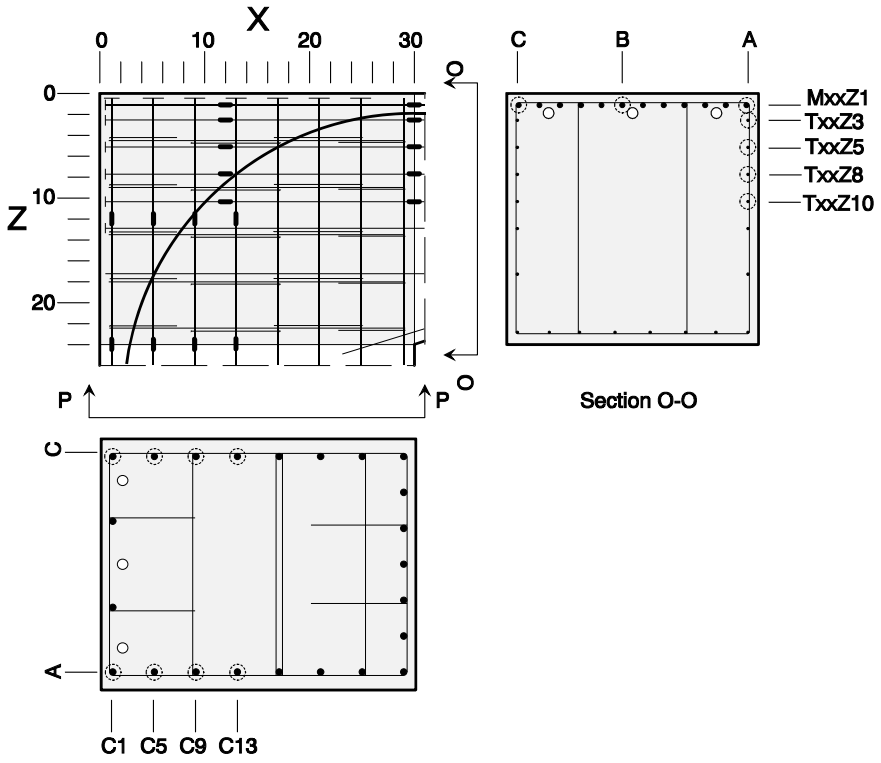

Overhang Longitudinal Reinforcement	Section X=13			Section X=30		
	A	**B**	**C**	**A**	**B**	**C**
Layer Z=1	M13Z1A	M13Z1B	M13Z1C	M30Z1A	M30Z1B	M30Z1C
Layer Z=3	T13Z3A			T30Z3A		
Layer Z=5	T13Z5A			T30Z5A		
Layer Z=8	T13Z8A			T30Z8A		
Layer Z=10	T13Z10A			T30Z10A		

Pier Longitudinal Reinforcement	Section X=12			Section X=24		
	A	**B**	**C**	**A**	**B**	**C**
Layer X=1	C1Z12A		C1Z12C	C1Z24A		C1Z24C
Layer X=5	C5Z12A		C5Z12C	C5Z24A		C5Z24C
Layer X=9	C9Z12A		C9Z12C	C9Z24A		C9Z24C
Layer X=13	C13Z12A		C13Z12C	C13Z24A		C13Z24C

Figure 4.143 POJ-PU-54-TH joint strain gage locations and labels

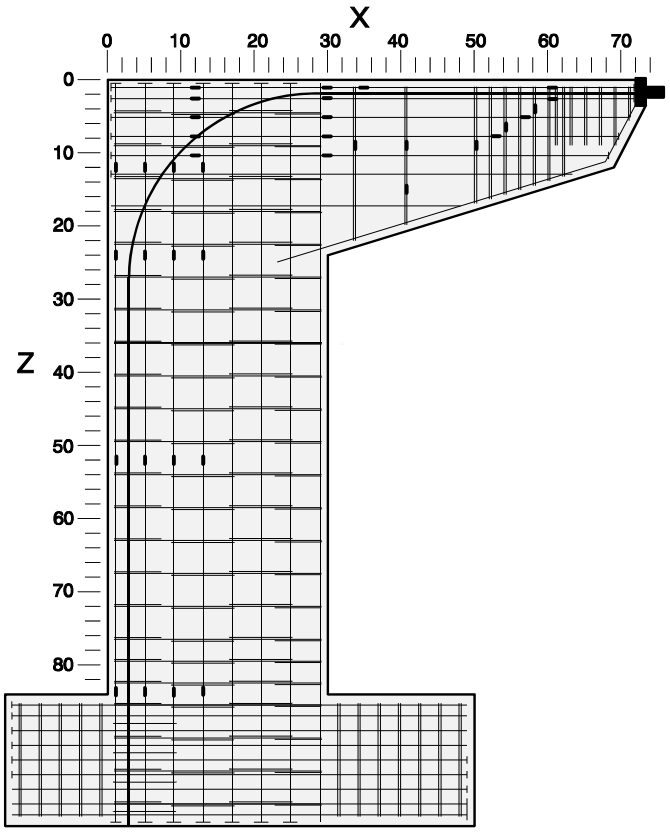

Pier Longitudinal Reinforcement	Section Z=52			Section Z=83		
	A	B	C	A	B	C
Level X1	C1Z52A		C1Z52C	C1Z83A		C1Z83C
Level X5	C5Z52A		C5Z52C	C5Z83A		C5Z83C
Level X9	C9Z52A		C9Z52C	C9Z83A		C9Z83C
Level X13	C13Z52A		C13Z52C	C13Z83A		C13Z83C

Figure 4.144 POJ-PU-54-TH overall strain gage locations and pier strain gage labels

4.3.2.4 Applied Moment vs. Strain Response–POJ-PU-54-TH

Applied moment vs. strain response for Specimen POJ-PU-54-TH included strain measurements for strain gages attached to primary longitudinal mild reinforcement in the overhang (Figure 4.145), transverse reinforcement in the overhang (Figure 4.146), and longitudinal pier reinforcement at layers X=1, 5, 9, and 13 (Figure 4.147 through Figure 4.150, respectively). Strain gages indicated abrupt changes in strain when cracking occurred in the vicinity of each of the gages.

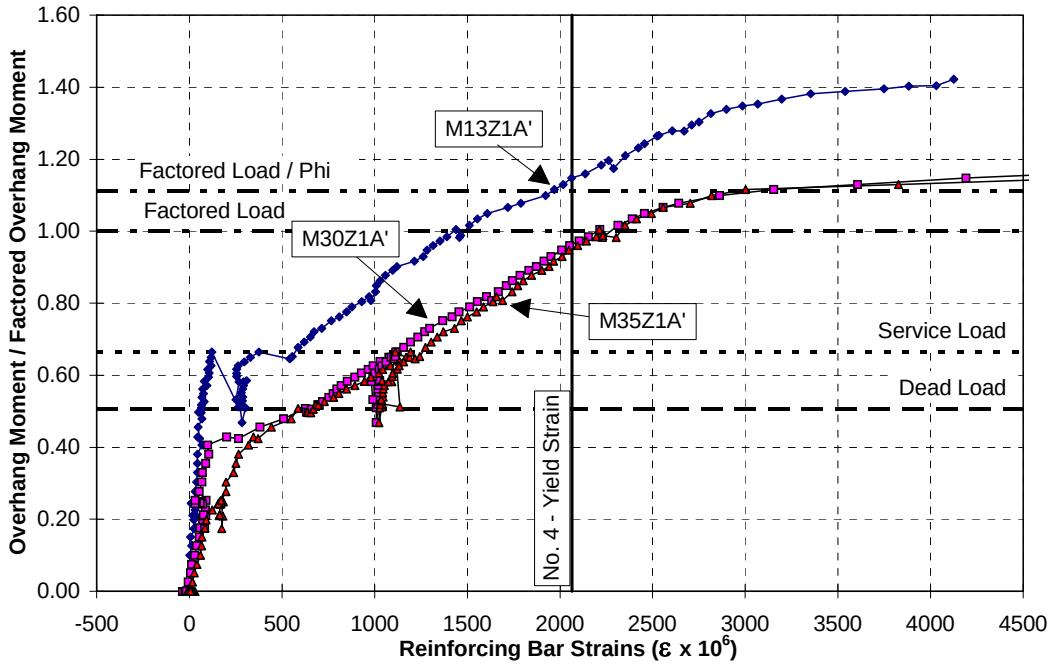

Figure 4.145 POJ-PU-54-TH strains in primary longitudinal mild reinforcement at Layer Z=1 in overhang

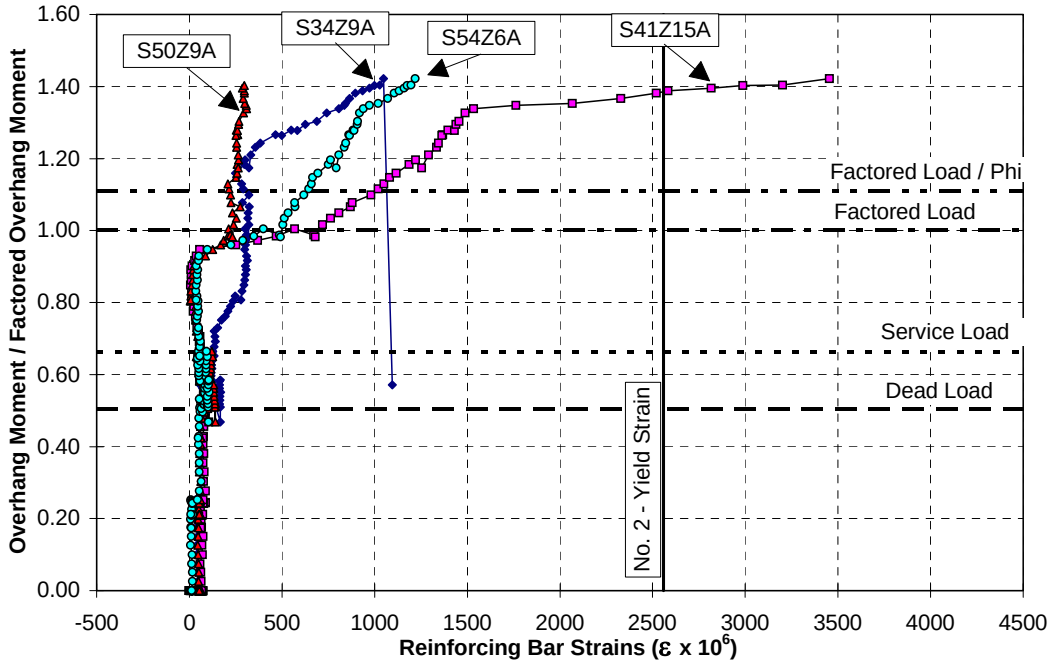

Figure 4.146 POJ-PU-54-TH strains in transverse reinforcement in overhang

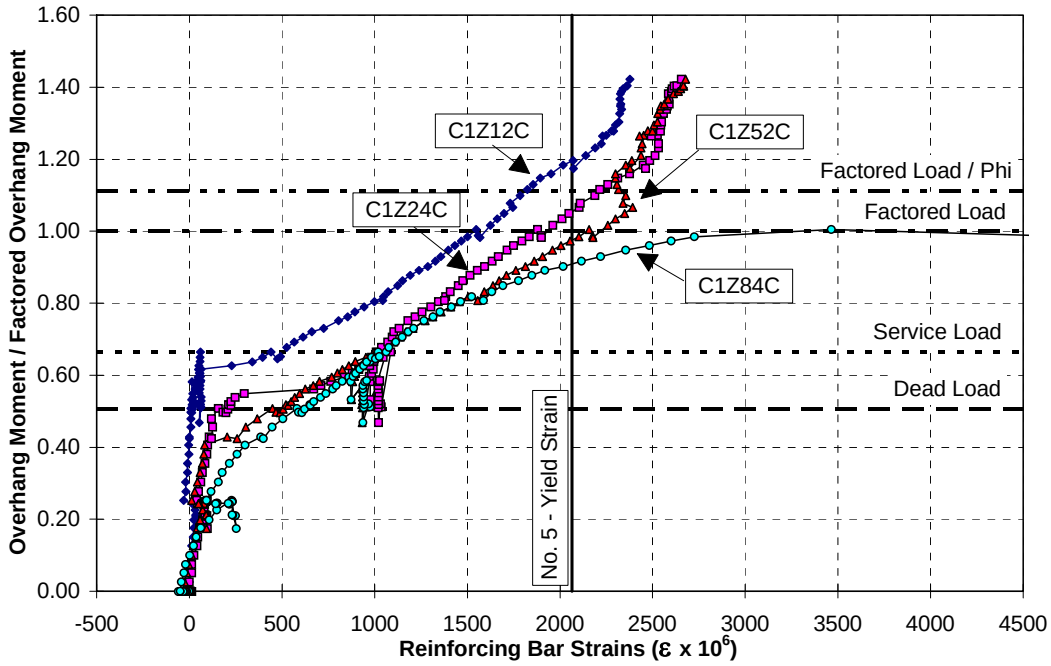

Figure 4.147 POJ-PU-54-TH strains in pier longitudinal reinforcement at Layer X=1

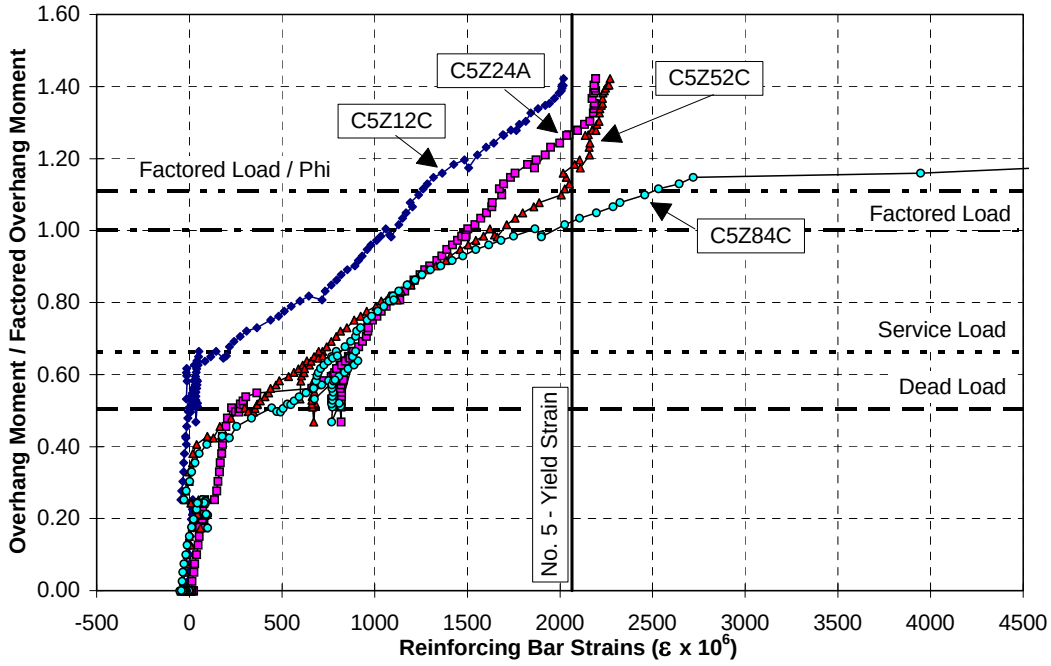

Figure 4.148 POJ-PU-54-TH strains in pier longitudinal reinforcement at Layer X=5

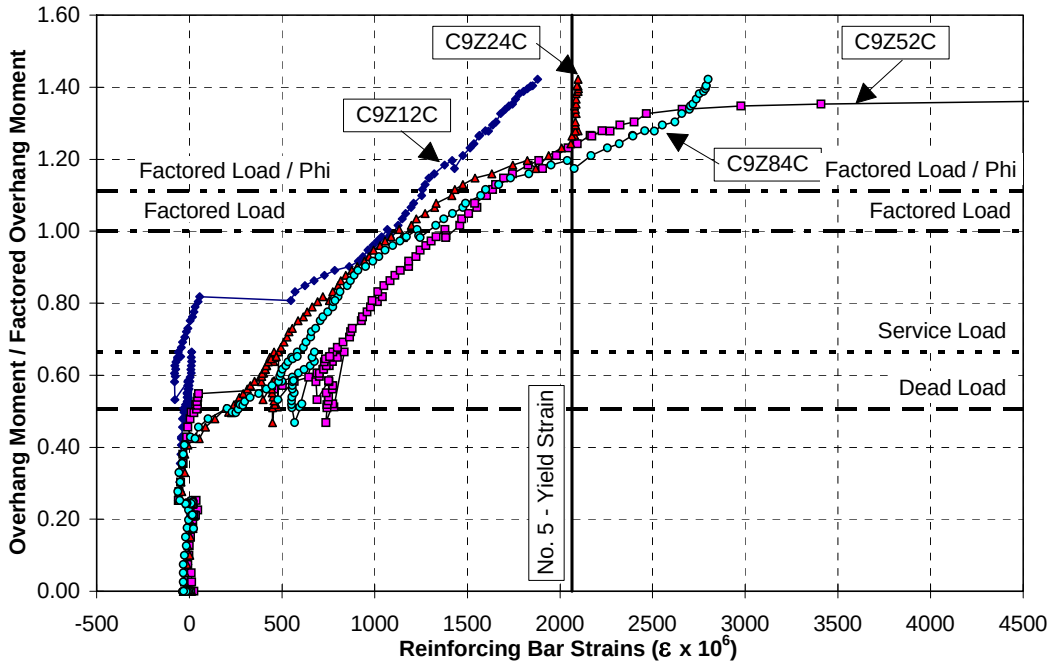

Figure 4.149 POJ-PU-54-TH strains in pier longitudinal reinforcement at Layer X=9

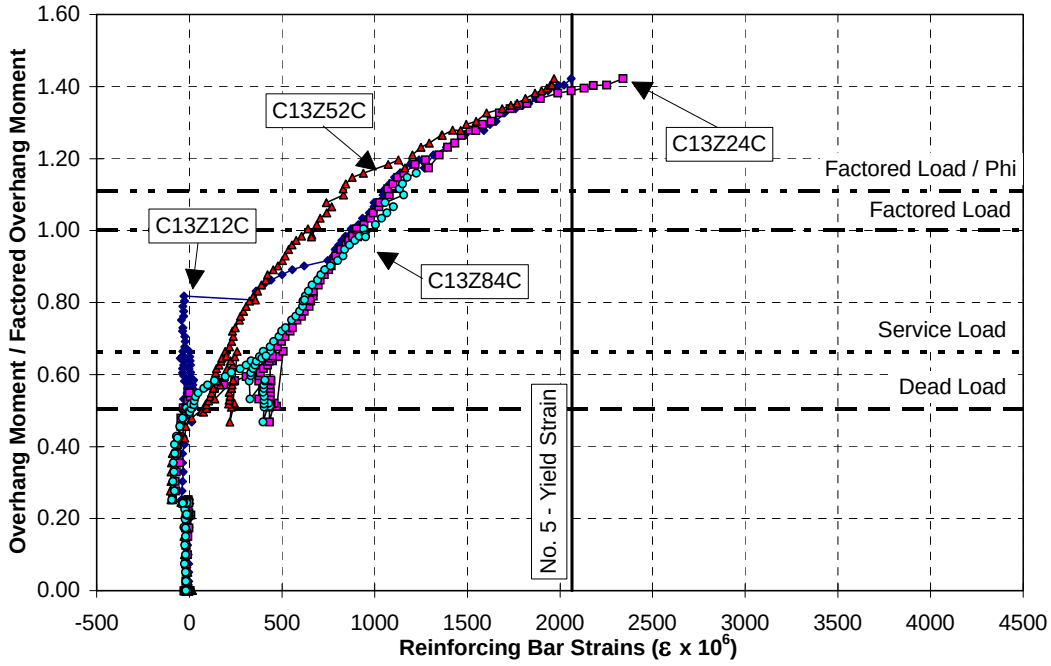

Figure 4.150 POJ-PU-54-TH strains in pier longitudinal reinforcement at Layer X=13

Strain measurements indicated the primary longitudinal reinforcement in the overhang (Layer Z=1, shown in Figure 4.145) yielded at the cross section closest to the column face (X=30) and the adjacent section (X=35) at a moment ratio of 0.98, or slightly less than factored load. Measured strain for the gage located in the joint (section X=13) reached yield strain at a moment ratio of 1.13.

Measured strains in the primary longitudinal mild reinforcement in the overhang were in excess of 10,000 με when the shear/compression failure occurred in the overhang.

Moment-strain response for transverse reinforcement (plotted in Figure 4.146) indicated first cracking occurred at a moment ratio of 0.96, or slightly less than factored load. Strain measurements for strain gage S41Z15A, attached to a closed transverse tie at section X=41, were equal to yield strain at a moment ratio of 1.40. After the concrete on the underside of the overhang (closest to the column face) spalled, a brittle failure mode developed because the capacity of the vertical tension tie in the overhang was not sufficient to support the outer load after the compression force path was lost.

Strains at Sections Z=24,54, and 84 for each layer of the pier longitudinal reinforcement were quite similar, as illustrated in Figure 4.147 through Figure 4.150. Measured strains at C9Z12C and C13Z12C showed sharp increases in strain of nearly 500 με when the critical diagonal joint crack formed at a moment ratio of 0.8, or DL+1.8LL. Strains in longitudinal reinforcement located in the joint reconfirmed the importance of positive anchorage of mild reinforcement in the joint.

4.3.2.5 Overhang and Pier Strain Profiles

Strain profiles in the overhang at Section X=30, and pier at Sections Z=12, 24, and 52 are presented in Figure 4.151 through Figure 4.154, respectively. Overhang strain profiles at section X=30 (Figure 4.151) were uniform through the depth of the cross section. As for Specimen POJ-RC-100-TH, this phenomenon was attributed to the small quantity of side-face reinforcement used because the largest crack widths at Section X=30 were located near mid-depth of the overhang. Strain profiles for the pier cross sections at Z=12, were irregular because of the cracking patterns in the joint. The strain profiles were expected to be fairly uniform across the section. Strain profiles for Sections Z=24 and 52 were nearly linear as a function of distance from the exterior face of the pier.

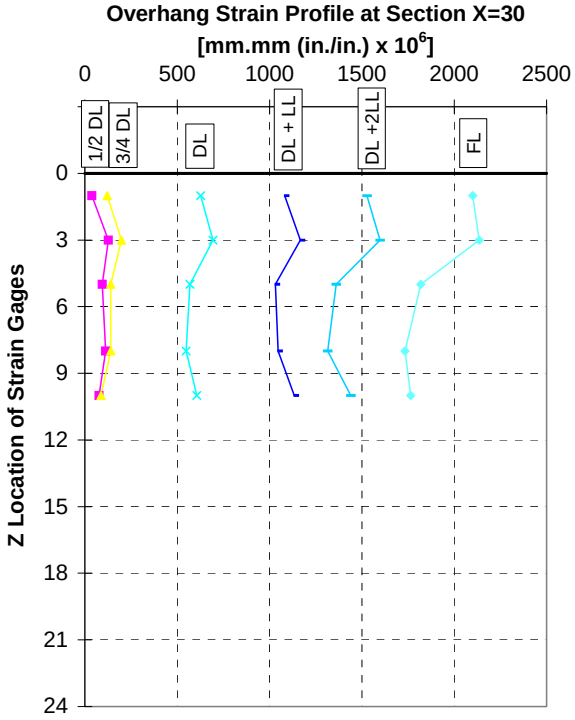

Figure 4.151 POJ-PU-54-TH strain profiles in overhang at Section X=30

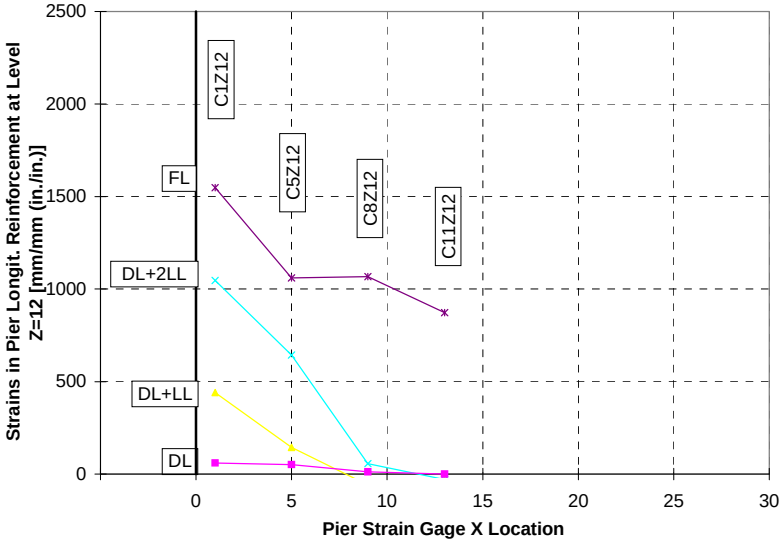

Figure 4.152 POJ-PU-54-TH strain profiles in pier at Section Z=12

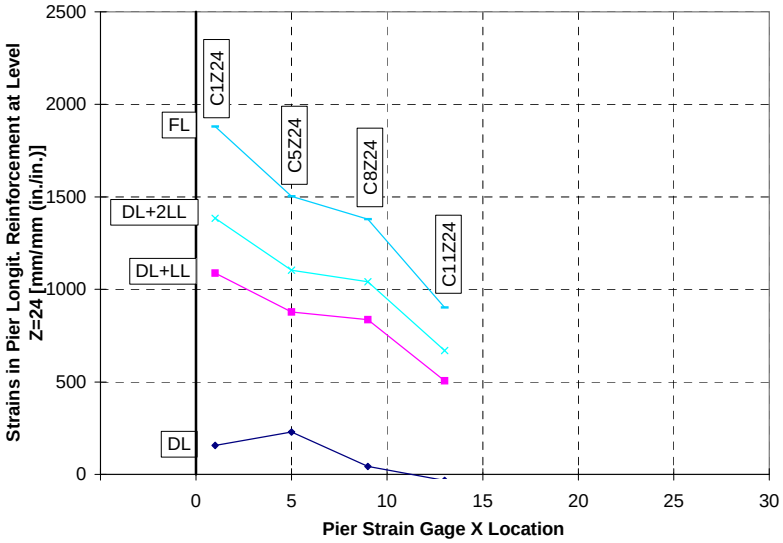

Figure 4.153 POJ-PU-54-TH strain profiles in pier at Section Z=24

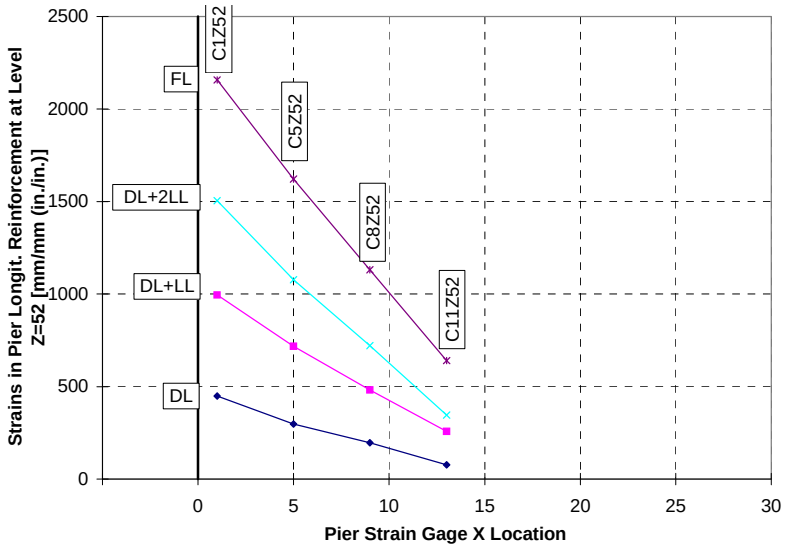

Figure 4.154 POJ-PU-54-TH strain profiles in pier at Section Z=52

4.3.3 74% Prestressed Design with T-Headed Reinforcement–POJ-PU-74-TH

Specimen POJ-PU-74-TH, like Specimen POJ-PU-54-TH, was designed using a strength-based design method which integrated post-tensioning tendons and T-headed mild reinforcement to resist factored loads and provide serviceability at design loads. Reinforcing details for Specimen POJ-PU-74-TH are presented in Figure 4.155.

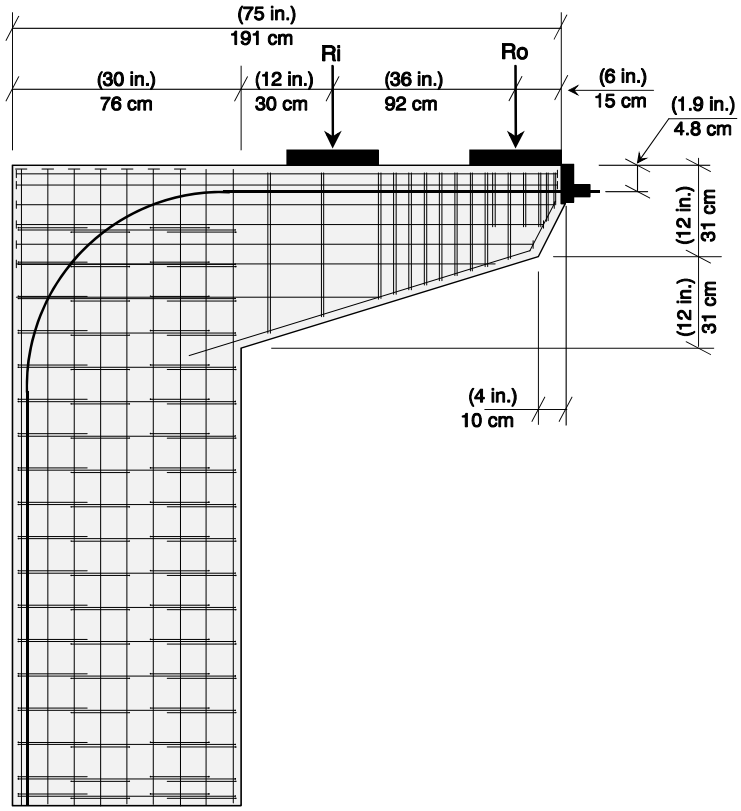

Figure 4.155 Reinforcement details for Specimen POJ-PU-74-TH

In Specimen POJ-PU-74-TH, 74% of the tension tie force required for strength was provided by Lo-Lax prestressing strand with an ultimate tensile stress of 1.8 GPa (270 ksi), and 26% was provided by T-headed mild reinforcement with a nominal yield stress of 413 MPa (60 ksi).

The joint corner detail for Specimen POJ-PU-74-TH (shown in Figure 4.156) illustrates the arrangement of T-headed reinforcement in the joint corner and location of the continuous post-tensioning. The interlaced T-headed reinforcement in the joint corner formed a compression node (see Figure 4.156) that developed the diagonal compression strut in the joint. Continuous prestressing through the joint region reduced concrete tensile stresses significantly and provided a bonded high-strength tensile tie in the region of potential diagonal cracking. A finite element analysis of the joint region confirmed the reduction of principal tensile stresses. Principal tensile stresses and principal compressive stresses are plotted as contours and vectors in Figure 4.157 and Figure 4.158, respectively. The percentage of post-tensioning was increased to 74% (54% was used in the previous specimen) to further reduce concrete tensile stresses at dead and service loads.

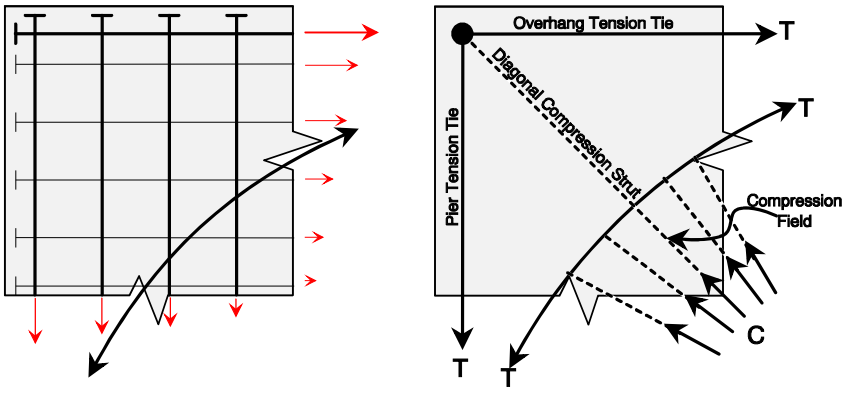

Figure 4.156 Joint corner detail for Specimen POJ-PU-74-TH

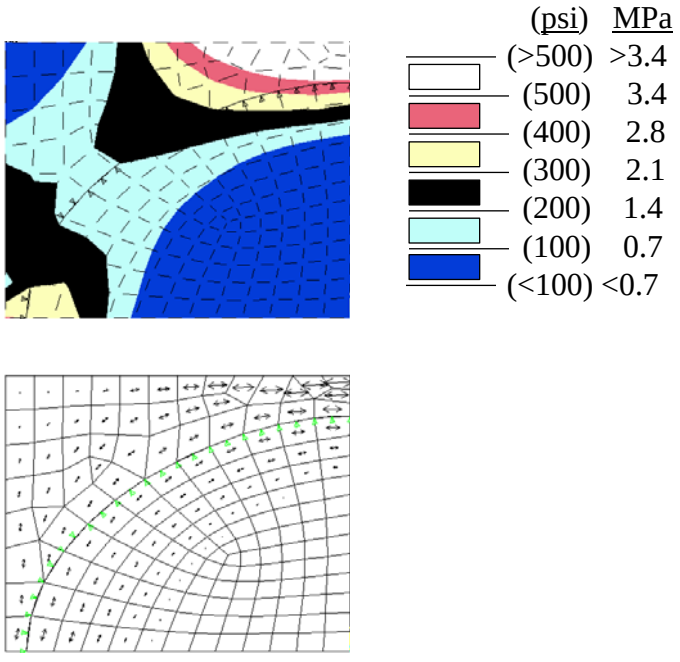

Figure 4.157 POJ-PU-74-TH joint principal tensile stresses and vectors at service load

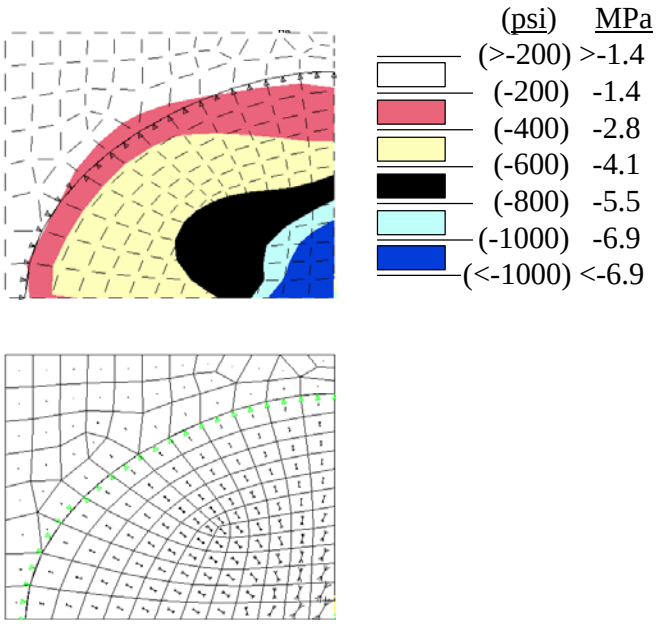

Figure 4.158 POJ-PU-74-TH joint principal compressive stresses and vectors at service load

Although the overhang and pier sections were expected to crack at dead load, the distribution of mild reinforcement and positioning of post-tensioned reinforcement were designed to limit the width of cracks that formed.

Specimen POJ-PU-74-TH was prestressed in stages after being cast and installed in the testing frame. The two outer 1.5 cm (0.6 in.) diameter tendons were each stressed to 1.1 GPa (160 ksi) before any load was applied to the specimen. The specimen was loaded in steps to ½DL at which point one-1.5 cm (0.6 in.) diameter tendon and the two-1.3 cm (0.5 in.) diameter tendons were stressed to 1.1 GPa (160 ksi). A lift off test was performed to verify that each tendon was stressed to 1.1 GPa (160 ksi). After the stressing operation was completed, applied load equivalent to ½DL was maintained on the overhang while the post-tensioning ducts were grouted. Testing continued once the grout reached a cube compressive strength of 10 MPa (1500 psi).

As applied load on the specimen was increased incrementally to dead load, the specimen was inspected for cracks after every other load step. After dead load was applied (load step 20), the first small cracks were identified. Crack widths were measured and cracking patterns were marked and labeled on the specimen and on a pencil sketch at DL, DL+½LL, and DL+LL (service load). After measuring crack widths at service load, the applied load was reduced to measure crack widths at dead load, after cracks from applied service load had formed. Crack widths were again measured at DL, DL+½LL, and DL+LL, and applied load was increased incrementally to DL+2LL where the last crack measurements were made.

A photograph of Specimen POJ-PU-74-TH at an applied load equivalent to factored load/phi is presented in Figure 4.159. Crack widths were well controlled at this point in the test. At DL+4LL, cracks in the overhang at the face of the pier extended nearly the full depth of the overhang. Some concrete spalling was noted on the underside of the overhang, but applied load was maintained. Maximum applied load on Specimen POJ-PU-74-TH was DL+6LL because of the reduced capacity of the strong floor anchor bolts (the specimen could not be loaded to failure). However, before testing was discontinued, large flexural cracks were observed in the overhang. A photograph of the north face of the specimen at maximum applied load is presented in Figure 4.160.

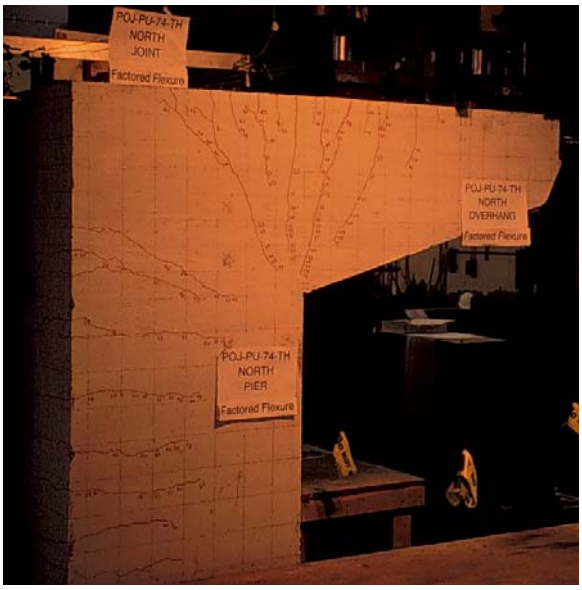

Figure 4.159 Photograph of cracking patterns on north face of Specimen POJ-PU-74-TH at factored load

Figure 4.160 Photograph of cracking patterns on north face of Specimen POJ-PU-74-TH at maximum applied load

4.3.3.1 Cracking Patterns and Maximum Crack Width Measurements–POJ-PU-74-TH

Overall cracking patterns on the north and south faces of Specimen POJ-PU-74-TH at dead load (presented in Figure 4.161 and Figure 4.162, respectively) and service load (presented in Figure 4.163 and Figure 4.164, respectively) indicated the post-tensioning reduced the number of cracks that would be visible under operational loads. Cracking patterns on the north and south faces at maximum applied load are presented in Figure 4.165 and Figure 4.166, respectively. Specimen POJ-PU-74-TH had a distributed cracking pattern, and all measured crack widths at service load were smaller than the maximum allowable crack width. Cracking patterns and maximum measured crack widths in the overhang, joint, and pier regions are detailed below.

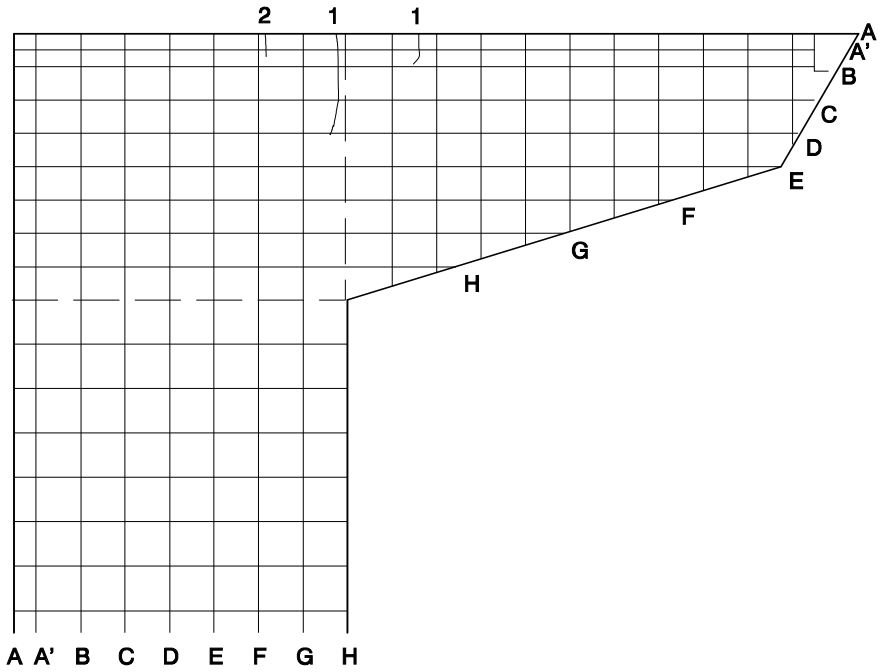

Figure 4.161 Cracking patterns on north face of Specimen POJ-PU-74-TH at dead load

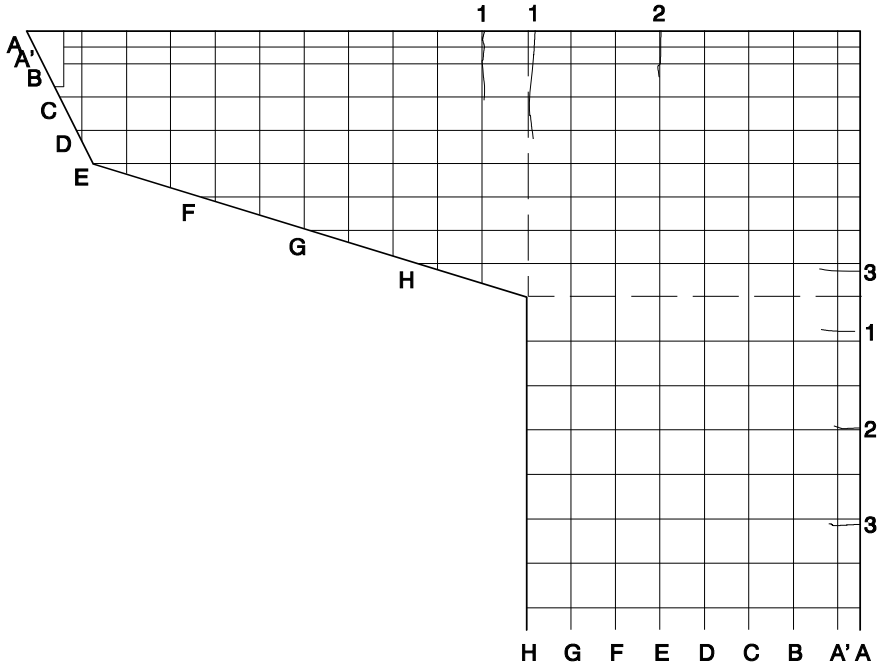

Figure 4.162 Cracking patterns on south face of Specimen POJ-PU-74-TH at dead load

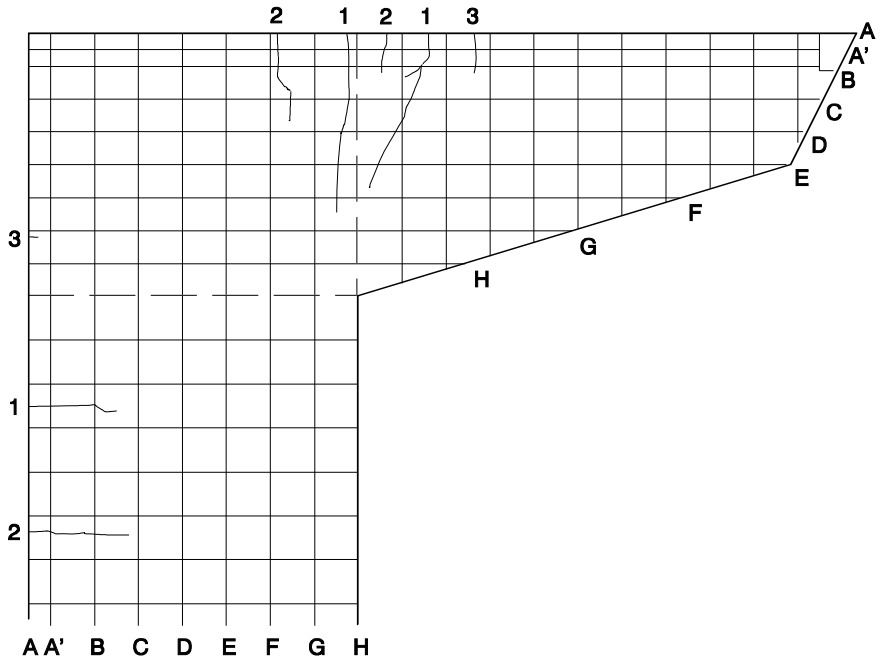

Figure 4.163 Cracking patterns on north face of Specimen POJ-PU-74-TH at service load

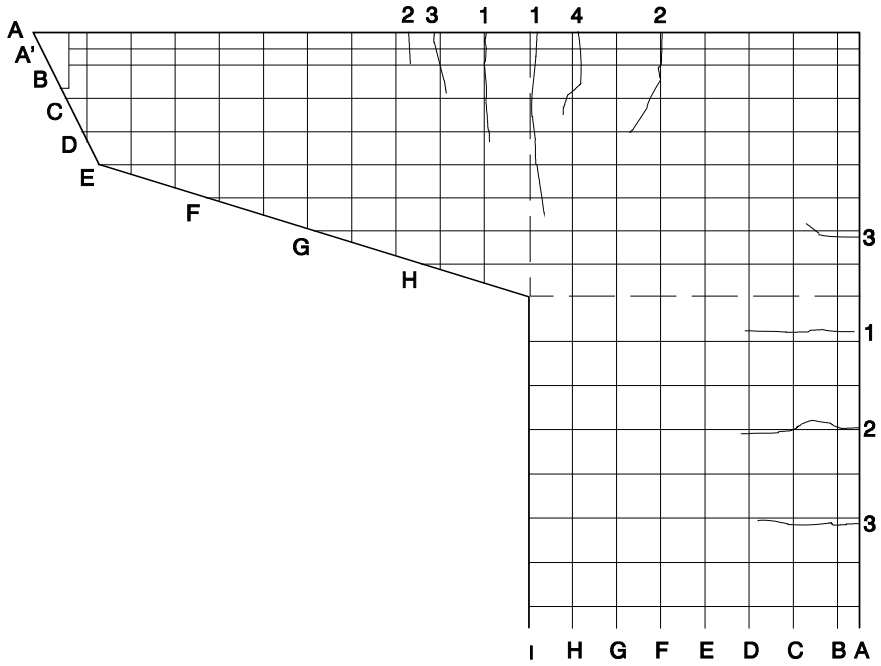

Figure 4.164 Cracking patterns on south face of Specimen POJ-PU-74-TH at service load

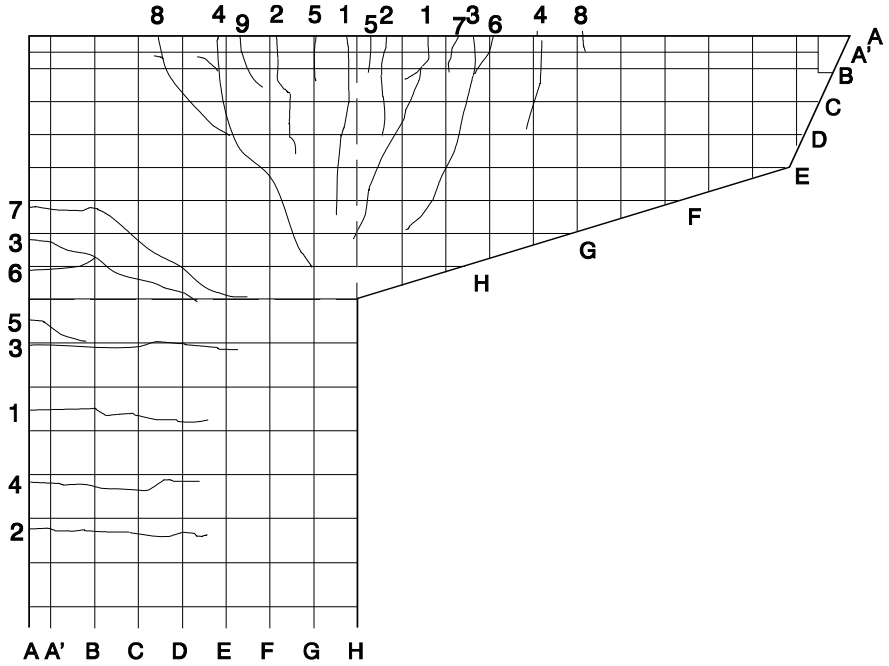

Figure 4.165 Cracking patterns on north face of Specimen POJ-PU-74-TH at end of test (no failure)

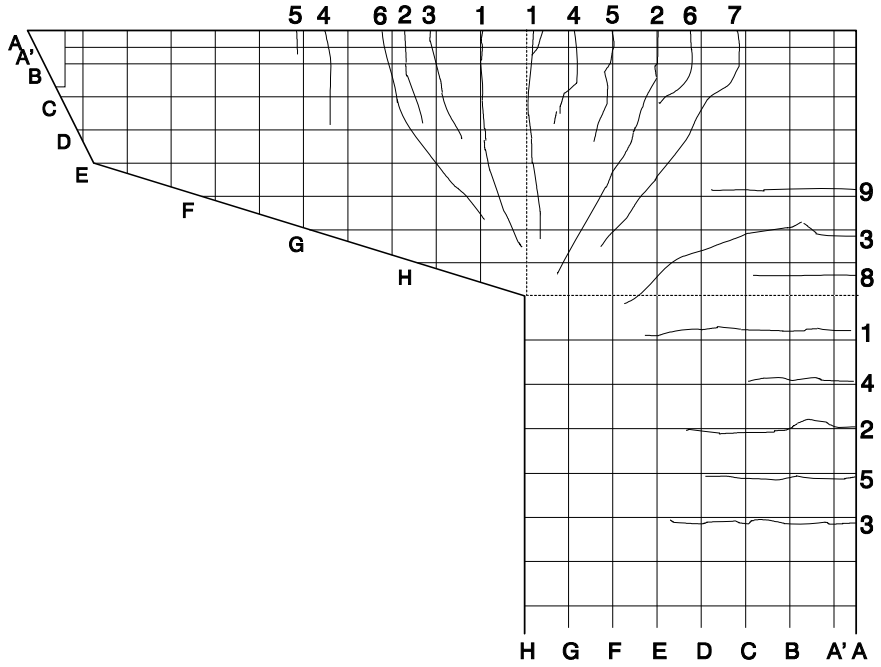

Figure 4.166 Cracking patterns on south face of Specimen POJ-PU-74-TH at end of test (no failure)

Crack patterns for the north and south faces of the overhang at dead load are presented in Figure 4.167 and Figure 4.169, respectively, and cracking patterns at service load are presented in Figure 4.168 and Figure 4.170, respectively. Maximum measured crack widths for the north face of the overhang are presented in Table A.45 and Table A.46 in SI and customary units, respectively. Maximum measured crack widths for the south face of the overhang are presented in Table A.47 and Table A.48 in SI and customary units, respectively. Crack widths in the overhang were well

controlled. The maximum measured crack width was 0.13 mm (0.050 in.) which is smaller than the maximum allowable crack width of 0.14 mm (0.0055 in.). Only three cracks developed on the side faces of the overhang at service loads. Cracks developed in the overhang in regions where principal tensile stresses (predicted by finite element analysis) were greater than $6\sqrt{f'_c}$ [2.9 MPa (425 psi)].

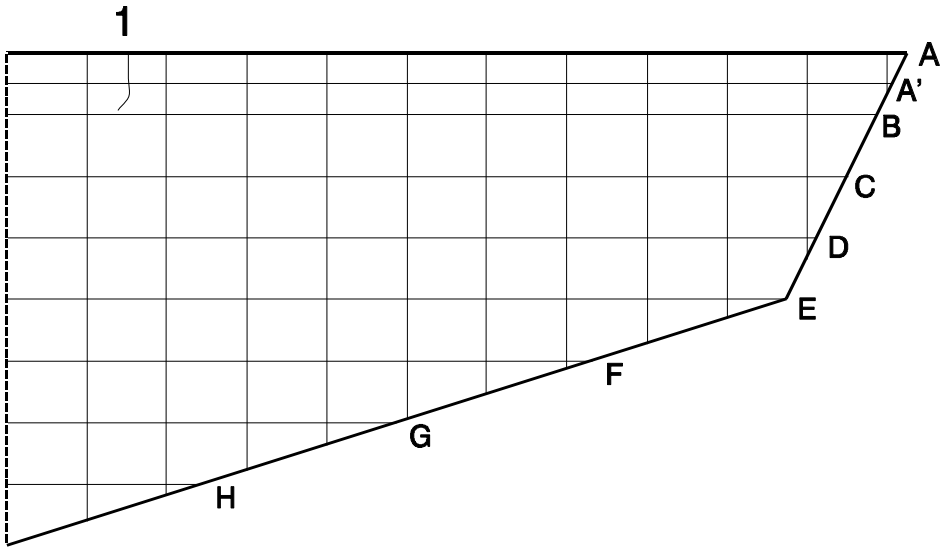

Figure 4.167 POJ-PU-74-TH cracking patterns on north face of overhang at dead load

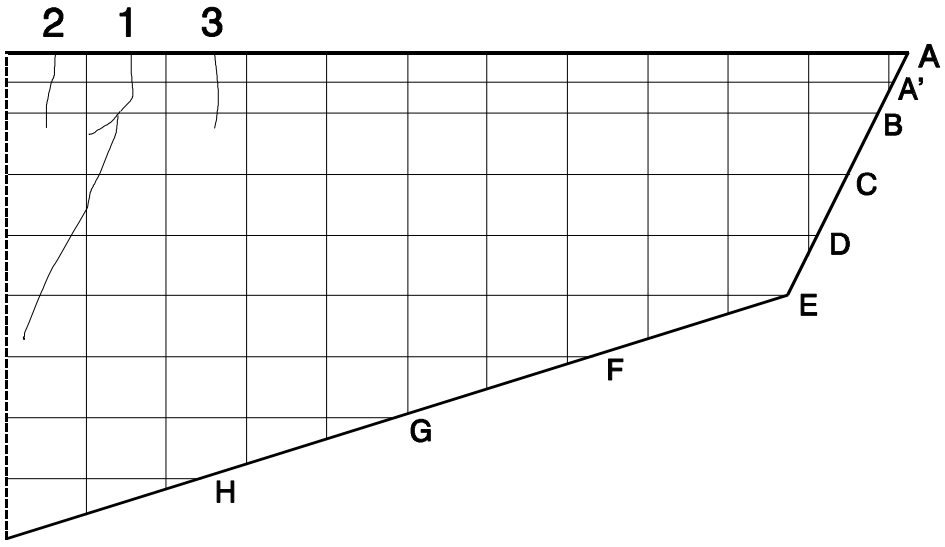

Figure 4.168 POJ-PU-74-TH cracking patterns on north face of overhang at service load

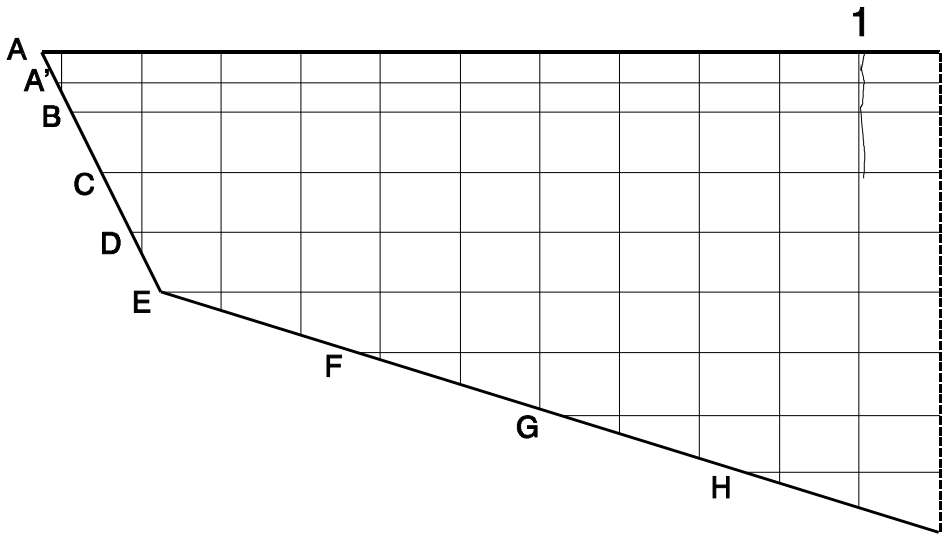

Figure 4.169 POJ-PU-74-TH cracking patterns on south face of overhang at dead load

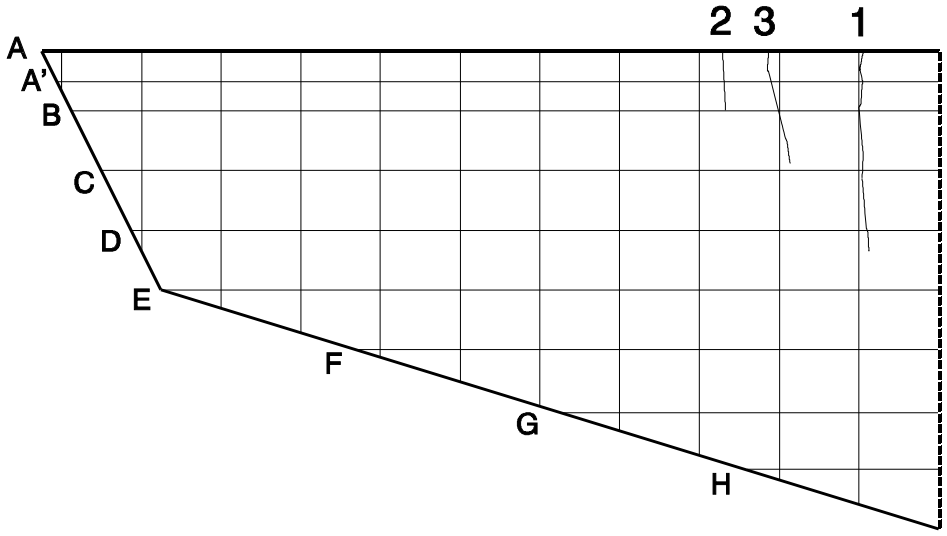

Figure 4.170 POJ-PU-74-TH cracking patterns on south face of overhang at service load

Cracking patterns for the north and south faces of the joint at dead load are presented in Figure 4.171 and Figure 4.173, respectively, and cracking patterns at service load are presented in Figure 4.172 and Figure 4.174, respectively. Maximum measured crack widths of 0.14 mm (0.0055 in.) occurred at crack (1) on both the north face of the joint (Table A.49 and Table A.50 in SI and customary units, respectively) and south face of the joint (presented in Table A.51 and Table A.52 in SI and customary units, respectively). Crack (1) was located near the joint/overhang interface (see Figure 4.172 and Figure 4.174). A major diagonal crack did not develop, even at applied loads well above factored loads.

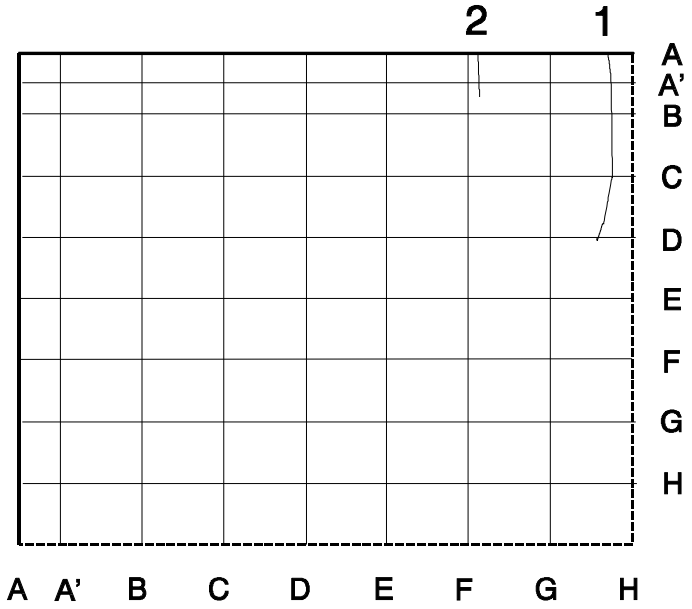

Figure 4.171 POJ-PU-74-TH cracking patterns on north face of joint at dead load

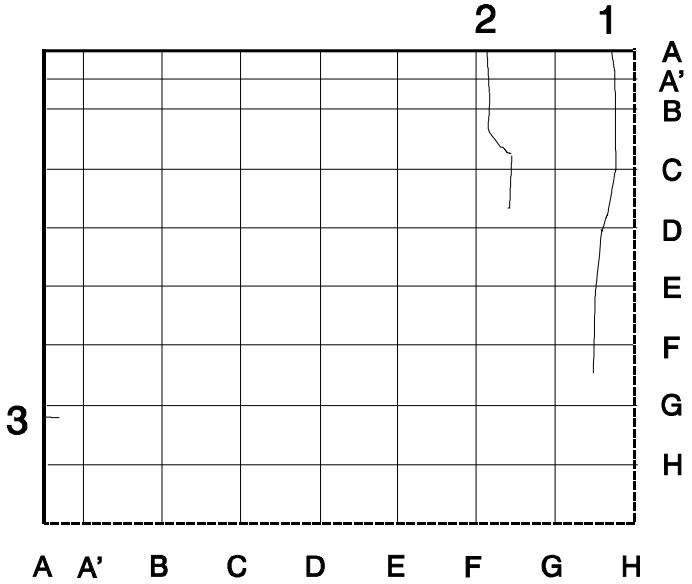

Figure 4.172 POJ-PU-74-TH cracking patterns on north face of joint at service load

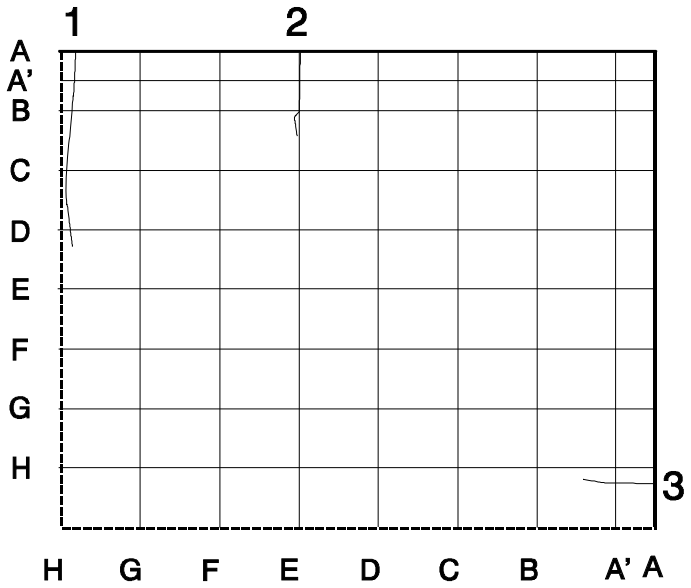

Figure 4.173 POJ-PU-74-TH cracking patterns on south face of joint at dead load

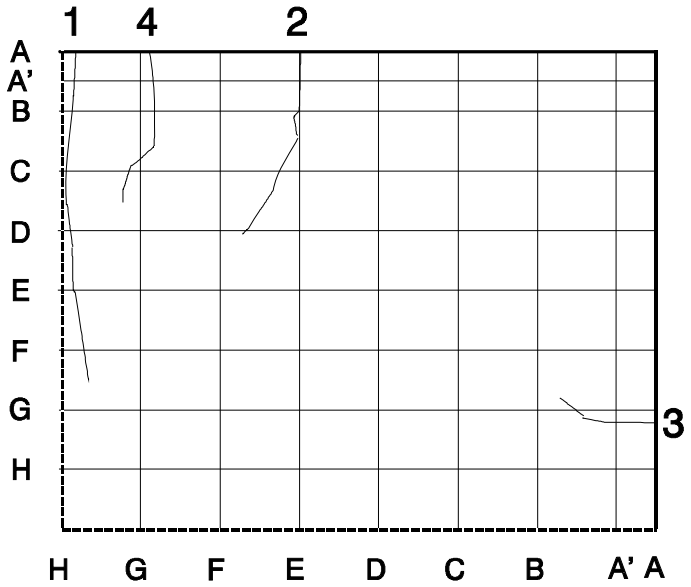

Figure 4.174 POJ-PU-74-TH cracking patterns on south face of joint at service load

No cracks were observed on the north face of the pier at dead load (shown in Figure 4.175), and two small cracks were visible at service load (Figure 4.176). The maximum measured crack width at service load for the north face of the pier was 0.08 mm (0.0030 in.) for both cracks (1) and (2). The south face of the pier had three visible cracks at dead load and service load (see Figure 4.177 and Figure 4.178, respectively). The maximum measured crack width at service load for the south face of the pier was 0.10 mm (0.0040 in.) which occurred at crack (3) (presented in Table A.55 and Table A.56 in SI and customary units, respectively).

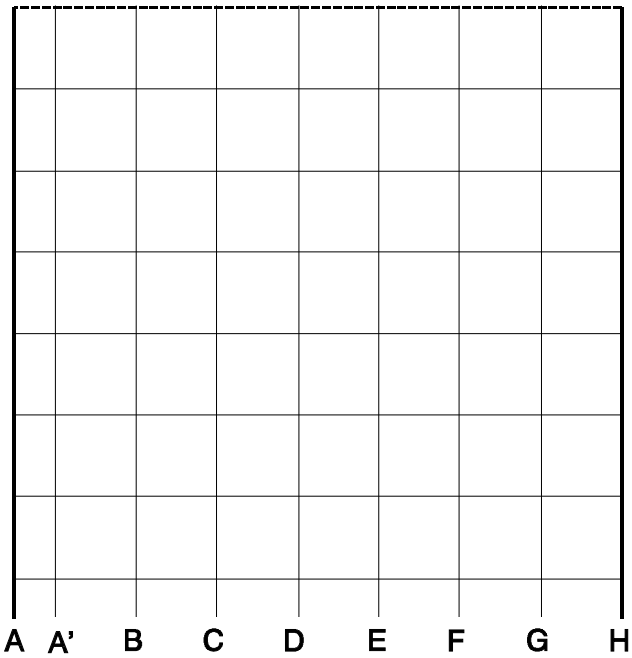

Figure 4.175 POJ-PU-74-TH cracking patterns on north face of pier at dead load

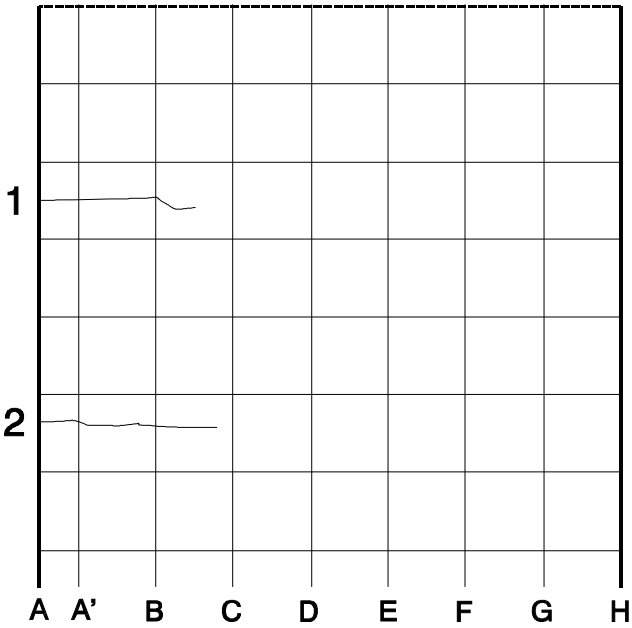

Figure 4.176 POJ-PU-74-TH cracking patterns on north face of pier at service loads

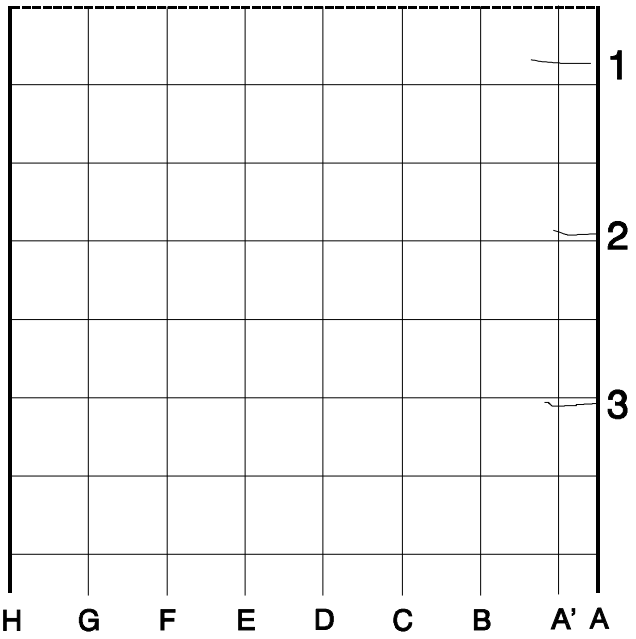

Figure 4.177 POJ-PU-74-TH cracking patterns on south face of pier at dead load

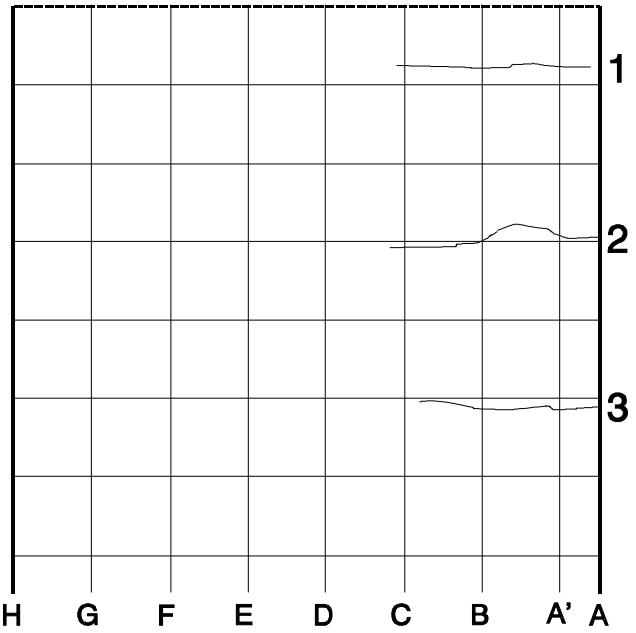

Figure 4.178 POJ-PU-74-TH cracking patterns on south face of pier at service load

It should be noted that the pier region had maximum crack widths that were 33% smaller than the expected maximum crack width [0.15 mm (0.0060 in.)]. It was assumed that friction-induced post-tensioning losses were smaller than calculated. In the design calculation, post-tensioning stresses at the stressing end (at the tip of the overhang) were 1.1 GPa (160 ksi), and stresses at the anchor (located at the base of the pier) were 0.85 GPa (123 ksi). When tendon stresses are assumed to be 1.1 GPa (160 ksi), the maximum predicted crack width is 0.10 mm (0.0040 in.). Unfortunately, post-

tensioning tendon strains were unavailable due to damaged gages, so it was not possible to verify the tendon stress.

4.3.3.2 Applied Overhang Moment vs. Deflection Response–POJ-PU-74-TH

Locations of the displacement transducers for Specimen POJ-PU-74-TH are presented in Figure 4.179. Transducers labeled A, B, or C were located on the south-side, center-line, or north-side of the specimen, respectively.

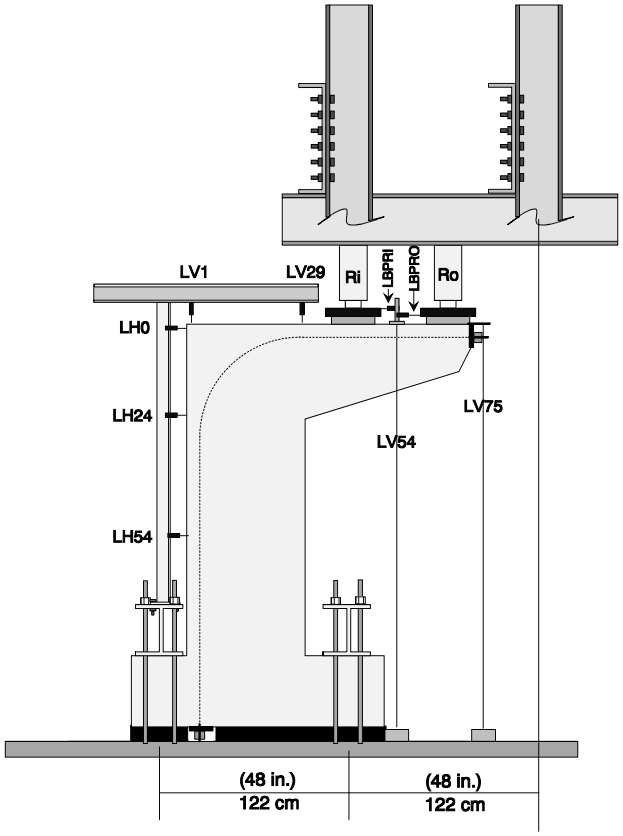

Figure 4.179 POJ-PU-74-TH location and identification of displacement gages

Plots of applied overhang moment vs. deflection response for Specimen POJ-PU-74-TH are presented in Figure 4.180 through Figure 4.183. As before, applied overhang moment is plotted as a fraction of factored moment. Displacements are labeled in both SI and customary units.

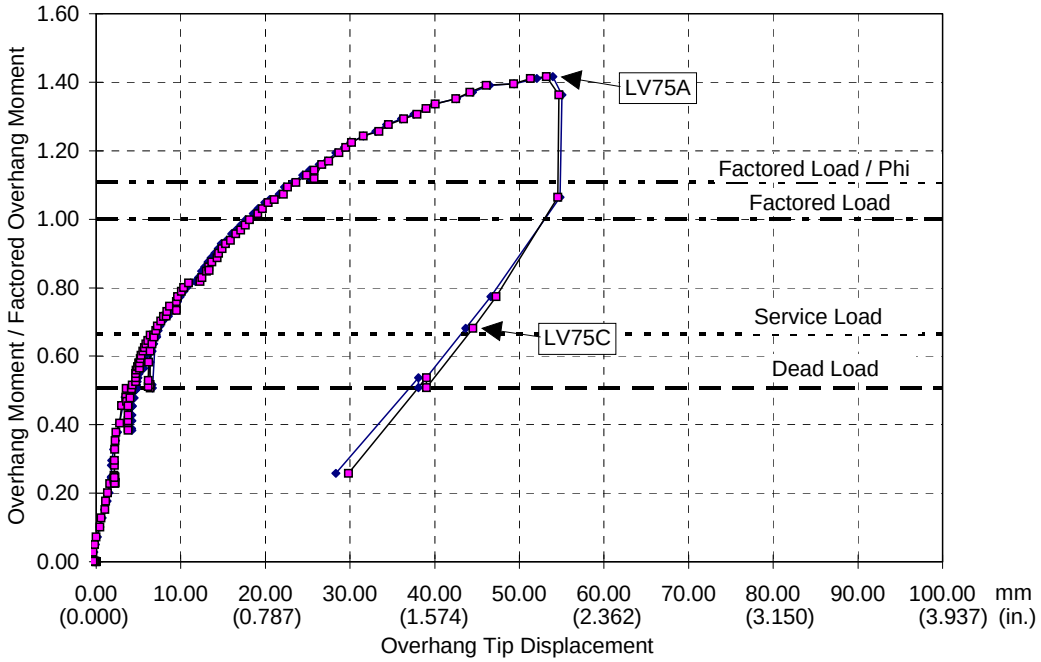

Figure 4.180 POJ-PU-74-TH tip deflection (LV 75)

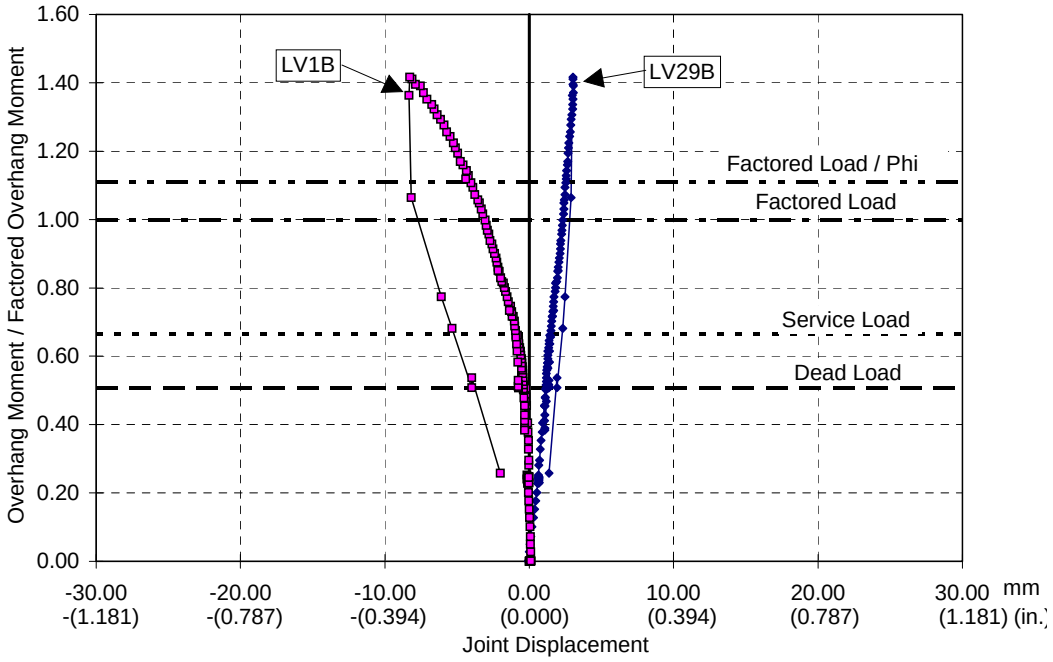

Figure 4.181 POJ-PU-74-TH vertical joint displacement

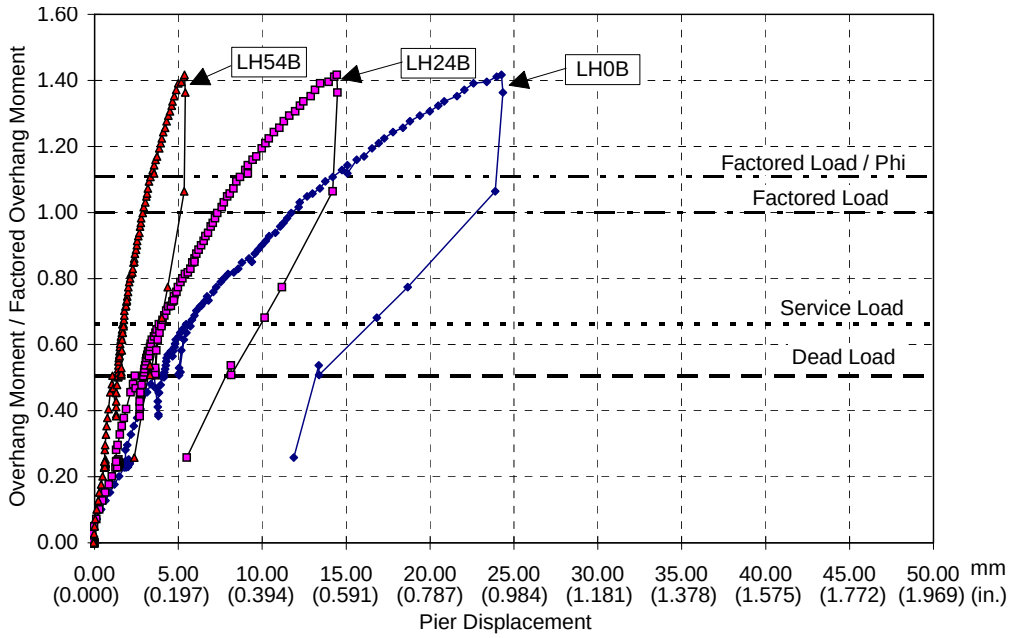

Figure 4.182 POJ-PU-74-TH pier horizontal deflection

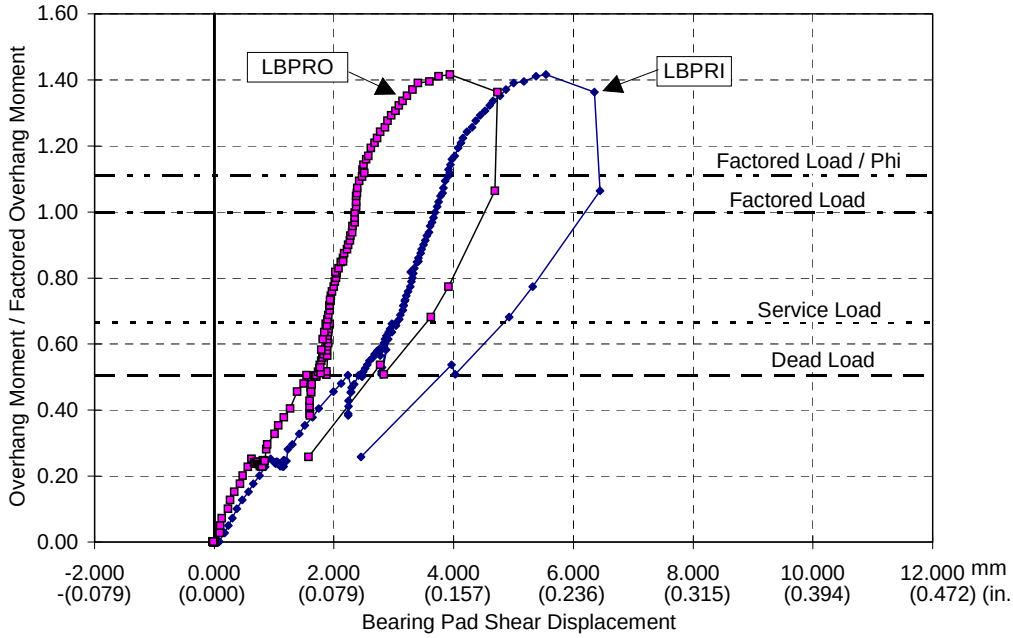

Figure 4.183 POJ-PU-74-TH bearing pad displacement

The moment-tip displacement response is plotted in Figure 4.180. The plot depicts the tip deflection response after the first two tendons were stressed (0 to an applied load of DL/2), and the response after all five tendons were stressed (DL/2 and higher). As in the previous tests, binding of the rams occurred due to the lateral displacement of the specimen and the load frame. The effects of the binding is clear from the loading-unloading response near dead load, and the elastic unloading after the maximum applied load of 1.4 times factored load was applied. As stated earlier, it was not possible to load the specimen to failure because of the limits of the strong-floor anchor bolts and capacity of the two hydraulic loading rams [889.6 MN (200 kips) capacity per ram]. After maximum load was applied, load was reduced incrementally until ½ dead load remained on the specimen.

Vertical displacement of the joint and elongation of the outer fiber of the pier is depicted in Figure 4.181. Horizontal displacement of the pier is plotted at three points (see Figure 4.179 for transducer labels) in Figure 4.182. Horizontal displacement of the bearing pads, shown in Figure 4.183, again depicts sway of the load frame due to eccentric loads from the loading rams (see Figure 4.179). Applied loads from the bearing pad shear deformation were not included in the moment calculations.

4.3.3.3 Location and Identification of Strain Gages–POJ-PU-74-TH

Strain gages for Specimen POJ-PU-74-TH were attached to the longitudinal and transverse reinforcement at points depicted in Figure 4.184 through Figure 4.186. As before, multiple strain gages were located at the same layer of reinforcement for redundancy in case a strain gage malfunctioned. Because the finite element analysis indicated principal tensile stresses in the joint were small, fewer strain gages were attached to the longitudinal reinforcement anchored in the joint. However, more strain gages were located in the region of the overhang where Specimen POJ-PU-54-TH failed. Locations and labels for strain gages located in the overhang of Specimen POJ-PU-74-TH are presented in Figure 4.184. Locations and labels for strain gages attached to the longitudinal reinforcement anchored in the joint region are presented in Figure 4.185. Overall strain gage locations and labels for the pier strain gages are presented in Figure 4.186.

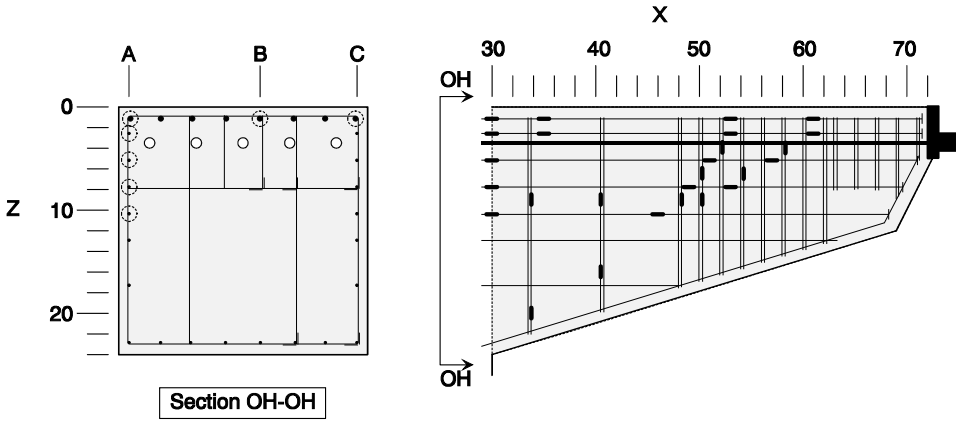

Primary Longitudinal Reinforcement	Section X=30			Section X=35			Section X=53		
	A	B	C	A	B	C	A	B	C
Layer Z=1	M30Z1A	M30Z1B	M30Z1C	M35Z1A	M35Z1B	M35Z1C	M53Z1A	M53Z1B	M53Z1C

Longitudinal Side-Face Reinforcement	Section X=30	Section X=35	Section X=46	Section X=49	Section X=51	Section X=53	Section X=61
Layer Z=3	T30Z3A	T35Z3A				T53Z3A	T61Z3A
Layer Z=5	T30Z5A				T51Z5A		
Layer Z=8	T30Z8A			T49Z8A		T53Z8A	
Layer Z=10	T30Z10A		T46Z10A				

Overhang Transverse Reinforcement	Section X=34	Section X=40	Section X=48	Section X=50	Section X=52	Section X=54	Section X=58
Level Z=4					S52Z4A		S58Z4A
Level Z=6				S50Z6A		S54Z6A	
Level Z=9	S34Z9A	S40Z9A	S48Z9A	S50Z9A			
Level Z=16		S40Z16A					
Level Z=20	S34Z20A						

Figure 4.184 POJ-PU-74-TH overhang strain gage locations and labels

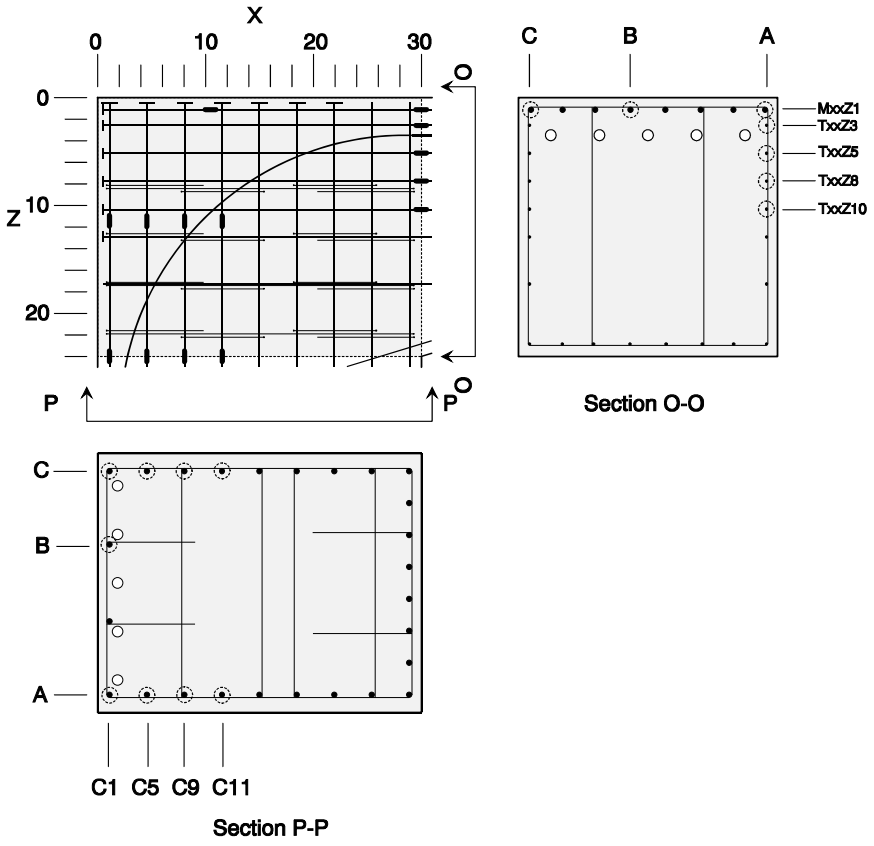

Overhang Longitudinal Reinforcement	Section X=11			Section X=30		
	A	**B**	**C**	**A**	**B**	**C**
Layer Z=1	M11Z1A	M11Z1B	M11Z1C	M30Z1A	M30Z1B	M30Z1C
Layer Z=3				T30Z3A		
Layer Z=5				T30Z5A		
Layer Z=8				T30Z8A		
Layer Z=10				T30Z10A		

Pier Longitudinal Reinforcement	Section Z=12			Section Z=24		
	A	B	C	A	B	C
Layer X=1	C1Z12A	C1Z12B	C1Z12C	C1Z24A	C1Z24B	C1Z24C
Layer X=5	C5Z12A		C5Z12C	C5Z24A		C5Z24C
Layer X=8	C8Z12A		C8Z12C	C8Z24A		C8Z24C
Layer X=11	C11Z12A		C11Z12C	C11Z24A		C11Z24C

Figure 4.185 POJ-PU-74-TH joint strain gage locations and labels

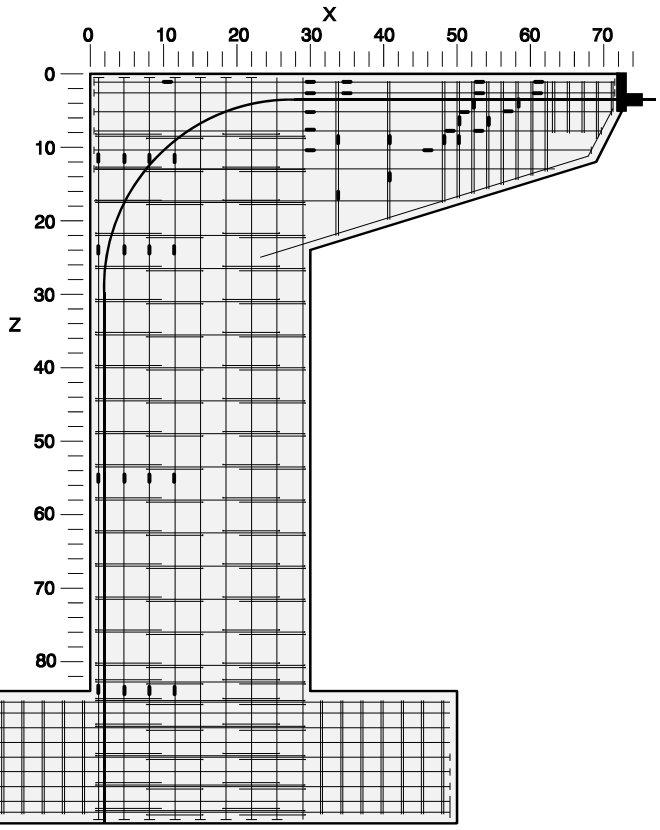

Pier Longitudinal Reinforcement	Section Z=55			Section Z=84		
	A	**B**	**C**	**A**	**B**	**C**
Layer X=1	C1Z55A	C1Z55B	C1Z55C	C1Z84A	C1Z84B	C1Z84C
Layer X=5	C5Z55A		C5Z55C	C5Z84A		C5Z84C
Layer X=8	C8Z55A		C8Z55C	C8Z84A		C8Z84C
Layer X=11	C11Z55A		C11Z55C	C11Z84A		C11Z84C

Figure 4.186 POJ-PU-74-TH overall strain gage locations and pier strain gage labels

It should be noted that a problem with the strain gage adhesive caused most of the strain gages to malfunction during the test. Strain gage readings are presented in Section 4.3.3.4 for gages that functioned for most of the test.

4.3.3.4 Overhang Moment vs. Strain Respons–POJ-PU-74-TH

As stated earlier, the strain gage adhesive did not properly bond the strain gages to reinforcement for the POJ-PU-74-TH test specimen. As a whole, strain gage readings were mostly unusable. Selected gages that functioned for most of the test are plotted in Figure 4.187 through Figure 4.192. Applied moment vs. strain response for the primary longitudinal mild reinforcement in the overhang is plotted in Figure 4.187. Strain response for the longitudinal side-face reinforcement and transverse reinforcement are plotted in Figure 4.188 and Figure 4.189, respectively. Strain responses for the longitudinal pier reinforcement are plotted in Figure 4.190 through Figure 4.192. In general, strain gages indicated abrupt changes in strain when cracking occurred in the vicinity of each of the gages.

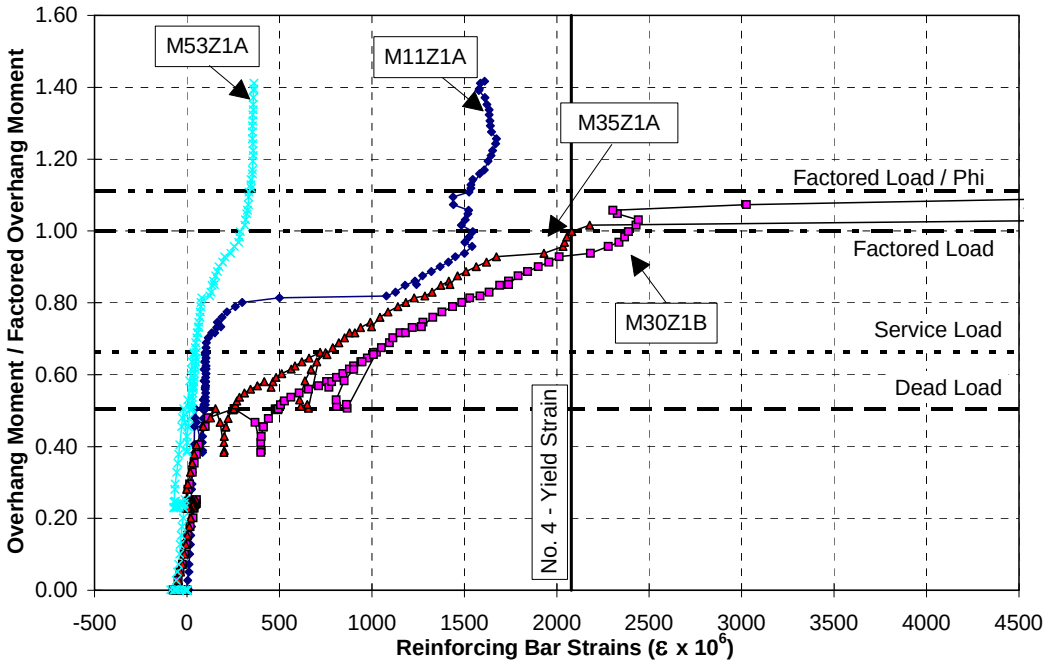

Figure 4.187 POJ-PU-74-TH strains in primary longitudinal mild reinforcement at Layer Z=1 in overhang

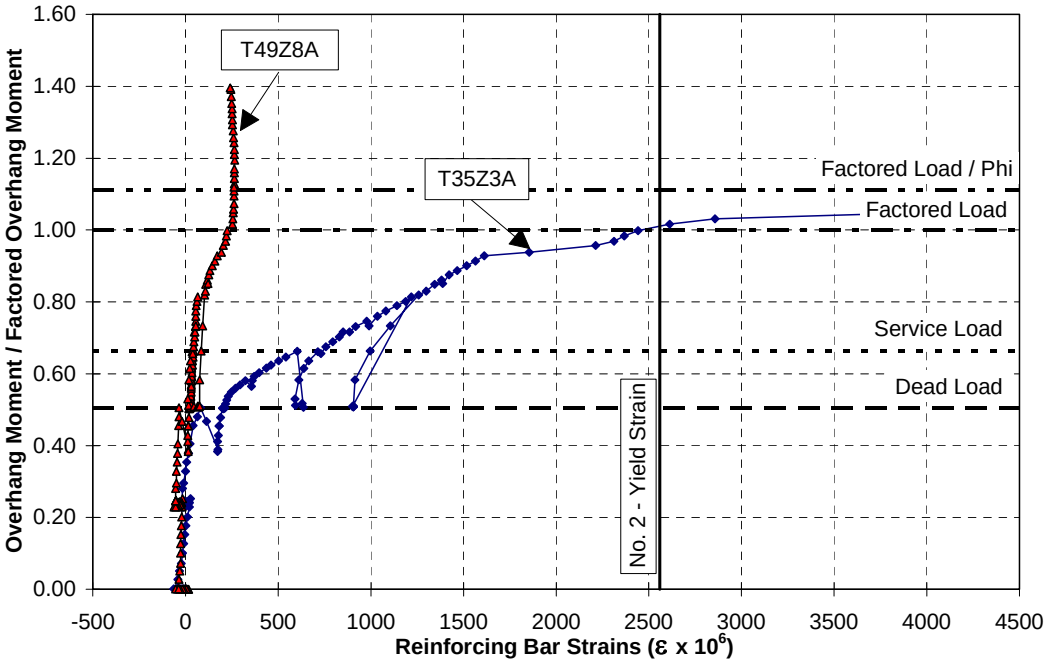

Figure 4.188 POJ-PU-74-TH strains in side-face longitudinal reinforcement in overhang

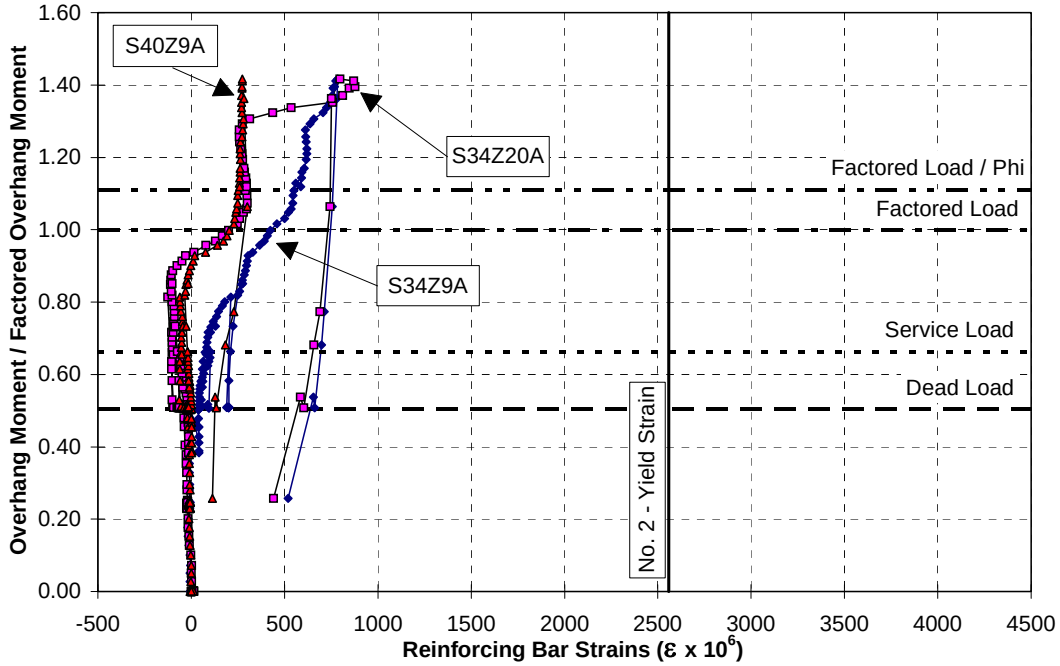

Figure 4.189 POJ-PU-74-TH strains in transverse reinforcement in overhang

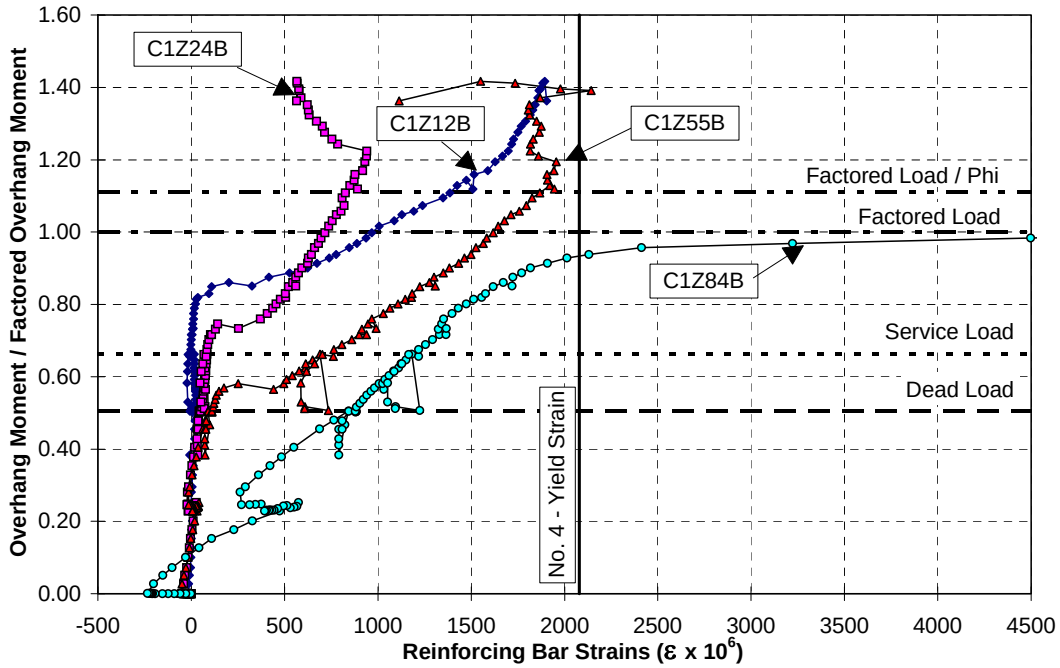

Figure 4.190 POJ-PU-74-TH strains in pier longitudinal reinforcement at Layer X=1

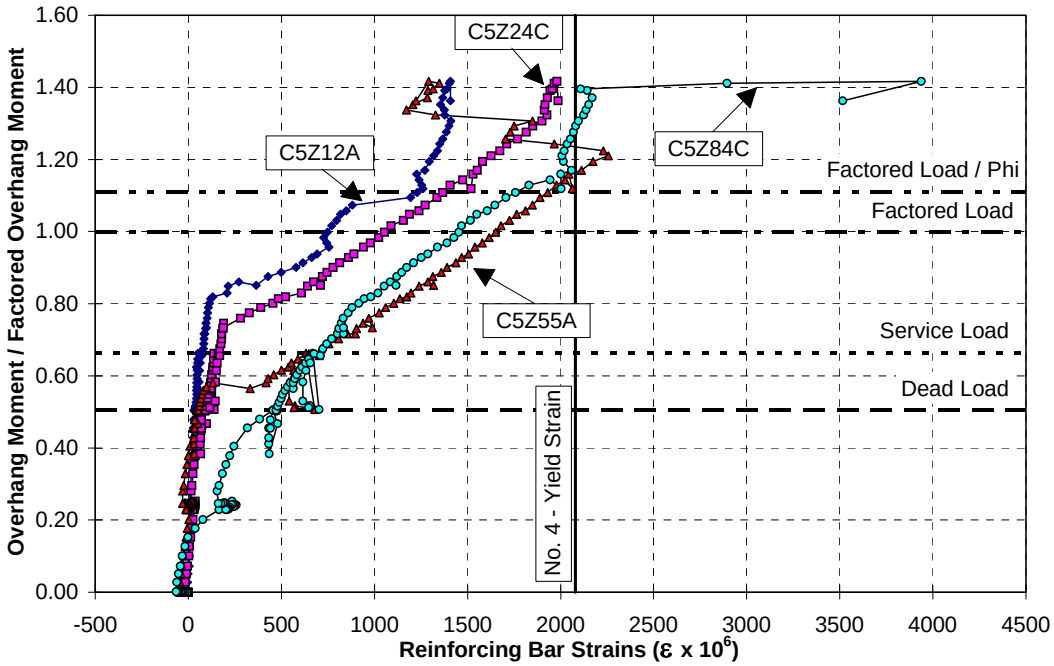

Figure 4.191 POJ-PU-74-TH strains in pier longitudinal reinforcement at Layer X=4

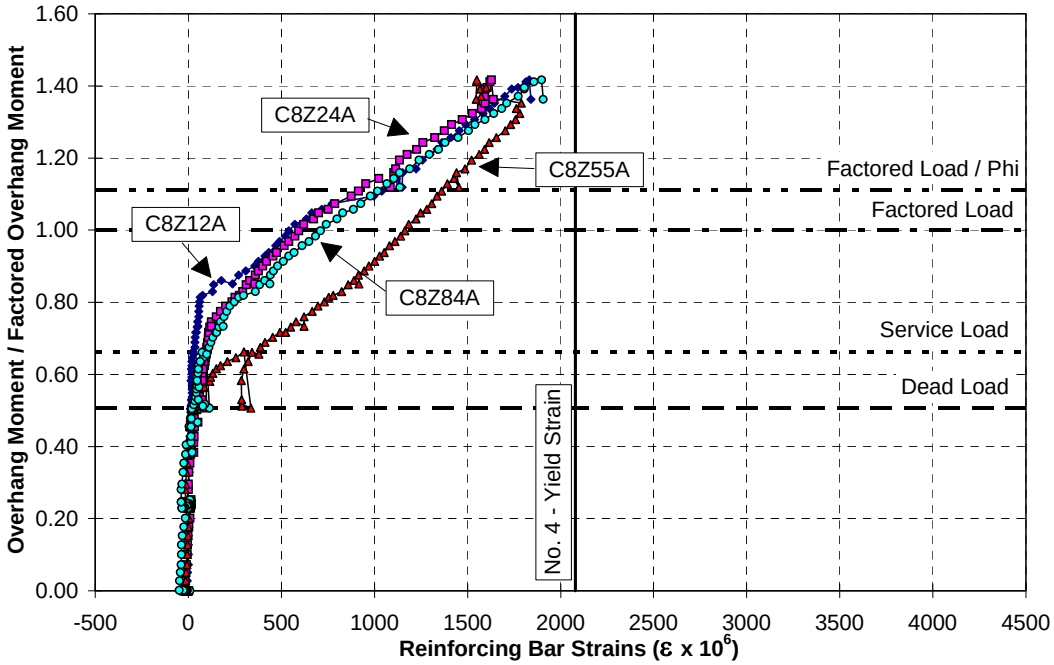

Figure 4.192 POJ-PU-74-TH strains in pier longitudinal reinforcement at Layer X=8

Strain measurements indicated the primary longitudinal mild reinforcement in the overhang (Layer Z=1, plotted in Figure 4.187) had similar strains at the different points gaged along the length. This response indicated the strut-and-tie model correctly predicted the constant state of stress in the primary overhang longitudinal reinforcement from the face of the pier to the exterior corner of the joint. This was considered to be confirmation that the longitudinal reinforcement required positive anchorage in the joint. The abrupt change in strain recorded for M11Z1A at a moment ratio of 0.8

indicated the formation of crack (7) on the south face of the joint. Strain gages M30Z1A and M35Z1A located on the top layer of longitudinal reinforcement in the overhang (at the joint/overhang interface and 5 inches away from the interface, respectively) indicated the primary longitudinal reinforcement yielded at moment ratios of 1.0 and 0.93, respectively.

The moment-strain response for strain gage T49Z8A (plotted in Figure 4.188) was attributed to the formation of crack (4) on the south face of the overhang. A similar moment-strain response measured by strain gage M53Z1A (located on the primary longitudinal reinforcement near crack (4) on the south face of the overhang) is shown in Figure 4.187. Large recorded strains for strain gage T35Z3A (plotted in Figure 4.188) at a moment ratio of 1.0 confirmed that primary longitudinal reinforcement yielded at/or near factored loads. Recorded strains in the transverse reinforcement located in the overhang (shown in Figure 4.189) were small and did not indicate imminent failure of the overhang.

Moment-strain response measured by strain gage C1Z84B (located at Layer X=1 near the hold-down beam) indicated changes in strain early in the test (see Figure 4.190). During installation of specimen POJ-PU-74-TH, the outer corbel stub (located at the base of the specimen) cracked as the specimen was being stressed to the strong floor. The onset of first cracking was expected to occur much later. Strain gages located at layers X=4 and X=8 (shown in Figure 4.191 and Figure 4.192, respectively) indicated the recorded strain for C1Z84B was a localized phenomenon.

4.3.3.5 Pier Strain Profiles–POJ-PU-74-TH

Strain profiles in the pier at Section Z=55 are presented in Figure 4.193. The strain profile was nearly linear, as expected, however the measured strains were smaller than expected assuming an effective post-tensioning stress of 850 MPa (123.4 ksi) in the pier. Further discussion and comparison of effective post-tensioning stresses in the pier are presented in Chapter 5.

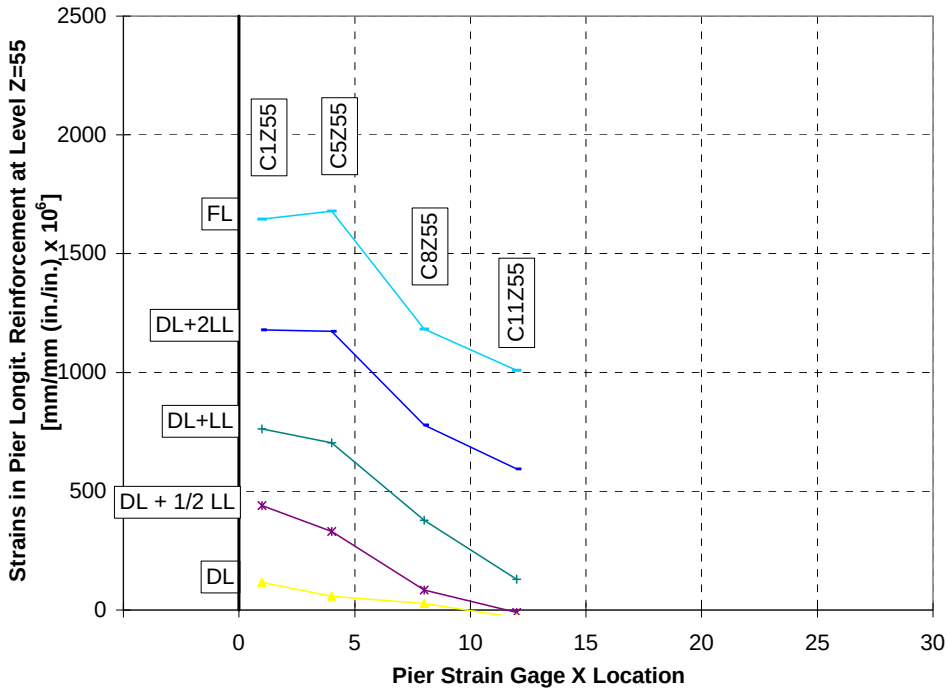

Figure 4.193 POJ-PU-74-TH strain profiles in pier at Section Z=55

CHAPTER 5

ANALYSIS OF TEST RESULTS

5.1 INTRODUCTION

Two prototype design specimens (POJ-RC-100 and POJ-PS-100) and three integrated design specimens (POJ-RC-100-TH, POJ-PU-54-TH, and POJ-PU-74-TH) were evaluated using the following criteria: strength, serviceability, constructibility, and estimated cost. The strength criterion was evaluated using the plots of experimental moment-deflection behavior and measured vs. predicted moment-strain profiles for each specimen. The service load evaluation included service load tip deflections, specimen cracking patterns and maximum crack-widths, and reinforcement tensile stress ranges. Ease or difficulty of constructing the model specimens provided the basis for evaluating constructibility of full-scale bents. Estimated costs for full-scale bents were based on material quantities used for the model specimens multiplied by the appropriate scale factor and material unit costs.

5.2 STRENGTH EVALUATION

Experimental results for the prototype and integrated design specimens clearly illustrate the strength deficiency of the prototype designs and increased strength obtained from the integrated design specimens. Each specimen was evaluated for strength and ductility by examining the moment-deflection response for applied loads above the factored load level, and by evaluating the observed failure mode. The predicted failure load and measured capacity were compared to evaluate the accuracy of the analytical models. Recorded and predicted strain-profiles for pier and overhang cross-sections were compared to evaluate the suitability of the assumed linear strain profile used in section analyses.

5.2.1 Comparison of Overhang Moment vs. Tip Deflection Response

The graph of the overhang moment versus tip displacement response, shown in Figure 5.1, illustrates the poor performance of the two prototype model specimens and the improved behavior of the three integrated design specimens. The maximum applied load for the model of the prototype reinforced concrete bent (POJ-RC-100) was slightly larger than DL+1.6LL, which was equivalent to 0.76 times factored loads. The specimen with the fully-prestressed overhang (POJ-PS-100) failed at a load equivalent to DL+0.5LL (0.58 times factored loads). Both prototype model bents failed in the joint region because anchorage of longitudinal reinforcement in the joint was insufficient after a diagonal crack developed in the joint.

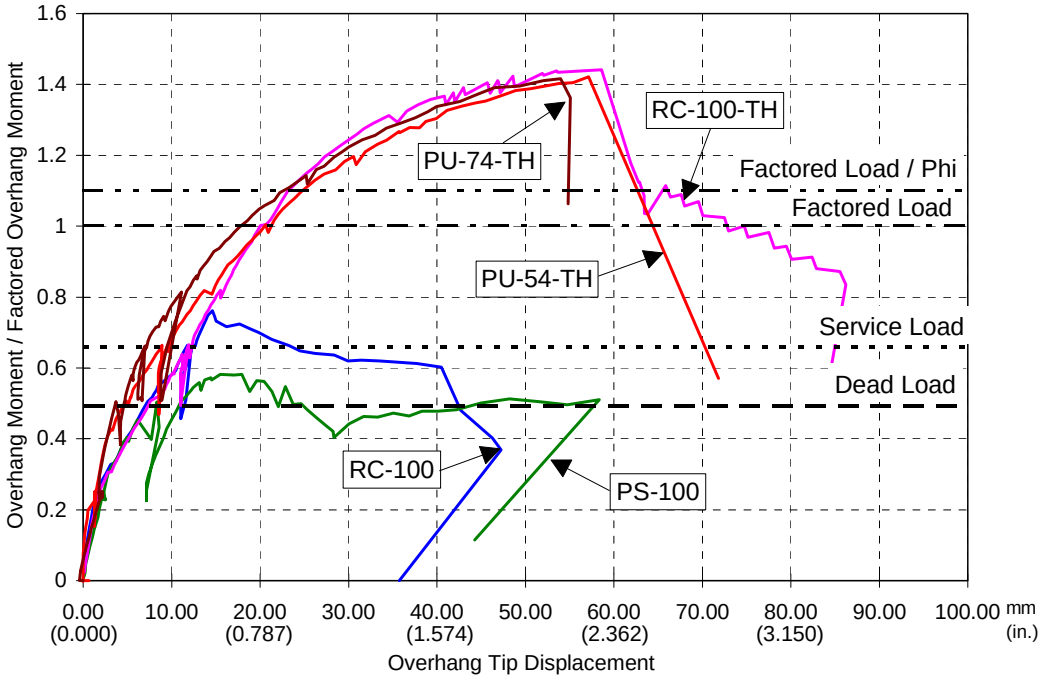

Figure 5.1 Moment vs. tip displacement response for pier-overhang-joint specimens

The reinforced concrete design with headed reinforcement (POJ-RC-100-TH) resisted an ultimate load of DL+5.9LL, which was equivalent to 1.44 times factored loads. The improved performance of the integrated design reinforced concrete specimen (POJ-RC-100-TH) over the prototype model reinforced concrete bent (POJ-RC-100) (shown in Figure 5.2) was attributed to the interlocked headed mild reinforcement used in the joint corner. Specimen POJ-RC-100-TH was constructed with 24.8% less steel than Specimen POJ-RC-100 because the design provided tensile reinforcement only in tensile regions identified by a strut-and-tie model.

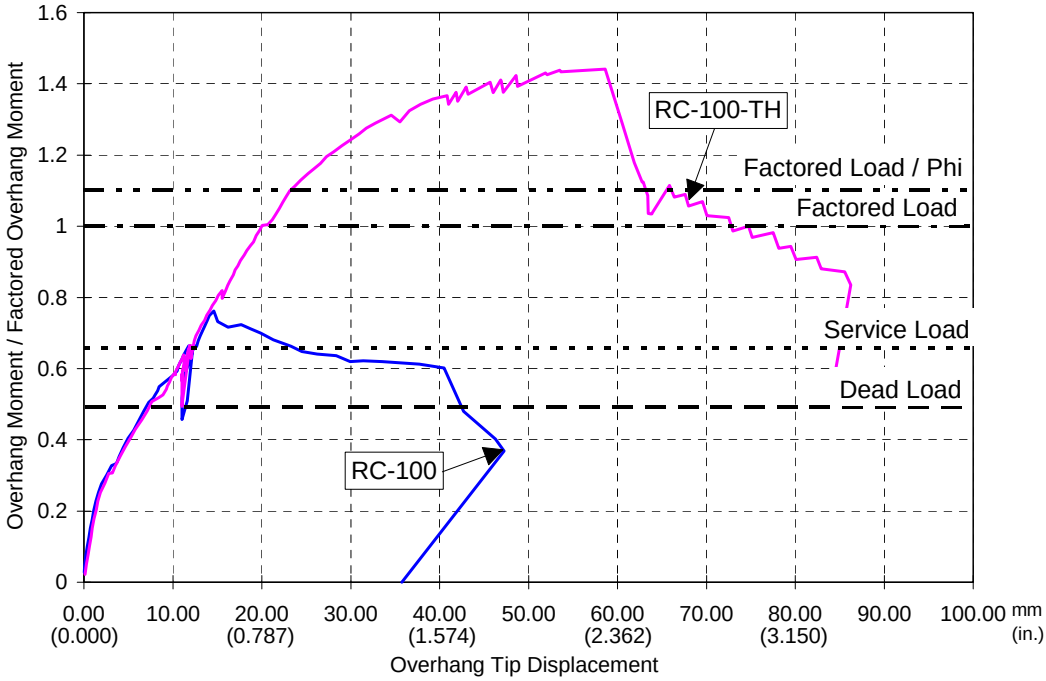

Figure 5.2 Comparison of moment vs. tip displacement response for specimens RC-100-TH and RC-100-TH

The partially-prestressed specimens (POJ-PU-54-TH and POJ-PU-74-TH) utilized headed mild reinforcement and continuous high-strength prestressed reinforcement to resist factored loads. Specimen POJ-PU-54-TH utilized a combination of prestressed reinforcement that provided 54% of the total tensile tie force in the overhang and mild reinforcement to resist factored loads. At ultimate, DL+5.8LL or 1.42 times factored loads, the underside of the overhang for Specimen POJ-PU-54-TH spalled at the face of the column, resulting in a brittle failure of the overhang. Specimen POJ-PU-74-TH utilized a larger fraction of prestressed reinforcement and also had a capacity well above factored loads. The specimen capacity was not determined because it exceeded the capacity of the testing frame (DL+6LL).

The three integrated design specimens had similar moment-deflection responses. Specimens were designed using a strut-and-tie model and a strain compatibility-based strength analysis, resulting in nearly identical capacities. Note that a portion of the overstrength demonstrated by the integrated design specimens can be attributed to the overstrength, ϕ, factors used in the design process. Overstrength factors were included to permit comparisons with models of prototype designs, and to facilitate realistic proportioning of specimens to permit evaluation of serviceability requirements.

5.2.2 Comparison of Measured and Predicted Strains

Recorded reinforcement strains were compared with predicted reinforcement strains at the column-overhang cross-section (X=30) and pier mid-height cross-section (Z=54), to evaluate the suitability of a linear strain-gradient used in analysis. Strain gage locations are depicted in Figure 5.3.

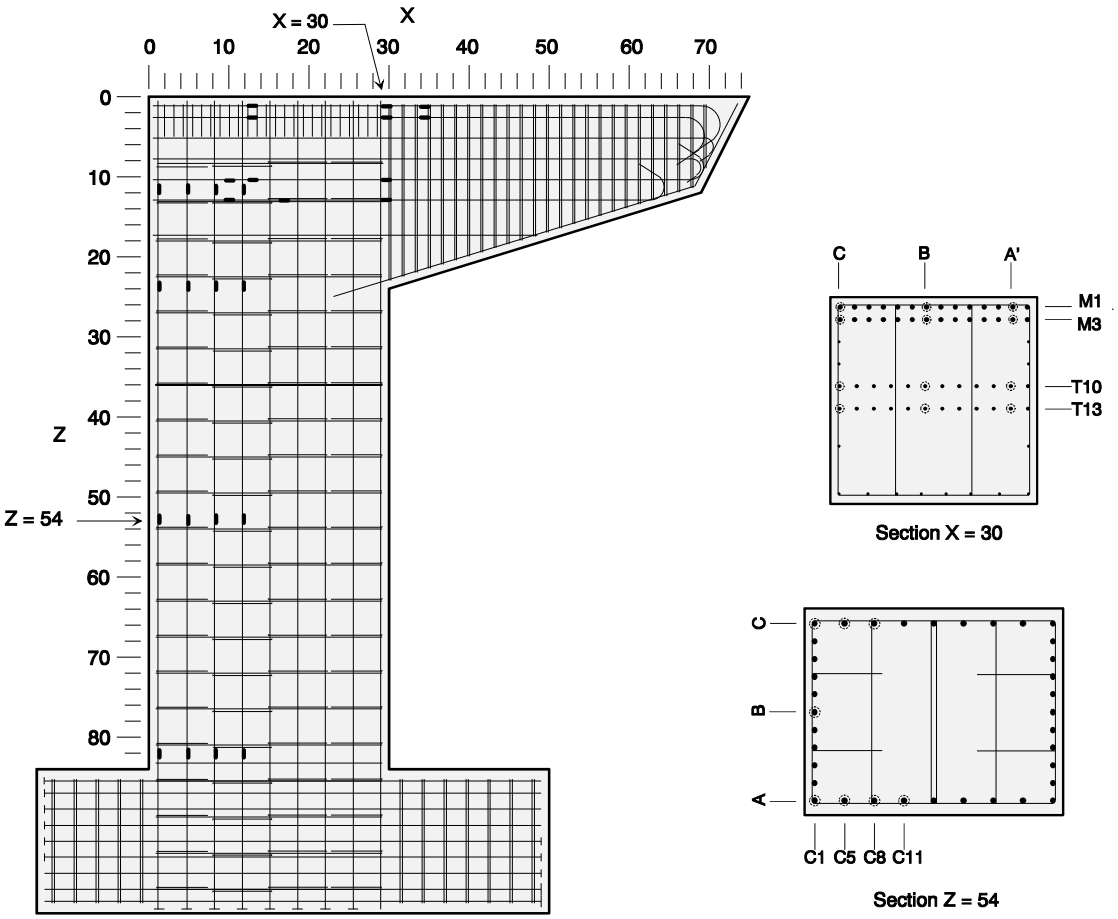

Figure 5.3 Strain gage locations for Specimen RC-100

Cross-section strain profiles at dead load (DL), service load (DL+LL), dead plus two live loads (DL+2LL), and factored load (FL) are presented in each graph. The experimental strains presented in each plot were determined by computing the arithmetic average of strain gage readings at the section (i.e., C1 determined from average of strain gage readings for gages A, B, and C). Predicted strains were computed using a spreadsheet-based strain-compatibility analysis. Cross-section strain profiles for Specimen POJ-PS-100 were not plotted due to the early failure of the specimen. Profiles for Specimen POJ-PU-74-TH were not plotted because strain gages malfunctioned.

Measured strain profiles for Specimen POJ-RC-100 (prototype model of reinforced concrete bent), shown in Figure 5.4 and Figure 5.5, correlated reasonably well with the analytical model. Due to the early failure in the joint region, the largest recorded applied load was only DL+1.6LL.

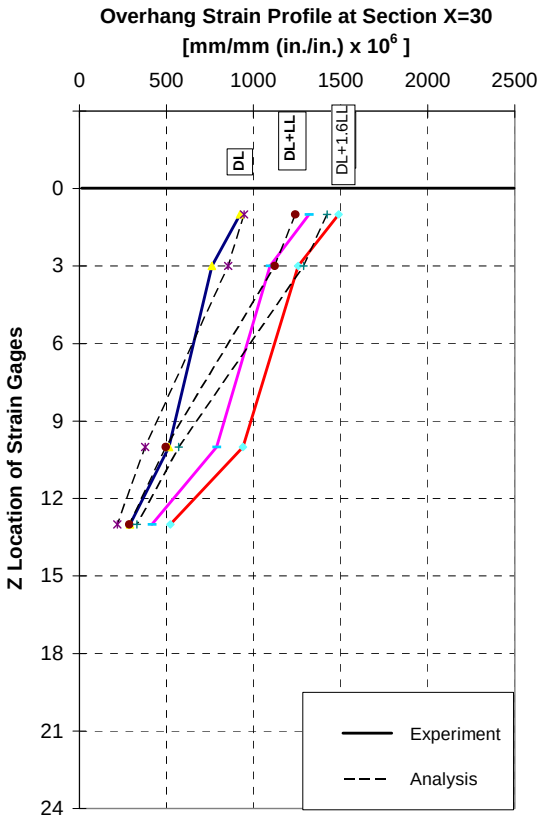

Figure 5.4 POJ-RC-100 comparison of analysis and test strain-profiles for the overhang at the face of the pier

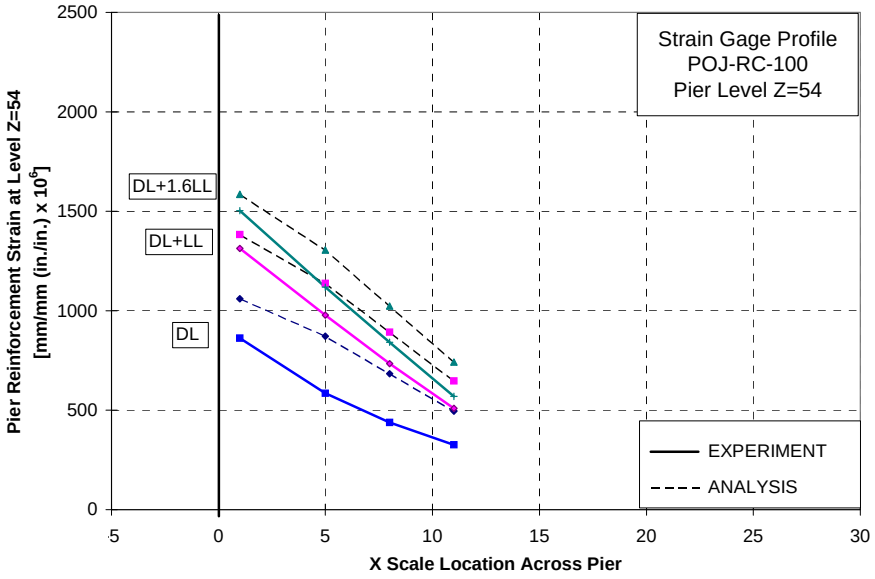

Figure 5.5 POJ-RC-100 comparison of analysis and test strain-profiles for a cross-section near mid-height of the pier

Experimental and predicted strains for Specimen POJ-RC-100-TH (integrated design reinforced concrete specimen with headed reinforcement), shown in Figure 5.6 and Figure 5.7, were in good agreement for the pier cross-section (Figure 5.7), but not for the overhang cross-section (Figure 5.6). The experimental results indicated strains in the side face reinforcement 33 cm (13 in.) from the top surface of the overhang were nearly twice what would be expected from a linear strain profile assumption. However, computed tensile stresses near the top fiber were in close agreement with computed values.

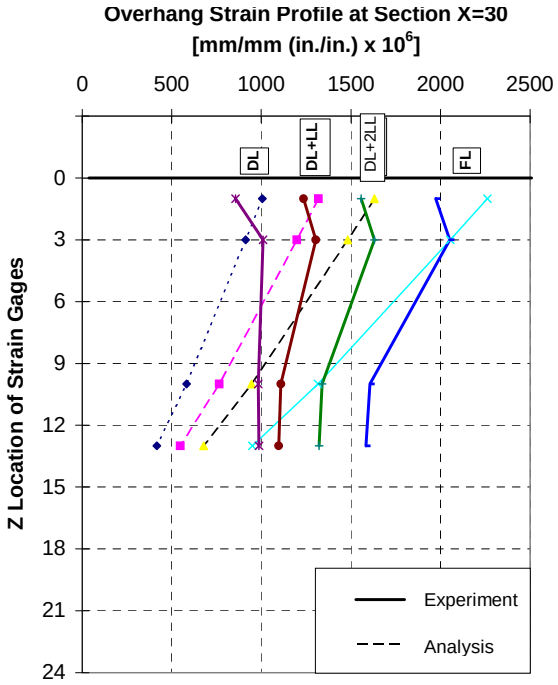

Figure 5.6 POJ-RC-100-TH Comparison of analysis and test strain-profiles for a cross-section of the overhang near the face of the pier

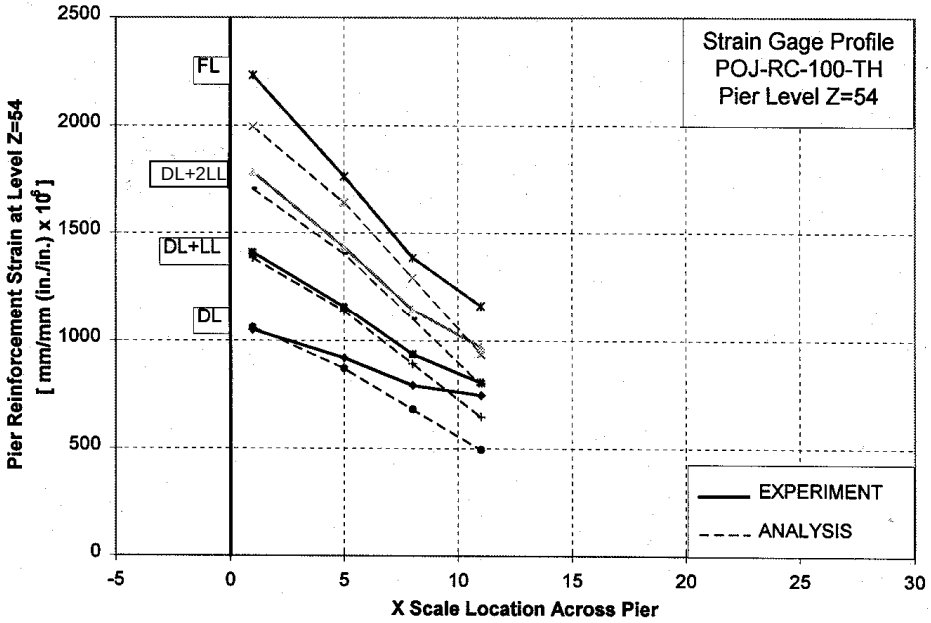

Figure 5.7 POJ-RC-100-TH comparison of analysis and test strain-profiles for a cross-section near mid-height of the pier

The recorded and predicted steel-strains for the overhang cross-section for Specimen POJ-PU-54-TH (Figure 5.8) were in good agreement near the top fibers, but the strain-profiles differed significantly. The strain-profiles at the overhang cross-section, shown in Figure 5.8, were computed assuming the prestress was 1100 MPa (160 ksi) in the overhang. The recorded strain profile indicated reinforcement strains 25 cm (10 in.) from the top of the overhang were nearly twice what would be expected using a linear strain profile.

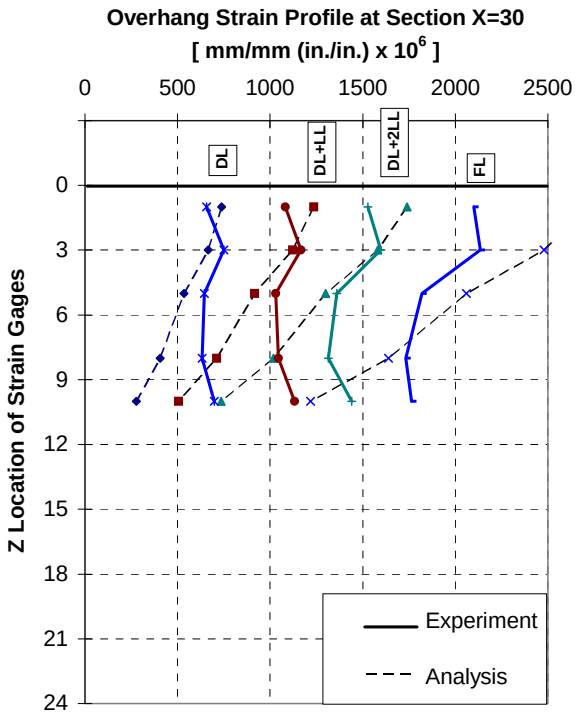

Figure 5.8 POJ-PU-54 comparison of analysis and test strain-profiles for a cross-section of the overhang near the face of the pier

Predicted strain profiles for the pier shown in Figure 5.9 were computed assuming a prestress of 850 MPa (123 ksi) in the pier region after losses occurred in the joint. The assumed pier post-tensioning corresponded with dead load on the bent. The predicted strain-profiles for the cross-section near mid-height of the pier (cross-section Z=54) did not agree with results from the strain gages. Predicted strains in the pier, using a post-tensioning stress of 850 MPa (123 ksi), over-estimated strains in the extreme tensile reinforcement by more than 500 με (which corresponds to a stress of 100 MPa (14.5 ksi)). The disparity in computed and measured results was attributed to smaller-than-expected post-tensioning losses.

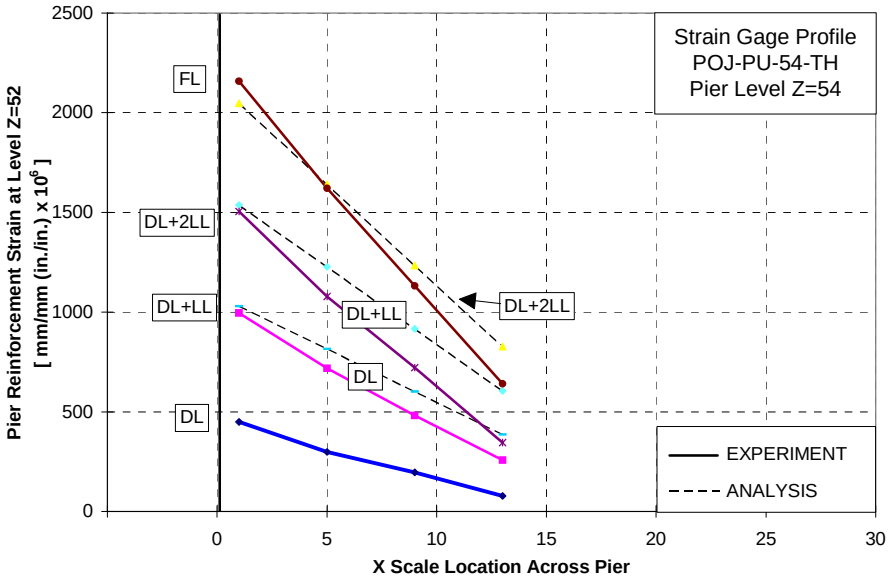

Figure 5.9 POJ-PU-54-TH pier analytical and experimental strain-profiles for a cross-section near mid-height of the pier

The plot of moment vs. measured post-tensioning stress at the base of the pier (shown in Figure 5.10) indicated the average post-tensioning stress was 926 MPa (134 ksi) at dead load [assuming a post-tensioning steel modulus of 193 GPa (28,000 ksi)]. The effective post-tensioning stress at dead load was estimated to be 1030 MPa (150 ksi) using recorded mild steel strains and a strain-compatibility analysis. This indicates the effective post-tensioning stress was larger than the post-tensioning stress assumed during design [850 MPa (123 ksi)]. The increased effective post-tensioning stress in the pier would have resulted in smaller-than-expected crack-widths. Crack-widths are discussed in Section 5.3.3.

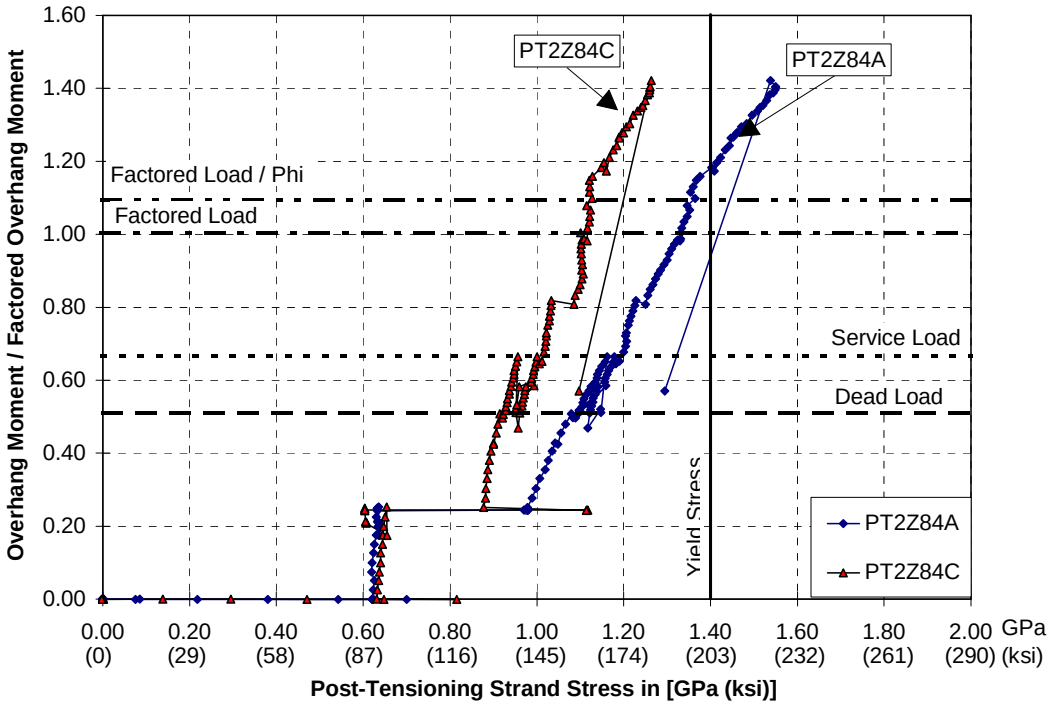

Figure 5.10 Pier post-tensioning stresses for Specimen POJ-PU-54-TH estimated from strain gage measurements

5.2.3 Comparison of Computed and Measured Capacities

The capacity for each specimen was calculated using both a section analysis (for flexural strength) and a joint bond-strength model. Nominal yield stress of the mild reinforcement [413 MPa (60 ksi)] was used for computing nominal flexural capacity of the overhang and pier, and the experimentally obtained stress-strain behavior of the mild reinforcement was used to estimate the ultimate flexural capacity of the same members. Nominal capacities are presented to illustrate the difference between ultimate capacities and nominal capacities used in design of the bents. The joint bond-strength model utilized a uniform bond-stress model, nominal yield of the mild reinforcement, and tensile strength of the bonded prestressing strands to determine the bent capacity.

The joint bond-strength model assumed a crack develops in the joint between the compression resultant and the joint corner opposite the compression resultant (Figure 5.11). The peak force developed by each bar in the prototype models that crosses the assumed diagonal crack was computed by utilizing the ratio of embedment length to development length in a uniform bond-stress model. For the integrated design specimens, reinforcement with T-headed anchors was assumed to develop yield strength. After computing the individual bar forces, the maximum applied load on the cantilever bent was computed by balancing the moments about the joint compression resultant.

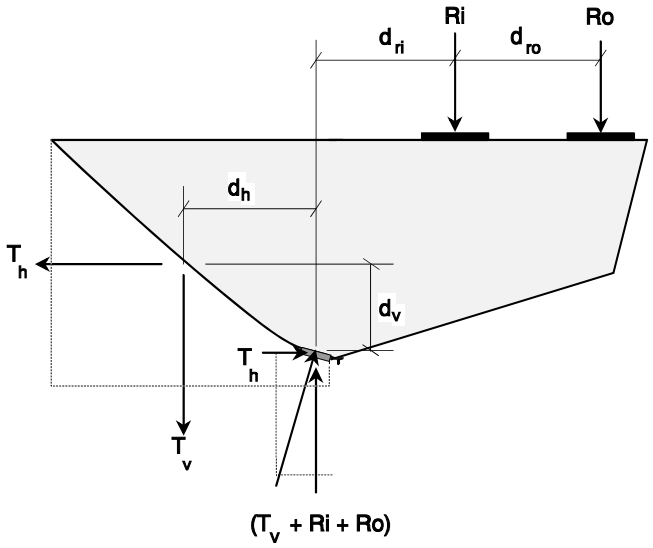

Joint Resistance = Applied Moment

$$T_h(d_v) + T_v(d_h) = Ri(d_{ri}) + Ro(d_{ro} + D_{RI})$$

Figure 5.11 Free body used to compute bent capacity

The force developed by each bar (non T-head) that crosses the diagonal crack assumed to propagate through the joint was computed by multiplying the nominal yield strength of the bar by the ratio of the embedment length beyond the crack, L, to the computed development length, l_d (see Figure 5.12). the basic bar development length, l_d, was computed using the ACI 318 (1963) development length equation (Equation 3-1 from Section 3.2.5.1). A nominal yield stress, f_y, of 414 MPa (60ksi) and a nominal concrete compressive strength, f'c, of 34.5 MPa (5000psi) were assumed. If the available anchorage length, L, was less than l_d, the maximum stress in the bar was computed as the fraction of the available anchorage length, L, divided by l_d, multiplied by the nominal yield stress, f_y. It was assumed that all reinforcing bars reached their respective computed maximum force simultaneously (i.e., when anchorage in the joint failed).

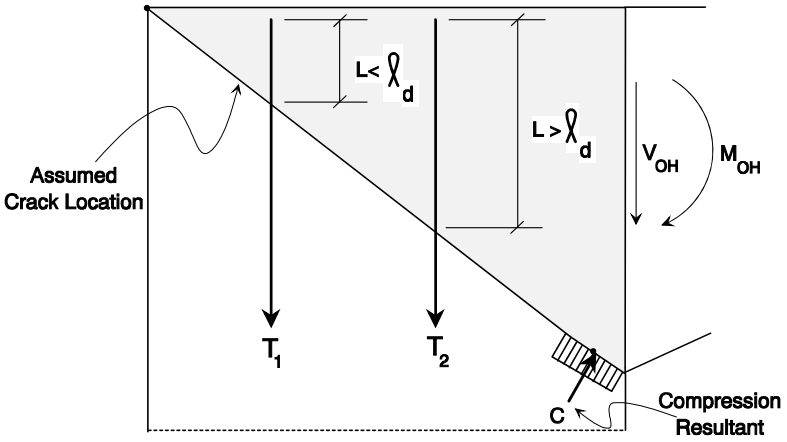

$$T_1 = \frac{L}{l_d} f_y A_s \text{ for } L < \ell_d$$

or

$$T_2 = f_y A_s \text{ for } L > \ell_d$$

Figure 5.12 Assumed joint crack and method for computing forces developed in longitudinal bars

At failure, shown in Figure 5.11, the overhand and a portion of the joint were assumed to act as a rigid-body. The maximum applied moment was determined by varying the applied load until equilibrium was achieved for the free body shown in Figure 5.11. Moments were summed about the compression centroid in the joint corner. The compression centroid (determined from the summation of the horizontal and vertical forces) was recomputed as the applied loads were varied, resulting in a change in the location of the compression centroid. The applied load that corresponded with joint failure was that which resulted in equilibrium of the free body.

Orientation of the critical joint crack corresponding with failure of the cantilever bent was not always obvious. Different locations of the crack eliminated effectiveness of some bars while increasing the embedment length of others. A trial-and-error approach was used to determine the correct location of the critical joint crack. Correct location of the crack corresponded with the minimum computed load on the overhang.

Details of the strength calculations performed for Specimens POJ-RC-100 and POJ-PS-100 using the joint bond-strength model are presented below. Calculations for the integrated design specimens were similar but somewhat simpler because T-heads on mild reinforcement facilitated development of the reinforcement.

A portion of the free body used to compute the capacity of Specimen POJ-RC-100 is shown in Figure 5.13. Capacities of bars that crossed the critical diagonal crack in the joint were determined, as outlined above, after determining the development length, l_d, and embedment length, L, for each bar. Capacity of the bent was determined by summing moments about the compression centroid. The size of the compression block and location of the resultant depended upon the magnitude of the applied load on the bent. The iterative analysis procedure resulted in the lowest computed capacity when the critical diagonal crack was assumed to propagate through the joint corner furthest from the compression resultant. A simplified free body diagram used to compute the bent capacity (where individual bar forces across the crack interface were replaced by vertical and horizontal resultants) is presented in Figure 5.14. The figure also contains the computation of the specimen capacity. The calculated capacity of Specimen POJ-RC-100, based on a uniform bond-stress model applied to the longitudinal reinforcement embedded in the joint, was DL+0.6LL.

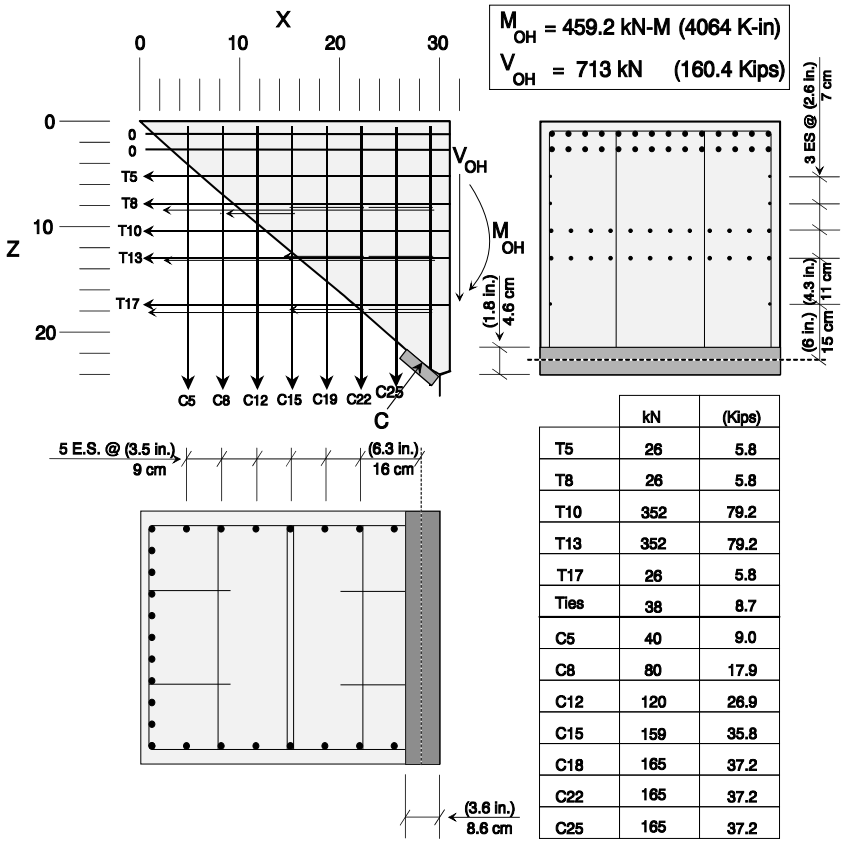

	kN	(Kips)
T5	26	5.8
T8	26	5.8
T10	352	79.2
T13	352	79.2
T17	26	5.8
Ties	38	8.7
C5	40	9.0
C8	80	17.9
C12	120	26.9
C15	159	35.8
C18	165	37.2
C22	165	37.2
C25	165	37.2

Figure 5.13 POJ-RC-100 free body and reinforcement locations used in joint strength model

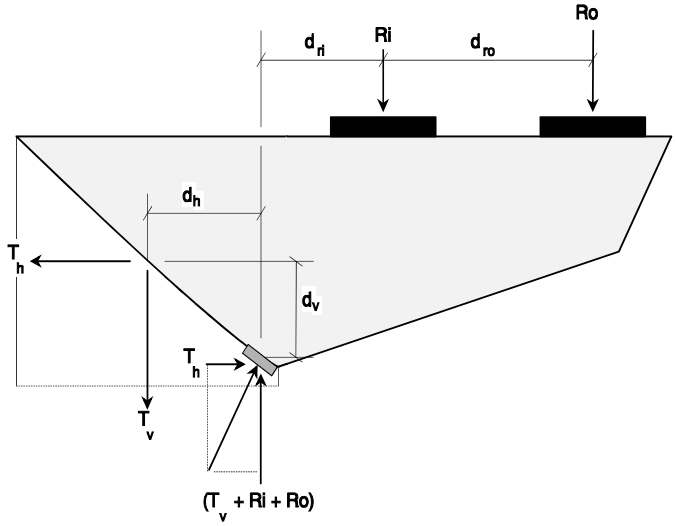

Joint Resistance = Applied Moment

$T_h(d_v) + T_v(d_h) = Ri(d_{ri}) + Ro(d_{ro} + d_{ri})$

(184.3 Kips)(11.6 in.) + (201.1 Kips)(10.9 in.) = (76.0 Kips)(13.8 in.) + (87.6 Kips)(37.8 in.)

820 kN (29.5 cm) + 895 kN (27.7 cm) = 338 kN (35.0 cm) + 389 kN (96.0 cm)

Figure 5.14 Free body used to compute capacity of Specimen POJ-RC-100

Once the test was completed, a post-mortem inspection of the joint region revealed two embedded lifting hooks in the top of the specimen had provided additional joint reinforcement that was not accounted for in the original capacity calculation. Accounting for the additional area of steel (4-No.3 mild reinforcing bars), the computed specimen capacity was increased to DL+1.6LL.

A portion of the free body used to compute the capacity of Specimen POJ-PS-100 is shown in Figure 5.15. A simplified free-body diagram (where individual bar forces on the crack interface were replaced by vertical and horizontal resultants) used to estimate the capacity is presented in Figure 5.16.

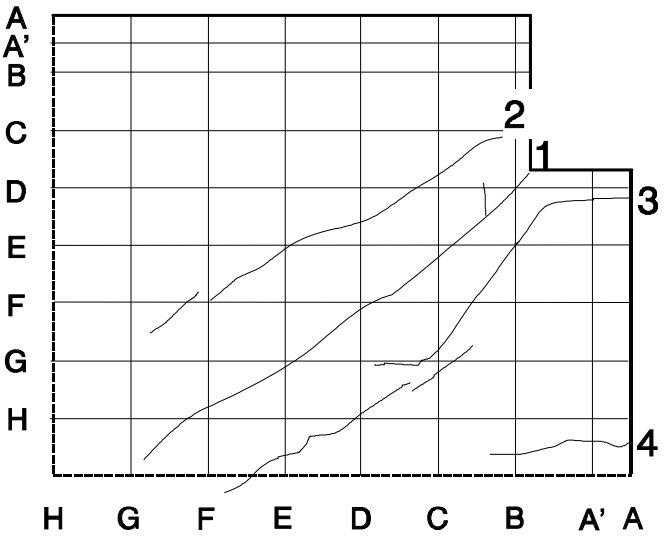

Figure 5.15 POJ-PS-100 cracking pattern on south face of joint at dead load

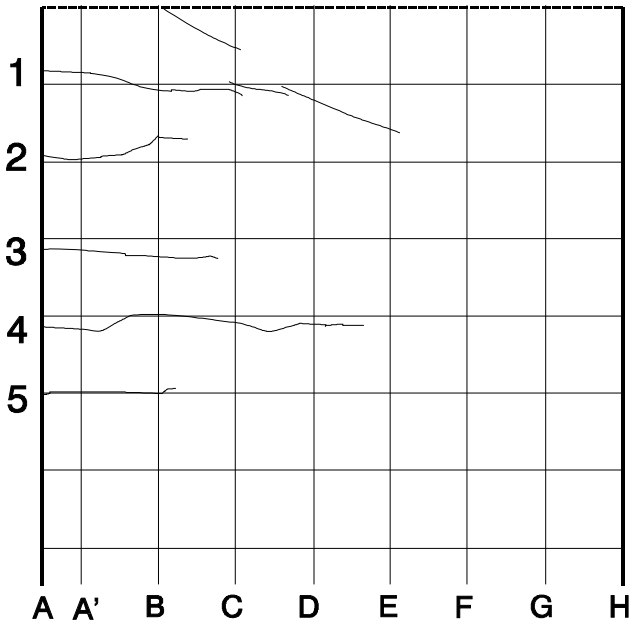

Figure 5.16 POJ-PS-100 cracking patterns on north face of pier at dead load

Table 5.1 lists the computed overhang, pier, and "joint" capacities as a fraction of the moment developed at the joint face at factored loads. The ratio of measured-to-predicted capacity was determined by dividing the measured capacity by the computed capacity associated with the observed failure mode. Specimen POJ-74-TH could not be loaded to failure, so the ratio of measured-to-predicted capacity is a lower-bound estimate based on the computed ultimate capacity of the overhang. These computed capacities are highlighted in Table 5.1. The proximity of these ratios to unity indicates that both the joint bond-strength model and analysis model for flexural strength provide reasonable strength predictions.

Table 5.1 Comparison of computed and measured capacities

	OVERHANG		**PIER**		**JOINT**			
	Nominal Capacity	Ultimate Capacity	Nominal Capacity	Ultimate Capacity	Computed Capacity	Measured Capacity	Measured/ Predicted Capacity	Failure Location
RC-100	1.36	1.49	1.27	1.39	**0.81**	0.76	0.94	Joint
PS-100	1.63	1.65	1.27	1.39	**0.54**	0.58	1.07	Joint
RC-100-TH	1.17	1.38	1.27	1.39	**1.26**	1.44	1.14	Joint
PU-54-TH	1.12	**1.24**	1.25	1.30	1.28	1.42	1.15	Overhang
PU-74-TH	1.13	**1.21**	1.31	1.35	1.35	>1.41	1.17	N/A

5.3 SERVICEABILITY EVALUATION

Three serviceability conditions were evaluated for each of the specimens: service load deflection, maximum crack-width at service load, and steel stress range. In addition, cracking patterns and crack-width frequency were also examined. Serviceability of the fully-prestressed overhang (POJ-PS-100) was not considered due to early failure of the specimen at DL+½LL.

5.3.1 Service-Level Tip Deflections

Service-level tip deflections (exceeding those after first application of dead load) for the models were compared with the L/300 displacement limit stated in AASHTO Section 8.9.3.2 for cantilever members (shown in Fig. 5.17). The allowable service-load deflection was 3.8 mm (0.15 in.) based on an overhang length of 114 cm (45 in.). The prototype reinforced concrete specimen (POJ-RC-100) and reinforced concrete specimen with headed bars (POJ-RC-100-TH) had unacceptable service level tip deflections that were equivalent to L/229 and L/266 respectively. The partially-prestressed Specimens, POJ-PU-54-TH and POJ-PU-74-TH, had acceptable service-level deflections of L/306 and L/497, respectively.

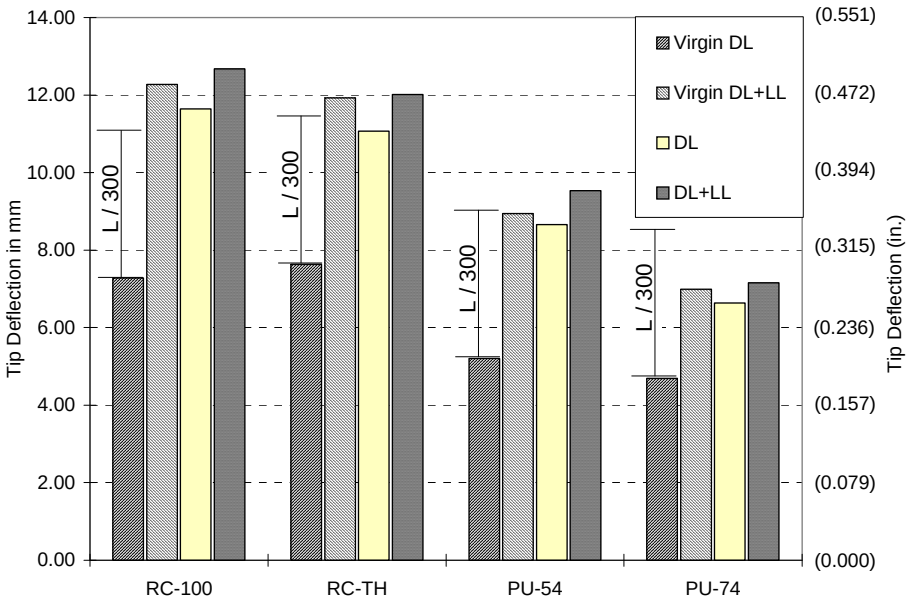

Figure 5.17 Service-level tip deflections

The service-level tip deflections shown in Figure 5.17 demonstrate the reduced deflections associated with increasing percentages of prestressed reinforcement. Dead load deflections following unloading from DL+LL were as much as 66% greater than the deflections resulting from first application of dead load. This may have been due to internal friction in the rams during unloading. Deflections resulting from reloading Specimen POJ-PU-54-TH to DL+LL resulted in unacceptable service-level tip deflections, equivalent to L/265. This was a 6% increase in deflection. Specimen POJ-PU-74-TH had an acceptable service level tip deflection equivalent to L/465.

5.3.2 Comparison of Service Load Cracking Patterns with Tensile Stresses from Finite Element Analyses

The service load crack patterns are shown with principal tensile stress contours computed by finite element analyses in Figure 5.18 through Figure 5.27. Elastic finite element analyses confirmed the large principal tensile stresses that existed at service load and dead load, respectively, in the joint regions of the model of the prototype reinforced concrete design (POJ-RC-100) and the model of the prototype fully-prestressed overhang design (POJ-PS-100) (Figs. 5.19 and 5.21, respectively). Due to poor detailing of the joint region in the prototype designs, large tensile stresses resulted in formation of critical diagonal joint cracks (heavier-weighted lines in Figure 5.18 and Figure 5.20) and premature failure of anchorage in the joint.

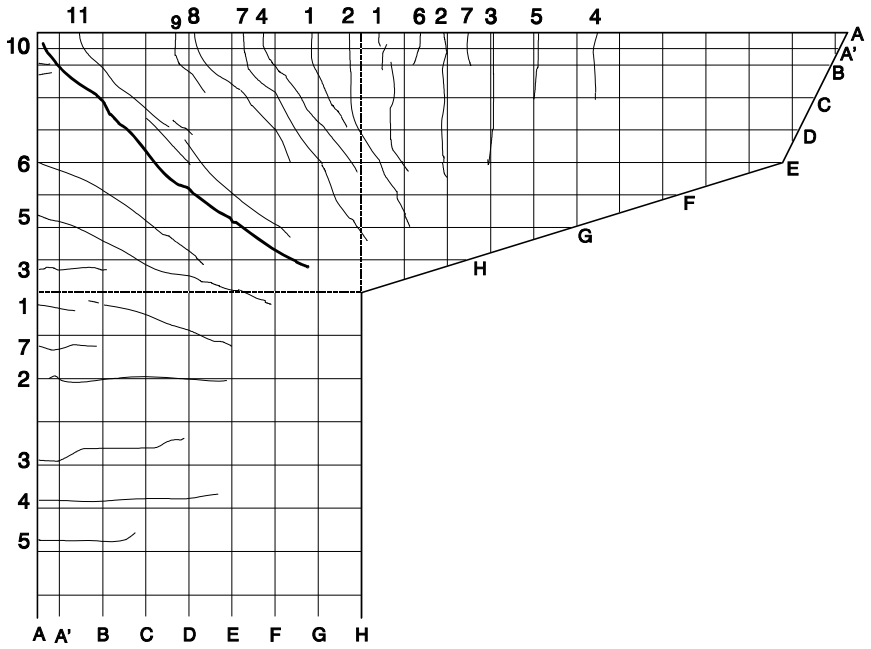

Figure 5.18 POJ-RC-100 service load crack pattern

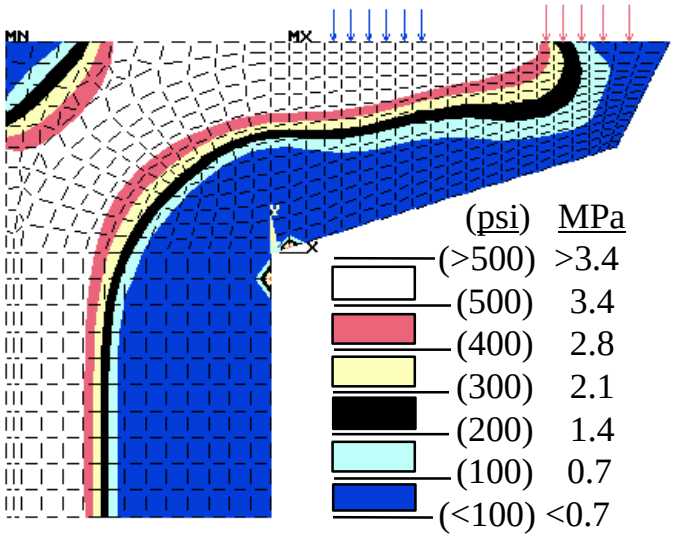

Figure 5.19 POJ-RC-100 principal tensile stress contours at service load

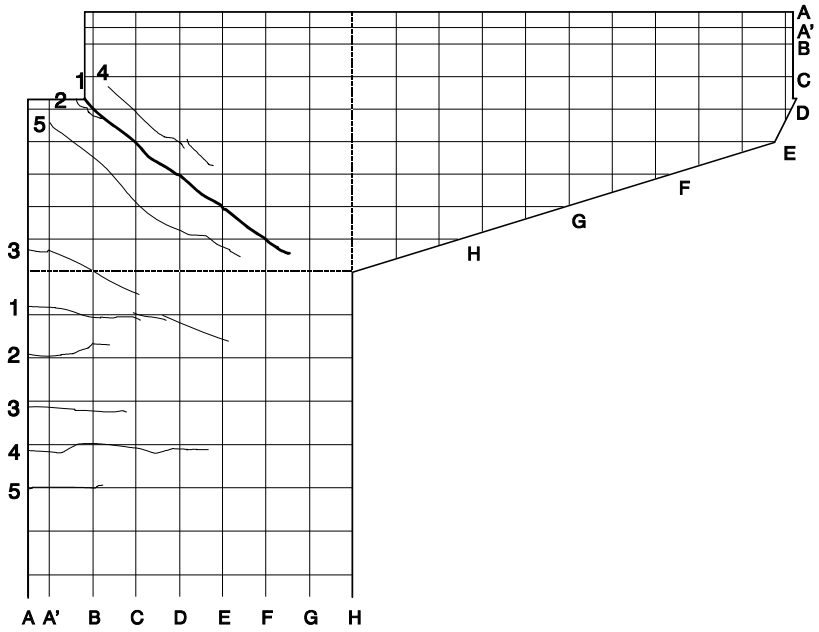

Figure 5.20 POJ-PS-100 dead load crack pattern

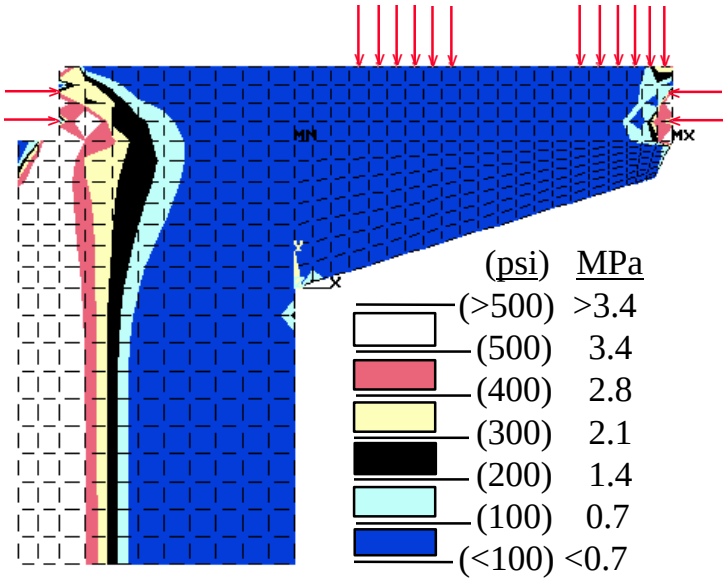

Figure 5.21 POJ-PS-100 principal tensile stress contours at dead load

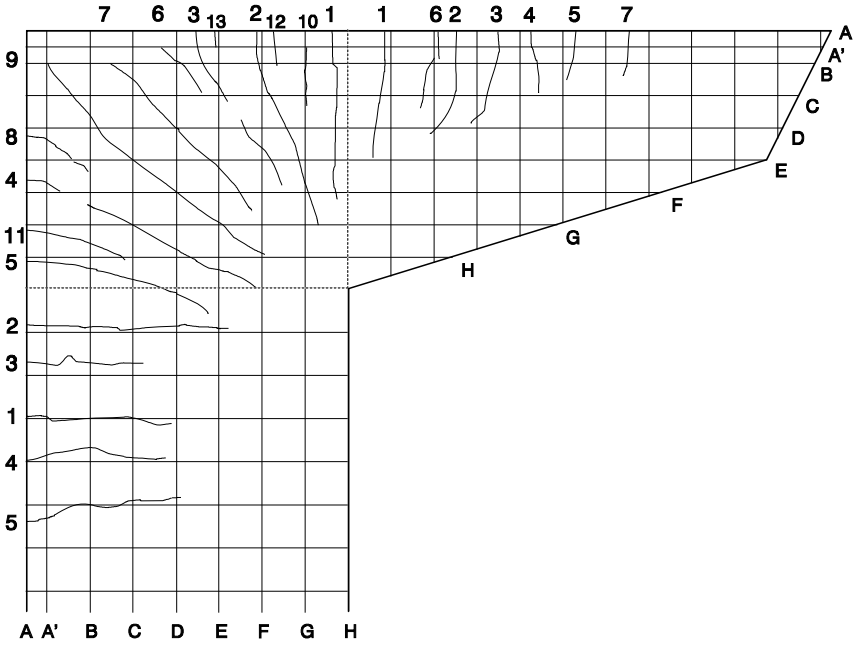

Figure 5.22 POJ-RC-100-TH service load crack pattern

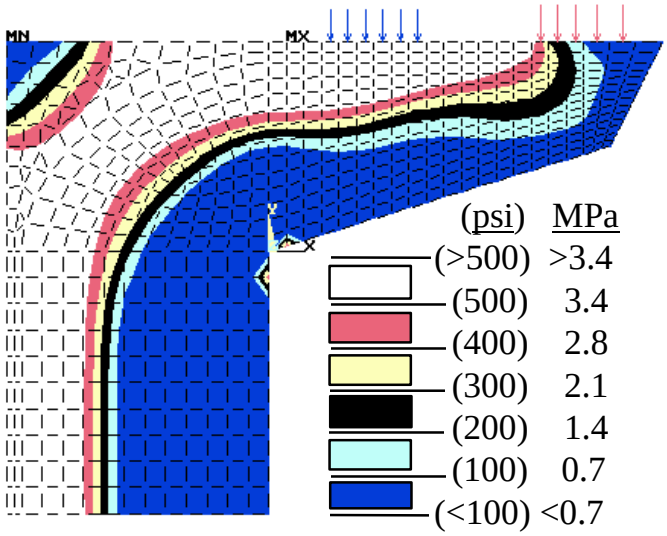

Figure 5.23 POJ-RC-100-TH principal tensile stress contours at service load

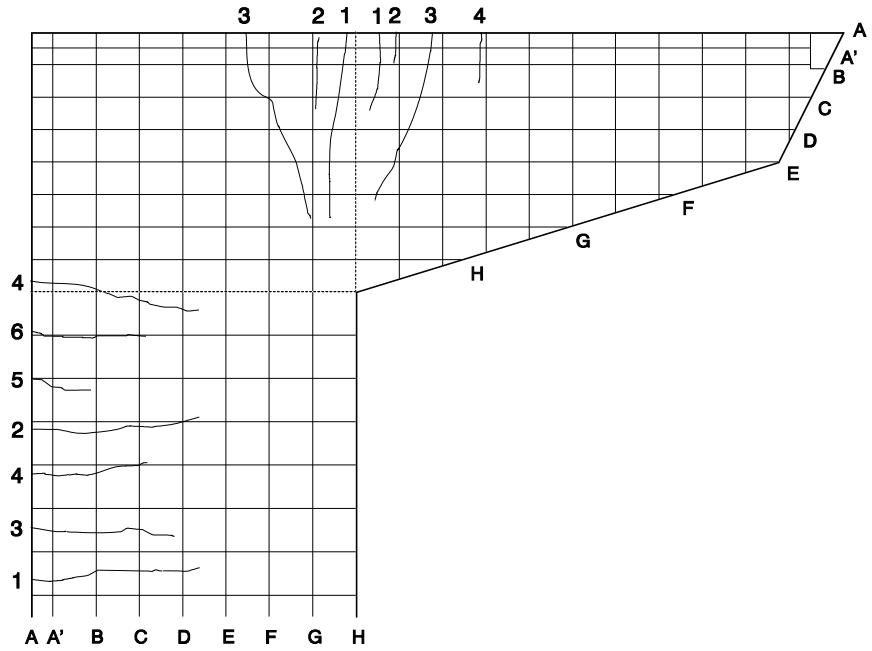

Figure 5.24 POJ-PU-54-TH service load crack pattern

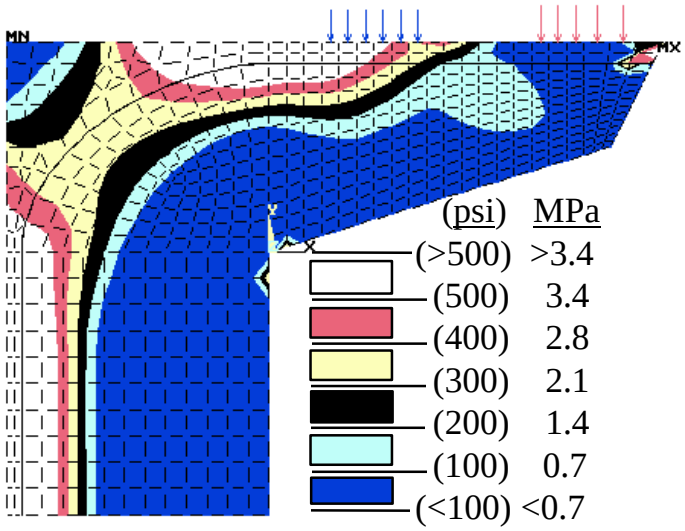

Figure 5.25 POJ-PU-54-TH principal tensile stress contours at service load

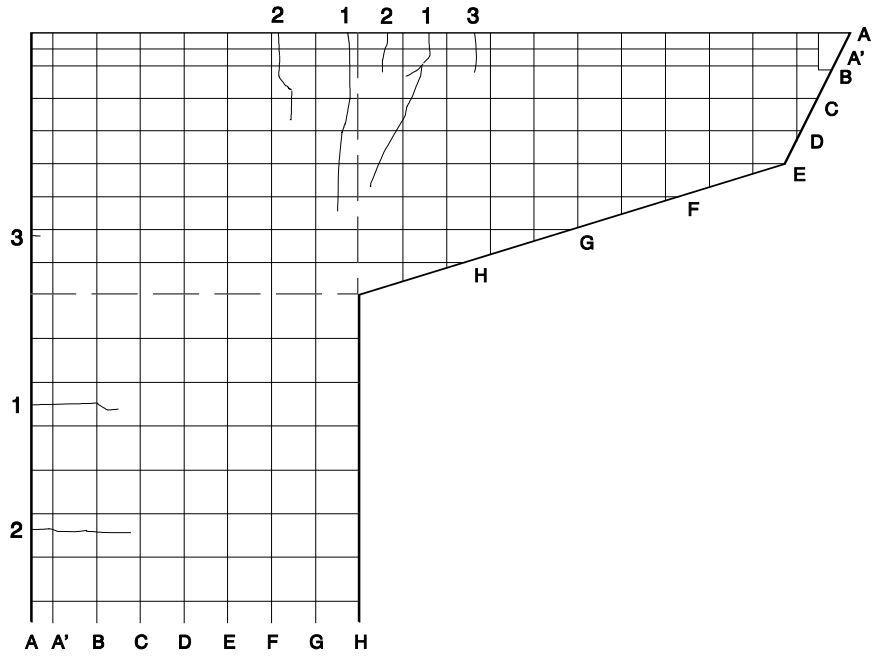

Figure 5.26 POJ-PU-74-TH service load crack pattern

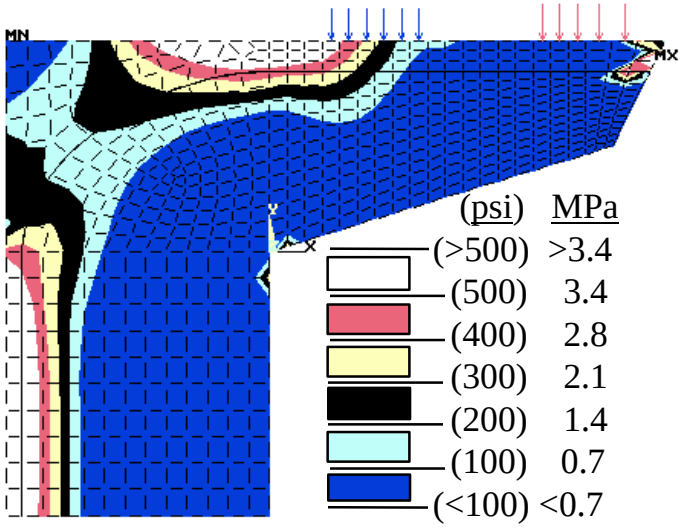

Figure 5.27 POJ-PU-74-TH principal tensile stress contours at service load

The finite element analysis for Specimen POJ-RC-100-TH at service-loads (Figure 5.23) indicated the principal tensile stresses in the overhang, joint, and pier regions were above the assumed concrete cracking stress of $7\sqrt{f'_c}$ (psi) [34.4 MPa (500 psi)]. During testing, the specimen developed 28 cracks (shown in Fig. 5.22) located within high tensile regions indicated by the finite element analysis. Cracks in the specimen were well-distributed throughout the tensile regions. Headed reinforcement in the joint corner prevented the diagonal crack (number 9 in Figure 5.22) from propagating to the exterior of the specimen. The pattern of joint cracking suggests additional side-face reinforcement should have been provided for adequate crack control.

The introduction of partial-prestressing had two benefits: it reduced the number of cracks observed at service-loads, and it reduced computed principal tensile stresses in the specimens. Specimen POJ-PU-54-TH had 14 cracks at service loads (Figure 5.24) and computed peak principal tensile stresses across the joint diagonal of 3.8 MPa (400 psi) at service loads (Figure 5.25). As expected, cracks were concentrated in the regions where computed principal tensile stresses were largest. Cracks were well-spaced in the overhang and pier regions, and very few cracks formed in the joint region. Specimen POJ-PU-74-TH had eight cracks at service loads (Figure 5.26) and peak computed principal tensile stresses across the joint diagonal of 1.7 MPa (200 psi) at service loads (Figure 5.27). Cracks in the overhang and pier regions formed in areas where computed principal tensile stresses exceeded the assumed cracking stress of $7\sqrt{f'_c}$ (psi) [34.4 MPa (500 psi)].

5.3.3 Evaluation of Crack Widths

Crack widths were measured at first cracking, dead load (DL), service load (DL+LL), and dead load plus two live loads (DL+2LL). Cracks in the overhang, joint, and pier were considered to be of an acceptable width if they were 0.14 mm (0.0055 in.) or smaller. The limiting crack width of 0.14 mm (0.0055 in.) was computed by dividing the 1992 AASHTO Standard Specifications [1] Z factor of 170 (which corresponds to a crack width of 0.039 mm (0.0155 in.)) by the 2.75 scale-factor used in the model. Crack widths were measured in inches using an optical crack-width comparitor with an accuracy of ±0.013 mm (± 0.0005 in.).

The maximum crack widths in the overhang, pier, and joint regions at the loads listed above were used to develop the maximum crack-width envelopes for these regions. Plots of moment versus maximum measured crack width for the three regions are shown in Figure 5.28 through Figure 5.30. Applied moment in the figures is non-dimensionalized using the factored moment, and the measured crack width is non-dimensionalized using the maximum allowable crack width of 0.14 mm (0.0055 in.).

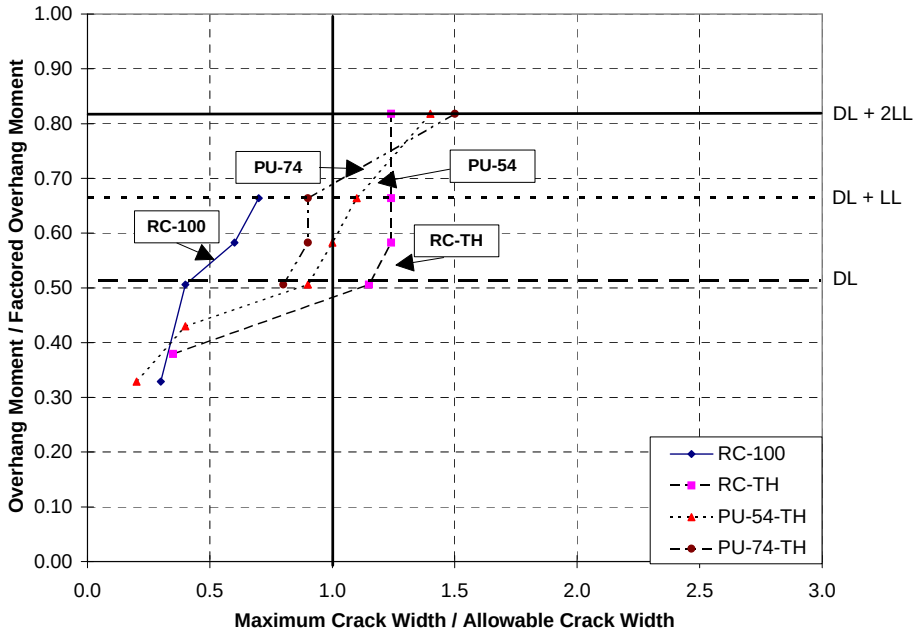

Figure 5.28 Crack-width envelopes for overhang region

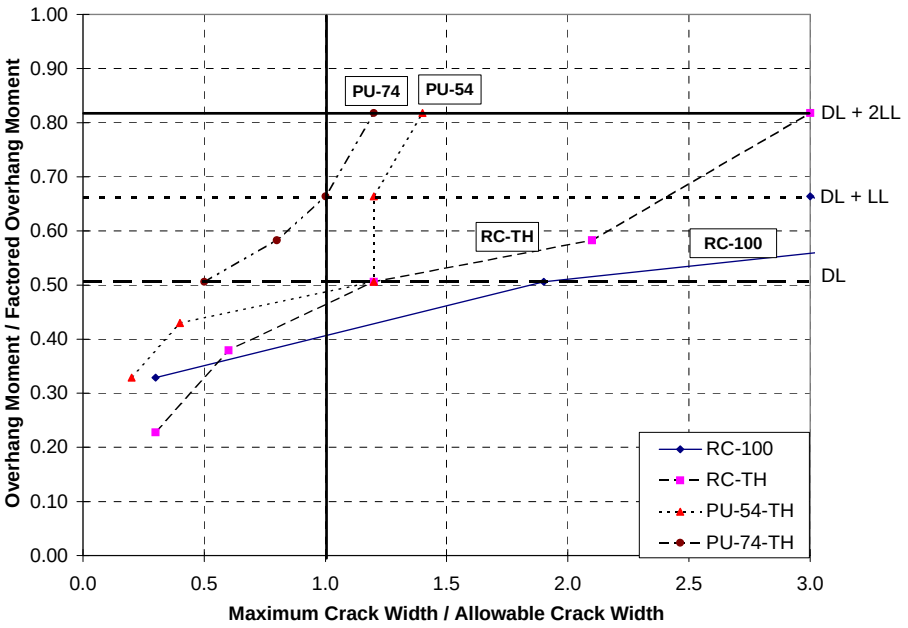

Figure 5.29 Crack-width envelopes for joint region

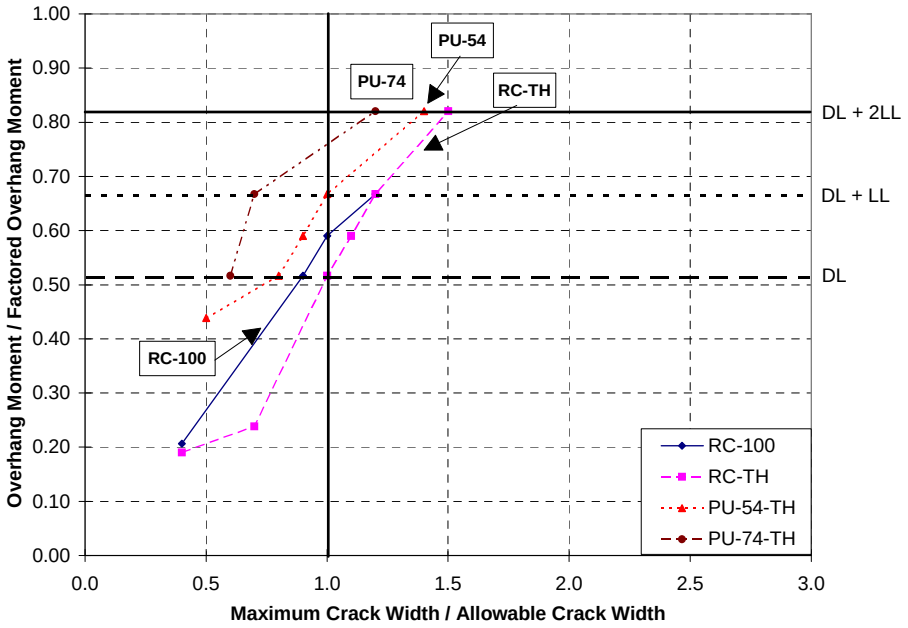

Figure 5.30 Crack-width envelopes for pier region

5.3.3.1 Overhang Crack-Width Envelopes

The crack-width envelope for the overhang region of each specimen is shown in Figure 5.28. The plot indicates the integrated design reinforced concrete specimen (POJ-RC-100-TH) and the 54% prestressed specimen (POJ-PU-54-TH) had maximum measured crack widths at loads at or below DL+LL that exceeded the maximum allowable crack width of 0.14 mm (0.0055 in.). Specimens POJ-RC-100-TH and POJ-PU-54-TH had maximum overhang crack-widths of 0.18 mm (0.007 in.) and 0.15 mm (0.006 in.), respectively, at service load. Both cracks were located at the extreme tensile fiber of the overhang. Frequency distribution plots, shown in Figure 5.32 and Figure 5.33,

indicate that only 0.4% and 1.1% of measured crack widths for Specimens POJ-RC-100-TH and POJ-PU-54-TH, respectively, were greater than the maximum allowable crack width.

5.3.3.2 Joint Crack-Width Envelopes

The joint crack-width envelopes, shown in Figure 5.29, indicate the prototype reinforced concrete model (POJ-RC-100), integrated reinforced concrete (POJ-RC-100-TH), and 54% prestressed (POJ-PU-54-TH) specimens had joint crack widths greater than the limiting crack width of 0.14 mm (0.0055 in.). Specimens POJ-RC-100 and POJ-RC-100-TH had 31 and 42 crack measurements, respectively, that exceeded the maximum allowable crack-width (which corresponds to 14.8% and 9.4% of all measured cracks, respectively). The maximum joint crack width in Specimen POJ-PU-54-TH [0.17 mm (0.0065 in.)] was measured in one location on the north side and two locations on the south side after loading to service load a second time. The crack-width frequency plots for Specimen POJ-PU-54-TH, shown in Figure 5.33, indicate only 1.8% of the measured joint crack widths exceeded the maximum allowable crack width.

At service load, both Specimens POJ-RC-100 and POJ-RC-100-TH had numerous cracks in the joint region with widths that exceeded the maximum allowable crack width. Joint cracks in Specimen POJ-RC-100 were indicative of the imminent bond failure that ultimately resulted due to the lack of adequate bar anchorage in the joint region. Joint cracks in Specimen POJ-RC-100-TH indicated the need for additional side-face reinforcement to improve serviceability. It was known prior to construction of this specimen that additional transverse reinforcement was needed in the joint. However, additional detailing reinforcement was not provided in order to isolate and evaluate the effect of headed mild reinforcement on the behavior of the specimen.

5.3.3.3 Pier Crack-Width Envelopes

Crack-width envelopes for the pier region, shown in Figure 5.30, indicate the reinforced concrete specimens (POJ-RC-100 and POJ-RC-100-TH) had crack widths that exceeded the maximum allowable crack width at service loads. The reinforced concrete piers had identical designs, and envelopes of the maximum crack widths were similar. Pier crack widths could have been reduced by replacing the longitudinal bars used in the piers with a greater number of smaller-diameter bars. Crack-width envelopes for the partially-prestressed specimens (POJ-PU-54-TH and POJ-PU-74-TH) indicated crack-widths were acceptable.

5.3.4 Crack-Width Frequency and Distribution at Service Loads

The crack-width frequency and distribution plots, shown in Figure 5.31 through Figure 5.34, indicate which regions of each specimen contained the widest cracks and/or the largest number of cracks. The plots depict the number of crack measurements (of a particular width) that occurred in the pier, overhang, and joint regions as a percentage of all crack-width measurements taken at service loads. Recall that crack widths were measured at 3 by 4 in. (75 by 100 mm) grid lines on both sides of the overhang, and 4 by 4 in. (100 by 100 mm) grid lines on the side faces of the pier. The plots were typically developed using the crack-width readings taken at "virgin" service loads and after reloading each specimen to service loads (Specimen POJ-RC-100 used only the readings taken at "virgin" service-loads). Crack-widths were measured in inches with 0.013 mm (0.0005 in.) accuracy.

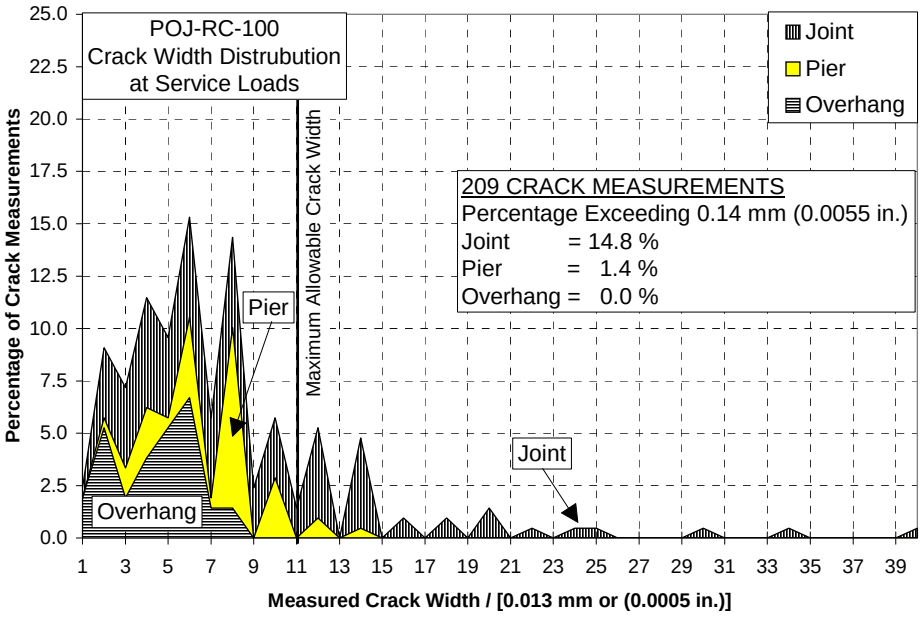

Figure 5.31 POJ-RC-100 crack-width frequency and distribution

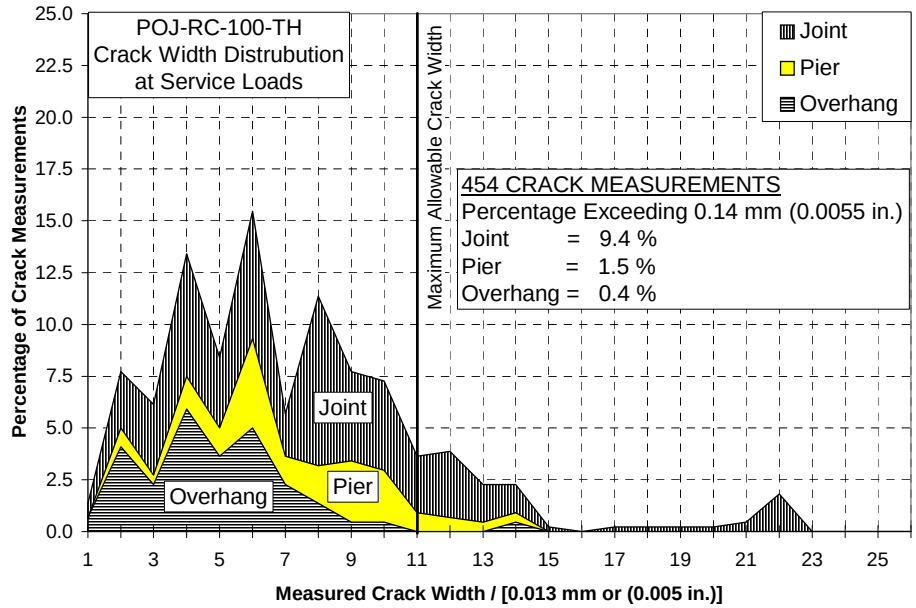

Figure 5.32 POJ-RC-100-TH crack-width frequency and distribution

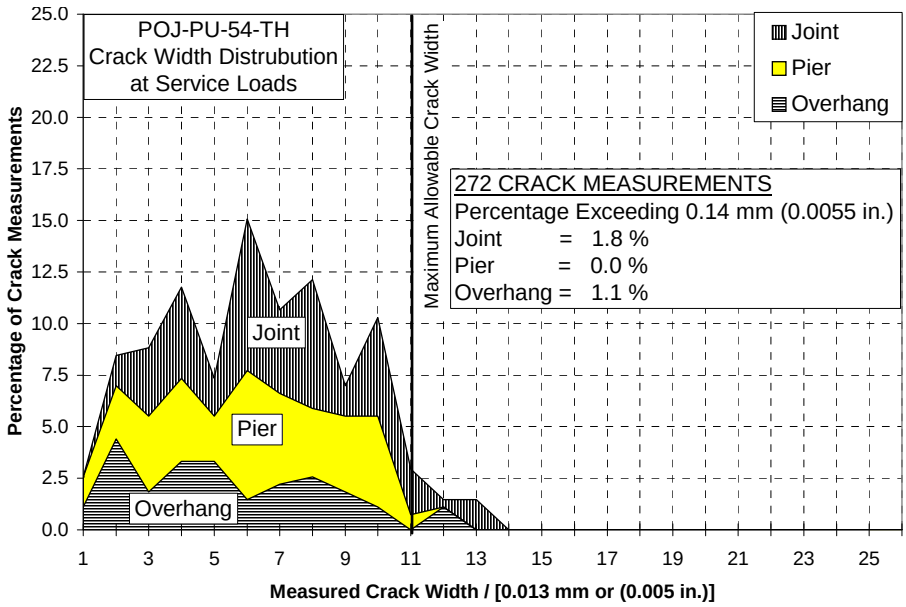

Figure 5.33 POJ-PU-54-TH crack-width frequency and distribution

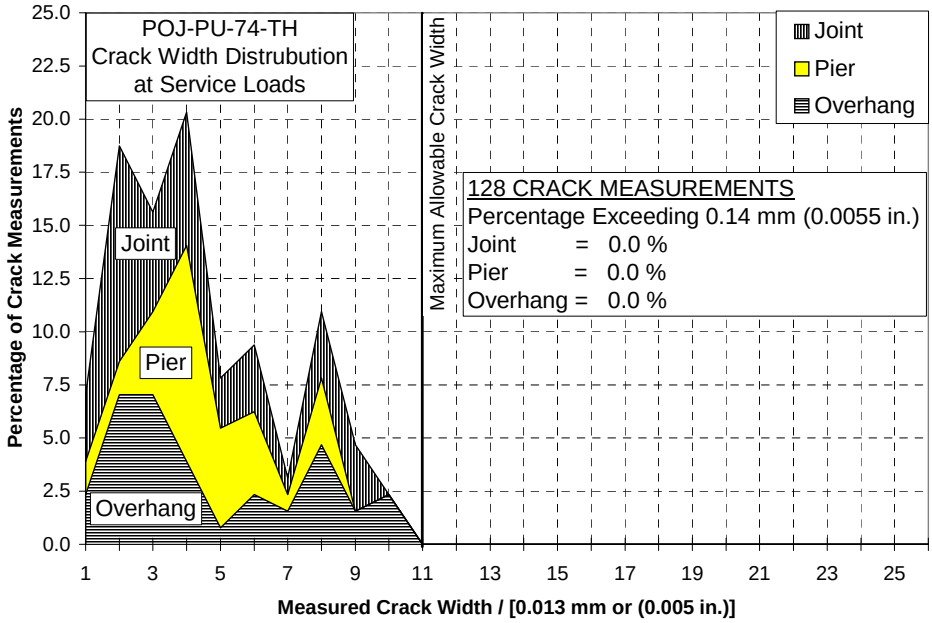

Figure 5.34 POJ-PU-74-TH crack-width frequency and distribution

The crack-width frequency and distribution for the prototype model reinforced concrete Specimen (POJ-RC-100), shown in Figure 5.31, was developed using one set of service load crack-width readings. At service loads, 209 crack widths were measured (112 on the north side and 97 on the south side of the specimen). Over 16% of all crack measurements for the specimen exceeded the maximum allowable crack width; 14.8% and 1.4% of the crack measurements at service load were in the joint and pier regions, respectively.

The frequency and distribution of crack widths within the different regions for the reinforced concrete specimen with T-headed bars (POJ-RC-100-TH) is shown in Figure 5.32. The north side had 231 crack-width measurements and the south side had 223 measurements at service-loads. The pier,

overhang, and joint regions of the specimen all had crack widths that exceeded the maximum allowable crack width of 0.14 mm (0.0055 in.). In the joint region, 42 crack measurements (9.4% of all measured cracks) exceeded the maximum allowable crack width. Only seven crack measurements in the pier and two in the overhang (1.5% and 0.4% of the measured crack-widths, respectively) exceeded the maximum allowable crack width at service loads.

The crack-width frequency and distribution plot for the specimen with a 54% prestressed overhang and headed bars (POJ-PU-54-TH) is shown in Figure 5.33. The north side had 130 crack-width measurements and the south-side had 142 crack-width measurements. Only 2.9% of the 272 crack widths measured exceeded the maximum allowable crack width at service load. The crack widths that exceeded the maximum allowable crack width were located in the joint region (five crack measurements or 1.8% of all measurements) and the overhang region (three crack measurements or 1.1%).

The crack-width frequency and distribution for the specimen with a 74% prestressed overhang and T-headed bars (POJ-PU-74-TH), shown in Figure 5.34, indicated all measured crack widths were less than the crack-width limit. The 128 crack-width measurements taken at service loads included 54 crack-width measurements on the north side and 74 crack-width measurements on the south side of the specimen. Crack widths on the north side of the specimen were fairly well distributed, while crack widths on the south side were small (typically less than 0.6 mm (0.025 in.)).

5.3.5 Comparison of Measured vs. Predicted Crack Widths

Values for the maximum measured crack widths and maximum predicted crack widths, shown in Figure 5.36 through Figure 5.39, are plotted at dead load (DL), service load (DL+LL), and DL+2LL for the overhang and pier regions. Predicted crack-widths were computed using the proposed crack width model (which will be presented shortly) and a strain compatibility analysis.

The accuracy of crack-width equations has been historically limited to ± 50% [16]. The rough appearance of the crack width on the surface, the distribution of cracks, and lack of repeatable experimental crack-width results make it difficult to accurately predict crack widths. Crack-width equations used in design determine the distribution of reinforcement in members. This serviceability check should produce members with controlled crack widths, resulting in aesthetically pleasing and durable structures.

The maximum allowable crack width of 0.14 mm (0.0055 in.) and the corresponding Z factor of 62 used for the study, were determined by dividing the full-scale maximum allowable crack width of 0.39 mm (0.0155 in.) and corresponding Z factor of 170 by the 2.75 scale factor. A Z factor of 170 provides protection for moderate exposure conditions and ensures cracks are not visible from a reasonable distance. If a more stringent limiting crack width for durability is specified for partially-prestressed members, the crack-width equation can be used to further limit crack widths.

Distribution of Tension Reinforcement:

The crack-width equation used in this study was similar to the formula in the 1992 AASHTO LRFD Specifications (Equation 5.7.3.4.2-1) [19] and was developed to predict maximum crack widths for the overhang specimens studied by Armstrong [3] and Salas [4]. The important variables in the equation are: steel tension stress, size of the tension block, and number of bars in the tension block. Steel tensile stress is determined using a cracked-section model. Size of the tension block is computed by determining the effective steel centroid of the mild and prestressed reinforcement. The number of steel reinforcing bars in the tension block as well as the number of bonded prestressing strands or grouted post-tensioning ducts were considered to help control crack widths.

Crack-Width Equation:

The crack-control equation used for the integrated design procedure, presented in Equation 3-29, is reformulated in Equation 5-1 to compute crack widths for direct comparison with maximum-measured crack widths. Variables for the crack-width equation (Equation 5-1) are illustrated in Figure 5.35 and are defined below:

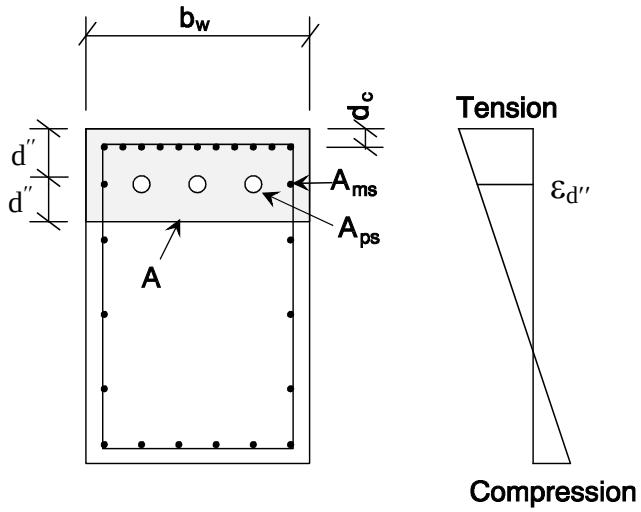

Figure 5.35 Illustration of crack-with equation variables

$$w = 0.000076\beta f_{sa} \left(d_c A\right)^{1/3} \qquad \textit{[5-1]}$$

where:

w = Maximum Crack-Width (in.)

β = Value of 1.2

f_{sa} = Average steel tensile stress (ksi) at a distance d'' from the extreme tensile fiber = $\varepsilon_{d'}$ (29,000 ksi) , where $\varepsilon_{d''}$ is the tensile strain at the effective steel centroid, d''

d_c = Distance from the extreme tension fiber to the centroid of the closest layer of primary tension reinforcement (in.)

A = Area of tension block (2 x d'' x b_w) (in^2) divided by the total number of mild reinforcing bars, bonded prestressing strands, and/or grouted post-tensioning ducts located within the tension block

$$d'' = \frac{\left[\sum A_{ps}\, d_{ps}\, f_{su} + \sum A_{ms}\, d_{ms}\, f_y\right]}{\left[\sum A_{ps}\, f_{su} + \sum A_{ms}\, f_y\right]} \qquad [5\text{-}2]$$

where:

d_{ps} = Distance from the extreme tension fiber to centroid of each layer of prestressed reinforcement in the tension zone

A_{ps} = Area of prestressed reinforcement at a layer

d_{ms} = Distance from extreme tension fiber to centroid of each layer of mild reinforcement in the tension zone

A_{ms} = Area of mild reinforcement at a layer.

The average steel tensile stress, f_{sa}, was computed by multiplying the strain, $\varepsilon_{d''}$, at the effective steel centroid by 29,000 ksi. Strain at the effective steel centroid, $\varepsilon_{d''}$, was determined using a strain compatibility analysis where stress in the bonded prestressed reinforcement was reduced to account for long-term losses. Computed crack widths in the overhang and pier for service loads, using Equation 5-1, are shown in Table 5.2 and Table 5.3, respectively.

Table 5.2 Computed overhang crack widths at service loads

	d	***d"***	***A***	f_{sa}	***w***	***w***
	(in.)	**(in.)**	**(in^2/#)**	**(ksi)**	**(in.)**	**mm**
RC-100	1.14	5.00	7.50	26.9	0.0050	0.13
RC-100-TH	1.14	1.86	3.19	36.5	0.0051	0.13
PU-54-TH	1.14	1.55	4.37	34.9	0.0054	0.14
PU-74-TH	1.14	2.85	8.05	28.6	0.0055	0.14

Table 5.3 Computed pier crack widths at service loads

	d	***d"***	***A***	f_{sa}	***w***	***w***
	(in.)	**(in.)**	**(in^2/#)**	**(ksi)**	**(in.)**	**mm**
RC-100	1.13	4.76	15.23	32.8	0.0077	0.20
RC-100-TH	1.13	4.76	15.23	32.8	0.0077	0.20
PU-54-TH	1.13	5.24	22.86	35.4	0.0095	0.24
PU-74-TH	1.11	3.29	14.36	33.5	0.0077	0.20

Maximum measured and predicted crack widths for the pier and overhang, shown in Figure 5.36 through Figure 5.39, are compared at dead load (DL), dead load plus one-half live load (DL+¾LL), service load (DL+LL), and dead-load plus two live loads (DL+2LL). The maximum crack widths were non-dimensionalized by dividing by the maximum allowable crack width of 0.14 mm (0.00055 in.), which corresponds with a Z factor of 62 (Z=170/2.75 scale factor).

For the prototype model reinforced concrete specimen (POJ-RC-100), maximum measured crack-widths in the overhang were slightly less than crack-widths predicted by Equation 5-1, as shown in Figure 5.36. Measured crack widths in the pier were in good agreement with predicted crack widths.

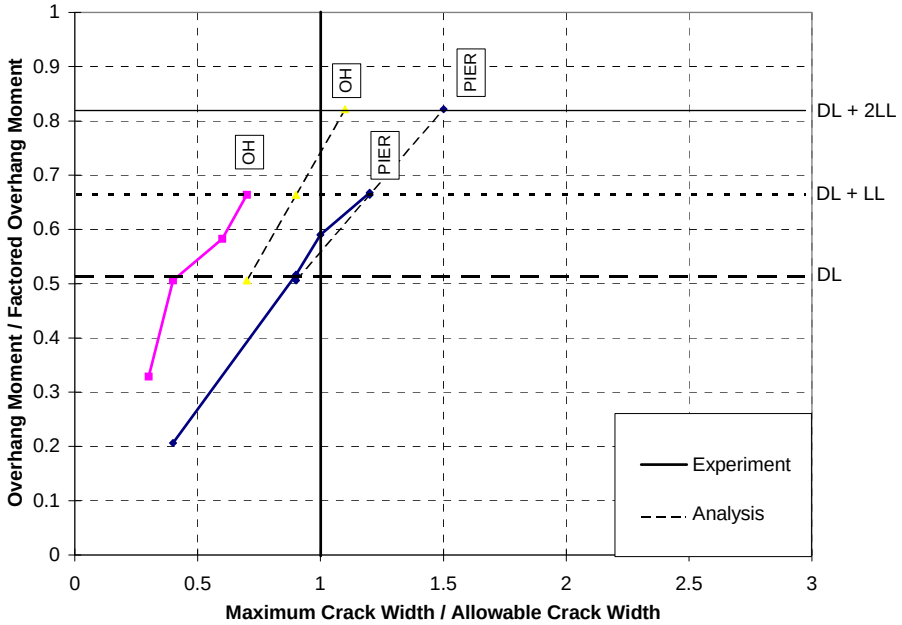

Figure 5.36 POJ-RC-100 maximum predicted and measured crack widths

For the reinforced concrete specimen with headed reinforcement (POJ-RC-100-TH), the maximum measured crack widths in the pier closely matched the crack-widths predicted by Equation 5-1. The maximum measured crack width in the overhang at service load was nearly 50% larger than the value predicted using Equation 5-1, but the maximum predicted and measured crack widths were in good agreement at DL+2LL. Figure 5.37 indicates a large crack developed at DL, but the crack width did not increase significantly with increased load to DL+2LL.

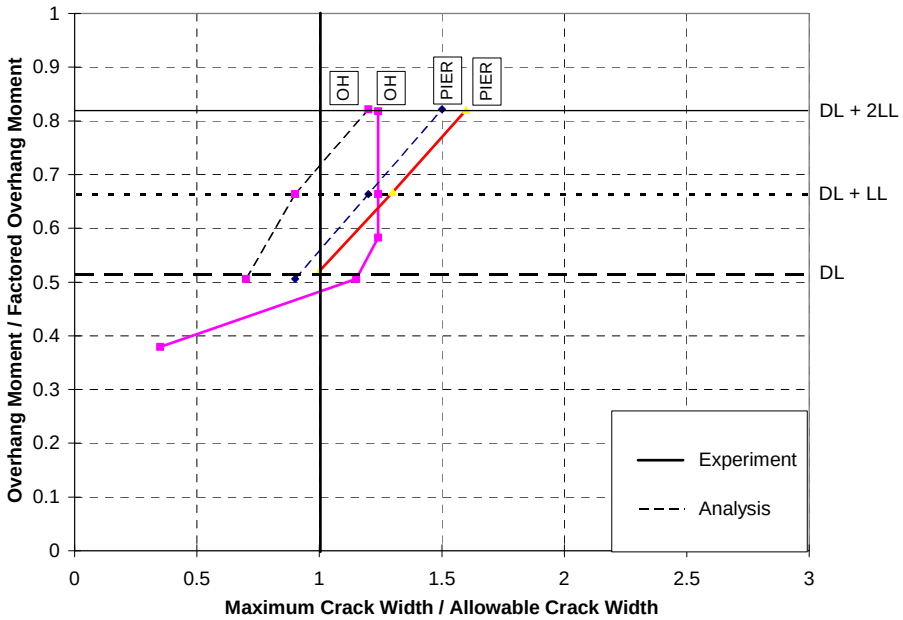

Figure 5.37 POJ-RC-100-TH maximum predicted and measured crack widths

The comparison of maximum measured and predicted crack widths for Specimen POJ-PU-54-TH are shown in Figure 5.38. The proposed crack-width equation over-estimated the pier region maximum measured crack width at service loads by 50%. The over-estimation was attributed to smaller-than-expected post-tensioning losses in the pier. The maximum crack width in the overhang was only 9% larger than the crack width predicted by Equation 5-1. Only three out of 66 crack measurements in the overhang exceeded the predicted maximum crack width at service loads.

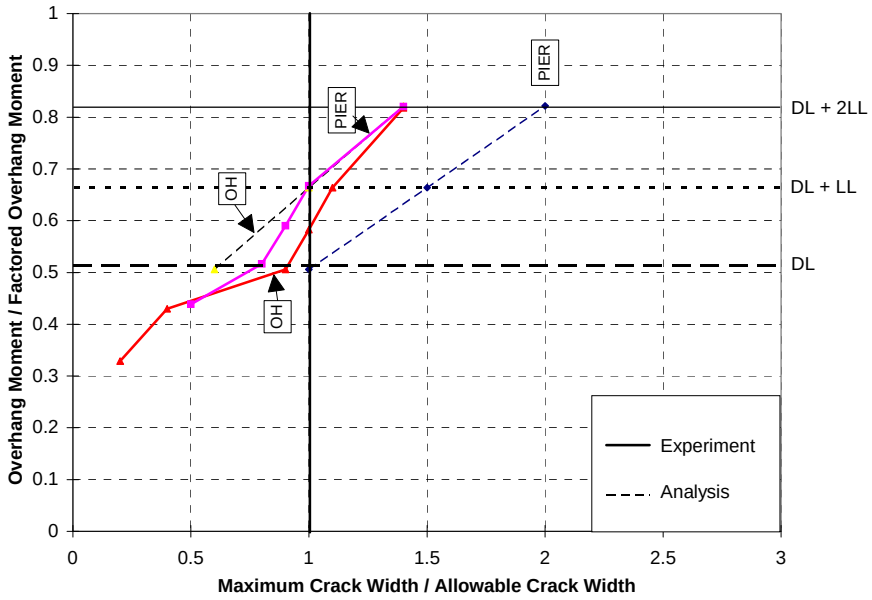

Figure 5.38 POJ-PU-54-TH maximum predicted and measured crack widths

The comparison of maximum measured and predicted crack widths for Specimen POJ-PU-74-TH is shown in Figure 5.39. Maximum measured crack-widths in the overhang region were similar to the maximum crack widths predicted by Equation 5-1. However, at service loads, the maximum measured crack width in the pier was 35% smaller than the predicted crack width. Once again, this was attributed to smaller-than-predicted losses in the post-tensioning.

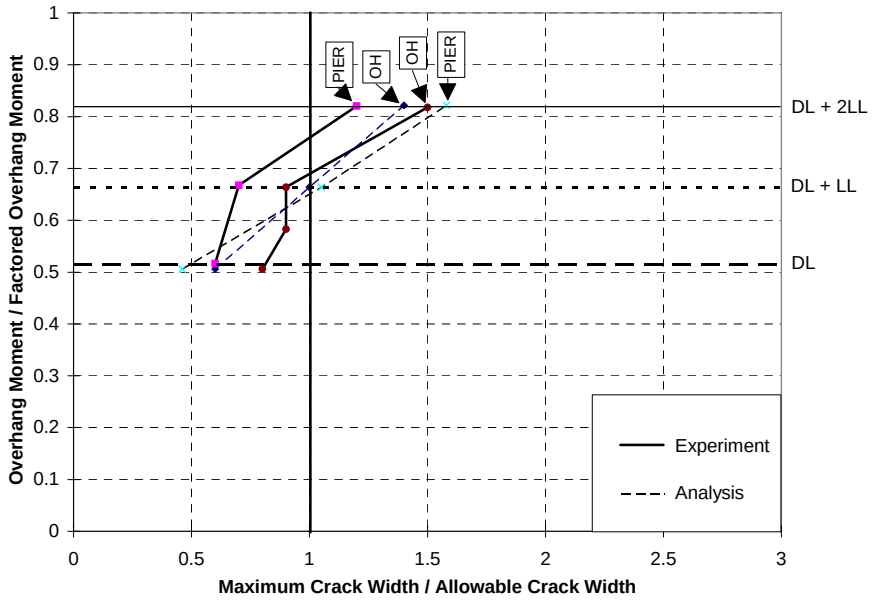

Figure 5.39 POJ-PU-74-TH maximum predicted and measured crack widths

In summary, maximum measured crack widths in the overhangs were in good agreement with crack widths predicted by Equation 5-1. The crack-width equation over-estimated pier crack widths for Specimens POJ-PU-54-TH and POJ-PU-74-TH by as much as 50%. This conservatism was attributed to the difficulty in determining the actual post-tensioning stress at dead load. The equation provided acceptable predictions of maximum crack widths; predicted crack widths were within the historically-accepted range of plus-or-minus 50%.

5.3.6 Evaluation of Reinforcement Stress Ranges

Calculated and measured stress ranges for the mild reinforcement and prestressed reinforcement are shown in Table 5.4 and Table 5.5. The calculated steel stress range was determined using a strain-compatibility analysis. The experimental stress range was computed by multiplying measured steel strains by 200 MPa (29,000 ksi).

Calculated stress ranges for mild reinforcement in the overhang were between 59 MPa (8.5 ksi) and 119 MPa (17.3 ksi), and were within the allowable limits stated in AASHTO Standard Specifications Equation (8-60), as detailed in table 5.4. The experimentally-obtained stress ranges were also smaller than the limiting mild reinforcement stress range. Calculated stress ranges for post-tensioning steel in the overhang of Specimens POJ-PU-54-TH and POJ-PU-74-TH were smaller than the limiting stress range of 100 MPa (14.5 ksi). Measured strains for the post-tensioning are not provided for Specimens POJ-PU-54-TH and POJ-PU-74-TH because strain gages were damaged during installation and/or stressing of the post tensioning.

Table 5.4 Computed and experimental stress ranges for overhangs

	Overhang Mild Steel Reinforcement						**Post Tensioning**	
	Allowable S_r		**Calculated S_r**		**Experimental S_r**		**Calculated S_r**	
	MPa	**(ksi)**	**MPa**	**(ksi)**	**MPa**	**(ksi)**	**MPa**	**(ksi)**
RC-100	99	14.4	59	8.5	90	13.1	N/A	N/A
PS-100	N/A	N/A	N/A	N/A	N/A	N/A	N/A	N/A
RC-100-TH	95	13.8	63	9.2	73	10.6	N/A	N/A
PU-54-TH	122	16.3	100	14.5	91	13.2	92	13.4
PU-74-TH	134	19.4	119	17.3	**	**	100	14.5

** Faulty gages

Calculated stress ranges for mild reinforcement in the pier were between 65 MPa (9.4 ksi) and 112 MPa (16.2 ksi), and were within the allowable limits stated in AASHTO Equation (8-60), as detailed in Table 5.5. The experimentally-obtained stress ranges were also smaller than the limiting mild reinforcement stress range, except for Specimen POJ-PU-54-TH, where the experimental reinforcement stress range was 8% greater than the limiting mild reinforcement stress range. The calculated stress range for post-tensioning steel in the pier of Specimen POJ-PU-54-TH was smaller than the limiting stress range of 100 MPa (14.5 ksi). As stated in Chapter 3, Specimen POJ-PU-74-TH had a stress range that was 3.5% larger than the limiting stress range. Measured strains for the post-tensioning are not provided for Specimens POJ-PU-54-TH and POJ-PU-74-TH because strain gages were damaged during installation and/or stressing of the post-tensioning.

Table 5.5 Computed and experimental stress ranges for piers

	Pier Mild Steel Reinforcement						Post-Tensioning	
	Allowable S_r		Calculated S_r		Experimental S_r		Calculated S_r	
	MPa	(ksi)	MPa	(ksi)	MPa	(ksi)	MPa	(ksi)
RC-100	112	13.2	65	9.4	90	13.1	N/A	N/A
PS-100	112	13.2	65	9.4	N/A	N/A	N/A	N/A
RC-100-TH	112	13.2	65	9.4	73	10.6	N/A	N/A
PU-54-TH	103	15.0	102	14.8	112	16.2	92	13.4
PU-74-TH	126	18.3	112	16.2	**	**	103	15.0

** Faulty gages

5.4 CONSTRUCTIBILITY AND COST ESTIMATION

5.4.1 Constructibility

Constructibility of the full-scale prototype and integrated-design bents was extrapolated from the scale-model specimens by considering the time and effort required to construct the model specimens. The ease of construction was graded on a scale of 1 to 10, where a rating of 1 corresponded with the highest degree of difficulty.

The prototype model reinforced concrete bent (POJ-RC-100) had closely-spaced longitudinal bars and numerous closed stirrups in the overhang, as well as a congested joint region. Congestion in the joint region was due to the maze of overlapping pier and overhang bars that were anchored in the joint region. The separate design of the overhang and pier cross sections meant that bars often had to be forced into place. Hooked longitudinal bars, located at the tip of the overhang, were difficult to place and tie together. Transverse reinforcement in the overhang was closely spaced and required substantial time to install. The difficult placement and overall number of bars that had to be placed and tied in Specimen POJ-RC-100 resulted in a rating of 4.

The prototype model prestressed overhang design (POJ-PS-100) was congested in the overhang and joint regions due to the number of shear friction bars, stirrups, and confinement reinforcement for the post-tensioning anchorages. The most difficult operation was the installation of the closely-spaced confinement reinforcement. After the specimen was cast, the Dywidag bars were stressed and the twelve ducts were grouted. The stressing and grouting operations were time-consuming and required many steps to complete. Because the construction of the reinforcing cage and post-tensioning operation were difficult, the specimen was given a constructibility rating of 3.

Headed mild reinforcement used for the integrated reinforced concrete T-head design (POJ-RC-100-TH) reduced assembly time and simplified placement of longitudinal reinforcement. The joint region was not congested because a reduced number of longitudinal bars were used. The well-spaced closed stirrups in the overhang were easy to install, and headed longitudinal reinforcement reduced congestion at the tip of the overhang. The ease of constructing this resulted in a constructibility rating of 9.

The integrated 54% prestressed specimen with headed mild reinforcement (POJ-PU-54-TH) did not require many reinforcing bars in the overhang and pier region, resulting in a rapid initial assembly of the cage. It took time to place the anchorage reinforcement and thread the three post-tensioning tendons through the cage and tie them into position. The post-tensioning operation went quickly, because only three strands were stressed and grouted. The additional time required to stress the specimen reduced the constructibility ranking to an 8.

The integrated 74% prestressed specimen with headed mild reinforcement (POJ-PU-74-TH) did not require many reinforcing bars, resulting in the quickest initial assembly of the mild reinforcement cage. Installation of the five post-tensioning ducts and tendons required some time, but placement of the anchorage reinforcement and grout ports went efficiently. The post-tensioning operation required more time than for the 54% prestressed specimen, and the additional grouting operations resulted in a ranking of 7.

A summary of constructibility ratings for the different bent types is presented in Table 5.6.

Table 5.6 Constructibility ratings for bent types

	Specimen	Rating
Prototype Designs	POJ-RC-100	4
	POJ-PS-100	3
Integrated Designs	POJ-RC-100-TH	9
	POJ-PU-54-TH	8
	POJ-PU-74-TH	7

5.4.2 Cost Estimation

Estimated costs for different bent types were calculated for full-scale bents. Material quantities for full-scale bents were determined by scaling up quantities for the scale models using the 2.75 factor. Concrete material and placement costs were not included in the cost estimates.

Material costs were estimated using the unit costs listed below. The prototype specimens were included to provide a base-line price comparison for the integrated design specimens. It should be noted that the prototype specimens did not provide factored-load resistance and were unacceptable design options.

The integrated design options utilized interlocking headed reinforcement in the joint corner to provide anchorage for the longitudinal reinforcement. Additional costs for steel plates used for the headed bars were included in a separate unit-cost item. The cost of friction welding the plates onto the ends of bars was included in the plate unit cost.

The unit costs used are as follows:

Mild Reinforcement-	
Closed Ties and Stirrups:	$0.50 / lb.
All Other:	$0.36 / lb.
Headed Reinforcement-	
5.5 in x 4.125 in. x 1.375 in. Plate:	$8.85 ea.
4.125 in. x 2.75 in. x 1.0 in. Plate:	$3.22 ea.
2.75 in. x 2.75 in. x 1.0 in. Plate:	$2.14 ea.
Strand Post-Tensioning Systems-	
Strand:	$1.00 / lb.
Multi-Strand Anchors:	$100 ea.
Plates:	$30 ea.
Bar Post-Tensioning Systems-	
Dywidag Bar:	$1.50 / lb.
Threaded Nuts:	$9.25 ea.
Plates:	$22.85 ea.

The estimated costs for the five full-scale bents are computed in Table 5.7 through 5.11. The bar chart of steel weights, shown in Figure 5.40, indicates the full-scale PU-74-TH bent would require the least steel [2091 kg (4610 lb.)]. The RC-100 bent would require the most steel [3476 kg (7665 lb.)].

Table 5.7 Full-scale POJ-RC-100 materials quantities and price estimates

POJ-RC-100

OVERHANG LONGITUDINAL REINFORCME						Total	Unit	Total
			Area	Length	Volume	Weight	Cost	Cost
		Number	(in^2)	(in.)	(in.^3)	(lbs.)		
	1	14	1.56	219	4793			
	2	14	1.56	214	4673			
	3	2	0.44	196	172			
	4	2	0.44	191	168			
	5	12	0.79	197	1867			
	6	12	0.79	210	1994			
	7	2	0.44	137	120			
	8	8	0.44	161	565			
					13787	3910	$0.36	$1,407.47

PIER LONGITUDINAL REINFORCEMENT							
			Area	Length	Volume	Weight	
	Number	(in^2)	(in.)	(in.^3)	(lbs.)		
1	11	2.25	225.5	5581			
2	2	2.25	225.5	1015			
3	2	2.25	225.5	1015			
4	2	2.25	225.5	1015			
5	2	2.25	225.5	1015			
6	2	2.25	225.5	1015			
7	2	2.25	225.5	1015			
8	2	2.25	225.5	1015			
9	11	2.25	225.5	5581			
				6089	1726	$0.36	$621.53

STIRRUPS							
		Outer	Inner				
	Area	Length	Length	Volume			
	(in^2)	(in.)	(in.)	(in.^3)			
1	0.44	254	181	191			
2	0.44	252	178	189			
3	0.44	249	175	186			
4	0.44	246	172	184			
5	0.44	243	169	182			
6	0.44	241	167	179			
7	0.44	238	164	177			
8	0.44	235	161	174			
9	0.44	232	158	172			
10	0.44	229	156	169			
11	0.44	227	153	167			
12	0.44	224	150	165			
13	0.44	221	147	162			
14	0.44	218	144	160			
15	0.44	216	142	157			
16	0.44	213	139	155			
17	0.44	210	136	152			
18	0.44	207	133	150			
19	0.44	204	131	147			
20	0.44	202	128	145			
21	0.44	199	125	143			
22	0.44	196	122	140			
23	0.44	193	120	138			
24	0.44	191	117	135			
25	0.44	188	114	133			
				4052	1149	$0.50	$574.45

PIER TIES					
		Area	Length	Volume	
	Number	(in^2)	(in.)	(in.^3)	
Outer	19	0.2	291.5	1108	314
Inner	38	0.2	177.38	1348	382
U's	38	0.2	85.25	648	184
				3104	880

SUB	Post Tensioning-		$0.00
TOTAL	T-Heads-		$0.00
	Mild Reinforcement-		$3,043.50
		TOTAL	$3,043.50

Table 5.8 Full-scale POJ-PS-100 material quantities and price estimates

POJ-PS-100

OVERHANG LONGIT. REINFORCMENT								
			Area	Length	Volume	Total Weight	Unit Cost	Total Cost
		Number	(in^2)	(in.)	(in.^3)	(lbs.)		
	1	9	0.31	179	500			
	2	2	0.31	179	111			
	3	9	0.79	179	1275			
	4	9	0.79	197	1400			
	5	2	0.44	210	185			
	6	2	0.44	137	120			
	7	8	0.44	161	565			
					3592	1018	$0.36	$366.64

STIRRUPS								
		Area	Outer Length	Inner Length	Volume			
		(in^2)	(in.)	(in.)	(in.^3)			
	1	0.44	254	181	191			
	2	0.44	252	178	189			
	3	0.44	249	175	186			
	4	0.44	246	172	184			
	5	0.44	243	169	182			
	6	0.44	241	167	179			
	7	0.44	238	164	177			
	8	0.44	235	161	174			
	9	0.44	232	158	172			
	10	0.44	229	156	169			
	11	0.44	227	153	167			
	12	0.44	224	150	165			
	13	0.44	221	147	162			
	14	0.44	218	144	160			
	15	0.44	216	142	157			
	16	0.44	213	139	155			
	17	0.44	210	136	152			
	18	0.44	207	133	150			
	19	0.44	204	131	147			
	20	0.44	202	128	145			
	21	0.44	199	125	143			
	22	0.44	196	122	140			
	23	0.44	193	120	138			
	24	0.44	191	117	135			
	25	0.44	188	114	133			
					4052	1149	$0.50	$574.45

ANCHORAGE								
						Area	Length	Volume	Total Weight	Unit Cost	Total Cost
						(in^2)	(in.)	(in.^3)	(lbs.)		
						0.44	7557	3325	943	$0.50	$471.44
POST TENSIONING BARS											
	1st Row	6	- 1-3/8 Dia. 200 in. Long Dywidag Bars							$0.71	$852.00
	2nd Row	6	- 1-3/8 Dia. 200 in. Long Dywidag Bars							$0.71	$852.00
		24	-1-3/8 in. Dia. Nuts							$9.25	$222.00
		24	- 7 in. x 9 in. x 2 .5 in. Plate							$22.85	$548.40
											$2,474.40

PIER LONGITUDINAL REINFORCEMENT						
			Area	Length	Volume	Total Weight
		Number	(in^2)	(in.)	(in.^3)	(lbs.)
	1	11	2.25	225.5	5581	
	2	2	2.25	225.5	1015	
	3	2	2.25	225.5	1015	
	4	2	2.25	225.5	1015	
	5	2	2.25	225.5	1015	
	6	2	2.25	225.5	1015	
	7	2	2.25	225.5	1015	
	8	2	2.25	225.5	1015	
	9	2	2.25	225.5	1015	
	9	11	2.25	225.5	5581	
					6089	1726

PIER TIES							
			Area	Length	Volume		
		Number	(in^2)	(in.)	(in.^3)		
	Outer	19	0.2	291.5	1108		
	Inner	38	0.2	177.38	1348		
	U's	38	0.2	85.25	648		
					3104	880	$0.50

			$0.36	$621.53
			$0.50	$440.04
SUB TOTAL	Post Tensioning- T-Heads			$2,474.40
				$0.00
	Mild Reinforcement-			$2,034.07
			TOTAL	**$4,508.47**

Table 5.9 Full-scale POJ-RC-100-TH material quantities and price estimates

POJ-RC-100-TH

OVERHANG LONGIT. REINFORCMENT						Total	Unit	Total
			Area	Length	Volume	Weight	Cost	Cost
		Number	(in^2)	(in.)	(in.^3)	(lbs.)		
	1	14	1.56	201	4384			
	2	14	1.56	201	4384			
	3	2	0.44	195	172			
	4	2	0.44	191	168			
	5	2	0.44	187	165			
	6	2	0.44	171	150			
	7	2	0.44	132	116			
	8	8	0.44	161	565			
					9540	2705	$0.36	$973.83

STIRRUPS								
			Outer	Inner				
		Area	Length	Length	Volume			
		(in^2)	(in.)	(in.)	(in.^3)			
	1	0.44	245	179	186			
	2	0.44	230	164	173			
	3	0.44	218	153	163			
	4	0.44	215	149	160			
	5	0.44	211	146	157			
	6	0.44	208	143	154			
	7	0.44	205	139	151			
	8	0.44	201	136	148			
	9	0.44	198	132	145			
	10	0.44	186	121	135			
					1574	446	$0.50	$223.23

PIER LONGITUDINAL REINFORCEMENT						Total	Unit	Total
			Area	Length	Volume	Weight	Cost	Cost
		Number	(in^2)	(in.)	(in.^3)	(lbs.)		
	1	11	2.25	225.5	5581			
	2	2	2.25	225.5	1015			
	3	2	2.25	225.5	1015			
	4	2	2.25	225.5	1015			
	5	2	2.25	225.5	1015			
	6	2	2.25	225.5	1015			
	7	2	2.25	225.5	1015			
	8	2	2.25	225.5	1015			
	9	11	2.25	225.5	5581			
					6089	1726	$0.36	$621.53

PIER TIES								
			Area	Length	Volume			
		Number	(in^2)	(in.)	(in.^3)			
	Outer	19	0.2	291.5	1108	314		
	Inner	38	0.2	177.38	1348	382		
	U's	38	0.2	85.25	648	184		
					3104	880	$0.50	$440.04

T-HEADS				
	Number		Description			
	46	- 5.5 in. x 4.125 in. x 1.375 in. Plate		$8.75	$402.50
	56	- 4.125 in. x 2.75 in. x 1.0 in. Plate		$4.95	$277.20
	16	- 2.75 in. x 2.75 in. x 1.0 in. Plate		$4.40	$70.40
					$750.10

SUB TOTAL	Post Tensioning- T-Heads		$0.00
			$750.10
	Mild Reinforcement-		$2,258.63
		TOTAL	**$3,008.73**

Table 5.10 Full-scale POJ-PU-54-TH material quantities and price estimates

			POJ-PU-54-TH															
OVERHANG LONGITUDINAL REINFORCME						Total	Unit	Total	POST TENSIONING									
			Area	Length	Volume	Weight	Cost	Cost		1st Row	3	- 7-0.6 & 1-0.5 in. Dia. 400 in. Strand				$0.50	$600.00
		Number	(in^2)	(in.)	(in.^3)	(lbs.)					6	-Mult-Strand Anchors				$100	$600.00
	1	12	1.56	201	3758						6	- Plates				$30	$180.00
	2	2	0.44	201	177												$1,380.00
	3	2	0.44	195	172												
	4	2	0.44	191	168				PIER LONGITUDINAL REINFORCEMENT						Total		
	5	2	0.44	187	165							Area	Length	Volume	Weight		
	6	2	0.44	171	150						Number	(in^2)	(in.)	(in.^3)	(lbs.)		
	7	2	0.44	132	116					1	4	2.25	225.5	2030			
	8	8	0.44	161	565					2	2	2.25	225.5	1015			
					4705	1334	$0.36	$480.35		3	2	2.25	225.5	1015			
										4	2	2.25	225.5	1015			
STIRRUPS										5	2	2.25	225.5	1015			
			Outer	Inner						6	2	2.25	225.5	1015			
		Area	Length	Length	Volume					7	7	2.25	225.5	3552			
		(in^2)	(in.)	(in.)	(in.^3)									4059	1151	$0.36	$414.36
	1	0.44	245	179	186												
	2	0.44	230	164	173				PIER TIES			Area	Length	Volume			
	3	0.44	218	153	163						Number	(in^2)	(in.)	(in.^3)			
	4	0.44	215	149	160					Outer	19	0.2	291.5	1108	314		
	5	0.44	211	146	157					Inner	38	0.2	177.38	1348	382		
	6	0.44	208	143	154					U's	38	0.2	85.25	648	184		
	7	0.44	205	139	151									3104	880	$0.50	$440.04
	8	0.44	201	136	148												
	9	0.44	198	132	145				T-HEADS								
	10	0.44	186	121	135						Number		Description				
					1574	446	$0.50	$223.23			28	- 5.5 in. x 4.125 in. x 1.375 in. Plate				$8.75	$245.00
											24	- 4.125 in. x 2.75 in. x 1.0 in. Plate				$4.95	$118.80
			Area	Length	Volume	Weight					18	- 2.75 in. x 2.75 in. x 1.0 in. Plate				$4.40	$79.20
			(in^2)	(in.)	(in.^3)	(lbs.)											$443.00
ANCHORAGES			0.2	294.25	59	17	$0.50	$8.34									
														SUB	Post Tensioning-		$1,380.00
														TOTAL	T-Heads		$443.00
															Mild Reinforcement-		$1,566.32
																TOTAL	**$3,389.32**

Table 5.11 Full-scale POJ-PU-74-TH material quantities price estimates

			POJ-PU-74-TH															
OVERHANG LONGITUDINAL REINFORCME						Total	Unit	Total	POST TENSIONING								Unit	Total
			Area	Length	Volume	Weight	Cost	Cost									Cost	Cost
	Number		(in^2)	(in.)	(in.^3)	(lbs.)				1st Row	3	- 7-0.6 in. Dia. 400 in. Long Strands					$0.43	$516.00
1	8		1.56	201	2505					1st Row	2	- 6-0.6 in. Dia. 400 in. Long Strands					$0.36	$288.00
2	2		0.44	201	177						10	-Mult-Strand Anchorage Hardware					$100	$1,000.00
3	2		0.44	195	172						10	- Plates					$30	$300.00
4	2		0.44	191	168													$2,104.00
5	2		0.44	187	165													
6	2		0.44	171	150				PIER LONGITUDINAL REINFORCEMENT							Total		
7	2		0.44	132	116								Area	Length	Volume	Weight		
8	8		0.44	161	565						Number		(in^2)	(in.)	(in.^3)	(lbs.)		
					3453	979	$0.36	$352.47		1	4		1.56	225.5	1407			
										2	2		1.56	225.5	704			
STIRRUPS										3	2		1.56	225.5	704			
			Outer	Inner						4	2		1.56	225.5	704			
	Area		Length	Length	Volume					5	2		1.56	225.5	704			
	(in^2)		(in.)	(in.)	(in.^3)					6	2		1.56	225.5	704			
1	0.44		245	179	186					7	2		1.56	225.5	704			
2	0.44		230	164	173					8	2		1.56	225.5	704			
3	0.44		225	159	169					9	8		1.56	225.5	2814			
4	0.44		218	153	163										4221	1197	$0.36	$430.93
5	0.44		215	149	160													
6	0.44		211	146	157				PIER TIES				Area	Length	Volume			
7	0.44		208	143	154						Number		(in^2)	(in.)	(in.^3)			
8	0.44		205	139	151					Outer	19		0.2	291.5	1108	314		
9	0.44		201	136	148					Inner	38		0.2	177.38	1348	382		
10	0.44		198	132	145					U's	38		0.2	85.25	648	184		
11	0.44		186	121	135										3104	880	$0.50	$440.04
					1743	494	$0.50	$247.19										
									T-HEADS									
			Area	Length	Volume	Weight					Number			Description				
			(in^2)	(in.)	(in.^3)	(lbs.)					0	- 5.5 in. x 4.125 in. x 1.375 in. Plate					$8.75	$0.00
ANCHORAGES			0.2	294.25	59	17	$0.50	$8.34			44	- 4.125 in. x 2.75 in. x 1.0 in. Plate					$4.95	$217.80
											18	- 2.75 in. x 2.75 in. x 1.0 in. Plate					$4.40	$79.20
																		$297.00
															SUB	Post Tensioning-		$2,104.00
															TOTAL	T-Heads		$297.00
																Mild Reinforcement-		$1,478.97
																	TOTAL	**$3,879.97**

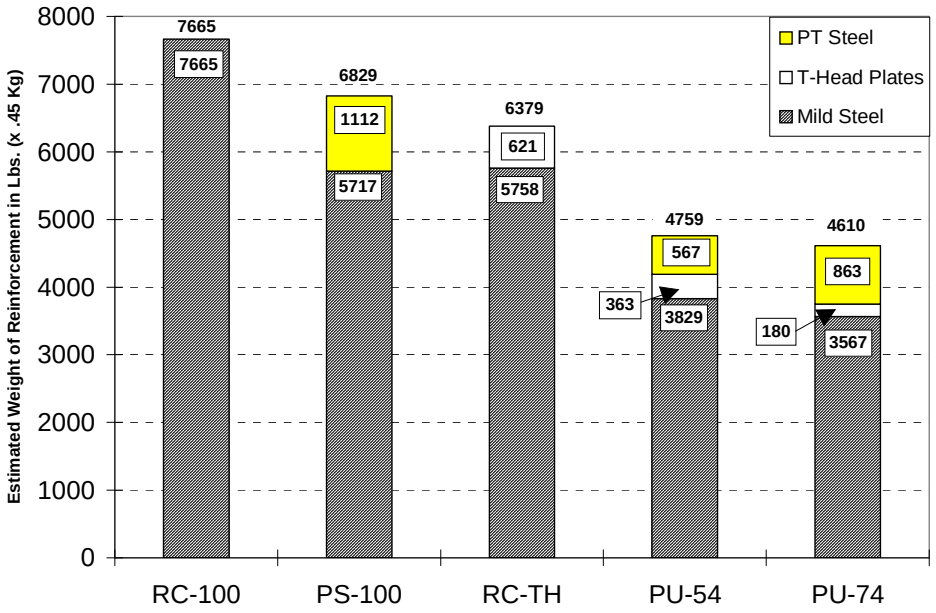

Figure 5.40 Material quantities for full-scale bents

The estimated costs for the full-scale specimens, shown in Figure 5.41, indicate the prototype reinforced concrete bent (RC-100) and reinforced concrete bent with headed bars were almost identical in price ($3043 and $3009, respectively). The premium price of $1/pound ($2.20/Kg) used to estimate the post-tensioning costs, plus the cost of multi-strand anchors, resulted in higher estimated costs for the 54% and 74% prestressed specimens. However, it must be noted that the RC-100 design would not support factored loads, and consideration of the additional costs associated with concrete placement in congested reinforcement cages would likely reduce or offset these cost differences. A fully-prestressed bent utilizing continuous post-tensioning, and designed to satisfy the current AASHTO Standard Specifications, would be significantly more expensive than any of the options listed (from 1.16 to 1.5 times more).

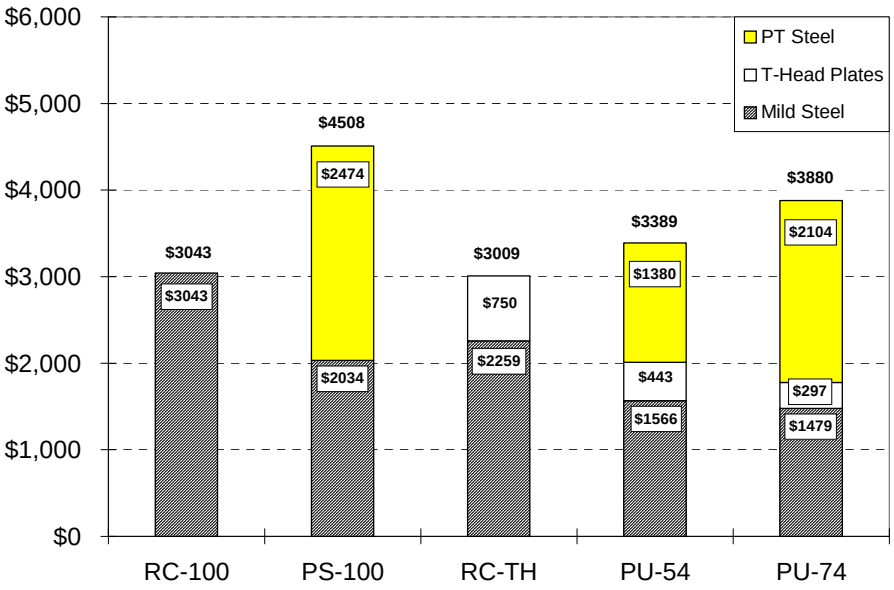

Figure 5.41 Material costs for full-scale bents

In considering serviceability and durability aspects, the 74% prestressed option exhibited only eight small cracks at service loads. The 54% prestressed option had 14 long cracks, and the reinforced concrete specimen with headed bars had 25 cracks. Although all of the integrated-design specimens would contain cracks at service loads, the 74% prestressed specimen limited the number and length of cracks that formed.

5.5 SUMMARY

The analytical and experimental results from the pier-overhang-joint study indicated the prototype model reinforced concrete and prototype model fully-prestressed overhang designs did not provide sufficient anchorage of longitudinal reinforcement in the joint region.

All integrated-design specimens provided sufficient strength to resist factored loads. Anchorage of reinforcement in the joint, and ultimately, integrity of the joint was assured by interlocking the headed mild reinforcement in the joint corner and by reducing the joint principal tensile stresses by providing continuous post-tensioning through the bent. Sufficient longitudinal and transverse reinforcement was provided in zones of high tensile stresses to resist factored loads.

Specimen POJ-RC-100-TH failed in the joint after the longitudinal reinforcement yielded and load on the specimen was above the predicted capacity. A transverse headed bar in the joint corner may have provided lateral joint confinement, but is not recommended because it would also cause unwanted congestion in the joint corner.

Spalling of the underside of the overhang that occurred for all the integrated design specimens suggested a larger amount of reinforcement should be provided in the compression zone. It was recognized that the overhang compression node was part of the critical force path that supported the outer superstructure reaction. Additional compressive reinforcement would provide added ductility to the specimens.

Service-load performance of the integrated design specimens was evaluated by measuring service-load crack widths. The partially-prestressed designs (POJ-PU-54-TH and POJ-PU-74-TH) provided adequate crack control in the different regions of the specimen, and reduced the number of cracks that formed. The integrated reinforced concrete design (POJ-RC-100-TH) had unacceptable crack-widths in the joint region at service load. It is recommended that a quantity of mild reinforcement be added to the joint region, based on detailing for a “bottle-shaped” compression field, shown in Figure 5.42 [8]. Additional detailing steel would provide additional strength and improve serviceability of the joint.

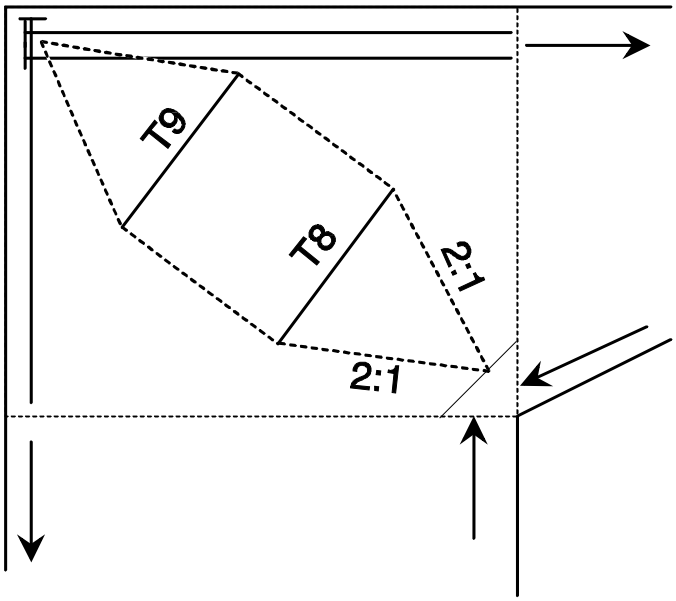

Figure 5.42 Bottle-shaped compression field for joint corner detail

Constructibility and construction costs of specimens indicated all integrated design models were economically feasible and practical design options. The prestressed options (POJ-PU-54-TH and POJ-PU-74-TH) had fewer visible cracks than the reinforced concrete option (POJ-RC-100-TH).

CHAPTER 6

PROPOSED DESIGN RECOMMENDATIONS

6.1 INTRODUCTION

Following review of the 1992 Proposed AASHTO Load and Resistance Factor Design (LRFD) Specifications [19] and the 1992 AASHTO Standard Specifications for Highway Bridges [1], it was determined that the proposed LRFD specifications provide a good initial framework for design recommendations for structural concrete. The LRFD Specifications unify the provisions and design equations for reinforced and prestressed concrete members into a single-set of specifications, and utilize a crack-width formula similar to that proposed in this study. In addition, the proposed LRFD specifications adopt the strut-and-tie model to proportion reinforcement near supports, concentrated loads, and for deep members. Rather than reproduce the complete specifications and commentary here, only sections for which modifications are proposed will be addressed. Proposed modifications are denoted by indented text and by sub-section numbers corresponding with Section 5, Concrete Structures, of the proposed LRFD specifications.

6.2 RECOMMENDED MODIFICATIONS TO PROPOSED AASHTO LRFD BRIDGE SPECIFICATIONS

Recommended modifications to Section 5 of the Proposed AASHTO LRFD Specifications are presented in this section. The modified subsections are presented in a format similar to that used in the April 16, 1992 draft of the specifications. Subsections related to research that is underway in other studies at The University of Texas at Austin will be noted. Recommendations for these subsections will be presented based on information that is available at this time and may be modified as more information becomes available.

5.6 *DESIGN CONSIDERATIONS*

.
.
.

5.6.3 *STRUT-AND-TIE MODEL*

5.6.3.1 *GENERAL*

Strut-and-tie models may be used to determine internal force effects near supports and points of application of concentrated loads <u>where nonlinear distributions of strain are expected</u> *at strength and extreme event limit states.*

The strut-and-tie model should be considered for the design of deep footings and pile caps or other situations in which the distance between the centers of applied load and the supporting reactions is less than about twice the member thickness.

5.6.3.2 STRUCTURAL MODELING

.
.
.

5.6.3.4 PROPORTIONING OF TENSION TIES

5.6.3.4.1 Strength of Tie

Tension tie reinforcement shall be anchored to the nodal zones by specified embedment lengths, hooks, or mechanical anchorages. The tension force shall be developed at the interface of the nodal zone.

The nominal resistance of a tension tie shall be taken as:

$$P_n = A_{st} f_y + A_{ps} f_{pu} \qquad (5.6.3.4.1\text{-}1)$$

where:

A_{st} = *total area of longitudinal mild steel reinforcement in the tie (IN^2)*

A_{ps} = *area of prestressing steel (IN^2)*

f_y = *yield strength of mild steel reinforcement (KSI*)

f_{pu} = *specified tensile strength of prestressed reinforcement (KSI).*

For transverse reinforcement:

$$P_n = A_{vs} f_y \qquad (5.6.3.4.1\text{-}2)$$

where:

P_n = *STM tie force (KIP)*

A_{vs} = *Total area of required shear reinforcement (IN^2)*

f_y = Nominal yield stress of shear reinforcement (KSI)

The transverse reinforcement A_{vs} should be distributed over a distance d in the region of the transverse tension tie.

C5.6.3.4.1

Equation 5.6.3.4.1-1 is intended to represent the strength of the combined mild steel/prestressed longitudinal steel tension tie. Studies have shown that the equation is a good approximation of the strength for a tension tie in deep beams.

The quantity of transverse reinforcement in beams can be computed using Equation 5.6.3.4.1-2.

Note that the transverse tension tie requirement is not reduced by a concrete contribution, even though a $1\sqrt{f_c'}\, b_w d$ contribution was used in the design of transverse tension ties in the intergrated design specimens. Excluding the concrete contribution will increase steel requirements only slightly, and as a result, provide additional safety with respect to shear strength of members.

5.7 *DESIGN FOR FLEXURAL AND AXIAL FORCE EFFECTS*

.
.
.

5.7.3.4 *CONTROL OF CRACKING BY DISTRIBUTION OF REINFORCEMENT*

The provisions specified herein shall apply to the reinforcement of all concrete components, except that of deck slabs designed in accordance with Article 9.7.2, in which tension in the cross-section exceeds 80% of the modulus of rupture, specified in Article 5.4.2.6, at applicable service limit state load combinations specificed in Table 3.4.1-1.

The following provisions shall be used for the distribution of tension reinforcement to control flexural cracking in members. For structures subject to very aggressive exposure, special investigations and precautions not specified herein shall be applied.

When the specified yield strength, f_y, for tension reinforcement exceeds 40.0 KSI, components shall be so proportioned that the tensile stress in the reinforcement at service loads, f_{sa} (KSI), does not exceed:

$$f_{sa} = \frac{C_{rk}}{\left(d_c A\right)^{1/3}} \qquad (5.7.3.4\text{-}1)$$

where

d = Distance from extreme compression fiber to centroid of primary tension reinforcement at the location of the tension tie (IN).

f_{sa} = Steel tensile stress at a distance d_e from the extreme tensile fiber = ε_{d_e} (29,000 KSI)

ε_{d_e} = Strain a distance d_e from the extreme tensile fiber based on a linear strain profile

C_{rk} = Limiting crack-width factor determined from exposure criteria. Values for C_{rk} from Table 5.7.3.4-1.shall be based on clear cover requirements specified in Table 5.12.3-1

Table 5.7.3.4-1 Values for C_{rk} for unprotected reinforcing steel (K/IN)

Exposure Conditions	**Cover (IN)**	**C_{rk} (K/IN)**
Moderate	≤ 2 IN	0.170
Moderate	> 2 IN	0.170 + 0.02(Cover - 2.0)
Moderate to Severe	≤ 2 IN	0.130
Moderate to Severe	> 2 IN	0.130 + 0.02(Cover - 2.0)

* For very severe exposure conditions, additional protection shall be furnished to provide additional corrosion resistance, in addition to satisfying Equation 5.7.3.4-1.

d_c = Distance from the extreme tension fiber to the centroid of the closest layer of primary tension reinforcement (IN)

A = Area of tension block (2 x $h - d_e$ x b_w) divided by the number of mild reinforcing bars, bonded strands, and/or grouted tendons located within the tension block [IN^2/# BARS]

d'' = Distance from extreme compression fiber to centroid of tensile reinforcement (IN)

$$d_e = \frac{[A_{ps}\ f_{ps}\ d_p + A_s\ f_y\ d_s]}{[A_{ps}\ f_{ps} + A_{s\ f_y}]} \qquad (5.7.3.4\text{-}2)$$

where:

d_p = Distance from extreme compression fiber to centroid of layer of prestressed reinforcement in the tension zone

A_{ps} = Area of prestressed reinforcement

d_s = Distance from extreme compression fiber to centroid of longitudinal mild reinforcement

A_s = Area of mild reinforcement.

The stress, f_{sa}, shall be computed using a cracked-section analysis. Bonded prestressing steel may be included in the calculation of f_{sa}. Prestressing stress should be reduced to account for long-term losses as specified in Section 5.9.5. The steel stress, f_{sa}, shall be determined at a distance d_e from the extreme compressionshall not exceed the limiting stress computed using Equation 5.7.3.4-1

C5.7.3.4.

In applying Equation 5.7.3.4-1ual cover, d_c, shall be used. Thicker or additional cover, exceeding 2.0 IN, provides additional corrosion protection. Values for C_{rk} provide a gradual transition in cover requirements from severe to moderate exposure conditions without a penalty for using more concrete cover.

Figure C5.7.3.4-1es the variables used for Equation 5.7.3.4-1

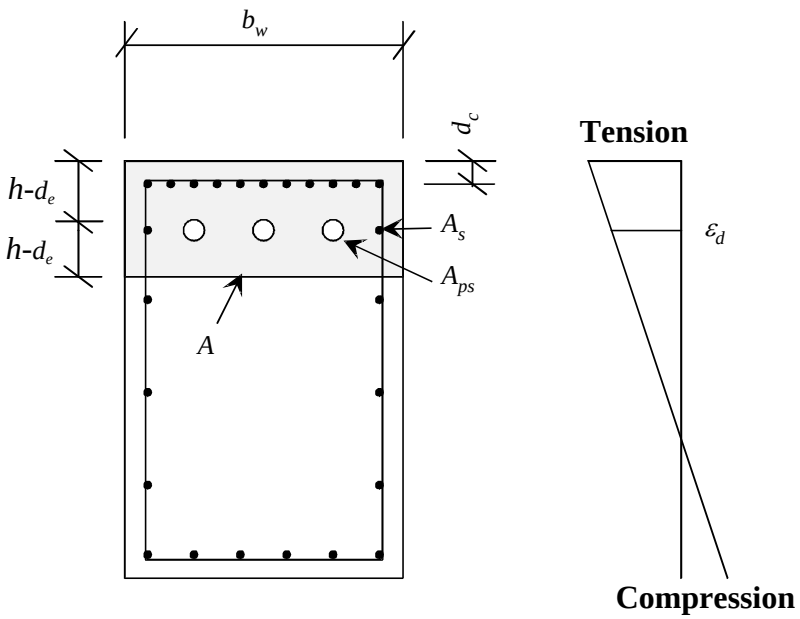

Figure C5.7.3.4-1 Identification of crack-width variables

6.3 SUMMARY

The proposed changes to the AASHTO LRFD Bridge Specifications incorporate many of the design criteria that were used in development of specimens tested in the cantilever-bent study. Shear friction provisions and design equations for deep beams, brackets, and corbels were retained but should be phased out as the strut-and-tie method becomes the design standard. Strut-and-tie models used in the study provided a thorough understanding of the flow of forces in disturbed regions, and resulted in concise requirements for designing reinforcement and checking concrete compressive stresses. Tests also demonstrated good behavior for specimens designed using strut-and-tie models.

A design example illustrating application of the proposed design provisions is included in Appendix B.

CHAPTER 7

SUMMARY AND CONCLUSIONS

7.1 SUMMARY

Large cantilever-bent specimens were designed and tested to evaluate AASHTO Standard Specifications, which provide separate treatment of design of reinforced and prestressed concrete elements. A specification is proposed here for an integrated design method for structural concrete. Two specimens that represent a prototype reinforced concrete bent and a prototype bent with a fully-prestressed overhang, and three integrated design specimens were designed and tested.

The model prototype reinforced concrete and fully-prestressed-overhang designs were structurally deficient. The reinforced concrete bent failed under applied loads equivalent to 0.76 times factored load, and the fully-prestressed overhang specimen failed under applied loads equivalent to 0.58 times factored load. A strength model that incorporated a uniform-bond stress model to compute bar anchorage in the joint was used to estimate the maximum applied load on the overhang. Computed capacities were within ± 10% of measured capacities.

The integrated-design specimens consisted of a reinforced concrete specimen, a 54% prestressed specimen, and a 74% prestressed specimen. The three-integrated design specimens incorporated headed longitudinal reinforcement, and the partially-prestressed specimens contained tendons that were continuous through the overhang, joint, and pier. All three integrated-design specimens had capacities exceeding factored design loads. The reinforced concrete and 54% prestressed specimens were tested to failure (1.44 and 1.41 times factored loads, respectively), and measured capacities were 14% greater than predicted capacities, indicating the design and analysis procedures provided conservative designs. Specimen POJ-PU-74-TH (the 74% prestressed specimen) was proof-tested to an applied load equivalent to 1.41 times factored loads.

The three integrated design specimens had superior strength because a strut-and-tie model was used to plan the flow of internal forces through the bent, and aid in detailing reinforcement. The strut-and-tie model indicated that the primary longitudinal reinforcement in the overhang and pier needed to be fully anchored in the joint corner. Headed reinforcement was used to fully anchor the longitudinal reinforcement, and continuous post-tensioning was placed through the joint.

Serviceability of the three integrated-design specimens was evaluated using maximum measured crack widths and deflections. Maximum measured crack widths were within the historically-accepted range of ± 50% of crack widths predicted using the proposed crack-width equation. It was clear from tests performed on integrated-design specimens that using a larger percentage of post-tensioning reduced the number of cracks that formed at service loads. The 74% prestressed specimen had excellent crack control and overall serviceability.

In order to develop design specifications for structural concrete, subtle changes to the AASHTO LRFD Specifications were recommended. The bulk of the LRFD specifications were in line with the procedures used in design of the integrated-design specimens. As use of the integrated-design method and strut-and-tie analysis procedure becomes more prevalent, some existing design provisions for corbels, deep beams, and shear friction reinforcement, as well as the AASHTO Standard Specifications, may be phased out.

In the experimental program, all integrated-design specimens were designed using resistance factors of 0.9 and 0.85 for flexure and shear, respectively. However, the AASHTO LRFD Specifications use resistance factors of 1.0 for flexure in prestressed concrete, 0.9 for flexure in reinforced concrete, and 0.9 for shear and torsion in reinforced or prestressed concrete. This research does not directly address the issue of resistance factors, but some consideration should be given to these factors. Results from three integrated-designs specimens support the conclusion that designs ranging from 72% prestressed to fully-reinforced concrete can be designed with similar ultimate capacities, and a resistance factor for "flexure and tension of structural concrete" should be proposed to replace the values for reinforced concrete and prestressed concrete. The shear resistance factor given in the AASHTO LRFD Specifications is 0.9 which is equal to the resistance factor for flexure in reinforced concrete. Clearly design conservatism is reduced on two fronts if a concrete contribution is included in the shear resistance calculation and an increased value for the resistance factor for shear is used. Maintaining the resistance factor for shear at the currently recognized value of 0.85 is more appropriate if a concrete contribution is included in the shear resistance equation. It is suggested to use a resistance factor of 0.9 for flexure and 0.85 for shear.

Based on the tests reported here, there is concern that the quantity of transverse reinforcement in the bents designed using the integrated design method was marginal because a concrete contribution for shear was included in the designs. However, it should be noted that the compression failure in the overhang preceded the shear failure of Specimen POJ-PU-54-TH and the overhang bents reported in Ref. 42. If compression reinforcement above the minimum required for creep and shrinkage had been used in the overhang of Specimen POJ-PU-54-TH, the bent capacity would have been higher. If the concrete contribution for shear is not included, it will result in slightly more congested reinforcing cages.

7.2 CONCLUSIONS AND RECOMMENDATIONS

1) Clearly, behavior of specimens designed using the integrated design procedure was superior to that of specimens designed using the AASHTO Standard Specifications. Integrated-design specimens attained factored design loads for which they were designed, while prototype model reinforced concrete and fully-prestressed overhang designs resisted only 76 and 58% of factored design loads, respectively.

2) Serviceability of the integrated-design specimens was excellent when larger quantities of prestressed reinforcement was used. The 74% prestressed bent (POJ-PU-74-TH) had excellent crack control for all regions of the bent, and limited service-level deflections. The 54% prestressed bent (POJ-PU-54-TH) had good crack control, and deflections that were slightly greater than the limiting service-level deflections. The reinforced concrete bent with T-headed reinforcement (POJ-RC-100-TH) had some large cracks in the joint region, and service-level deflections were larger than the accepted limit. Modifications were proposed to improve serviceability of these bents.

3) Costs of integrated-design bents were estimated to be equal to the structurally deficient reinforced concrete prototype bent. Congestion of reinforcement was greatly reduced through the use of partially-prestressed designs and headed mild reinforcement. Estimated cost of the deficient prototype fully-prestressed overhang design was 2.1 times more than the deficient prototype reinforced concrete design.

4) Costs, based on current construction cost estimates, increased with additional post-tensioning, however reduced reinforcement congestion should reduce concrete placement costs. Additionally, the premium associated with construction of prestressed concrete structures should decrease as more construction companies become adept at installing and stressing post-tensioned reinforcement. The superior serviceability and strength of Specimen POJ-PU-75-TH is well worth the small increase in cost for additional post-tensioned reinforcement.

5) Headed reinforcement reduced congestion and facilitated anchorage of reinforcement in the joint region. Anchor heads provide ideal nodes for anchoring tension ties and compression struts as visualized in strut-and-tie models.

6) Strut-and-tie modeling was the key analysis tool used in this study. It helped identify the flow of forces through the bent, and identified critical anchorage details in the joint region. Inclusion of the strut-and-tie design method in the AASHTO LRFD Specifications is a clearly-needed improvement over the AASHTO Standard Specifications.

7) The proposed crack-width equation provided conservative estimates of crack widths, within the historically accepted range. The equation proved to be a valuable tool when it was used to evaluate serviceability of various designs and to compute the required number of reinforcing bars to control crack widths. Integrated design specimens had excellent crack control when post-tensioning was located in regions of high tensile stresses. Given the uncertainty associated with crack-width measurements in general, it is understood that limits applied to crack widths should be conservative to prevent unsightly cracks from developing and to provide corrosion protection. An amendment to the AASHTO LRFD Specifications is provided.

8) Anchorage details used in the joint of prototype model bents were inadequate and resulted in premature failure of the bent. A uniform bond-stress model was demonstrated to adequately represent at failure, the anchorage capacity of bars anchored in the joint region. The uniform bond-stress model simply assumed that each bar could resist a force equal to the ratio of anchorage length to development length times the nominal capacity of the bar. In practice, equations from Orangun [29] or the ACI Committee 408 Summary Report [30] should be used to compute bar development lengths. The model utilized to estimate some specimen capacities assumed that all reinforcement reached its capacity at maximum loads. Estimated capacities of the prototype model reinforced concrete and prestressed concrete bents were within ±10% of measured bent capacities.

9) Linear elastic finite element analyses proved invaluable for identification of peak tensile stress regions and determination of first-cracking load.

APPENDIX A
MEASURED CRACK WIDTHS

Table A.1 POJ-RC-100 maximum crack widths in mm for north face of overhang

Load Step	North-Overhang	Ri kN	Ro kN	Moment kN-M	1 mm		2 mm		3 mm		4 mm		5 mm		6 mm		7 mm	
11	First Crack	161	161	196.3	0.04	A	0.03	A										
13		190	190	232.1	0.04	A	0.04	A										
20	Dead Load	293	293	357.4	0.05	A	0.05	A	0.05	A'	0.03	A	0.01	A	0.03	A		
27	DL+1/2 LL	318	344	411.7	0.08	A	0.06	A'	0.05	A'	0.04	A	0.04	A	0.04	A		
34	Service	343	399	468.9	0.08	A	0.08	A	0.08	A	0.05	A	0.05	A'	0.05	A	0.03	A
35	Dead Load	293	293	357.4	0.06	C	0.06	B	0.05	B	0.06	A	0.05	A'	0.06	A	0.05	A
42	DL+1/2 LL	318	344	411.7	0.08	C	0.08	B	0.06	B	0.05	A	0.05	A'	0.03	A	0.04	A
49	Service	343	399	468.9	0.08	C	0.10	B	0.06	B	0.08	A	0.08	A'	0.05	A	0.05	A
60	DL+2 LL	409	496	577.9														

Table A.2 POJ-RC-100 maximum crack widths in (in.) for north face of overhang

Load Step	North-Overhang	Ri (kips)	Ro (kips)	Moment (k-in.)	1 (in.)		2 (in.)		3 (in.)		4 (in.)		5 (in.)		6 (in.)		7 (in.)	
11	First Crack	36.2	36.2	1738	0.0015	A	0.0010	A										
13		42.8	42.8	2054	0.0015	A	0.0015	A										
20	Dead Load	65.9	65.9	3163	0.0020	A	0.0020	A	0.0020	A'	0.0010	A	0.0005	A	0.0010	A		
27	DL+1/2 LL	71.4	77.4	3643	0.0030	A	0.0025	A'	0.0020	A'	0.0015	A	0.0015	A	0.0015	A		
34	Service	77	89.6	4150	0.0030	A	0.0030	A	0.0030	A	0.0020	A	0.0020	A'	0.0020	A	0.0010	A
35	Dead Load	65.9	65.9	3163	0.0025	C	0.0025	B	0.0020	B	0.0025	A	0.0020	A'	0.0025	A	0.0020	A
42	DL+1/2 LL	71.4	77.4	3643	0.0030	C	0.0030	B	0.0025	B	0.0020	A	0.0020	A'	0.0010	A	0.0015	A
49	Service	77	89.6	4150	0.0030	C	0.0040	B	0.0025	B	0.0030	A	0.0030	A'	0.0020	A	0.0020	A
60	DL+2 LL	92	111	5114														

Table A.3 POJ-RC-100 maximum crack widths in mm for south face of overhang

Load Step	South Overhang	Ri kN	Ro kN	Moment kN-M	1 mm		2 mm		3 mm		4 mm		5 mm		6 mm		7 mm		8 mm	
11	First Crack	161	161	196.3	0.06	A	0.04	A												
13		190	190	232.1	0.05	B	0.03	A												
20	Dead Load	293	293	357.4	0.05	A	0.05	A	0.04	A	0.03	A	0.01	A						
27	DL+1/2 LL	318	344	411.7	0.06	B	0.06	A'	0.09	A	0.05	A	0.03	A'	0.06	A				
34	Service	343	399	468.9	0.10	C	0.08	B	0.08	B	0.05	A	0.05	A	0.08	A	0.05	A	0.01	A
35	Dead Load	293	293	357.4	0.05	B	0.08	B	0.09	C	0.06	A	0.04	A	0.06	A	0.04	A	0.01	A
42	DL+1/2 LL	318	344	411.7	0.09	C	0.08	C	0.09	C	0.05	A	0.06	A	0.08	A	0.05	A	0.03	B
49	Service	343	399	468.9	0.10	C	0.09	C	0.10	C	0.08	A	0.05	A	0.08	A	0.05	A	0.03	B
60	DL+2 LL	409	496	577.9																

Table A.4 POJ-RC-100 maximum crack widths in (in.) for south face of overhang

Load Step	South Overhang	Ri (kips)	Ro (kips)	Moment (k-in.)	1 (in.)		2 (in.)		3 (in.)		4 (in.)		5 (in.)		6 (in.)		7 (in.)		8 (in.)	
11	First Crack	36.2	36.2	1738	0.0025	A	0.0015	A												
13		42.8	42.8	2054	0.0020	B	0.0010	A												
20	Dead Load	65.9	65.9	3163	0.0020	A	0.0020	A	0.0015	A	0.0010	A	0.0005	A						
27	DL+1/2 LL	71.4	77.4	3643	0.0025	B	0.0025	A'	0.0035	A	0.0020	A	0.0010	A'	0.0025	A				
34	Service	77	89.6	4150	0.0040	C	0.0030	B	0.0030	B	0.0020	A	0.0020	A	0.0030	A	0.0020	A	0.0005	A
35	Dead Load	65.9	65.9	3163	0.0020	B	0.0030	B	0.0035	C	0.0025	A	0.0015	A	0.0025	A	0.0015	A	0.0005	A
42	DL+1/2 LL	71.4	77.4	3643	0.0035	C	0.0030	C	0.0035	C	0.0020	A	0.0025	A	0.0030	A	0.0020	A	0.0010	B
49	Service	77	89.6	4150	0.0040	C	0.0035	C	0.0040	C	0.0030	A	0.0020	A	0.0030	A	0.0020	A	0.0010	B
60	DL+2 LL	92	111	5114																

Table A.5 POJ-RC-100 maximum crack widths in mm for north face of joint

Load Step	North Joint	Ri KN	Ro KN	Moment KN-M	1 mm		2 mm		3 mm		4 mm		5 mm		6 mm		7 mm		8 mm		9 mm		10 mm		11 mm	
13	First Crack	190	190	232.1	0.01	A																				
20	Dead Load	293	293	357.4	0.05	A	0.05	A	0.04	A'	0.04	A'	0.13	A'	0.08	A'										
27	DL+1/2 LL	318	344	411.7	0.09	A	0.09	A	0.08	A	0.08	B	0.13	A'	0.17	A										
34	Service	343	399	468.9	0.10	A	0.10	A'	0.09	A	0.13	B	0.15	A'	0.18	A	0.10	B	0.14	A'	0.13	A'	0.36	A'	0.18	C
35	Dead Load	293	293	357.4	0.10	A	0.08	A	0.13	A'	0.08	B	0.15	A'	0.17	B	0.10	A'	0.14	B	0.10	A'	0.51	A'	0.15	B
42	DL+1/2 LL	318	344	411.7	0.10	A	0.08	A	0.11	A'	0.09	B	0.18	B	0.18	B	0.10	B	0.17	B	0.11	A'	0.39	A'	0.20	B
49	Service	343	399	468.9	0.13	A	0.08	A	0.09	A'	0.10	B	0.18	B	0.20	B	0.10	B	0.17	C	0.10	A'	0.43	A'	0.19	B
60	DL + 2 LL	409	496	577.9																						

Table A.6 POJ-RC-100 maximum crack widths in (in.) for north face of joint

Load Step	North Joint	Ri (Kips)	Ro (Kips)	Moment (K-in.)	1 (in.)		2 (in.)		3 (in.)		4 (in.)		5 (in.)		6 (in.)		7 (in.)		8 (in.)		9 (in.)		10 (in.)		11 (in.)	
13	First Crack	42.8	42.8	2054	0.0005	A																				
20	Dead Load	65.9	65.9	3163	0.0020	A	0.0020	A	0.0015	A'	0.0015	A'	0.0050	A'	0.0030	A'										
27	DL+1/2 LL	71.4	77.4	3643	0.0035	A	0.0035	A	0.0030	A	0.0030	B	0.0050	A'	0.0065	A										
34	Service	77	89.6	4150	0.0040	A	0.0040	A'	0.0035	A	0.0050	B	0.0060	A'	0.0070	A	0.0040	B	0.0055	A'	0.0050	A'	0.0140	A'	0.0070	C
35	Dead Load	65.9	65.9	3163	0.0040	A	0.0030	A	0.0050	A'	0.0030	B	0.0060	A'	0.0065	B	0.0040	A'	0.0055	B	0.0040	A'	0.0200	A'	0.0060	B
42	DL+1/2 LL	71.4	77.4	3643	0.0040	A	0.0030	A	0.0045	A'	0.0035	B	0.0070	B	0.0070	B	0.0040	B	0.0065	B	0.0045	A'	0.0155	A'	0.0080	B
49	Service	77	89.6	4150	0.0050	A	0.0030	A	0.0035	A'	0.0040	B	0.0070	B	0.0080	B	0.0040	B	0.0065	C	0.0040	A'	0.0170	A'	0.0075	B
60	DL + 2 LL	92	111	5114																						

Table A.7 POJ-RC-100 maximum crack widths in mm for south face of joint

Load Step	South Joint	Ri kN	Ro kN	Moment kN-M	1 mm		2 mm		3 mm		4 mm		5 mm		6 mm		7 mm		8 mm		9 mm		10 mm	
13	First Crack	190	190	232.1	0.04	A	0.01	A																
20	Dead Load	293	293	357.4	0.09	A	0.13	C	0.08	A	0.15	A'	0.04	A	0.08	A								
27	DL+1/2 LL	318	344	411.7	0.10	A	0.15	C	0.09	A	0.20	B	0.05	A	0.13	A	0.20	D	0.33	A'	0.05	A	0.08	A'
34	Service	343	399	468.9	0.10	A	0.15	C	0.13	A	0.23	B	0.06	A	0.13	A	0.28	D	0.43	A'	0.05	A	0.06	A
35	Dead Load	293	293	357.4	0.09	A	0.13	C	0.10	A	0.28	B	0.08	A	0.11	A	0.30	E	0.38	A'	0.05	A	0.05	A'
42	DL+1/2 LL	318	344	411.7	0.10	A	0.17	C	0.13	A	0.25	B	0.09	A	0.18	A	0.30	E	0.51	B	0.08	A	0.05	A'
49	Service	343	399	468.9	0.10	A	0.13	C	0.13	A	0.25	B	0.10	A	0.13	A	0.23	E	0.41	B	0.05	A	0.05	A'
60	DL+2 LL	409	496	577.9																				

Table A.8 POJ-RC-100 maximum crack widths in (in.) for south face of joint

Load Step	South Joint	Ri (kips)	Ro (kips)	Moment (k-in.)	1 (in.)		2 (in.)		3 (in.)		4 (in.)		5 (in.)		6 (in.)		7 (in.)		8 (in.)		9 (in.)		10 (in.)	
13	First Crack	42.8	42.8	2054	0.0015	A	0.0005	A																
20	Dead Load	65.9	65.9	3163	0.0035	A	0.0050	C	0.0030	A	0.0060	A'	0.0015	A	0.0030	A								
27	DL+1/2 LL	71.4	77.4	3643	0.0040	A	0.0060	C	0.0035	A	0.0080	B	0.0020	A	0.0050	A	0.0080	D	0.0130	A'	0.0020	A	0.0030	A'
34	Service	77	89.6	4150	0.0040	A	0.0060	C	0.0050	A	0.0090	B	0.0025	A	0.0050	A	0.0110	D	0.0170	A'	0.0020	A	0.0025	A
35	Dead Load	65.9	65.9	3163	0.0035	A	0.0050	C	0.0040	A	0.0110	B	0.0030	A	0.0045	A	0.0120	E	0.0150	A'	0.0020	A	0.0020	A'
42	DL+1/2 LL	71.4	77.4	3643	0.0040	A	0.0065	C	0.0050	A	0.0100	B	0.0035	A	0.0070	A	0.0120	E	0.0200	B	0.0030	A	0.0020	A'
49	Service	77	89.6	4150	0.0040	A	0.0050	C	0.0050	A	0.0100	B	0.0040	A	0.0050	A	0.0090	E	0.0160	B	0.0020	A	0.0020	A'
60	DL+2 LL	92	111	5114																				

Table A.9 POJ-RC-100 maximum crack widths in mm for north face of pier

Load Step	North-Pier	Ri kN	Ro kN	Moment kN-M	1 mm		2 mm		3 mm		4 mm		5 mm	
13	First Crack	190	190	232.1	0.06	A	0.04	A'						
20	DL	293	293	580.8	0.08	A'	0.08	A	0.10	A	0.08	B	0.05	A
27	DL+1/2 LL	318	344	663.9	0.09	A'	0.09	B	0.10	A	0.05	B	0.10	A
34	DL+LL	343	399	751.3	0.18	A'	0.10	A	0.15	A	0.10	B	0.13	A'
35	Dead Load	293	293	580.8	0.10	A'	0.08	B	0.13	A	0.10	A	0.10	A
42	DL+1/2 LL	318	344	663.9	0.08	B	0.09	B	0.09	A	0.06	A	0.13	A
49	DL+LL	343	399	751.3	0.13	B	0.10	B	0.10	A	0.08	A	0.10	A
60	DL+2 LL	409	496	922.7										

Table A.10 POJ-RC-100 maximum crack widths in (in.) for north face of pier

Load Step	North-Pier	Ri (kips)	Ro (kips)	Moment (k-in.)	1 (in.)		2 (in.)		3 (in.)		4 (in.)		5 (in.)	
13	First Crack	42.8	42.8	2054	0.0025	A	0.0015	A'						
20	DL	65.9	65.9	5140	0.0030	A'	0.0030	A	0.0040	A	0.0030	B	0.0020	A
27	DL+1/2 LL	71.4	77.4	5875	0.0035	A'	0.0035	B	0.0040	A	0.0020	B	0.0040	A
34	DL+LL	77	89.6	6649	0.0070	A'	0.0040	A	0.0060	A	0.0040	B	0.0050	A'
35	Dead Load	65.9	65.9	5140	0.0040	A'	0.0030	B	0.0050	A	0.0040	A	0.0040	A
42	DL+1/2 LL	71.4	77.4	5875	0.0030	B	0.0035	B	0.0035	A	0.0025	A	0.0050	A
49	DL+LL	77	89.6	6649	0.0050	B	0.0040	B	0.0040	A	0.0030	A	0.0040	A
60	DL+2 LL	92	111	8165										

Table A.11 POJ-RC-100 maximum crack widths in mm for south face of pier

Load Step	South Pier	Ri kN	Ro kN	Moment kN-M	1 mm		2 mm		3 mm		4 mm		5 mm		6 mm	
13	First Crack	190	190	232.1	0.06	A	0.04	A								
20	Dead Load	293	293	580.8	0.10	A'	0.08	A	0.01	A	0.06	A	0.08	A	0.06	A
27	DL+1/2 LL	318	344	663.9	0.11	A	0.11	A	0.13	A	0.09	A	0.10	A	0.09	A
34	Service	343	399	751.3	0.10	A	0.13	A	0.13	A	0.13	B	0.13	A	0.10	A
35	Dead Load	293	293	580.8	0.09	B	0.10	A	0.08	A	0.10	A	0.10	A	0.10	A
42	DL+1/2 LL	318	344	663.9	0.11	B	0.13	A	0.14	A	0.10	A	0.13	A	0.10	A
49	Service	343	399	751.3	0.10	B	0.13	A	0.13	A	0.10	A	0.13	A	0.10	A
60	DL+2 LL	409	496	922.7												

Table A.12 POJ-RC-100 maximum crack widths in (in.) for south face of pier

Load Step	South Pier	Ri (kips)	Ro (kips)	Moment (k-in.)	1 (in.)		2 (in.)		3 (in.)		4 (in.)		5 (in.)		6 (in.)	
13	First Crack	42.8	42.8	2054	0.0025	A	0.0015	A								
20	Dead Load	65.9	65.9	5140	0.0040	A'	0.0030	A	0.0005	A	0.0025	A	0.0030	A	0.0025	A
27	DL+1/2 LL	71.4	77.4	5875	0.0045	A	0.0045	A	0.0050	A	0.0035	A	0.0040	A	0.0035	A
34	Service	77	89.6	6649	0.0040	A	0.0050	A	0.0050	A	0.0050	B	0.0050	A	0.0040	A
35	Dead Load	65.9	65.9	5140	0.0035	B	0.0040	A	0.0030	A	0.0040	A	0.0040	A	0.0040	A
42	DL+1/2 LL	71.4	77.4	5875	0.0045	B	0.0050	A	0.0055	A	0.0040	A	0.0050	A	0.0040	A
49	Service	77	89.6	6649	0.0040	B	0.0050	A	0.0050	A	0.0040	A	0.0050	A	0.0040	A
60	DL+2 LL	92	111	8165												

Table A.13 POJ-PS-100 maximum crack widths in mm for north face of joint

Load Step	South Joint	Ri kN	Ro kN	Moment kN-M	1 mm		2 mm		3 mm		4 mm		5 mm	
10	DL/2	146	146	178.4	0.05	C								
10'	DL/2 Ovnt	146	146	178.4	0.15	C	0.14	D						
12		176	176	214.2	0.19	C	0.19	D						
14		205	205	250.0	0.29	E	0.32	D						
16		234	234	285.8	0.38	E	0.39	E	0.04	A				
18		264	264	321.6	0.43	C	0.58	B	0.06	A'	0.05	D		
20	DL	293	293	357.4	0.41	E	1.12	B	0.05	A	0.08	D	0.11	C
20'	DL Ovrnt	293	293	357.4	0.41	E	0.71	D	0.09	A	0.10	D	0.20	C

Table A.14 POJ-PS-100 maximum crack widths in (in.) for north face of joint

Load Step	South Joint	Ri (kips)	Ro (kips)	Moment (k-in.)	1 (in.)		2 (in.)		3 (in.)		4 (in.)		5 (in.)	
10	DL/2	32.9	32.9	1579	0.0020	C								
10'	DL/2 Ovnt	32.9	32.9	1579	0.0060	C	0.0055	D						
12		39.5	39.5	1896	0.0075	C	0.0075	D						
14		46.1	46.1	2213	0.0115	E	0.0125	D						
16		52.7	52.7	2530	0.0150	E	0.0155	E	0.0015	A				
18		59.3	59.3	2846	0.0170	C	0.0230	B	0.0025	A'	0.0020	D		
20	DL	65.9	65.9	3163	0.0160	E	0.0440	B	0.0020	A	0.0030	D	0.0045	C
20'	DL Ovrnt	65.9	65.9	3163	0.0160	E	0.0280	D	0.0035	A	0.0040	D	0.0080	C

Table A.15 POJ-PS-100 maximum crack widths in mm for south face of joint

Load Step	South Pier	Ri kN	Ro kN	Moment kN-M	1 mm		2 mm		3 mm		4 mm	
10	DL/2	146	146	290.0	0.08	C'						
10'	DL/2	146	146	290.0	0.25	D						
12		176	176	348.2	0.25	D						
14		205	205	406.3	0.25	D						
16		234	234	464.5	0.51	D	0.05	D	0.05	E	0.04	A
18		264	264	522.7	0.46	D	0.09	D	0.13	E	0.08	A
20	DL	293	293	580.8	0.69	D	0.13	E	0.18	F	0.10	A
20'	DL	293	293	580.8	0.66	C	0.13	C	0.36	F	0.08	A

Table A.16 POJ-PS-100 maximum crack widths in (in.) for south face of joint

Load Step	South Pier	Ri (kips)	Ro (kips)	Moment (k-in.)	1 (in.)		2 (in.)		3 (in.)		4 (in.)	
10	DL/2	32.9	32.9	2566	0.0030	C'						
10'	DL/2	32.9	32.9	2566	0.0100	D						
12		39.5	39.5	3081	0.0100	D						
14		46.1	46.1	3596	0.0100	D						
16		52.7	52.7	4111	0.0200	D	0.0020	D	0.0020	E	0.0015	A
18		59.3	59.3	4625	0.0180	D	0.0035	D	0.0050	E	0.0030	A
20	DL	65.9	65.9	5140	0.0270	D	0.0050	E	0.0070	F	0.0040	A
20'	DL	65.9	65.9	5140	0.0260	C	0.0050	C	0.0140	F	0.0030	A

Table A.17 POJ-PS-100 maximum crack widths in mm for north face of pier

Load Step	North Pier	Ri kN	Ro kN	Moment kN-M	1 mm		2 mm		3 mm		4 mm		5 mm	
10	DL/2	146	146	290.0										
10'	DL/2	146	146	290.0										
12		176	176	348.2										
14		205	205	406.3										
16		234	234	464.5	0.04	A	0.04	A	0.06	A	0.04	A'	0.05	A'
18		264	264	522.7	0.05	A	0.05	A	0.08	A	0.08	B	0.08	A'
20	DL	293	293	580.8	0.08	D	0.06	A'	0.08	A	0.06	B	0.09	A
20'	DL	293	293	580.8	0.05	A	0.05	A	0.10	A	0.06	C	0.09	A'

Table A.18 POJ-PS-100 maximum crack widths in (in.) for north face of pier

Load Step	North Pier	Ri (kips)	Ro (kips)	Moment (k-in.)	1 (in.)		2 (in.)		3 (in.)		4 (in.)		5 (in.)	
10	DL/2	32.9	32.9	2566										
10'	DL/2	32.9	32.9	2566										
12		39.5	39.5	3081										
14		46.1	46.1	3596										
16		52.7	52.7	4111	0.0015	A	0.0015	A	0.0025	A	0.0015	A'	0.0020	A'
18		59.3	59.3	4625	0.0020	A	0.0020	A	0.0030	A	0.0030	B	0.0030	A'
20	DL	65.9	65.9	5140	0.0030	D	0.0025	A'	0.0030	A	0.0025	B	0.0035	A
20'	DL	65.9	65.9	5140	0.0020	A	0.0020	A	0.0040	A	0.0025	C	0.0035	A'

Table A.19 POJ-PS-100 maximum crack widths in mm for south face of pier

Load Step	South Pier	Ri kN	Ro kN	Moment kN-M	1 mm		2 mm		3 mm		4 mm		5 mm	
10	DL/2	146	146	290.0										
10'	DL/2	146	146	290.0										
12		176	176	348.2										
14		205	205	406.3										
16		234	234	464.5	0.05	A	0.05	A	0.04	A'	0.05	A'	0.04	A
18		264	264	522.7	0.06	A	0.08	A	0.05	A	0.06	A	0.08	A
20	DL	293	293	580.8	0.10	C	0.10	A	0.08	A	0.08	A	0.05	A
20'	DL	293	293	580.8	0.09	C	0.10	A	0.05	A	0.06	B	0.06	A

Table A.20 POJ-PS-100 maximum crack widths in (in.) for south face of pier

Load Step	South Pier	Ri (kips)	Ro (kips)	Moment (k-in.)	1 (in.)		2 (in.)		3 (in.)		4 (in.)		5 (in.)	
10	DL/2	32.9	32.9	2566										
10'	DL/2	32.9	32.9	2566										
12		39.5	39.5	3081										
14		46.1	46.1	3596										
16		52.7	52.7	4111	0.0020	A	0.0020	A	0.0015	A'	0.0020	A'	0.0015	A
18		59.3	59.3	4625	0.0025	A	0.0030	A	0.0020	A	0.0025	A	0.0030	A
20	DL	65.9	65.9	5140	0.0040	C	0.0040	A	0.0030	A	0.0030	A	0.0020	A
20'	DL	65.9	65.9	5140	0.0035	C	0.0040	A	0.0020	A	0.0025	B	0.0025	A

Table A.21 POJ-RC-100-TH maximum crack widths in mm for north face of overhang

Load Step	North-Overhang	Ri kN	Ro kN	Moment kN-m	1 mm		2 mm		3 mm		4 mm		5 mm		6 mm		7 mm		8 mm	
9	First Crack	132	132	161.1	0.05	A														
15		220	220	267.9	0.08	A	0.03	A												
20	Dead Load	293	293	357.4	0.15	A	0.06	A												
27	DL+1/2 LL	318	344	411.7	0.18	A	0.08	C	0.05	B	0.04	A	0.04	A	0.04	A				
34	Service	343	399	468.9	0.18	A	0.09	A	0.06	A	0.06	A	0.05	A	0.06	A	0.03	A		
35	Dead Load	293	293	357.4	0.17	A	0.10	D	0.05	A	0.04	A'	0.05	A	0.05	A	0.04	A		
42	DL+1/2 LL	318	344	411.7	0.17	A	0.09	E	0.05	A	0.04	A'	0.05	A	0.05	A	0.03	A		
49	Service	343	399	468.9	0.18	A	0.10	E	0.05	A	0.05	A	0.05	A	0.08	A	0.05	A		
60	DL+2 LL	409	496	577.9	0.18	A	0.15	E	0.09	B	0.06	A'	0.08	A	0.10	A	0.09	A'	0.05	C

Table A.22 POJ-PU-54-TH maximum crack widths in (in.) for north face of overhang

Load Step	North Overhang	Ri (kips)	Ro (kips)	Moment (k-in.)	1 (in.)		2 (in.)		3 (in.)		4 (in.)		5 (in.)		6 (in.)		7 (in.)		8 (in.)	
17	First Crack	56	56	2688	0.0005	A														
20	Dead Load	65.9	65.9	3163	0.0035	A														
27	DL+1/2 LL	71.4	77.4	3643	0.0035	A	0.0010	A'	0.0030	A										
34	Service	77	89.6	4150	0.0045	A	0.0010	A	0.0045	C	0.0025	A								
35	Dead Load	65.9	65.9	3163	0.0045	A	0.0010	A	0.0035	C	0.0015	A								
42	DL+1/2 LL	71.4	77.4	3643	0.0045	A	0.0010	A	0.0045	C	0.0020	A								
49	Service	77	89.6	4150	0.0050	A	0.0010	A	0.0050	C	0.0025	A'								
60	DL+2 LL	92	111	5114	0.0065	A	0.0020	A	0.0070	C	0.0050	B	0.0010	A'	0.0020	A.	0.0020	A'	0.0015	A

Table A.23 POJ-RC-100-TH maximum crack widths in mm for south face of overhang

Load Step	South-Overhang	Ri kN	Ro kN	Moment kN-m	1 mm		2 mm		3 mm		4 mm		5 mm		6 mm		7 mm		8 mm		9 mm	
9	First Crack	132	132	161.1	v	A	v	A														
15		220	220	267.9	v	A	0.05	A	0.05	A												
20	Dead Load	293	293	357.4	v	A	0.09	A	0.08	A	0.05	A	0.05	A'	0.04	A	0.03	A				
27	DL+1/2 LL	318	344	411.7	v	A	0.11	A	0.08	A	0.08	A	0.06	A	0.05	A	0.06	A				
34	Service	343	399	468.9	v	A	0.11	A	0.09	A	0.06	A	0.09	A	0.05	A	0.09	A	0.03	A		
35	Dead Load	293	293	357.4	v	A	0.08	A	0.10	A	0.06	A	0.10	A	0.05	A	0.08	A	0.03	A		
42	DL+1/2 LL	318	344	411.7	v	A	0.10	A	0.13	A	0.06	A	0.08	A	0.08	A	0.08	A	0.03	A		
49	Service	343	399	468.9	v	A	0.13	A	0.10	A	0.08	A	0.08	A	0.08	A	0.06	A	0.08	A	0.03	A
60	DL+2 LL	409	496	577.9	v	A	0.18	A	0.15	A	0.11	C	0.14	A	0.11	C	0.13	A	0.05	A	0.09	C

Table A.24 POJ-RC-100-TH maximum crack widths in (in.) for south face of overhang

Load Step	South-Overhang	Ri (kips)	Ro (kips)	Moment (k-in.)	1 (in.)		2 (in.)		3 (in.)		4 (in.)		5 (in.)		6 (in.)		7 (in.)		8 (in.)		9 (in.)	
9	First Crack	29.7	29.7	1426	v	A	v	A														
15		49.4	49.4	2371	v	A	0.0020	A	0.0020	A												
20	Dead Load	65.9	65.9	3163	v	A	0.0035	A	0.0030	A	0.0020	A	0.0020	A'	0.0015	A	0.0010	A				
27	DL+1/2 LL	71.4	77.4	3643	v	A	0.0045	A	0.0030	A	0.0030	A	0.0025	A	0.0020	A	0.0025	A				
34	Service	77	89.6	4150	v	A	0.0045	A	0.0035	A	0.0025	A	0.0035	A	0.0020	A	0.0035	A	0.0010	A		
35	Dead Load	65.9	65.9	3163	v	A	0.0030	A	0.0040	A	0.0025	A	0.0040	A	0.0020	A	0.0030	A	0.0010	A		
42	DL+1/2 LL	71.4	77.4	3643	v	A	0.0040	A	0.0050	A	0.0025	A	0.0030	A	0.0030	A	0.0030	A	0.0010	A		
49	Service	77	89.6	4150	v	A	0.0050	A	0.0040	A	0.0030	A	0.0030	A	0.0030	A	0.0025	A	0.0030	A	0.0010	A
60	DL+2 LL	92	111	5114	v	A	0.0070	A	0.0060	A	0.0045	C	0.0055	A	0.0045	C	0.0050	A	0.0020	A	0.0035	C

Table A.25 POJ-RC-100-TH maximum crack widths in mm for north face of joint

North-Joint	Ri KN	Ro KN	Moment KN-M	1 mm		2 mm		3 mm		4 mm		5 mm		6 mm		7 mm		8 mm		9 mm		10 mm		11 mm		12 mm		13 mm	
First Crack	132	132	161.1	0.03	A																								
	220	220	267.9	0.08	A	0.08	D	0.04	A																				
Dead Load	293	293	357.4	0.10	A	0.10	D	0.10	A	0.10	A'	0.10	A'	0.03	B	0.05	C												
DL+1/2 LL	318	344	411.7	0.14	A	0.09	C	0.13	B	0.15	B	0.13	A	0.06	B	0.14	C	0.08	A	0.23	C	0.04	A'	0.04	A				
Service	343	399	468.9	0.15	A	0.10	D	0.11	A	0.14	A	0.13	A	0.05	A	0.18	D	0.10	A	0.28	C	0.04	B	0.05	A	0.10	A	0.03	A
Dead Load	293	293	357.4	0.14	A	0.10	C	0.10	D	0.15	B	0.13	A	0.06	A	0.17	C	0.08	A'	0.30	C	0.04	B	0.08	A	0.10	A	0.03	A
DL+1/2 LL	318	344	411.7	0.15	A	0.14	C	0.11	D	0.15	B	0.14	A	0.06	B	0.18	C	0.08	A'	0.30	C	0.04	B	0.05	A	0.08	A	0.03	A
Service	343	399	468.9	0.15	A	0.15	C	0.11	A	0.14	B	0.13	A'	0.08	B	0.18	C	0.10	A	0.28	B	0.04	B	0.08	A	0.11	A	0.04	A
DL + 2 LL	409	496	577.9	0.20	A	0.17	A	0.19	A	0.19	B	0.14	A	0.11	A	0.28	D	0.11	A	0.43	C	0.04	B	0.08	A	0.17	A	0.04	A

Table A.26 POJ-RC-100-TH maximum crack widths in (in.) for north face of joint

North-Joint	Ri (Kips)	Ro (Kips)	Moment (K-in.)	1 (in.)		2 (in.)		3 (in.)		4 (in.)		5 (in.)		6 (in.)		7 (in.)		8 (in.)		9 (in.)		10 (in.)		11 (in.)		12 (in.)		13 (in.)	
First Crack	29.7	29.7	1426	0.0010	A																								
	49.4	49.4	2371	0.0030	A	0.0030	D	0.0015	A																				
Dead Load	65.9	65.9	3163	0.0040	A	0.0040	D	0.0040	A	0.0040	A'	0.0040	A'	0.0010	B	0.0020	C												
DL+1/2 LL	71.4	77.4	3643	0.0055	A	0.0035	C	0.0050	B	0.0060	B	0.0050	A	0.0025	B	0.0055	C	0.0030	A	0.0090	C	0.0015	A'	0.0015	A				
Service	77	89.6	4150	0.0060	A	0.0040	D	0.0045	A	0.0055	A	0.0050	A	0.0020	A	0.0070	D	0.0040	A	0.0110	C	0.0015	B	0.0020	A	0.0040	A	0.0010	A
Dead Load	65.9	65.9	3163	0.0055	A	0.0040	C	0.0040	D	0.0060	B	0.0050	A	0.0025	A	0.0065	C	0.0030	A'	0.0120	C	0.0015	B	0.0030	A	0.0040	A	0.0010	A
DL+1/2 LL	71.4	77.4	3643	0.0060	A	0.0055	C	0.0045	D	0.0060	B	0.0055	A	0.0025	B	0.0070	C	0.0030	A'	0.0120	C	0.0015	B	0.0020	A	0.0030	A	0.0010	A
Service	77	89.6	4150	0.0060	A	0.0060	C	0.0045	A	0.0055	B	0.0050	A'	0.0030	B	0.0070	C	0.0040	A	0.0110	B	0.0015	B	0.0030	A	0.0045	A	0.0015	A
DL + 2 LL	92	111	5114	0.0080	A	0.0065	A	0.0075	A	0.0075	B	0.0055	A	0.0045	A	0.0110	D	0.0045	A	0.0170	C	0.0015	B	0.0030	A	0.0065	A	0.0015	A

Table A.27 POJ-RC-100-TH maximum crack widths in mm for south face of joint

Load Step	South-Joint	Ri KN	Ro KN	Moment KN-M	1 mm		2 mm		3 mm		4 mm		5 mm		6 mm		7 mm		8 mm		9 mm		10 mm		11 mm		12 mm	
9	First Crack	132	132	161.1	0.04	A																						
15		220	220	267.9	0.08	B	0.09	A	0.04	A	0.04	A																
20	Dead Load	293	293	357.4	0.10	D	0.11	C	0.08	A	0.09	A	0.11	A	0.18	C	0.11	A	0.13	A	0.08	A						
27	DL+1/2 LL	318	344	411.7	0.10	C	0.10	A	0.05	A	0.10	A	0.11	A	0.20	D	0.14	A	0.17	A'	0.17	A'	0.18	B	0.10	A	0.04	A
34	Service	343	399	468.9	0.13	D	0.11	A	0.06	A	0.10	A	0.15	A	0.19	D	0.15	A	0.17	A	0.17	A	0.28	B	0.13	A	0.10	A
35	Dead Load	293	293	357.4	0.13	D	0.13	A	0.08	A'	0.11	B	0.14	A'	0.15	E	0.11	A	0.15	A	0.13	A	0.28	B	0.10	A	0.08	A
42	DL+1/2 LL	318	344	411.7	0.10	E	0.10	A	0.08	A'	0.11	A	0.13	A	0.18	D	0.14	A	0.15	A'	0.18	A	0.27	B	0.10	A	0.08	A
49	Service	343	399	468.9	0.13	D	0.15	C	0.10	A'	0.14	A	0.15	A'	0.17	D	0.18	A	0.17	A	0.13	A	0.28	D	0.13	A	0.08	A
60	DL + 2 LL	409	496	577.9	0.17	A	0.14	A	0.11	A	0.14	A	0.20	A	0.25	E	0.18	A	0.22	A	0.19	A	0.43	D	0.13	B	0.15	A

Table A.28 POJ-RC-100-TH maximum crack widths in (in.) for south face of joint

Load Step	South-Joint	Ri (Kips)	Ro (Kips)	Moment (K-in.)	1 (in.)		2 (in.)		3 (in.)		4 (in.)		5 (in.)		6 (in.)		7 (in.)		8 (in.)		9 (in.)		10 (in.)		11 (in.)		12 (in.)	
9	First Crack	29.7	29.7	1426	0.0015	A																						
15		49.4	49.4	2371	0.0030	B	0.0035	A	0.0015	A	0.0015	A																
20	Dead Load	65.9	65.9	3163	0.0040	D	0.0045	C	0.0030	A	0.0035	A	0.0045	A	0.0070	C	0.0045	A	0.0050	A	0.0030	A						
27	DL+1/2 LL	71.4	77.4	3643	0.0040	C	0.0040	A	0.0020	A	0.0040	A	0.0045	A	0.0080	D	0.0055	A	0.0065	A'	0.0065	A'	0.0070	B	0.0040	A	0.0015	A
34	Service	77	89.6	4150	0.0050	D	0.0045	A	0.0025	A	0.0040	A	0.0060	A	0.0075	D	0.0060	A	0.0065	A	0.0065	A	0.0110	B	0.0050	A	0.0040	A
35	Dead Load	65.9	65.9	3163	0.0050	D	0.0050	A	0.0030	A'	0.0045	B	0.0055	A'	0.0060	E	0.0045	A	0.0060	A	0.0050	A	0.0110	B	0.0040	A	0.0030	A
42	DL+1/2 LL	71.4	77.4	3643	0.0040	E	0.0040	A	0.0030	A'	0.0045	A	0.0050	A	0.0070	D	0.0055	A	0.0060	A'	0.0070	A	0.0105	B	0.0040	A	0.0030	A
49	Service	77	89.6	4150	0.0050	D	0.0060	C	0.0040	A'	0.0055	A	0.0060	A'	0.0065	D	0.0070	A	0.0065	A	0.0050	A	0.0110	D	0.0050	A	0.0030	A
60	DL + 2 LL	92	111	5114	0.0065	A	0.0055	A	0.0045	A	0.0055	A	0.0080	A	0.0100	E	0.0070	A	0.0085	A	0.0075	A	0.0170	D	0.0050	B	0.0060	A

Table A.29 POJ-RC-100-TH maximum crack widths in mm for north face of pier

Load Step	North-Pier	Ri kN	Ro kN	Moment kN-m	1 mm		2 mm		3 mm		4 mm		5 mm	
20	Dead Load	293	293	580.8	0.08	A'	0.08	A	0.08	A	0.10	A	0.08	A
27	DL+1/2 LL	318	344	663.9	0.10	A'	0.08	A'	0.10	A	0.13	A	0.10	A'
34	Service	343	399	751.3	0.11	A	0.09	A	0.11	A	0.14	A	0.13	A
35	Dead Load	293	293	580.8	0.10	A	0.08	A	0.11	A'	0.13	A	0.13	A
42	DL+1/2 LL	318	344	663.9	0.11	A	0.08	A'	0.11	A'	0.13	A	0.14	A
49	Service	343	399	751.3	0.13	A'	0.08	A	0.11	A	0.13	A	0.18	A
60	DL+2 LL	409	496	922.7	0.17	A	0.10	A	0.18	A'	0.18	A	0.19	A

Table A.30 POJ-RC-100-TH maximum crack widths in (in.) for north face of pier

Load Step	North-Pier	Ri (kips)	Ro (kips)	Moment (k-in.)	1 (in.)		2 (in.)		3 (in.)		4 (in.)		5 (in.)	
20	Dead Load	65.9	65.9	5140	0.0030	A'	0.0030	A	0.0030	A	0.0040	A	0.0030	A
27	DL+1/2 LL	71.4	77.4	5875	0.0040	A'	0.0030	A'	0.0040	A	0.0050	A	0.0040	A'
34	Service	77	89.6	6649	0.0045	A	0.0035	A	0.0045	A	0.0055	A	0.0050	A
35	Dead Load	65.9	65.9	5140	0.0040	A	0.0030	A	0.0045	A'	0.0050	A	0.0050	A
42	DL+1/2 LL	71.4	77.4	5875	0.0045	A	0.0030	A'	0.0045	A'	0.0050	A	0.0055	A
49	Service	77	89.6	6649	0.0050	A'	0.0030	A	0.0045	A	0.0050	A	0.0070	A
60	DL+2 LL	92	111	8165	0.0065	A	0.0040	A	0.0070	A'	0.0070	A	0.0075	A

Table A.31 POJ-RC-100-TH maximum crack widths in mm for south face of pier

Load Step	South-Pier	Ri kN	Ro kN	Moment kN-m	1 mm		2 mm		3 mm		4 mm		5 mm	
12	First Crack	176	176	214.2	0.05	A	0.04	A	0.01	A	0.01	A		
15		220	220	267.9	0.06	C	0.08	A	0.10	A	0.08	A	0.08	A'
20	Dead Load	293	293	580.8	0.10	A	0.13	A	0.10	A	0.11	A'	0.08	A
27	DL+1/2 LL	318	344	663.9	0.14	A	0.13	A	0.11	A	0.15	A	0.10	B
34	Service	343	399	751.3	0.13	A	0.15	A	0.14	A	0.15	A'	0.11	B
35	Dead Load	293	293	580.8	0.13	A'	0.13	A	0.08	A'	0.14	A'	0.09	A'
42	DL+1/2 LL	318	344	663.9	0.13	A'	0.15	A	0.14	A	0.14	A	0.09	B
49	Service	343	399	751.3	0.13	A	0.18	A	0.17	A	0.17	A	0.14	C
60	DL+2 LL	409	496	922.7	0.18	A'	0.22	A	0.18	A	0.18	A	0.18	C

Table A.32 POJ-RC-100-TH maximum crack widths in (in.) for south face of pier

Load Step	South-Pier	Ri (kips)	Ro (kips)	Moment (k-in.)	1 (in.)		2 (in.)		3 (in.)		4 (in.)		5 (in.)	
12	First Crack	39.5	39.5	1896	0.0020	A	0.0015	A	0.0005	A	0.0005	A		
15		49.4	49.4	2371	0.0025	C	0.0030	A	0.0040	A	0.0030	A	0.0030	A'
20	Dead Load	65.9	65.9	5140	0.0040	A	0.0050	A	0.0040	A	0.0045	A'	0.0030	A
27	DL+1/2 LL	71.4	77.4	5875	0.0055	A	0.0050	A	0.0045	A	0.0060	A	0.0040	B
34	Service	77	89.6	6649	0.0050	A	0.0060	A	0.0055	A	0.0060	A'	0.0045	B
35	Dead Load	65.9	65.9	5140	0.0050	A'	0.0050	A	0.0030	A'	0.0055	A'	0.0035	A'
42	DL+1/2 LL	71.4	77.4	5875	0.0050	A'	0.0060	A	0.0055	A	0.0055	A	0.0035	B
49	Service	77	89.6	6649	0.0050	A	0.0070	A	0.0065	A	0.0065	A	0.0055	C
60	DL+2 LL	92	111	8165	0.0070	A'	0.0085	A	0.0070	A	0.0070	A	0.0070	C

Table A.33 POJ-PU-54-TH maximum crack widths in mm for north face of overhang

Load Step	North Overhang	Ri kN	Ro kN	Moment kN-m	1 mm		2 mm		3 mm		4 mm		5 mm		6 mm		7 mm		8 mm	
17	First Crack	249	249	303.7	0.01	A														
20	Dead Load	293	293	357.4	0.09	A														
27	DL+1/2 LL	318	344	411.7	0.09	A	0.03	A'	0.08	A										
34	Service	343	399	468.9	0.11	A	0.03	A	0.11	C	0.06	A								
35	Dead Load	293	293	357.4	0.11	A	0.03	A	0.09	C	0.04	A								
42	DL+1/2 LL	318	344	411.7	0.11	A	0.03	A	0.11	C	0.05	A								
49	Service	343	399	468.9	0.13	A	0.03	A	0.13	C	0.06	A'								
60	DL+2 LL	409	496	577.9	0.17	A	0.05	A	0.18	C	0.13	B	0.03	A'	0.05	A.	0.05	A'	0.04	A

Table A.34 POJ-PU-54-TH maximum crack widths in (in.) for north face of overhang

Load Step	North Overhang	Ri (kips)	Ro (kips)	Moment (k-in.)	1 (in.)		2 (in.)		3 (in.)		4 (in.)		5 (in.)		6 (in.)		7 (in.)		8 (in.)	
17	First Crack	56	56	2688	0.0005	A														
20	Dead Load	65.9	65.9	3163	0.0035	A														
27	DL+1/2 LL	71.4	77.4	3643	0.0035	A	0.0010	A'	0.0030	A										
34	Service	77	89.6	4150	0.0045	A	0.0010	A	0.0045	C	0.0025	A								
35	Dead Load	65.9	65.9	3163	0.0045	A	0.0010	A	0.0035	C	0.0015	A								
42	DL+1/2 LL	71.4	77.4	3643	0.0045	A	0.0010	A	0.0045	C	0.0020	A								
49	Service	77	89.6	4150	0.0050	A	0.0010	A	0.0050	C	0.0025	A'								
60	DL+2 LL	92	111	5114	0.0065	A	0.0020	A	0.0070	C	0.0050	B	0.0010	A'	0.0020	A.	0.0020	A'	0.0015	A

Table A.35 POJ-PU-54-TH maximum crack widths in mm for south face of overhang

Load Step	South Overhang	Ri kN	Ro kN	Moment kN-m	1 mm		2 mm		3 mm		4 mm		5 mm	
13	First Crack	190	190	232.1	0.03	A								
17		249	249	303.7	0.05	A								
20	Dead Load	293	293	357.4	0.10	A								
27	DL+1/2 LL	318	344	411.7	0.10	A	0.03	A	0.05	A				
34	Service	343	399	468.9	0.15	A	0.05	A	0.10	A				
35	Dead Load	293	293	357.4	0.13	A	0.05	A	0.08	A				
42	DL+1/2 LL	318	344	411.7	0.14	A	0.05	A	0.09	A				
49	Service	343	399	468.9	0.15	A	0.06	A	0.11	A				
60	DL+2 LL	409	496	577.9	0.20	A	0.14	A	0.17	A'	0.06	A	0.01	A

Table A.36 POJ-PU-54-TH maximum crack widths in (in.) for south face of overhang

Load Step	South Overhang	Ri (kips)	Ro (kips)	Moment (k-in.)	1 (in.)		2 (in.)		3 (in.)		4 (in.)		5 (in.)	
13	First Crack	42.8	42.8	2054	0.0010	A								
17		56	56	2688	0.0020	A								
20	Dead Load	65.9	65.9	3163	0.0040	A								
27	DL+1/2 LL	71.4	77.4	3643	0.0040	A	0.0010	A	0.0020	A				
34	Service	77	89.6	4150	0.0060	A	0.0020	A	0.0040	A				
35	Dead Load	65.9	65.9	3163	0.0050	A	0.0020	A	0.0030	A				
42	DL+1/2 LL	71.4	77.4	3643	0.0055	A	0.0020	A	0.0035	A				
49	Service	77	89.6	4150	0.0060	A	0.0025	A	0.0045	A				
60	DL+2 LL	92	111	5114	0.0080	A	0.0055	A	0.0065	A'	0.0025	A	0.0005	A

Table A.37 POJ-PU-54-TH maximum crack widths in mm for north face of joint

Load Step	North Joint	Ri kN	Ro kN	Moment kN-m	1 mm		2 mm		3 mm		4 mm		5 mm		6 mm		7 mm		8 mm		9 mm		10 mm	
17	First Crack	249	249	303.7	0.03	A																		
20	Dead Load	293	293	357.4	0.05	C	0.05	A																
27	DL+1/2 LL	318	344	411.7	0.08	C	0.08	A	0.09	A	0.10	A												
34	Service	343	399	468.9	0.08	A	0.10	A	0.15	A	0.17	A												
35	Dead Load	293	293	357.4	0.08	E	0.09	A	0.13	A	0.17	A												
42	DL+1/2 LL	318	344	411.7	0.08	B	0.09	A	0.10	C	0.15	A												
49	Service	343	399	468.9	0.08	B	0.13	A	0.13	A	0.17	A												
60	DL+2 LL	409	496	577.9	0.11	A'	0.14	A	0.17	D	0.18	A	0.14	A	0.06	A'	0.20	A	0.05	A'	0.11	A	0.10	A

Table A.38 POJ-PU-54-TH maximum crack widths in (in.) for north face of joint

Load Step	North Joint	Ri (kips)	Ro (kips)	Moment (k-in.)	1 (in.)		2 (in.)		3 (in.)		4 (in.)		5 (in.)		6 (in.)		7 (in.)		8 (in.)		9 (in.)		10 (in.)	
17	First Crack	56	56	2688	0.0010	A																		
20	Dead Load	65.9	65.9	3163	0.0020	C	0.0020	A																
27	DL+1/2 LL	71.4	77.4	3643	0.0030	C	0.0030	A	0.0035	A	0.0040	A												
34	Service	77	89.6	4150	0.0030	A	0.0040	A	0.0060	A	0.0065	A												
35	Dead Load	65.9	65.9	3163	0.0030	E	0.0035	A	0.0050	A	0.0065	A												
42	DL+1/2 LL	71.4	77.4	3643	0.0030	B	0.0035	A	0.0040	C	0.0060	A												
49	Service	77	89.6	4150	0.0030	B	0.0050	A	0.0050	A	0.0065	A												
60	DL+2 LL	92	111	5114	0.0045	A'	0.0055	A	0.0065	D	0.0070	A	0.0055	A	0.0025	A'	0.0080	A	0.0020	A'	0.0045	A	0.0040	A

Table A.39 POJ-PU-54-TH maximum crack widths in mm for south face of joint

Load Step	South Joint	Ri kN	Ro kN	Moment kN-m	1 mm		2 mm		3 mm		4 mm		5 mm		6 mm		7 mm		8 mm		9 mm	
13	First Crack	190	190	232.1	0.03	A																
17		249	249	303.7	0.05	A																
20	Dead Load	293	293	357.4	0.08	A	0.08	A	0.03	A												
27	DL+1/2 LL	318	344	411.7	0.10	A	0.10	C	0.05	A	0.04	A	0.13	A								
34	Service	343	399	468.9	0.11	A	0.14	A	0.13	C	0.05	A	0.14	A	0.09	A						
35	Dead Load	293	293	357.4	0.10	A	0.10	A	0.13	C	0.05	A	0.14	A	0.06	A'						
42	DL+1/2 LL	318	344	411.7	0.11	A	0.13	A	0.13	C	0.05	A	0.14	A	0.08	A						
49	Service	343	399	468.9	0.13	A	0.13	A	0.13	D	0.06	A	0.17	A	0.13	A						
60	DL+2 LL	409	496	577.9	0.17	A	0.18	A	0.15	C	0.13	A'	0.17	A'	0.10	A'	0.19	C	0.18	A'	0.09	A

Table A.40 POJ-PU-54-TH maximum crack widths in (in.) for south face of joint

Load Step	South Joint	Ri (kips)	Ro (kips)	Moment (k-in.)	1 (in.)		2 (in.)		3 (in.)		4 (in.)		5 (in.)		6 (in.)		7 (in.)		8 (in.)		9 (in.)	
13	First Crack	42.8	42.8	2054	0.0010	A																
17		56	56	2688	0.0020	A																
20	Dead Load	65.9	65.9	3163	0.0030	A	0.0030	A	0.0010	A												
27	DL+1/2 LL	71.4	77.4	3643	0.0040	A	0.0040	C	0.0020	A	0.0015	A	0.0050	A								
34	Service	77	89.6	4150	0.0045	A	0.0055	A	0.0050	C	0.0020	A	0.0055	A	0.0035	A						
35	Dead Load	65.9	65.9	3163	0.0040	A	0.0040	A	0.0050	C	0.0020	A	0.0055	A	0.0025	A'						
42	DL+1/2 LL	71.4	77.4	3643	0.0045	A	0.0050	A	0.0050	C	0.0020	A	0.0055	A	0.0030	A						
49	Service	77	89.6	4150	0.0050	A	0.0050	A	0.0050	D	0.0025	A	0.0065	A	0.0050	A						
60	DL+2 LL	92	111	5114	0.0065	A	0.0070	A	0.0060	C	0.0050	A'	0.0065	A'	0.0040	A'	0.0075	C	0.0070	A'	0.0035	A

Table A.41 POJ-PU-54-TH maximum crack widths in mm for north face of pier

Load Step	North Pier	Ri kN	Ro kN	Moment kN-m	1 mm		2 mm		3 mm		4 mm		5 mm		6 mm	
17	First Crack	249	249	493.6	0.04	A	0.05	A								
20	Dead Load	293	293	580.8	0.06	A'	0.06	A	0.04	A	0.05	A	0.05	A		
27	DL+1/2 LL	318	344	663.9	0.08	A	0.08	A'	0.06	A	0.08	A	0.08	A	0.03	A
34	Service	343	399	751.3	0.11	A	0.09	A	0.08	A	0.13	A	0.11	A	0.08	A
35	Dead Load	293	293	580.8	0.09	A	0.09	A'	0.08	A	0.09	A	0.10	A	0.06	A
42	DL+1/2 LL	318	344	663.9	0.10	A	0.10	A	0.10	A	0.10	A	0.10	A	0.05	A
49	Service	343	399	751.3	0.11	A	0.10	A'	0.09	A	0.13	A	0.11	A	0.08	A
60	DL+2 LL	409	496	922.7	0.15	A	0.13	A	0.18	A	0.18	A	0.18	A	0.11	A

Table A.42 POJ-PU-54-TH maximum crack widths in (in.) for north face of pier

Load Step	North Pier	Ri (kips)	Ro (kips)	Moment (k-in.)	1 (in.)		2 (in.)		3 (in.)		4 (in.)		5 (in.)		6 (in.)	
17	First Crack	56	56	4368	0.0015	A	0.0020	A								
20	Dead Load	65.9	65.9	5140	0.0025	A'	0.0025	A	0.0015	A	0.0020	A	0.0020	A		
27	DL+1/2 LL	71.4	77.4	5875	0.0030	A	0.0030	A'	0.0025	A	0.0030	A	0.0030	A	0.0010	A
34	Service	77	89.6	6649	0.0045	A	0.0035	A	0.0030	A	0.0050	A	0.0045	A	0.0030	A
35	Dead Load	65.9	65.9	5140	0.0035	A	0.0035	A'	0.0030	A	0.0035	A	0.0040	A	0.0025	A
42	DL+1/2 LL	71.4	77.4	5875	0.0040	A	0.0040	A	0.0040	A	0.0040	A	0.0040	A	0.0020	A
49	Service	77	89.6	6649	0.0045	A	0.0040	A'	0.0035	A	0.0050	A	0.0045	A	0.0030	A
60	DL+2 LL	92	111	8165	0.0060	A	0.0050	A	0.0070	A	0.0070	A	0.0070	A	0.0045	A

Table A.43 POJ-PU-54-TH maximum crack widths in mm for south face of pier

Load Step	South Pier	Ri kN	Ro kN	Moment kN-m	1 mm		2 mm		3 mm		4 mm		5 mm		6 mm	
17	First Crack	249	249	493.6	0.08	A	0.06	A								
20	Dead Load	293	293	580.8	0.09	A'	0.09	A	0.08	A.	0.04	A	0.05	A		
27	DL+1/2 LL	318	344	663.9	0.11	A	0.11	A	0.06	A	0.06	A	0.08	A		
34	Service	343	399	751.3	0.13	A	0.13	A	0.13	A	0.10	A	0.10	A	0.04	A
35	Dead Load	293	293	580.8	0.11	A	0.10	A	0.08	A	0.09	A	0.11	A	0.03	A'
42	DL+1/2 LL	318	344	663.9	0.13	A	0.11	A	0.10	A	0.09	A	0.09	A	0.03	A'
49	Service	343	399	751.3	0.14	A	0.13	A	0.13	A	0.11	A	0.13	A	0.04	A
60	DL+2 LL	409	496	922.7	0.18	A	0.17	A	0.20	A	0.15	A	0.15	A	0.09	A

Table A.44 POJ-PU-54-TH maximum crack widths in (in.) for south face of pier

Load Step	South Pier	Ri (kips)	Ro (kips)	Moment (k-in.)	1 (in.)		2 (in.)		3 (in.)		4 (in.)		5 (in.)		6 (in.)	
17	First Crack	56	56	4368	0.0030	A	0.0025	A								
20	Dead Load	65.9	65.9	5140	0.0035	A'	0.0035	A	0.0030	A.	0.0015	A	0.0020	A		
27	DL+1/2 LL	71.4	77.4	5875	0.0045	A	0.0045	A	0.0025	A	0.0025	A	0.0030	A		
34	Service	77	89.6	6649	0.0050	A	0.0050	A	0.0050	A	0.0040	A	0.0040	A	0.0015	A
35	Dead Load	65.9	65.9	5140	0.0045	A	0.0040	A	0.0030	A	0.0035	A	0.0045	A	0.0010	A'
42	DL+1/2 LL	71.4	77.4	5875	0.0050	A	0.0045	A	0.0040	A	0.0035	A	0.0035	A	0.0010	A'
49	Service	77	89.6	6649	0.0055	A	0.0050	A	0.0050	A	0.0045	A	0.0050	A	0.0015	A
60	DL+2 LL	92	111	8165	0.0070	A	0.0065	A	0.0080	A	0.0060	A	0.0060	A	0.0035	A

Table A.45 POJ-PU-74-TH maximum crack widths in mm for north face of overhang

Load Step	North Overhang	Ri kN	Ro kN	Moment kN-m	1 mm		2 mm		3 mm		4 mm		5 mm	
10	DL/2	146	146	178.4										
20	Dead Load	293	293	357.4	0.03	A								
27	DL+1/2 LL	318	344	411.7	0.05	A	0.05	A						
34	Service	343	399	468.9	0.13	A	0.09	A	0.03	A				
35	Dead Load	293	293	357.4	0.11	A	0.06	A	0.03	A				
42	DL+1/2 LL	318	344	411.7	0.11	A	0.09	A	0.03	A				
49	Service	343	399	468.9	0.13	A	0.10	A	0.04	A				
60	DL+2 LL	409	496	577.9	0.22	A	0.14	A	0.13	B	0.04	A	0.04	A

Table A.46 POJ-PU-74-TH maximum crack widths in (in.) for north face of overhang

Load Step	North Overhang	Ri (kips)	Ro (kips)	Moment (k-in.)	1 (in.)		2 (in.)		3 (in.)		4 (in.)		5 (in.)	
10	DL/2	32.9	32.9	1579										
20	Dead Load	65.9	65.9	3163	0.0010	A								
27	DL+1/2 LL	71.4	77.4	3643	0.0020	A	0.0020	A						
34	Service	77	89.6	4150	0.0050	A	0.0035	A	0.0010	A				
35	Dead Load	65.9	65.9	3163	0.0045	A	0.0025	A	0.0010	A				
42	DL+1/2 LL	71.4	77.4	3643	0.0045	A	0.0035	A	0.0010	A				
49	Service	77	89.6	4150	0.0050	A	0.0040	A	0.0015	A				
60	DL+2 LL	92	111	5114	0.0085	A	0.0055	A	0.0050	B	0.0015	A	0.0015	A

Table A.47 POJ-PU-74-TH maximum crack widths in mm for south face of overhang

Load Step	South Overhang	Ri kN	Ro kN	Moment kN-m	1 mm		2 mm		3 mm		4 mm		5 mm		6 mm	
10	DL/2	146	146	178.4												
20	Dead Load	293	293	357.4	0.05	A										
27	DL+1/2 LL	318	344	411.7	0.08	A										
34	Service	343	399	468.9	0.11	A	0.03	A	0.04	A						
35	Dead Load	293	293	357.4	0.10	A	0.03	A	0.04	A						
42	DL+1/2 LL	318	344	411.7	0.13	A	0.03	A	0.04	B						
49	Service	343	399	468.9	0.13	A	0.03	A	0.05	A						
60	DL+2 LL	409	496	577.9	0.20	A	0.09	C	0.13	A	0.03	A	0.03	A	0.09	A

Table A.48 POJ-PU-74-TH maximum crack widths in (in.) for south face of overhang

Load Step	South Overhang	Ri (kips)	Ro (kips)	Moment (k-in.)	1 (in.)		2 (in.)		3 (in.)		4 (in.)		5 (in.)		6 (in.)	
10	DL/2	32.9	32.9	1579												
20	Dead Load	65.9	65.9	3163	0.0020	A										
27	DL+1/2 LL	71.4	77.4	3643	0.0030	A										
34	Service	77	89.6	4150	0.0045	A	0.0010	A	0.0015	A						
35	Dead Load	65.9	65.9	3163	0.0040	A	0.0010	A	0.0015	A						
42	DL+1/2 LL	71.4	77.4	3643	0.0050	A	0.0010	A	0.0015	B						
49	Service	77	89.6	4150	0.0050	A	0.0010	A	0.0020	A						
60	DL+2 LL	92	111	5114	0.0080	A	0.0035	C	0.0050	A	0.0010	A	0.0010	A	0.0035	A

Table A.49 POJ-PU-74-TH maximum crack widths in mm for north face of joint

Load Step	North Joint	Ri kN	Ro kN	Moment kN-m	1 mm		2 mm		3 mm		4 mm		5 mm		6 mm		7 mm	
10	DL/2	146	146	178.4														
20	Dead Load	293	293	357.4	0.08	A	0.03	A										
27	DL+1/2 LL	318	344	411.7	0.10	A	0.06	A										
34	Service	343	399	468.9	0.13	A	0.13	A										
35	Dead Load	293	293	357.4	0.10	A	0.10	A										
42	DL+1/2 LL	318	344	411.7	0.11	A	0.10	A										
49	Service	343	399	468.9	0.14	A	0.11	A										
60	DL+2 LL	409	496	577.9	0.15	A	0.18	A	0.08	A	0.15	A	0.05	A	0.08	B	0.08	B

Table A.50 POJ-PU-74-TH maximum crack widths in (in.) for north face of joint

Load Step	North Joint	Ri (kips)	Ro (kips)	Moment (k-in.)	1 (in.)		2 (in.)		3 (in.)		4 (in.)		5 (in.)		6 (in.)		7 (in.)	
10	DL/2	32.9	32.9	1579														
20	Dead Load	65.9	65.9	3163	0.0030	A	0.0010	A										
27	DL+1/2 LL	71.4	77.4	3643	0.0040	A	0.0025	A										
34	Service	77	89.6	4150	0.0050	A	0.0050	A										
35	Dead Load	65.9	65.9	3163	0.0040	A	0.0040	A										
42	DL+1/2 LL	71.4	77.4	3643	0.0045	A	0.0040	A										
49	Service	77	89.6	4150	0.0055	A	0.0045	A										
60	DL+2 LL	92	111	5114	0.0060	A	0.0070	A	0.0030	A	0.0060	A	0.0020	A	0.0030	B	0.0030	B

Table A.51 POJ-PU-74-TH maximum crack widths in mm for south face of joint

Load Step	South Joint	Ri kN	Ro kN	Moment kN-m	1 mm		2 mm		3 mm		4 mm		5 mm		6 mm		7 mm		8 mm	
10	DL/2	146	146	178.4																
20	Dead Load	293	293	357.4	0.05	A	0.03	A	0.03	A										
27	DL+1/2 LL	318	344	411.7	0.10	A	0.04	A	0.03	A	0.04	A								
34	Service	343	399	468.9	0.13	C	0.06	A	0.05	A	0.08	B	0.06	A						
35	Dead Load	293	293	357.4	0.10	A	0.06	A	0.05	A	0.09	B	0.05	A						
42	DL+1/2 LL	318	344	411.7	0.11	C	0.06	A	0.04	A	0.06	B	0.04	A						
49	Service	343	399	468.9	0.14	A	0.06	A	0.05	A	0.09	A	0.05	A						
60	DL+2 LL	409	496	577.9	0.18	A	0.15	D	0.13	A	0.13	A	0.09	A	0.08	A	0.10	A'	0.05	A

Table A.52 POJ-PU-74-TH maximum crack widths in (in.) for south face of joint

Load Step	South Joint	Ri (kips)	Ro (kips)	Moment (k-in.)	1 (in.)		2 (in.)		3 (in.)		4 (in.)		5 (in.)		6 (in.)		7 (in.)		8 (in.)	
10	DL/2	32.9	32.9	1579																
20	Dead Load	65.9	65.9	3163	0.0020	A	0.0010	A	0.0010	A										
27	DL+1/2 LL	71.4	77.4	3643	0.0040	A	0.0015	A	0.0010	A	0.0015	A								
34	Service	77	89.6	4150	0.0050	C	0.0025	A	0.0020	A	0.0030	B	0.0025	A						
35	Dead Load	65.9	65.9	3163	0.0040	A	0.0025	A	0.0020	A	0.0035	B	0.0020	A						
42	DL+1/2 LL	71.4	77.4	3643	0.0045	C	0.0025	A	0.0015	A	0.0025	B	0.0015	A						
49	Service	77	89.6	4150	0.0055	A	0.0025	A	0.0020	A	0.0035	A	0.0020	A						
60	DL+2 LL	92	111	5114	0.0070	A	0.0060	D	0.0050	A	0.0050	A	0.0035	A	0.0030	A	0.0040	A'	0.0020	A

Table A.53 POJ-PU-74-TH maximum crack widths in mm for north face of pier

Load Step	North Pier	Ri kN	Ro kN	Moment kN-m	1 mm		2 mm		3 mm		4 mm		5 mm	
10	DL/2	146	146	290.0										
20	Dead Load	293	293	580.8										
27	DL+1/2 LL	318	344	663.9	0.03	A	0.04	A						
34	Service	343	399	751.3	0.10	A	0.06	A						
35	Dead Load	293	293	580.8	0.08	A'	0.05	A						
42	DL+1/2 LL	318	344	663.9	0.08	A	0.05	A						
49	Service	343	399	751.3	0.08	A	0.08	A						
60	DL+2 LL	409	496	922.7	0.13	A	0.10	A	0.10	A	0.10	A	0.04	A

Table A.54 POJ-PU-74-TH maximum crack widths in (in.) for north face of pier

Load Step	North Pier	Ri (kips)	Ro (kips)	Moment (k-in.)	1 (in.)		2 (in.)		3 (in.)		4 (in.)		5 (in.)	
10	DL/2	32.9	32.9	2566										
20	Dead Load	65.9	65.9	5140										
27	DL+1/2 LL	71.4	77.4	5875	0.0010	A	0.0015	A						
34	Service	77	89.6	6649	0.0040	A	0.0025	A						
35	Dead Load	65.9	65.9	5140	0.0030	A'	0.0020	A						
42	DL+1/2 LL	71.4	77.4	5875	0.0030	A	0.0020	A						
49	Service	77	89.6	6649	0.0030	A	0.0030	A						
60	DL+2 LL	92	111	8165	0.0050	A	0.0040	A	0.0040	A	0.0040	A	0.0015	A

Table A.55 POJ-PU-74-TH maximum crack widths in mm for south face of pier

Load Step	South Pier	Ri kN	Ro kN	Moment kN-m	1 mm		2 mm		3 mm		4 mm		5 mm	
10	DL/2	146	146	290.0										
20	Dead Load	293	293	580.8	0.03	A	0.04	A	0.03	A				
27	DL+1/2 LL	318	344	663.9	0.05	A	0.04	A	0.05	A	0.03	A		
34	Service	343	399	751.3	0.05	A	0.08	A	0.10	A	0.04	A		
35	Dead Load	293	293	580.8	0.05	A	0.08	A'	0.09	A	0.04	A		
42	DL+1/2 LL	318	344	663.9	0.05	A	0.06	A	0.08	A	0.04	A		
49	Service	343	399	751.3	0.06	A'	0.06	A	0.10	A	0.04	A		
60	DL+2 LL	409	496	922.7	0.17	A	0.10	A	0.17	A	0.09	A	0.06	A

Table A.56 POJ-PU-74-TH maximum crack widths in (in.) for south face of pier

Load Step	South Pier	Ri (kips)	Ro (kips)	Moment (k-in.)	1 (in.)		2 (in.)		3 (in.)		4 (in.)		5 (in.)	
10	DL/2	32.9	32.9	2566										
20	Dead Load	65.9	65.9	5140	0.0010	A	0.0015	A	0.0010	A				
27	DL+1/2 LL	71.4	77.4	5875	0.0020	A	0.0015	A	0.0020	A	0.0010	A		
34	Service	77	89.6	6649	0.0020	A	0.0030	A	0.0040	A	0.0015	A		
35	Dead Load	65.9	65.9	5140	0.0020	A	0.0030	A'	0.0035	A	0.0015	A		
42	DL+1/2 LL	71.4	77.4	5875	0.0020	A	0.0025	A	0.0030	A	0.0015	A		
49	Service	77	89.6	6649	0.0025	A'	0.0025	A	0.0040	A	0.0015	A		
60	DL+2 LL	92	111	8165	0.0065	A	0.0040	A	0.0065	A	0.0035	A	0.0025	A

APPENDIX A

CANTILEVER BENT DESIGN EXAMPLE

Selection of Full-Scale Prototype Superstructure Loads

A review of the substructures supporting the 7.9 m (26 ft) wide entrance-ramp girder indicated that both reinforced concrete and fully-prestressed concrete designs were implemented. In most cases, if the two superstructure loads were positioned on the overhang, and truck clearance beneath the overhang was not a concern, designers used a reinforced concrete design. In areas where the maximum depth of the overhang was restricted, a fully-prestressed design was used. It was clear that only a small difference in the design flexural capacity of the members drove the design away from a reinforced concrete design to the more conservative fully-prestressed design. For these cases, a mixture of high-strength prestressing steel and mild reinforcing steel (partial prestressing) could be used to reduce steel congestion, provide supplemental tensile reinforcement to resist factored loads, and provide good serviceability. It was decided to create a design example for a bent supporting a 7.9 m (26 ft) wide box girder superstructure. A schematic of the bent is presented in Figure A.1.

The design loads shown in Table A.1 were computed for a four span continuous 7.9 m (26 ft) box girder superstructure with spans of 33.5 m (110 ft). The substructure under consideration in this study was the second pier. Because the superstructure was continuous, the support reactions based on a tributary span length were amplified by a 1.10 dead load continuity multiplier and a 1.22 live load continuity multiplier. The multipliers were computed for the lane loading on the bridge superstructure shown in Figure A.2. Lane loads were applied on the box girder cross section as shown in Figure A.3. Inside reactions (nearest the column), Ri, and outside reactions (nearest the overhang tip), Ro, for dead load (DL) and live load plus impact (LL) are listed in Figure A.3. These reactions do not include the continuity multipliers, and were computed using the typical span length of 33.5 m (110 ft). The reactions including continuity multipliers, are listed in Table A.1 for five load cases.

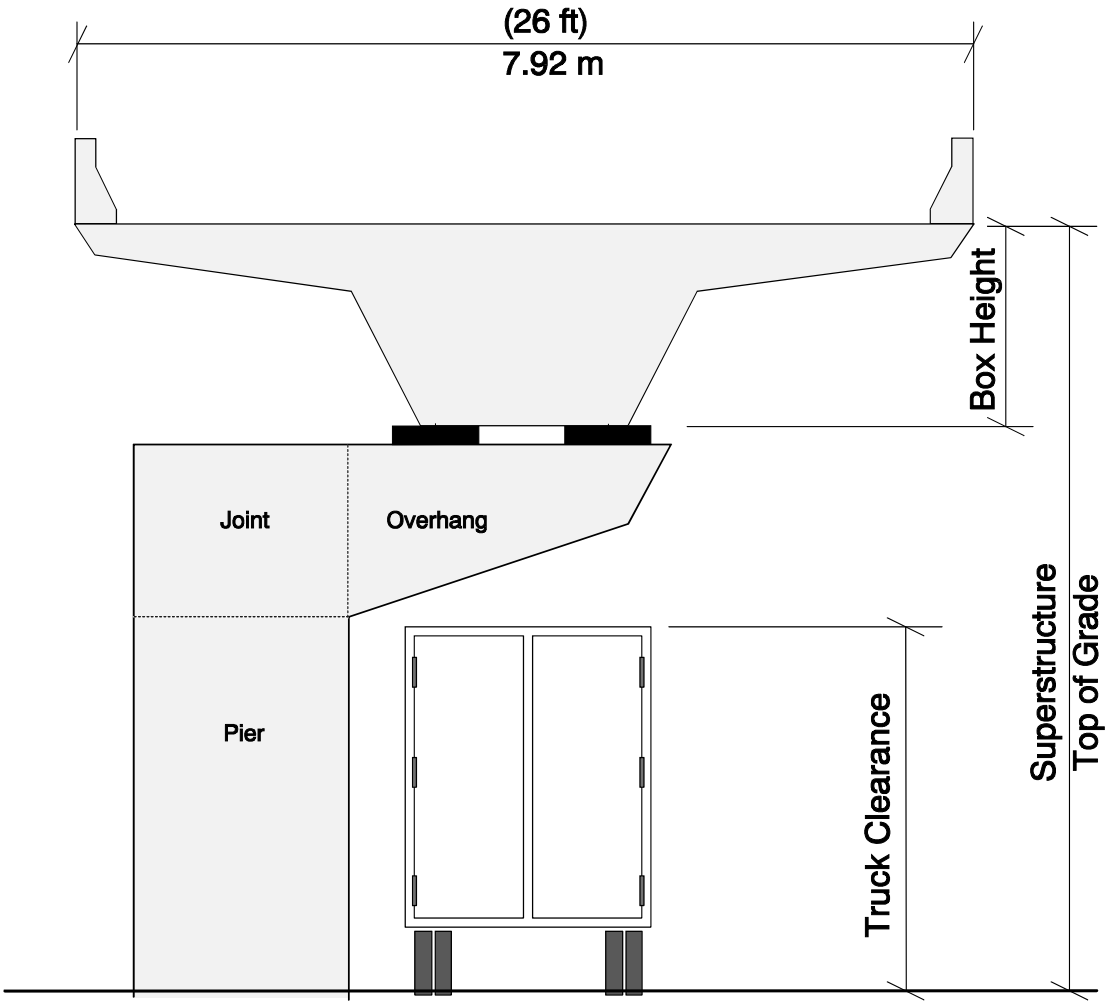

Figure A.1 Substructure Schematic

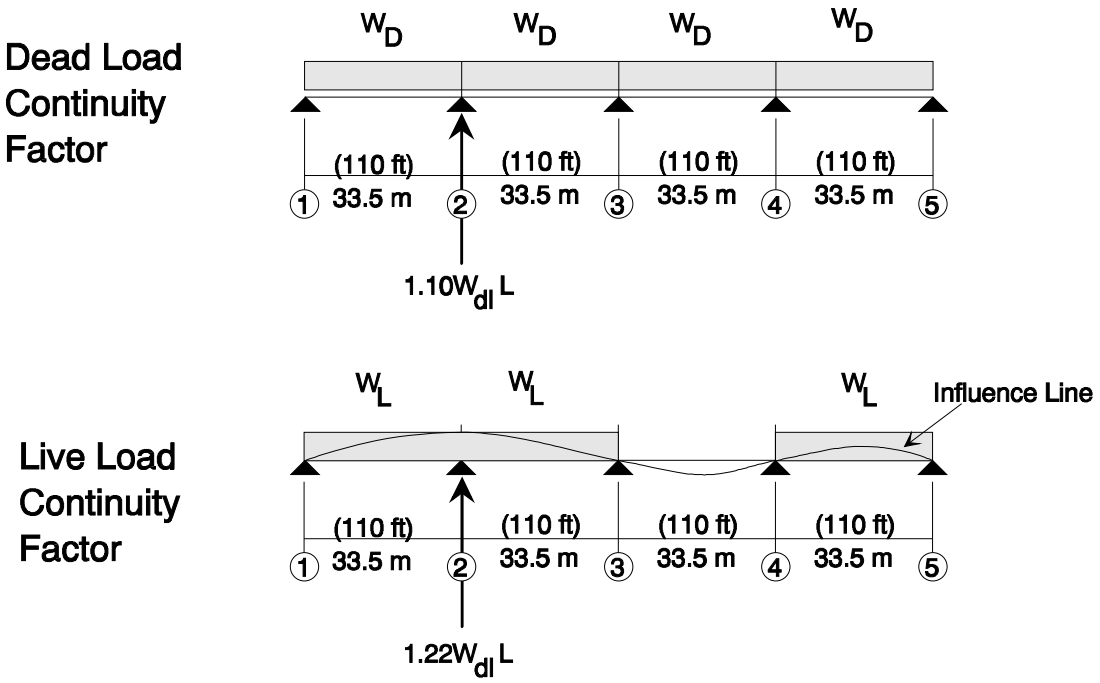

Figure A.2 Pier Location and Continuity Factors

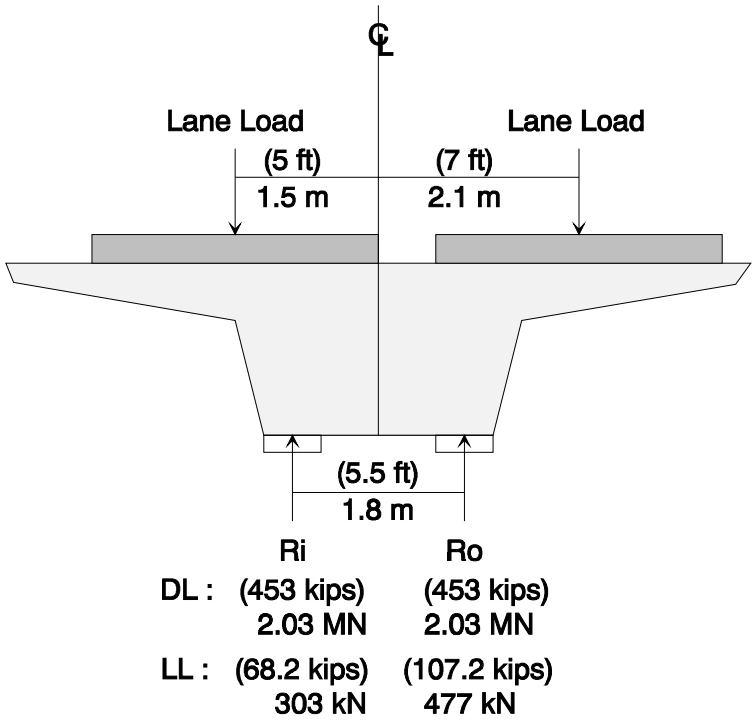

Figure A.3 Full-Scale Prototype Loads Without Continuity Factors
Table A.1 Full-Scale Substructure Loads for a 7.9 m (26 ft) Wide Girder

Load Description	Load Abbreviation	Ri		Ro	
		kN	(kips)	kN	(kips)
Dead Load	DL	2217	498.3	2217	498.3
Dead Load +1/2 Live Load	(DL + 1/2 LL)	2362	531.1	2616	588.1
Service Load	(DL+LL)	2589	582.0	3015	677.8
Dead Load + 2 Live Load	(DL+2LL)	2961	665.7	3813	857.3
Factored Load	(1.3DL + 2.17LL)	3690	829.5	4614	1037.2
Factored Load / Φ	(1.3DL +2.17LL)/Φ	4100	921.7	5126	1152.4

Design of Cantilever Bent using Strut-and-Tie Model Design Procedure

Height and width of the overhang were set equal to the distance between superstructure reaction points (168 cm (66 in.)). Applied loads Ri and Ro were assumed to act 0.5h and 1.5h from the column face, respectively. Bent geometry was established to be similar to the C11-C substructure presented in Chapter 3. Bent geometry is presented in Figure A.4 along with the strut-and-tie model. Self weight of the overhang is included in the strut-and-tie model shown in Figure A.4. Numerical values for some of the strut and ties are presented in Figure A.5.

Selection of Post-Tensioned Reinforcement:

The quantity of post-tensioned steel was provided by two tendons with 19-15 mm (0.6 in.) diameter strands located 24 cm (9.5 in.) from the extreme tension fiber. Nineteen strand tendons were used because they were typical for bents in the San Antonio 'Y' project. The goal was to design an example problem where 75% of the overhang tension tie force was resisted by post-tensioned reinforcement. The location and spacing of the post-tensioning ducts is presented in Figure A.6 and Figure A.7.

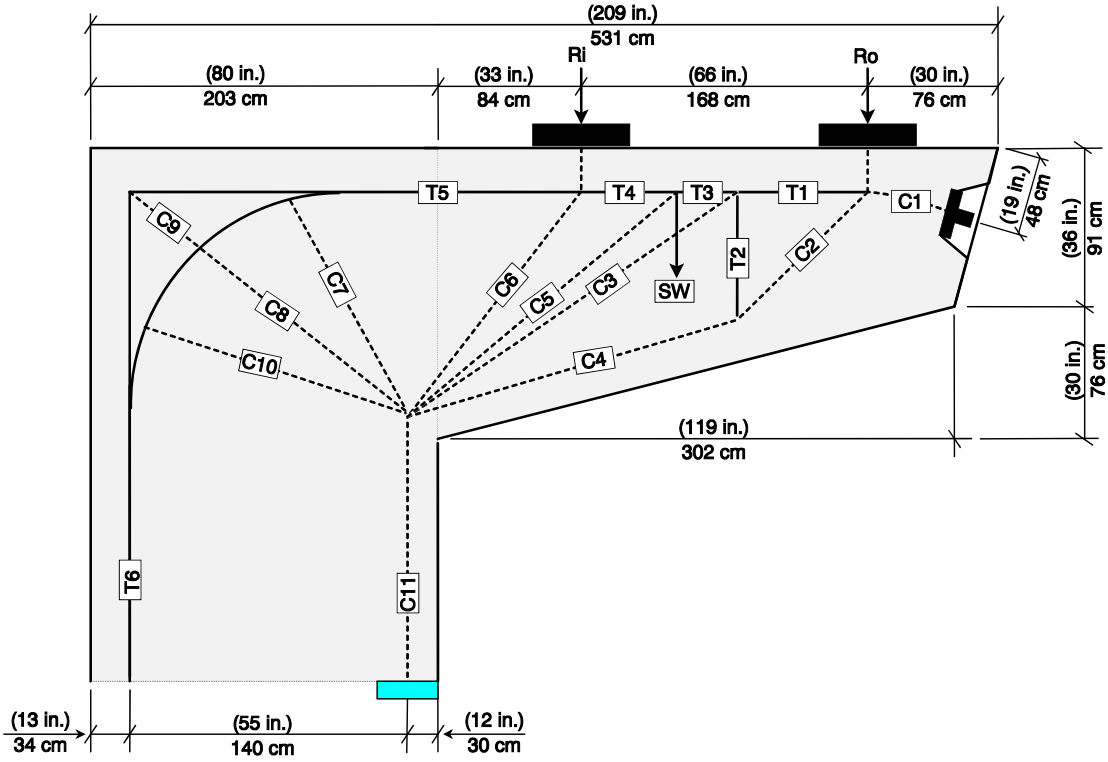

Figure A.4 Strut-and-Tie Model

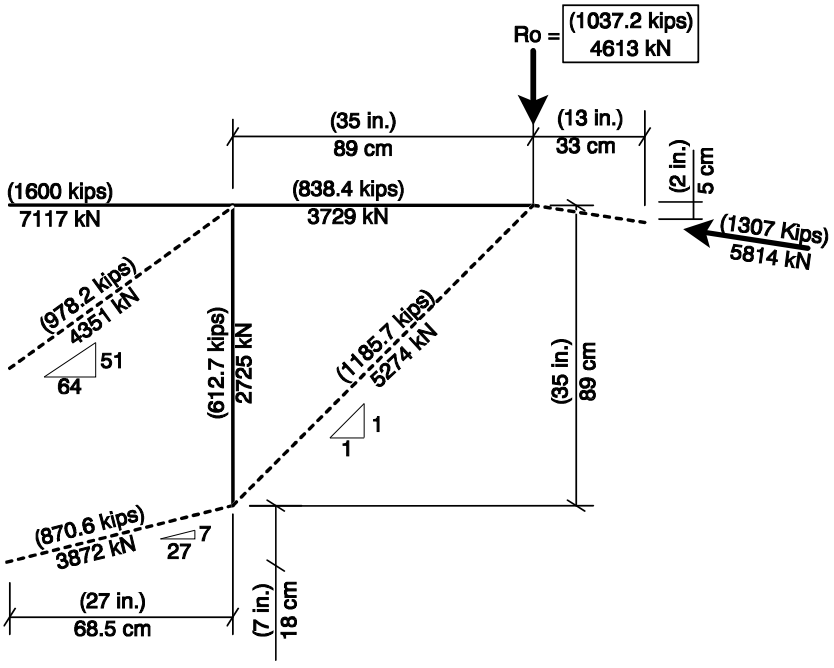

Figure A.5 Details for Strut-and-Tie Model of Vertical Tie T2

Longitudinal Reinforcement in the Overhang:

The amount of longitudinal reinforcement in the overhang was determined using the maximum force in the top cord (Tension Tie T5) of the strut-and-tie model (shown in Figure A.4). The amount of reinforcement required to resist the model factored loads was computed by:

$$T5 \le \Phi\left(A_{ms} f_y + A_{ps} f_{pu}\right) \qquad \textbf{[A-1]}$$

where:

T5	=	STM tension tie force =11462 kN (2577 kips).
Φ	=	Phi factor = 0.9
A_{ms}	=	Area of mild steel primary flexural reinforcement
	=	71 cm^2 (11.0 in^2)
f_y	=	Nominal yield stress of mild reinforcement = 414 MPa (60 ksi)
A_{ps}	=	Area of prestressed primary flexural reinforcement
	=	52.7 cm^2 (8.17 in^2)
f_{pu}	=	Prestressing steel stress at Ultimate Load =1860 MPa (270 ksi).

The quantity of mild steel provided 23 % of the tension tie force (T5), and the quantity of prestressing steel provided 77% of the tension tie force. Based on the strut-and-tie model, there was no need to provide shear-friction reinforcement. Side-face reinforcement was determined using the Frantz and Breen [10] relationship:

$$\rho_{sk} \ge 0.00024(d - 30) \qquad \text{For d} \le \text{(100 in.)} \qquad \textbf{[A-2]}$$

where:

d	=	Full Scale distance from extreme compression fiber to main tensile reinforcement in (in.)
	=	159 cm (62.5 in.)

and :

$$\rho_{sk} = \frac{A_{sk}}{2\,[d/2 \cdot 2d_c]} \qquad \textbf{[A-3]}$$

where:

ρ_{sk}	=	Skin reinforcement ratio = 0.0078
A_{sk}	=	Area of skin reinforcement = 21.6 cm^2 (3.34 in^2)
d_c	=	Distance from skin steel centroid to nearest outside face of the concrete of the model = 8.7 cm (3.43 in.).

Side-face reinforcement consisted of three rows of No. 7 reinforcing bars equally spaced at 30 cm (11.8 in.) on each outer face of the overhang. Quantity of side-face

reinforcement was computed to be 23 cm^2 (3.6 in^2) and was slightly greater than required by Eq. A-3. Details of the longitudinal overhang reinforcement at the cross section adjacent to the pier are shown in Figure A.7.

Transverse Reinforcement in Overhang:

Only one vertical tie was considered in the STM for the overhang. The quantity of transverse reinforcement required to resist the tension tie force (T2) of 2725 kN (612.7 kips) (shown in Figure A.5) was computed using:

$$T2 \le \Phi\left(A_{vs} f_y + 1\sqrt{f_c'}\ b_w d\right) \qquad \textbf{[A-4]}$$

where:

T2	=	STM tie force = (612.7 kips) 2725 kN
Φ	=	0.85
A_{vs}	=	Total area of required shear reinforcement = (10.75 in^2) 69.3 cm^2
f_y	=	Nominal yield stress of shear reinforcement = (60 ksi) 414 MPa
f_c'	=	Nominal concrete compressive stress (psi) = (5000 psi) 34.5 MPa
b_w	=	Beam width (in.) = 66 in. (168 cm)
d	=	Distance from extreme compression fiber to centroid of primary tension reinforcement at the location of the tension tie (in.) = (40 in.) 101.6 cm.

Transverse reinforcement provided consisted of six - No. 6 bar double stirrups spaced at 20.3 cm (8.0 in.) resulting in transverse reinforcement area equal to 68.1 cm^2 (10.6 in^2). Post-tensioning reduced the tension tie force by 881 kN (198 kips), based on the results of the strut-and-tie model. Transverse reinforcement was space uniformly over a distance equal to the effective depth, d, of the section at the tension tie.

Minimum transverse reinforcement was designed in accordance with:

$$s_{max} = \frac{A_v\left(f_y\right)}{50 b_w} \le d/2 \ \textit{and}\ (24\ \textit{in.}) \qquad \textbf{[A-5]}$$

where:

s_{max}	=	Maximum transverse reinforcement spacing (in.) = (20 in.) 51 cm
A_v	=	Area of transverse reinforcement (in^2) = (1.76 in^2) 11.4 cm^2
f_y	=	Nominal yield stress of transverse reinforcement (ksi) = (60 ksi) 414 MPa
b_w	=	Beam width in (in.) = (66 in.) 168 cm^2.

The maximum spacing of 51 cm (20 in.) was determined for an effective depth, d, of 102 cm (40 in.). Transverse reinforcement details are presented in Figure A.6.

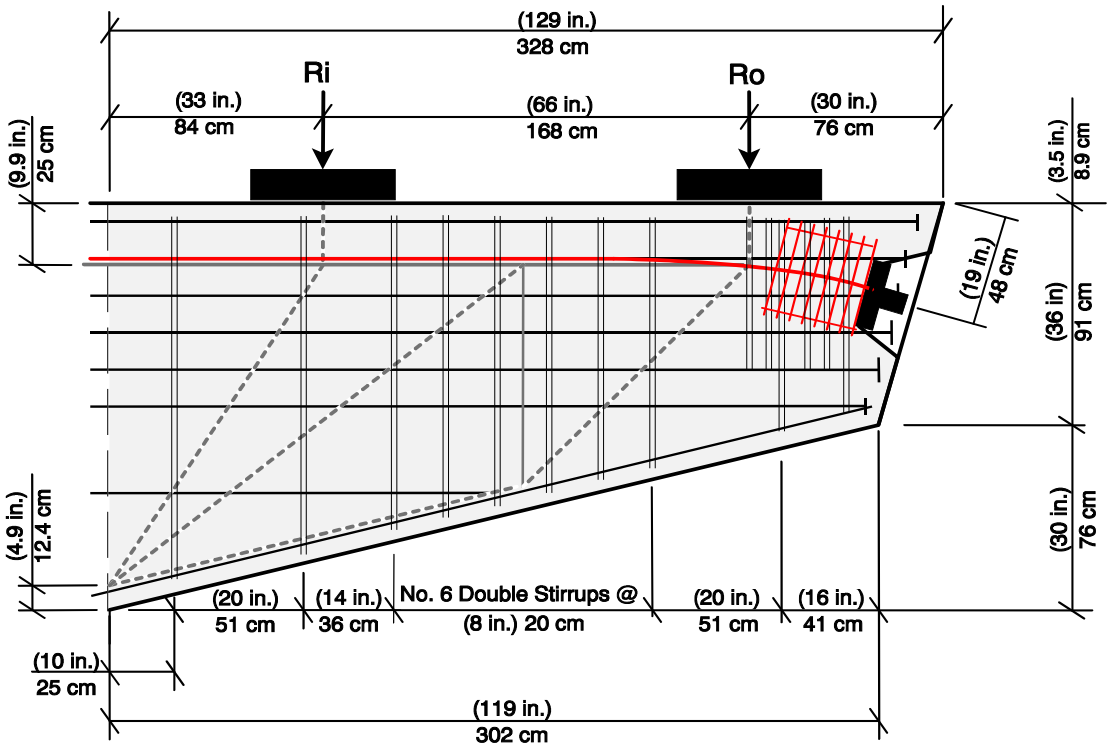

Figure A.6 Transverse Reinforcement Details for Example Problem

Overhang Serviceability Provisions:

Once the amount of side face reinforcement was computed, a cracked-section analysis (considering all longitudinal reinforcement) was conducted to determine steel stresses at service and dead loads. Steel stresses were used to check crack widths and determine the maximum stress range.

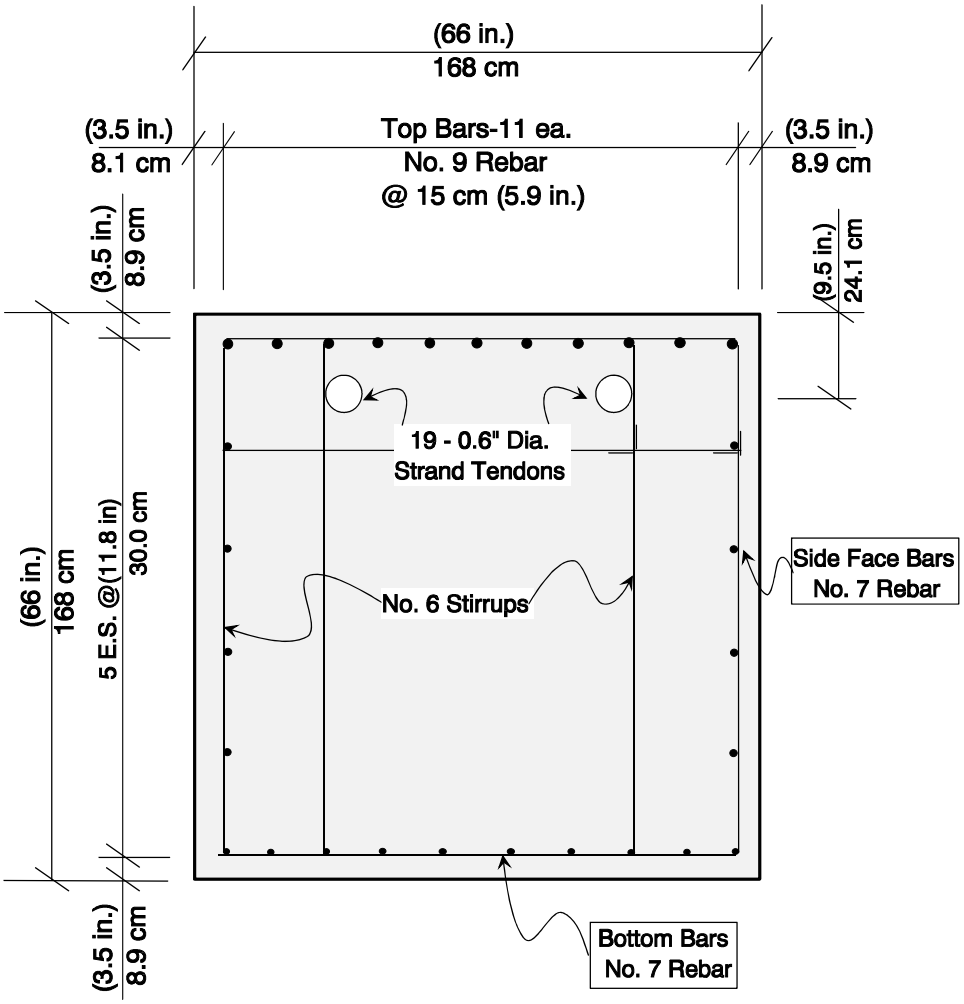

Figure A.7 Overhang Cross Section for Example Problem

Size of crack widths are intended to be controlled by the relationship presented in Eq. A-3. Variables used for the following equation are depicted in Figure A.8, and are defined as follows:

$$f_{sa} \le f_{sl} = \frac{Crk}{\left(d_c A\right)^{1/3}} \qquad \textbf{[A-6]}$$

where:

f_{sa} = Steel tensile stress at a distance d′′ from the extreme tensile fiber = $\varepsilon_{d''}$ (29,000 ksi) = (23.4 ksi) 161.8 MPa

$\varepsilon_{d''}$ = Strain a distance d′′ from the extreme tensile fiber based on a linear strain profile = 0.0008069 (in./in.) mm/mm

f_{sl} = Computed Limiting steel stress (ksi) = 25.3 ksi (174 MPa)

Crk = Crack width limiting factor based on exposure criteria
= 170

d_c = Distance from the extreme tension fiber to the centroid of the closest layer of primary tension reinforcement (in.)
= (3.5 in.) 8.9 cm

A = Area of tension block (2 x d″ x b_w) = (1307 in^2) 8431 cm^2 divided by the number of Prestressing strands and/or mild reinforcing bars located within the tension block [in^2/# bars] = (87.13 in^2/bar)

d″ = Distance from extreme tensile fiber to centroid of tensile reinforcement. (Areas of prestressed reinforcement, A_{ps}, located a distance, d_{ps}, from the extreme tensile fiber and/or areas of mild reinforcement, A_{ms}, located a distance, d_{ms}, from the extreme tensile fiber are considered in the equation.).
= (9.9 in.) 25.1 cm

$$d'' = \frac{\left[\sum (A_{ps}\ f_{su})\, d_{ps} + \sum (A_{ms}\ f_{y})\, d_{ms}\right]}{\left[\sum A_{ps}\ f_{su} + \sum A_{ms}\ f_{y}\right]} \qquad \textbf{[A-7]}$$

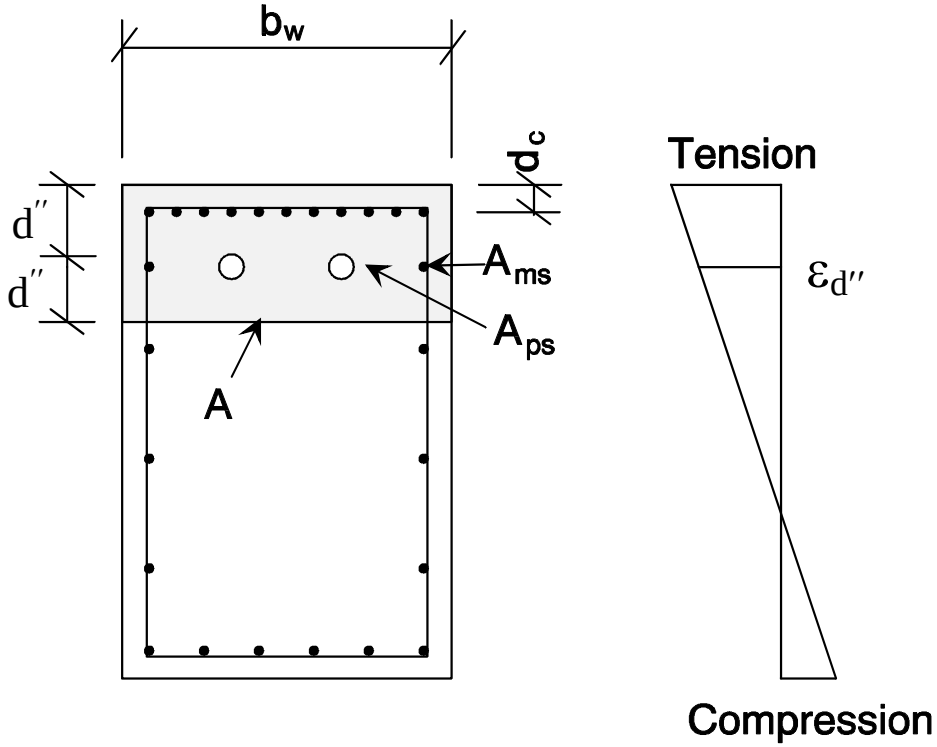

Figure A.8 Identification of Crack-Width Control Variables

Average steel stress due to service loads was computed to be 161 MPa (23.4 ksi), and was less than the stress, f_{sl} , of 174 MPa (25.3ksi) associated with the limiting crack width.

The fatigue stress range was determined by computing the difference in steel stresses in the top-most reinforcing bars resulting from service loads and dead loads. Stress in the top reinforcing bars was 74.5 MPa (10.8 ksi) due to dead loads and 193 MPa (28.0 ksi) due to service loads. The resulting 118.5 MPa (17.2 ksi) stress range was within the allowable fatigue stress range of 137 MPa (19.8 ksi) determined by Eq. 3-31. Peak stress in the reinforcement of 193 MPa (28.0 ksi) due to service loads was less than the 0.6 fy = 248 MPa (36 ksi) limiting steel stress.

Stress in the prestressing tendons was 1000 MPa (160 ksi) due to dead loads and 1187 MPa (174.3 ksi) due to service loads. The resulting 98 MPa (14.3 ksi) stress range was within the allowable fatigue stress range of 100 MPa (14.5 ksi).

Pier Design

Pier longitudinal reinforcement was determined using a strut-and-tie model and cracked-section analysis. The quantity of post-tensioned steel, determined from the overhang design, was two tendons with 19-15 mm (0.6 in.) diameter strands. Because the prestressing tendons were continuous through the specimen, the percentage of prestress in the pier was less than 77% of the total tension tie force.

Longitudinal Reinforcement:

The quantity of longitudinal reinforcement in the pier was based on the tie force, T6 , of the STM illustrated in Figure A.4. The amount of reinforcement required to resist factored loads was computed by:

$$T6 \le \Phi\left(A_{ms} f_y + A_{ps} f_{pu}\right) \qquad \textbf{[A-8]}$$

where:

T6	=	STM tension tie force =11621 kN (2612.7 kips).
Φ	=	Phi factor = 0.8
A_{ms}	=	Area of mild steel primary flexural reinforcement
	=	142 cm^2 (22 in^2)
f_y	=	Nominal yield stress of mild reinforcement = 414 MPa (60 ksi)

A_{ps} = Area of prestressed primary flexural reinforcement
= 52.7 cm^2 (8.17 in^2)
f_{pu} = Prestressing steel stress at Ultimate Load =1860 MPa (270 ksi).

The quantity of mild steel provides 35% of the tension tie force (T6) and the quantity of prestressing steel provided 65 % of the (T6) tension tie force. A cracked-section analysis was conducted to determine steel stresses due to service and dead loads to check crack widths and maximum stress range. The cracked-section analysis was conducted assuming a reduced tendon force, T_x = 850 MPa (123.4 ksi), computed using Eq. 3-42 in Section 3.4.4.4.

The total area of longitudinal mild reinforcement in the pier, 232 cm^2 (36 in^2), provides a column reinforcement ratio of 0.72 %. The design provided a realistic combination of mild reinforcement, based on a potential relaxation of the 1% minimum column reinforcement provision, and prestressing steel, based on strength design.

Transverse Reinforcement:

Transverse reinforcement was detailed using AASHTO LRFD Article 5.10.6.2. Transverse tie spacing was 30.5 cm (12 in.) using No. 4 reinforcement. Tie longitudinal spacing was 30.5 cm (12 in.). Detailing of transverse reinforcement and the distribution of longitudinal reinforcement are shown in Figure A.9.

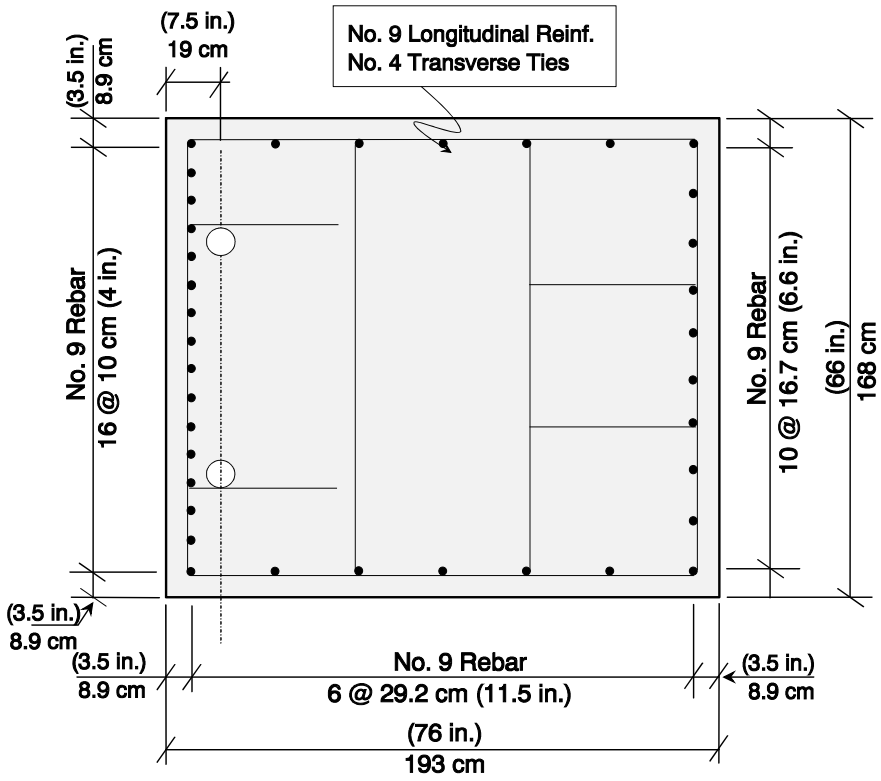

Figure A.9 Pier Reinforcement Details for Example Problem

Serviceability Provisions:

Crack widths in the pier were controlled by the relationship presented in Eq. A-6. The average steel stress due to service loads was computed to be 198.6 MPa (28.8 ksi), which was slightly less than the limiting stress, f_{sl} , of 200 MPa (29.0 ksi) associated with the limiting crack width. In order to satisfy the equation, sixteen No. 9 longitudinal reinforcing bars were used. The clear distance between bars of 7.1 cm (2.8 in.) is small, but it satisfies code required minimum clear spacing of 6.7 cm (2.65 in.) (1.5 times the assumed maximum aggregate size of 4.5 cm (1.75 in.)).

The fatigue stress range was determined by computing the difference in steel stresses in the extreme tensile reinforcing bars resulting from service loads and dead loads. Stress in the reinforcing bars was 135 MPa (19.6 ksi) due to dead loads and 226 MPa (32.8 ksi) due to service loads. The resulting stress range of 91 MPa (13.2 ksi) was within the allowable fatigue stress range of 117 MPa (16.9 ksi) computed using Eq. A-6. Peak stress in the

reinforcement at service loads was 226 MPa (32.8 ksi), which was less than $0.6f_y$ =248 MPa (36 ksi).

Stress in the prestressing tendons was 851 MPa (123.4 ksi) due to dead loads and 932 MPa (135.2 ksi) due to service loads. The resulting stress range in the prestressing of 81 MPa (11.8 ksi) was within the allowable fatigue stress range of 100 MPa (14.5 ksi)

Joint Design

Bar Anchorage:

Use of headed reinforcement in the joint region assured development of longitudinal reinforcement beginning at the face of the steel plate. This facilitated the formation of tension ties through the joint region and a diagonal compression strut between the interlocking heads and opposite (compression) corner of the joint. Continuous post-tensioning through the joint reduced tensile stresses in the joint significantly. In addition to reducing tensile stresses, the post-tensioning steel provided a high-strength tensile tie across any potential diagonal joint crack. The computed specimen strength, using the analysis model described in Section 7.2, was 1.4 times the strength required to resist applied factored loads. Reinforcement details for the joint and complete specimen are illustrated in Figure A.10 and Figure A.11, respectively.

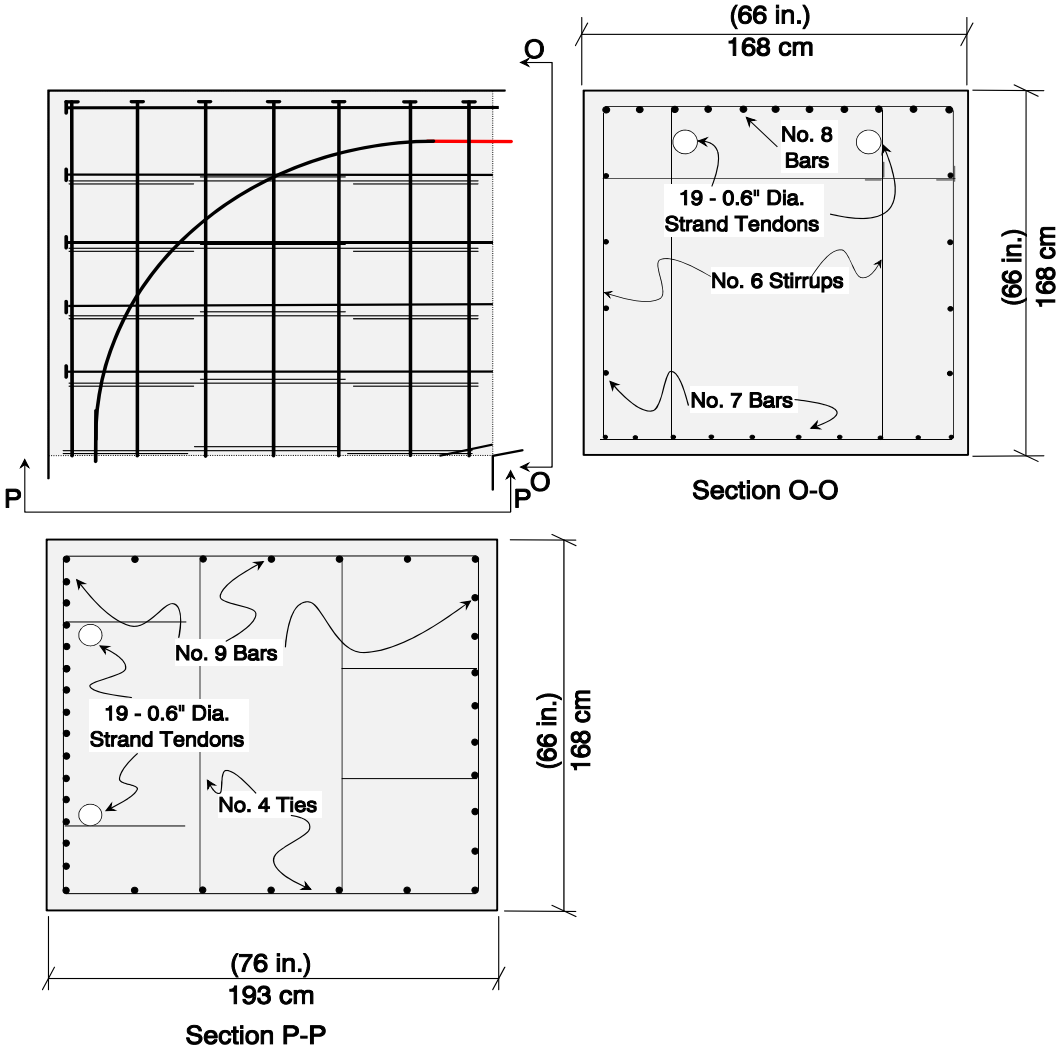

Figure A.10 Joint Reinforcement Details for Example Problem

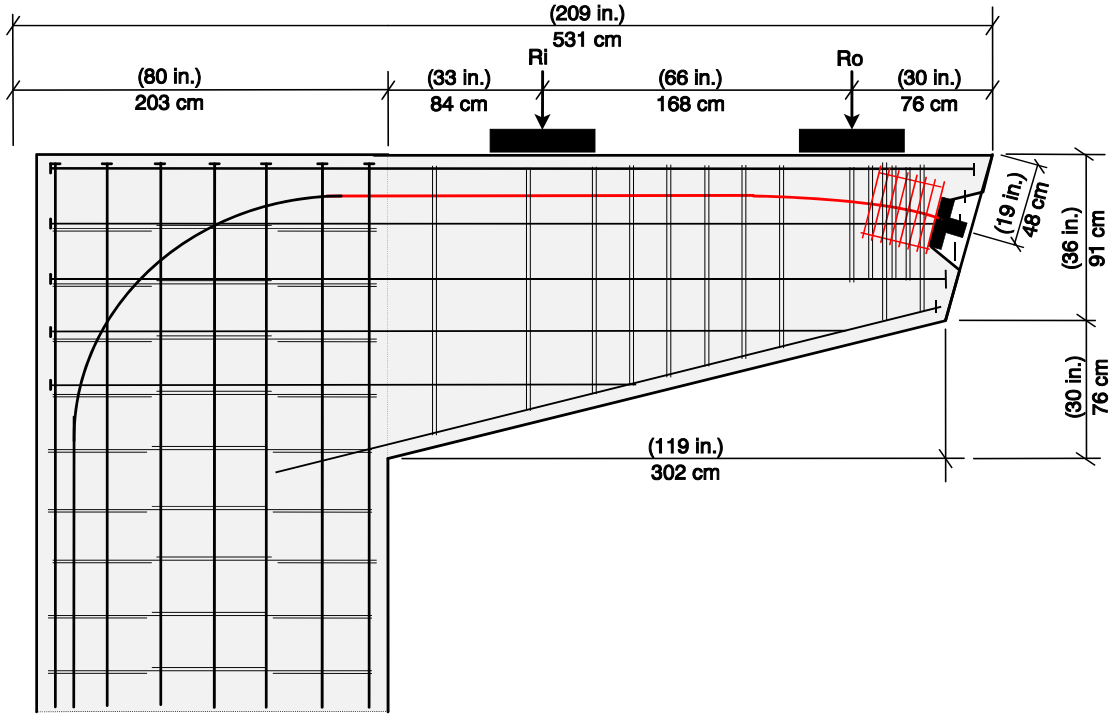

Figure A.11 Overall Reinforcement Details for Example Problem

APPENDIX B

CANTILEVER BENT DESIGN EXAMPLE

SELECTION OF FULL-SCALE PROTOTYPE SUPERSTRUCTURE LOADS

A review of typical substructures supporting the 7.9 m (26 ft) wide entrance-ramp girder indicated that both reinforced concrete and fully-prestressed concrete designs were implemented. In most cases, if the two superstructure loads were positioned on the overhang, and truck clearance beneath the overhang was not a concern, designers used a reinforced concrete design. In areas where the maximum depth of the overhang was restricted, a fully-prestressed design was used. It was clear that only a small difference in the design flexural capacity of the members forced the design away from a reinforced concrete design to the more conservative fully-prestressed design. For these cases, a mixture of high-strength prestressing steel and mild reinforcing steel (partial prestressing) could be used to reduce steel congestion, provide supplemental tensile reinforcement to resist factored loads, and provide good serviceability. In order to demonstrate the design provisions recommended in Chapter 6, a partially prestressed design example was created for a bent supporting a 7.9 m (26 ft) wide box girder superstructure. A schematic of the bent is presented in Figure B.1.

The design loads shown in Table B.1 were computed for a four-span continuous 7.9 m (26 ft) box girder superstructure with spans of 33.5 m (110 ft). The substructure under consideration in this study was the second pier. Because the superstructure was continuous, the support reactions based on a tributary span length were amplified by a 1.10 dead load continuity multiplier and a 1.22 live load continuity multiplier. The multipliers were computed for the lane loading on the bridge superstructure shown in Figure B.2. Lane loads were applied on the box girder cross section as shown in Figure B.3. Inside reactions (nearest the column), Ri, and outside reactions (nearest the overhang tip), Ro, for dead load (DL) and live load plus impact (LL) are listed in Figure B.4. These reactions do not include the continuity multipliers, and were computed using the typical span length of 33.5 m (110 ft). The reactions, including continuity multipliers, are listed in Table B.1 for five load cases.

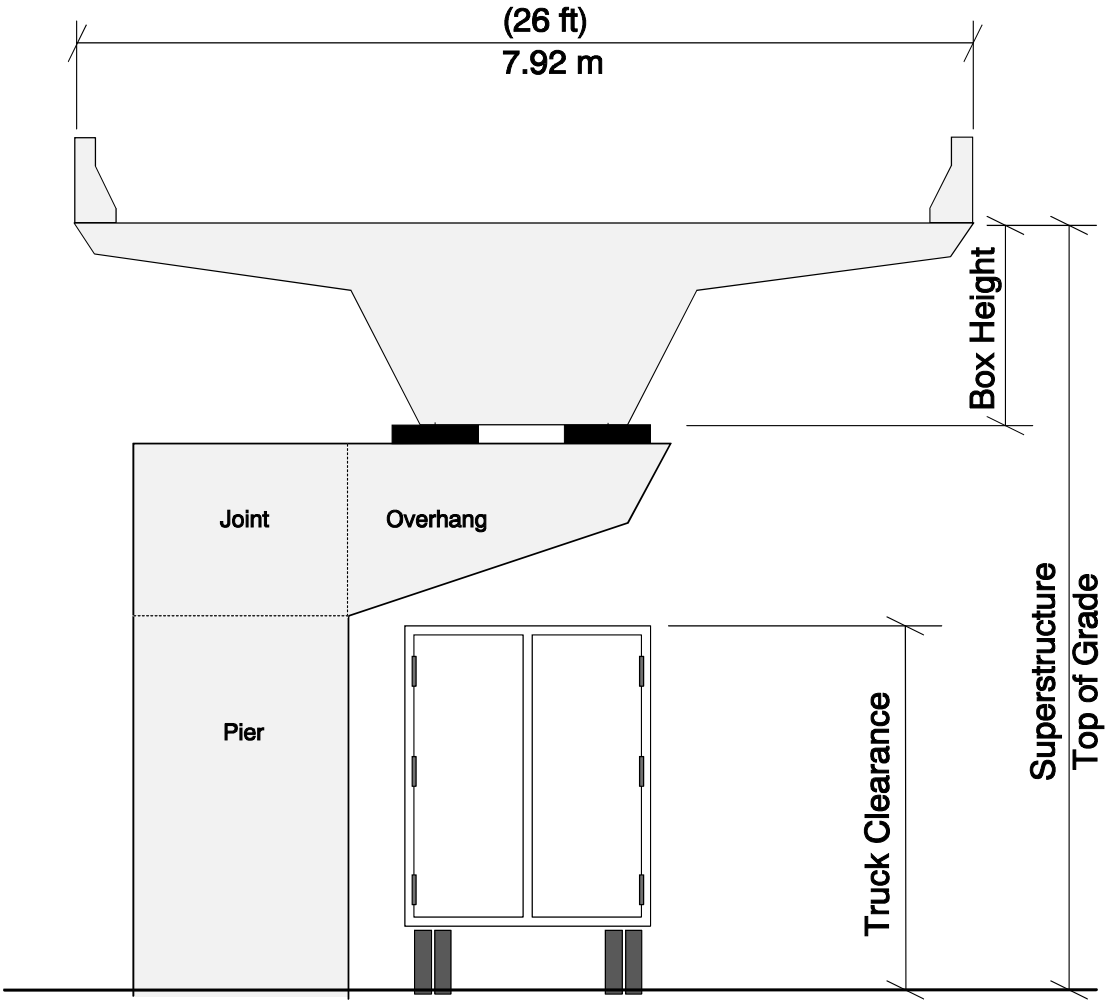

Figure B.1 Substructure Schematic

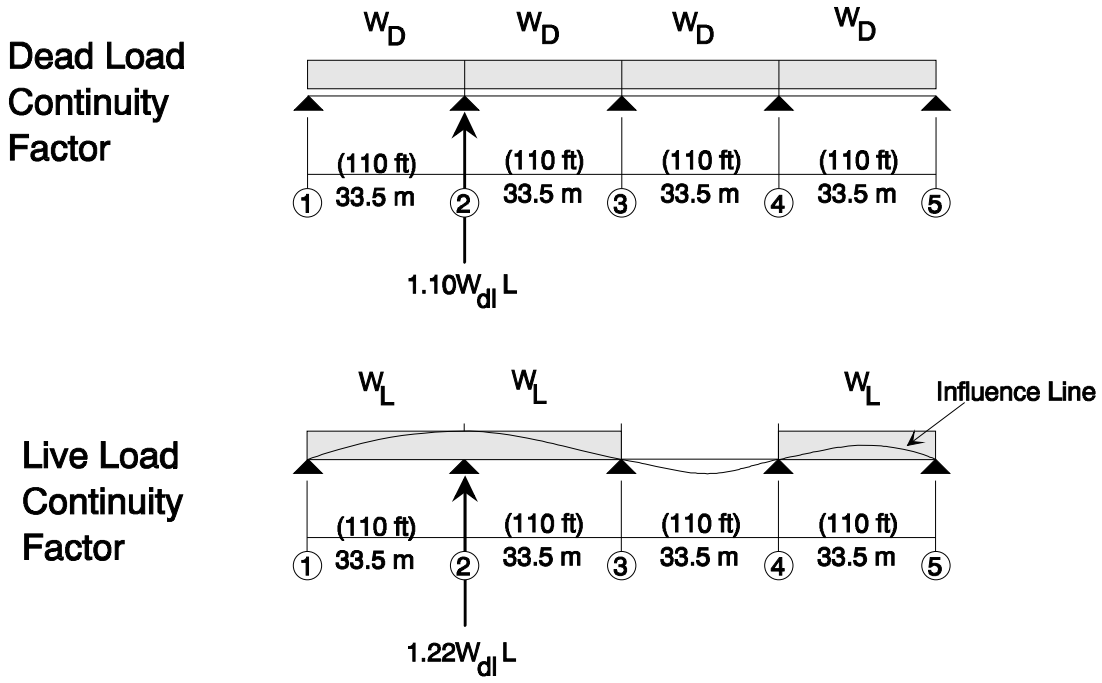

Figure B.2 Pier Location and Continuity Factors

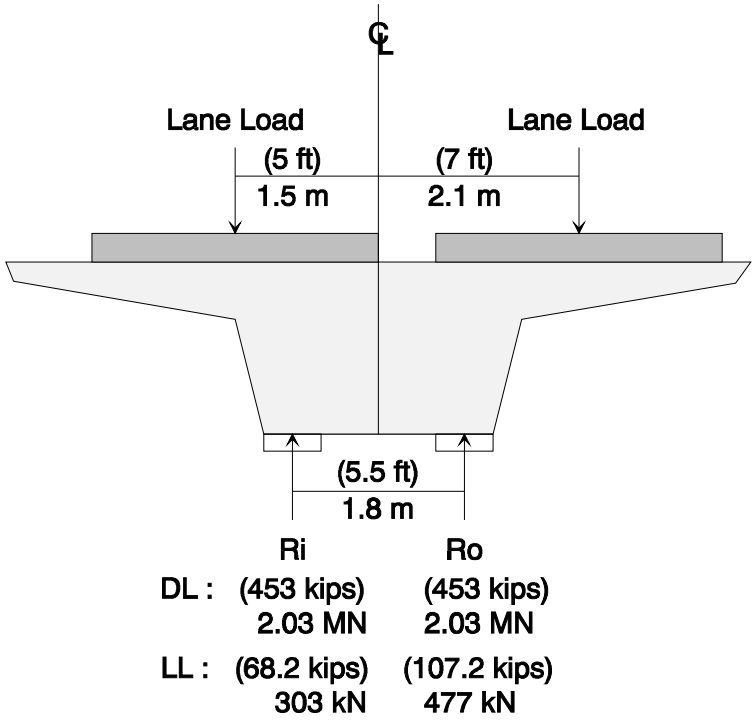

Figure B.3 Full-Scale Prototype Loads Without Continuity Factors

Table B.1 Full-Scale Substructure Loads for a 7.9 m (26 ft) Wide Girder

Load Description	Load Abbreviation	Ri		Ro	
		kN	(kips)	kN	(kips)
Dead Load	DL	2217	498.3	2217	498.3
Dead Load +1/2 Live Load	(DL + 1/2 LL)	2362	531.1	2616	588.1
Service Load	(DL+LL)	2589	582.0	3015	677.8
Dead Load + 2 Live Load	(DL+2LL)	2961	665.7	3813	857.3
Factored Load	(1.3DL + 2.17LL)	3690	829.5	4614	1037.2
Factored Load / Φ	(1.3DL +2.17LL)/Φ	4100	921.7	5126	1152.4

DESIGN OF CANTILEVER BENT USING STRUT-AND-TIE MODEL DESIGN PROCEDURE

Height and width of the overhang were set equal to the distance between superstructure reaction points (168 cm (66 in.)). Applied loads Ri and Ro were assumed to act 0.5h and 1.5h from the column face, respectively. Bent geometry was established to be similar to the C11-C substructure presented in Chapter 3. Bent geometry is presented in Figure B.4 along with the strut-and-tie model. Self weight of the overhang is included in the strut-and-tie model shown in Figure B.4. Numerical values for some of the struts and ties are presented in Figure B.5.

Selection of Post-Tensioned Reinforcement

The quantity of post-tensioned steel was provided by two tendons with 19-15 mm (0.6 in.) diameter strands located 24 cm (9.5 in.) from the extreme tension fiber. Nineteen-strand tendons were used because they were typical for bents in the San Antonio 'Y' project. The goal was to design an example where 75% of the overhang tension tie force was resisted by post-tensioned reinforcement. The location and spacing of the post-tensioning ducts is presented in Figure B.6 and Figure B.7.

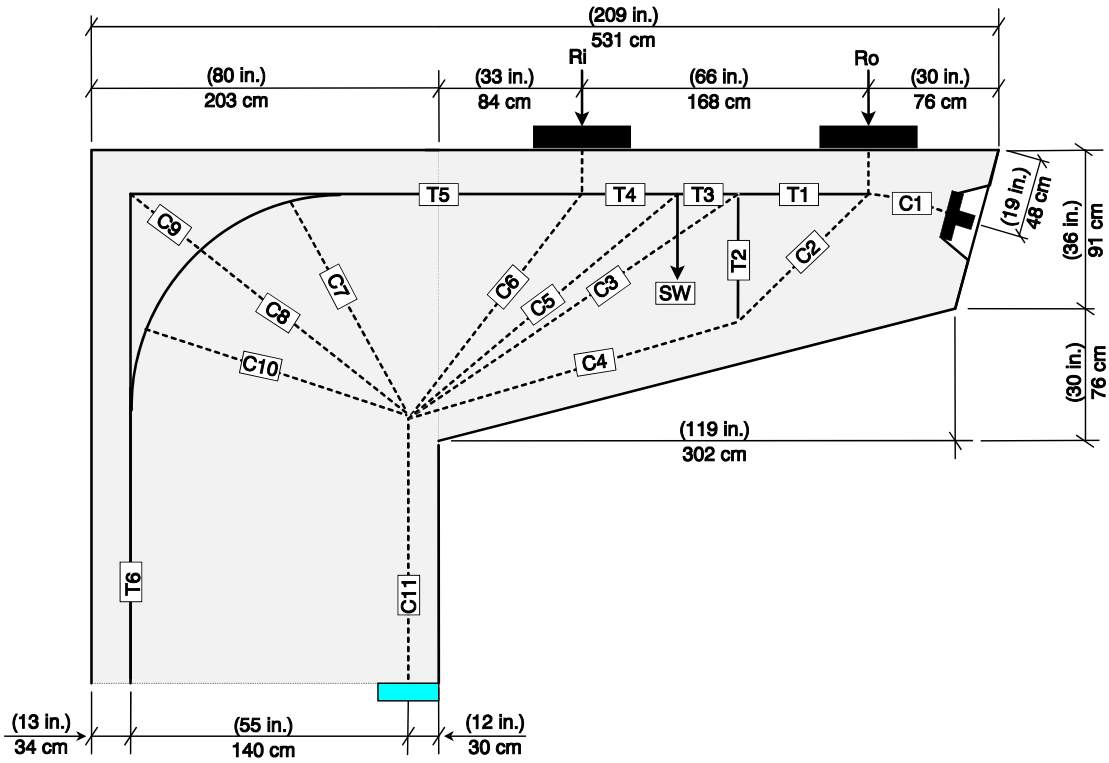

Figure B.4 Strut-and-Tie Model

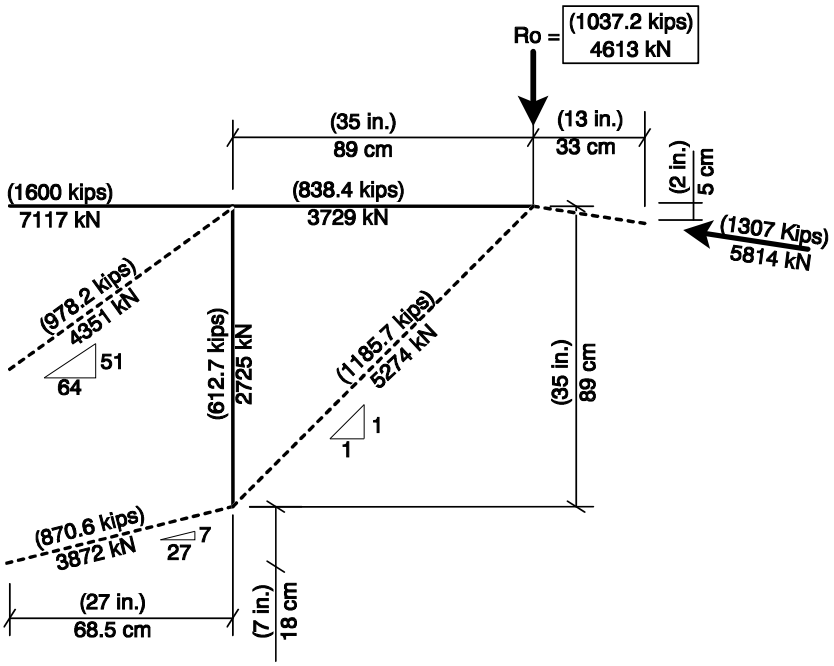

Figure B.5 Details for Strut-and-Tie Model of Vertical Tie T2

Longitudinal Reinforcement in the Overhang

The amount of longitudinal reinforcement in the overhang was determined using the maximum force in the top cord (Tension Tie T5) of the strut-and-tie model (shown in Figure B.4). The amount of reinforcement required to resist the model factored loads was computed by:

$$T5 \le \Phi\left(A_{ms} f_y + A_{ps} f_{pu}\right) \quad \textbf{[B-1]}$$

where:

T5	=	STM tension tie force =11462 kN (2577 kips).
Φ	=	Phi factor = 0.9
A_{ms}	=	Area of mild steel primary flexural reinforcement
	=	71 cm^2 (11.0 in^2)
f_y	=	Nominal yield stress of mild reinforcement = 414 MPa (60 ksi)
A_{ps}	=	Area of prestressed primary flexural reinforcement
	=	52.7 cm^2 (8.17 in^2)
f_{pu}	=	Prestressing steel stress at Ultimate Load =1860 MPa (270 ksi).

The quantity of mild steel provided 23% of the tension tie force (T5), and the quantity of prestressing steel provided 77% of the tension tie force. Based on the strut-and-tie model, there was no need to provide shear-friction reinforcement. Side-face reinforcement was determined using the Frantz and Breen [10] relationship:

$$\rho_{sk} \ge 0.00024(d - 30) \quad \text{For d} \le (100 \text{ in.}) \quad \textbf{[B-2]}$$

where:

d	=	Full Scale distance from extreme compression fiber to main tensile reinforcement in (in.)
	=	159 cm (62.5 in.)

and :

$$\rho_{sk} = \frac{A_{sk}}{2\,[d/2 \cdot 2d_c]} \quad \textbf{[B-3]}$$

where:

ρ_{sk}	=	Skin reinforcement ratio = 0.0078
A_{sk}	=	Area of skin reinforcement = 21.6 cm^2 (3.34 in^2)
d_c	=	Distance from skin steel centroid to nearest outside face of the concrete of the model = 8.7 cm (3.43 in.).

Side-face reinforcement consisted of three rows of No. 7 reinforcing bars equally spaced at 30 cm (11.8 in.) on each outer face of the overhang. Quantity of side-face reinforcement was computed to be 23 cm^2 (3.6 in^2) and was slightly greater than required by Eq. B-3. Details of the longitudinal overhang reinforcement at the cross section adjacent to the pier are shown in Figure B.7.

Transverse Reinforcement in Overhang

Only one vertical tie was considered in the STM for the overhang. The quantity of transverse reinforcement required to resist the tension tie force (T2) of 2725 kN (612.7 kips) (shown in Figure B.5) was computed using:

$$T2 \le \Phi\left(A_{vs} f_y + 1\sqrt{f_c'}\; b_w d\right) \quad \textbf{[B-4]}$$

where:

T2	=	STM tie force = (612.7 kips) 2725 kN
Φ	=	0.85
A_{vs}	=	Total area of required shear reinforcement = (10.75 in^2) 69.3 cm^2
f_y	=	Nominal yield stress of shear reinforcement = (60 ksi) 414 MPa
f_c'	=	Nominal concrete compressive stress (psi) = (5000 psi) 34.5 MPa
b_w	=	Beam width (in.) = 66 in. (168 cm)
d	=	Distance from extreme compression fiber to centroid of primary

tension reinforcement at the location of the tension tie (in.)
= (40 in.) 101.6 cm.

Transverse reinforcement provided consisted of six - No. 6 bar double stirrups spaced at 20.3 cm (8.0 in.) resulting in transverse reinforcement area equal to 68.1 cm^2 (10.6 in^2). Post-tensioning reduced the tension tie force by 881 kN (198 kips), based on the results of the strut-and-tie model. Transverse reinforcement was spaced uniformly over a distance equal to the effective depth, d, of the section at the tension tie.

Minimum transverse reinforcement was designed in accordance with:

$$s_{max} = \frac{A_v(f_y)}{50 b_w} \le d/2 \text{ and } (24 \text{ in.}) \qquad \textbf{[B-5]}$$

where:

s_{max} = Maximum transverse reinforcement spacing (in.) = (20 in.) 51 cm
A_v = Area of transverse reinforcement (in^2) = (1.76 in^2) 11.4 cm^2
f_y = Nominal yield stress of transverse reinforcement (ksi) = (60 ksi) 414 MPa
b_w = Beam width in (in.) = (66 in.) 168 cm^2.

The maximum spacing of 51 cm (20 in.) was determined for an effective depth, d, of 102 cm (40 in.). Transverse reinforcement details are presented in Figure B.6.

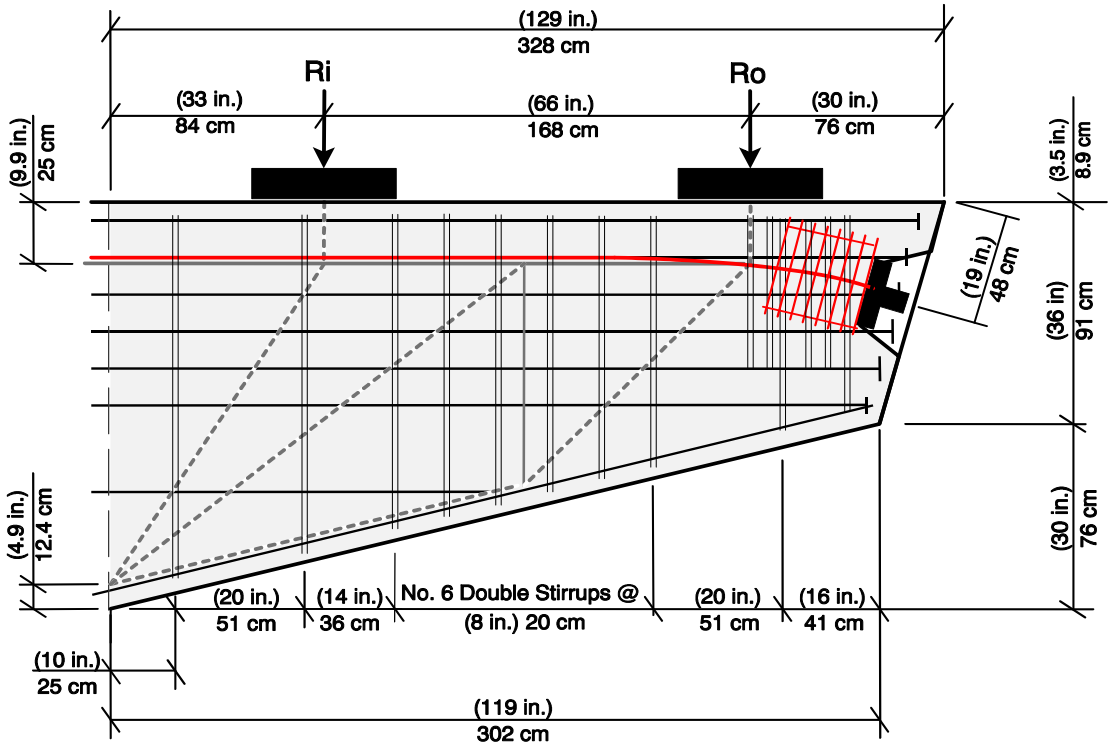

Figure B.6 Transverse Reinforcement Details for Example Problem

Overhang Serviceability Provisions

Once the amount of side face reinforcement was computed, a cracked-section analysis (considering all longitudinal reinforcement) was conducted to determine steel stresses at service and dead loads. Steel stresses were used to check crack widths and determine the maximum stress range.

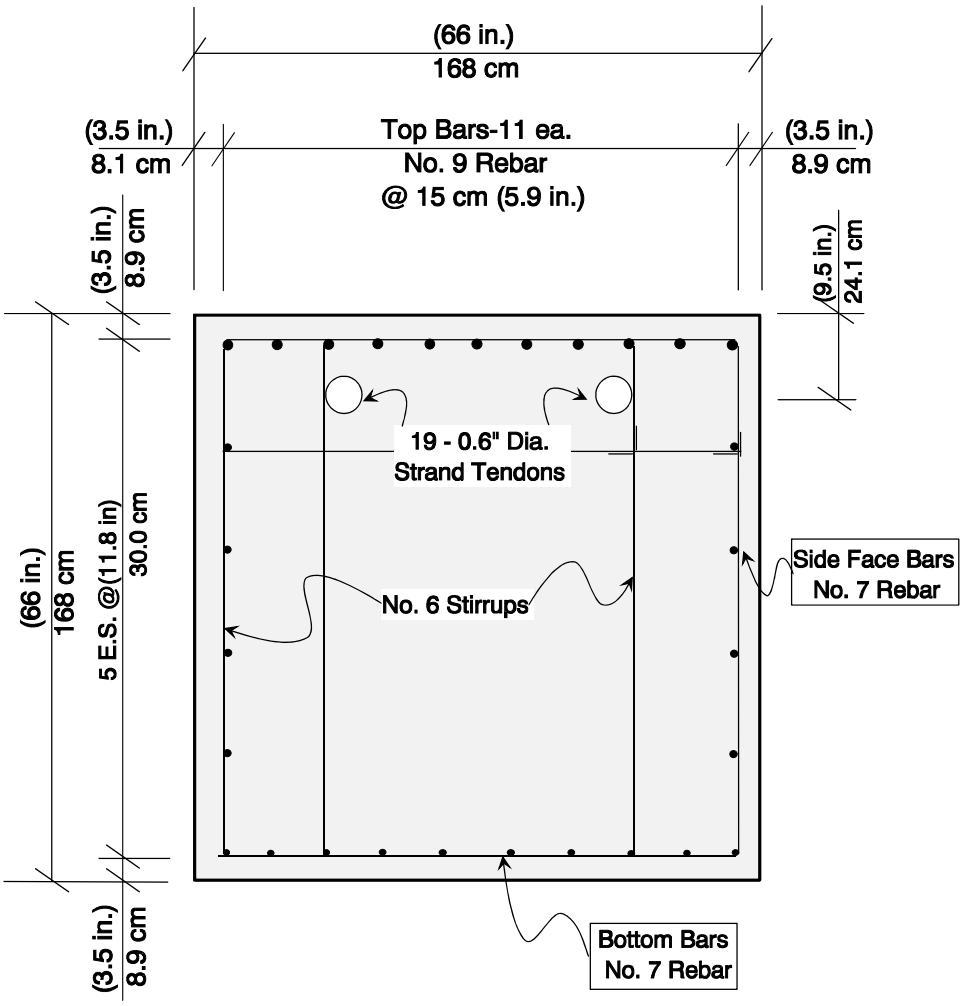

Figure B.7 Overhang Cross Section for Example Problem

Size of crack widths is intended to be controlled by the relationship presented in Eq. B-3. Variables used for the following equation are depicted in Figure B.8, and are defined as follows:

$$f_{sa} \le f_{sl} = \frac{Crk}{(d_c A)^{1/3}} \qquad \textbf{[B-6]}$$

where:

f_{sa}	=	Steel tensile stress at a distance d″ from the extreme tensile fiber = $\varepsilon_{d''}$ (29,000 ksi) = (23.4 ksi) 161.8 MPa
$\varepsilon_{d''}$	=	Strain a distance d″ from the extreme tensile fiber based on a linear strain profile = 0.0008069 (in./in.) mm/mm
f_{sl}	=	Computed Limiting steel stress (ksi) = 25.3 ksi (174 MPa)
Crk	=	Crack width limiting factor based on exposure criteria = 170
d_c	=	Distance from the extreme tension fiber to the centroid of the closest layer of primary tension reinforcement (in.) = (3.5 in.) 8.9 cm
A	=	Area of tension block (2 x d″ x b_w) = (1307 in^2) 8431 cm^2 divided by the number of Prestressing strands and/or mild reinforcing

bars located within the tension block [in^2/# bars] = (87.13 in^2/bar)

d″ = Distance from extreme tensile fiber to centroid of tensile reinforcement. (Areas of prestressed reinforcement, A_{ps}, located a distance, d_{ps}, from the extreme tensile fiber and/or areas of mild reinforcement, A_{ms}, located a distance, d_{ms}, from the extreme tensile fiber are considered in the equation.).
= (9.9 in.) 25.1 cm

$$d'' = \frac{\left[\sum (A_{ps}\ f_{su})\, d_{ps} + \sum (A_{ms}\ f_y)\, d_{ms}\right]}{\left[\sum A_{ps}\ f_{su} + \sum A_{ms}\ f_y\right]} \qquad \textbf{[B-7]}$$

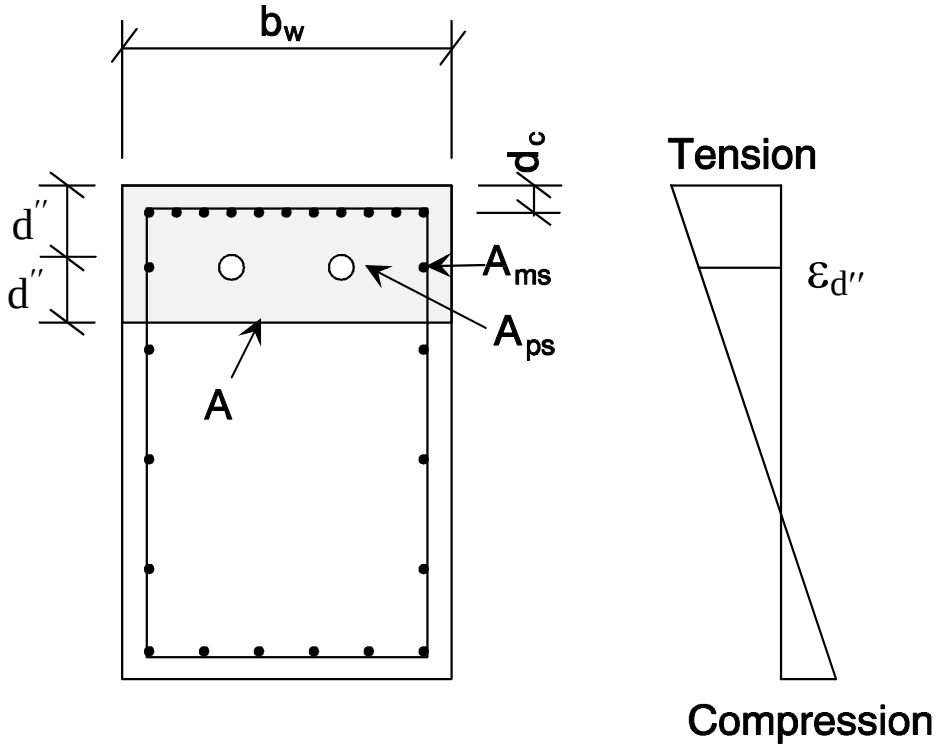

Figure B.8 Identification of Crack-Width Control Variables

Average steel stress due to service loads was computed to be 161 MPa (23.4 ksi), and was less than the stress, f_{sl}, of 174 MPa (25.3ksi) associated with the limiting crack width.

The fatigue stress range was determined by computing the difference in steel stresses in the top-most reinforcing bars resulting from service loads and dead loads. Stress in the top reinforcing bars was 74.5 MPa (10.8 ksi) due to dead loads and 193 MPa (28.0 ksi) due to service loads. The resulting 118.5 MPa (17.2 ksi) stress range was within the allowable fatigue stress range of 137 MPa (19.8 ksi) determined by Eq. 3-31. Peak stress in the reinforcement of 193 MPa (28.0 ksi) due to service loads was less than the 0.6 fy = 248 MPa (36 ksi) limiting steel stress.

Stress in the prestressing tendons was 1000 MPa (160 ksi) due to dead loads and 1187 MPa (174.3 ksi) due to service loads. The resulting 98 MPa (14.3 ksi) stress range was within the allowable fatigue stress range of 100 MPa (14.5 ksi).

PIER DESIGN

Pier longitudinal reinforcement was determined using a strut-and-tie model and cracked-section analysis. The quantity of post-tensioned steel, determined from the overhang design, was two tendons with 19-15 mm (0.6 in.) diameter strands. Because the prestressing tendons were continuous through the specimen, the percentage of prestress in the pier provided less than 77% of the total tension tie force.

Longitudinal Reinforcement

The quantity of longitudinal reinforcement in the pier was based on the tie force, T6 , of the STM illustrated in Figure B.4. The amount of reinforcement required to resist factored loads was computed by:

$$T6 \le \Phi\left(A_{ms} f_y + A_{ps} f_{pu}\right) \qquad \textbf{[B-8]}$$

where:

T6	=	STM tension tie force =11621 kN (2612.7 kips).
Φ	=	Phi factor = 0.8
A_{ms}	=	Area of mild steel primary flexural reinforcement
	=	142 cm^2 (22 in^2)
f_y	=	Nominal yield stress of mild reinforcement = 414 MPa (60 ksi)
A_{ps}	=	Area of prestressed primary flexural reinforcement
	=	52.7 cm^2 (8.17 in^2)
f_{pu}	=	Prestressing steel stress at Ultimate Load =1860 MPa (270 ksi).

The quantity of mild steel provides 35% of the tension tie force (T6) and the quantity of prestressing steel provided 65% of the (T6) tension tie force. A cracked-section analysis was conducted to determine steel stresses due to service and dead loads to check crack widths and maximum stress range. The cracked-section analysis was conducted assuming a reduced tendon force, T_x = 850 MPa (123.4 ksi), computed using Eq. 3-42 in Section 3.4.4.4.

The total area of longitudinal mild reinforcement in the pier, 232 cm^2 (36 in^2), provides a column reinforcement ratio of 0.72%. The design provided a realistic combination of mild reinforcement, based on a potential relaxation of the 1% minimum column reinforcement provision, and prestressing steel, based on strength design.

Transverse Reinforcement

Transverse reinforcement was detailed using AASHTO LRFD Article 5.10.6.2. Transverse tie spacing was 30.5 cm (12 in.) using No. 4 reinforcement. Tie longitudinal spacing was 30.5 cm (12 in.). Detailing of transverse reinforcement and the distribution of longitudinal reinforcement are shown in Figure B.9.

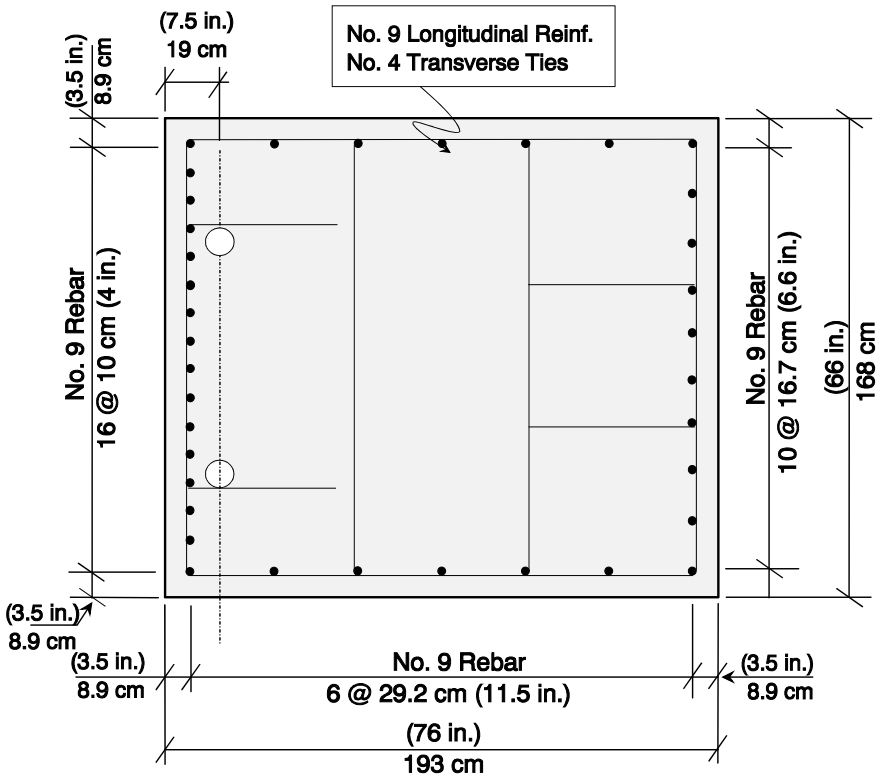

Figure B.9 Pier Reinforcement Details for Example Problem

Serviceability Provisions

Crack widths in the pier were controlled by the relationship presented in Eq. B-6. The average steel stress due to service loads was computed to be 198.6 MPa (28.8 ksi), which was slightly less than the limiting stress, f_{sl}, of 200 MPa (29.0 ksi) associated with the limiting crack width. In order to satisfy the equation, sixteen No. 9 longitudinal reinforcing bars were used. The clear distance between bars of 7.1 cm (2.8 in.) is small, but it satisfies code required minimum clear spacing of 6.7 cm (2.65 in.) (1.5 times the assumed maximum aggregate size of 4.5 cm (1.75 in.)).

The fatigue stress range was determined by computing the difference in steel stresses in the extreme tensile reinforcing bars resulting from service loads and dead loads. Stress in the reinforcing bars was 135 MPa (19.6 ksi) due to dead loads and 226 MPa (32.8 ksi) due to service loads. The resulting stress range of 91 MPa (13.2 ksi) was within the allowable fatigue stress range of 117 MPa (16.9 ksi) computed using Eq. B-6. Peak stress in the reinforcement at service loads was 226 MPa (32.8 ksi), which was less than $0.6f_y$ =248 MPa (36 ksi).

Stress in the prestressing tendons was 851 MPa (123.4 ksi) due to dead loads and 932 MPa (135.2 ksi) due to service loads. The resulting stress range in the prestressing of 81 MPa (11.8 ksi) was within the allowable fatigue stress range of 100 MPa (14.5 ksi).

JOINT DESIGN

Bar Anchorage

Use of headed reinforcement in the joint region assured development of longitudinal reinforcement beginning at the face of the steel plate. This facilitated the formation of tension ties through the joint region and a diagonal compression strut between the interlocking heads and opposite (compression)

corner of the joint. Continuous post-tensioning through the joint reduced tensile stresses in the joint significantly. In addition to reducing tensile stresses, the post-tensioning steel provided a high-strength tensile tie across any potential diagonal joint crack. The computed specimen strength was 1.4 times the strength required to resist applied factored loads. Reinforcement details for the joint and complete specimen are illustrated in Figure B.10 and Figure B.11, respectively.

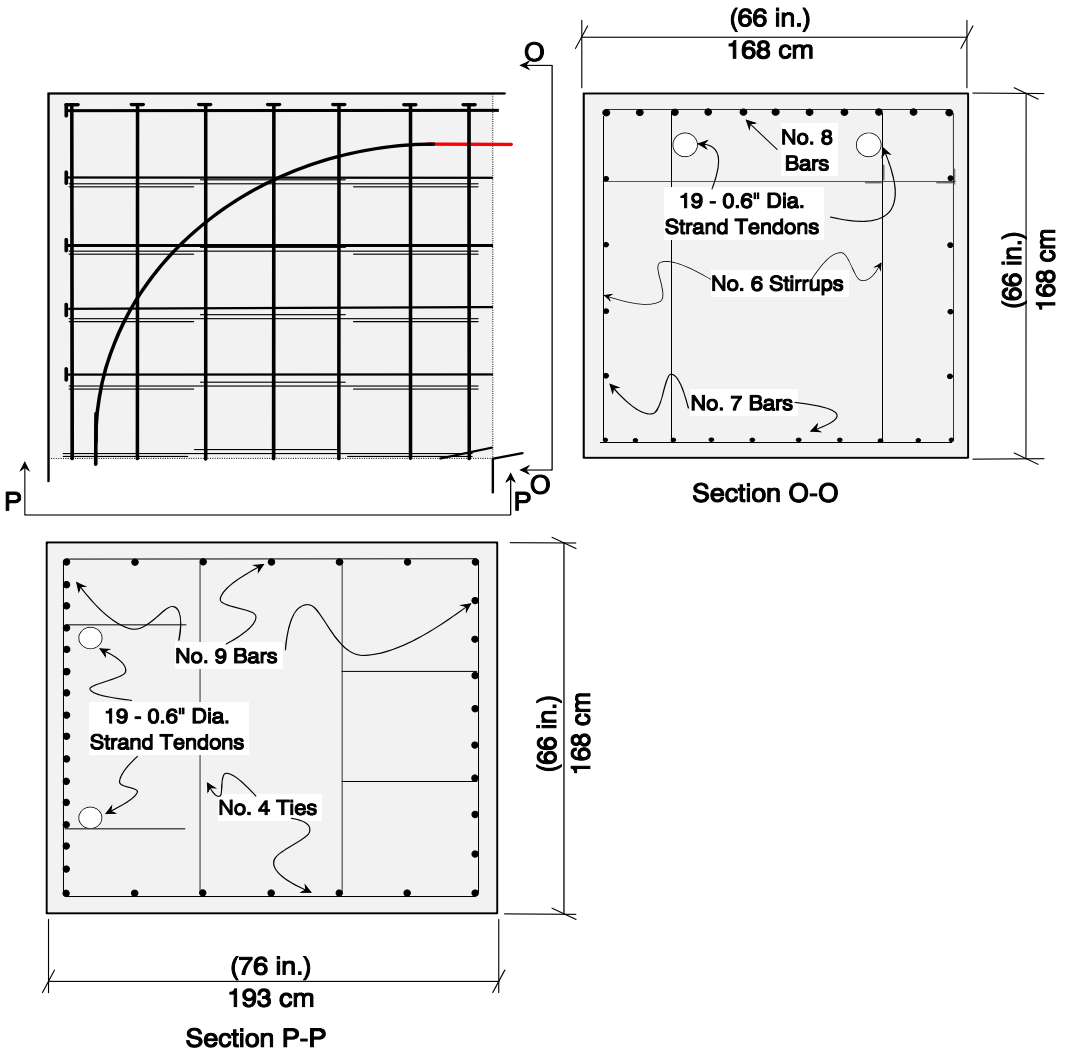

Figure B.10 Joint Reinforcement Details for Example Problem

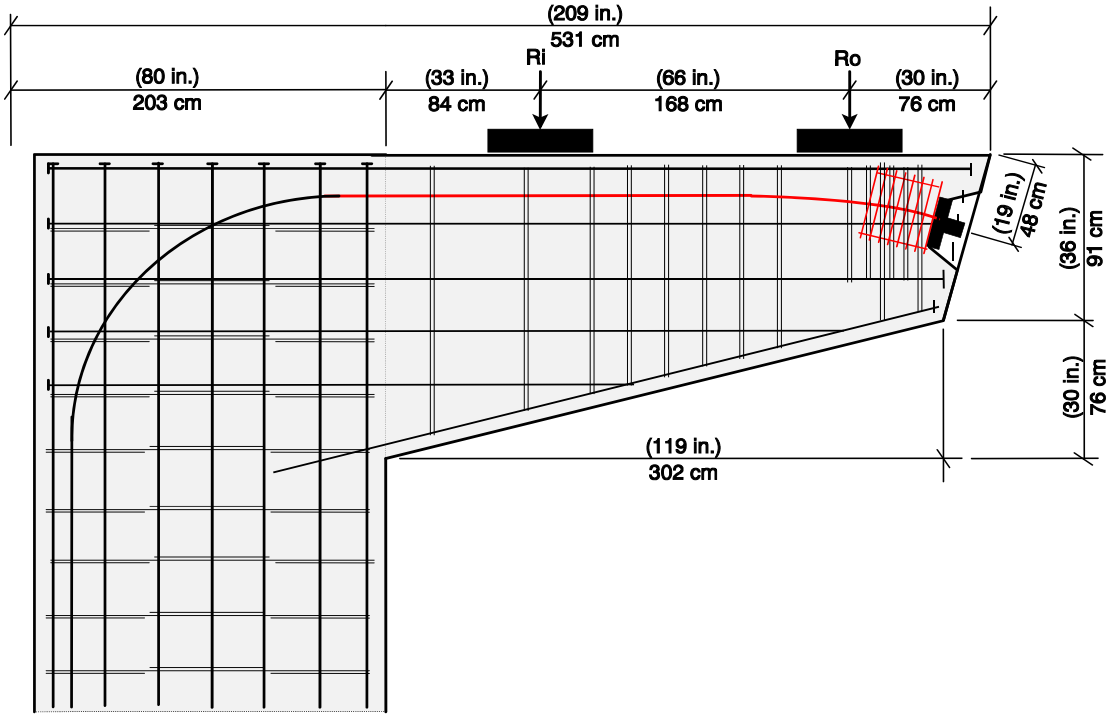

Figure B.11 Overall Reinforcement Details for Example Problem

REFERENCES

[1] American Association of State Highway Transportation Officials (AASHTO), Standard Specifications for Highway Bridges, Thirteenth Edition, 1983.

[2] Bergmeister, K, Breen, J.E., Jirsa, J.O., and Kreger, M.E., "Detailing for Structural Concrete," Research Report 1127-3F Center for Transportation Research, The University of Texas at Austin, October 1990.

[3] Armstrong, S.D., "Design and Behavior of Large Cantilever Overhangs with Combinations of Prestressed and Non-Prestressed Reinforcement," Unpublished Masters Thesis, The University of Texas at Austin, August 1994.

[4] Salas Pereira, R.M., "Behavior of Structural Concrete Cantilever Piers Using T-Headed Reinforcing Bars and Varied Prestressing Design Criteria," Unpublished Masters Thesis, The University of Texas at Austin, August 1994.

[5] Billington, S.L., "Behavior of Two-Span Continuous Pier Caps with Varying Levels of Prestress," Unpublished Masters Thesis, The University of Texas at Austin, December 1994.

[6] Scott, S.E., "An Evaluation of Repair Methods for Cantilever Bridge Piers," Unpublished Masters Thesis, The University of Texas at Austin, May 1997.

[7] American Association of State Highway Transportation Officials (AASHTO), Standard Specifications for Highway Bridges, Fourteenth Edition, 1989.

[8] Schlaich, J., Schafer, K., and Jennewein, M., "Toward a Consistent Design of Reinforced and Prestressed Concrete Structures," PCI Journal, Vol. 32, No. 3, May-June 1987, pp. 74-151.

[9] Breen, J.E., Burdet, O., Roberts, C., Sanders, D., and Wollmann, G., "Anchorage Zone Reinforcement for Post-Tensioned Concrete Girders," National Cooperative Highway Research Program, Report No. 356, August 1991.

[10] Frantz G.C., and Breen J.E., "Control of Cracking on the Side Faces of Large Reinforced Concrete Beams," Research Report 198-1F Center for Transportation Research, The University of Texas at Austin, August 1992.

[11] "Reinforced Concrete Column Investigation - Tentative Final Report of Committee 105," *ACI Journal*, Proceedings V. 20, No. 5, Feb. 1933, pp. 275-282.

[12] Zeihl, P., "Minimum Mild Reinforcing Requirements for Concrete Columns," Unpublished Masters Thesis, The University of Texas at Austin, December 1997.

[13] DeVries, R.A., "Anchorage of Headed Reinforcement in Concrete," Unpublished Doctoral Dissertation, The University of Texas at Austin, December 1996.

[14] Dyken, T., and Kepp B., "Properties of T-Headed Reinforcing Bars in High Strength Concrete," Norway.

[15] Suri K.M. and Dilger W.H., "Crack Width of Partially Prestressed Concrete Members," *ACI Journal*, September-October, 1986.

[16] Gergely P., and Lutz L.A., "Maximum Crack Width in Reinforced Concrete Flexural Members," *Causes, Mechanism and Control of Cracking in Concrete*, ACI Publication SP-20, American Concrete Institute, Detroit, 1973, pp. 87-117.

[17] Yip, T.S.C. , "Discussion of Equations for Prediction of Flexural Crack Width in Prestressed Members," Departmental Report, the University of Texas at Austin, December 1995.

[18] American Concrete Institute (ACI), *Building Code Requirements for Reinforced Concrete and Commentary - 318-93*, Detroit, 1993.

[19] American Association of State Highway and Transportation Officials (ASSHTO) LRFD Bridge Specifications and Commentary, April 1994.

[20] West, J.D., "Durability Design of Post-Tensioned Substructure Elements," Unpublished Doctoral Dissertation, The University of Texas at Austin, December 1997.

[21] Posten, R.W., "Improving Durability of Bridge Decks by Transverse Prestressing," Doctoral Dissertation, The University of Texas at Austin, December 1984.

[22] Borges, F. and Lima, A., "Crack and Deformation Similitude in Reinforced Concrete," *RILEM*, No. 7, June 1960.

[23] Sabnis, G.M., Harris, H.G., White, R.N., and Mirza, M.S., *Structural Modeling and Experimental Techniques*, Prentice-Hall Civil Engineering and Engineering Mechanics Series, 1983

[24] Abeles, P.W., "Static and fatigue tests on partially prestressed concrete," *ACI Journal*, December 1954.

[25] Abeles, P.W., "Philosophy of Partial Prestressing," *American Concrete Institute SP-59*, from 1976 Symposium on "Concrete Design: U.S. and European Practices", 1979, pp. 287-304.

[26] Wollmann, G.P. , Yates, D.L., Breen, J.E., and Kreger, M.E., "Fretting Fatigue in Post-Tensioned Concrete," The University of Texas at Austin, Center for Transportation Research, Report No. 465-2F, November 1988.

[27] "Cracks in Columns Force Closing on I-10", *San Antonio Express-News*, 5 April 1995, 2B.

[28] "Eight Columns on Freeway Set to be Repaired", *San Antonio Express-News*, 8 June 1995, 2B.

[29] *ACI*, "Building Code Requirements for Reinforced Concrete and Commentary - 318-63," Detroit, 1963.

[30] Orangun, C.O., Jirsa, J.O, and Breen, J.E. “A Reevaluation of Test Data on Development Length and Splices,” *ACI Journal*, Proceedings V. 74, Mar. 1977, pp. 114-122.

[31] ACI Committee 408, “Bond Stress - The State of the Art,” *ACI Journal*, Proceedings V. 63, No. 11, Nov. 1966, pp. 1161-1188.

[32] Wang, C, Salmon, C.G., *Reinforced Concrete Design*, Fourth Edition, Harper & Row, New York 1985, pp. 208-211.

[33] “ANSYS 5.0 Engineering Analysis System Command Reference Manual,” Swanson Analysis Systems Inc., Houston, PA, June 8, 1992.

[34] Microsoft Excel Version 5.0, Microsoft Corporation, 1994.

[35] Price Quotation for T-headed Bars, David Mitchell, Headed Reinforcement Canada, Inc. Mt. Pearl, Newfoundland, Canada, February 1996.

[36] Price Quotation for Dywidag Hardware, Micki L. Torres, Dywidag-Systems International, February 1996.

[37] Procedure to Install Internal Post-Tensioning and Price Estimate, Gary Greenfield, Fosrock Inc., May 1995.

[38] Price Quotation for Maxi Bolt Undercut Anchors, Chris Heinz, Drillco Devices LTD, Long Island City, NY, February 1996.

[39] Price Quotation for Threaded Through-Anchors, Phone Quotation, Austin Bolt, February 1996.

[40] Conversation w/ Scott Armstrong, TxDOT.